Welcome Message from the Chair –

IEEE PES Student Activities Subcommittee

On behalf of the Student Activities Subcommittee, I welcome you to the Student Poster Contest at the 2011 IEEE Power and Energy Society's General Meeting held at Detroit, MI, USA on July 25, 2011.

At the time of printing this book, we have 177 extended abstracts from students from different parts of the world confirmed to participate in the 2011 IEEE PES GM student poster contest. This book of extended abstracts is aimed at documenting the many outstanding research projects, some at their early stages, and providing a glimpse of some of the activities of interest to our society at various educational institutions around the world which is presented at this meeting in form of posters by students. The research topics of these abstracts (posters) fall into twelve categories, namely:

- Distribution Systems
- Electricity Markets
- Electric Vehicles in Power Systems
- Microgrids
- Modeling and Simulation
- Power System Analysis
- Power System Operations
- Power System Protection, and Fault Analysis and Detection
- Power System Stability and Control
- Reactive Power Compensation
- Renewable Energy
- Transmission Systems

All students are invited to attend the Student Industry Faculty luncheon to be held on July 27, 2011 from 12 pm to 1.30 pm. The student poster contest winners will be announced at the luncheon.

Continuous support from the Grainger Foundation, and IEEE Power and Energy Society, and its members, especially, Power and Energy Education Committee (PEEC) for the student activities is gratefully acknowledged.

Ganesh Kumar Venayagamoorthy, PhD

Missouri University of Science and Technology, USA

IEEE PES Student Activities Subcommittee

Chair
Dr. Ganesh Kumar Venayagamoorthy
Director of the Real-Time Power and Intelligent Systems Laboratory &
Professor of Electrical and Computer Engineering (eff. 9/11)
Missouri University of Science and Technology
301 W. 16th Street, Rolla, MO 65409, USA
gkumar@ieee.org
http://web.mst.edu/~ganeshv
http://rtpis.org

Vice-Chair
Dr. Siddarth Suryanarayanan
Assistant Professor
Department of Electrical and Computer Engineering
Colorado State University
Fort Collins, CO, USA
sid.suryanarayanan@ieee.org
http://www.engr.colostate.edu/~ssuryana

Secretary
Dr. Anurag K Srivastava
Assistant Professor
School of Electrical Engineering and Computer Science
Washington State University
PO Box 642752
EME 102
Spokane St Pullman
Washington 99164-2752, USA
asrivast@eecs.wsu.edu

LIST OF PARTICIPANTS AND POSTER TITLES

Distribution Systems

Page #	Poster #	Student Name (Last Name)	Student Name (First Name)	Affiliation	Poster Title
21	5001	Akinbode	Oluwaseyi	Arizona State University, Tempe, AZ	The Development and Application of a Distribution-class Locational Marginal Pricing Index for Future Distribution Systems
22	5002	Alam	Md. Jan-E-	University of Wollongong, New South Wales, Australia	Assessment of Distributed Generation Impacts on Distribution Networks Using Unbalanced Three-Phase Power Flow Analysis
23	5003	Alvehag	Karin	KTH - Royal Institute of Technology, Stockholm, Sweden	A Reliability Model for Distribution Systems Incorporating Seasonal Variations in Severe Weather
24	5004	Berardino	Jonathan	Drexel University, Philadelphia, PA	Economic Demand Dispatch for Demand Response via Control of Building Electric Loads
25	5005	Bin Humayd	Abdullah	University of Waterloo, Waterloo, ON, Canada	Comprehensive Multi-Year Distribution System Planning Using Back-Propagation Approach
26	5006	Chehreghani Bozchalui	Mohammad	University of Waterloo, ON, Canada	Optimal Operation of Residential Energy Hubs in Smart Grids
27	5007	Chennuri	Manasaveena	West Virginia University, Morgantown, WV	Agent Based Load Management System for a Smart Power Distribution System
28	5008	Contreras	Gustavo	Kansas State University, Manhattan, KS	Analysis of Animal-Caused Outages in Distribution Systems
29	5009	Douglin	Richard	Texas A&M University, College Station, TX	Addition of Smart Meter to a Reconfigured IEEE 34 Node Test Feeder
30	5010	Dyapa	Swathi	New Mexico Institute of Mining and Technology, Socorro, NM	Analysis, Modeling and Forecasting of Electric Load of a Town using linear regression model
31	5011	Halling	Todd	Kansas State University, Manhattan, KS	Feasibility of Community Wind Generation in Rural Western Kansas
32	5012	Kankanala	Padmavathy	Kansas State University, Manhattan, KS	Analysis of Outages Due to Wind and Lightning on Overhead Distribution Feeders

33	5013	Kefayati	Mahdi	The University of Texas at Austin, Austin, TX	Providing Efficient Incentives for Coordinated Energy Delivery to Flexible Electric Loads
34	5014	Meng	Fanjun	Missouri University of Science and Technology, Rolla, MO	Economic Loading of Renewable DG and Storage in Competitive Distribution Markets
35	5015	Montoya	Luis	University of Wisconsin, Milwaukee, WI	Power Quality Assessment of a Distribution Feeder connected with a wind generator based on a Doubly-Fed configuration
36	5016	Moradzadeh	Benyamin	University of Tennessee, Knoxville, TN	Optimal Distribution System Reconfiguration and Restoration without Heuristics
37	5017	Natarajan	Sudarshan A	Colorado State University, Fort Collins, CO	To Establish Bounds on Numerical Growth of the Feeder Reconfiguration Problem
38	5018	Tareila	Colin	Kansas State University, Manhattan, KS	A D-STATCOM Custom Inverter for Single Phase Wind and Solar Installations
39	5019	Venkatesan	Naveen	West Virginia University, Morgantown, WV	Demand Response Model and its Effects on Voltage Profile of a Distribution System
40	5020	Yan	Ruifeng	The University of Queensland, St. Lucia, Brisbane, Australia	Investigation of Voltage Variations in Unbalanced Distribution Systems due to High Photovoltaic Penetrations

Electricity Markets

Page #	Poster #	Student Name (Last Name)	Student Name (First Name)	Affiliation	Poster Title
41	5021	Dai	Ting	University of Nebraska-Lincoln, Lincoln, NE	Optimal Participation of Wind Power in the Liberalized Power Market
42	5022	Gonzalez	Nestor	Morelia Institute Technologic , Morelia, Mexico	Nodal Pricing for Multiple Types Class With Effect Assessment of Demand Response
43	5023	Hasan	Kazi Nazmul	The University of Queensland, Brisbane, Australia	Tradeoffs in Planning Renewable Power Generation Entry to the Electricity Market
44	5024	Liang	Jiaqi	Georgia Institute of Technology, Atlanta, GA	Combining the Reserve Market for Wind
45	5025	Morais	Hugo	Polytechnic Institute of Porto, R. Dr. António Bernardino de Almeida, Porto, Portugal	Multi-Agents VPP Aggregation
46	5026	Nappu	Muhammad Bachtiar	The University of Queensland, Brisbane, Australia	Evaluation of GENCO's Strategy in Creating a Congested System for Exercising Market Power
47	5027	Sharma	Satish	Malaviya National Institute of Technology Jaipur, India	Payment Cost Minimization Auction in Electricity Markets

Electric Vehicles in Power Systems

Page #	Poster #	Student Name (Last Name)	Student Name (First Name)	Affiliation	Poster Title
48	5028	Bangalore	Pramod	Chalmers University of Technology, Gothenburg, Sweden	Extension of Test System For Distribution System Reliability Analysis with Integration of Electric Vehicles in Distribution System
49	5029	Chakravarty	Priyam	Missouri University of Science and Technology, Rolla, MO	Optimum SOC of Grid-Connected SmartParks
50	5030	Clarke	Andrew	Clemson University, Clemson, SC	Plug in Hybrid Electric Vehicle Penetration on the Electric Grid
51	5031	Desai	Kaushal	University of North Carolina Charlotte, NC	Micro-turbine Based Intelligent Hybrid Vehicle with Vehicle to Grid (V2G) Capability
52	5032	He	Dawei	Georgia Inistitute of Technology, Atlanta, GA	Isolated Phase-shift Bidirectional DC/DC Converter Design for Plug-in Hybrid Electric Vehicle (PHEV) Applications
53	5033	ISLAM	F R	The University of New South Wales at Australian Defence Force Academy, Canberra, Australia	V2G Technology to Improve Wind Power Quality
54	5034	Li	Qiao	Carnegie Mellon University, Pittsburgh, PA	Large-scale Optimal Coordinated Charging of Electric Vehicles in Power Systems
55	5035	Maigha	Fnu	Missouri University of Science and Technology, Rolla, MO	Future Challenges in PHEV Implementation for Transport Electrification
56	5036	Sortomme	Eric	University of Washington, Seattle, WA	Optimal Unidirectional Vehicle-to-Grid Scheduling: Benefits for Utilities and Customers
57	5037	Wu	Di	Iowa State University, Ames, IA	Integrating Plug-in Electric Vehicles into the Electric Power System
58	5038	Yoon	Minhan	Korea University, Seoul, Korea	Operation of Electric Vehicle Management System based on V2G-Contract

Microgrids

Page #	Poster #	Student Name (Last Name)	Student Name (First Name)	Affiliation	Poster Title
59	5039	Fernandez	Juan	Florida International University, Miami, FL	Real-Time Monitoring, Operation and Control of Laboratory Test-Bed Micro Power System
60	5040	Gautam	Prajwal	Missouri University of Science and Technology, Rolla, MO	Real-Time Simulation of a Micro Grid with Unbalanced Sources
61	5041	Jimenez	Juan	Drexel University, Philadelphia, PA	Nonlinear Observability Issues Associated with Multiconverter Shipboard Power Systems
62	5042	Liu	Yang	Missouri University of Science and Technology, Rolla, MO	Intelligent Energy Management Controller for a Photovoltaic-Battery System
63	5043	Olivares	Daniel	University of Waterloo, Waterloo, ON, Canada	A Centralized Optimal Energy Management System for Microgrids
64	5044	Shariatzadeh	Farshid	Washington State University, Pullman, WA	Real Time Modeling and Simulation of Microgrid Reconfiguration
65	5045	Xu	Ling	University of South Florida, Tampa, FL	Control of a Battery to Improve the Operation of a Microgrid

Modeling and Simulation

Page #	Poster #	Student Name (Last Name)	Student Name (First Name)	Affiliation	Poster Title
66	5046	Ahmed	Danial	American University of Sharjah, Sharjah, UAE	Harnessing Mechanical Energy on Highways and Walkways to Generate Electric Power
67	5047	Arghandeh	Reza	Virginia Polytechnic Institute and State University, Arlington, VA	A Tool for Design and Simulation of Flywheels for Ride-through Applications in Data Centers
68	5048	Bevis	Troy	Florida State University, Tallahassee, FL	Development of an Architecturally Flexible Multiagent System Test Bed
69	5049	Cai	Chengrui	Iowa State University, Ames, IA	Modeling distributed photovoltaic generation for power system analysis
70	5050	Dang	Jie	Georgia Institute of Technology, Atlanta, GA	Induction Machine Model using Flux Linkage as State Variables Including Saturation
71	5051	Faria	Pedro	Polytechnic Institute of Porto, R. Dr. António Bernardino de Almeida, Porto, Portugal	LMP Triggered Demand Response Events Validation Using PSCAD
72	5052	Guo	Shaotong	Washington State University, Pullman, WA	Parameter Identification of DFIG Using Online Measurement Data
73	5053	Hernandez	Ronald	Northeastern University, Boston, MA	Adaptive Near-Optimal Compensation Applied to Linear and Nonlinear Loads
74	5054	Jadav	Raj	University of Queensland, St Lucia, QLD, Australia	Understanding Moisture Diffusion Process in Oil-Impregnated Pressboard Insulation of Transformer
75	5055	Jayasuriya	Sachi	Drexel University, Philadelphia, PA	Simulation of a DC-DC Buck-Boost Converter with Measurement Delay Errors
76	5056	Kim	Janghoon	University of Wisconsin, Madison, WI	The Relation Between Undervoltages, Line Outages and Load Shed in Cascading Failure
77	5057	Kim	Heejin	Yonsei University, Seoul, South Korea	Research on Dynamic Interaction among multiple Static Var Compensator
78	5058	Mohamed	Ahmed	Florida International University, Miami, FL	Bi-Directional AC-DC/DC-AC Converter for Power Sharing of Hybrid AC/DC Systems

79	5059	Munoz	Juan	University of Waterloo, Waterloo, ON, Canada	Alternative Techniques for Power Flow Solutions Based on Affine Arithmetic
80	5060	Nam	Taesik	Yonsei University, Seoul, Korea	Modeling of Electric Arc Furnace using PSCAD based on Measurement Data
81	5061	Nasiruzzaman	A. B. M.	The University of New South Wales at Australian Defence Force Academy, Canberra, Australia	Complex Network Framework Based Centrality Approach to Find Critical Nodes in a Power System
82	5062	Nejadpak	Arash	Florida International University, Miami, FL	Online Gain Scheduling of Multi-Resolution Wavelet-Based Controller for Acoustic Noise and Vibration Reduction in Sensorless Control of PMSM at low speed
83	5063	Pai	Gurudatha	University of Wyoming, Laramie, WY	Non-parametric System Identification of western North American Power System with its Statistics
84	5064	Paudyal	Sumit	University of Waterloo, Waterloo, ON, Canada	Three-phase Distribution OPF in Smart Grids: Optimality versus Computational Burden
85	5065	Pirnia	Mehrdad	University of Waterloo, Waterloo, ON, Canada	A Novel Optimization Approach to Solve Power Flow Problem Using Complementarity
86	5066	Potluri	Tejaswi	Arizona State University, Tempe, AZ	Network Topology Optimization with ACOPF
87	5067	Price	Alexandra	University of Queensland, St Lucia, QLD, Australia	Computational Tool to Derive Short-Circuit Network Equivalents
88	5068	Solanki	Ashishkumar	University of Wisconsin Milwaukee, Milwaukee, WI	Power Smoothing Technique using Battery in Double Fed Induction Generator
89	5069	Tao	Ye	Georgia Institute of Technology, Atlanta, GA	Three-Phase Optimal Power Flow
90	5070	Yu	Pengfei	Iowa State University, Ames, IA	A Novel Method to Control Step Size of Continuation Power Flow
91	5071	Ying	Xichun	North Carolina State University, Raleigh, NC	A Spatial, Temporal and Event Simulator of a Smart Grid

92	5072	Zhang	Hui	Arizona State University, Tempe, AZ	Effect of Various Parameters on the Inductive Induced Voltage and Current on Pipelines
93	5073	Zhao	Junhui	Wayne State University, Detroit, MI	Modeling and Control of Discrete Event Systems Using Finite State Machines with Parameters and Their Applications in Power Grids
94	5074	Zhao	Yue	University of Nebraska-Lincoln, Lincoln, NE	A Third-Order Sliding-Mode Controller for DC/DC Converters with Constant Power Loads

Power System Analysis

Page #	Poster #	Student Name (Last Name)	Student Name (First Name)	Affiliation	Poster Title
95	5075	Allen	Alicia	University of Texas at Austin, Austin, TX	Understanding Power System Oscillations Using Time-Domain Simulations
96	5076	Asprou	Markos	University of Cyprus, Nicosia, Cyprus	An enhanced hybrid state estimator for wide area monitoring of power systems
97	5077	Cao	Zheng	University of Wyoming, Laramie, WY	Electromechanical Mode Estimation Validation using Recursive Residual Whiteness Testing
98	5078	Farantatos	Evangelos	Georgia Institute of Technology, Atlanta, GA	A Predictive Out of Step Protection Scheme based on PMU enabled Dynamic State Estimation
99	5079	Haughton	Daniel	Arizona State University, Tempe, AZ	A synchrophasor based distribution system state estimator for increased observability and control
100	5080	Jiang	Xinyu Tony	Rensselaer Polytechnic Institute, Troy, NY	A Flexible Integrated Phasor System Design for PMU Data Concentrating
101	5081	Luitel	Bipul	Missouri University of Science and Technology, Rolla, MO	Scalable Integrated Situational Awareness Systems for Smart Grids
102	5082	Shrestha	Binod	University of Saskatchewan, Saskatoon, SK, Canada	Fast Out-of-Step Detection in Large Power System Using State Plane Analysis
103	5083	Wilson	Ralph	Florida State University, Tallahassee, FL	Multi-channel methodology for a system wide measure of complex dynamics in power systems
104	5084	Yan	Jie	Iowa State University, Ames, IA	PMU-Based Monitoring of Rotor Angle Dynamics

Power System Operations

Page #	Poster #	Student Name (Last Name)	Student Name (First Name)	Affiliation	Poster Title
105	5085	Abdullah	M Abu	University of Wollongong, Wollongong, New South Wales, Australia	Quantification of Emission Reduction from Electricity Network with the Integration of Renewable Resources
106	5086	Abrahamsson	Lars	Royal Institute of Technology (KTH), Teknikringen, Stockholm, Sweden	Railway power supply investment decisions considering the voltage drops -- assuming the future traffic to be known -- an MINLP formulation
107	5087	Most. Nahida	Akter	Rajshahi University of Engineering & Technology, Rajshahi, Bangladesh	Student Friendly Economic Dispatch Problem Analysis Toolbox in Power System
108	5088	Bordin	Bordeerath	National University of Singapore, Singapore	Techniques for Improving Precision and Construction Efficiency of a Pattern Classifier in Composite System Reliability Assessment
109	5089	Timothy	Carter	Wayne State University, Detroit, MI	Pollutant Emission Modeling for Sustainable Water Delivery
110	5090	Indrajit	Das	University of Waterloo, Waterloo, ON, Canada	Determination of Critical Sensitivity Indices for Large Scale Solar PV Investment Models
111	5091	Andrew	Drees	Michigan Technological University, Houghton, MI	Campus-Wide Power Infrastructure: Preliminary Study into Smart Grid Application
112	5092	Bamdad	Falahati	Mississippi State University, Mississippi State, MI	Reliability Assessment of Cyber-Physical Power Systems
113	5093	Che	Guan	University of Connecticut, Storrs, CT	Dual-tree M-band Wavelet Transform and Composite Very Short-term Load Forecasting
114	5094	Yiyun	Guo	University College London, London, United Kingdom	The Impact of Integrating Distributed Generation on the Losses in the Smart Grid
115	5095	Jesse	Hill	Drexel University, Philadelphia, PA	System Constraints Effects on Optimal Dispatch Schedule for Battery Storage Systems

116	5096	Qinran	Hu	University of Tennessee, Knoxville, TN	Heuristic Optimal Restoration Based on Constructive Algorithms for Smart Grids
117	5097	Yen-Yu	Lee	University of Texas at Austin, Austin, TX	A Two-stage Stochastic Economic Dispatch Model with Minimum Frequency Constraints
118	5098	Guodong	Liu	University of Tennessee, Knoxville, TN	Quantifying Spinning Reserve in Systems with Significant Wind Power Penetration
119	5099	Diego	Mejia	Iowa State University, Ames, IA	Affine Decision Rules-Based Power Systems Planning under Multiple Uncertainties
120	5100	Chihaya	Murakami	Waseda University, Tokyo, Japan	Generator-Transmission Maintenance Planning Prioritization Method with Pareto Optimal Set
121	5101	Ajinkya	Paralikar	Arizona State University, Tempe, AZ	Toward a More Flexible Generator Cost Function: A U-Shaped Supply Function
122	5102	Isha	Sharma	University of Waterloo, Waterloo, ON, Canada	Coordinated Operation of Energy Hubs in Smart Grids
123	5103	Karen	Studarus	University of Washington, Seattle, WA	Modeling the impact of wind ramping events on thermal power plant emissions
124	5104	Auswin	Thomas	Iowa State University, Ames, IA	Integrated Retail and Wholesale Power System Operation with Smart Grid Functionality
125	5105	Jerry	Thompson	West Virginia University, Morgantown, WV	Hardware Prototype of a Multi-Agent Grid Management System
126	5106	Qin	Wang	Iowa State University, Ames, IA	New Security Tools for Real-Time Operation of Power System
127	5107	Peng	Xiong	National University of Singapore, Singapore	The Stochastic Unit Commitment with Reliability Constraints
128	5108	Junpeng	Zhan	University of Liverpool, Liverpool , UK	Integrated Maintenance Scheduling of Generators and Transmission Lines Based on Fast Group Searching Optimizer

Power System Protection, and Fault Analysis and Detection

Page #	Poster #	Student Name (Last Name)	Student Name (First Name)	Affiliation	Poster Title
129	5109	Gong	Xiang	University of Nebraska-Lincoln, Lincoln, NE	Wind Turbine Imbalance Fault Detection Using Current Signals
130	5110	Hong	Junho	University College Dublin, Ireland	An Intrusion and Defense Testbed in a Cyber-Power system Environment
131	5111	Howard	Dustin	Georgia Institute of Technology, Atlanta, GA	Fault Current Contribution of Type I Wind Turbine-Generators
132	5112	Jo	Yonghwan	Myongji University, South Korea	A User Interface technique for HMI of IED based on IEC 61850
133	5113	Korad	Akshay	Arizona State University, Tempe, AZ	Special Protection Schemes (SPSs) with Smart Transmission Switching
134	5114	Lacy	Clark	University of Nebraska-Lincoln, Lincoln, NE	Wind Turbine Imbalance Fault Detection Using the Hilbert-Huang Transform
135	5115	Lee	Won-seok	Myongji University, South Korea	Selective Ground Fault Protection Algorithm For DC Traction Systems
136	5116	Leelaruji	Rujiroj	Royal Institute of Technology (KTH), Stockholm, Sweden	Coordination of Protection and VSC-HVDC Systems for Mitigating Cascading Failures
137	5117	Long	Xun	University of Alberta, Edmonton, AB, Canada	A New Technique of Faults Detection in De-Energized Distribution Feeders
138	5118	Lu	Dingguo	University of Nebraska-Lincoln, Lincoln, NE	Stator Current-Based Fault Diagnosis of Wind Turbines using ALE & Wiener Filter
139	5119	Martin	Russell	University of Wyoming, Laramie, WY	Detection of Forced-Response Distrubances in Power Systems
140	5120	Ruiz	Jose	University of Tennessee at Chattanooga, Chattanooga, TN	Testing POTT Scheme Based on International Electrotechnical Commission (IEC) 61850
141	5121	Ryan	Shane	University College Dublin, Belfield, Dublin, Ireland	Trending and Condition Monitoring of Wind Turbine SCADA data
142	5122	Subedi	Laxman	Kansas State University, Manhattan, KS	Trouble Call Analysis Using Artificial Immune System Techniques
143	5123	Yin	Yujuan	Zhejiang University, Hangzhou, Zhejiang, China	Multi-Kernel Support Vector Classifier for Fault Diagnosis of Transformers

Power System Stability and Control

Page #	Poster #	Student Name (Last Name)	Student Name (First Name)	Affiliation	Poster Title
144	5124	Chompoobutrgool	Yuwa	KTH Royal Institute of Technology, Stockholm, Sweden	Linear Analysis of the KTH-NORDIC32 System
145	5125	Dahal	Sudarshan	The University of Queensland, Australia	An Approach to Control Photovoltaic Generator to Damp Low Frequency Oscillations in Emerging Distribution Systems
146	5126	Follum	Jim	University of Wyoming, Laramie, WY	Relating Residuals to Mode Estimate Accuracy for Stability Analysis
147	5127	Hadidi	Ramtin	Memorial University of Newfoundland, St. John's, NL, Canada	A Real-Time Wide-Area Excitation Control to Enhance Transient and Oscillatory Stabilities
148	5128	Hassani Variani	Maryam	University of Tennessee, Knoxville, TN	Flatness-Based Automatic Generation Control with High Penetration of Wind Energy
149	5129	Huang	Yulong	South China University of Technology, Guangzhou, China	Optimal Transient Stability Control Based on OMIB Equivalents and Trajectory Sensitivities
150	5130	Liu	Qixing	Carnegie Mellon University, Pittsburgh, PA	Toward Modeling and Control of Synchrophasor-enabled Frequency Regulation in the Electric Energy Systems
151	5131	Mahmud	Md. Apel	The University of New South Wales at Australian Defence Force Academy, Canberra, Australia	Observer-based Nonlinear Excitation Control of Power Systems
152	5132	Makasa	Kangombe	Missouri University of Science and Technology, Rolla, MO	Adaptive Dynamic Programming for SVC Secondary Voltage Control in a Smart Grid
153	5133	Modi	Nilesh	The University of Queensland, Brisbane, Australia	Performance of Power Oscillation Damping Controllers with Different Static Load Characteristics
154	5134	Nasr Azadani	Ehsan	University of Waterloo, Waterloo, ON, Canada	Modeling and Stability Analysis of a Microturbine as a Distributed Energy Resource

155	5135	Ogahara	Ryuichi	Waseda University, Tokyo, Japan	Time Evaluation of Voltage Stability for System Planning Study
156	5136	Olulope	Paul	Missouri University of Science and Technology, Rolla, MO	TRANSIENT STABILITY PREDICTION USING RECURRENT NEURAL NETWORK
157	5137	Pajuelo	Eli	University of Saskatchewan, Saskatoon, SK, Canada	Coordination of Underexcitation Limiter, Loss of Excitation Protection and Generator Control
158	5138	Pirooz Azad	Sahar	University of Toronto, Toronto, ON, Canada	Large Area Small Signal Stability Enhancement of AC Networks Based on Multi-Infeed HVDC Configuration
159	5139	Puthenpurayil Kunjumuhammed	Linash	Imperial College London, UK	Simulation Platform to Study the Effect of Large Scale Integration of Wind Power in Small Signal Stability
160	5140	Segundo Sevilla	Felix Rafael	Imperial College London, UK	Fault-Tolerant Wide-Area Control of Power Systems
161	5141	Xu	Guoyi	Queen's University of Belfast, Belfast, UK	Wind turbines with energy storage for power smoothing and FRT enhancement
162	5142	Zhang	Zhe	University of Nebraska-Lincoln, Lincoln, NE	A Novel Energy-Based Dissipative Excitation Control for Synchronous Generators

Reactive Power Compensation

Page #	Poster #	Student Name (Last Name)	Student Name (First Name)	Affiliation	Poster Title
163	5143	Aziz	Tareq	The University of Queensland, Australia	A Grid Compatible Methodology for Reactive Power Compensation in Renewable Based Distribution System
164	5144	Dvorkin	Yury	University of Washington, Seattle, WA	Reactive Power Compensation in Low-Power Mode: Implementing Controlled Shunt Reactors
165	5145	GopiReddy	Lakshmi	Texas A&M University, College Station, TX	Thermal impact on IGBTs of Grid-connected STATCOM
166	5146	Roy	N K	Waseda University, Tokyo, Japan	Low Voltage Profile - a Big Problem for Dispersed Generation
167	5147	Somayajula	Deepak	Colorado State University, Fort Collins, CO	Ultra-capacitor Integration to Improve Dynamic Real and Reactive Power Conditioning
168	5148	Suzuki	Ken	The University of Texas at Austin, Austin, TX	Shunt Capacitor Renewal Planning with a Cost Leveling Strategy using the Condition Age Model
169	5149	Wang	Yurong	Kansas State University, Manhattan, KS	Reactive Power Planning using Different VAr Devices

Renewable Energy

Page #	Poster #	Student Name (Last Name)	Student Name (First Name)	Affiliation	Poster Title
170	5150	Adhikari	Sarina	University of Waterloo, Waterloo, ON, Canada	Voltage and PQ Control with Inverter-based Photovoltaic Systems
171	5151	Amin	Mahmoud	National University of Singapore, Singapore	A Novel High Frequency Multi-Port Power Converter for Hybrid Sustainable Energy Conversion Systems
172	5152	Chen	Xia	Arizona State University, Tempe, AZ	LCC Based MTDC for Grid Integration of Large Onshore Wind Farms in Northwest China
173	5153	Eftekharnejad	Sara	Wichita State University, Wichita, KS	Impact of Large Scale Penetration of Photovoltaic Systems on Power System Performance
174	5154	El-Mazariky	Amr	University of Tennessee, Knoxville, TN	Analysis of Wind Generation Impacts on Ontario System Operation
175	5155	Fan	Miao	University of Tennessee, Knoxville, TN	Probabilistic Power Flow in Transmission System with Photovoltaic Generation
176	5156	Finnie	Preston	University of Nebraska-Lincoln, Lincoln, NE	Renewable and Modular Micro-Source for Smart-Grid Applications
177	5157	Gu	Yingzhong	Texas A&M University, College Station, TX	Assessment of Wind Generation Curtailment
178	5158	Hlaing	Aye	Waseda University, Tokyo, Japan	A Selection Method of Output Control Generators Considering Voltage Stability for Large Penetration of PVs
179	5159	Mohanpurkar	Manish	Colorado State University, Fort Collins, CO	A Framework for the Investigation of Impacts of Wind Energy Penetration on Unscheduled Flows in Bulk Interconnections
180	5160	Najera	Yazmin	The University of Texas at Austin, Austin, TX	Image Processing Tools for Predicting the Time of Cloud Shadow Arrivals to Photovoltaic Systems
181	5161	Ochs	David	Kansas State University, Manhattan, KS	Renewable Energy-Based Power Electronics Teaching Lab
182	5162	Shamseldein	Mohamed	University of Waterloo, Waterloo, ON, Canada	Novel Configurations for Photovoltaic Farms to Reduce Partial Shading Losses

183	5163	Shu	Zhen	National University of Singapore, Singapore	Latin Hypercube Sampling Techniques for Power Systems Reliability Analysis with Renewable Energy Sources
184	5164	Sinha	Anubhav	Arizona State University, Tempe, AZ	Multi-State Representation of Variable Wind Generation Profiles for Power System Reliability Studies
185	5165	Tamtam	Perlekar	Wichita State University, Wichita, KS	Steady-State Analysis of a Renewable Energy Inverter
186	5166	Wei	Yanli	University of Tennessee, Knoxville, TN	Impact to the Volatility of Electricity Price under High-Penetration Wind Power
187	5167	Xu	Yao	University of Tennessee, Knoxville, TN	Payment Cost Minimization Considering Wind Energy Effects and Transmission Constrains
188	5168	Zeng	Jianwu	University of Nebraska-Lincoln, Lincoln, NE	Short-Term Solar Power Prediction Using an RBF Neural Network

Transmission System

Page #	Poster #	Student Name (Last Name)	Student Name (First Name)	Affiliation	Poster Title
189	5169	Barrows	Clayton	Penn State University, University Park, PA	Transmission Switching Forensics
190	5170	Chen	Hao	Iowa State University, Ames, IA	Low-Frequency AC Transmission for Offshore Wind Power
191	5171	Elkington	Katherine	Royal Institute of Technology, Sweden	Operation of Doubly Fed Induction Generators with VSC-HVDC Transmission
192	5172	He	Lina	University College Dublin, Belfield, Dublin, Ireland	Impact of AC Grid Faults on VSC-HVDC Off-Shore Wind Network
193	5173	Lessa	Leonardo	University of São Paulo, State, Ilha Solteira, Brazil	Analyses of the modifications in the p circuits for inclusion of frequency influence in transmission line representation
194	5174	Bui	Minh	The University of Queensland, Brisbane, Australia	Dynamic simulation of HVDC interconnection in large power system
195	5175	Langella	R	Second University of Naples	Preliminary Analysis of MV Cable Lines Models for High Frequency Harmonic Penetration Studies
196	5176	Xing	Luhua	Shandong University, Shandong Jinan, China	A New Protection Principle for HVDC Transmission Lines Based on Fault component of Voltage and Current
197	5177	Yin	Haiping	University of South Florida, Tampa, FL	Coordination between DFIG-based Wind Farm and LCC-HVDC Transmission Considering Limiting Factors

The Development and Application of a Distribution-class Locational Marginal Pricing Index for Future Distribution Systems

Oluwaseyi Akinbode and Kory Hedman
School of Electrical, Computer and Energy Engineering, Arizona State University, Tempe, AZ 85287-5706, USA
Email: oakinbod@asu.edu and kory.hedman@asu.edu

***Abstract*—With the implementation of smart grid objectives, it is expected that the deployment of distributed generation resources, energy storage systems and responsive loads in distribution systems in the near future will become substantial. Consequently, the distribution system operational paradigm will expand to include real-time operating strategies for distributed resources and system optimization. Additionally, there will be increased focus on economic efficiency. To adequately support these functions, a new price signal called the distribution-class locational marginal pricing index (D-LMP) is being proposed for use in distribution systems. The D-LMP is an extension of the LMP concept to distribution systems. In this paper a case is made for the D-LMP as a better pricing signal than the rate structures that can be obtained in today's distribution systems and a better facilitator of the smart grid objectives. The paper highlights D-LMP's capability to capture the time-varying nature of the marginal cost of energy and the locational effect of congestion and system losses on the cost of delivered energy. Developing a model for the D-LMP will provide the added benefit of creating a model around the new resources in the distribution grid. The behavior of these resources, which will include responsiveness to price levels, can be funneled back to the transmission system for the benefit of the competitive bulk energy system.**

I. KEY FIGURE

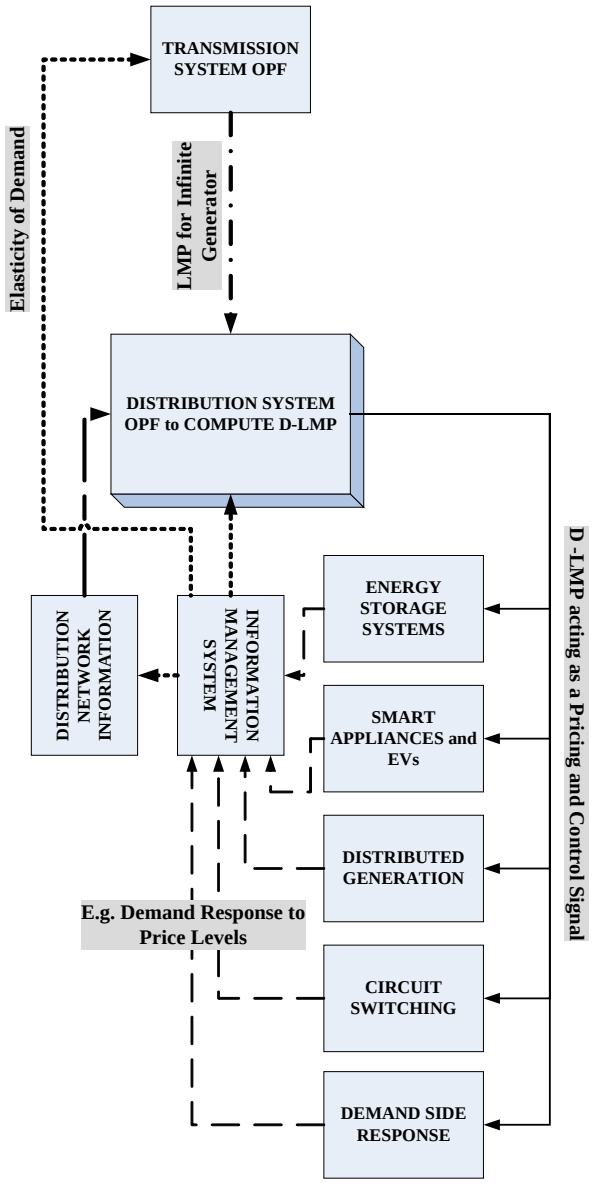

Figure 1. D-LMP Calculation and Application Framework

Assessment of Distributed Generation Impacts on Distribution Networks Using Unbalanced Three-Phase Power Flow Analysis

Md. Jan-E-Alam, K. M. Muttaqi, and D. Sutanto
Integral Energy Power Quality and Reliability Centre, School of Electrical, Computer and Telecommunications Engineering, University of Wollongong, Wollongong, New South Wales, 2522, Australia,
Email: mjea982@uowmail.edu.au

***Abstract*— Impacts of Distributed Generation (DG) resources on distribution networks have been studied. A Newton-Raphson algorithm based three phase power flow program has been developed to incorporate the effects of system unbalance and single phase DG injection. Power flow equations have been formulated and solved in phase coordinate form. Effects of substation load-tap changer, voltage regulator, shunt capacitor and different type of load models have been considered in the development of the program. Phase asymmetry of distribution networks has been treated by modifying the Jacobian matrix. The proposed technique has been tested on IEEE 34 bus distribution test system for assessment of DG impacts in the networks and results have been presented.**

I. KEY EQUATIONS

Equations used for development of the three-phase load flow program and impact assessment of DG resources on distribution network are:

$$P_k^{ph} = V_k^{ph}\left(\sum_{i=k}^{m} V_i^{i} \sum_{j=a,b,c} V_i^{i}\left[\begin{matrix} G_{k-i}^{ph-j}\cos\left(\delta_k^{ph}-\delta_i^{j}\right)+ \\ B_{k-i}^{ph-j}\sin\left(\delta_k^{ph}-\delta_i^{j}\right)\end{matrix}\right]\right) \quad (1)$$

$$Q_k^{ph} = V_k^{ph}\left(\sum_{i=k}^{m} V_i^{i} \sum_{j=a,b,c} V_i^{i}\left[\begin{matrix} G_{k-i}^{ph-j}\sin\left(\delta_k^{ph}-\delta_i^{j}\right)- \\ B_{k-i}^{ph-j}\cos\left(\delta_k^{ph}-\delta_i^{j}\right)\end{matrix}\right]\right)$$

$$\begin{bmatrix}(\Delta P)_{abc}\\(\Delta Q)_{abc}\end{bmatrix} = \begin{bmatrix}\left(\frac{\partial P}{\partial \delta}\right)_{abc} & \left(\frac{\partial P}{\partial V}V\right)_{abc}\\ \left(\frac{\partial Q}{\partial \delta}\right)_{abc} & \left(\frac{\partial Q}{\partial V}V\right)_{abc}\end{bmatrix}\begin{bmatrix}(\Delta\delta)_{abc}\\ \left(\frac{\Delta V}{V}\right)_{abc}\end{bmatrix} \quad (2)$$

$$\left[(\Delta V)_{abc}\right] = \left[\left(\frac{\partial P}{\partial V}\right)_{abc} - \left(\frac{\partial P}{\partial \delta}\right)_{abc}\left(\frac{\partial P}{\partial \delta}\right)_{abc}^{-1}\left(\frac{\partial Q}{\partial V}\right)_{abc}\right]^{-1}\left[(\Delta P)_{abc}\right] \quad (3)$$

II. KEY FIGURES

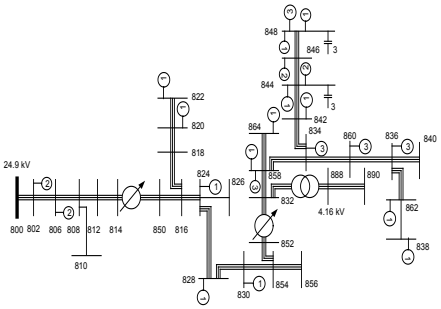

Figure 1. IEEE 34 bus distribution test system with DG locations

III. KEY RESULTS

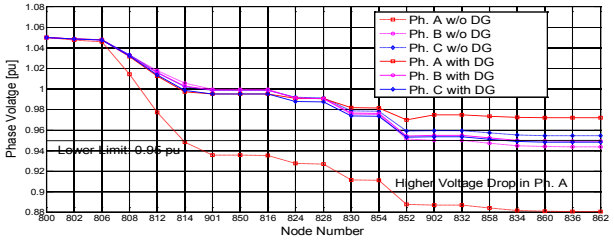

Figure 2. Voltage support by DG resources

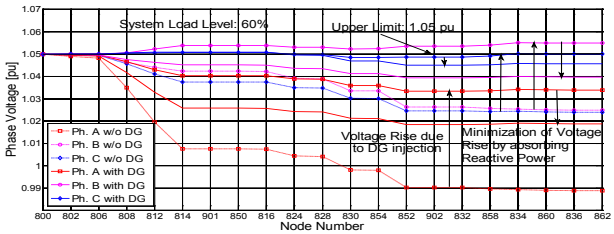

Figure 3. Voltage rise effect without regulator and possible minimization by absorbing reactive power by DG

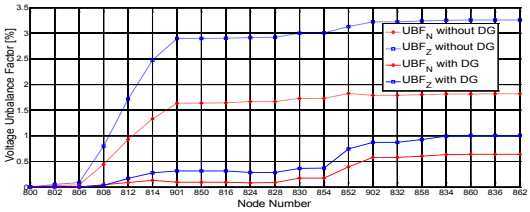

Figure 4. Voltage unbalance factors with and without DG (without regulator)

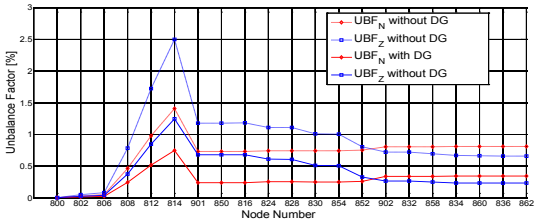

Figure 5. Voltage unbalance factors with and without DG (with regulator)

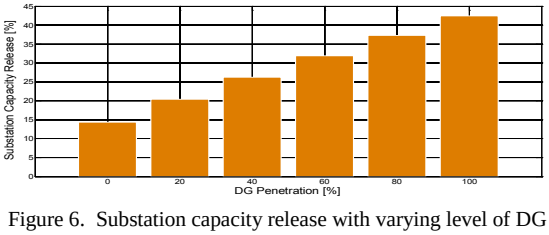

Figure 6. Substation capacity release with varying level of DG penetration

A Reliability Model for Distribution Systems Incorporating Seasonal Variations in Severe Weather

Karin Alvehag and Lennart Söder
Department of Electric Power Systems, KTH - Royal Institute of Technology, Stockholm, Sweden
Email: karin.alvehag@ee.kth.se

Paper published in IEEE TRANSACTIONS ON POWER DELIVERY, VOL. 26, NO. 2, APRIL 2011

***Abstract*— In distribution system planning and operation, accurate assessment of reliability performance is essential for making informed decisions. Also, performance-based regulation accompanied by quality regulation increases the need to understand and quantify differences in reliability performance between networks. Distribution system reliability performance indices exhibit a stochastic behavior due to the impact of severe weather. In this paper a new reliability model is presented which incorporates the stochastic nature of the severe weather intensity and duration to model variations in failure rate and restoration time. The model considers the impact of both high winds and lightning and can be expanded to account for more types of severe weather. Furthermore, the modeling approach considers when severe weather is likely to occur during the year by using a non-homogeneous Poisson process (NHPP). The proposed model is validated and applied to a test system to estimate reliability indices. Results show that the stochasticity in weather has a great impact on the variance in the reliability indices.**

I. KEY EQUATIONS

The weather intensity levels during high winds and lightning are modeled through the wind speed *w* and the ground flash density *Ng*, respectively. A constant failure rate during normal weather λ_n is assumed. The time-dependent failure rate for overhead lines is defined as:

$$\lambda(w(t), N_g(t)) = \lambda_{hw}(w(t)) + \lambda_l(N_g(t)) + \lambda_n(w(t), N_g(t)) \quad (1)$$

The restoration time for overhead lines is modeled as a function of weather intensity through a weight factor, f_w. The effect of hourly and daily variations in availability of repair crew is modeled by f_d and f_h. The restoration time during normal weather conditions is r_{norm}. The restoration time for overhead lines is defined as:

$$r(t) = f_w(w(t), N_g(t))\ f_d(t)\ f_h(t)\ r_{norm} \quad (2)$$

II. KEY RESULTS

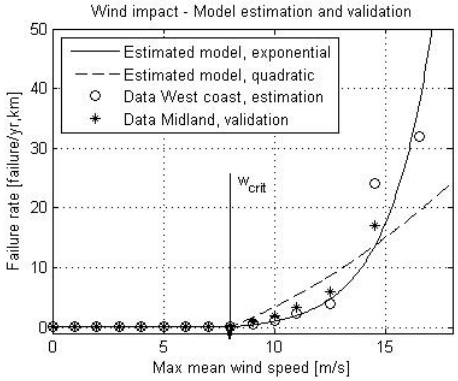

Figure 1. Failure rate as a function of maximum mean wind speed.

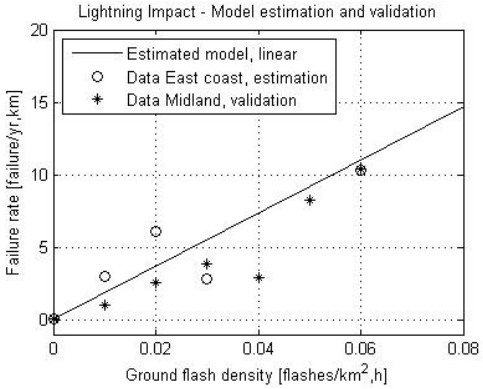

Figure 2. Failure rate as a function of ground flash density

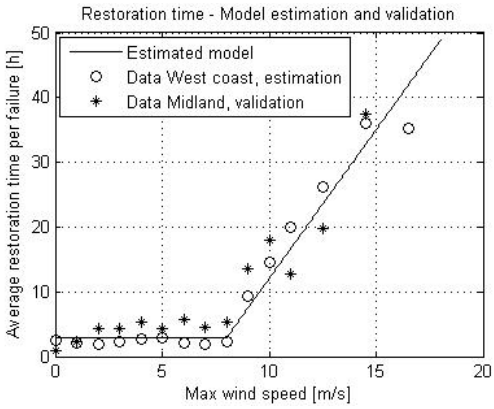

Figure 3. The average restoration time per overhead line failure for each wind speed class.

Economic Demand Dispatch for Demand Response via Control of Building Electric Loads

Jonathan Berardino, Chika Nwankpa, and Karen Miu
Center for Electric Power Engineering, Electrical and Computer Engineering Department, Drexel University, Philadelphia, PA 19104, USA,
Email: jnb38@drexel.edu, nwankpa@ece.drexel.edu, and miu@ece.drexel.edu

***Abstract*— This poster presents a method for determining the economic dispatch of the controllable electric load (demand) of a group of buildings for demand response purposes. A generic problem formulation to minimize a facility's overall electricity cost is developed with a focus on defining the overall problem and certain assumptions that are derived from real-world building issues. The problem is simplified so it can be solved as a linear programming problem, and a specific example is presented to demonstrate this approach. This example will compare the proposed method to possible approaches by a building manager attempting to shed load via on-site building management systems. This work is a part of efforts at Drexel University aimed at developing a "Smart Campus".**

I. Key Equations

The generic economic demand dispatch problem is formulated as a constrained nonlinear minimization problem as shown below:

$$\min C\left(P_{HVAC,it}\right) = \alpha\left(\sum_{i=1}^{m}\sum_{t=1}^{T} P_{L,it} + \sum_{i=1}^{m}\sum_{t=1}^{T} P_{HVAC,it} + \sum_{i=1}^{m}\sum_{t=1}^{T} P_{Loss,it}\left(P_{HVAC,it}\right)\right) \quad (1)$$

$$s.t. \quad B_L - \sum_{i=1}^{m} P_{HVAC,i} - \sum_{i=1}^{m} P_{L,i} - \sum_{i=1}^{m} P_{Loss,i}\left(P_{HVAC,i}\right) = P_D \quad (2)$$

$$\Theta_{\min,i} \le \Theta_i \le \Theta_{\max,i} \quad (3)$$

$$0 \le P_{HVAC,i}\left(\Theta_i\right) \le P_{rated,i} \quad (4)$$

$$\Delta t_i \le \Delta t_{required,i} \quad (5)$$

II. Key Figures

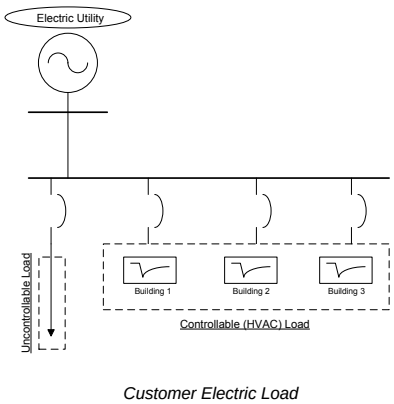

Figure 1. Physical setup for 3 building demand dispatch example

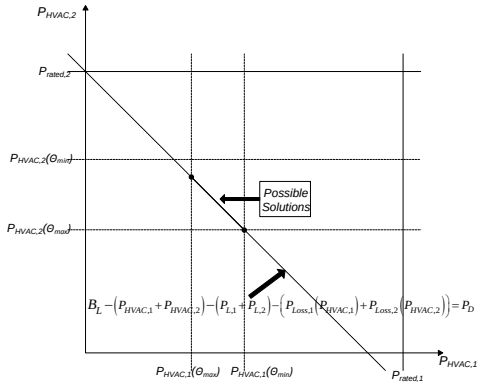

Figure 2. Generic depiction of constrained LP problem for 2 buildings

III. Key Results

TABLE 1. LP Dispatch Example Solution

	Building #	1	2	3
Interval 1	P_{HVAC} (kW)	97.93	102.38	133.02
	Θ (degF)	52.56	54.93	46.96
	Δ P_{HVAC} (kW)	-2.07	2.38	-46.98
	Δ Θ (degF)	2.56	-2.07	6.96
Interval 2	P_{HVAC} (kW)	96.26	97.43	111.08
	Θ (degF)	54.79	58.98	52.12
	Δ P_{HVAC} (kW)	-1.68	-4.95	-21.95
	Δ Θ (degF)	2.23	4.05	5.16
Interval 3	P_{HVAC} (kW)	106.56	114.02	150.85
	Θ (degF)	40.26	43.68	39.68
	Δ P_{HVAC} (kW)	10.30	16.59	39.77
	Δ Θ (degF)	-14.54	-15.30	-12.44
Interval 4	P_{HVAC} (kW)	90.90	90.95	94.35
	Θ (degF)	54.92	57.14	49.59
	Δ P_{HVAC} (kW)	-15.66	-23.07	-56.50
	Δ Θ (degF)	14.67	13.47	9.91

Comprehensive Multi-Year Distribution System Planning Using Back-Propagation Approach

Abdullah S. Bin Humayd, and Kankar Bhattacharya
Department of Electrical and Computer Engineering,
University of Waterloo, Waterloo, ON, Canada N2L 3G1
Email: abinhuma@uwaterloo.ca and kankar@ece.uwaterloo.ca

***Abstract*— Distribution system design and planning is facing a major change in paradigm because of deregulation of the power industry and with rapid penetration of distributed generation (DG) sources. This paper presents a comprehensive multi-year distribution system planning approach. A new heuristic approach based on a back-propagation algorithm combined with cost-benefit analysis is presented. It incorporates various energy supply options for discos such as DG, substations and feeders and determines the size, placement and upgrade plan. The optimal size and location of distribution system component upgrades for the plan terminal year are first found using cost-benefit analysis combined with an optimization model. This provides a compatible set of upgrade and investment to the distribution system. Then the year of commissioning are then determined for the obtained optimal parameters. To show the effectiveness of the proposed approach sensitivity analysis is presented in order to examine the change of the results to changes in energy prices and demand.**

I. KEY EQUATIONS

- The objective function aims to minimize the investment and operating cost of the distribution company which includes DG units, substation and feeders and the cost of the unserved energy.
- Subject to:
    1. Nodal power balance
    2. Feeder capacity limits
    3. Substation capacity limits
    4. DG capacity limits
    5. Budget limits

II. KEY RESULTS

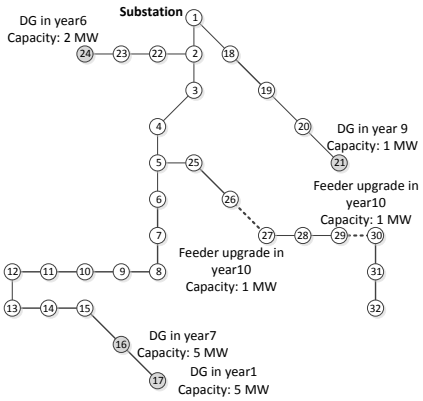

Figure 2. Optimal distribution system plan

III. KEY FIGURES

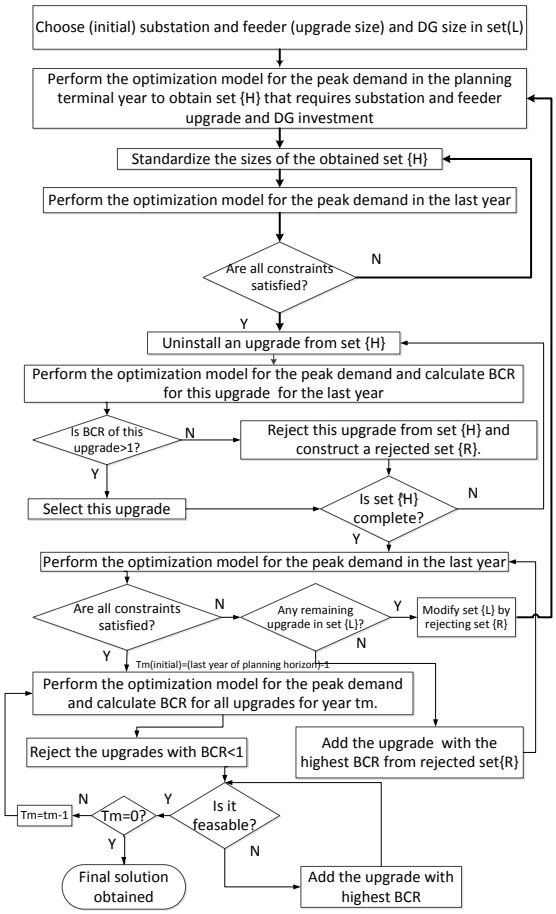

Figure 1. Schematic of the proposed approach

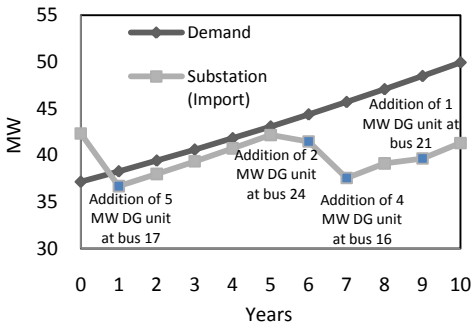

Figure 3. Distribution company demand and imported energy via substation

Optimal Operation of Residential Energy Hubs in Smart Grids

Mohammad C. Bozchalui, Syed A. Hashmi, Hussin Hassen, Claudio A. Cañizares and Kankar Bhattacharya
Department of Electrical and Computer Engineering, University of Waterloo, Waterloo, ON N2L 3G1, Canada,
Email: {mchehreg, ccanizar, kankar}@uwaterloo.ca

***Abstract*— This paper presents mathematical optimization models of residential energy hubs which can be readily incorporated into automated decision making technologies in Smart Grids, and can be solved efficiently in a real-time frame to optimally control all major residential energy loads, storage and production components while properly considering the customer preferences and comfort level. Mathematical models for major household demand, i.e., fridge, freezer, dishwasher, washer and dryer, stove, water heater, hot tub, and pool pumps are formulated. Also, mathematical models of other components of a residential energy system including lighting, heating, and air-conditioning are developed, and generic models for solar PV panels and energy storage/generation devices are proposed. The developed mathematical models result in a Mixed Integer Linear Programming (MILP) optimization problem, which the objective is to minimize demand, total cost of electricity and gas, emissions and peak load over the scheduling horizon while considering end-user preferences. The presented simulation results demonstrates the application of this model to a real household, showing savings of up to 20% on energy costs and 50% on peak demand, while maintaining the household owner's desired comfort levels.**

I. KEY EQUATIONS

The general form of the optimization model for optimal operation of residential energy hubs is as follows:

$$\begin{aligned} \min \quad & J \\ \text{s.t.} \quad & \text{peak power constraint} \\ & \text{devices' operational constraints} \end{aligned} \tag{1}$$

where J denotes the objective functions such as temperature deviations, total energy consumption, and total costs.

II. KEY FIGURES

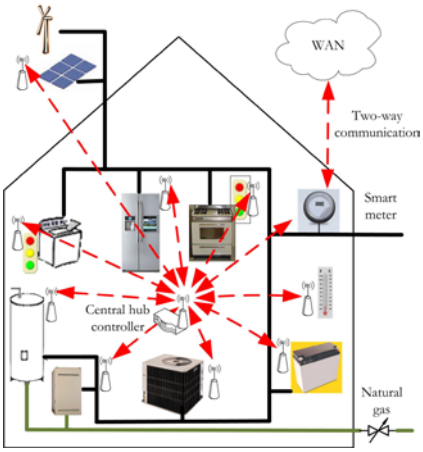

Figure 1. Residential energy hub.

III. KEY RESULTS

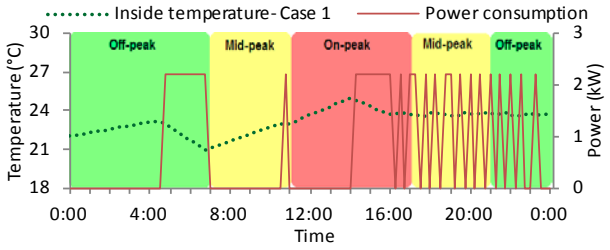

Figure 2. Operational schedule of AC during a typical summer day.

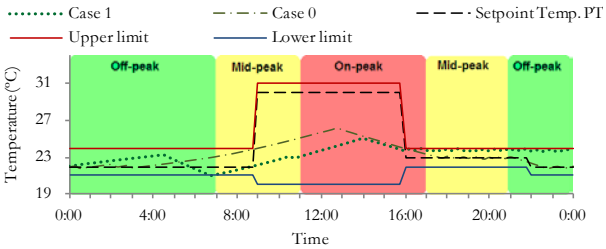

Figure 3. Comparison of indoor household temperatures.

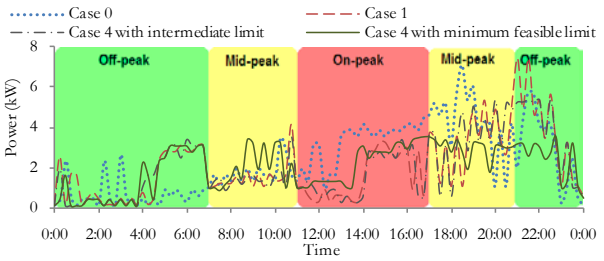

Figure 4. Effect of peak load constraints on household demand.

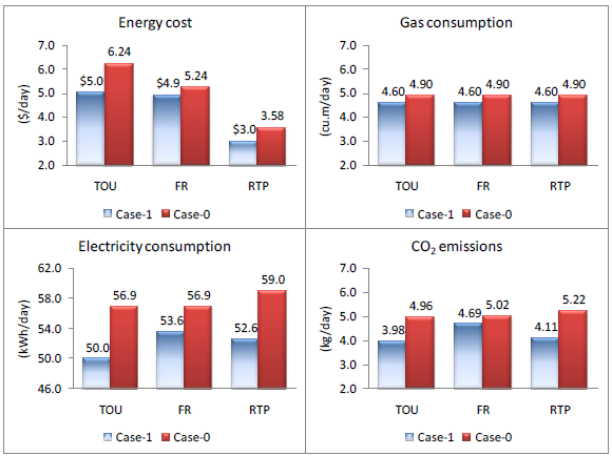

Figure 5. Comparison o energy costs, energy consumption, gas consumption, and emissions for TOU, FR, and RTP prices for a summer day

Agent Based Load Management System for a Smart Power Distribution System

Manasaveena Chennuri
Advance Power and Electric Research Center, Lane Department of Computer Science and Electrical Engineering, West Virginia University, Morgantown, WV 26505, USA,
Email: *mchennur@mix.wvu.edu*

***Abstract*— Smart Grid initiative by various power industrial units around the globe brought a revolutionary change to impart intelligence and robust technology into the existing electric grid to make it highly reliable with effective capacity utilization. Improving the performance of the distribution system by imparting intelligence and communication is very vital to make the grid smart. This paper presents a novel approach to accommodate distributed generation resources in the power distribution system helping to reduce the peak power demand by 15 percent. Demand dispatch; a novel approach to demand response is implemented to achieve peak demand reduction. Multi-agent system is adopted to embed intelligence into the system by managing the load through agent communication. Distribution system load is forecasted in MATLAB and multi-agents programmed using Java Agent DEvelopment framework (JADE) utilize the forecasted load data to dispatch the load in such a way so as to reduce the peak demand. The dispatch algorithm makes use of controllable loads which can be turned on and off with unnoticeable interruption. Real time historical system data is used in the load forecast. Agents are located at load management level, zone level, load aggregator level, and DG level. These agents communicate and negotiate to dispatch the load appropriately based on resources and load availability.**

I. KEY FIGURES

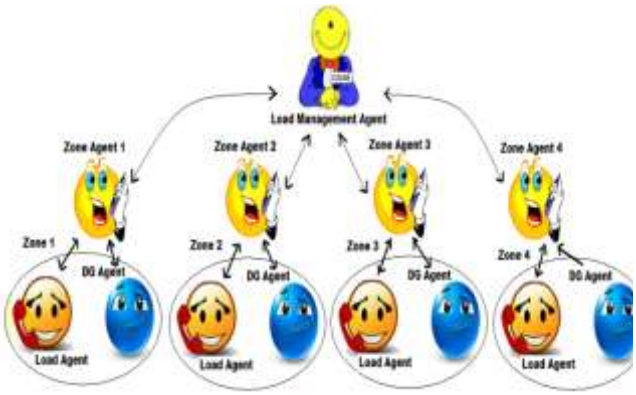

Figure 1. Proposed Multi-Agent System Architecture

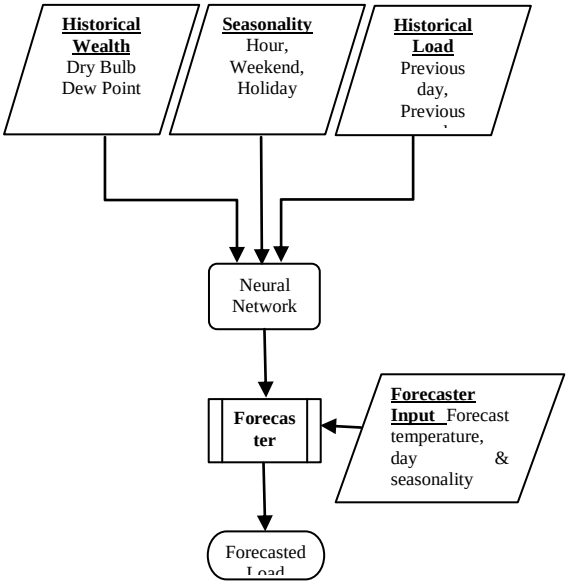

Figure 2. Load Forecasting Flowchart

II. KEY RESULTS

Time of the Day	System Load Before Peak Management (MW)	System Load After Peak Management (MW)
1	21.2208	19.89222819
2	20.1878	19.773
3	19.3578	19.009
4	18.6598	18.4947
5	18.3294	18.482
6	18.6346	19.8057649
7	19.4703	19.8057649
8	20.4247	19.8057649
9	20.9876	19.8057649
10	21.7635	19.8057649
11	22.5264	19.8057649
12	22.9449	19.8057649
13	23.3009	19.8057649
14	23.1674	19.8057649
15	23.0896	19.8057649
16	22.9185	19.8057649
17	22.3871	19.8057649
18	22.0426	19.8057649
19	21.4414	19.8057649
20	21.2354	19.8057649
21	20.7774	19.8057649
22	19.8053	19.805764
23	18.7465	19.2759
24	17.5666	18.1565

Figure 3. Load Forecast Predicted by Neural Network Model and Load Dispatch Schedule by MAS

Analysis of Animal-Caused Outages in Distribution Systems

G. Contreras, *Student Member, IEEE,* and A. Pahwa, *Fellow, IEEE,* and S. Das, *Non-Member*

Department of Electrical and Computer Engineering, Kansas State University, Manhattan, KS 66502, USA,
Email: *gaczt6@ksu.edu, Pahwa@ksu.edu and sdas@ksu.edu*

***ABSTRACT*-- One of many caused outages in distribution systems is caused by animals, mainly squirrels. Detail outage records have been provided for four different cities in the state of Kansas. In this paper, three different types of graphs are illustrated with the information of the number of animal outages in distributions systems. The first graph indicates the number of animal outages vs. each month. The second graph indicates the number of animal outages vs. different time frames. The third graph indicates the number of animal outages vs. the type of equipment affected. The graphs are illustrated with five years of historical data from 2005 to 2009 for the cities of Manhattan, Topeka, Wichita, and Lawrence. This information will be used to verify previously published models for representation of animal-related outages and to develop new models for future research.**

I. MODEL EQUATIONS

NONE

II. KEY FIGURES & RESULTS

MANHATTAN

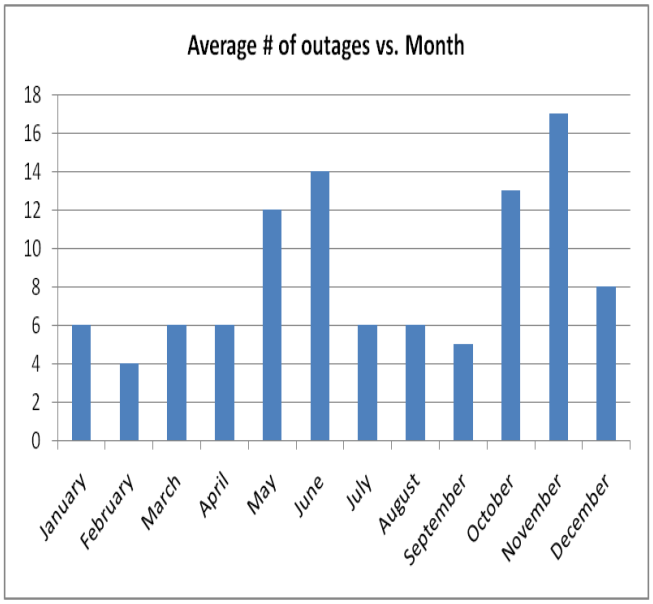

Fig 1: Average # of outages vs. Months

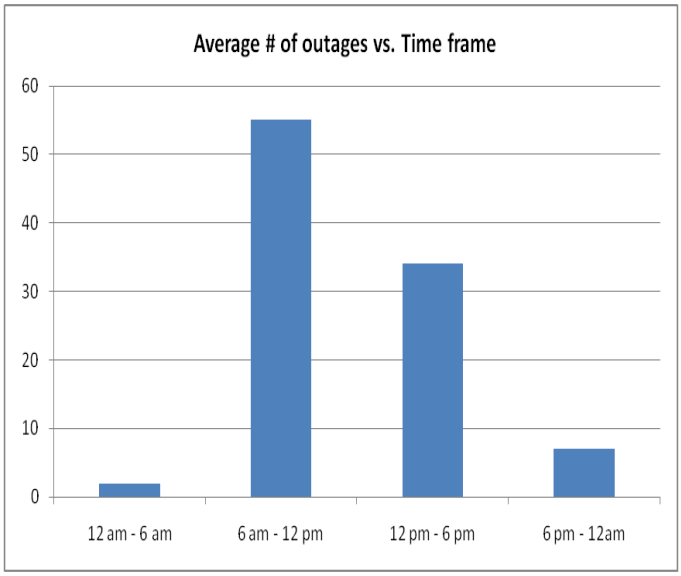

Fig. 2: Average # of outages vs. Time frame

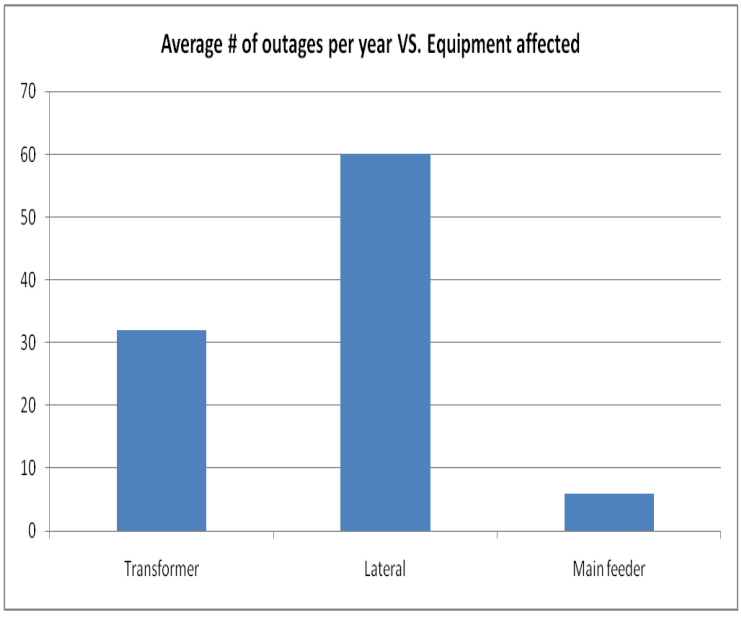

Fig 3: Average # of outages vs. Equipment affected

Addition of Smart Meter to a Reconfigured IEEE 34 Node Test Feeder

Fred A. Ituzaro, Richard H. Douglin, and Karen L. Butler-Purry
Power Systems Automation Laboratory, Department of Electrical and Computer Engineering, Texas A&M University, College Station, TX 77843-3128, USA,
Email: fgyekum@tamu.edu, rdouglin@tamu.edu and klbutler@tamu.edu

***Abstract*—Governmental policies and technological growth has seen many electric utilities implementing Advanced Metering Infrastructure (AMI) on their network as an important step towards a smart grid development. This effort is to actively encourage customer participation while enhancing utility performance. In this poster, we present how the existing IEEE 34 node distribution test feeder has been modified into a multi-feeder that incorporates smart meters. Loads on the test feeder are classified as commercial, residential and industrial to provide a basis for the allocation of smart meters. The modified test feeder will allow for the study of various impact that smart meters could have on the utility grid stemming from potential cyber security issues to demand response, as well as load forecasting and fault predictions. This system has been implemented in the PSCAD/EMTDC environment.**

I. KEY FIGURES

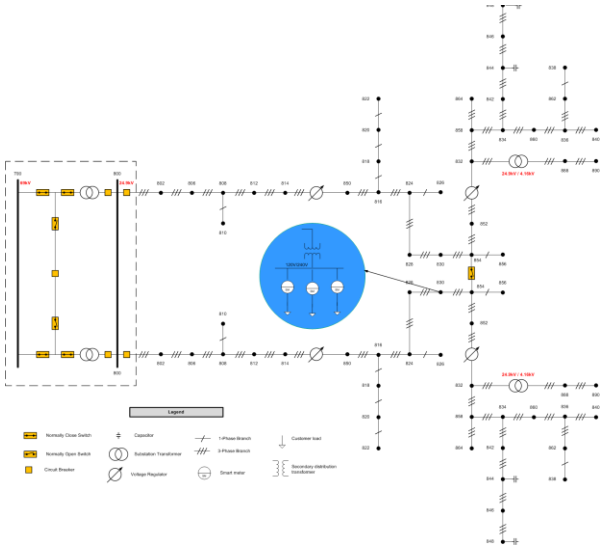

Figure 1: A multi-feeder IEEE 34 node with smart meter

Spot Loads								
Node	Load Model	Ph-1		Ph-2		Ph-3		Load Class
		kW	kVAr	kW	kVAr	kW	kVAr	
860	Y-PQ	20	16	20	16	20	16	I
840	Y-I	9	7	9	7	9	7	I
844	Y-Z	135	105	135	105	135	105	C
848	D-PQ	20	16	20	16	20	16	C
890	D-I	150	75	150	75	150	75	I
830	D-Z	10	5	10	5	25	10	R
Total		344	224	344	224	359	229	

Table 1: Classification of spot loads I=industrial, C=commercial, R=residential

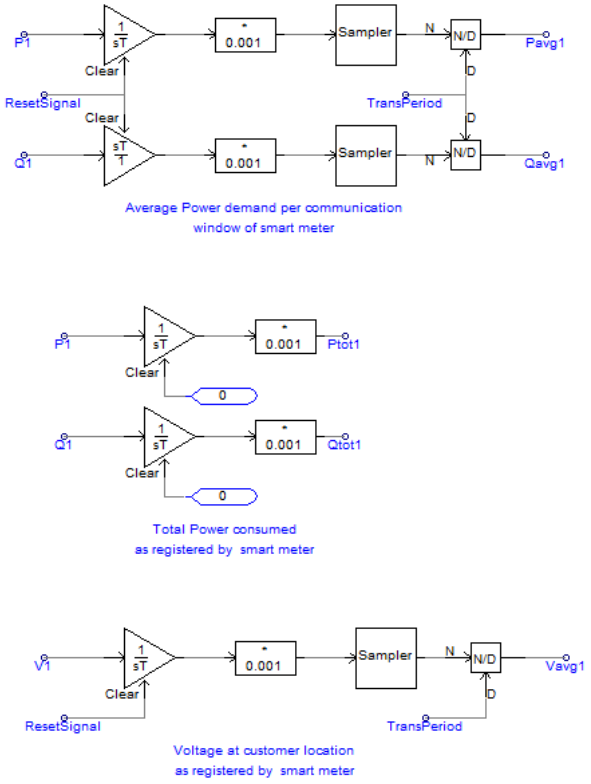

Figure 2: Implementation of some smart meter functionalities in PSCAD

Distributed Loads									Load Class
Node	Node	Load Model	Ph-1		Ph-2		Ph-3		
A	B		kW	kVAr	kW	kVAr	kW	kVAr	
802	806	Y-PQ	0	0	30	15	25	14	R
808	810	Y-I	0	0	16	8	0	0	R
818	820	Y-Z	34	17	0	0	0	0	R
820	822	Y-PQ	135	70	0	0	0	0	R
816	824	D-I	0	0	5	2	0	0	R
824	826	Y-I	0	0	40	20	0	0	R
824	828	Y-PQ	0	0	0	0	4	2	R
828	830	Y-PQ	7	3	0	0	0	0	R
854	856	Y-PQ	0	0	4	2	0	0	R
832	858	D-Z	7	3	2	1	6	3	R
858	864	Y-PQ	2	1	0	0	0	0	R
858	834	D-PQ	4	2	15	8	13	7	R
834	860	D-Z	16	8	20	10	110	55	R
860	836	D-PQ	30	15	10	6	42	22	R
836	840	D-I	18	9	22	11	0	0	R
862	838	Y-PQ	0	0	28	14	0	0	R
842	844	Y-PQ	9	5	0	0	0	0	R
844	846	Y-PQ	0	0	25	12	20	11	R
846	848	Y-PQ	0	0	23	11	0	0	R
Total			262	133	240	120	220	114	

Table 2: Classification of distributed loads R=residential

Analysis, Modeling and Forecasting Electric Load of a town using Multiple Linear Regression Model

Swathi R. Dyapa and Kevin Wedeward
Department of Electrical Engineering, New Mexico Institute of Mining and Technology, Socorro, NM 87801, USA,
Email: sdyapa@nmt.edu *and* wedeward@ee.nmt.edu

***Abstract*— In recent years, the interest in electric load modeling and forecasting has been continuously increasing, and the power system load has become a new area for researching into power system. Nowadays, with the promotion of smart grid technologies load forecasting is of greater importance due to its application in the planning of demand side management. In this paper we present an investigation for the short-term load forecasting of the demand for the Magdalena town power system using a multiple linear regression (MLR) model. MLR analysis for load forecasting uses the technique of weighted least-squares estimation. Based on this analysis, the usage of polynomial terms and the steps to compose the MLR model, which shows the statistical relationship between the total load, the weather variables like temperature and the calendar variables such as hour of the day and day of the week influences, is explained. As a case study, historical data consisting of half hourly load demand and temperatures of Magdalena town power system is used, to forecast the short-term load. This model proposes a new approach for modern utilities to perform load-forecasting tasks.**

I. Key Equations

The general linear regression model with normal error terms is :

$$Y_i = \beta_0 + \beta_1 X_{i1} + \beta_2 X_{i2} + \ldots + \beta_{n-1} X_{i,\,n-1} + e_i \qquad (1)$$

The polynomial regression model with one predictor Variable with the polynomial order 3 is defined as

$$Y_i = \beta_0 + \beta_1 X_i + \beta_2 X_i^2 + \beta_3 X_i^3 + e_i \qquad (2)$$

$$Y = \beta_0 + \beta_1 x\text{HourxT} + \beta_2 x\text{HourxT}^2 + \beta_3 x\text{HourxT}^3 + \beta_4 x\text{DayxHour} \qquad (3)$$

II. Key Figures

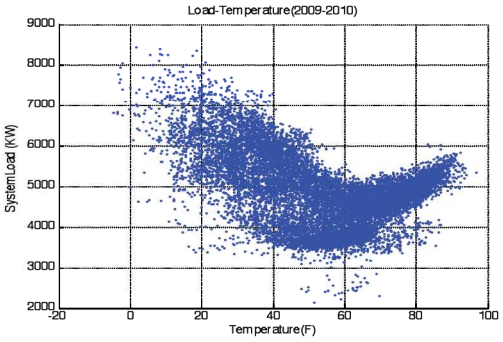

Figure 1. Load-Temperature scatter plot (2009-2010)

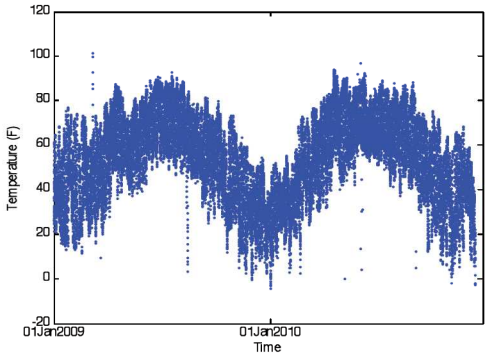

Figure 2. Temeperature series (2009-=2010)

Feasibility of Community Wind Generation in Rural Western Kansas

Todd Halling and Dr. Anil Pahwa (Advisor)
Department of Electrical and Computer Engineering, Kansas State University, Manhattan, KS 66502, USA,
Email: *hallingt@k-state.edu*

***Abstract*— Energy costs are rising, supplies of fossil fuels are diminishing, and environmental concerns surrounding power generation in the United States are at an all time high. The United States is continuing to push all states for energy reform and where better for Kansas to look than wind energy. Kansas is third among all states in wind generation potential, but the best wind generation sites are located in predominantly sparsely populated areas creating energy transportation problems. Because of these issues, large wind farms can only do so much and interest in community wind projects has been increasing. This paper will examine a distribution system in rural western Kansas where interest in community wind exists, and perform a feasibility study based on economic factors and current grid constraints. Since a good portion of the load in this area is from pivot point irrigation systems load distributions were created based on temperature ranges instead of a linear progression of concurrent days. The feasibility of various types and sizes of wind generators will be examined and recommendations made on key economic factors and grid requirements.**

I. KEY EQUATIONS

Not yet established, will be completed before July 15, 2011

II. KEY FIGURES

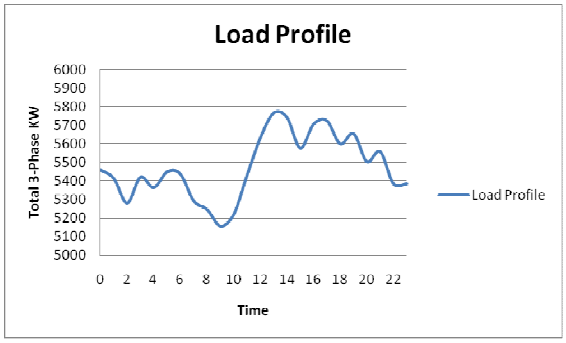

Figure 1. Load Profile of the Distribution Network

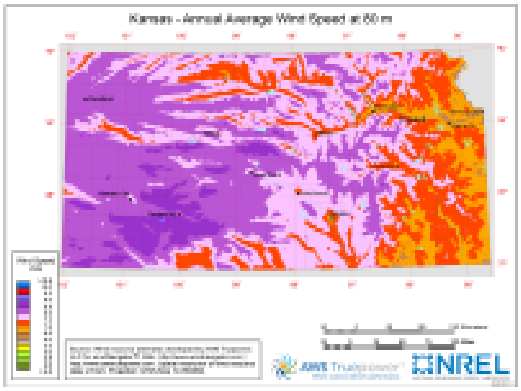

Figure 2. Annual Average Wind Speed Map at 80 Meters (www.windpoweringamerica.gov)

III. KEY RESULTS

Not yet established, will be completed before July 15, 2011

Analysis of Outages Due to Wind and Lightning on Overhead Distribution Feeders

P. Kankanala, *Student Member, IEEE,* and A. Pahwa, *Fellow, IEEE,* and S. Das, *Non-Member*

Department of Electrical and Computer Engineering, Kansas State University, Manhattan, KS 66502, USA,
Email: *pk150@ksu.edu, Pahwa@ksu.edu and sdas@ksu.edu*

***Abstract*-- Different environmental factors including weather, trees, animals cause a large number of outages in distribution systems. Wind and lighting continue to be the major weather related causes of outages on overhead power distribution lines. This paper present a method based on regression models to study and analyze outages due to wind and lightning on overhead distribution feeders in different districts in Kansas from 2005 to 2009. Two different sets of data, one for lightning strikes within 200 m on either side of the distribution feeders and the other within 400 m on either side of the distribution feeders, are considered. Performance of six regression models to estimate outages are compared to identify the best model gathering. Results obtained from these models are compared with each other to determine the most suitable model for representing the effects of wind and lightning. All the models, however, seems to underestimate when the observed outages are in the higher range and overestimate when they are in the lower range. Therefore, to estimate the outages more accurately, intelligent models based on learning will be applied in the future work.**

I. Model Equations

Model 1:

$$O = \beta_1 Li + \beta_2 Wd$$

Model 2:

$$O = \beta_1 Li + \beta_2 Wd + \beta_3 Wd^2$$

Model 3:

$$O = \beta_1 Li + \beta_2 Wd + \beta_3 Wd^2 + \beta_4 Li^2$$

Model 4:

$$O = \beta_1 Li + \beta_2 Wd + \beta_3 WdLi + \beta_4 Wd^2 + \beta_5 Li^2$$

Model 5:

$$O = exp(\beta_0 + \beta_1 Li + \beta_2 Wd + \beta_3 (Wd * Li))$$

Model 6:

$$O = \exp(\beta_0 + \beta_1 \ln(Li) + \beta_2 Wd + \beta_3 (Wd * \ln(li))$$

II. Key Figures & Results

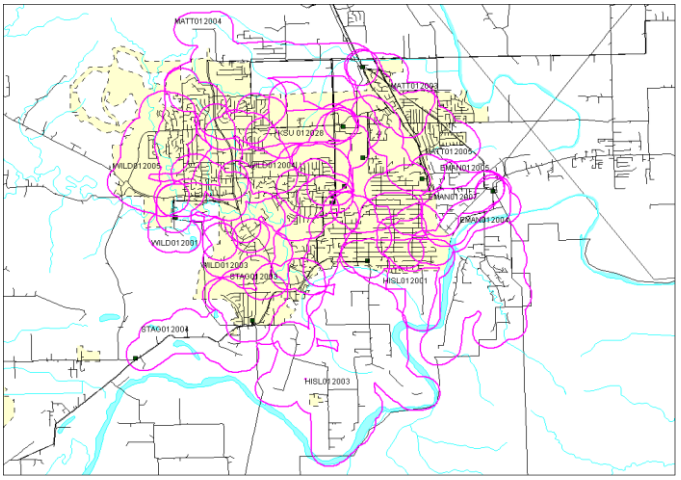

Fig 1: Map for Manhattan 400 m.

Table I: Summary of regression models for Manhattan

	200 m			400 m		
	Manhattan					
	AAE	MSE	R^2	AAE	MSE	R^2
Model 1	2.36	15.82	0.62	2.39	15.60	0.57
Model 2	2.32	15.73	0.66	2.37	15.51	0.63
Model 3	2.28	15.33	0.67	2.28	14.90	0.66
Model 4	2.24	14.76	0.77	2.25	14.28	0.75
Model 5	2.28	14.79	0.75	2.31	14.30	0.73
Model 6	5.48	58.62	0.55	5.61	57.06	0.58

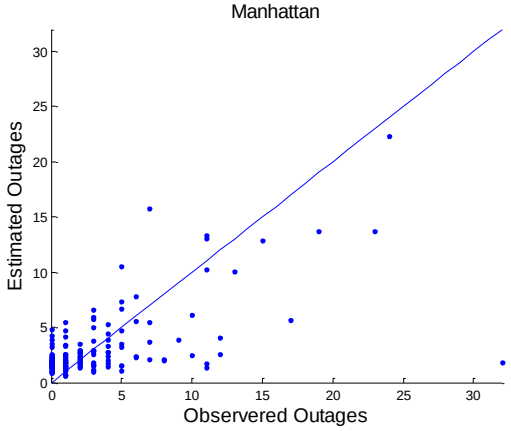

Fig. 2: Estimated and observed outages for Manhattan

Providing Efficient Incentives for Coordinated Energy Delivery to Flexible Electric Loads

Mahdi Kefayati and Ross Baldick
Department of Electrical and Computer Engineering, The University of Texas at Austin, Austin, TX 78712, USA.
Email: *kefayati@utexas.edu* and *baldick@ece.utexas.edu*

***Abstract*— Recent research has shown that dynamic pricing of electricity based on wholesale prices does not necessarily lead to a desired behavior of the aggregate load at the distribution level. On the other hand, the proposed methods for coordinating energy delivery to flexible electrical loads are shown to provide effective control over the aggregate load behavior besides substantial reductions in costs and increased reliability; however, designing efficient methods to practically induce the desired behavior such as pricing mechanisms poses a challenging problem.**

In this work, we introduce a novel method for pricing energy delivery to flexible loads called Energy Delivery Transaction Pricing (EDTP), which provides the efficient incentives for the demands to reveal their true flexibility and facilitates demand-side cost-comfort analysis. In contrast with conventional dynamic pricing methods where the electric power is priced at every time instant, our method is based on viewing the energy delivery process as a whole calling it an Energy Delivery Transaction (EDT). We price EDTs based on the price of electricity in the wholesale market, distribution level congestion status, arrival time and flexibility of the demand.

Our method is presented in the context of a coordinated load scheduling problem we considered before, where an Energy Services Company (ESCo) contracts flexible loads such as EVs for delivering certain amount of energy by their desired deadlines, and consequently participates in the wholesale electricity market to satisfy its contracted demand. The ESCo also contracts the distribution network (DN) to only use its spare capacity. Moreover, the ESCo can utilize the flexibility of its contracted load to provide reserves back to the grid by controlling the energy delivery process of each load. The purchasing and charging decisions are obtained by a computationally efficient scheduler called LP Scheduler which is also used in pricing of EDT requests. To provide efficient incentives in this context, we proposed differential pricing, where each new request is priced based on its incremental cost to the total schedule and therefore, more flexibility would translate to lower costs.

We evaluate the performance of EDTP in terms of the total cost of energy delivery, network level effects and user acceptance versus conventional consumption and optimal opportunistic response to real-time prices at different distribution network congestion levels. Our results show that EDTP exhibits strong performance advantage especially at and below moderate congestion levels and offers an advantageous option for most users while observing reliability of the distribution system and offering substantial amounts of reserves.

I. KEY FIGURES

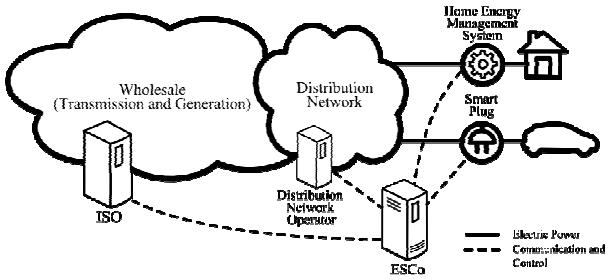

Figure 1. ESCo Interaction Model.

II. KEY RESULTS

Table 1. Total cost of energy delivery.

Load Level	Low	Med.	High
EDTP	$182	$182	$224
Convectional	$317	$319	$317
Opportunistic	$229	$218	$226

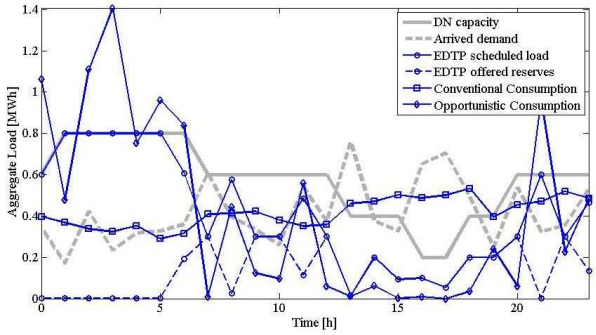

Figure 2. Sample aggregate load profile at high loads and relative performance of EDTP versus conventional and opportunistic consumption.

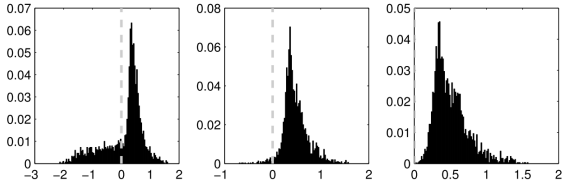

(a) High Load (b) Med. Load (c) Low Load

Figure 3. Empirical histogram of the unit price difference between EDTP and opportunistic consumption at different load levels.

Economic Loading of Renewable DG and Storage in Competitive Distribution Markets

Fanjun Meng, *Student Member IEEE* and Badhrul H. Chowdhury, *Senior Member IEEE*
Department of Electrical and Computer Engineering,
Missouri University of Science and Technology, Rolla, MO 65409, USA,
Email: *fmtx9@mst.edu and bchow@ieee.org*

***Abstract*—A new methodology to calculate distribution locational marginal prices (DLMP) is introduced for future smart distribution systems with renewable energy resources as the primary energy supply. The proposed DLMP calculates the marginal energy cost for renewable generations and storage, as well as the marginal congestion and loss cost in order to determine optimal economic operations in the system. The DLMP can be used as a pricing signal to achieve maximum system social surplus and environmental benefits by encouraging utilization of renewable distributed generation and energy storage in a competitive distribution market.**

I. DLMP FORMULATION IN OPF MODEL

$$\text{Max: } SS(P_S,P_B)=\underbrace{\sum_{i=1}^{M}(DLMP_i-S_i)P_{S,i}}_{\text{supplier's surplus}}+\underbrace{\sum_{j=1}^{N}(B_j-DLMP_j)P_{B,j}}_{\text{customer's surplus}}$$

$$s.t.\ \ G(P_S,P_B)=\sum_{i=1}^{M}P_{S_j}-\sum_{j=1}^{N}P_{B_i}=0\longleftrightarrow\lambda_G$$

$$H(P_S,P_B)=LF_l^{Max}-\sum_{k=1}^{K}GSF_{l-k}\times(P_{S,k}-P_{B,k})\geq 0\longleftrightarrow\mu_l$$

$$J(P_{S,i},Q_{S,i},Vm_i,\theta_i)\leq 0\longleftrightarrow\gamma^+,\gamma^-$$

$$DLMP_i=\frac{\partial L}{\partial P_i}=\underbrace{\lambda_G}_{MEC}+\underbrace{\frac{\partial P_{loss}}{\partial P_i}\lambda_G}_{MLC}+\underbrace{\sum_{k=1}^{M}GSF_{k-i}\times\mu_k}_{MCC}$$

II. GENRATION ENVIRONMENTAL FACTOR

$$ECF_i=\frac{P_{Gen,i}}{MVA_{base}}\times\left(GF_i-(1-GF_i)\right)=\frac{P_{Gen,i}}{MVA_{base}}\left(2\times GF_i-1\right)$$

$$GEF_i=W_A\times\left(1-\frac{1}{1+e^{-W_S\times ECF_i}}\right)$$

III. SIMULATION RESULTS

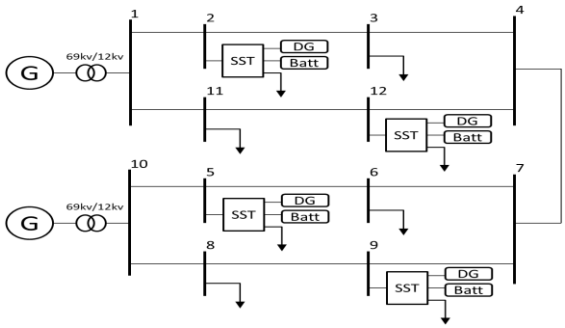

Figure 1 12-bus distribution system test bed

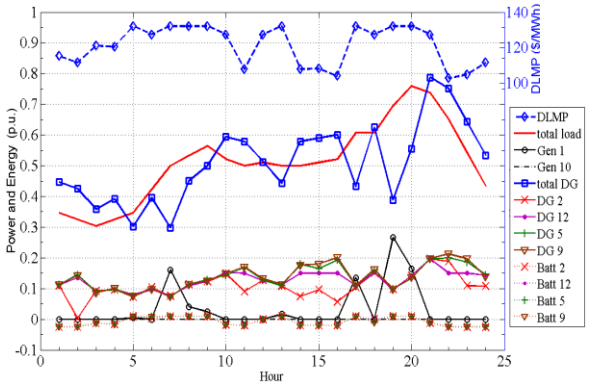

Figure 2. Simulation results of power and energy dispatch and DLMPs in a 24-hour period

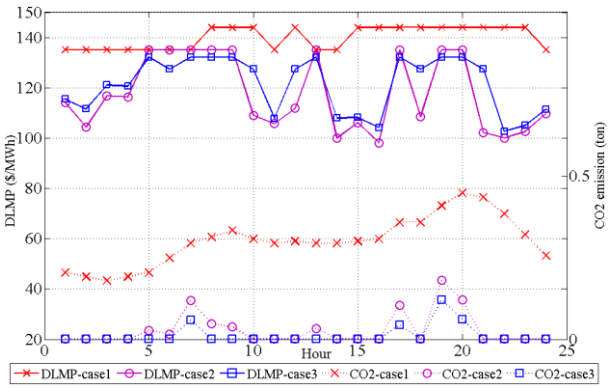

Figure 3 Simulation results of DLMPs and CO2 emissions of three cases (case 1 only has legacy grid supply; case 2 includes renewable DGs; case 3 add energy storages with DGs).

IV. CONCLUSION:

A new methodology of distribution economic operation is proposed to meet the requirement of the future distribution system using Distribution LMP as economic control signal. The proposed algorithm could find the optimal economic operation that minimize DLMPs and maximize total social surplus. From test bed simulations, the renewable DGs and energy storages could improve social and environmental welfare significantly, however, the benefits are limited by weather-dependent DG generation and high capital cost of hardware at present. The DLMPs also indicate marginal generation and marginal loads which is important for distribution system control of generation power routing, storage energy management, and infrastructure expansion. Future work may continue on:

- Reliability analysis and generation reserve for distribution system.
- Development of a practical infrastructure model for financial instruments in distribution system.
- Cost to benefit analysis for hardware investment and operation.
- Generation reserve and stability analysis of microgrid

Power Quality Assessment of a Distribution Feeder connected with a wind generator based on a Doubly-Fed configuration

Luis Fernando Montoya Sanchez. IEEE Student Member
Department of Electrical and Computer Engineering
University of Wisconsin Milwaukee USA
Email: montoyas@uwm.edu

***Abstract*—the study shows the power quality assessment developed for a wind generator connected to a Distribution test feeder-IEEE 13 Node Test Feeder which consumes 2.3MVA - . The wind generator selected operates under a 3-phase doubly fed configuration, with a rated power of 850kW and includes the rotor side converter model to operate the generator; the grid side converter of this configuration was omitted so far and will be included in the model for future study. The wind generator represents roughly 37% of the requirement. Two points were selected to connect the wind generator, according to its unbalanced, and both connections were selected, so that at the nodes where connected three-phase balanced loads.**

Two standards were considered for this assessment: pEN 50160-2006, IEEE Std. 519. Both standards supply limits for voltage and current waveform distortion, flicker, sags, and voltage unbalanced; measurements which were covered for the assessment. The measurement and limitation of power quality factors is essential for an accurate grid operation. For instance, voltage sags which happen at the utility supply can cause malfunction in the operation of a DFIG. Even though, this assessment shows relevant results according to the wind generator point of connection, it has to be mention that the GSC (Grid side Converter) will be included, and the results will be part of a future paper publication.

I. KEY EQUATIONS

Principal equations for the power at the stator of a DFIG:

$$Ps = -3\omega_s \varphi_s i_{rq} \qquad (1)$$

$$Qs = 3\omega_s \varphi_s \left\{ \frac{\varphi_s}{L_M} - i_{rd} \right\} \qquad (2)$$

Summary of the Control Strategy used for the DFIG:

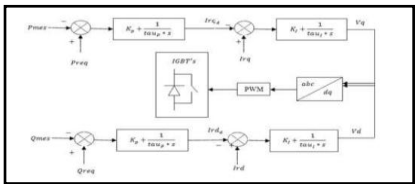

Figure 1. Control strategy for the DFIG.

II. KEY FIGURES

For the DFIG a wind profile was assumed, and also was repeating for every hundred seconds until three minutes of simulation were completed.

Two points of connection were chosen due to the unbalance- guarantying in this way that the generator could operate. The two points of connection are shown below:

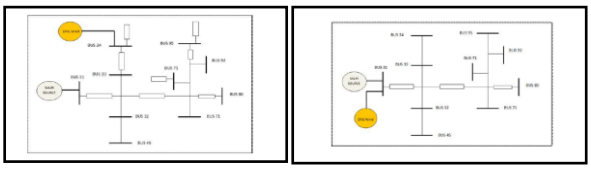

Figure 3. Scenario No.2 of assessment.

III. KEY RESULTS

In summary, there is a correlation between the point of connection of the Wind farm, and the unbalanced resulting before the connection was changed. Another aspect counts on pst, which was increased out of bounds. All these cases are summarized on Table.1 according to the standard, and point of connection preselected.

Power Quality	Scenario No. 1 BUS 31	Scenario No. 2 BUS 33
Voltage Unbalance	0.28% Note: Voltage unbalanced measured at this scenario without DFIG was 0.4 % (using voltage deviation method)	1.2 % Note: Voltage unbalanced measured at this scenario without DFIG was 0.6% (using voltage deviation method)
Voltage Distortion	**Harmonics:** fulfills Std EN 50160. Inter-harmonics: fulfills Std IEC 61000-4-7. Sub-harmonics: Do not fulfill Std 61000-4-7.	**Harmonics:** fulfills Std EN 50160. Inter-harmonics: fulfills Std IEC 61000-4-7. Sub-harmonics: fulfill Std 61000-4-7.
Current Distortion	**Harmonics:** fulfills Std IEEE 519. **Inter-harmonics:** Do not fulfill Suggested standard. Std IEEE 519. **Sub-harmonics:** Do not fulfill Suggested standard. Std IEEE 519	**Harmonics:** fulfills Std IEEE 519. **Inter-harmonics:** fulfills Suggested standard. Std IEEE 519. **Sub-harmonics:** fulfill Suggested standard. Std IEEE 519
Disconnection of the Utility source	DFIG maintains the same power reference.	DFIG does not maintain the same power reference, losses the reference and goes to zero.
PST	Pst calculated < 1. fulfills Std. pr-EN 50160:2006	Pst calculated > 1. Does not Fulfill Std. pr-EN 50160:2006
Sags	Depth: DFIG maintains its power reference during the sag. Duration: Dramatic sag of 1 sec and 10% residual voltage causes a higher transient when the utility recovers. But the DFIG maintains its output.	Depth: DFIG losses its power reference Duration: DFIG losses its power reference for any duration sag.

Table 1. Summary of the results developed for the assessment

Optimal Distribution System Reconfiguration and Restoration without Heuristics

Benyamin Moradzadeh and Kevin Tomsovic
Department of Electrical Engineering and Computer Science, University of Tennessee, Knoxville, TN 37996, USA,
Email: bmoradza@utk.edu *and* tomsovic@tennessee.edu

***Abstract*— In this paper, a general approach based on Mixed Integer Programming (MIP) is proposed to formulate the reconfiguration problem for a radial/weakly meshed distribution network or restoration following a fault. Two objectives considered in this study are to minimize the number of switching operations, and to minimize the active power loss with respect to operational constraints, such as load balance, line flow limits, and radiality of the network. The latter is the most challenging issue in solving the problem by MIP. Performance of Mixed-Integer Linear Programming (MILP) and Mixed-Integer Quadratic programming including quadratic constraints (MIQP) are investigated and compared. A novel approach based on Depth-First Search (DFS) algorithm is implemented to avoid cycles and loops in the system. Using the proposed strategy, it is easy to formulate the reconfiguration problem with various objectives for any given distribution system. Recent improvements in MIP algorithms and processor speed have dramatically improved computational time, allowing the approach to be practical for online application. Numerical simulations of the proposed method on single-feeder 33-bus system model demonstrate the feasibility of the proposed algorithm.**

I. KEY EQUATIONS

Objective: Loss minimization

$$\text{Min}\left(\sum_{i=1}^{n_l} R_i .\left(P_{f,i}^2 + Q_{f,i}^2\right)\right) \quad (1)$$

Objective: Minimizing switching actions

$$\text{Min}\left(\sum_{i\in NO} x_i - \sum_{i\in NC} x_i + \sum_{i=1}^{n_l} R_i .\left(P_{f,i}^2 + Q_{f,i}^2\right)\right) \quad (2)$$

S.t.

- Power flow constraints:

$$A^T P_f = P \quad (3)$$

$$A^T Q_f = Q \quad (4)$$

$$P_f^2 + Q_f^2 \le x_i I_{\max}^2 \quad (5)$$

$$x_i \in \{0,1\}$$

- Radiality constraint

$$\sum_{i=1}^{N_j} x_i \le N_j - 1 \quad (6)$$

II. KEY FIGURES

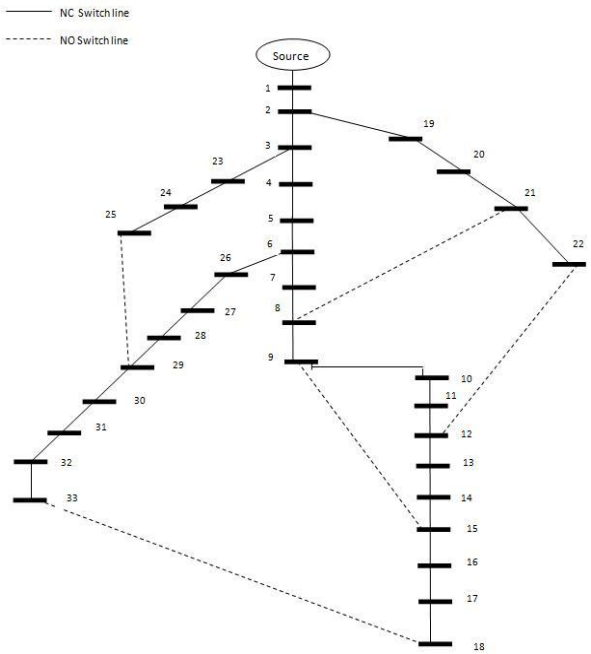

Figure 1. Test System

III. KEY RESULTS

TABLE I
RECONFIGURATION RESULT FOR LOSS MINIMIZATION

Parameter	MILP	MIQP	MIQP (Reduced model)
Optimal solution (open switches)	8-21,10-11, 13-14, 16-17,28-29	7-8,9-10, 14-15, 25-29,32-33	7-8,9-10, 14-15, 25-29, 32-33
Initial system loss	202.4		
System loss with new configuration	161.58	139.55	139.55
Minimum voltage (initial system)	0.913		
Minimum voltage with new configuration	0.927	0.938	0.938
MIP processing time (s)	0.028	74.96	0.04

To Establish Bounds on Numerical Growth of the Feeder Reconfiguration Problem

Sudarshan Natarajan
Advanced Power Engineering Laboratory, Department of Electrical and Computer Engineering,
Colorado State University, Fort Collins, CO 80521, USA.
Email: Sudarshan.Natarajan@colostate.edu

***Abstract*— Traditionally, electric distribution power systems have been designed to operate in a radial fashion. Simplicity of design, and economics of protection systems were the main inspirations for this. Current trends of growing demand for higher reliability of supply, compounded by the need for increased deployment of distributed generation (DG) and energy storage, has forced utilities to look for means to upgrade existing systems, with justifiable cost overheads. The Smart Grid Initiative, the official policy to modernize the US power grid, identifies one of the important steps towards achieving the aforementioned objectives is to optimize distribution network resources; this may be achieved by optimal reconfiguration of the legacy grid. Several techniques have been explored for this such as dynamic switch (sectionalizing) reconfiguration.**

The distribution feeder reconfiguration problem aims to redesign the existing radial feeder network into an interconnected network to improve reliability of system, with increased DG penetration. The motivation of this work is to establish bounds on the growth of the distribution feeder reconfiguration problem so that it maybe classified in *P or NP.* A problem is classified as having computational complexity of 'P' (polynomial time) if it can be solved in polynomial time by some algorithm and 'NP' (non-deterministic polynomial time) if there exists no known algorithm that can solve it 'quickly'. Classifying a problem in NP justifies the use of heuristic or meta-heuristic based algorithms, to find a solution to the problem. The technique explored in this work involves addition of new lines, called inter-ties, in the system between existing feeders. This creates a meshed network at the distribution end.

In order to not deviate from the problem to find the computational complexity of the feeder reconfiguration problem, DG's are treated as ideal power sources. Also, it is assumed that the feeder reconfiguration is a static problem i.e., the objectives are known in advance and inter-ties are added permanently to the system. This is a reasonable assumption to make without loss of generality of the problem. The feeder reconfiguration problem has been analyzed by many authors, who have suggested various algorithms to find 'a solution'. A closer examination reveals that these algorithms use an underlying heuristic based technique or have adapted some form of heuristic algorithm. To the best of our knowledge, no work, till date, has conclusively proved the need for such algorithms over the more popular conventional polynomial time algorithms.

Proof that the feeder reconfiguration problem has an exponential growth rate has been shown, and it establishes the minimum and maximum bounds on the growth rate. Also, it is shown, under realistic assumptions, that even in a simple test case, the subspace of the problem is extremely large. An implication may be that any known polynomial time algorithm cannot find a solution in reasonable time. However, this remains to be proved in future work.

Establishing bounds on the problem growth rate helps classify the computational complexity and hence provides some justification for the use of heuristic algorithms in optimization of assets such as feeder interties.

I. KEY EQUATIONS

It is found that the feeder reconfiguration problem has exponential growth rate given by

$$2^{(x-1)} \leq T \leq 2^{x(x-1)/2} \quad (1)$$

where: 'x' is the total number of buses (excluding slack) in the system under the assumption of equal number of buses on feeders.

This proves that the problem at hand could potentially become intractable as the system under consideration grows in size.

II. KEY RESULTS

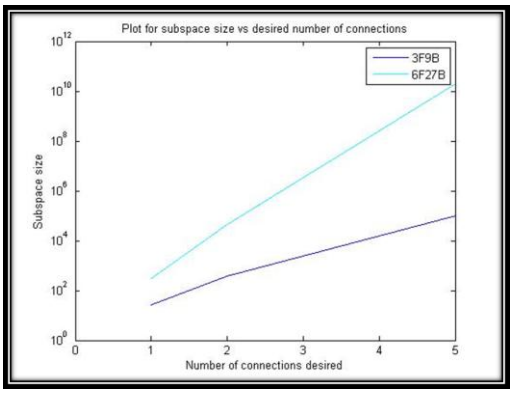

Figure 1. Graph depicting the growth of the subspace with increase in number of desired connections for two feeder configurations.

A D-STATCOM Custom Inverter for Single Phase Wind and Solar Installations

Colin Tareila and Ruth Douglas Miller
Power Systems Laboratory, Department of Electrical and Computer Engineering, Kansas State University, Manhattan, KS 66506, USA,
Email: tareilac@ksu.edu, *and* rdmiller@ksu.edu

***Abstract*— Currently many utilities are resistant to the idea of increasing the penetration of distributed energy sources on distribution systems and feeder lines. This is in part due to the added technical difficulties associated with maintaining compliance with IEEE standards. The large majority of distribution systems in the United States are radial and provide utilities with no communication or feedback on the low-voltage side of the substation. This makes the dynamic control of feeder lines very limited with time steps that are well above the variable power output of wind turbines and solar installations. This poster presents the design of a D-STATCOM inverter for small to mid sized (10kW-20kW) permanent magnet wind or solar installations. The proposed inverter can actively regulate VARs on individual feeder lines at a programmable output while providing the variable output power of the renewable energy source. The aim is to provide utilities with distributive control of VAR compensation and power factor correction on feeder lines. The designed inverter utilizes a multi-level voltage-source converter (VSC) topology. Reactive power control is achieved by modulation index control. Active power control is achieved by phase-shift-angle control and VSC harmonics are eliminated by the optimized harmonic stepped waveform technique (OHSW). All simulations were done in MATLAB's SimPowerSystems toolbox.**

I. Key Equations

The guiding equations for power flow are:

$$P = \frac{mV_c V_{line} Sin(\delta)}{X} \quad (1)$$

$$Q = V_{line} \frac{V_{line} - mV_c Cos(\delta)}{X} \quad (2)$$

I. Key Figures

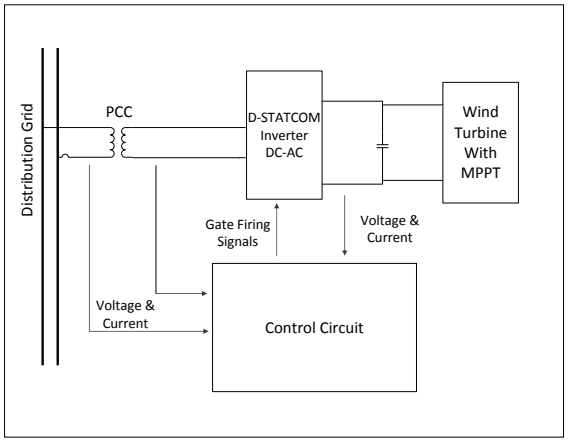

Figure 1: Block Diagram of System

II. Key Results

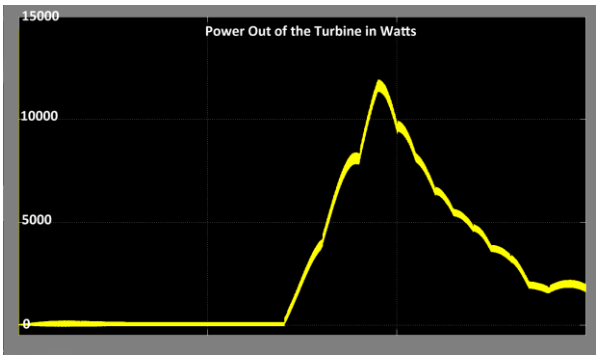

Figure 3. 15 second simulation of the power out of a wind turbine. The turbine is turned on at the 8 seconds.

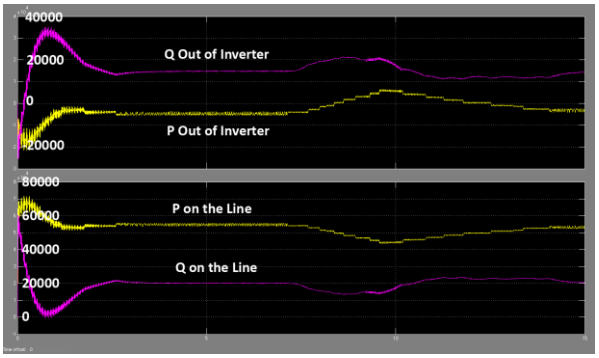

Figure 4. Performance Comparison between PSO and AIS Based Controller for 20 MW/40 MVAR Pulsed Load

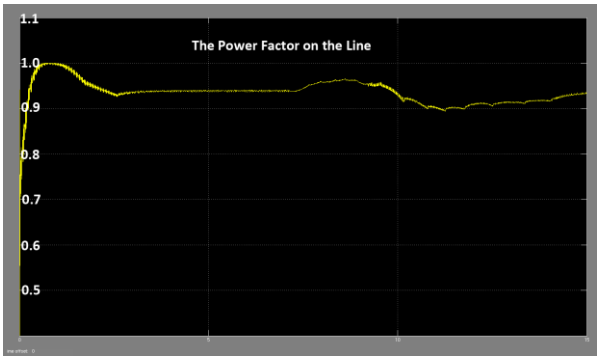

Figure 5, The Power Factor on the distribution line. The original load on the line was 50 + j34 kVA with a power factor of 0.8. The D-STATCOM was set to deliver a target power factor of 0.9.

Demand Response Model and its Effects on Voltage Profile of a Distribution System

Naveen Venkatesan, Jignesh Solanki and Sarika Khushalani Solanki
Lane Department of Computer Science and Electrical Engineering, West Virginia University
Morgantown, WV 26505, USA
Email: nvenkate@mix.wvu.edu and Jignesh.Solanki@mail.wvu.edu

***Abstract*— This paper develops a model for Demand Response (DR) by utilizing consumer behavior modeling considering different scenarios and levels of consumer rationality. Consumer behavior modeling has been done by developing extensive demand-price elasticity matrices for different types of consumers such as Long Range (LR) consumer, Short Range (SR) consumer and Real World (RW) consumer. These Price Elasticity Matrices (PEMs) are utilized to calculate the level of demand response for a given consumer. DR thus obtained is applied to a real world distribution network considering a day-ahead real time pricing scenario to study the effects of demand reduction on system voltage. Results show considerable boost in system voltage that paves way for further demand curtailment through demand side management techniques like Volt/Var Control (VVC).**

I. KEY EQUATIONS

The guiding equations for developing DR model are:

Self Elasticity Coefficient:

$$E(i,i) = \frac{\Delta d(t_i)/d_0}{\Delta p(t_i)/p_0} \quad (1)$$

Cross Elasticity Coefficient:

$$E(i,j) = \frac{\Delta d(t_i)/d_0}{\Delta p(t_j)/p_0} \quad (2)$$

Demand reduction for each hour:

$$\Delta d(t_i) = \sum_{j=1}^{24} E(i,j) * \left(\Delta p_j/p_0\right) * d_0 \quad (3)$$

II. KEY FIGURES

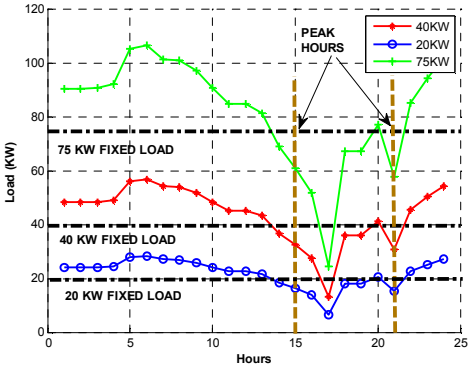

Fig 1: Daily demand curve for a LR consumer

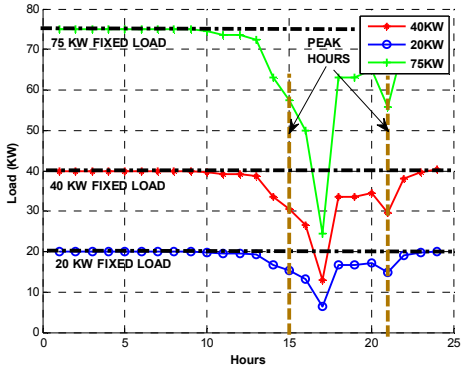

Fig 2: Daily demand curve for a SR consumer

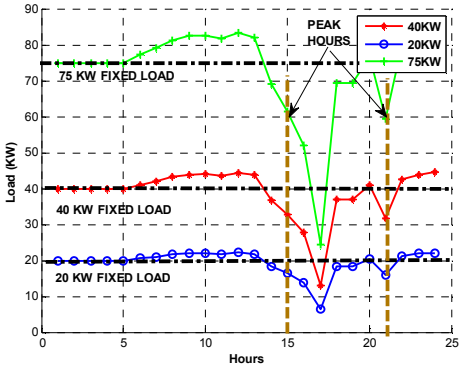

Fig 3: Daily demand curve for a RW consumer

III. KEY RESULTS

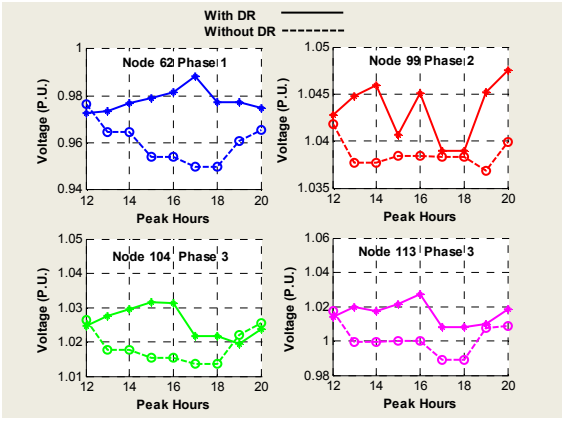

Figure 4. Comparison of Voltage profile of system nodes with and without DR

Investigation of Voltage Variations in Unbalanced Distribution Systems due to High Photovoltaic Penetrations

Ruifeng Yan and Tapan Kumar Saha
School of Information Technology & Electrical Engineering, The University of Queensland,
St. Lucia, Brisbane, Australia,
Email: ruifeng@itee.uq.edu.au and saha@itee.uq.edu.au

***Abstract*— Photovoltaic (PV) power in distribution systems is increasing rapidly due to government incentives and public's expectation on environment. This raises utilities' concern on voltage rise and voltage fluctuation in distribution networks when PV power fluctuates with fast changing weather conditions. In the literature, many studies have been conducted on these issues based on balanced systems with transposed lines; however few of them concentrate on analysis of unbalanced networks. Low voltage distribution systems have an unbalanced nature and uneven mutual coupling, which result in different voltage drop for each phase. Therefore, traditional balanced assumption may not be adequate for analyses of distribution systems with a high PV penetration level. This paper proposes a method of analyzing voltage variations of an unbalanced distribution system caused by PV power fluctuations due to changes in sun irradiation.**

I. KEY EQUATIONS

The equation for an unbalanced distribution system is:

$$\begin{bmatrix} \overrightarrow{V_{632\,a}} \\ \overrightarrow{V_{632\,b}} \\ \overrightarrow{V_{632\,c}} \end{bmatrix} = \begin{bmatrix} \overrightarrow{V_{rg60\,A}} \\ \overrightarrow{V_{rg60\,B}} \\ \overrightarrow{V_{rg60\,C}} \end{bmatrix} - \begin{bmatrix} \overrightarrow{Z_{11}} & \overrightarrow{Z_{12}} & \overrightarrow{Z_{13}} \\ \overrightarrow{Z_{12}} & \overrightarrow{Z_{22}} & \overrightarrow{Z_{23}} \\ \overrightarrow{Z_{13}} & \overrightarrow{Z_{23}} & \overrightarrow{Z_{33}} \end{bmatrix} \begin{bmatrix} \overrightarrow{S^*_{632\,a}/V^*_{632\,a}} \\ \overrightarrow{S^*_{632\,b}/V^*_{632\,b}} \\ \overrightarrow{S^*_{632\,c}/V^*_{632\,c}} \end{bmatrix} \quad (1)$$

II. KEY FIGURES

The figures of phase voltage variations due to photovoltaic power fluctuations are:

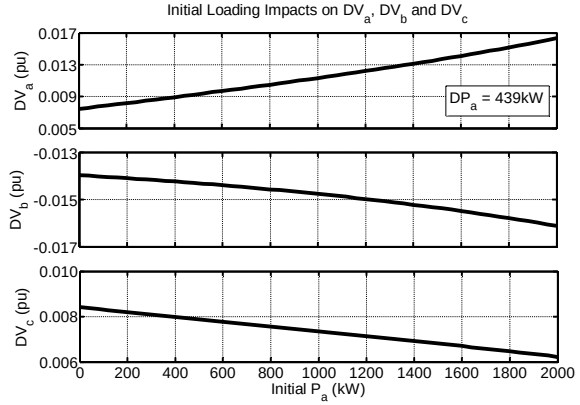

Fig. 1. $P_{632\,a}$ initial value impacts on voltage variations ($\Delta V_{632\,abc}$) when $|\Delta P_{632\,a}| = 439kW$

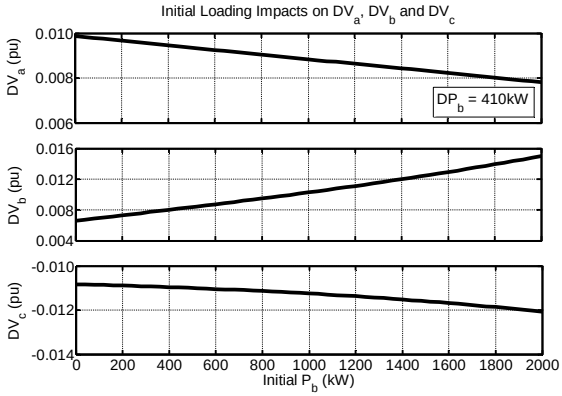

Fig. 2. $P_{632\,b}$ initial value impacts on voltage variations ($\Delta V_{632\,abc}$) when $|\Delta P_{632\,b}| = 410kW$

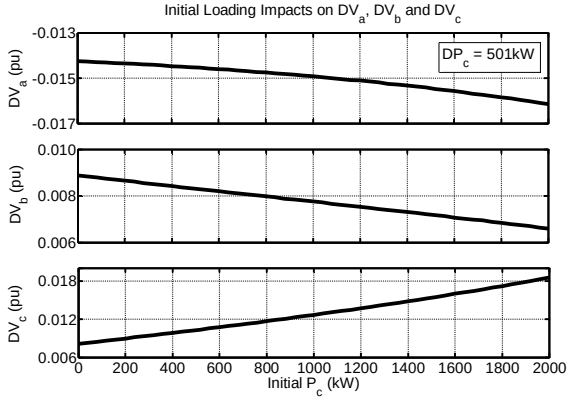

Fig. 3. $P_{632\,c}$ initial value impacts on voltage variations ($\Delta V_{632\,abc}$) when $|\Delta P_{632\,c}| = 501kW$

III. KEY RESULTS

Based on the look-up graphs in Section II, phase voltage variations due to PV power fluctuations can be analyzed and estimated as demonstrated in Table I.

TABLE I
TOTAL AND INDIVIDUAL CONTRIBUTIONS OF PV POWER FLUCTUATIONS TO NETWORK VOLTAGE VARIATIONS

Voltage variations from Superposition				
Downstream Voltage	$P_{632\,a} \downarrow only$ $(\Delta = 439kW)$	$P_{632\,b} \downarrow only$ $(\Delta = 410kW)$	$P_{632\,c} \downarrow only$ $(\Delta = 501kW)$	$Total\ \Delta V$
$\Delta V_{632\,a}\ (pu)$	$+0.0120$	$+0.0089$	-0.0152	$+0.0057$
$\Delta V_{632\,b}\ (pu)$	-0.0149	$+0.0100$	$+0.0074$	$+0.0025$
$\Delta V_{632\,c}\ (pu)$	$+0.0072$	-0.0112	$+0.0142$	$+0.0102$

Optimal Participation of Wind Power in the Liberalized Power Market

Ting Dai and Wei Qiao
Department Electrical Engineering, University of Nebraska-Lincoln
Lincoln, NE 68588-0511 USA
Email: *ting.dai@huskers.unl.edu and wqiao@engr.unl.edu*

***Abstract*— While installing wind power into the liberalized power market can reduce the operation and fuel costs of the power system, it also increases the imbalance cost and need for reserve. Due to this contradictory, there is a need for planning the amount of wind power in the power system. This paper proposes a model following American power market rules to find the optimal participation of wind power. This model assumes that wind power producer can bid into both day-ahead and real-time market and pay imbalance cost due to wind power prediction errors. A case study will be presented where the proposed model will be tested with simulation results on a practical power system.**

I. KEY EQUATIONS

The Key Equations of this Market models are:

$$Max\ V_{obj} = \sum_{t\in T}\sum_{i\in I} p^{LMP} * P_{i,t} - \sum_{t\in T}\sum_{i\in I} F_{i,t} * f_{i,t}^{Price} - \sum_{l\in R}\sum_{t\in T} c_{l,t}^{startup} - \sum_{l\in R} b_l^{price} * R_l \quad (1)$$

$$\sum_{i\in I^{Dispatch}} P_{i,t}^{Day-Ahead} + p_t^{Bid-Wind} = d_t^{Bid} \quad (2)$$

$$\sum_{l\in I^{Reserve}} (R_{l,t}^{+} - R_{i,t}^{-}) = p_t^{Bid-Wind} - p_t^{Actual-wind} + d_t^{realized} - d_t^{Bid} + d_t^{shedding} \quad (3)$$

$$\sum_{l\in I^{Reserve}} (R_{l,t}^{+} + R_{i,t}^{-}) \le R_{\max} \quad (4)$$

$$0 \le p^{bid-wind} \le w * P_{total} \quad (5)$$

II. KEY FIGURES

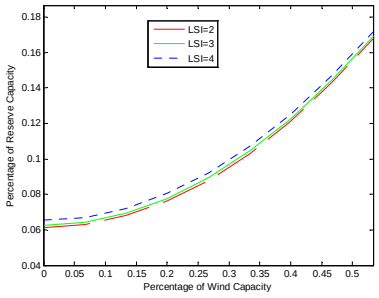

Figure 1. The required system reserve level against the level of wind power penetration

III. KEY RESULTS

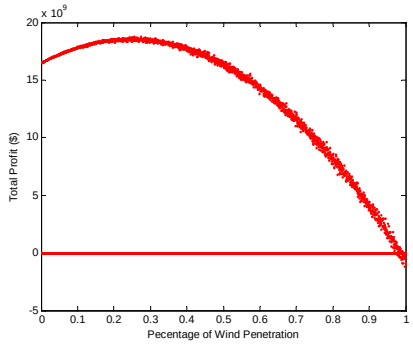

Figure 2. The relationship between wind penetration and total profit of the CAISO: base case.

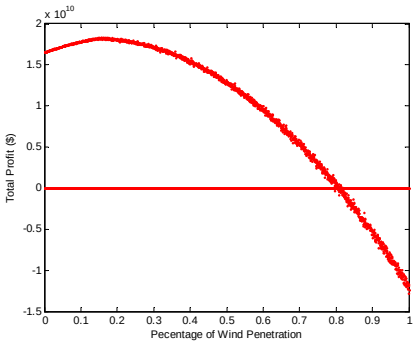

Figure 3. The relationship between wind penetration and total profit of the CASIO: considering the influence of the LMP.

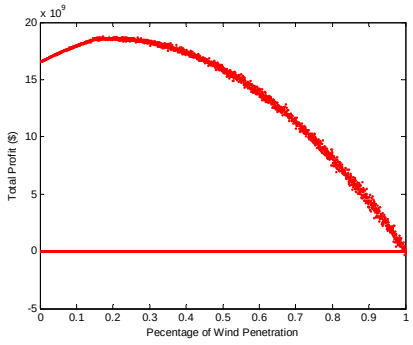

Figure 4. The relationship between wind penetration and total profit: considering the influence of CAES.

Nodal Pricing for Multiple Types Class With Effect Assessment of Demand Response

Nestor Gonzalez IEEE student member, Guillermo Gutierrez
Ggraduate Program and Research in Electrical Engineering, Master Science of Electrical Engineering ,Morelia, Morelia Institute Technologic , Morelia, Mich.58120 ,MEX,
Email: acapulco1393@yahoo.com.mx and ggutier@itmorelia.edu.mx

Abstract— **evolution of electricity market deregulation provides opportunities to implement emergent telecommunications technologies for electric service management. Some users are more sensitive to changes in electricity prices and would be more interested in reducing costs and are willing to accept lower-ability level of reliability as their activities do not require continuous use of electricity. Obviously some customers will be more sensitive to changes in electricity prices and thus are willing to accept a lower level of reliability because they do not required continuous use of electricity. For this reason, the service outage for any contingency or any set schedule will affect both those consumers willing to accept a minimum level of reliability as well as consumers interested in contracts based on load curtailment. This paper evaluates the effect assessment of demand respond (DR) programs on nodal prices considering customers' electricity contracts by differentiating multiple types of classes based on the desired risk level, n-1 and n-2 element outage. Load elasticity information reported in demand response projects is adopted to evaluate the non-dispatchable load reduction due to dynamic pricing.**

I. KEY EQUATIONS

We consider a market model where customers select electricity contracts by differentiating electricity in multiple availability types and multiple types of classes based on desired risk level. For system state *j* (only considering n-1 and n-2), the nodal prices and load shed considering customer requirements can be solved mathematically for each period of time *t* as:

$$Min = \sum_{i=1}^{Ng} C_{si,t}^{j} Pg_{si,t}^{j} + \sum_{i=1}^{Nb} OC_{i,t}^{j}\left(LC_{pi,t}^{j}\right) - \sum_{i=1}^{Nb} C^{j}{}_{bi,t} Pd_{bi,t}^{j}$$

$$S.to \quad \sum_{i=1}^{n}\left(Pg_{si,t}^{j} - Pd_{bi,t}^{j} + LC_{pi,t}^{j}\right) = \sum_{i=1}^{n} P_{i,t}^{j}\left(V,\theta\right) \qquad (2)$$

$$\sum_{i=1}^{n}\left(Qg_{si,t}^{j} - Qd_{bi,t}^{j} + LC_{qi,t}^{j}\right) = \sum_{i=1}^{n} Q_{i,t}^{j}\left(V,\theta\right) \qquad (3)$$

$$\left(P_{ig,t}^{j,\min} \le P_{ig,t}^{j} \le P_{ig,t}^{j,\max}\right) \qquad (4)$$

$$\left(Q_{ig,t}^{j,\min} \le Q_{ig,t}^{j} \le Q_{ig,t}^{j,\max}\right) \qquad (5)$$

$$\left(V_{i,t}^{j,\min} \le V_{i,t}^{j} \le V_{i,t}^{j,\max}\right) \qquad (6)$$

$$\left(P_{im,t}^{j} \le P_{im,t}^{j,\max}\right) \qquad (7)$$

$$\left(LC_{pi,t}^{j} \le LC_{pi,t}^{j,\max}\right) \qquad (8)$$

$$\alpha_d = \left(\frac{dQ}{dP}\right)\left(\frac{P}{Q}\right) = \left(\frac{\Delta Q}{\Delta P}\right)\left(\frac{P}{Q}\right) \qquad (9)$$

II. KEY FIGURES

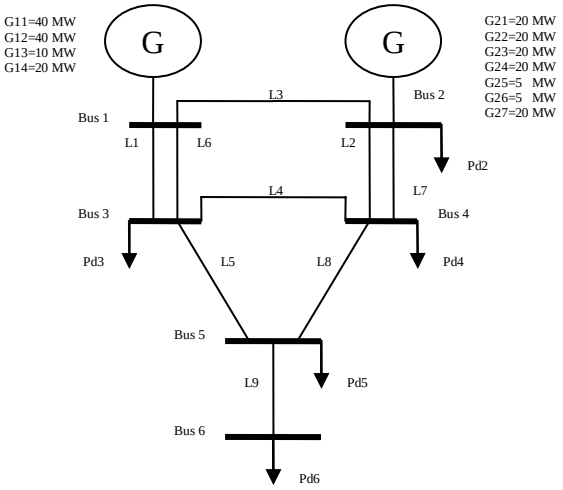

Figure 1. Test System

III. KEY RESULTS

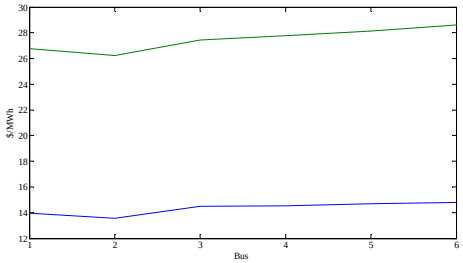

Figure 2 Nodal pricing by class in base case (Green line is the expected value of class B and blue line is the expected value by class A)

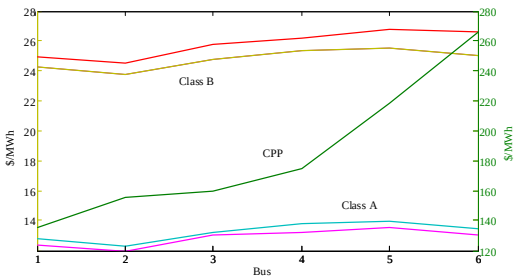

Figure 3 Expected nodal prices per class, when is applied different elasticity, by a day with Critical Peak Pricing.

Tradeoffs in Planning Renewable Power Generation Entry to the Electricity Market

Kazi Nazmul Hasan, Tapan Kumar Saha, and Mehdi Eghbal
The University of Queensland, Brisbane, Queensland 4072, Australia

***Abstract*—Renewable intensive bulk power system planning and operation considerations are getting high importance due to huge pressure imposed by environment-friendly policies and uncertainties in the fossil-fuel based investments. This paper addresses a number of influential economic and reliability issues for renewable generation entry to a deregulated electricity market. Geothermal power penetration, wind intermittency, load volatility, price variation and dynamic bidding are considered here in the optimal power flow simulation. A modified IEEE-RTS is simulated, through MATPOWER/MATLAB and CRUSE software, while considering the Australian National Electricity Market (NEM) data for generation technologies and costs. Locational marginal prices (LMP), system minutes and Expected Energy Not Supplied (EENS) are presented here considering gas, wind, geothermal and geothermal/wind generation-mix. The simulation results confirm high potential of geothermal power as a new generation entry to the Australian NEM.**

I. Key Equations

A simplified cost function of a generator can be represented as follows (1-3):

$$C = \sum_{i \in n_g} f_P^i\left(P_g^i\right) \tag{1}$$

$$f_P^i\left(P_g^i\right) = a_i {P_g^i}^2 + b_i P_g^i + c_i \tag{2}$$

$$f_{P,\min}^i\left(P_g^i\right) \le f_P^i\left(P_g^i\right) \le f_{P,\max}^i\left(P_g^i\right) \qquad i \in n_g \tag{3}$$

$$System\min utes = \frac{60 \times \sum_k \sum_{j \in LC} L_{kj} D_{kj} f_j}{L_S} \quad sys-\min \tag{4}$$

$$EENS = \sum_k \sum_{j \in LC} P_j L_{kj} D_j \qquad MWh \tag{5}$$

II. Key Results

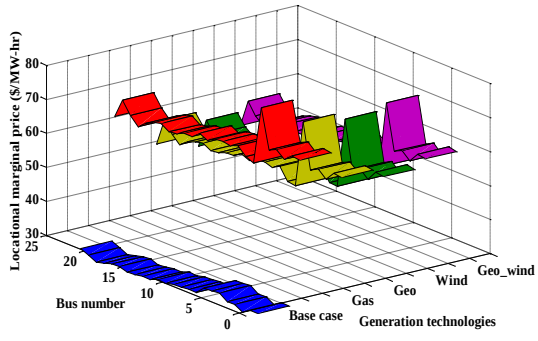

Fig.1 LMPs for different generation technologies

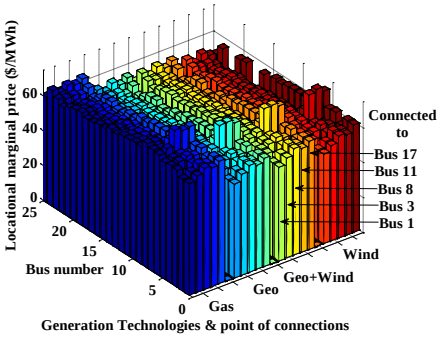

Fig.2 LMPs for different point of connection scenarios

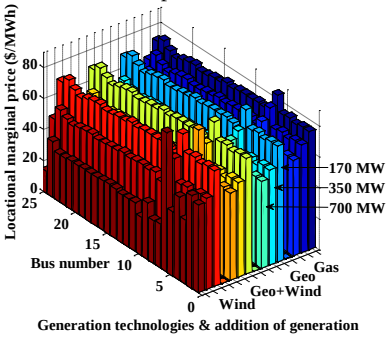

Fig.3 LMPs for different amount of generation scenarios

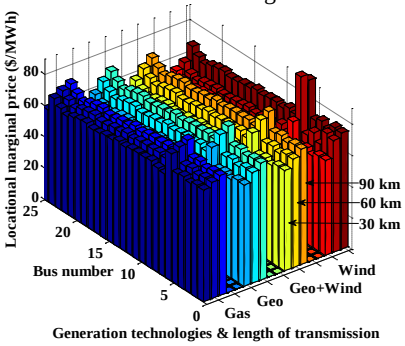

Fig.4 LMPs for different transmission length scenarios

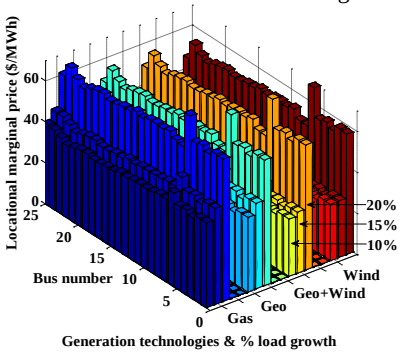

Fig.5 LMPs for different load growth scenarios

Combining the Reserve Market for Wind Power Trading

Jiaqi Liang, Santiago Grijalva, and Ronald G. Harley
School of Electrical and Computer Engineering
Georgia Institute of Technology, Atlanta, GA 30332, USA.
Email: jliang@gatech.edu, sgrijalva@ece.gatech.edu, and rharley@gatech.edu

***Abstract*— Due to the variability and limited predictability of wind power, wind producers participating in most electricity markets are subject to significant deviation penalties during market settlements, and system operators need to schedule additional reserve to balance the unpredicted wind power variations. This paper proposes a combined energy and regulation reserve market model to encourage wind producers to regulate their short-term outputs. With a reserve market designed with lower deviation penalties, wind producers can increase their revenue by optimally bidding in the energy and reserve markets to reduce their deviation penalties. Meanwhile, part of the intra-hour wind variations, which would have appeared in the system energy balance, is diverted into the system regulation reserve. The system then benefits from facing less wind energy intra-hour variations, demanding less short-term reserve for wind variations, and having additional fast, although variable, regulation reserve from wind plants, which are likely to enhance grid security and operations in high wind penetration scenarios. A test case is studied to demonstrate the effectiveness of the proposed market model and bidding strategy on increasing the wind plant revenue and grid security.**

I. Key Equations

By bidding in to both the day-ahead energy and reserve market, with a bidding scheme of (P_{cE}, P_{cUR}), a wind plant receives the following revenue:

$$R(P_t \mid P_{cE}, P_{cUR}) = \begin{cases} \pi_{E+}P_t + (\pi_E - \pi_{E+})P_{cE} + (\pi_{UR} - \pi_{E+})P_{cUR} & P_t \in [P_{cE} + P_{cUR}, P_{t\max}] \\ \pi_{UR-}P_t - (\pi_{UR-} - \pi_E)P_{cE} - (\pi_{UR-} - \pi_{UR})P_{cUR} & P_t \in [P_{cE}, P_{cE} + P_{cUR}) \\ \pi_{E-}P_t - (\pi_{E-} - \pi_E)P_{cE} - (\pi_{UR-} - \pi_{UR})P_{cUR} & P_t \in [0, P_{cE}) \end{cases}$$

where P_t is the actual available wind power. π_X's are prices for energy, reserve, and their deviations. Optimizing the expected revenue gives the optimal day-ahead bidding scheme.

II. Key Figures

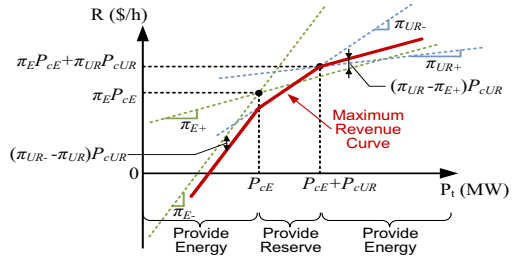

Figure 1. Wind plant maximum revenue vs. available wind power

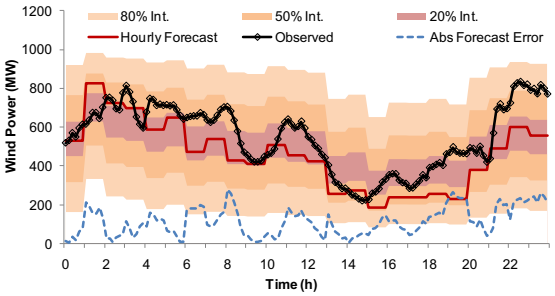

Figure 2. Day-ahead hourly wind power forecasts

III. Key Results

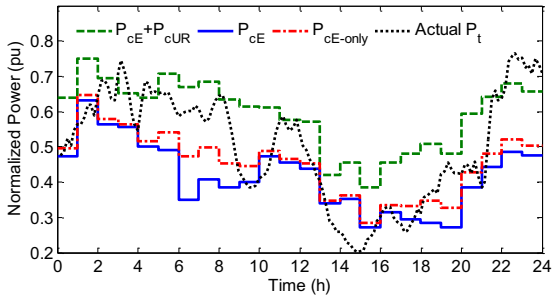

Fig. 8. Optimal committed energy and reserve when bidding in both markets (P_{cE} and P_{cUR}) and in only the energy market ($P_{cE\text{-}only}$).

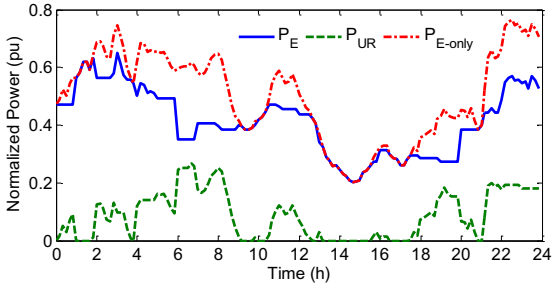

Figure 3. Output energy and reserve during the actual delivery day: bidding in both markets and bidding in only the energy market.

TABLE II
2006 Monthly Average Revenue (No Curtailment)

	$R_{E\&UR}$ (k$/h)	$R_{E\text{-}only}$ (k$/h)	R Inc. (%)		$R_{E\&UR}$ (k$/h)	$R_{E\text{-}only}$ (k$/h)	R Inc. (%)
Jan	11.23	10.81	3.88	Aug	4.96	4.63	7.25
Feb	9.36	8.99	4.06	Sep	4.92	4.49	9.59
Mar	13.08	12.70	2.97	Oct	7.80	7.42	5.07
Apr	13.32	12.96	2.76	Nov	9.02	8.64	4.38
May	6.53	6.12	6.71	Dec	8.48	8.15	4.12
Jun	10.06	9.71	3.62	Yearly Avg.	8.82	8.44	**4.96**
Jul	7.04	6.69	5.10				

Multi-Agents VPP Aggregation

Hugo Morais and Zita Vale
Knowledge Engineering and Decision Support Research Center, School of Engineering, Polytechnic Institute of Porto,
R. Dr. António Bernardino de Almeida, 431, 4200-072 Porto, Portugal,
Email: hgvm@isep.ipp.pt and zav@isep.ipp.pt

***Abstract*—** This paper presents a negotiation methodology for the creation and management of coalitions of producers and consumers in Electricity Markets environmental. This approach is tested using the multi-agent market simulator MASCEM, taking advantage of its ability to provide the means to model and simulate Virtual Power Players (VPP). VPPs are represented as coalitions of agents, with the capability of negotiating both in the market (Electricity and others), and internally, with their members, in order to combine and manage their individual specific characteristics and goals, with the strategy and objectives of the VPP itself.

Coalition formation is an important form of interaction in multi-agent systems. Coalition formation is the coming together of a number of distinct, autonomous agents in order to act as a coherent grouping in which they increase their individual gains by collaborating. Coalition formation process can be viewed as being composed of three main activities:

1) Coalition structure generation: forming coalitions of agents such that those within a coalition coordinate their activities, but those in different coalitions do not;

2) Optimization of the value of each coalition: pooling the resources and tasks of the agents in a given coalition to maximize the coalition value;

3) Payoff distribution: dividing each coalition's value among its members.

Coalitions have been advocated in e-commerce (where buyers may pool their requirements in order to obtain bigger discount groups [10]), in grid computing (where multi-institution virtual organizations are viewed as being central to coordinated resources sharing and problem solving), and in e-business (where agile groupings of agents need to be formed in order to satisfy particular markets niches [11]). In all of these cases, the formation of coalitions aims to increase the agents' abilities to satisfy goals and to maximize their personal, or the system's, outcomes.

In a first approach each VPP define a set of objectives to classify the producers and to select the best candidates to join their coalitions, and offer better contract conditions to the most appropriate ones, attempting to convince them to join the aggregation; less favorable contracts to less suitable candidates.

Besides the revenues that VPPs offer in their contracts, they also try to convince the best candidates (candidates with high classification) to join their coalition by presenting other conditions, such as increasing payments based on the reliability that candidates may present on the future.

The candidates that are awarded with best contract proposals are the ones that are most highly classified, taking into account their characteristics and objectives' suitability to the VPP.

On the other hand, the candidates that have applied to several aggregations choose among the proposals that interested VPPs offered, by comparing: the offered payments by produced energy; the expected increasing in future contracts with each VPP; the similar players with similar characteristics' history of improvement in contracts with each VPP; and the non-payment related issues that each VPP offers, such as CO2 emissions that this coalition members present. After analyzing the contract conditions, the candidates can send counter-proposals to the VPPs, starting the negotiation process which will culminate in an eventual entrance of the candidates in the VPP for which the achieved deal most pleases both parts.

Once the coalitions are formed, as the time evolves, if a VPP finds that its actual situation could be improved by adding a new company to its aggregation, it can, at any time, offer a contract proposal to a desired company, trying to convince it to join the coalition. Also, if an independent company finds itself in a similar situation throughout the time, it can apply to VPPs that present higher profits perspectives.

Some negotiation process experimental findings, resulting from MASCEM simulations, are presented in the Case Study, including the players' participation in the market. The agents used in case study are based in real producers in Spain and are considered 100 producers and 10 VPP. The negotiation process, with special emphasis on its timings is presented in the Figure 1.

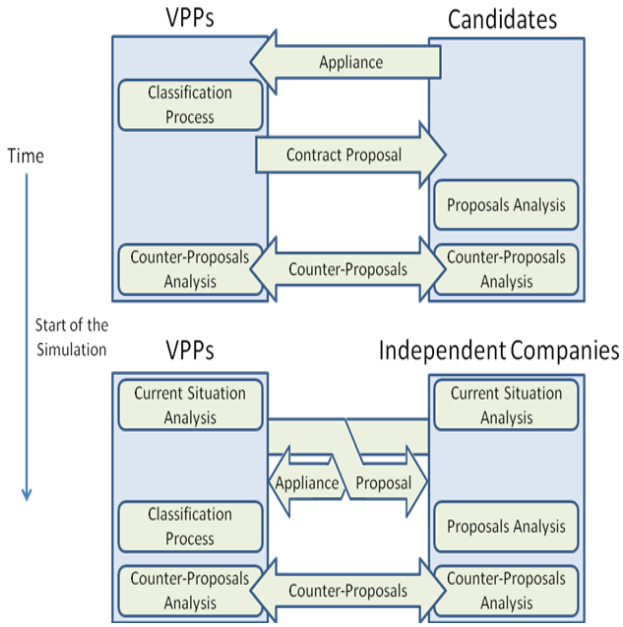

Figure 1. Negotiation Process

Evaluation of GENCO's Strategy in Creating a Congested System for Exercising Market Power

Muhammad Bachtiar Nappu and Ramesh C. Bansal
School of Information Technology and Electrical Engineering
The University of Queensland, Brisbane, QLD 4072, Australia
Email: *bachtiar@ieee.org* and *bansal@itee.uq.edu.au*

***Abstract*— An independent system operator must be able to simulate market performance and to identify participants which have potential points to exercise market power with the purpose of guarantee a safe, transparent and fair competition among market participants. This manuscript recognises the impact of bidding strategy taken by prospective generation company within the potential region to be congested. In this paper a composite method for investigating market power under congestion condition is proposed, which employs shift-factor optimal power flow based *LMP-lossless* scheme. A 24-bus IEEE Reliability Test system (IEEE-RTS) is employed as the case study to investigate some financial implications of market power under congestion circumstances.**

I. Key Equations

The guiding equations for market power investigation are:

$$\mathrm{HHI} = \sum_{i=1}^{N} (\xi_i)^2 \quad (1)$$

$$\rho_i = \lambda + \sum_{m} \mu_{min,flow,m} \cdot S_{m,n} - \sum_{m} \mu_{max,flow,m} \cdot S_{m,n} \quad (2)$$

$$r_G = \sum_{i=1}^{N} \rho_i P_i \quad (3)$$

$$c_G = \sum_{i=1}^{N} \left[\frac{1}{2} m_i (P_i)^2 + B_i P_i\right] \quad (4)$$

$$\pi_G = r_G - c_G \quad (5)$$

$$c_D = \sum_{i=1}^{N} \rho_i D_i \quad (6)$$

II. Key Figures

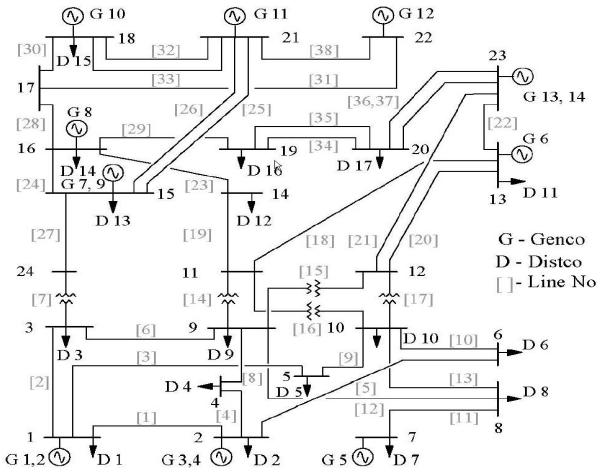

Figure 1. Single Line Diagram of IEEE 24-Bus Reliability Test System

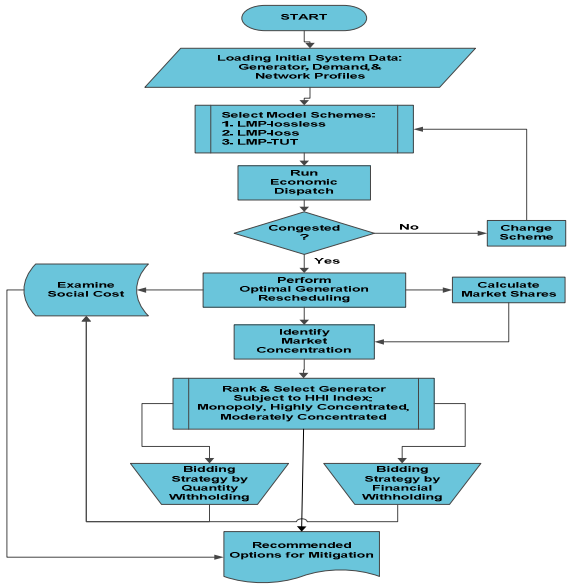

Figure 2. The proposed composite method for market power investigation

III. Key Results

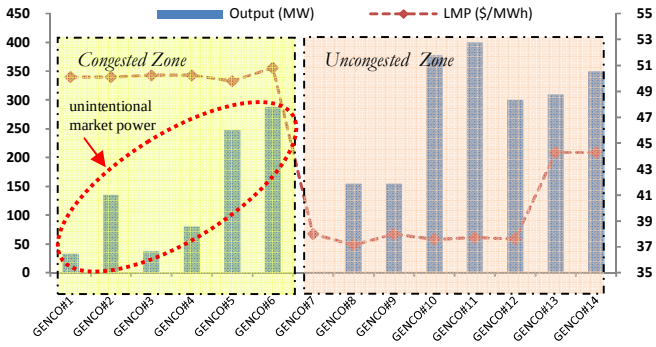

Figure 3. GENCOs Output vs. LMP with Congestion

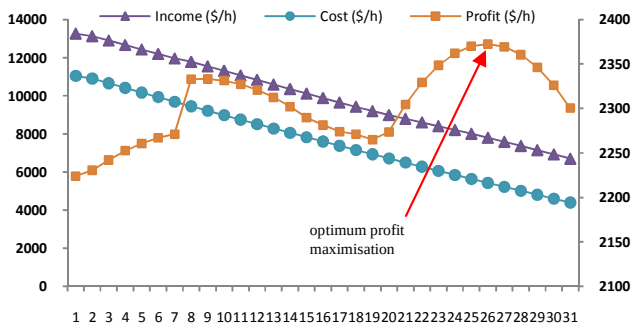

Figure 4. The behavior of GENCO #6 by quantity withholding strategy

Payment Cost Minimization Auction in Electricity Markets

Satish Sharma and Rohit Bhakar
Department of Electrical Engineering,
Malaviya National Institute of Technology Jaipur,
India,
Email: satishsharma1500@gmail.com and
rohitbhakar@gmail.com

N. P. Padhy and H. O. Gupta
Department of Electrical Engineering,
Indian Institute of Technology Roorkee, India
Email: nppeefee@iitr.ernet.in and
harifee@iitr.ernet.in

***Abstract*— In deregulated electricity markets, offer cost minimization auction is used to minimize the total bid cost for selecting offer and demand bids. But a uniform market clearing price (MCP) is used for consumer payments. Hence, the minimized bid cost is different from settlement cost. The problem has a non-separable objective function and the bid curves are non-continuous. This paper proposes a combination theory based model to consider all possible combination of suppliers who can participate in auction for hourly system demand. These combinations are compared for minimum payment cost. Decision variables such as power levels, MCP and startup cost are included for calculation of minimum payment cost. Simulations reflect that the method is efficient and the payment cost for payment cost minimization auction is substantially lower than the payment cost for offer cost minimization auction, for a particular set of offer bids pertaining to certain demand.**

I. Key Equations

The objective function for offer cost minimization auction is:

$$\min_{\{p_i(t)\}} J \quad \text{with } J \equiv \sum_{t=1}^{T}\sum_{i=1}^{I} c_i(t)p_i(t) + S_i(t) \tag{1}$$

Under the payment cost minimization auction mechanism, payment costs of buyers are directly minimized. The problem is:

$$\min_{\{MCP(t)\},\{p_i(t)\}} J \quad \text{with } J \equiv \sum_{t=1}^{T}\sum_{i=1}^{I} MCP(t)p_i(t) + S_i(t) \tag{2}$$

Both the above auctions are subjected to following constraints:

$$P_d(t) - \sum_{i=1}^{I} p_i(t) = 0 \tag{3}$$

$$p_i(t) = 0, \text{ if } u_i(t) = 0 \tag{4}$$

$$p_{i\min}(t) \le p_i(t) \le p_{i\max}(t), \text{ if } u_i(t) = 1 \tag{5}$$

$$MCP(t) = \max(c_i(t)), \forall i \ \ s.t.\ p_i(t) > 0 \tag{6}$$

II. Key Algorithim

The algorithm is as:

Step 1: Initial data from bids submitted for auction and from hourly demand.

Step 2: Calculate total number of combinations of bidding generators.

Step 3: Discard the combinations unable to supply the minimum system demand.

Step 4: Calculate the payment cost for the resulting combinations from (2).

Step 5: Compare the payment cost for each combination and determine the minimum payment cost combination.

Step 6: For minimum payment cost combination, determine the MCP and power level of generators at that hour.

Step 7: For next hour dispatch, go to the step 4.

Step 8: Dispatch the MCP and power levels for day-ahead electricity market for all hours

III. Key Results

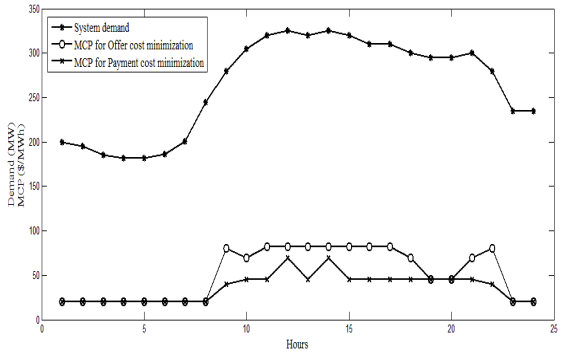

Fig. 1. Hourly demand and MCP for both auctions.

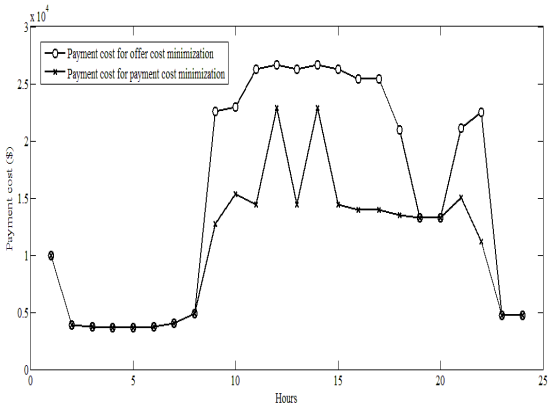

Fig. 2. Hourly payment cost for both auctions.

Extension of Test System For Distribution System Reliability Analysis with Integration of Electric Vehicles in Distribution System

Pramod Bangalore and Lina Bertling
Department of Energy and Environment, Chalmers University of Technology, Gothenburg, 41296, Sweden,
Email: *pramod@student.chalmers.se and lina.bertling@chalmers.se*

***Abstract*— Over the years the electric power system has seen an exponential growth in terms of size and technology. A similar growth and development has taken place in the terms of probabilistic applications used to analyze the power systems. A literature survey was done to analyze the existing widely used test systems; IEEE RTS and RBTS. Conclusions have been drawn towards how these test systems can be updated or modified to be sufficient with respect to the modern power systems "Smart Grid". Extensions to Bus-2 distribution system of RBTS have been proposed to include the integration of Electric Vehicles into the distribution system. A sample study investigating the effect of Vehicle to Grid supply on the Energy Not Supplied in the system has been carried out the results for the same have been presented. The aim of the work is to be able to provide a test system with electric vehicles for probabilistic reliability applications.**

I. KEY EQUATIONS

The main equation used in calculating Energy Not Supplied to the system is :

ENS = Average load connected to the load point * Annual outage time (1)

II. KEY FIGURES

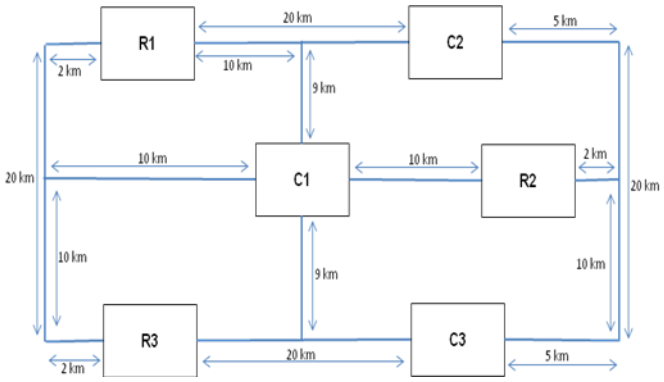

Figure 1. Proposed Geography for the Distribution Test System

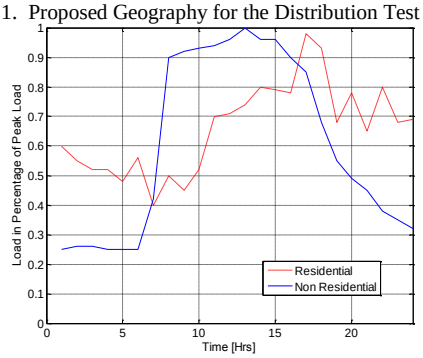

Figure 2. Daily Load curves for residential and non-residential customers

III. KEY RESULTS

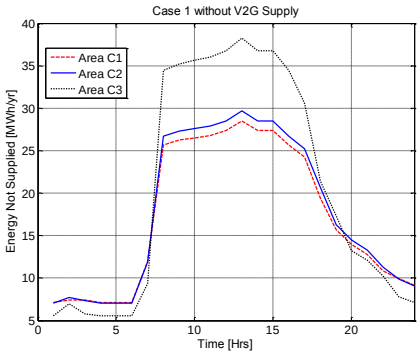

Figure 3 ENS for the commercial complexes C1, C2 and C3 without V2G supply

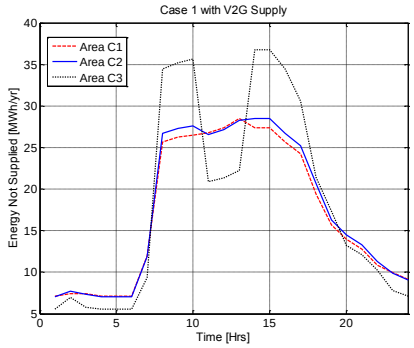

Figure 4. ENS of commercial complexes C1, C2 and C3 with V2G supply with 30% EV penetration

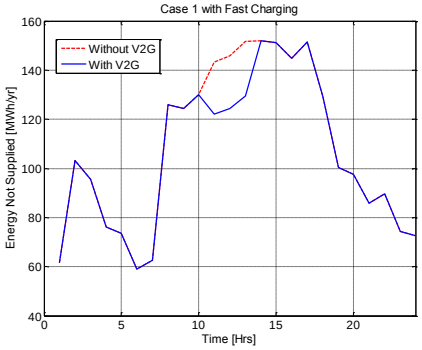

Figure 5. ENS of total system with and without V2G supply with 30% EV penetration

Figures 3 and 4 show the difference in the value of ENS when Vehicle to Grid (V2G) supply is considered. As can be observed from the latter figure, the value of ENS is reduced due to addition of EVs as a source of power.

Optimum SOC of Grid-Connected SmartParks

Priyam Chakravarty and Ganesh K. Venayagamoorthy
Real-Time Power and Intelligent Systems Laboratory
Missouri University of Science and Technology, Rolla, MO 65409, USA
Email: pc5gd@mst.edu and gkumar@ieee.org

***Abstract*— When a smart grid composed of plug-in vehicle parking lots (SmartParks) and wind farm is subjected to variable wind power ($P_{wind}(t)$) penetration, there are fluctuations in power flow through transmission lines ($P_{1\text{-}6}(t)$, $P_{6\text{-}4}(t)$) connected to the wind farm bus. These fluctuations although minimized by the presence of SmartParks as shock absorber, can cause power deficit or wastage when the SmartParks are at undercharged or overcharged state, respectively. In order to avoid this, it is necessary to maintain a dynamic optimum state of charge ($SOC(t)$) at the SmartParks which changes based on variations in wind speed ($Wsp(t)$). In this study, an action dependent heuristic dynamic programming (ADHDP) type adaptive critic design (ACD) based controller is proposed that uses a mean variance optimization (MVO) algorithm as an actor to generate the charge/discharge command ($P_{comm}(t)$) based on the cost-to-go function ($J(t)$) determined by the critic depending on the system states ($X(t)$). A performance index ($U(t)$) guides the critic learning, which depends on oscillations in power flow ($P_{1\text{-}6}(t)$, $P_{6\text{-}4}(t)$) from their reference power ($P_{1\text{-}6\text{-}ref}$, $P_{6\text{-}4\text{-}ref}$) and deviations in SOC(t) from a dynamic reference state of charge ($SOCref(t)$) which is a function of predicted change in wind speed ($\Delta Wsp(t)$) over a time period (T).The results demonstrate that the ACD controller maintains an optimum $SOC(t)$ in the SmartParks that minimizes transmission line power flow fluctuations in the system under variable wind speed conditions.**

I. Key Equations

The guiding equations for determining optimum charge/discharge command ($P^*_{comm}(t)$) for SmartParks:

$$X(t) = [SOC(t), P_{wind}(t), P_{1-6}(t), P_{6-4}(t)] \quad (1)$$

$$\Delta Wsp(t) = \sum_{t=0}^{T} \{Wsp(t) - Wsp(t+1)\} \quad (2)$$

$$SOCref(t) = \frac{SOC_{\max} + SOC_{\min}}{2} - \{\frac{\Delta Wsp(t)}{Wsp(t)} \times 100\} \quad (3)$$

$$U(t) = \alpha_1 |P_{1-6}(t) - P_{1-6-ref}| + \alpha_2 |P_{6-4}(t) - P_{6-4-ref}| + \alpha_3 |SOC(t) - SOCref(t)| \quad (4)$$

II. Key Figures

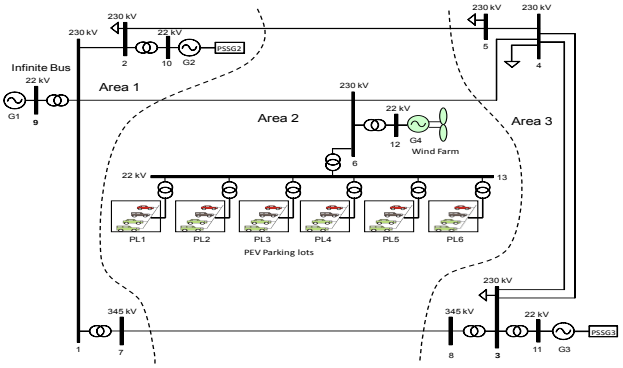

Figure 1. Modified 12-bus system with wind farm & SmartParks

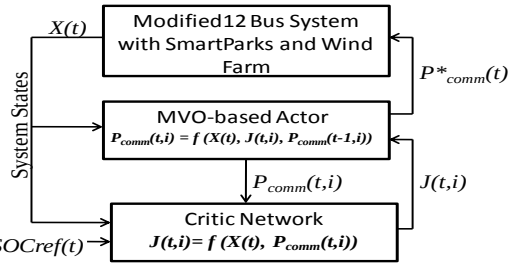

Figure 2. ACD based charge/discharge command ($P^*_{comm}(t)$) controller (dispatch cycle t, MVO iteration i)

III. Key Results

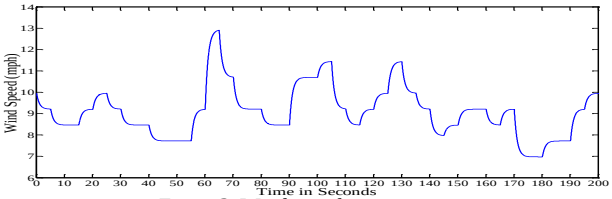

Figure 3. Wind speed variations

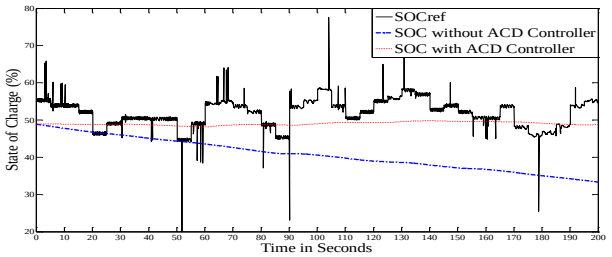

Figure 4. Comparison of SOC of SmartParks. SOC declines from 48% to 20% in 15 minutes without ACD controller as compared to 45% with ACD controller

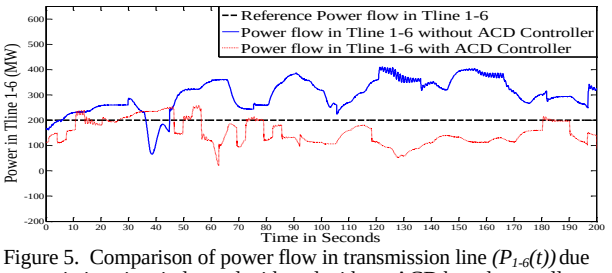

Figure 5. Comparison of power flow in transmission line ($P_{1\text{-}6}(t)$) due to variations in wind speed with and without ACD based controller

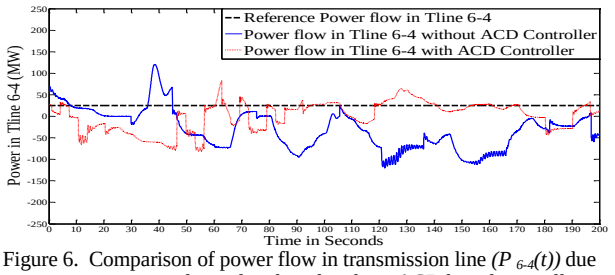

Figure 6. Comparison of power flow in transmission line ($P_{6\text{-}4}(t)$) due to variations in wind speed with and without ACD based controller

Plug In Hybrid Electric Vehicle Penetration on the Electric Grid

Andrew Clarke
Department of Electrical and Computer Engineering, Clemson University, Clemson, SC 29634 USA
Email: *adclark@clemson.edu*

***Abstract*—Plug in hybrid electric vehicle (PHEV) technology is becoming a promising alternative to traditional internal combustion engine (ICE) vehicle technology due to its increased fuel efficiency and lower emissions. Before individual ownership PHEV penetration significantly increases, the consequences of connecting the vehicles to the grid must be examined. In order to demonstrate the effect uncontrolled PHEV charging will have on the electric grid, vehicle's charging stations will be placed in several areas of an electric distribution grid and vehicles will be charged at a variety of times. Simulation of adding PHEVs to a distribution grid, shown in Figure 3, will be conducted using PSCAD. Studies will include the simulation of different PHEV charging penetrations at various places in the system at a variety of times for connection of the PHEV to the grid. Also included will be the effect of varying the load profile for the system based on time of day and seasonal changes. Seasonal changes in load profile as well as transformer cooling and overloading problems will be examined to determine acceptable PHEV charging times and the potential impacts on an electric distribution grid. Figure 1, found in [1], shows how a household load profile varies based on seasonal changes. Results will include bus voltages and distribution line flows. Figure 2, found in [2], shows the average charging profile of a PHEV that will be used in simulation.**

I. REFERENCES

[1]. Shao, Shengnan, et. Al. *Challenges of PHEV Penetration to the Residential Distribution Network.* Retrieved from IEEE Xplore.

[2]. Taylor, Jason, et. al. *Evaluations of Plug-in Electric Vehicle Distribution System Impacts.* Retrieved from IEEE Xplore.

II. SIMULATION

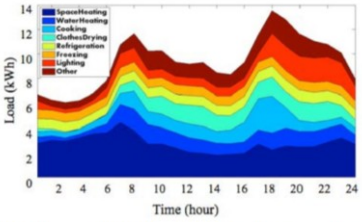

Fig. 1. Hourly winter load seen by a 25kVA distribution transformer, serving five homes.

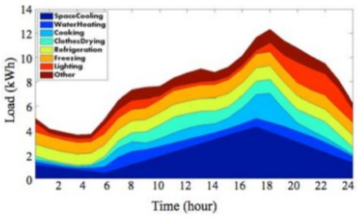

Fig.2. Hourly summer load seen by a 25kVA distribution transformer, serving five homes.

FIGURE 1, SEASONAL FIVE HOUSEHOLD LOAD PROFILE FROM [1]

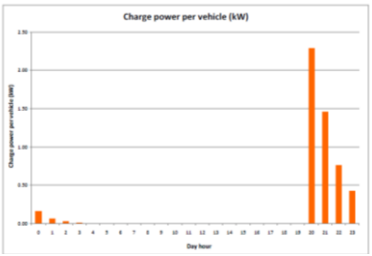

FIGURE 2, PHEV CHARGING PROFILE FROM [2]

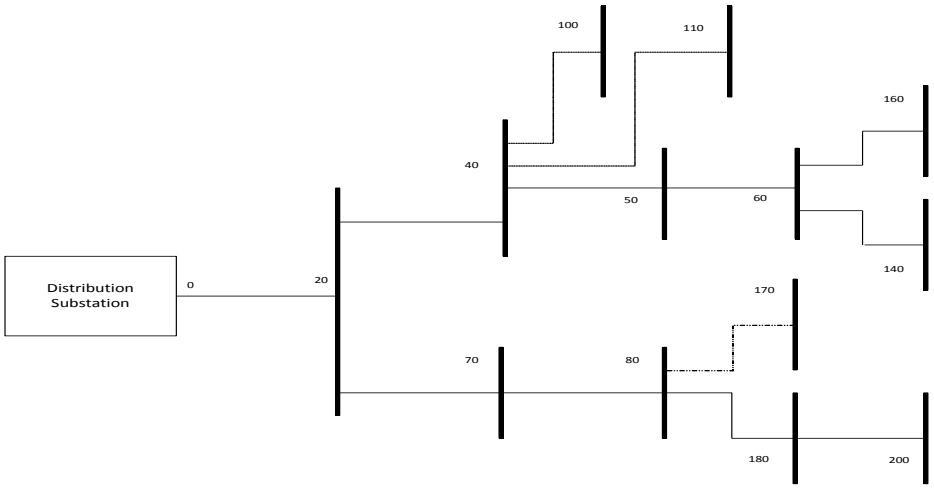

FIGURE 3, DISTRIBUTION SYSTEM USED FOR SIMULATION

Micro-turbine Based Intelligent Hybrid Vehicle with Vehicle to Grid (V2G) Capability

Kaushal Desai and Sukumar Kamalasadan
Power, Energy and Intelligent Systems Laboratory, Department of Electrical and Computer Engineering,
University of North Carolina Charlotte, NC 28223, USA,
Email: *kdesai22@uncc.edu* and *skamalas@uncc.edu*

***Abstract*— Hybrid electric vehicles have increasingly become significant in today's scenario owing to the need for reduced dependence on traditional fossil fuels due to economical and environmental concerns. This research proposes a hybrid electric vehicle drive-train topology, with the difference being that instead of the internal combustion engine, this model proposes the use of more efficient micro-turbine generator (MTG) as the main power source, with a battery-ultra-capacitor combination for energy storage and regeneration. It introduces a novel control algorithm, with an intelligent supervisory control for the power flow in the system, and also provides for the micro-turbine generator to be used for vehicle to grid (V2G) operation.**

I. KEY EQUATIONS

The equations for the micro-turbine, permanent magnet generator, battery and ultra-capacitor are:

Turbine Torque Equation

$$\tau = K_{HHV}\left(W_{f2} - 0.23\right) + 0.5(1 - N)\ \ (Nm) \tag{1}$$

Equations for the Permanent Magnet Synchronous Generator

$$V_{qs}^{r} = -(R_s + pL_{qs})i_{qs}^{r} - \omega_e i_{ds}^{r} L_{ds} + \omega_e \lambda_m \tag{2}$$
$$V_{ds}^{r} = -(R_s + pL_{ds})i_{ds}^{r} + \omega_e i_{qs}^{r} L_{qs} \tag{3}$$
$$T_e = \frac{3P}{4}\left(L_{ds} - L_{qs}\right)i_{ds}^{r} i_{qs}^{r} + i_{qs}^{r}\lambda_m \tag{4}$$
$$\frac{d\omega_m}{dt} = \tau_m - \tau_e \tag{5}$$
$$\frac{d\theta_m}{dt} = \omega_m \tag{6}$$

Equations for the Battery Model

$$z_{k+1} = z_k - \left(\frac{\eta_i \Delta t}{C_n}\right) i_k \tag{7}$$
$$y_k = K_0 - i_k R - \frac{K_1}{z_k} - K_2 z_k + K_3 \ln(z_k) + K_4 \ln(1 - z_k) \tag{8}$$

Equations for the Ultra-capacitor model

$$Rf = \frac{2N}{3} ESR \tag{9}$$
$$Cf = \frac{1.05}{N} C_0 \tag{10}$$
$$Rm = \frac{2N}{3} \phi^{-(2k-1)} ESR \tag{11}$$
$$Cm = \frac{1.05}{N} \phi^{(2j+1)} C_0 \tag{12}$$
$$Rs = \frac{2N}{3} \phi^{-(2k+1)} ESR \tag{13}$$
$$Cs = \frac{1.05}{N} \phi^{(2j-1)} C_0 \tag{14}$$

II. KEY FIGURES

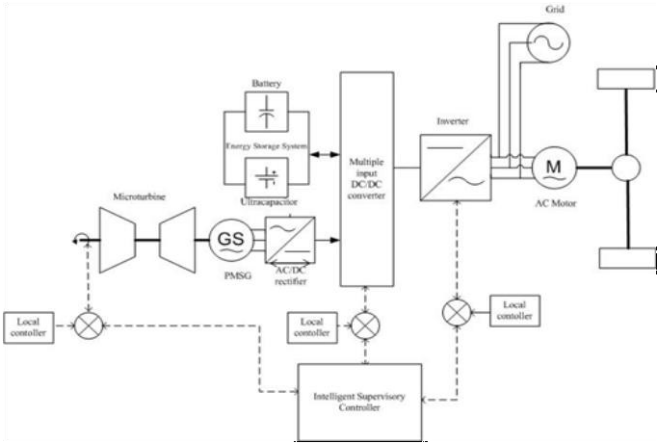

Figure 1. Overall System Block Diagram

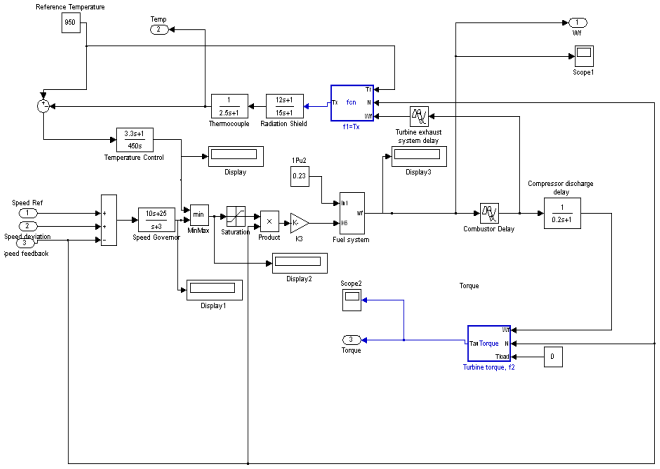

Figure 2. Micro-turbine System Simulink Diagram

III. PRELIMINARY RESULTS

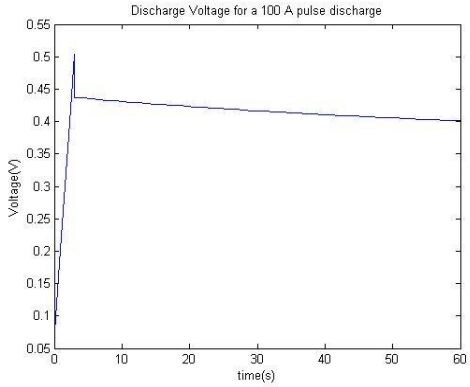

Figure5: Ultra-capacitor output voltage for a 100 A pulse discharge

Isolated Phase-shift Bidirectional DC/DC Converter Design for Plug-in Hybrid Electric Vehicle (PHEV) Applications

Dawei He, Shenghui Cui and Thomas Habetler
Department of Electrical and Computer Engineering, Georgia Inistitute of Technology, Atlanta, GA 30332, USA,
Email: hedawei.david@gmail.com

***Abstract*— This paper presents a new isolated bidirectional DC/DC converter for auxiliary power supply in PHEV where light weight, small size and high power density are required. According to reference [1], compared to conventional isolated bidirectional converters, besides the characters such as bidirectional power flow control, electric isolation and voltage disparity, this new circuit, which should be called modified isolated bidirectional converter, minimizes device current stresses over a wider input voltage range under proper PWM plus phase-shift control strategy. However, different from these two existed modified converters proposed in [1], [2], it processes higher power density with minimum number of devices. These advantages make the new topology competitive for high power applications. Also, a theoretical design principle for an isolated bidirectional DC/DC converter used in PHEV is provided in this paper. Proof of concept is realized through a prototype.**

I. KEY FIGURES

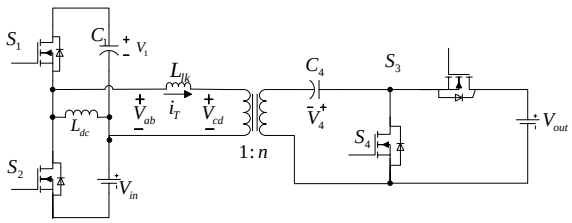

Figure 1. Modified circuit proposed in this work.

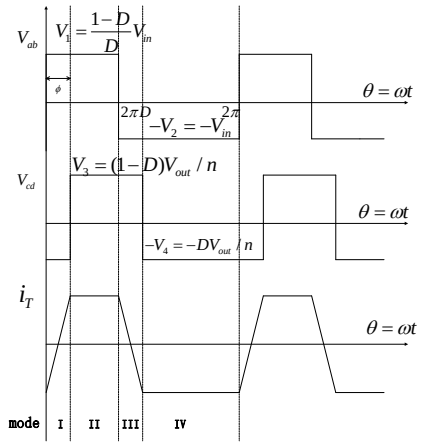

Figure 2. Diagram of Principles.

In mode I: S1, S4 are on, while S2, S3 are off,

$$i_T(\theta) = \frac{V_1 + V_4}{\omega L_1}\theta + i_T(0)$$

In mode II: S1, S3 are on, while S2, S4 are off,

$$i_T(\theta) = \frac{V_1 - V_3}{\omega L_1}(\theta - \phi) + i_T(\phi_1)$$

In mode III: S2, S3 are on, while S1, S4 are off,

$$i_T(\theta) = \frac{-V_2 - V_3}{\omega L_1}(\theta - 2\pi D) + i_T(2\pi D)$$

In mode IV: S2, S4 are on, while S1, S3 are off,

$$i_T(\theta) = \frac{-V_2 + V_4}{\omega L_1}(\theta - 2\pi D - \phi) + i_T(2\pi D + \phi)$$

Power flows through transformer can be calculated by

$$P_0 = \frac{\int_0^{T_s} i_T V_{ab}\,dt}{T_s} = \frac{\phi[4\pi(1-D) - \frac{1}{D}\phi]}{4\pi\omega L_{lk} D} V_{in}^2 .$$

II. KEY RESULTS

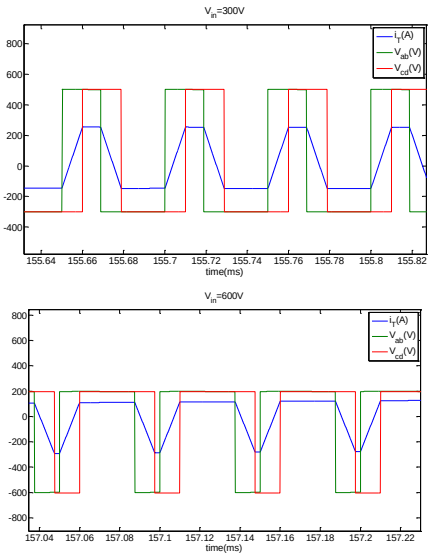

Figure 3. Simulation Result

III. REFERENCE

[1] Han, S., & Divan, D. (2008). Bi-directional DC/DC converters for plug-in hybrid electric vehicle (PHEV) applications. *Proc 23rd IEEE Applied Power Electronics Conference and Exposition* (p. 784-789).

[2] Hui Li; Fang Zheng Peng; Lawler, J.; , "Modeling, simulation, and experimental verification of soft-switched bi-directional DC-DC converters," *Applied Power Electronics Conference and Exposition, 2001. APEC 2001. Sixteenth Annual IEEE* , vol.2, no., pp.736-742 vol.2, 2001.

V2G Technology to Improve Wind Power Quality

F. R. Islam, H. R. Pota, and A. B. M. Nasiruzzaman
School of Engineering and Information Technology (SEIT), The University of New South Wales at Australian Defence Force Academy (UNSW@ADFA), Canberra, ACT 2600, Australia.
E-mail: F.M.Islam@student.adfa.edu.au, H.Pota@adfa.edu.au and A.Nasiruzzaman@student.adfa.edu.au

***Abstract*— This paper presents the use of PHEVs in wind farm as an implementation of V2G technology for power smoothing in generation systems, where power flow variations can occur. A system model with wind farm and a dynamic model of PHEVs are introduced here based on third order battery model. A feed forward compensating control strategy is presented to improve the wind farm's performance, a simple battery scheme is proposed for the, control of the charging and discharging of the PHEVs using a power electronic interface. Simulations have been carried out and demonstrate that the PHEVs have the potential to control the wind farm's output power to a constant value. Scope of such analysis will cover the performance of wind generation with PHEVs, to demonstrate that use of PHEVs as battery energy storage system, can improve overall dynamic response of a wind farm.**

I. KEY EQUATIONS

The most important equations for the controller are:

$$\dot{m} = \left(Km\left(V_{ref} - V_s\right) - m\right)\Big/T \tag{1}$$

$$\dot{x}_\alpha = K_i\left(V_{ref} - V_s\right)\Big/X_L \tag{2}$$

$$0 = K_p\left(V_{ref} - V_s\right)\Big/X_L + x_\alpha - \alpha \tag{3}$$

The link with AC network will be:

$$p_s = -\frac{V_t V_s}{x_T}\sin(\theta_s - \theta_t) = V_{dc} I \tag{5}$$

$$q_s = \frac{V_s^2}{x_T} - \frac{V_s K m V_{dc}}{x_T}\sqrt{1 - \left(\frac{x_T I}{K m V_s}\right)^2} \tag{6}$$

A third-order single cage induction generator model has been used here. The dynamic equations for lead acid battery of PHEVs are:

$$\dot{q}_e = i_{dc}/T_s \tag{7}$$

$$\dot{i}_m = (i_{dc} - i_m)/T_m \tag{8}$$

$$\dot{\theta} = -[P_s - (\theta - Q_a)/R_\theta]/C_\theta \tag{9}$$

$$V_{dc} = E_m - V_p(q_e, i_m) - v_e e^{-\beta q_e} - R_0 i_{dc} \tag{10}$$

$$V_p = \begin{cases} \dfrac{R_p i_m + K_p q_e}{SOC} & if \quad i_m > 0 \quad (Discharge) \\ \dfrac{R_p i_m}{q_e + 0.1} + \dfrac{K_p q_e}{SOC} & if \quad i_m < 0 \quad (Charge) \end{cases} \tag{11}$$

II. KEY FIGURES

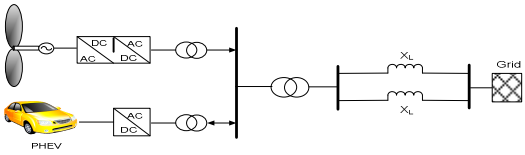

Figure 1. Test System

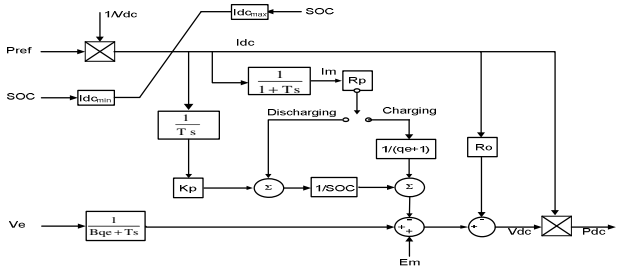

Figure 2. Proposed Battery Scheme

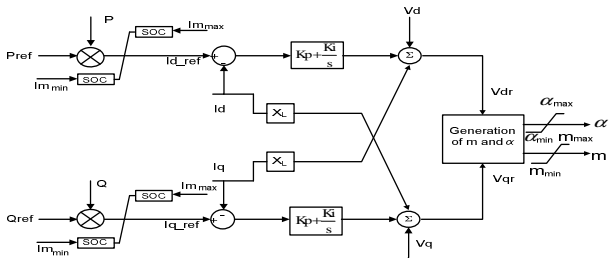

Figure 3. Modified Decoupled PQ Controller

III. KEY RESULTS

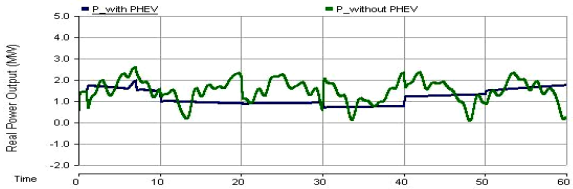

Figure 4. Real Power Output with and without PHEV

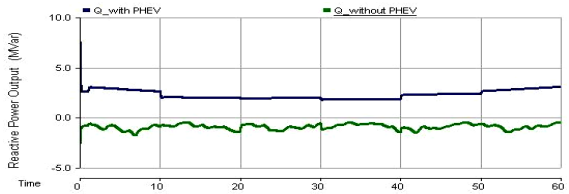

Figure 5. Reactive Power Output with and without PHEV

Large-scale Optimal Coordinated Charging of Electric Vehicles in Power Systems

Qiao Li, Tao Cui, Rohit Negi, Franz Franchetti and Marija D. Ilić
Department of Electrical and Computer Engineering
Carnegie Mellon University
5000 Forbes Avenue, Pittsburgh, PA 15213
Email: {qiaol, tcui, negi, franzf, milic}@ece.cmu.edu

***Abstract*—We consider large-scale coordinated electric vehicle (EV) charging problem in power systems. The overall goal is to achieve the highest level of EV penetration, subject to power system constraints, such as branch capacity and voltage profiles. In this work, we propose a novel EV charging algorithm, which is *throughput optimal*. That is, it achieves the highest level of EV penetration among *all possible* EV charging algorithms. Further, the algorithm is *online*, which does not require any statistics of the non-EV loads or EV driving pattern. All that is required is that an EV owner submits the charging goal when an EV is plugged into the power grid. Thus, as compared to the existing algorithms in the literature, where coordinated charging is preplanned based on predicted loads, our algorithm can achieve robust performance with respect to the changes in the load profiles. Finally, the performance of the algorithm is verified by simulation results.**

I. Key Equations

Queueing equation for EV charging:

$$Q_k(n) = [Q_k(n-1) - \sigma_k(n)]^+ + A_k(n) \tag{1}$$

where $A_k(n)$ is the (aggregated) newly arrived EV charging jobs during time slot n at bus k, which are submitted by EV owners. $\sigma_k(n)$ is the EV charging schedule at time slot n at bus k. It is further required that $\sigma_k(n) \in \mathcal{D}_k(\phi_k(n))$, where $\phi_k(n)$ is the number of EVs that are currently plugged-in at bus k, and $\mathcal{D}_k(\cdot)$ is a discrete set representing total charging powers options at bus k.

Optimal EV charging algorithm:

$$\begin{aligned}
\text{maximize}_{\boldsymbol{\sigma}} \quad & \boldsymbol{Q}(n)^T \boldsymbol{\sigma} && (2)\\
\text{subject to} \quad & S_k^{\text{non-EV}}(n) + \sigma_k = \sum_{l \in \mathcal{N}_k} S_{kl}, \forall k \in \mathcal{N} && (3)\\
& S_{kl} \le S_{kl}^{\max}, \forall (k,l) \in \mathcal{E} && (4)\\
& V_k^{\min} \le V_k \le V_k^{\max}, \forall k \in \mathcal{N} && (5)\\
& \sigma_k \in \mathcal{D}_k(\phi_k(n)), \forall k \in \mathcal{N} && (6)
\end{aligned}$$

II. Key Figures

We simulate the charging algorithm in the standard IEEE 13 node test feeder. The EV charging simulation results are shown in Fig. 1 and the corresponding voltage results are shown in Fig. 2 .

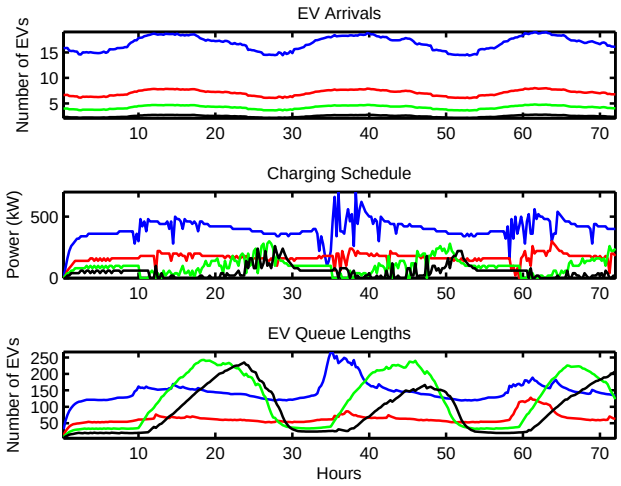

Fig. 1. The EV charging simulation results at selected buses in the IEEE 13 node test feeder. The blue, red, green and black curves correspond to loads 671.a.b.c, 675.a, 675.c and 611.c respectively.

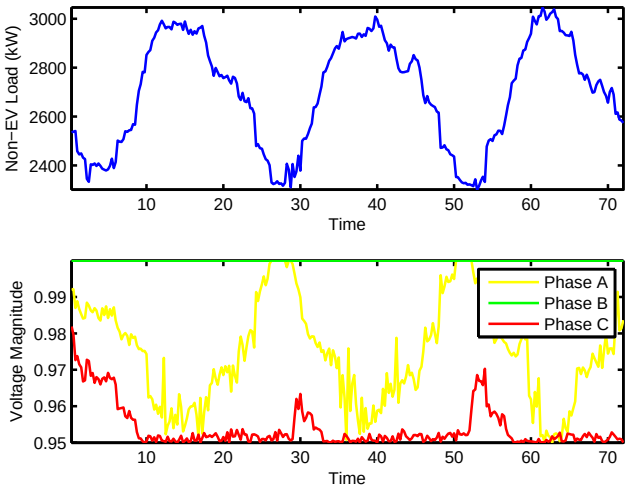

Fig. 2. The voltage simulation results in the IEEE 13 node test feeder.The top figures shows the total load, and the bottom figure shows the minimum voltages.

Future Challenges in PHEV Implementation for Transport Electrification

.Maigha and Mariesa Crow
Department of Electrical and Computer Engineering, Missouri University of Science and Technology, Rolla, MO 65401, USA
Email: mmck6@mst.edu and crow@ieee.org

***Abstract*— Sky-rocketing fuel prices, diminishing reserves of fossil fuels, greenhouse gas emissions and resulting political unrest, have driven the attraction of the researchers into finding environment friendly solutions to these problems. The synthesis of electricity and transportation, they being the core of any infrastructure, has been found as a feasible solution, but with considerable tradeoffs. The HEV (Hybrid Electric Vehicles) have been seen as solutions to the everyday reduction in the limited reserves of non-renewable energy sources. Further, with the enhanced battery technology, the BEV (Battery Electric Vehicles) have shown the potential of being used in coherence with the intermittent, renewable energy sources like wind and solar, thereby strengthening their position in the future markets as distributed energy sources. Presently, the PHEV (Plug-in Hybrid Electric Vehicles) have attracted much attention due to their potential to provide two-way transfer of electric energy, called the G2V (Grid-to-Vehicle) and V2G (Vehicle-to-Grid) technologies respectively in the Smart grid terminology. It is crucial to analyze their effect on the current grid structure in terms of system-wide as well as component-wide effects. On one hand, they have been found profitable in providing ancillary services, while on the other, they have been found taxing when analyzed for servicing the base load.**

It is to be noted that, the degree of penetration of the PHEVs is governed by innumerable factors. To name a few, the list includes federal laws, incentives to customers, usage of AMI (Advanced Metering Infrastructure), aggregator designing, improved power electronics, communication security, pricing structures and standardization. Open challenges in their implementation include, the change in the load curves due to additional load, leading to the degradation of distribution transformer lives, battery charging modes, profiles and times, tracking and aggregating the vehicles for being used as a substantial power source, cost incurred versus the revenues earned by the end user, reliability of power supplied and the uncertainty in integration due to the variability in the human element involved. Even though they have been under research for more than two decades, there is still no comprehensive tool to assess their overall effect on the grid. Moreover, the probabilistic human behavior and requirement of an aggregator in the mid layer has raised the questions on any optimal design of the same. This poster aims at providing an overview of the current challenges in the electrification of transportation. We outline some impending questions, thus briefing the pros and cons of their future implementation.

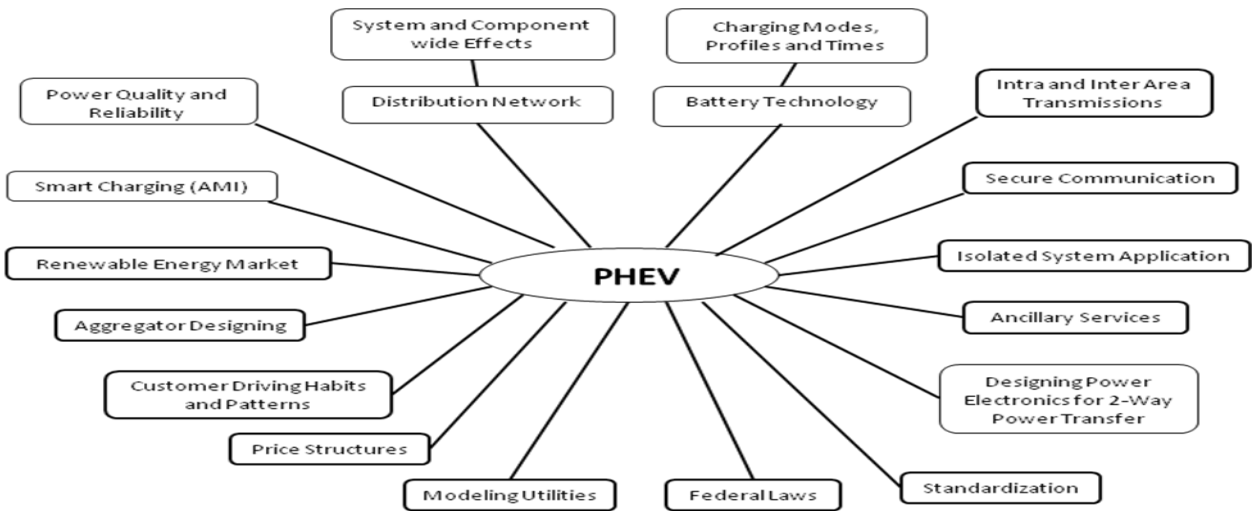

Optimal Unidirectional Vehicle-to-Grid Scheduling: Benefits for Utilities and Customers

Eric Sortomme and Mohamed A. El-Sharkawi
Smart Energy Laboratory, Department of Electrical Engineering, University of Washington, Seattle, WA 98195, USA,
Email: eric.sortomme@gmail.com and melshark@u.washington.edu

Abstract— **Vehicle-to-Grid (V2G) is a way for EVs to provide valuable services to the electric grid while plugged in. Unidirectional V2G is a logical first step in V2G adoption because it requires no aftermarket hardware nor will it void EV battery warrantees. In order to bid ancillary services under unidirectional V2G, the capacities of many EVs must be aggregated. This can be done by a utility or a third party. In this poster, the benefits of optimal scheduling of ancillary services under unidirectional V2G are explored. Two case studies demonstrate the benefits for utilities and customers. One case study shows how optimal unidirectional V2G can provide emission free intra hour wind balancing with minimal peak load increases. Another case study highlights the profit potential for utilities and the resulting lower prices for customers.**

I. KEY EQUATIONS

The Optimal Combined Bidding Algorithm (OptComb):

$$\underset{POP_i(t),RegD_i(t),RegU_i(t),ResR_i(t)}{\text{maximize}} \quad In \tag{1}$$

Subject to:

$$In = \sum_i \sum_t \left(\begin{pmatrix} \alpha \begin{pmatrix} P_{RU}(t) RegU_i(t) \\ +P_{RD}(t) RegD_i(t) \\ +P_{RR}(t) ResR_i(t) \end{pmatrix} \\ +\beta\left(E(PD_i(t))\right) \end{pmatrix} EVPer(t) \right) \tag{2}$$

$$\sum_t \left(E(PD_i(t))Comp_i(t)\right)Ef_i + SOC_{I,i} - Trip_i \le MaxC_i \tag{3}$$

$$\sum_{t=1}^{T_{trip,i}} \left(E(PD_i(t))Comp_i(t)\right)Ef_i + SOC_{I,i} \le MaxC_i \tag{4}$$

$$\left(RegD_i(t) + POP_i(t)\right)Comp_i(t) \le MaxP_i(t) \tag{5}$$

$$RegU_i(t) \le POP_i(t) \tag{6}$$

$$ResR_i(t) + RegU_i(t) \le POP_i(t) \tag{7}$$

$$RegU_i(t) \ge 0 \tag{8}$$

$$RegD_i(t) \ge 0 \tag{9}$$

$$ResR_i(t) \ge 0 \tag{10}$$

II. KEY FIGURES

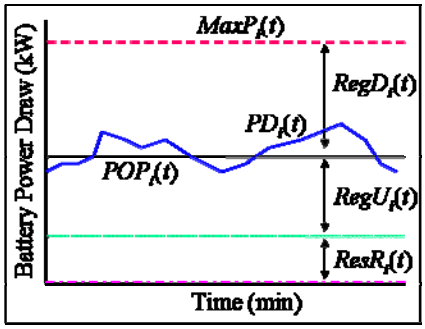

Figure 1.Graphical depiction of unidirectional V2G charging.

III. KEY RESULTS

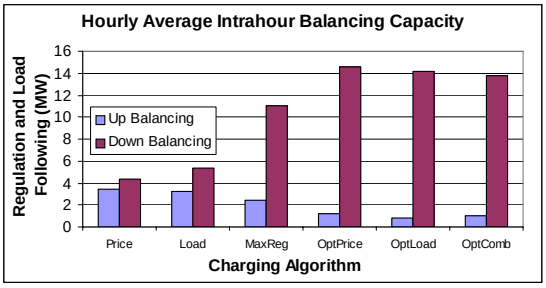

Figure 2. Hourly average wind balancing capacity by V2G algorithm.

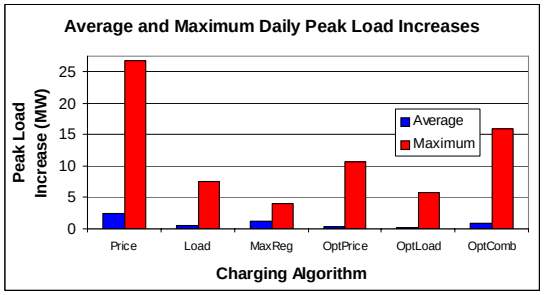

Figure 3. Daily average and maximum peak load increase by V2G algorithm.

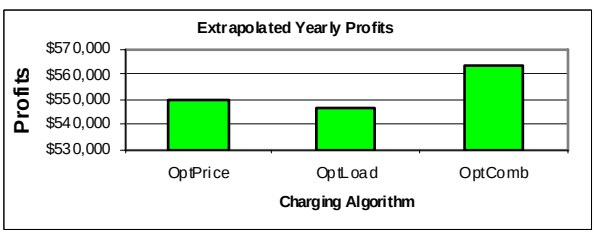

Figure 4. Extrapolated yearly profits by optimal V2G algorithm

Integrating Plug-in Electric Vehicles into the Electric Power System

Di Wu, Dionysios Aliprantis, Konstantina Gkritza and Lei Ying
Department of Electrical and Computer Engineering, Iowa State University, Ames, IA 50011, USA,
Email: {dwu, dali, nadia, leiying}@iastate..edu

***Abstract*— Plug-in Electric Vehicles (PEVs) have been recognized as a key part of solution to energy and environmental problems. An expectation has been made for one million PEVs on U.S. road by 2015. The emerging fleet of PEVs will introduce a considerable amount of additional load on the power system. We estimate the power consumption by light-duty PEVs in different charging scenarios using the travel patterns obtained from the 2009 National Household Travel Survey (NHTS). Also, we propose scheduling and dispatch algorithms for PEV aggregators to minimize the expected electric energy cost according to price variation and charging demand. Simulation results are used to evaluate the proposed algorithms, and to demonstrate the potential impact of an aggregated PEV fleet on the power system.**

I. KEY EQUATIONS

The guiding equations in the analytical method to estimate the electric energy consumption are:

$$E(\epsilon) = \frac{1}{\eta} E(\xi) E(h_{tr}) E(m_{cd}) \tag{1}$$

$$\sigma(\epsilon) = \sqrt{E(\xi^2) E(h_{tr}^2) E(m_{cd}^2) / \eta^2 - E^2(\epsilon)} \tag{2}$$

$$f_{m_{cd}}(x) = f_m(x) \int_x^{\infty} f_d(v) dv + f_d(x) \int_x^{\infty} f_m(u) du \tag{3}$$

II. KEY RESULT

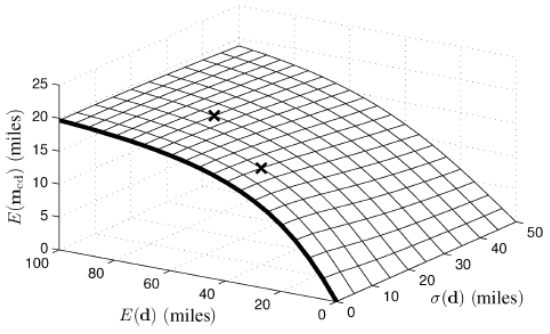

Figure 1. $E(m_{cd})$ versus $E(d)$ and $\sigma(d)$

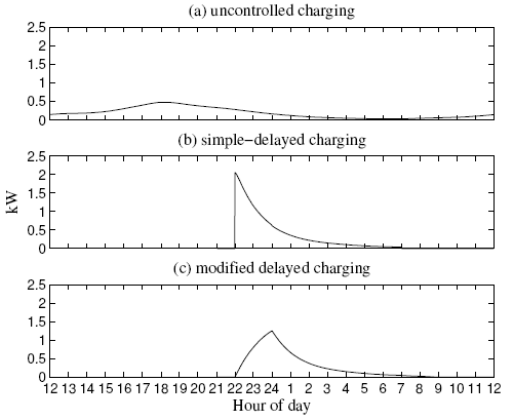

Figure 2. Average power consumption per PEV (in an urban area on a weekday)

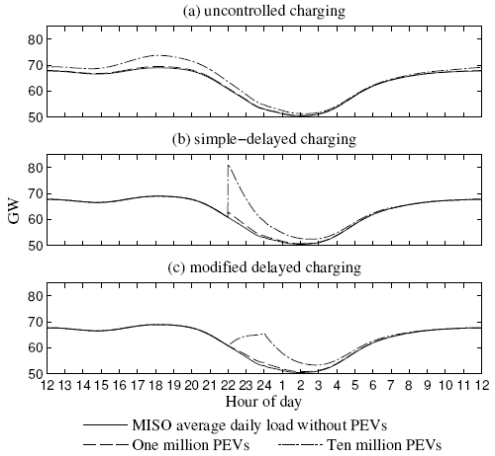

Figure 3. PEV fleet power load superimposed on MISO load curve

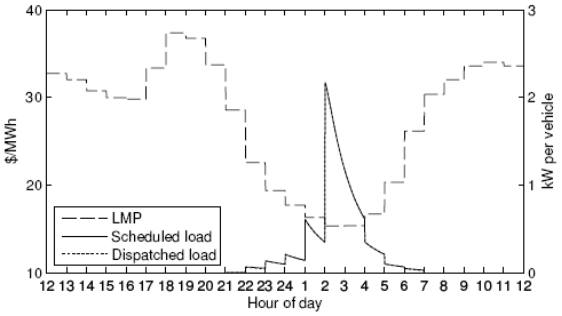

Figure 4. Scheduling and dispatch results

Operation of Electric Vehicle Management System based on V2G-Contract

Minhan Yoon and Gilsoo Jang
Power and Energy Laboratory, Department of Electrical Engineering, Korea University, Seoul, Korea
Email: radiance0@korea.ac.kr and gjang@korea.ac.kr

***Abstract*— The number of Electric Vehicle (EV) in Korea is expected to increase exponentially in the next several decades. The introduction of large EV amounts on the power system can significantly impact the operation of power system at utility side, spinning reserve, load estimation, etc. The variable consumption & generation of EV (V2G) must be maintained within the standard limits to make ISO sustain stable operation. In this paper, the impact of EV on the future Korean power system is analyzed and an V2G operation based on V2G-Contract system is introduced to determine the electricity dispatch planning. Even though, the speculated analysis has not been validated for real cases, the stochastic analysis based on Weibull distribution is considering the estimation data from several research institutes in Korea which have public confidence. As a result shows, the enough V2G-Contract amount and reliable Keeping Rate could help ISO be sure of electricity dispatch with high penetration of a large amount of EV.**

I. KEY EQUATIONS

The distribution function considering V2G-contract follows:

$$f(x;\lambda,k)=\frac{k}{\lambda}\left(\frac{x}{\lambda}\right)^{k-1} e^{-(x/\lambda)^k} \qquad x \geq 0 \quad (1)$$

$$\lambda = V2G\_Contract \quad (2)$$

$$k = V2G\_Contract^{(1+Keeping\_Rate)} \quad (3)$$

$$V2G\_Capacity = V2G\_Contract \pm Deviation(Keeping\_Rate) \quad (4)$$

II. KEY FIGURES

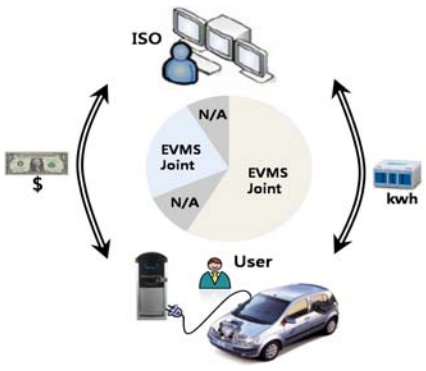

Figure 1. The concept of V2G-Contract system

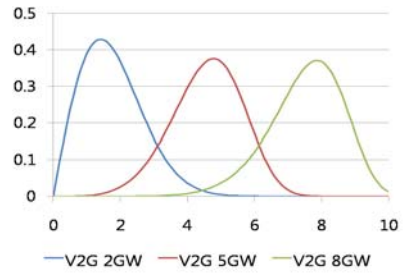

Figure 2. PDF of V2G support at base case

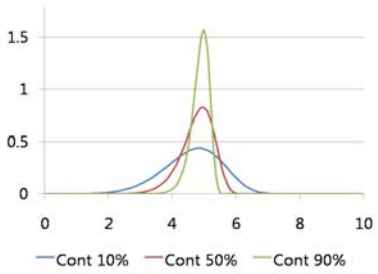

Figure 3. PDF of 5GW V2G-Contract support at variable Keeping Rate

III. KEY RESULTS

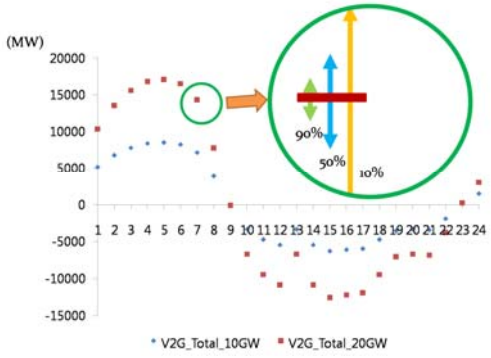

Figure 4. V2G Capacity for load curve stabilization

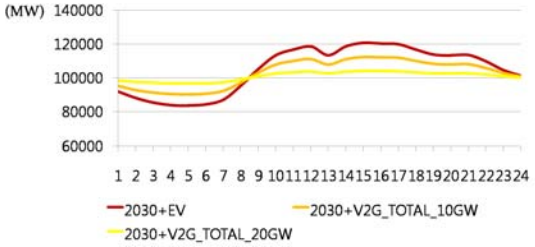

Figure 5. Daily load pattern comparison regarding V2G capacity

Real-Time Monitoring, Operation and Control of Laboratory Test-Bed Micro Power System

Juan F. Fernandez, Vahid Salehi, Ali Mazloomzadeh, Osama Mohammed
Energy Systems Research Laboratory, Department of Electrical and Computer Engineering, Florida International University, Miami, FL 33174, USA
Email: jfern014@fiu.edu, vsale001@fiu.edu, amazl001@fiu.edu, and mohammed@fiu.edu

***Abstract*— The Energy System Research Group at Florida International University is working on constructing and implementing of a small-scale power system test-bed which has the different capabilities for experimental research and educational purposes. By having this kind of power system, engineers and researchers are capable to implement their own idea about power system phenomenon in a practical way. The developed power system uses several power generation stations as a small scaled model of conventional power plants which can model different types of slack and PV buses. This paper presents the application created to synchronize generators connected to the test bed power system, as well as the real-time controlling and monitoring of the generators and buses. The control strategy for the proper synchronization of the generators on the test bed is done by an algorithm created in LabView. Furthermore, a compatible GUI was created for the operator to monitor and control the power system in real-time. The system uses several different Data Acquisition units (DAQs) to gather voltage and current waveforms from corresponding transducers, which allows calculations of power, frequency, true RMS/ amplitude/ phasor and vectors of positive, negative and zero sequences, at each point of observation in our power system. The calculated results were proven by means of certified measurement devices. With the ability to read data in a real-time format, alongside with a graphical user interface, this allows not only the power system test bed to synchronize generators automatically, but also to set the power output of each generation station, while giving the user the ability to control and monitor the behavior of the power system on both the generation and load side.**

I. KEY FIGURES

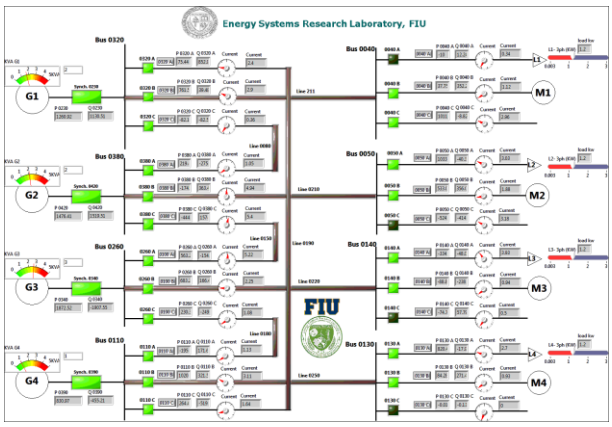

Figure 1. Switching Control Front Panel

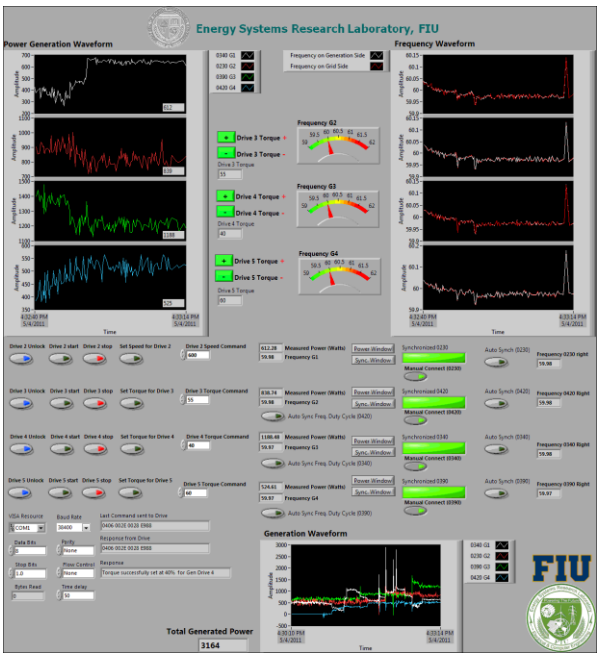

Figure 2. Generation Control Front Panel

II. KEY RESULTS

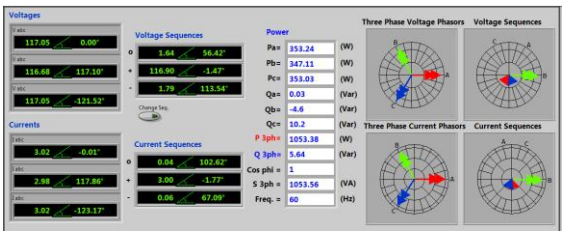

Figure 3. 0040 Feeder C Software Analysis

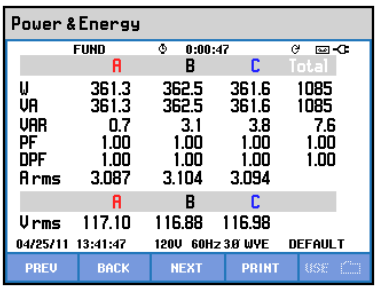

Figure 4. 0040 Feeder C Fluke 435 Measurements

Real-Time Simulation of a Micro Grid with Unbalanced Sources

Prajwal K. Gautam and Ganesh K. Venayagamoorthy
Real-Time Power and Intelligent Systems Laboratory,
Missouri University of Science and Technology, Rolla, MO 65409, USA,
Email: pkgg28@mst.edu and gkumar@ieee.org

***Abstract*— A micro grid system may comprise of different types of balanced and unbalanced power generations. This paper presents real time simulation of a micro grid consisting of three phase solar modules and single phase wind turbine. Energy storage system (ESS) is modeled to compensate single phase wind generation by injecting unbalanced currents into the micro grid. Inverter controls implement synchronous reference frame transformation of voltage and current signals into direct axis (d), quadratic axis (q) quantities. PI controller senses error in grid voltage comparing with Vref* and generates commanded current Icmd*. Output of PI controller is normalized to generate three phase duty cycles and compared with triangular wave to produce gate drive signals to fire IGBTs of 3 phase inverter. ESS control maintains the positive sequence voltage at a fixed level in the q axis and all other components at zero.**

I. KEY FIGURE

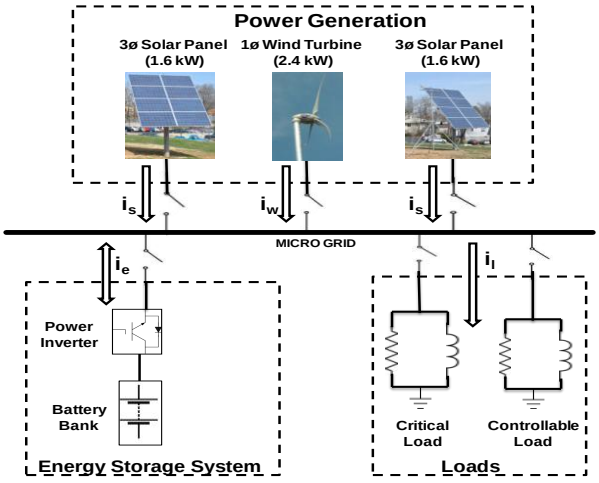

Figure 1. Micro Grid System

II. KEY EQUATIONS

The guiding three phase equations for the ESS control are:

$$i_{ae}(\theta_e) = i_{al}(\theta_e) - i_{as}(\theta_e) - i_w(\theta_e) \quad (1)$$

$$i_{be}(\theta_e) = i_{bl}(\theta_e) - i_{bs}(\theta_e) + i_w(\theta_e) \quad (2)$$

$$i_{ce}(\theta_e) = i_{cl}(\theta_e) - i_{cs}(\theta_e) \quad (3)$$

$$p_e(\theta_e) = p_l(\theta_e) - p_s(\theta_e) - p_w(\theta_e) \quad (4)$$

III. ENERGY STORAGE SYSTEM CONTROL

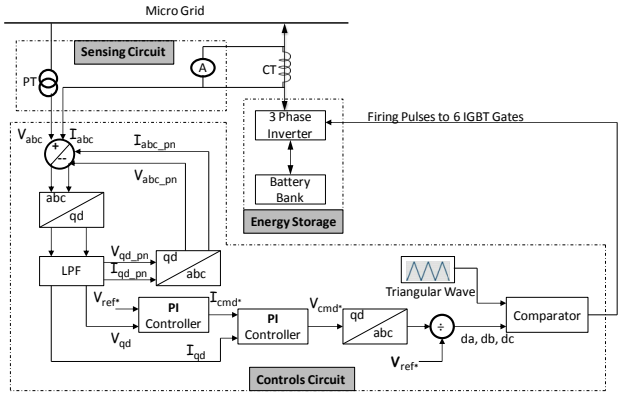

Figure 2. Control Schematics for Energy Storage System

IV. KEY RESULTS

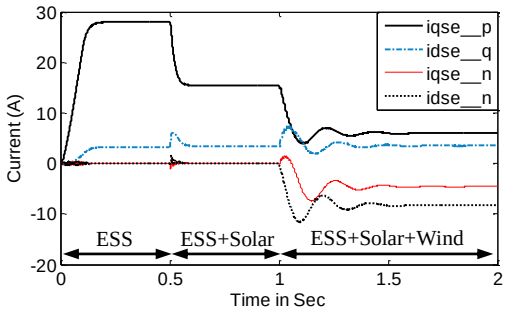

Figure 3. Positive and Negative Sequence Currents for 7 kW Load

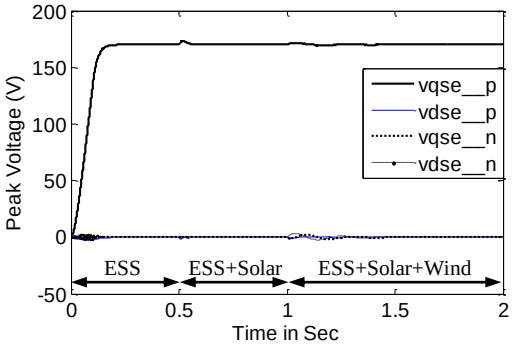

Figure 4. Positive and Negative Sequence Voltages

Nonlinear Observability Issues Associated with Multiconverter Shipboard Power Systems

Juan C. Jimenez and Chika O. Nwankpa
Center for Electric Power Engineering, Department of Electrical and Computer Engineering, Drexel University
Philadelphia, PA 19104, USA,
Email: jcj26@drexel.edu and con22@drexel.edu

***Abstract*— Perturbations in shipboard power systems can make controllers useless if improper control strategies are used. Incorporating the nonlinear dynamics of the shipboard power system in the control methodology is the solution to this problem. Before this solution is designed, the concept of nonlinear observability should be first investigated. A measure of observability of such systems will allow one to quantify their operational performance. This work attempts to account for an observability measure of these multiconverter systems through the inclusion of other dynamics such as electromechnical behavior of generators and loads, providing a more comprehensive view of system performance. In the example section the observability threshold will lead to an indicator of how far the system is from being unobservable based on the system load profile.**

I. KEY EQUATIONS

The general model used to investigate power system dynamics is that of the Differential Algebraic Equations (DAE) type:

$$\begin{aligned} \dot{x} &= f(x,u,N) \\ 0 &= g(x,u,N) \\ p &= h(x,N) \end{aligned} \tag{1}$$

The observability formulation is derived by reforming (1) as:

$$\begin{aligned} F(\dot{x},x,N) &= Bu \\ p &= h(x,N) \end{aligned} \tag{2}$$

The observability formulation derived from (2) is given in terms of the Jacobian:

$$J_O = \begin{bmatrix} G_x & G_{\dot{x}} & G_w \\ H_x & H_{\dot{x}} & H_w \end{bmatrix} \tag{3}$$

$$G = \begin{bmatrix} F(\dot{x},x,N) \\ F_x(\dot{x},x,N)\dot{x} + F_{\dot{x}}(\dot{x},x,N)\ddot{x} \\ \vdots \\ \left(F(\dot{x},x,N)\right)^{(s)} \end{bmatrix} = \begin{bmatrix} u \\ u^{(1)} \\ \vdots \\ u^{(s)} \end{bmatrix} \tag{4}$$

$$H = \begin{bmatrix} h(x,N) \\ h_x(\dot{x},x,N)\dot{x} \\ \vdots \\ h(x,N)^{(r)} \end{bmatrix} = \begin{bmatrix} p \\ \dot{p} \\ \vdots \\ p^{(r)} \end{bmatrix} \tag{5}$$

Using this Jacobian, the system is observable if the following two conditions hold:

$$\begin{aligned} &1: rank(J_O) = n + rank\begin{bmatrix} G_{\dot{x}} & G_w \\ H_{\dot{x}} & H_w \end{bmatrix} \\ &2: rank(J_O) \text{ is constant rank on S} \\ &\mathrm{S}: \{0 = g(x,u,N)\} \end{aligned} \tag{6}$$

II. KEY FIGURES

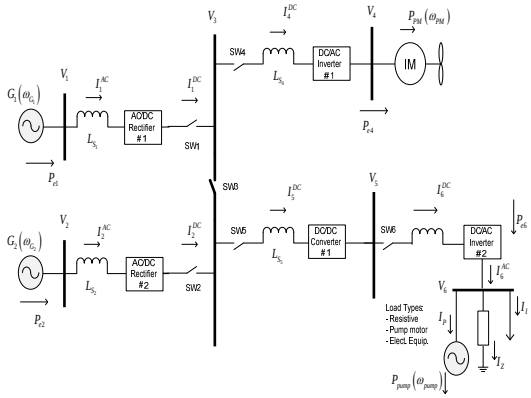

Figure 1. Representation of a multiconverter shipboard power system

III. KEY RESULTS

TABLE I
A SET OF MEASUREMENTS TO DECLARE OBSERVABILITY

$p: h(x,N)$	$\left[\tau_{G_1}\omega_{G_1}, \tau_{G_2}\omega_{G_2}, \tau_{PM}\omega_{PM}, \tau_{pump}\omega_{pump}\right]^T$
$\frac{dh}{dx}$	$\left[diag\left(\tau_{G_1}, \tau_{G_2}, \tau_{PM}, \tau_{pump}\right) \quad \mathbf{0}^{4\times 1}\right]$
$\frac{dh^{(1)}}{dx}$	$\left[\mathbf{0}^{4\times 5}\right]$
$\dim(J_O)$	18x15
$n + rank\begin{bmatrix} G_{\dot{x}} & G_w \\ H_{\dot{x}} & H_w \end{bmatrix}$	14
$rank(J_O)$	14

Intelligent Energy Management Controller for a Photovoltaic-Battery System

Yang Liu and Ganesh K. Venayagamoorthy
Real-Time Power and Intelligent Systems Laboratory
Missouri University of Science and Technology, Rolla, MO 65409, USA
Email: yl2p2@mst.edu and gkumar@ieee.org

Abstract— **The development and implementation of an intelligent energy management controller (IEMC) for grid-independent photovoltaic-battery (PVB) system is presented. The PVB system consists of four subsystems namely: the PV collector arrays, battery storage (B_{SOC}), programmable load and the IEMC. The programmable load has two types of loads, a priority load (L_{PL})that need to be met always and a controllable load(L_{CL}) that will vary over time. The objective of the IEMC is threefold – first, to supply PV energy (E_{pv}) to meet the needs of the priority loads (E_{PL}); secondly, to maintain a sufficient battery state of charge (E_B) to meet the priority load demand in hours of short or no PV outputs; and thirdly, with the first and second objectives met, maximize supply to controllable load (E_{CL}). This multi-objective energy dispatch control is implemented using an optimal fuzzy logic controller (FLC) whose rules and internal parameters are evolved using the mean-variance optimization (MVO) algorithm.**

I. KEY EQUATIONS

$$E_{PL}(t) = f_1(E_{PV}(t), L_{PL}(t), B_{SOC}(t)) \quad (1)$$

$$E_B(t) = f_2(E_{PV}(t), L_{PL}(t), B_{SOC}(t), E_{PL}(t)) \quad (2)$$

$$E_{CL}(t) = f_3(E_{PV}(t), L_{PL}(t), B_{SOC}(t), L_{CL}(t), E_{PL}(t), E_B(t)) \quad (3)$$

$$U(t) = \alpha * E_{PL}(t) + \beta * E_B(t) + \gamma * E_{CL}(t) \quad (4)$$

II. KEY FIGURES

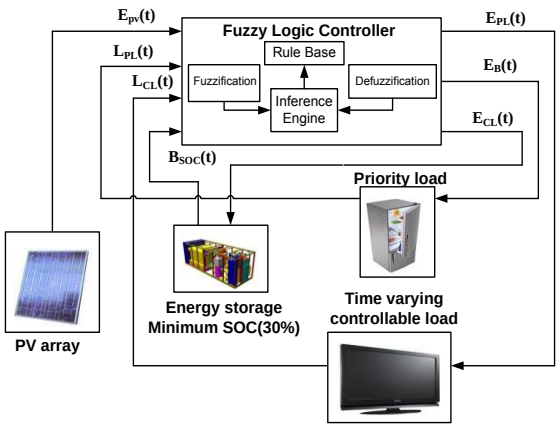

Figure. 1 . Schematic of photovoltaic-battery system with IEMC using an optimized FLC based on MVO

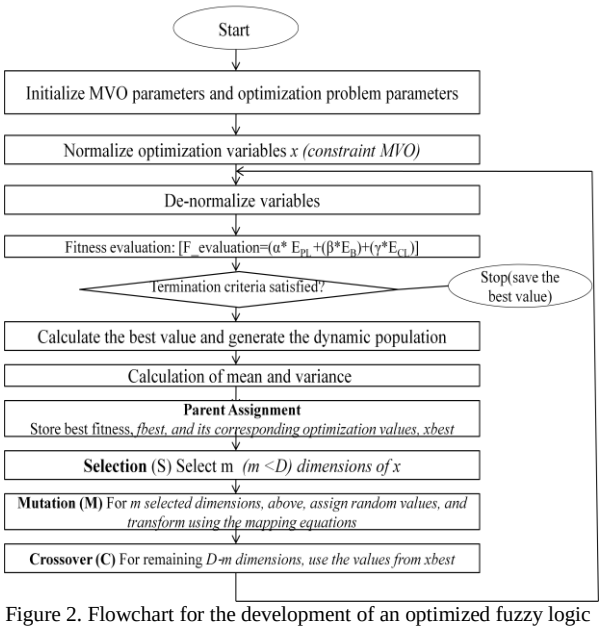

Figure 2. Flowchart for the development of an optimized fuzzy logic based IEMC using MVO

The structural development of IEMC to achieve the threefold objective mentioned above is based on the combination of two intelligent approaches- fuzzy logic controller(FLC) and mean variance optimization (MVO). An optimal FLC requires intelligent design of three main modules: fuzzification process, inference engine (rule base), and the defuzzification process. The membership functions and rules of FLC are optimized using MVO. To compare the performance IEMC, two other energy management controllers are introduced: a naïve fuzzy logic controller and a PV-priority controller. Results show that proposed IEMC can power more priority load and also maintain a higher battery SOC

III. KEY RESULTS

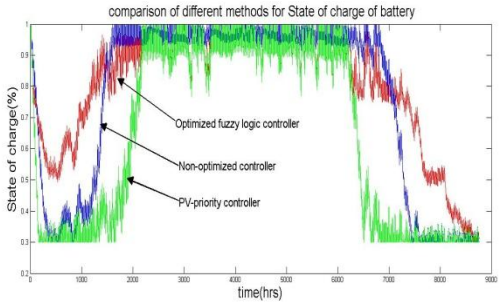

Figure. 3 Comparison between different methods of battery SOC

A Centralized Optimal Energy Management System for Microgrids

Daniel E. Olivares, Claudio A. Cañizares and Mehrdad Kazerani
Power and Energy Systems Group, Department of Electrical and Computer Engineering, University of Waterloo, Waterloo, Ontario, Canada,
Email: *dolivare@uwaterloo.ca*

***Abstract*— The issue of controlled and reliable integration of distributed energy resources into microgrids and large power grids has recently gained considerable attention. The microgrid concept, which basically corresponds to the coordinated operation of a cluster of loads, distributed generators and energy storage systems, is quite appealing due to its flexibility, controllability and energy management capabilities. In order to provide uninterruptible power supply to the loads, microgrids are expected to operate in both grid-connected and stand-alone modes, and economically meet the demand on an instantaneous basis. The problem of optimal management of the resources in a microgrid is being widely investigated and recent studies have proposed the application of both centralized and distributed control schemes by using multi-agent systems, heuristic methods and optimization algorithms. This work focuses on the conceptual design of a centralized energy management system (EMS) and its desirable attributes for a microgrid in stand-alone mode of operation. A number of test protocols are proposed to analyze the performance of the system, as well as the impacts of relevant parameters.**

I. Proposed Architecture

A centralized EMS architecture and a block diagram with its relevant components and interactions are shown in Figs. 1 and 2.

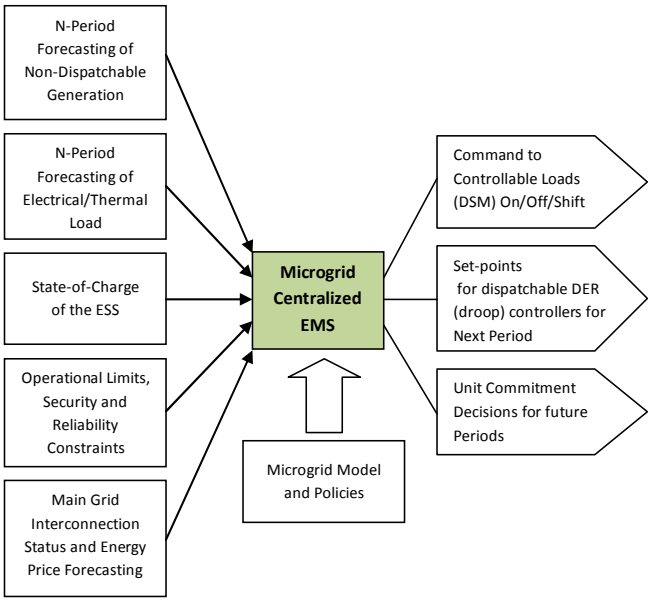

Figure 1. Typical centralized EMS architecture for microgrids

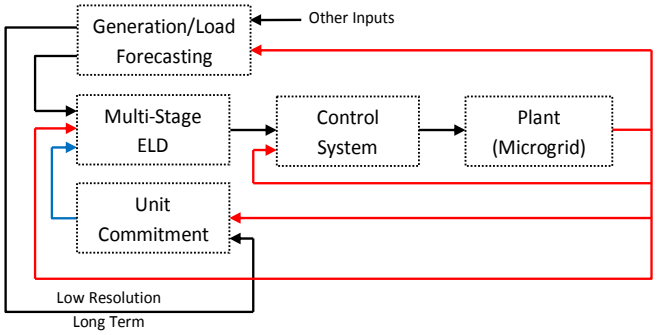

Figure 2. Centralized EMS block diagram

II. Calibration Procedures

A. *Multi-stage ELD horizon vs ESS capacity*

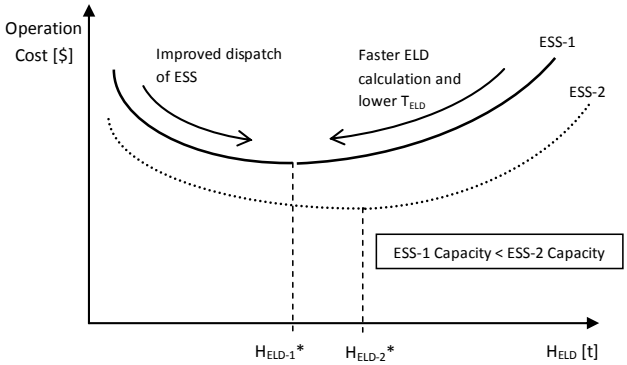

Figure 3. Trade-off in selection of ELD horizon

B. *Impact of Forecasting Accuracy*

Evaluation of 3 different scenarios:

- Persistence model (worst case)
- Perfect forecasting (best case)
- Uncertain forecast (realistic case)

III. References

[1] R. H. Lasseter, "MicroGrids," in *Proc. IEEE-PES Winter Meeting*, vol. 1, Jan. 2002, pp. 305-308.

[2] E. Alvarez, A. C. Lopez, J. Gómez-Aleixandre, and N. de Abajo, "On-line minimization of running costs, greenhouse gas emissions and the impact of distributed generation using microgrids on the electrical system," in *Proc. IEEE PES/IAS Conference on Sustainable Alternative Energy (SAE)*, Sept. 2009, pp. 1-10.

[3] M. Korpas and A. T. Holen, "Operation planning of hydrogen storage connected to wind power operating in a power market," *IEEE Transactions on Energy Conversion*, vol. 21, no. 3, Sept. 2006, pp. 742-749.

Real Time Modeling and Simulation of Microgrid Reconfiguration

Farshid Shariatzadeh and Anurag K. Srivastava
Smart Grid Demonstration and Research Investigation Lab (SGDRIL), The School of Electrical Engineering and Computer Science, Washington State University, Pullman, WA 99163, USA
Email: *fshariat@eecs.wsu.edu* and *asrivast@eecs.wsu.edu*

***Abstract*— Reconfiguration is the process of modifying the microgrid's topological by changing the status (open/close) of circuit breakers or switches. Reconfiguration is critical to maintain the availability of energy to the connected loads in the microgrid and to interrupt the smallest portion of the microgrid under any abnormal conditions either to restore service to a section or to meet some operational requirements. Several research works have been reported by researchers in the past on reconfiguration of distribution systems, which need to be further, investigated for microgrid. Microgrids are distribution systems, generally including distributed generation and energy storage, and can operate in both in-grid and off-grid modes. In this work, a developed reconfiguration algorithm has been tested on two microgrids, 8-bus shipboard power system (SPS) and modified CERTS. SPS provides energy to navigation and operation systems as well as weapons and communication systems, and most of the time works in islanded or off-grid mode. CERTS microgrid is a test case developed in 1999 for testing and validating developed tools and technologies. Unlike the SPS, CERTS microgrid can operate in both modes. Conventional reconfiguration algorithms for distribution systems are not completely suitable for microgrids because of their unique features. Transition between grid-connected and islanded mode and operation for both modes should be considered in microgrids. In this work, genetic algorithm (GA) and graph theory based methodologies were used to reconfigure a network, satisfying the operational requirements and priorities of loads. Application of the GA for reconfiguration was implemented in MATLAB and tested for 8-bus shipboard power system (SPS) and modified CERTS microgrids with consideration of distributed generation and islanding operation. Developed algorithm was also validated in real time using real-time digital simulator (RTDS) and dSPACE controller as hardware in the loop (HIL). Satisfactory simulations results were obtained for several possible test case scenarios in a real-time and off-line for both SPS and modified CERTS microgrid.**

I. KEY FIGURES

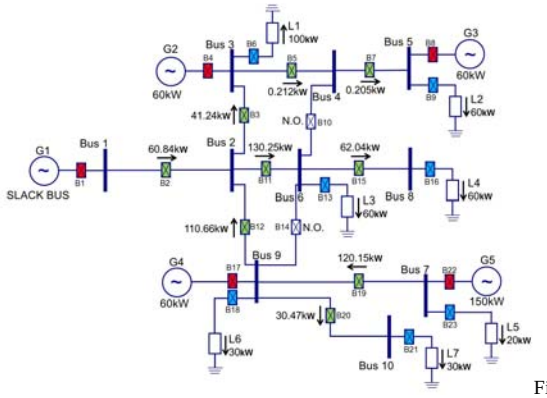

Figure 1. Modified CERTS microgrid

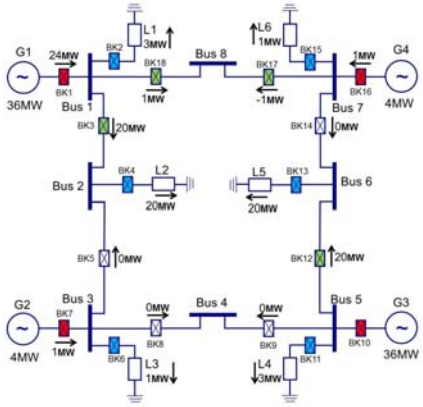

Figure 2. 8-Bus SPS

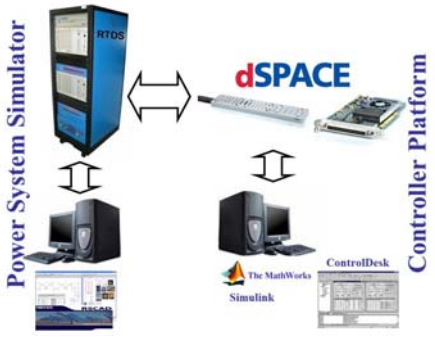

Figure 2. Hardwares Configuration in Real-Time Implementation

Control of a Battery to Improve the Operation of a Microgrid

Ling Xu, *Student Member, IEEE*, Zhixin Miao, *Senior Member, IEEE*, and Lingling Fan, *Senior Member, IEEE*
Department of Electrical Engineering, University of South Florida, Tampa, FL 33620, USA,
Email: lxu@mail.usf.edu

***Abstract*—Microgrids have two operating modes: grid-connected and islanding mode. Energy storage system would benefit microgrid on both modes. This paper focuses on the effect on microgrid due to integration of energy storage component. An AC voltage and frequency control approach provided by energy storage during islanding mode is developed. A microgrid consisting of a detailed battery model with inverter, passive loads and an induction machine is built in PSCAD/EMTDC. The behaviors of battery and microgrid on different operating modes are investigated, which demonstrates that both AC voltage and frequency are improved if the proposed control strategy is applied during islanding.**

I. KEY EQUATIONS

The normal operation controller of inverter for battery is designed based on:

$$v_{d1} = -(Ri_d + L\frac{di_d}{dt}) + \omega_s L i_q + v_d \quad (1)$$

$$v_{q1} = -(Ri_q + L\frac{di_q}{dt}) - \omega_s L i_q \quad (2)$$

$$v_{dc}(C\frac{dv_{dc}}{dt} + i_{dc2}) = v_d i_d \rightarrow \frac{dv_{dc}}{dt} = \frac{v_d i_d}{v_{dc} C} - \frac{i_{dc2}}{C} \quad (3)$$

The islanding operation controller of inverter for battery is designed based on:

$$V_{d1} = \omega_s L I_q + V_d \quad (4)$$

$$V_{q1} = -\omega_s L I_d \quad (5)$$

II. KEY FIGURES

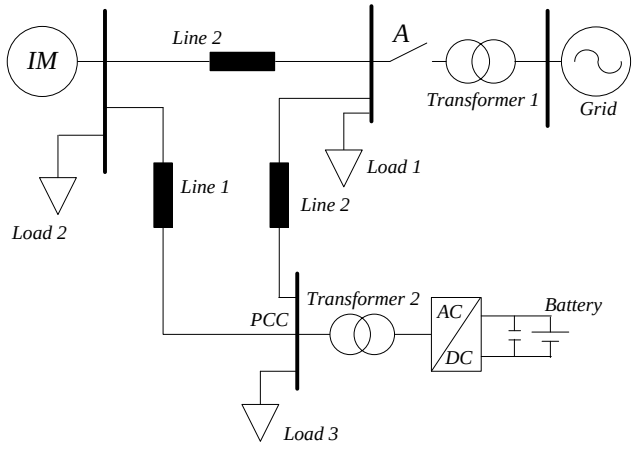

Figure 1. A microgrid with battery system

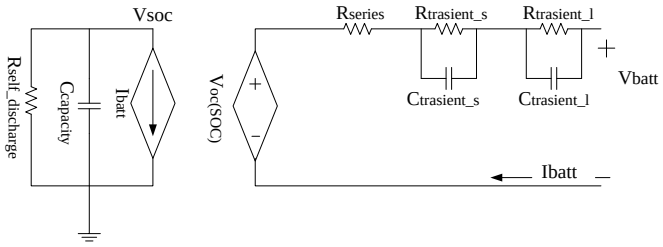

Figure 2. A detailed battery model

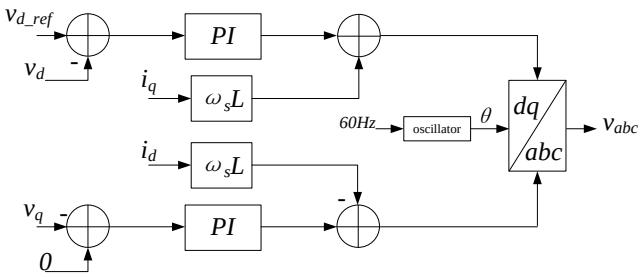

Figure 3. Islanding controller of inverter for battery

III. KEY RESULTS

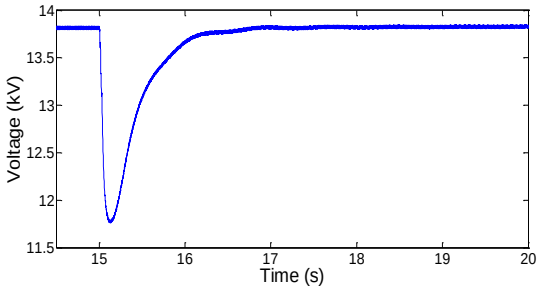

Figure 4. RMS voltage of PCC during islanding event

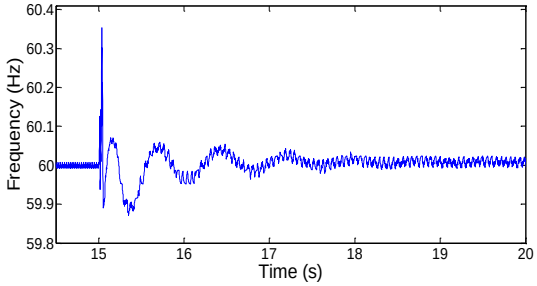

Figure 5. Frequency at PCC during islanding event

Harnessing Mechanical Energy on Highways and Walkways to Generate Electric Power

Danial Ahmed, Arsalan Muhammad, Muhammad Atiq and Dr. Ahmed Osman
Department of Electrical Engineering, American University of Sharjah, Sharjah, 2666, UAE,
Email: b00030066@aus.edu, b00032400@aus.edu, b00029387@aus.edu and aosmanahmed@aus.edu

***Abstract*— Green house gas emission has surfaced as one of the crucial debatable topic for environmentalists and scientists. According to most of the environmentalist one of the main causes of green house gas emission is due to power generation using fossilized material such as coal, oil and natural gas. Green house gases have contributed a great deal towards the well known phenomena 'global warming'. This poster presents an innovative solution to decrease carbon footprint and contribute towards green energy. Piezoelectric generates electric power on experiencing mechanical stress. Extending this concept of power generation an innovative power generation system which uses vehicle and pedestrian movement on roads and pavement respectively to generate electric energy have been designed. The system is divided into two sub systems. The first system converts wasted mechanical energy in to electrical energy using piezoelectric ceramic. Several modifications are proposed in the existing system to increase the power efficiency of the system. The second subsystem uses Switch Synchronous Harvesting on Inductors (SSHI) to step up power generation up to 250%. To evaluate the performance of the system and validate our design the system is developed in MATLAB/SIMULINK and PSPICE. The performance of the system is examined for different piezoelectric ceramics and load conditions.**

I. KEY EQUATIONS

The guiding equations of the piezoelectric power generation system are:

$$C_{stack} = \frac{\varepsilon_o \varepsilon_r A}{h_{piezo}} \quad (1)$$

$$R_{loss} = \frac{\tan\delta}{\omega C_{stack}} \quad (2)$$

$$V_{stack} = k_{33}\sqrt{\frac{2W_{mech}}{C_{stack}}} \quad (3)$$

$$P = i_{stack}^2 R_{loss} \quad (4)$$

II. KEY FIGURES

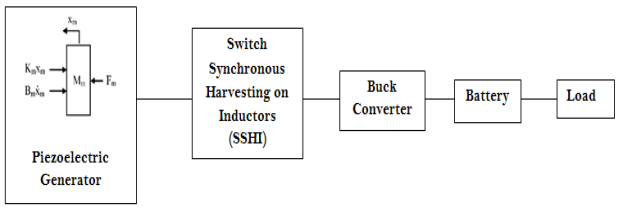

Figure 1. Piezoelectric Power Generation System

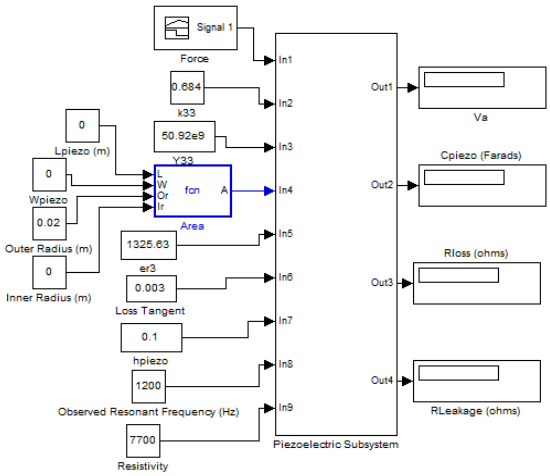

Figure 2. Simulation of power generation system in MATLAB

III. KEY RESULTS

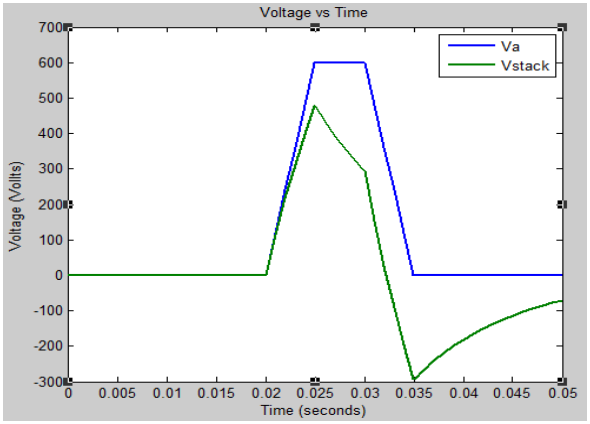

Figure 3. Input pulse (Va) of 600 V vs. output voltage (Vstack) of 500V for cylindrical ceramic plate with 0.006m outer radius

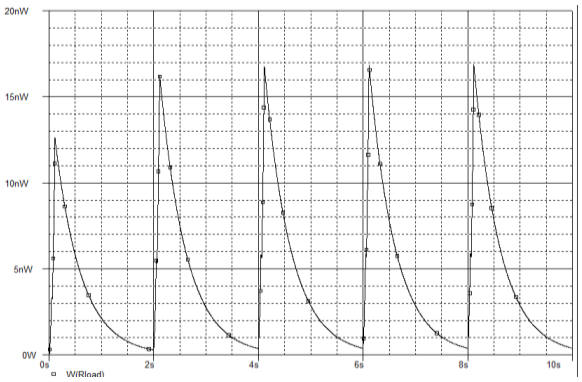

Figure 4. Output Power through SSHI circuit

A Tool for Modeling and Simulation of Flywheels for Ride-through Applications in Data Centers

R. Arghandeh, M. Pipattanasomporn and S. Rahman
Virginia Polytechnic Institute and State University - Advanced Research Institute, Arlington, VA 22203, USA,
Email: reza6@vt.edu , mpipatta@vt.edu , srahman@vt.edu

***Abstract*—Due to technological advancements, the FES becomes a promising alternative compared with other battery storage technologies. This poster aims at developing the modeling and simulation tool to demonstrate the use of FES units to secure sensitive loads in a data center. The FES is modeled, simulated and evaluated in the MATLAB/SIMULINK® environment. A case study of a data center is presented. It illustrates how a FES can help improve load serving capability and provide a short ride-through time to critical loads during a utility disturbance. In comparison with the batteries, the application of FES for power security is newer on the horizon. Therefore, the availability of experimental data for flywheels is limited. The proposed software tool can compensate for the lack of real FES operational data through modeling and simulations.**

I. KEY EQUATIONS

The basic equations of the flywheel energy storage system are:

$$J = \frac{1}{2} \cdot \pi \cdot \rho \cdot l \cdot r^4 \quad (1)$$

$$\omega(t) = \omega_{\max} \cdot e^{-\frac{K_1}{J} \cdot t} \quad (2)$$

$$E = \frac{1}{2} \cdot J \cdot \omega_{\max}^2 \cdot e^{-\frac{2K_1}{J} \cdot t} \quad (3)$$

$$P = K_2 \cdot \omega_{\max}^2 \cdot e^{-\frac{2K_1}{J} \cdot t} \quad (4)$$

II. KEY FIGURES

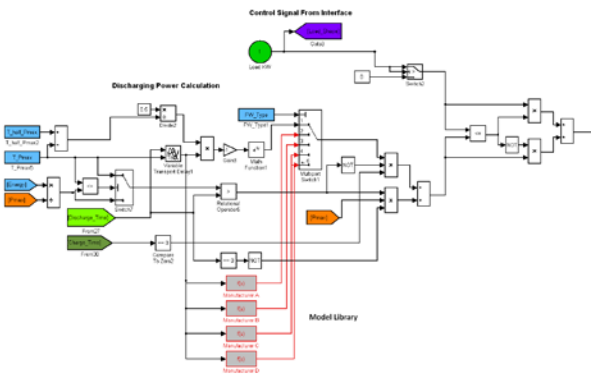

Fig. 1. Discharging section of the flywheel model in the Matlab/Simulink

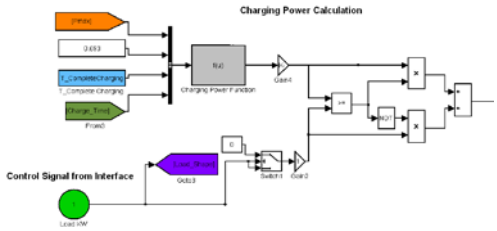

Fig. 2. Charging section of the flywheel model in the Matlab/Simulink

III. KEY RESULTS

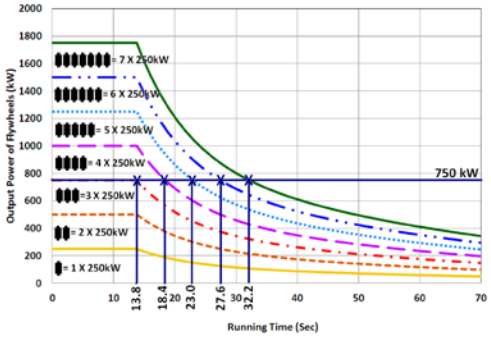

Fig 3. Simulation results for different numbers of the parallel flywheels to support 750 kW critical loads.

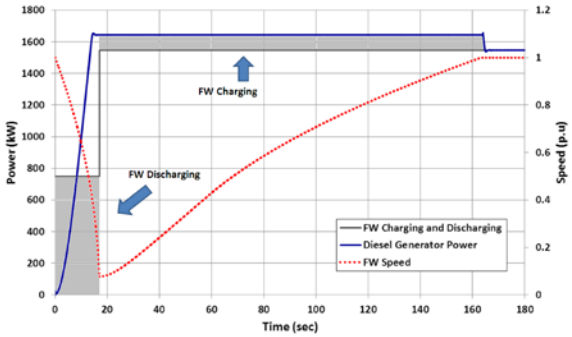

Fig 4. Model output during discharging and charging; flywheel speed (red), critical load power (gray), diesel generator power (solid blue)

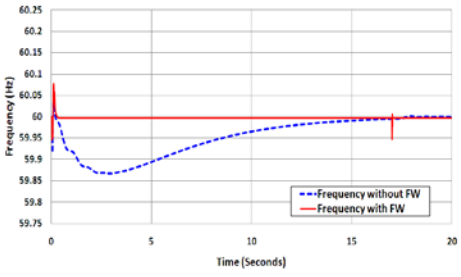

Fig 5. The frequency deviations of the critical loads after the power outage with flywheels (solid line) and without flywheels (dashed line).

Development of an Architecturally Flexible Multiagent System Test Bed

Troy Bevis and Dr. Sanjeev Srivastava
Center for Advanced Power Systems, Department of Electrical and Computer Engineering, Florida State University, Tallahassee, FL 32310, USA.
Email: bevis@caps.fsu.edu and sanjeev@caps.fsu.edu

***Abstract*— The multiagent system test bed is a distributed control test bed designed for the implementation of a flexible multiagent architecture. The goal is to provide a test bed architecture that allows an agent programmer to focus solely on agent implementation and not the underlying communication protocol or hardware implementation, thus leading to shorter development time. The multiagent systems will be capable of interfacing with numerous systems, both in simulations and actual hardware, including MATLAB/Simulink from Mathworks and the Real-Time Digital Simulator from RTDS Technologies. The capability of controlling a real, physical system via the test bed is desired to convey the usefulness of multiagent systems for various projects. Equipped with analog and digital I/O, as well as standard communication peripherals such as RS-232, CAN, and Ethernet, the test bed can be implemented as distributed control and interfaced with various Digital Signal Processors, FPGAs, and other embedded controllers. The multiagent system will be utilized as a high-level control system in a multi-converter test bed that represents a scaled electric ship system, enabling optimization and control at the system level.**

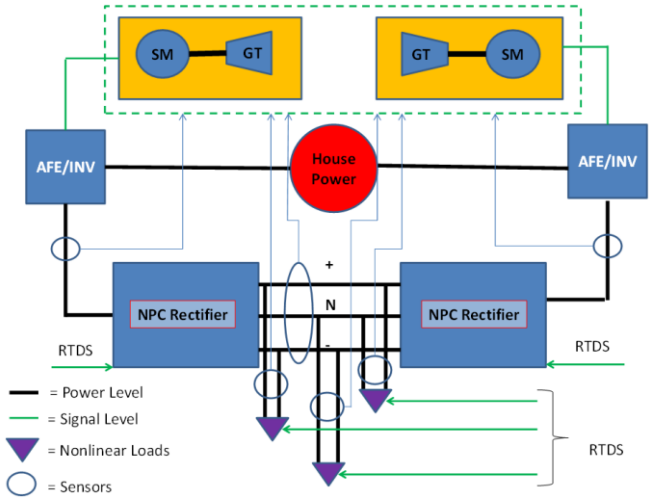

Figure 2. Scaled Ship System with Nonlinear Dynamic Loads

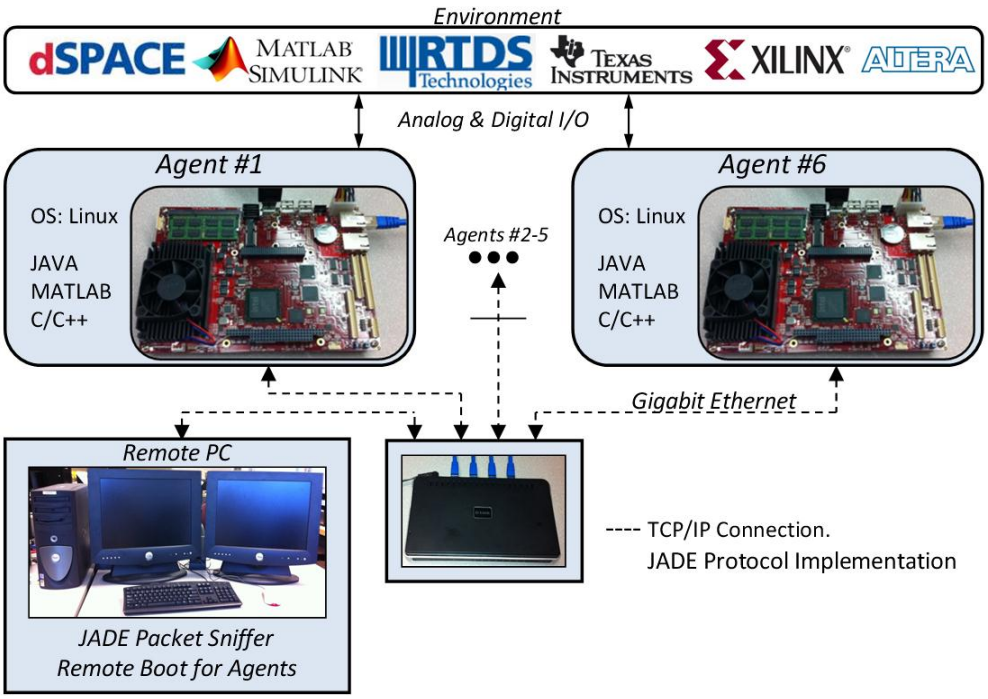

Figure 1. Multigent Test Bed Architecture

Modeling distributed photovoltaic generation for power system analysis

Chengrui Cai *IEEE student member*, Dionysios Aliprantis *IEEE senior member*
Department of Electrical and Computer Engineering, Iowa State University, Ames, IA 50010, USA,
Email: ccai@iastate.edu *and* dali@iastate.edu

***Abstract*— Photovoltaic (PV) generation is one important form of renewable energy generation and it has been applied around the world. With an increasing interest on the PV generation and continuously deceasing module cost, the large PV generation system begins to raise an increasing concern of its impact both on the local distribution grid and the regional transmission grid. The objective of this paper is to propose a comprehensive approach to build the aggregated model of the large distributed PV generation system for power system analysis. Due to the geographical diversity of distributed PV system, the actual variability of the aggregated power output will be smaller compared with the estimated power output using single point radiation measurement. To properly address this issue, cloud patterns are generated at first using fractal surface method and then the facing condition of PV panels is also taken account for a more realistic modeling of the solar radiation received by a titled surface. Then a new MPPT surface energy conversion model is proposed, which can convert the environment condition variables to power output quickly and accurately. A setup of experimental PV generation and monitoring platform is then presented. This platform is designed to collect environmental condition data with high temporal resolution (1 second interval), enabling the analysis of solar radiation variability at the second level and the PV panel response under fast changing radiation condition. Finally, how to use the high temporal resolution data to improve the proposed aggregated PV generation model is discussed.**

I. METHODOLOGY OF DEVELOPING OF THE AGGREGATED PV GENERATION MODEL

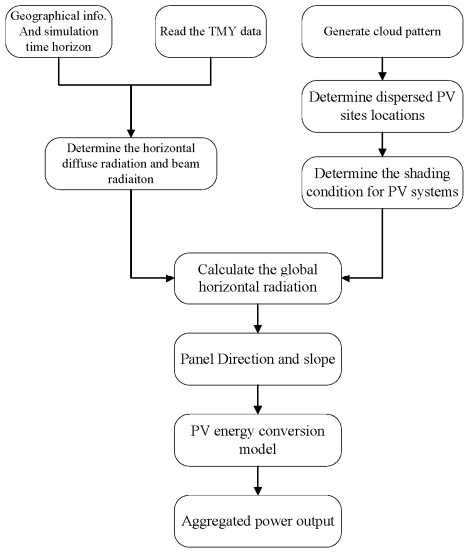

Figure 1 Approach flow chart

II. KEY FIGURES AND RESULT

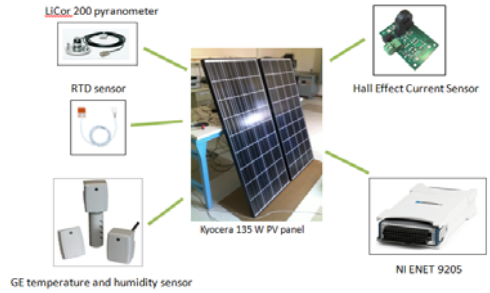

Figure 2 Experimental setup

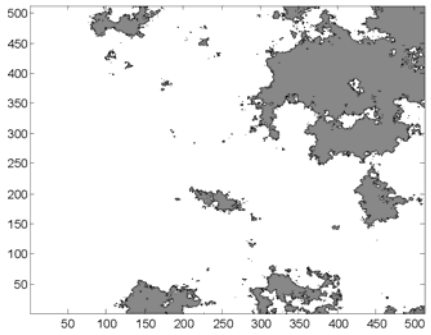

Figure 3 Generated cloud with 20% coverage

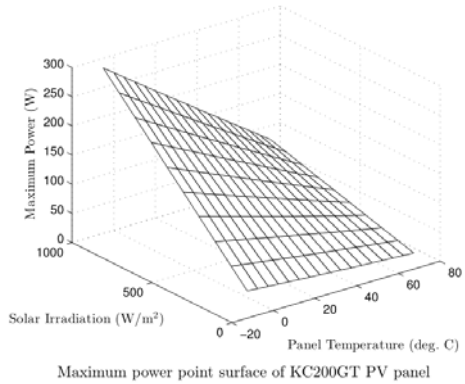

Figure 4 MPPT surface energy conversion model

Induction Machine Model using Flux Linkage as State Variables Including Saturation

Jie Dang, J. Restrepo and Ronald G. Harley
School of Electrical and Computer Engineering, Georgia Institute of Technology, Atlanta, GA 30332-0250, USA,
Email: jiedang05@gmail.com, joserestrepoz@gmail.com and rharley@ece.gatech.edu

***Abstract*—With the development of wind generation, wind generator --- induction machine modeling has drawn a lot of attention these years. Classic induction machine models, like dq model, use current as state variables. When induction machine is connected with inductive external networks, such models which use current as interface with external networks, come up with some problems. This poster presents an induction machine model which uses flux linkage as state variables, which improves calculation efficiency and accuracy greatly. Besides that, for modeling including saturation, using magnetizing current as an arctangent function of magnetizing flux linkage matches better with the saturation curve, comparing with using magnetizing flux linkage as a polynomial function of magnetizing current. Such conclusion is verified through MALAB/SIMULINK simulation, for three phase and single phase ground short circuit fault, and PLECS library induction machine is used for reference because of it provides a dynamic effect on the machine's state variables. Fault simulation is studied using different time steps to better support the advantages of the model presented in this poster.**

I. KEY EQUATIONS

Instead of fitting the saturation curve with polynomial, the magnetizing current as a function of magnetizing flux linkage can be presented using an arctangent function, which matches with saturation curve better:

$$f(\lambda_m) = \frac{2M_d}{\pi}[(\lambda_m - \lambda_T)\arctan(\tau_T(\lambda_m - \lambda_T)) - \lambda_T \arctan(\tau_T\lambda_T)] + \frac{M_d}{\pi\tau_T}[\ln(1+\tau_T{}^2\lambda_T{}^2) - \ln(1+\tau_T{}^2(\lambda_m - \lambda_T)^2)] + M_a\lambda_m$$

II. KEY FIGURES

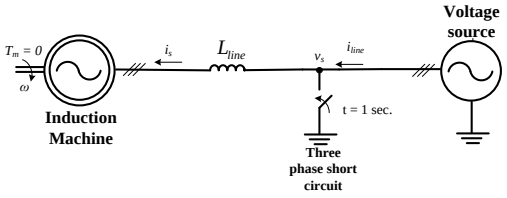

Figure 1. Three phase short circuit fault

Fi

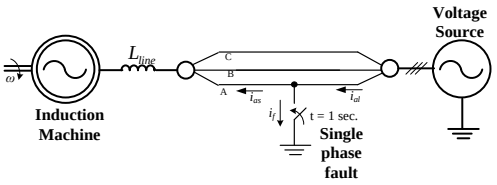

Figure 2. Single phase short circuit fault

III. KEY RESULTS

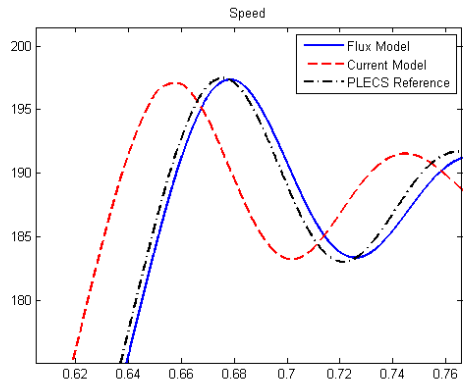

Figure 3. Start up speed comparison between different models

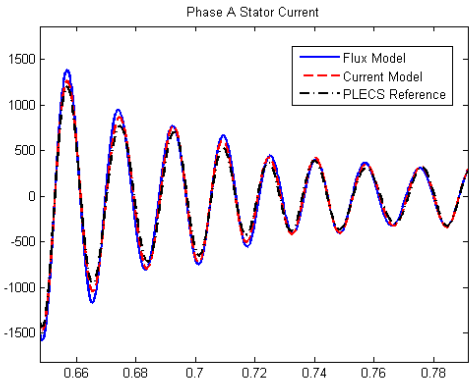

Figure 4. Phase A stator current comparison between different models

LMP Triggered Demand Response Events Validation Using PSCAD

Pedro Faria and Zita Vale
Knowledge Engineering and Decision Support Research Center, School of Engineering, Polytechnic Institute of Porto,
R. Dr. António Bernardino de Almeida, 431, 4200-072 Porto, Portugal,
Email: pnf@isep.ipp.pt and zav@isep.ipp.pt

***Abstract*— Recent changes in power systems, mainly due to the substantial increase of distributed generation and to the operation in competitive environments, have created new challenges to operation and planning.**
The present work considers a Virtual Power Player (VPP) that manages a set of energy resources, including the capacity from Demand Response (DR) programs activation and considering the energy that may be bought in day-ahead and real-time markets.
A DR program for which the event trigger depends on the Locational Marginal Price (LMP) used by the New England Independent System operator (ISO-NE) inspired the way that DR is used in this work.
After calculating the energy component value of LMP, if this is higher than the a priori determined trigger value, a new resource scheduling is performed, using GAMS software, including the DR capacity. The resulting load curtailment scheduling is validated through a simulation of the network in PSCAD. The analysis of the resultant curves allows evaluating the impact of the load curtailment in the implemented 32 bus distribution network and consequently deciding on the technical validation of the load curtailment schedule.

I. KEY FIGURE

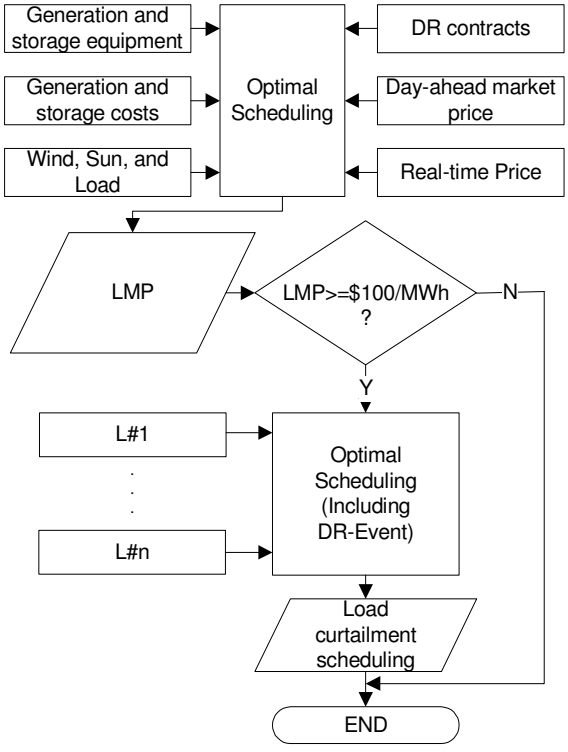

Figure 1. Test System

II. KEY EQUATION

The objective function of the resource scheduling is:

$$Minimize\ f = Min \left(\begin{array}{l} P_{Day-ahead} \times c_{Day-ahead} + P_{Real-time} \times c_{Real-time} \\ + \sum_{gt=1}^{ngt} (P_{Gen(gt)} \times c_{Gen(gt)}) \\ - P_{StorageCharge} \times c_{StorageCharge} \\ + P_{StorageDischarge} \times c_{StorageDischarge} \\ + U_{ndeliveredEnergy} \times c_{UndeliveredEnergy} \\ + E_{xcessGeneratedEnergy} \times c_{ExcessGeneratedEnergy} \\ + \sum_{b=1}^{nb} \left(\begin{array}{l} P_{DR-Event(b)} \times c_{DR-Event(b)} \\ + P_{DR-Contract(b)} \times c_{DR-Contract(b)} \end{array} \right) \end{array} \right) \quad (1)$$

III. KEY RESULTS

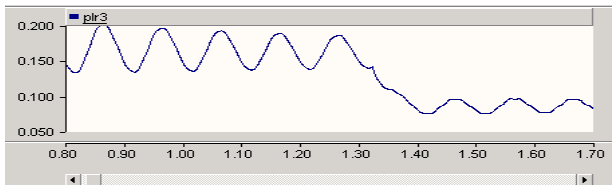

Figure 2. Active power consumption, in bus 3, before and after the event occurred at instant 1.30.

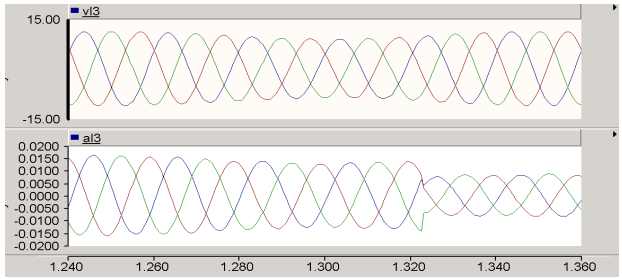

Figure 3. Three-phase voltage (up) and current (down), in bus 3, before and after the event occurred at instant 1.30.

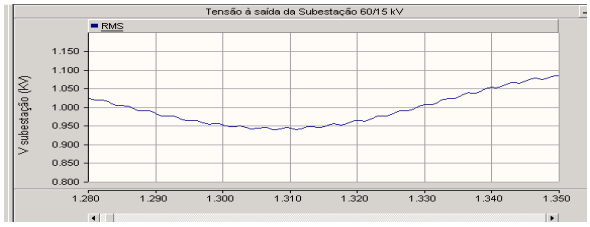

Figure 4. RMS voltage in the substation, after and before the event.

Parameter Identification of DFIG Using Online Measurement Data

Shaotong GUO and Anjan BOSE
Department of Electrical Engineering and Computer Science, Washington State University, Pullman, WA 99163, USA,
Email: sguo@eecs.wsu.edu and bose@wsu.edu

***Abstract*— Doubly-feed Induction Generators (DFIG) are increasingly used in wind farms and better operational tools are needed to control this renewable generation. This project mainly focuses on identifying both the types of wind turbines and the number of each type in operation, by using online measurement data from PMUs. The following will be presented on the poster: First, we derive the desired state equations from the 5th order DFIG model and determine the types of variables needed from measurements. Then we build up a DFIG subsystem and in-cooperate it into Kundur's 2-area 4 Generators test system, simulate the operating condition and store the necessary data. Third, different parameter identification methods (Recursive Output Error (ROE) Method and Recursive Pseudo-Linear Regression (RPLR) Method) are applied, and the performances of these algorithms are compared.**

I. KEY EQUATIONS

The 5th order DFIG model used for parameter Identification is:

$$\dot{x}(t) = A(t)*f(x(t)) + B(t)*u(t)$$

where

$$u(t) = \begin{bmatrix} u_{ds}(t) \\ u_{qs}(t) \\ u_{dr}(t) \\ u_{qr}(t) \end{bmatrix} \quad x(t) = \begin{bmatrix} I_{ds}(t) \\ I_{qs}(t) \\ I_{dr}(t) \\ I_{qr}(t) \\ pw_r(t) \end{bmatrix} \quad f(x(t)) = \begin{bmatrix} I_{ds}(t) \\ I_{qs}(t) \\ I_{dr}(t) \\ I_{qr}(t) \\ pw_r(t) \\ I_{ds}(t)I_{qr}(t) \\ I_{ds}(t)pw_r(t) \\ I_{qs}(t)I_{dr}(t) \\ I_{qs}(t)pw_r(t) \\ I_{dr}(t)pw_r(t) \\ I_{qr}(t)pw_r(t) \end{bmatrix}$$

$$A(t) = \begin{bmatrix} A_{1,1} & 0 & A_{1,3} & 0 & 0 & 0 & 0 & 0 & A_{1,9} & 0 & A_{1,11} \\ 0 & A_{2,2} & 0 & A_{2,4} & 0 & 0 & A_{2,7} & 0 & 0 & A_{2,10} & 0 \\ A_{3,1} & 0 & A_{3,3} & 0 & 0 & 0 & 0 & 0 & A_{3,9} & 0 & A_{3,11} \\ 0 & A_{4,2} & 0 & A_{4,4} & 0 & 0 & A_{4,7} & 0 & 0 & A_{4,10} & 0 \\ 1 & 1 & 1 & 1 & 1 & 1 & 1 & 1 & 1 & 1 & 1 \end{bmatrix}$$

$$A_{1,1} = \frac{-Rs}{M*Ls} = A_{2,2} \qquad A_{1,3} = \frac{Lh*Rr}{M*Ls*Lr} = A_{2,4}$$

$$A_{1,9} = \frac{Lh^2}{M*Lr*Ls} = -A_{2,7} \qquad A_{1,11} = \frac{Lh}{M*Ls} = -A_{2,10} \qquad A_{3,1} = \frac{-Rr}{M*Lr} = A_{4,2}$$

$$B(t) = \begin{bmatrix} B_{1,1} & 0 & B_{1,3} & 0 \\ 0 & B_{2,2} & 0 & B_{2,4} \\ B_{3,1} & 0 & B_{3,3} & 0 \\ 0 & B_{4,2} & 0 & B_{4,4} \\ 1 & 1 & 1 & 1 \end{bmatrix}$$

$$B_{1,1} = \frac{1}{M*Ls} = B_{2,2}$$

$$B_{1,3} = \frac{-Lh}{M*Ls*Lr} = B_{2,4} = B_{3,1} = B_{4,2}$$

$$B_{3,3} = \frac{1}{M*Lr} = B_{4,4}$$

II. KEY FIGURES

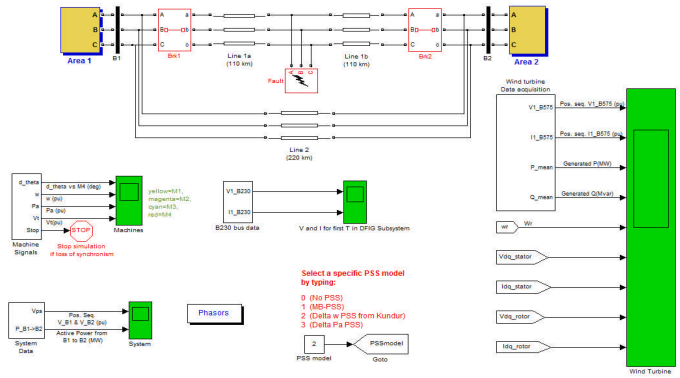

Figure 1. Kundur's 2-area Test System

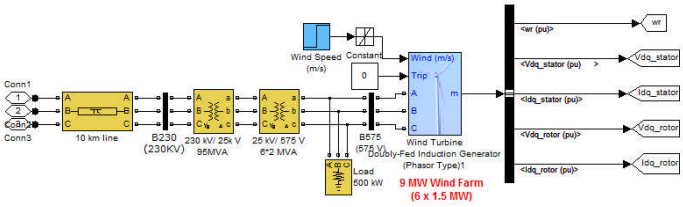

Figure 2. DFIG subsystem which is in-cooperate into Kundur's 2area system

III. KEY RESULTS

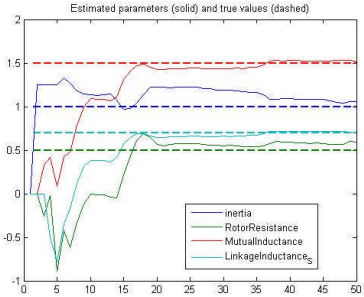

Figure 3. Parameter identification using Recursive Output Error (ROE)Method

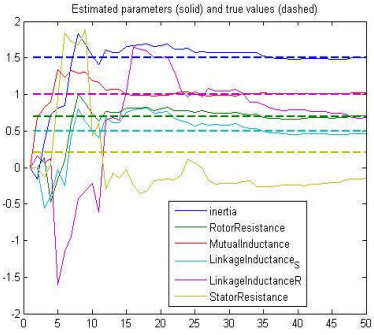

Figure 4. Parameter identification using Recursive Pseudo-Linear Regression (RPLR) Method

Adaptive Near-Optimal Compensation Applied to Linear and Nonlinear Loads

Ronald D. Hernández and Hanoch Lev-Ari
Department of Electrical and Computer Engineering
Northeastern University
Boston, MA 02115. USA
Email: {rhernand, levari}@ece.neu.edu

Aleksandar M. Stanković
Department of Electrical and Computer Engineering
Tufts University
Medford, MA 02155. USA
Email: astankov@ece.tufts.edu

***Abstract*—The role of compensation in power system efficiency optimization is to reduce the power consumption of the source (line) impedance, so that most of the source power is delivered to the load. A classical result by Fryze is used in the case when the voltage drop across the line is negligible in comparison with the load voltage. However, when the source impedance becomes significant the traditional Fryze current is no longer the smallest line current that supplies the same real power to the load as the original load current. An optimal solution considering significant line impedance has been already obtained in our recent works. Unfortunately, it relies on network and load parameters that are not easy to determine during operation. This motivated our approach in searching for an adaptive near-optimal compensator that relies only on measurements of the load voltage and current so as to allow precise control of P_{comp}, the real power flowing out of the compensator, as well as P_{cload}, the real power delivered to the compensated load (i.e., $P_{cload} = P_{load} - P_{comp}$), while reducing P_{line}, the power consumed by the line impedance, to within a few percent of its theoretical minimum.**

We have already demonstrated that a near-optimal performance in the presence of significant source impedance can be achieved with the implementation of the *quadrature Fryze* compensation $i_s(t) = \alpha v(t) - \beta\mathcal{H}\{v(t)\}$ where α, β are real-valued coefficients and $\mathcal{H}\{\cdot\}$ represents the Hilbert transform of a signal. We have developed an adaptive-iterative implementation of this quad-Fryze compensator and presented results for just linear loads. In this poster we present the results under the presence of a nonlinear load represented by a three phase induction motor supplied with unbalanced voltages. The corresponding linear load results are also presented for comparison purposes.

I. Key Equations

The most important equations are the following:

$$\mathcal{I}_s = [\alpha + j\beta]\,\mathcal{V} \tag{1}$$

$$\mathcal{I}_{comp}(k+1) = \mathcal{I}(k) - [\alpha(k) + j\beta]\,\mathcal{V}(k) \tag{2}$$

$$\alpha(k) = \frac{\Re\{\mathcal{I}(k)\mathcal{V}^H(k)\} - P_{comp,desired}}{\|\mathcal{V}(k)\|^2} \tag{3}$$

$$\beta_{i+1} = \beta_i - \frac{\beta_i - \beta_{i-1}}{\bar{P}_{cload,\,i} - \bar{P}_{cload,\,i-1}}\left[\bar{P}_{cload,\,i} - \bar{P}_{cload,\,desired}\right] \tag{4}$$

II. Key Figure

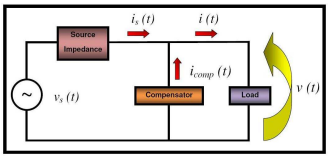

Fig. 1. Load compensation in a power delivery system.

III. Key Results

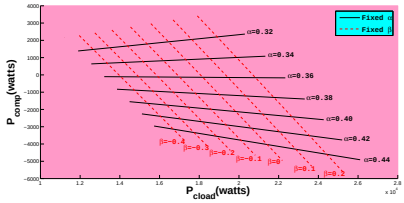

Fig. 2. Mapping of α,β into P_{comp}-P_{cload} plane – Linear Load.

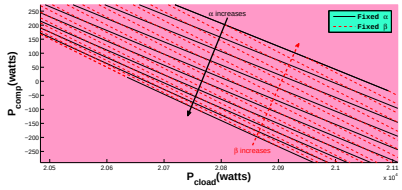

Fig. 3. Mapping of α,β into P_{comp}-P_{cload} plane – Nonlinear Load.

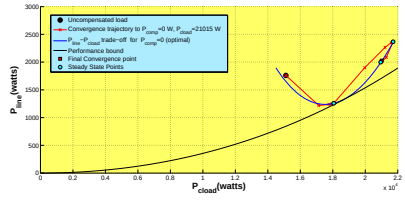

Fig. 4. Convergence trajectory – Linear Load.

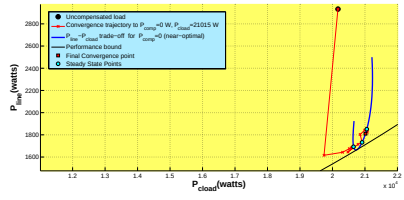

Fig. 5. Convergence trajectory – Nonlinear Load.

Understanding Moisture Diffusion Process in Oil-Impregnated Pressboard Insulation of Transformer

Raj B. Jadav, Tapan K. Saha and Chandima Ekanayake
School of Information Technology and Electrical Engineering, University of Queensland,
St Lucia, QLD, Australia – 4102.
Email: r.jadav@uq.edu.au, saha@itee.uq.edu.au and chandima@itee.uq.edu.au

***Abstract*— Moisture is one of the most influencing parameters, which accelerates solid insulation degradation and ageing process in transformers. Correct estimation of the moisture within solid insulation of transformer is still a challenge due to temperature driven complex moisture dynamics between oil and paper insulation. This paper investigates moisture diffusion process in oil-impregnated pressboard samples at different temperatures to understand the moisture diffusion process of transformers. Mathematical model for moisture diffusion is developed and numerical calculations are carried out using finite volume method. In experimental method, moisture diffusion process in oil-impregnated pressboard sample is investigated by continuous measurement of dissipation factor (Tan δ) at different temperatures. Finally, simulation results obtained from the moisture model are verified with the experimental method.**

I. KEY EQUATIONS

The key equations for moisture diffusion model are:

$$\frac{\partial C(x,t)}{\partial t} = \frac{\partial}{\partial x}\left[D.\frac{\partial C(x,t)}{\partial x}\right] \quad (1)$$

$$D = D_0 e^{\left[k.c + E_a\left(\frac{1}{T_0}-\frac{1}{T}\right)\right]} \quad (2)$$

Initial and boundary conditions are:

$$c_{(x,t=0)} = c_0\,,\ c_0 < 0.5\% \quad (3)$$

$$c_{(x=0,t)} = c_{cs} \quad (4)$$

$$\frac{\partial c_{(x=l,t)}}{\partial x} = 0 \quad (5)$$

II. KEY FIGURES

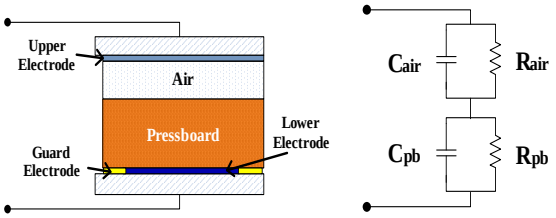

Fig. 1 (a) Electrode arrangement in the test cell (b) Equivalent R-C circuit for air and PB sample

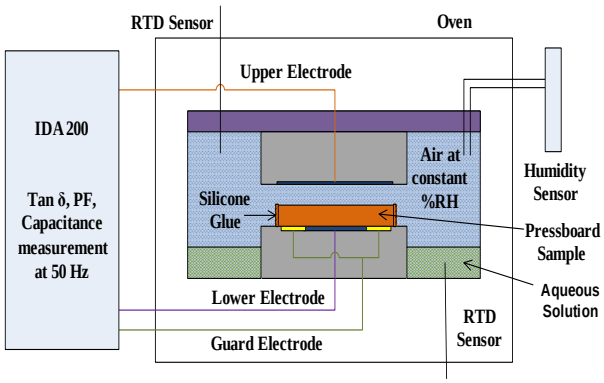

Fig.2 Schematics of the experimental set up

III. KEY RESULTS

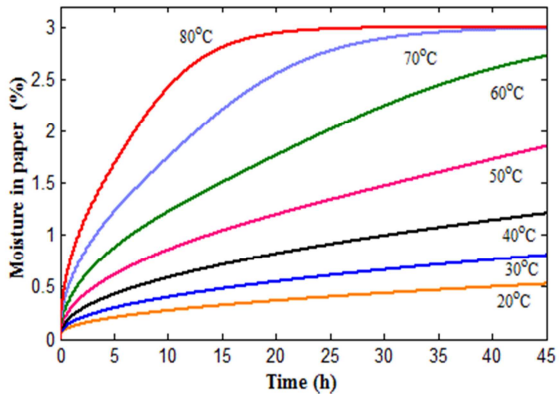

Fig.3 Simulated results of moisture diffusion with 1 mm oil-impregnated pressboard sample at different temperature levels.

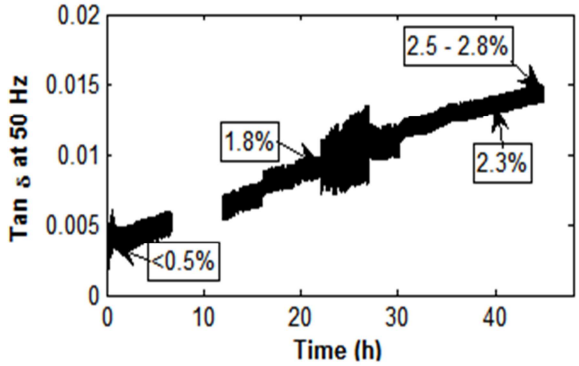

Fig.4. Change in dissipation factor (Tan δ) due to moisture absorption by 1 mm pressboard sample kept at 30% humidity and 60°C.

Simulation of a DC-DC Buck-Boost Converter with Measurement Delay Errors

Sachi Jayasuriya[1], Saichol Chudjuarjeen[1,2], Juan C. Jimenez[1], Chika O. Nwankpa[1], Karen Miu[1] and Anawach Sangswang[2]

Electrical and Computer Engineering Department, Drexel University, Philadelphia, PA 19104, USA[1]

Department of Electrical Engineering, King Mongkut's University of Technology Thonburi, Bangkok, Thailand[2]

Email: sj336@drexel.edu, c_somchai2@hotmail.com, jcj26@drexel.edu, chika@mail.ece.drexel.edu, karen@coe.drexel.edu and anawach.san@kmutt.ac.th

***Abstract*— Power electronic converters are an important feature of many systems such as renewable energy systems, dc distribution systems and shipboard systems. The operations of such systems are highly reliant on their embedded communication infrastructures. Communication delays in delivering converter measurements across a computer controlled network can affect the accuracy of these measurements as viewed by remote hosts. With the preceding as motivation, this poster presents the simulation of an information embedded buck-boost converter which observes measurement errors that result from delays in delivering the measurements. The embedded information network will be represented two ways; by an exponential model and a logistic growth model. Results will concentrate on the effect of delays on the overall analysis of the converter.**

I. KEY EQUATIONS

Conventional averaged model of the buck-boost converter:

$$\left.\begin{aligned}\frac{di_L}{dt} &= \frac{1}{L}\left[-v_C + V_{ref}v_C - k_1 i_L v_C - k_2 v_C^2 + V_{ref}E - k_1 i_L E - k_2 v_C E\right]\\ \frac{dv_C}{dt} &= \frac{1}{C}\left[i_L - V_{ref} i_L + k_1 i_L^2 + k_2 i_L v_C - \frac{v_C}{R}\right]\end{aligned}\right\} \quad (1)$$

Exponential network model:

$$\left.\begin{aligned}\frac{dmi_L}{dt} &= \frac{1}{r}(i_L - mi_L)\\ \frac{dmv_C}{dt} &= \frac{1}{r}(v_C - mv_C)\end{aligned}\right\} \quad (2)$$

Logistic growth network model:

$$\left.\begin{aligned}\frac{dmi_L}{dt} &= \frac{mi_L}{a}\left(1 - \frac{mi_L}{i_L}\right)\\ \frac{dmv_C}{dt} &= \frac{mv_C}{a}\left(1 - \frac{mv_C}{v_C}\right)\end{aligned}\right\} \quad (3)$$

II. KEY FIGURES

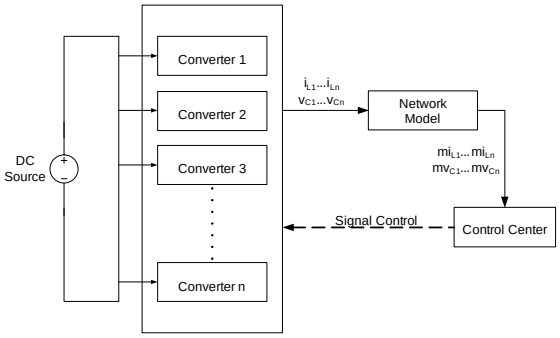

Figure 1. Networked multi-converter system

III. KEY RESULTS

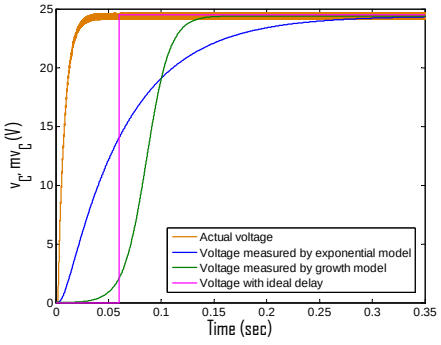

Figure 2. Time domain analysis of the buck-boost converter

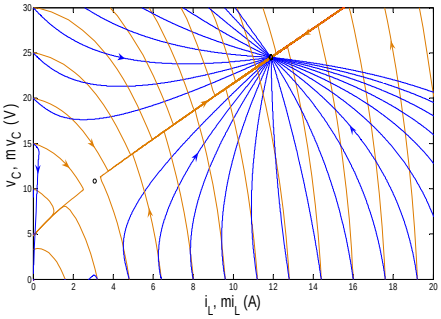

Figure 3. Phase portrait of the buck-boost converter with exponential network model

The Relation Between Undervoltages, Line Outages and Load Shed in Cascading Failure

Janghoon Kim and Ian Dobson
Department of Electrical and Computer Engineering, University of Wisconsin, Madison, WI 53706, USA
Email: jhkim25@wisc.edu

***Abstract*— In cascading blackouts of the power grid, initial outage of some components causes the successive outages of other components, and load shed. There are various types of outages or events such as bus undervoltages, line outages, generator trips, and load shed. All of these can be used as indicators of the blackout size. Previous research on cascading usually focuses on only one indicator and the relative importance of the various indicators and the relations between them is not well known. In this poster, we suggest a method to relate the indicators based on processing cascading failure data.**

Load shed is chosen as the indicator of most interest since it is directly related to the impact on the customers. However, more data or precursor data may be available for the other indicators. We seek to quantify how the load shed depends on the other indicators by applying least square regression methods. Correlation coefficients are used to identify the other indicators that more strongly contribute to load shed. Then the best linear model for the load shed as function of the strongly contributing indicators is determined. The coefficients in the linear model quantify how much the other indicators contribute to load shed and their relative importance. The linear model gives a means of better predicting load shed from other quantities that are easier to monitor and available as precursor data in cascading events in which no load is shed. We test the methods on cascading failure data produced by a detailed simulation of cascading failure on an industry test case.

I. KEY EQUATIONS

Finding relation between indicators:

$$\text{Load shed} = \text{f}(\text{Line outages}, \text{Voltage Violation})$$

Find f using The Least Squares Method:

$$\min \quad \sum(y_i - \text{f}(\text{x}_\text{i}, \text{b}))^2 \qquad (1)$$

II. KEY TABLES

	Line	Voltage	Together
Correlation	0.40	0.54	0.60

Table 1 Correlation coefficient of three cases
Result is checked by correlation.

III. KEY RESULTS

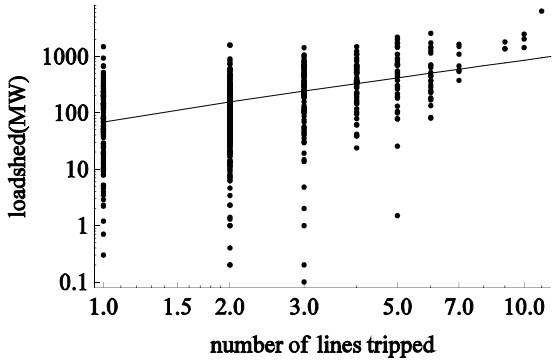

Figure 1 Relation of line outages to load shed

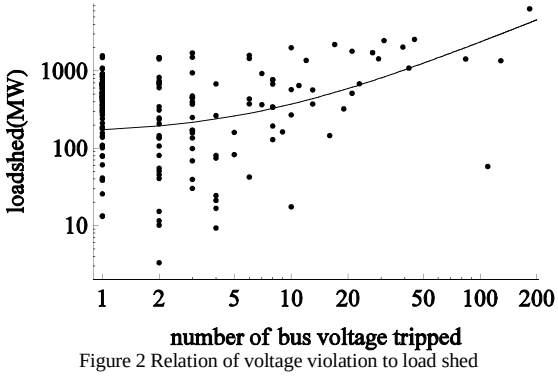

Figure 2 Relation of voltage violation to load shed

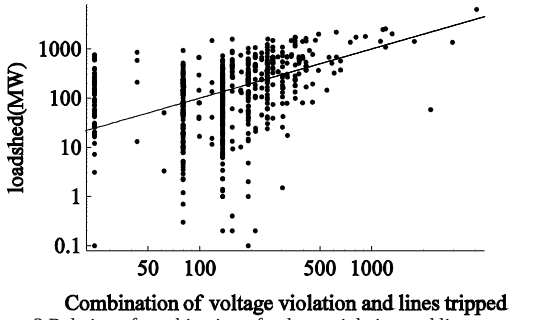

Figure 3 Relation of combination of voltage violation and line outages to load shed

Research on Dynamic Interaction among multiple Static Var Compensator

Heejin Kim
School of Electrical and Electronic Engineering, Yonsei University, Seoul, South Korea,
Email: jimmykim07@gmail.com

***Abstract*— Flexible AC Transmission System (FACTS) has been deployed to strengthen the existing grid and build the Smart grid. Static Var Compensation (SVC) is the most popular FACTS device to support voltage stability and generate reactive power. However, adverse interactions among multiple SVC controllers may occur when they are not properly coordinated with each other. These interactions can amplify oscillations and even destabilize the system by influencing the damping properties of individual SVC controllers or increasing voltage deviations. This poster presents a survey on the existing cases and underlying mechanism of diverse interactions among multiple SVC controllers. We show PSS/e simulation result with Kundur's 2-area 4-machine system.**

I. KEY FIGURE

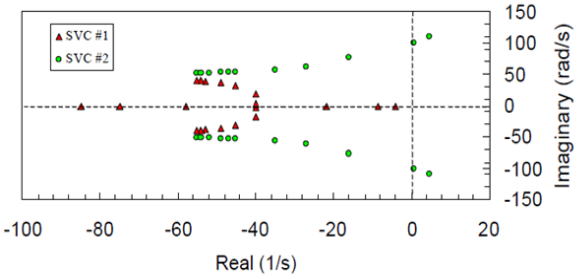

Figure 1. Root locus in the case for SVC interaction

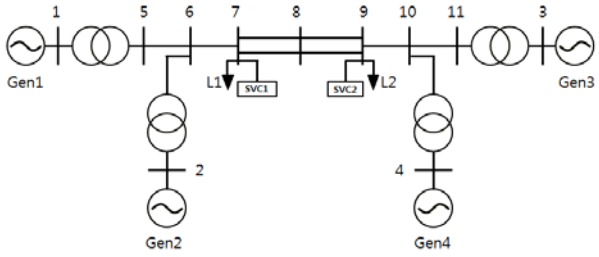

Figure 2 Kundur's 2-area, 4-machine system

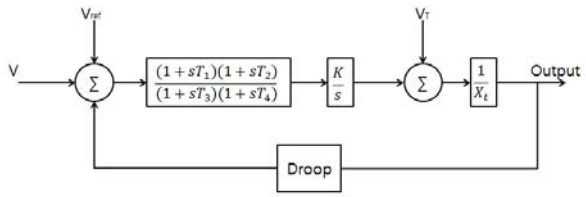

Figure 3. Block diagram of SVC controller

II. KEY RESULTS

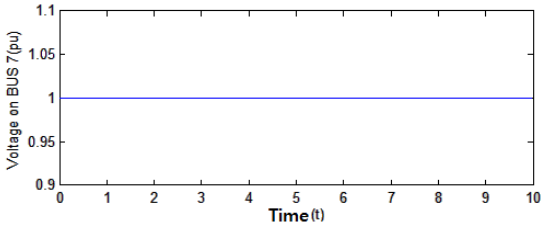

Figure 4. Voltage on Bus 7 (Droop=0.03, K=100 for SVC 1 and SVC 2)

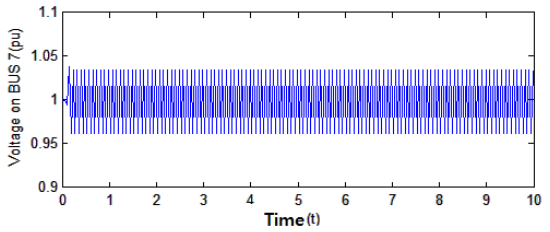

Figure 5. Voltage on Bus 7 (Droop=0.03, K=250 for SVC 1, Droop=0.03, K=100 for SVC 2)

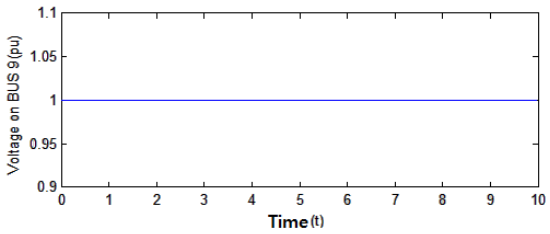

Figure 6. Voltage on Bus 9 (Droop=0.03, K=100 for SVC 1 and SVC 2)

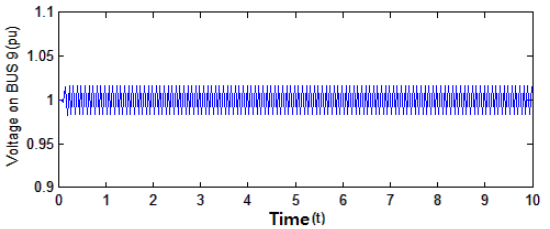

Figure 7. Voltage on Bus 9 (Droop=0.03, K=250 for SVC 1, Droop=0.03, K=100 for SVC 2)

Bi-Directional AC-DC/DC-AC Converter for Power Sharing of Hybrid AC/DC Systems

A. Mohamed, *Student Member, IEEE*, M. Elshaer, *Student Member, IEEE*
Energy Systems Research Laboratory, Department of Electrical and Computer Engineering
Florida International University
Miami, Florida, USA

***Abstract*— In this paper, some of the aspects related to the connectivity of DC microgrids to the main grid are investigated. A prototype system has been designed and implemented to address these aspects. The described system is dependent mainly on sustainable energy sources. Hence, a special care has been given to dealing with this kind of sources while designing different components of the system. Certain features had to be maintained in the system in order to assure efficient integration of different sources such as, efficient and reliable load-feeding capability and full controllability of voltage and power flow among various buses in the system. Two different converters have been investigated; firstly, a fully controlled rectifier has been designed to tie the DC grid with the AC one. A vector decoupling controlled sinusoidal pulse width modulation (SPWM) technique has been used to allow the designed rectifier to maintain a constant output voltage while being able to control the active and reactive power drawn from the grid independently. Hence, this controlled rectifier acts as a voltage regulator for the DC microgrid and has a uni-directional power flow capability from the AC grid to the DC microgrid. Moreover, in order to allow bi-directional power flow, a bi-directional AC-DC/DC-AC converter has also been designed. The Bi-directional AC-DC/DC-AC converter controls the active power transferred from the DC grid to the AC grid while operating at unity power factor. In addition, it controls the active power transferred from the AC grid to the DC grid while operating at unity power factor. Both simulation and experimental results verify the validity of the proposed system.**

I. KEY EQUATIONS

The complete dynamic model of the system is,

$$\begin{bmatrix} \frac{di_q}{dt} \\ \frac{di_d}{dt} \\ \frac{dv_{dc}}{dt} \end{bmatrix} = \begin{bmatrix} \frac{-R}{L} & w & \frac{-S_q}{L} \\ w & \frac{-R}{L} & \frac{-S_d}{L} \\ \frac{3S_q}{2C} & 0 & \frac{-1}{CR_L} \end{bmatrix} \begin{bmatrix} i_q \\ i_d \\ v_{dc} \end{bmatrix} + \begin{bmatrix} \frac{1}{L} & 0 & 0 \\ 0 & 0 & 0 \\ 0 & 0 & 0 \end{bmatrix} \begin{bmatrix} e_q \\ 0 \\ 0 \end{bmatrix} \quad (1)$$

The power balance equation of the system assuming that it is lossless is as given by (2),

$$\frac{3}{2} v_{rq} i_q = v_{dc} C \frac{d}{dt} v_{dc} + \frac{{v_{dc}}^2}{R_L} \quad (2)$$

Where, $v_{rq} = \frac{S_q \cdot v_{dc}}{2}$ and $v_{rd} = \frac{S_d \cdot v_{dc}}{2}$

$$v_{rq}^{cont} = wLi_d + e_q + K_p\left(i_q^{ref} - i_q\right) + K_i \int (i_q^{ref} - i_q) dt \quad (3)$$

$$v_{rd}^{cont} = -wLi_q + K_p\left(i_d^{ref} - i_d\right) + K_i \int (i_d^{ref} - i_d) dt \quad (4)$$

II. KEY FIGURES

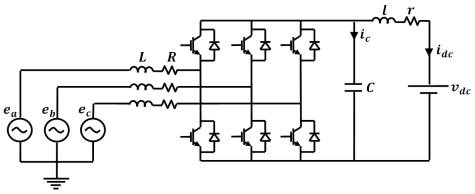

Fig. 1. The three phase bi-directional AC-DC/DC-AC used in the proposed system.

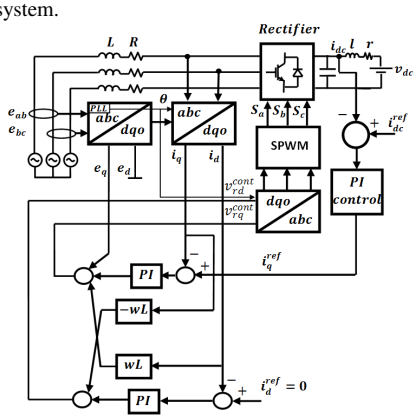

Fig. 2. Vector decoupling control (operation at unity PF)

I. KEY RESULTS

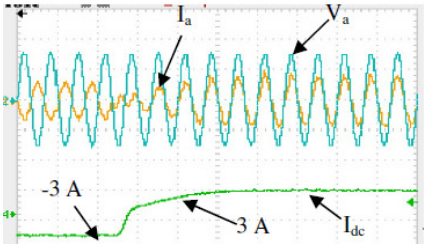

Fig. 3. Controlled Bi-directional response to DC current reference change (-3)-(3) Amps (Power direction reverses)

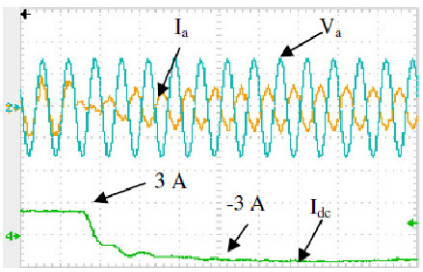

Fig. 4. Controlled Bi-directional response to DC current reference change (3)-(-3) Amps (Power direction reverses)

Alternative Techniques for Power Flow Solutions Based on Affine Arithmetic

J.C. Muñoz*, *Student Member, IEEE,* C. Cañizares*, *Fellow, IEEE,* K. Bhattacharya*, *Senior Member, IEEE* and A. Vaccaro**, *Senior Member, IEEE.*
*Department of Electrical and Computer Engineering, University of Waterloo, Waterloo, ON N2L3G1, Canada.
**Department of Engineering of the University of Sannio, Benevento, Italy
Email: jcmunozg@uwaterloo.ca , ccanizar@uwaterloo.ca, kankar@ece.uwaterloo.ca, vaccaro@unisannio.it

***Abstract*— Affine Arithmetic (AA) is a numerical analysis technique where the variables of interest are represented as affine combinations of data uncertainties and/or approximation errors. This technique keeps track of the sources of error in such a way that the computed quantities are automatically bounded. Recently, AA has been successfully applied to solve the load flow problem by considering uncertainties in the load and generation levels [1]. It represents a more computational efficient method than the Monte Carlo approach commonly used in probabilistic load flow studies to study system uncertainties. This work presents a comparative analysis of two different methods used to solve the load flow problem based on AA. In addition, different strategies to deal with the non-affine operations are proposed and discussed. Simulations are carried out by using Matlab with the aim of testing the effectiveness of the AA load flow solution strategies, based on the IEEE- 30 bus benchmark system with uncertainties in the loading and generation levels. The corresponding results are compared with those obtained via Monte Carlo simulations.**

I. KEY EQUATIONS

- Affine forms for bus voltages and angles:

$$\hat{v}_i = v_{oi} + \sum_{j\in nP} \frac{\partial v_i}{\partial P_j} \varepsilon_{Pj} + \sum_{k\in nQ} \frac{\partial v_i}{\partial Q_k} \varepsilon_{Qk} \quad (1)$$

$$\hat{\delta}_i = \delta_{oi} + \sum_{j\in nP} \frac{\partial \delta_i}{\partial P_j} \varepsilon_{Pj} + \sum_{k\in nQ} \frac{\partial \delta_i}{\partial Q_k} \varepsilon_{Qk} \quad (2)$$

- Power equations in polar form:

$$\hat{P}_i = \sum_{j=1}^{n} \hat{v}_i \hat{v}_j \left(G_{ij} cos\left(\hat{\delta}_i - \hat{\delta}_j\right) + B_{ij} sin\left(\hat{\delta}_i - \hat{\delta}_j\right) \right) \quad (3)$$

$$\hat{Q}_i = \sum_{j=1}^{n} \hat{v}_i \hat{v}_j \left(G_{ij} sin\left(\hat{\delta}_i - \hat{\delta}_j\right) - B_{ij} cos\left(\hat{\delta}_i - \hat{\delta}_j\right) \right) \quad (4)$$

- Power equations in rectangular form:

$$\hat{P}_i = \sum_{j=1}^{n} \hat{e}_i \left(\hat{e}_j G_{ij} - \hat{f}_j B_{ij}\right) + \hat{f}_i \left(\hat{f}_j G_{ij} + \hat{e}_j B_{ij}\right) \quad (5)$$

$$\hat{Q}_i = \sum_{j=1}^{n} \hat{f}_i \left(\hat{e}_j G_{ij} - \hat{f}_j B_{ij}\right) - \hat{e}_i \left(\hat{f}_j G_{ij} + \hat{e}_j B_{ij}\right) \quad (6)$$

II. KEY FIGURES & RESULTS

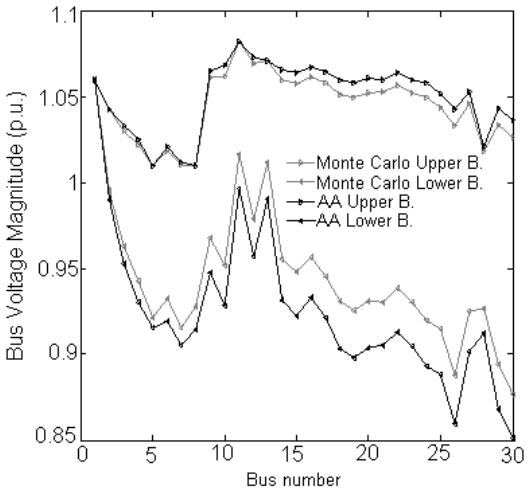

Figure 1. AA based load flow in polar form.

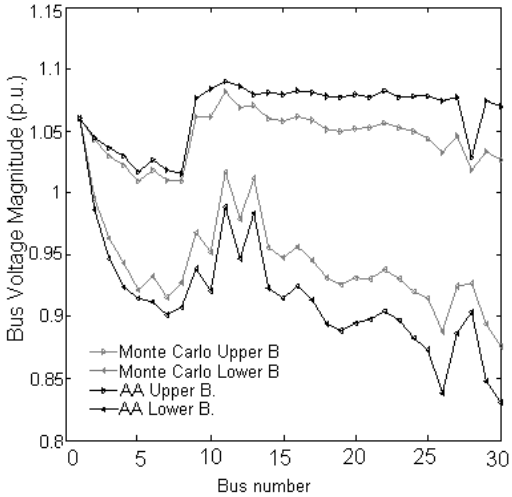

Figure 2. AA based load flow in rectangular form.

III. REFERENCES

[1] A. Vaccaro, C.A. Canizares, and D. Villacci, "An Affine Arithmetic-Based Method for Reliable Power Flow Analysis in the Presence of Data Uncertainty," *IEEE Trans. Power Syst.*, vol. 25, no. 2, pp. 624-632, May. 2010.

Modeling of Electric Arc Furnace using PSCAD based on Measurement Data

Taesik Nam
Smart Grid Laboratory, Department of Electrical and Electronic Engineering, Yonsei University, Seoul, Korea,
Email: tsnam@yonsei.ac.kr

***Abstract*— An arc furnace is a severe non-linear load causing the adverse effects of power quality to the electrical power supply grid : voltage and current harmonics, voltage and current imbalances, low power factor, and voltage flicker. Purpose of this paper is modeling of the three phase electric arc furnace with PSCAD and its voltage harmonic mitigation using Static Var Compensator (SVC) : Thyristor Controlled Reactor combined with a Fixed Capacitor bank (TCR/FC). Also, this paper examines compensation of voltage imbalance caused by electric arc furnace and shows to reduce Total Harmonic Distribution (THD) obtained by experimental data to harmonic standard. In addition, we verify the compensation of reactive power with instantaneous injection of electric load using SVC.**

I. SIMULATION PARAMETERS

Table 1. Simulation Setting Parameter

Short circuit power at PCC	5700MVA	Filter rating at 22kV	140MVA
Rated voltage at PCC	154kV	2nd filter rating	30MVA
Rated power at transformer	150MVA	3rd filter rating	54MVA
Rated capacity at Arc Furnace	140MVA	4th filter rating	56MVA
TCR rating at 22kV	140MVA	Each filters Quality factor	80

II. KEY FIGURES

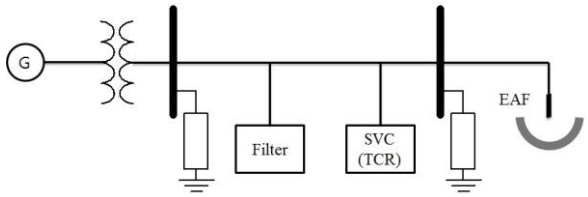

Figure 1. Arc Furnace System

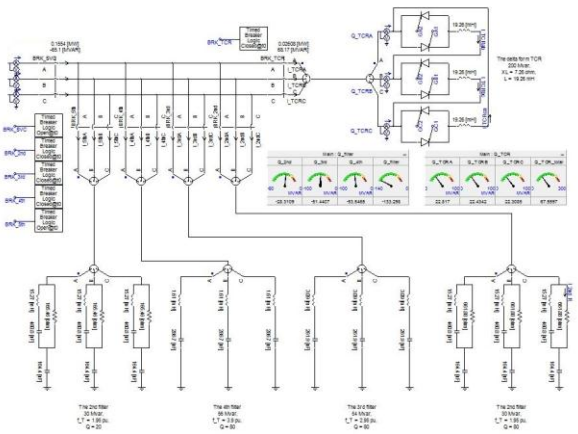

Figure 2. TCR and Filter in Arc Furnace System

III. KEY RESULTS

Table 2. Compare the Harmonic Distribution

Before applying the filter		After applying the filter	
Order	%	Order	%
1st	100%	1st	100%
2nd	7.7%	2nd	1.8%
3rd	5.8%	3rd	0.2%
4th	2.5%	4th	0.1%
5th	4.2%	5th	1.8%
7th	3.1%	7th	1.1%
THD	11.2%	THD	2.85%

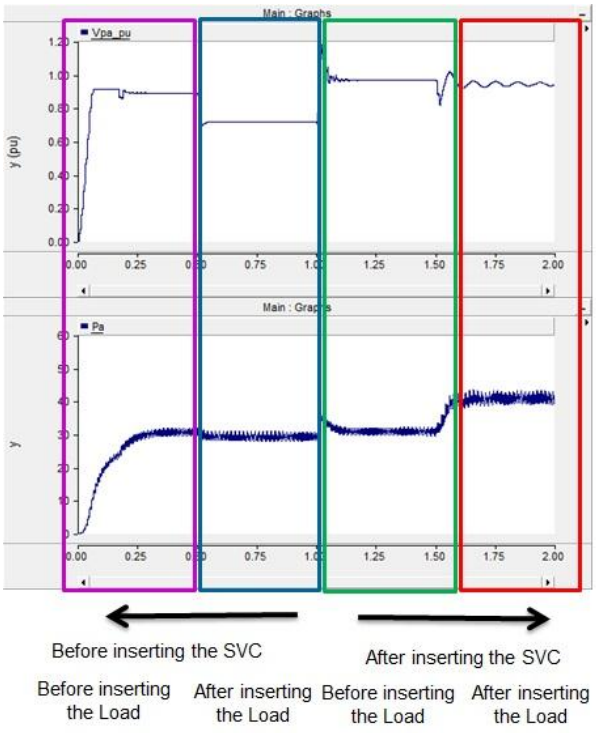

Figure 3. Variation of RMS value of the Voltage Wave Form according to Injecting SVC and Electric Load

Complex Network Framework Based Centrality Approach to Find Critical Nodes in a Power System

A. B. M. Nasiruzzaman and H. R. Pota
School of Engineering and Information Technology, University of New South Wales at the Australian Defence Force Academy, Northcott Drive, Canberra, 2600, Australia,
Email: nasiruzzaman@ieee.org and h.pota@adfa.edu.au

***Abstract*— Power system plays an indispensible role in modern society. However, there have been several large scale blackouts around the world in recent years, in spite of technological progress and huge investment in system reliability and security. There are some critical nodes in power systems which are very vulnerable to attacks. If these nodes can be identified beforehand, system reliability and security can be improved to a large extent by regular monitoring and servicing. Complex network framework based betweenness centrality can be used to identify critical nodes in a power system. When a node is located on the power transmission path linking pairs of other nodes, the previously mentioned node is central. A node in such a position can influence the network when removed from the system either intentionally or accidentally. A new betweenness index is proposed to identify critical nodes in a power system. To evaluate the performance of the proposed index IEEE 30 bus test system is simulated in MATLAB. The effectiveness of the proposed index is examined by calculating the network efficiency with removal of nodes from the system one after another in descending order of their betweenness.**

I. KEY EQUATIONS

The guiding equations of betweenness centrality and network efficiency are:

$$C_B^k = \frac{\sum_{s=1}^{N}\sum_{l=1}^{N} F_k^{sl}}{\sum_{s=1}^{N}\sum_{l=1}^{N} F_G^{sl}} \quad , s \neq l \neq k \in V \qquad (1)$$

$$J = \frac{1}{N(N-1)} \sum_{i \neq j \in V} \frac{1}{x_{ij}} \qquad (2)$$

II. KEY FIGURES

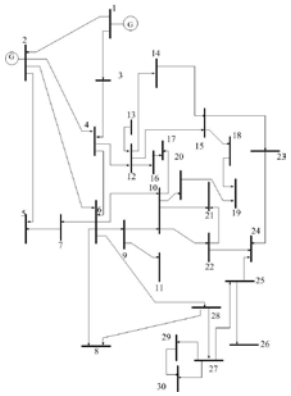

Figure 1. IEEE 30 Bus test system

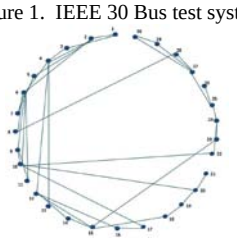

Figure 2. Physical topology graph of IEEE 30 bus test system

III. KEY RESULTS

Table I: Top 6 Critical Nodes in IEEE 30 Bus System

Node	Betweenness	Node	Betweenness
5	0.8012	12	0.3510
6	0.6210	14	0.3410
11	0.5501	13	0.2100

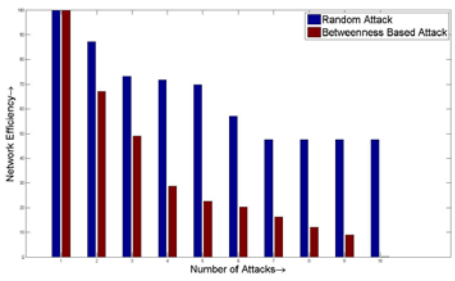

Figure 3. Performance comparison of random node removal and betweenness based node removal

Online Gain Scheduling of Multi-Resolution Wavelet-Based Controller for Acoustic Noise and Vibration Reduction in Sensorless Control of PMSM at low speed

Arash Nejadpak, Ahmed Mohamed, Osama A. Mohammed, *Fellow, IEEE*
Energy Systems Research Laboratory, Department of Electrical and Computer Engineering, Florida International University, Miami, Florida, USA
Email: arash.nejadpak@gmail.com , mohammed@fiu.edu

***Abstract*— An online gain scheduling of the Wavelet-based controller coefficients is presented in this paper for the purpose of reducing noise and vibration resulting from a sensorless control of PM machines at low speeds. The Wavelet-based controller decomposes the whole frequency spectrum into several sub-bands. Each sub-band has a unique effect on the position and speed estimation error in the transient and steady state conditions. The high frequency bands mostly affect the noise and vibration of the system. In this study, parameters which belong to the wavelet-based controller are optimized with hardware in the loop in order to reduce the steady state errors and increase the estimation precision. For the optimization procedure, the GA (Genetic Algorithm) was implemented. The performance of the optimized controller was verified trough the simulation and laboratory experimentation.**

I. KEY EQUATIONS

The guiding equation of the proposed wavelet-based multi resolution controller is as follows:

$$u = K_{d^1} e_{d^1} + K_{d^2} e_{d^2} + \cdots + K_{d^N} e_{d^N} \quad (1)$$

Where gains $K_{d^1}, K_{d^2}, \ldots, K_{d^N}$ are used to tune high and medium frequency components of the error signal (e_{d^1} , e_{d^2}, . . . , e_{d^N}) and N is the number of decomposition levels

The optimization algorithm, used in this paper, is the problem of minimizing fitness function given by:

$$O(t) = \sum_{t=0}^{T_s} \alpha_1 . |\Delta\theta(t)|^2 + \sum_{t=0}^{T_s} \alpha_2 . |\Delta w(t)|^2 + \sum_{t=0}^{T_s} \alpha_3 . |V|^2 \quad (2)$$

II. KEY FIGURES

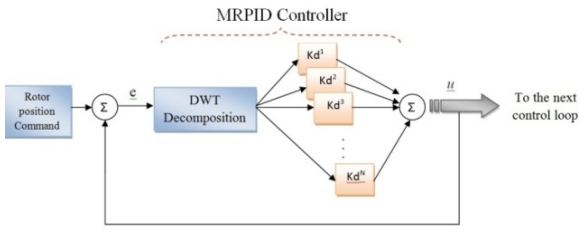

Fig. 1.Implementation of Wavelet-based Multi-resolution controller

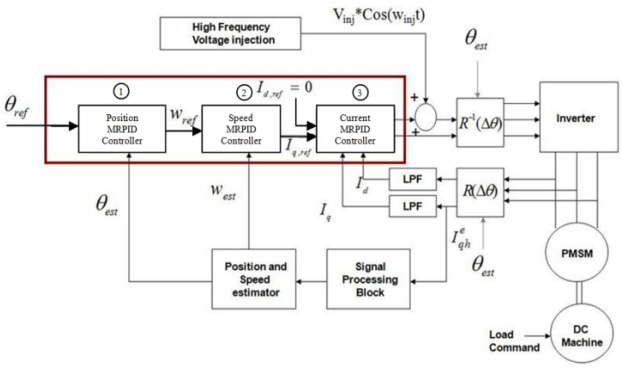

Figure 2. Block diagram of the system for sensorless control of PMSM

III. KEY RESULTS

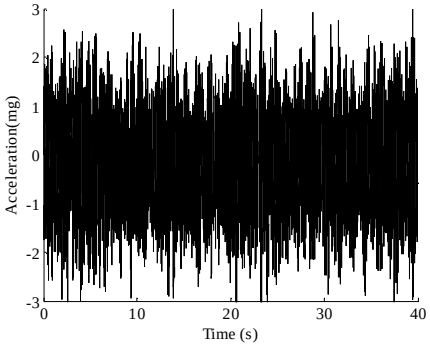

Figure 3. Accelerometer results before optimization

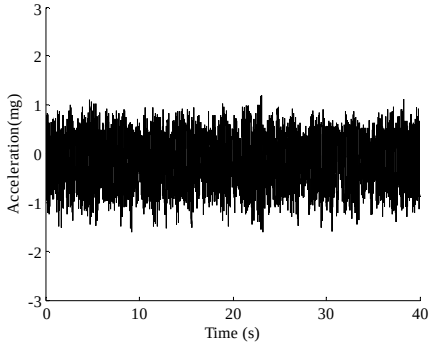

Figure 4. Accelerometer results after optimization.

Non-parametric System Identification of western North American Power System with its Statistics

Gurudatha Pai K (gpai@uwyo.edu)
Department of Electrical and Computer Engineering
University of Wyoming, Laramie, WY 82070

Prof. John W. Pierre (pierre@uwyo.edu)
Department of Electrical and Computer Engineering
University of Wyoming, Laramie, WY 82070

***Abstract*—Measurement based small signal stability analysis of power systems has gained increasing attention in recent times. This particular work relates to non-parametric system identification using measured power system data while probing with multiple cycles of a multi-sine probing signal. In this scheme, multiple cycles of a low level multi-sine probing signal are modulated onto the Pacific DC Intertie, acting as an excitation to the western North American power system. The time-synchronized (using PMUs) response is recorded at various points on the power grid and is analyzed.**

The non-parametric system identification method used is called the *Empirical Transfer Function Estimate (ETFE)*. ETFE is one of the many "first step" methods used to analyze power system probing test data. It provides an estimate of the power system frequency response from excitation input to each measured output.

The multi-sine probing signal used in these probing tests is very typical of system identification experiments. It is composed of a sum of sinusoidal signals of varying frequencies; in this case .01Hz to 2Hz. In a typical power system probing test multiple cycles of this signal are used.

This work specifically extends the ETFE magnitude and phase response estimates to estimates of their statistical bias and variances. ETFE's variance is shown to decrease with probing signal amplitude and the number of cycles used. These results are validated using Monte-Carlo analysis on the linearized power system models and is applied to WECC system-wide test data from 2006. This work also provides a method of estimating the ambient noise spectrum in the presence of multiple cycles of multi-sine probing signal. By using a large number of cycles of the multi-sine probing signal, the variance of ETFE can be reduced significantly whilst keeping the system well within its operating point. These features make ETFE a very viable, fast, intuitive and accurate-enough tool for some base-line estimation of power system frequency response; with the standard deviations in both magnitude and phase response estimates.

I. KEY EQUATIONS

The statistical moments of the magnitude and phase response estimates are given by:

$$E\left[|\hat{G}(\omega)|\right] \approx |G_0(\omega)|\left(1+\frac{1}{4}\frac{\sigma^2(\omega)}{|G_0(\omega)|^2}\right) \tag{1}$$

$$VAR\left[|\hat{G}(\omega)|\right] \approx \frac{\sigma^2(\omega)}{2} - \frac{1}{16}\frac{\sigma^4(\omega)}{|G_0(\omega)|^2} \tag{2}$$

$$E[\angle\hat{G}(\omega)] = \angle G_0(\omega) \tag{3}$$

$$VAR[\angle\hat{G}(\omega)] \approx \frac{\sigma^2(\omega)}{2|G_0(\omega)|^2} \tag{4}$$

$$\hat{\sigma}^2(\omega) = \frac{\hat{\Phi}_V(\omega)}{|U(\omega)|^2} \tag{5}$$

$\Phi_V(\omega)$ is the power spectrum of the ambient noise.

II. KEY FIGURES

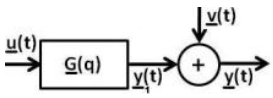

Fig. 1. Block diagram of a LTI system; defining the signals used

III. KEY RESULTS

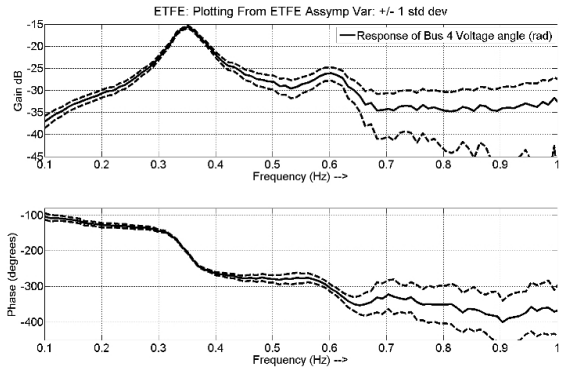

Fig. 2. A typical estimate of the transfer function +/- one std devn.; from probing input to bus 4 of the model.

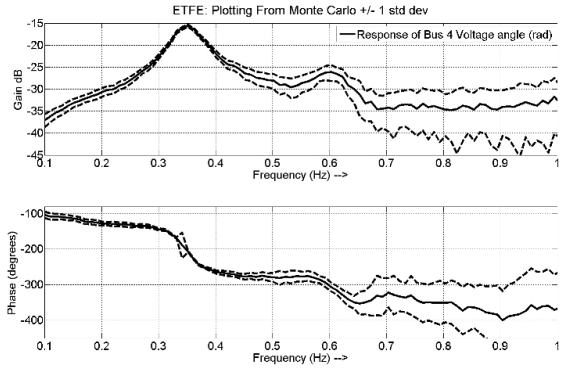

Fig. 3. Monte Carlo calculations of the transfer function +/- one std devn.; from probing input to bus 4 of the model.

Three-phase Distribution OPF in Smart Grids: Optimality versus Computational Burden

Sumit Paudyal, Claudio A. Cañizares, and Kankar Bhattacharya
Department of Electrical and Computer Engineering, University of Waterloo, Waterloo, Ontario, N2L 3G1, Canada
E-mail: spaudyal@uwaterloo.ca, ccanizar@uwaterloo.ca, kankar@uwaterloo.ca

***Abstract*—Existing Mixed Integer Non-linear Programming (MINLP) solution methods and commercially available solvers lack computational efficiency and robustness for solving three-phase Distribution Optimal Power Flow (DOPF) programs, given their computational complexity associated with the large number of continuous and integer variables encountered in practical applications. A heuristic sub-optimal approach to solve this problem was previously proposed by the authors in [1], in which a compromise is made between optimality and computational burden. In the present work, a Genetic Algorithm (GA) based method is used to determine the optimal solution to the three-phase DOPF problem, and the proposed heuristic method is compared with the GA in terms of both optimality and computational burden. Two distribution feeders, namely, the IEEE 13-node feeder and a practical feeder from Hydro One are used for these comparisons. The results show that the GA-based method yields superior solutions in terms of optimality but at a rather large computational cost, making it unsuitable for practical implementation. The heuristic method is shown to yield solutions reasonably close to the global optima at a significantly reduced computational burden. The results demonstrate that the proposed heuristic solution method has the potential to improve distribution system operation in practical real-time applications.**

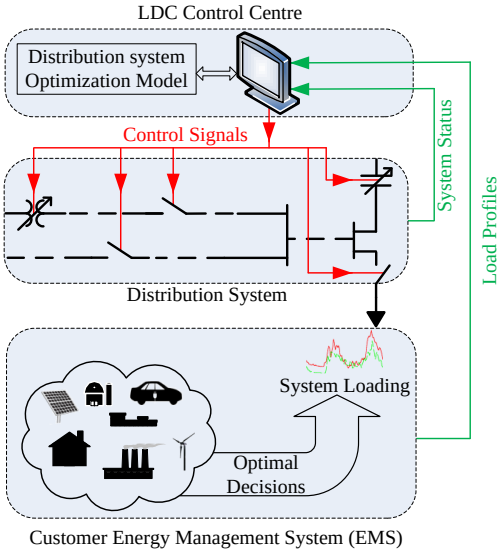

Fig. 1. Schematic diagram of the proposed approach for optimal operation of distribution systems in the context of Smart Grids.

I. Key Figure

Figure 1, depicts the schematics of a distribution feeder in the context of Smart Grids, with its various components and features illustrating the scope of the present work. It demonstrates application of the proposed three-phase DOPF as a core mathematical framework for centralized optimization-based control of distribution systems, and also illustrate need for the efficient DOPF solution methods for real-time applications.

II. Key Equations

The following equation represents the objective function considered in the proposed DOPF mathematical model, which is the minimization of a weighted sum of energy drawn from the sub-station and the number of switching operations of Load Tap Changers (LTCs) and Switched Capacitors (SCs):

$$J = \alpha \sum_{h} Psub_h + \sum_{p} \sum_{t} \left(\beta_t \sum_{h=2}^{24} \left| tap_{p,t,h} - tap_{p,t,h-1} \right| \right) + \sum_{p} \sum_{C} \left(\gamma_C \sum_{h=2}^{24} \left| cap_{p,C,h} - cap_{p,C,h-1} \right| \right) \quad (1)$$

where index C represents the set of SCs, h represents hours, p represents phases, and t represents controllable tap changers. The variable cap represents the number of capacitor banks switched in SCs, J represents the objective function, $Psub$ represents the power drawn from the substation, and tap represents tap positions. The parameters α, β_t, and γ_C are the weights attached to the energy drawn from the substation, LTC switchings and SC switchings, respectively.

The following equation represents the augmented objective function used in the heuristic method, which is obtained by adding a quadratic penalty term to the objective function (1); so that the original MINLP problem is transformed into a standard NLP problem.

$$J' = J + \sum_{ni} K_{ni} \left(w_{ni} - round(w_{ni}) \right)^2 \quad (2)$$

where ni represents the number of integer variables, w_{ni} represents the tap and cap variables, and K_{ni} represents constant multipliers.

Reference

[1] S. Paudyal, C. Cañizares, K. Bhattacharya, "Optimal Operation of Distribution Feeders in Smart Grids," *IEEE Trans. Industrial Electronics*, Early Access. Apr. 2011.

A Novel Optimization Approach to Solve Power Flow Problem Using Complementarity

Mehrdad Pirnia, Kankar Bhattacharya, Claudio Canizares
Power and Energy Systems Group, Department of Electrical and Computer Engineering, University of Waterloo, Ontario, Canada, N2L 3G1,
Email: mpirnia@uwaterloo.ca , Kankar@uwaterloo.ca , ccanizares@uwaterloo.ca

***Abstract*—A novel optimization based solution to the power flow problem, using complementarity conditions which tracks the generator bus voltage level changes when its minimum or maximum reactive power limits have been attained is proposed. In order to test the accuracy of the model, this has been tested on IEEE 14-bus, 30-bus, 57-bus, 118-bus and 300-bus test systems, using GAMS PATHNLP solver, and has been benchmarked against the standard Newton-Raphson method, which is the most well-known power flow solution methodology today. The proposed model converges in a few iterations, with the same results as the Newton-Raphson solver, using UWPflow [1]. To investigate the robustness of this approach, the proposed model has been tested on a large 1200-bus real system, which can be classified as an ill-conditioned power flow problem when using a flat start. Using the proposed complementarity method, the problem converges from a flat start in a few iterations, while Newton-Raphson method diverges.**

I. KEY EQUATIONS

The proposed optimization model for power flow problem with complementarity conditions can be written as [2]:

$$\min \quad \sum_i \Delta P^2{}_i + \Delta Q^2{}_i \tag{1}$$

s.t.

$$\Delta P_i(\delta, V, P_i) = P_i - \sum_i P_{ij}(\delta, V) \quad \forall i \tag{2}$$

$$\Delta Q_i(\delta, V, Q_i) = Q_i - \sum_i Q_{ij}(\delta, V) \quad \forall i \tag{3}$$

$$0 \le \left(Q_{gen_i} - Q_{gen_i}^{Min}\right) \perp V_{a_i} \ge 0 \quad \forall i \in \{gen, slack\} \tag{4}$$

$$0 \le \left(Q_{gen_i}^{Max} - Q_{gen_i}\right) \perp V_{b_i} \ge 0 \quad \forall i \in \{gen, slack\} \tag{5}$$

$$V_{gen_i} = V_{i_0} + V_{a_i} - V_{b_i} \quad \forall i \in \{gen, slack\} \tag{6}$$

$$V_{gen_i}, V_{a_i}, V_{b_i} \ge 0 \quad \forall i \in \{gen, slack\} \tag{7}$$

II. KEY RESULTS

Proposed Model (Flat Start)		
System	Major Iterations	Total time (Seconds)
IEEE 14bus	7	0.046
IEEE 30bus	3	0.047
IEEE 57bus	5	0.109
IEEE 118bus	9	0.375
IEEE 300bus	9	0.515
Real 1211bus	11	12.281

Table 1. Performance Evaluation for PF-CC with Flat Start

Newton-Raphson (Flat Start)	
System	Major Iterations
IEEE 14bus	5
IEEE 30bus	6
IEEE 57bus	4
IEEE 118bus	5
IEEE 300bus	12
Real 1211bus	Doesn't converge

Table 2. Performance Evaluation for Newtone-Raphson Method with Flat start

REFERENCES

[1] "UWPFLOW: Continuation and Direct Methods to Locate Fold Bifurcations in AC/DC/FACTS Power Systems". Available: http://www.power.uwaterloo.ca.

[2] W. Rosehart, C. Roman, and A. Schellenberg, "Optimal Power Flow With Complementarity Constraints," *IEEE Transactions On Power Systems*, vol. 20, no. 2, 2005.

Network Topology Optimization with ACOPF

Tejaswi Potluri and Kory W. Hedman
School of Electrical, Computer and Energy Engineering, Arizona State University, Tempe, AZ 85287, USA
Email: tpotluri@asu.edu and khedman@asu.edu

Abstract*— The Alternating Current Optimal Power Flow (ACOPF) problem is a non convex optimization problem used to determine the optimal generation dispatch. The flow of electricity is governed by Kirchhoff's laws and is subject to certain non-linear constraints some of which involve trigonometric functions. The ACOPF problem solved to optimality subject to these constraints results in the least cost solution. It is a non-convex, non-linear optimization problem and hence difficult to be solved. This research focuses on incorporating transmission switching into the ACOPF problem and consequently examining the cost reduction in the network. The network topology optimization technique proposed to be implemented incorporates a binary variable to represent the switching of lines in the ACOPF. This makes the ACOPF a mixed integer non-linear problem (MINLP) and brings forth the question of the ability of currently available optimization software to handle large scale MINLP. The concept of transmission switching, at first glance, sounds counter-intuitive, questioning the wisdom in opening branches on an everyday basis. However, it has been shown by Hedman et al. that co-optimizing the network topology along with generation leads to significant cost reductions. This research focuses on further investigating transmission switching with an ACOPF problem. It also focuses on examining the effect of transmission switching on the voltage and reactive power profiles of the network which cannot be observed in a DCOPF formulation. The most optimal branch to be opened is determined based on the ranking using a heuristic. This heuristic is based the algorithm proposed by David J. Fuller for fast transmission switching in DCOPF. The ACOPF is performed on the test data and all the branches on the network are rated from the highest ranking to the lowest based on the product of the LMP difference and branch flow. The highest ranking branch is opened and the ACOPF problem is solved with the branch open. The new objective value is compared with the previous objective and if there is any improvement the branch remains open for all future calculations. If there is no improvement, the branch is closed back and the next highest ranking branch is opened. This process is continued iteratively until the most optimal solution is reached. The aim of this research is to show that even a small percentage of cost reduction achieved through controlled topology optimization contributes to major savings in an industry dealing in billions of dollars.

I. KEY EQUATIONS

The mathematical equation used to calculate the rank for the heuristic is given below:

$$\text{Rank}_k = (LMP_n - LMP_m) \times P_k \quad (1)$$

where

LMP_m = Locational marginal price of the from bus of branch k

LMP_n = Locational marginal price of the to bus of branch k

P_k = real power flow on branch k

I. KEY FIGURES

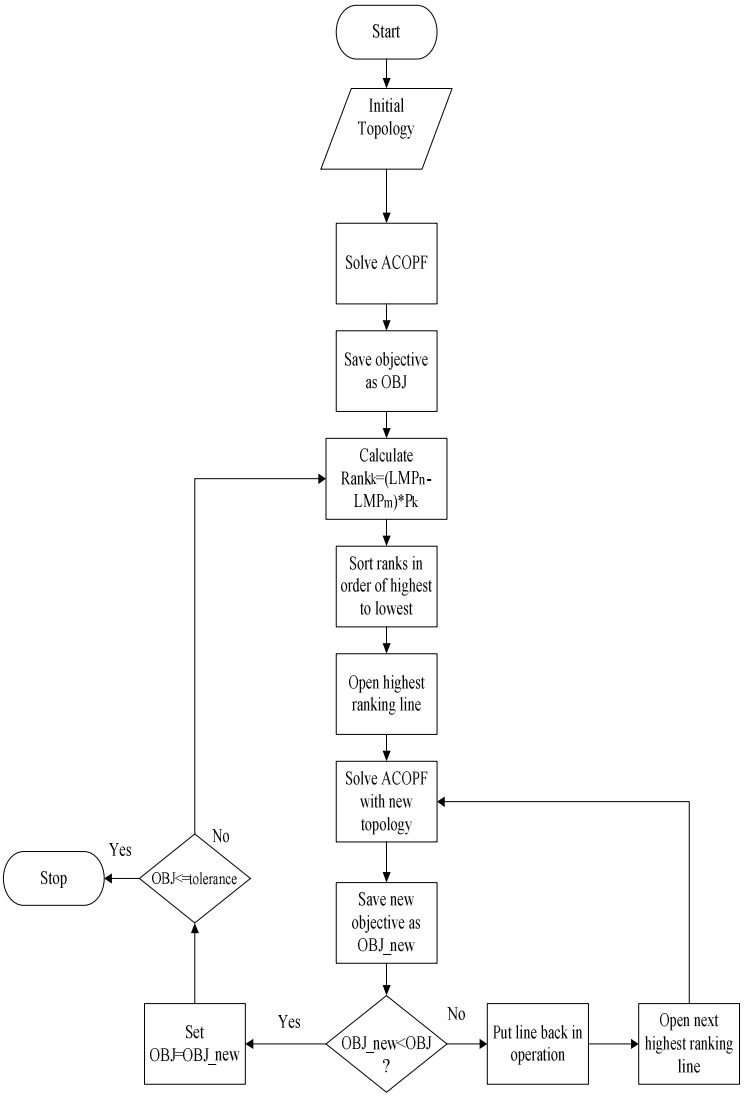

Figure 1. Flow chart of ACOPF with heuristic

Computational Tool to Derive Short-Circuit Network Equivalents

Alexandra Price and Tapan Saha
School of Information Technology and Electrical Engineering, University of Queensland, St Lucia, QLD 4075, Australia,
Email: a.price@ieee.org and saha@itee.uq.edu.au

***Abstract*— A computational tool to aid in network reduction for short-circuit analysis is presented. The tool calculates an equivalent network and plots the transient current profile of the network in a timely and user friendly manner. The tool is able to calculate an equivalent network with a transformer and the user can easily convert between SI units and per unit quantities. The equivalent network parameters and plots are displayed in Microsoft Excel with many functions developed using Visual Basic programming language. The results produced were verified by conducting case studies in PSS®E and PSCAD®. The tool reduces the network to a simple equivalent circuit containing a series combination of a resistor and an inductor. The tool can be used to estimate the impact of increasing the resistance and/or the inductance when analyzing complex devices such as fault current limiters.**

I. KEY EQUATIONS

The guiding equations for fault calculations are:

$$k = \frac{I_{peak}}{\sqrt{2} \times I_{rms}} \quad (1)$$

$$\frac{X}{R} = -3/ln\left(\frac{k - 1.02}{0.98}\right) \quad (2)$$

$$I_{1\varphi,rms} = \frac{cU_n}{\sqrt{3}|R + jX|} \quad (4)$$

The principal equations used for transient current analysis are:

$$|R + jX| = \sqrt{(R_1 + R_2 + R_0)^2 + (X_1 + X_2 + X_0)^2} \quad (5)$$

$$i(t) = \hat{I}\left[\sin(\omega t + \varphi + \theta) - e^{-t/\tau}\sin(-\varphi + \theta)\right] \quad (6)$$

I. KEY FIGURES

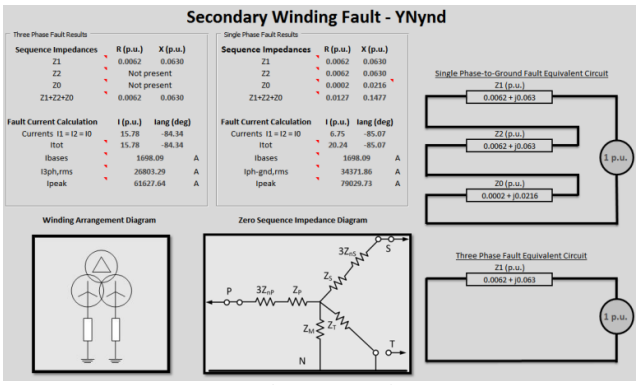

Fig. 1. Secondary winding fault results for a YNyn connected transformer

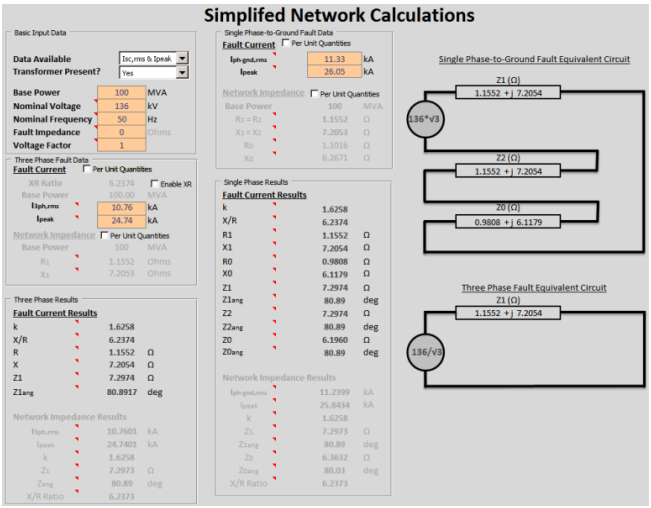

Fig. 2. Basic Input Data Tab of computational tool

II. KEY RESULTS

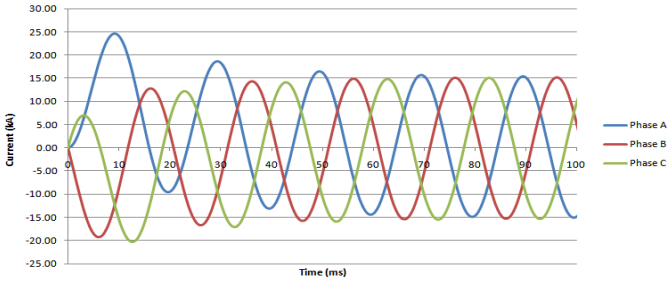

Fig. 3. Case 1 transient current profile produced from PSCAD®

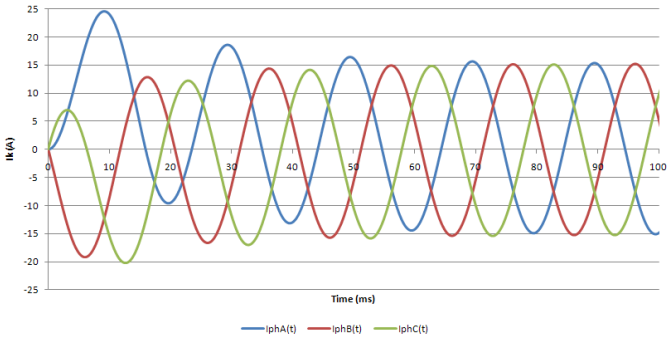

Fig. 4. Case 1 transient current profile from computational tool

Power Smoothing Technique using Battery in Double Fed Induction Generator

Ashish K Solanki and guided by Prof. David Yu
Department of Electrical Engineering, University of Wisconsin Milwaukee, Milwaukee
Email: solanki@uwm.edu , yu@uwm.edu

***Abstract*: Wind can play major role to meet increasing demand of Energy. Doubly Fed induction Generator is very commonly used in Wind Energy because of many advantages like small scale power converters, direct connection with the Grid and many more. We always want to extract the maximum power available in the wind. Due to a fluctuation of wind the power feeding to the gird or micro grid will also fluctuate. However, we always want to feed the power which is asked by the control unit in the grid or micro grid. This poster proposed a scheme to provide the power which will be demanded from the control unit and also extract maximum power from the wind. This scheme used Storage Battery with the inverter to smooth the power injection to the grid. If the generated power is more than demanded power, the additional power is used to charge the battery.**

I. KEY EQUATIONS

$$P_w = \frac{\rho}{2} C_p(\lambda, \beta) A v_w^3 \quad (1)$$

$$P_s = v_{ds} \cdot i_{ds} + v_{qs} \cdot i_{qs} \quad (2)$$

$$Q_s = v_{qs} \cdot i_{ds} - v_{ds} \cdot i_{qs} \quad (3)$$

$$P_r = v_{dr} \cdot i_{dr} + v_{qr} \cdot i_{qr} \quad (4)$$

$$Q_r = v_{qr} \cdot i_{dr} - v_{dr} \cdot i_{qr} \quad (6)$$

$$T_{em} = \frac{3}{2} \cdot \frac{P}{2} \cdot (\lambda_{ds} \cdot i_{qs} - \lambda_{qs} \cdot i_{ds}) \quad (7)$$

II. KEY FIGURES

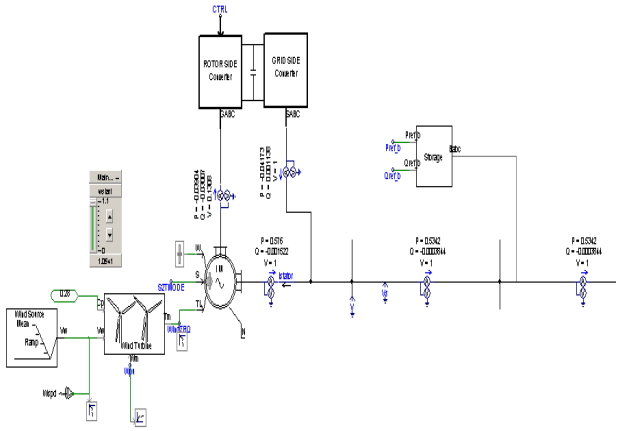

Figure1. DFIG and Battery connected to grid

III. KEY RESULTS

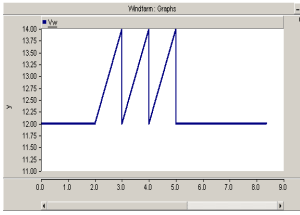

Figure2: Wind Profile

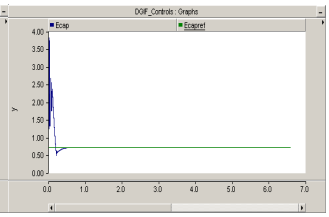

Figure3: DC Bus Voltage

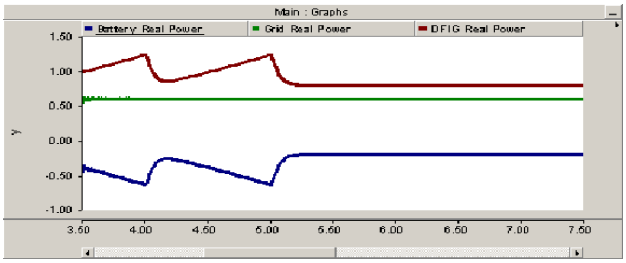

Figure 4: Real Power generated by DFIG, Real power of the storage and Grid Real Power

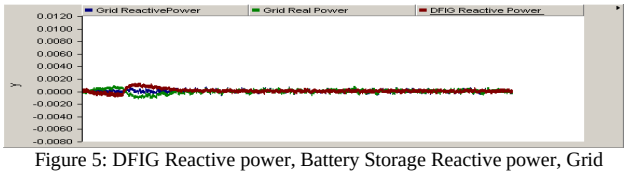

Figure 5: DFIG Reactive power, Battery Storage Reactive power, Grid Reactive power(with battery storage)

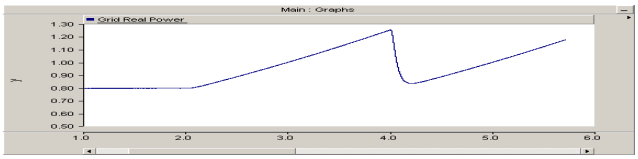

Figure 6:Grid power without Battery storage

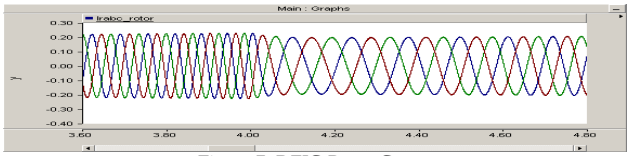

Figure 7: DFIG Rotor Current

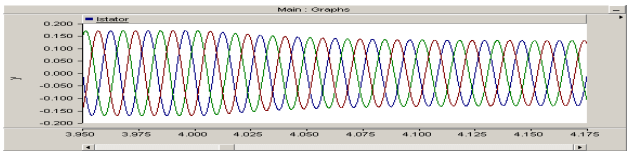

Figure:8: DFIG Stator Curret

The ramp in the wind speed is picked up by the battery and the power feed to the grid become smooth.

Three-Phase Optimal Power Flow

Ye Tao and A. P. Sakis Meliopoulos
Power Systems Control and Automation Laboratory, School of Electrical and Computer Engineering, Georgia Institute of Technology, Atlanta, GA 30332, USA,
Email: taoye99@gatech.edu and sakis.m@gatech.edu

***Abstract*— a major goal of smart grid technologies is to extend transmission grid analysis and control methods to distribution systems. Hence, Distribution Management Systems (DMS) for the smart grid need to include functions such as state estimation and optimal power flow (OPF) which are common in Energy Management Systems. Since distribution systems operate in general in unbalanced conditions, three-phase optimal power flow (TOPF) is required rather than the traditional single-phase OPF. This work proposes a TOPF formulation and a solution algorithm that operates in the infeasible region and moves the operating point to a feasible and optimal point via a sequential method.**

I. KEY EQUATIONS

The TOPF problem is formulated as follows:

$$\min \; J(\mathbf{x},\mathbf{u}) = \mu \sum \left(|\mathbf{I}_m| \right) + \sum_{k=1}^{N} \sum_{j=1}^{M(k)} \left(a_{k,j} + b_{k,j} P_{k,j} + c_{k,j} P_{k,j}^2 \right)$$

$$s.t. \qquad \mathbf{g}(\mathbf{x},\mathbf{u},\mathbf{I}_m) = 0$$

$$\mathbf{h}^{\min} \le \mathbf{h}(\mathbf{x},\mathbf{u}) \le \mathbf{h}^{\max}$$

$$\mathbf{u}^{\min} \le \mathbf{u} \le \mathbf{u}^{\max}$$

where **x** is the state variable vector, **u** is the control variable vector, and $\mathbf{I}_m$ is the mismatch current vector. The method introduces the mismatch variables that allow any operating point to be optimal but infeasible. The equations **g** represent Kirchoff's current law at each node of the system. A general node is shown below.

II. KEY FIGURES

The figure below shows a general node that may include generators, transformers, loads, capacitor bank, reactor, SVC, etc. The sum of currents equals zero at each node, yielding equations **g**.

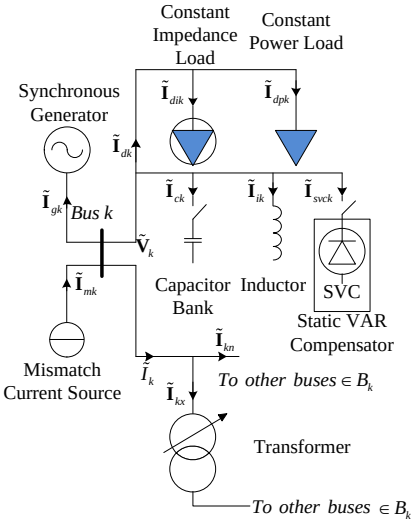

The solution algorithm is shown in the figure below. The solution method operates on infeasible but optimal points and with each iteration moves the point closer to the feasible and optimal point by minimizing the mismatches.

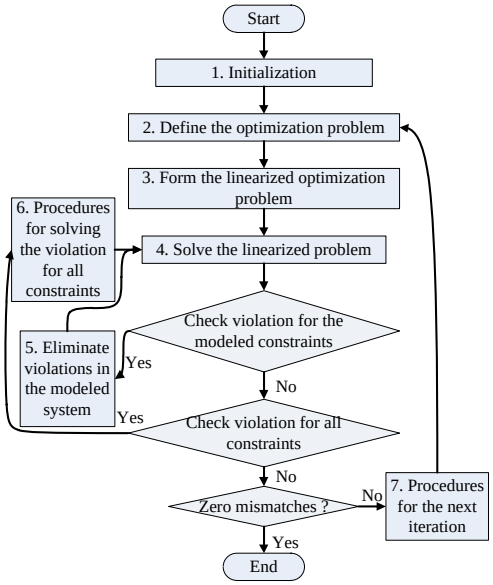

III. KEY RESULTS

The method is demonstrated in a simple three generator system shown in the figure below.

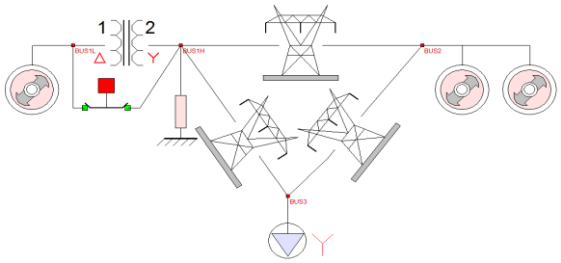

The figures below show the value of the objective function (actual cost plus penalty for mismatches) and the actual cost of the system as the solution iterations progress.

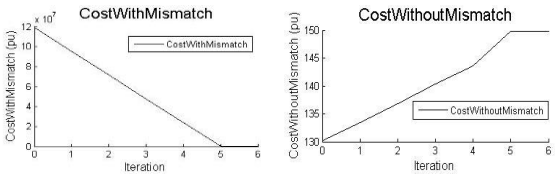

IV. CONCLUSIONS

This work presents a robust and highly efficient sequential algorithm to solve the TOPF. Experimental results show that this algorithm provides the optimal unbalanced solution and it converges in a few iterations (five to six iterations) independently of system complexity. Future work will focus on incorporating discrete variables and extension to larger power systems.

A Novel Method to Control Step size of Continuation Power Flow

Pengfei Xu[1], Xiaoru Wang[1] and Venkataramana Ajjarapu[2]

1. Department of Electrical Engineering, Southwest Jiaotong University, Chengdu, Sichuan 610000, China.
2. Department of Electrical and Computer Engineering, Iowa State University, Ames, IA 50010, USA,

Email: pengfeix@iastate.edu, xrwang@home.swjtu.edu.cn, and vajjarap@iastate.edu

***Abstract*— The continuation algorithm is used to find a path of equilibrium solutions of a set of nonlinear equations, and has been combined with power flow technique to come up with continuation power flow algorithm, which has been widely used in the field of steady state analysis of power systems including assessment of voltage stability. Control of step size plays a key role in computational efficiency of continuation power flow. Small step size gives too many solution points, large step size gives too many iteration in corrector and may cause divergence, both cases of which are time consuming. Method to control step size is proposed. Last step size and information from the corrector and trigger condition of operation devices of systems are applied to predict next step size. Possible divergence is detected at the beginning in each one of the correctors. The proposed methodology needs less number of solution points. Identification of Limit induced bifurcation becomes by product of this methodology.**

I. KEY EQUATIONS

The formulation of continuation power flow can be

$$\boldsymbol{f}(\boldsymbol{x},\lambda)=0,\boldsymbol{x}\in\boldsymbol{R}^n,\lambda\in[0,\lambda_{critical}] \quad (1)$$

Step size $\Delta\lambda_v$ to ensure convergence for each one of correctors are

$$\Delta\lambda_v^m=\left(\frac{\left\|\overline{\Delta\boldsymbol{x}}^0(\lambda_v)\right\|\cdot(\sqrt{2}-1)}{\left\|\hat{\boldsymbol{x}}(\lambda_v)-\overline{\boldsymbol{x}}(\lambda_v)\right\|\cdot 2\overline{\Theta}_0(\lambda_v)}\right)^{0.5}\Delta\lambda_{v-1},m=1 \quad (2)$$

$$\Delta\lambda_v^m=\sqrt{0.57}\Delta\lambda_v^{i-1},\ \ m>1, \quad (3)$$

Let $\Delta\lambda_{vGi}$ and $\Delta\lambda_{vci}$ be the limited step size for actuation of Q-limit and switch of shunt compensators then step size $\Delta\lambda_v^m$ in the predictor can be selected by

$$\Delta\lambda_v^m\rightarrow\min\left\{\Delta\lambda_v^m,\Delta\lambda_{vGi},\Delta\lambda_{vci}\right\}. \quad (4)$$

Parameter λ is selected as continuation at the beginning. In the neighborhood of critical point, one of components of $\boldsymbol{x}$ may be selected as continuation parameter. Let $\boldsymbol{y}:=(\boldsymbol{x},\lambda)\in\boldsymbol{R}^{n+1}$, the method of choosing continuation parameter y_k is

$$y_k:\left|dy_k\right|=\max\left\{\left|dy_1\right|,\left|dy_2\right|,\cdots,\left|dy_{n+1}\right|\right\} \quad (5)$$

where, dy_k is the k^{th} component of $\boldsymbol{dy}$, $\boldsymbol{dy}\in\boldsymbol{R}^{n+1}$ is the tangent obtained in predictor.

II. KEY FIGURES

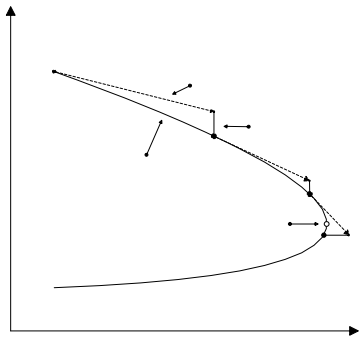

Fig. 1 An illustration of the predictor-corrector scheme in the continuation power flow

III. KEY RESULTS

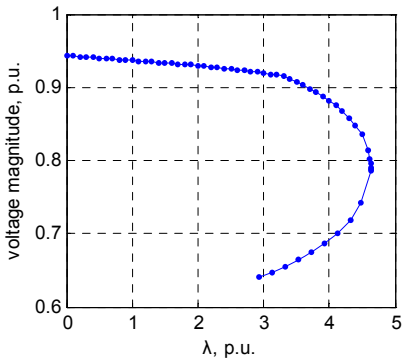

Fig. 2 voltage magnitude response of bus 526 in IEEE 300 system with fixed step size under global load increasing

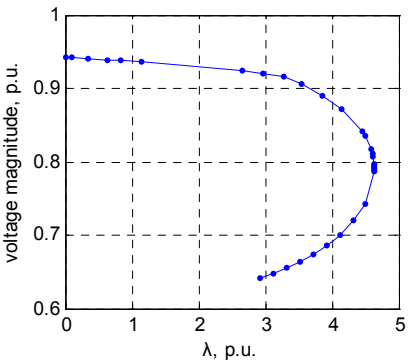

Fig. 3 voltage magnitude response of bus 526 in IEEE 300 system with proposed step size under global load increasing(It needs less number of iterations compared to fig.1)

A Spatial, Temporal and Event Simulator of a Smart Grid

Xichun Ying and Mo-Yuen Chow
Advanced Diagnosis Automation and Control Lab, Department of Electrical and Computer Engineering,
North Carolina State University, Raleigh, NC 27606, USA,
Email: xying@ncsu.edu and chow@ncsu.edu

***Abstract*— An innovative and comprehensive Smart Grid software simulator is essential to facilitate the analysis and the development of the control, energy management, fault management and communication in a smart grid environment. This simulator will be integrated with heterogeneous systems and spatial, temporal and event information. It will be designed as modularized, library-based and user-friendly. Multi-rate sampling will be used in the simulator. This poster introduces the objective, motivation in developing this simulator, suggests the desired features, architecture and modules of the simulator and presents a diagram as a showcase of a future power system with spatial, temporal and event information.**

I. KEY FIGURES

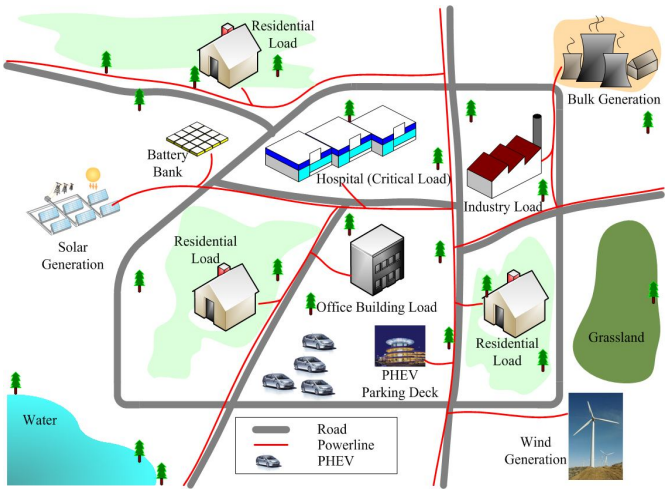

Figure 1. A showcase of a future power system with Spatial, Temporal and Event Information

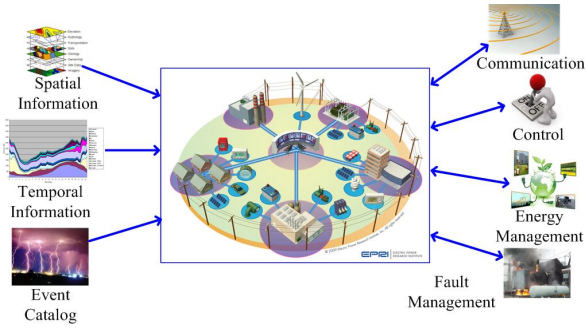

Figure 2. Architecture of the Smart Grid simulator

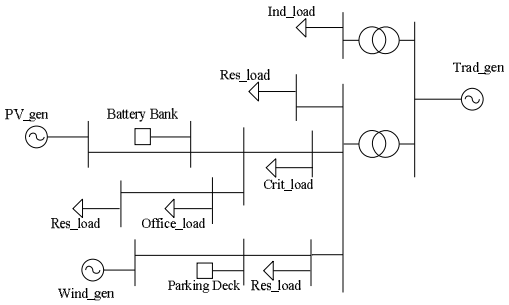

Figure 3. A power system one-line diagram

Effect of Various Parameters on the Inductive Induced Voltage and Current on Pipelines

Hui Zhang George G. Karady and Jim Hunt
Department of Electrical and Engineering, Arizona State University, Tempe, AZ 85287, USA,
Email: hui.zhang@asu.edu, karady@asu.edu and jim.hunt@srpnet.com

***Abstract*— Considerable research has been conducted on the issues of induced voltage on the pipelines which are close to the high voltage power lines. It has been found that the induced voltage and current on the pipeline are determined by many parameters. This paper presents a comprehensive study on how the various parameters affect the induced voltage and current on the pipelines. In the system modeling part, a circuit model for multiple-pipeline section-model is employed. In this model, not only the perfect parallel case, but also a more realistic case with approaches, crossing as well as removals is considered. 2 cases are studied in this paper. The results of steady state induced voltage and current have demonstrated the effect of different parameters.**

I. KEY EQUATIONS

The guiding equations are:

$$V(x) = -Z_C\left(K_1 e^{\gamma x} - K_2 e^{-\gamma x}\right) \quad (1)$$

$$I(x) = K_1 e^{\gamma x} + K_2 e^{-\gamma x} + \frac{E_{ind}}{z} \quad (2)$$

where $r_1 = \frac{Z_1 - Z_C}{Z_1 + Z_C}$ and $r_2 = \frac{Z_2 - Z_C}{Z_2 + Z_C}$ are defined as reflection factors. The coefficient K_1 and K_2 is given by

$$K_1 = \frac{E_{ind}}{2z} \cdot \frac{(1+r_1)r_2 - (1+r_2)e^{\gamma L}}{e^{2\gamma L} - r_1 r_2} \quad (3)$$

$$K_2 = \frac{E_{ind}}{2z} \cdot \frac{(1+r_2)r_1 e^{\gamma L} - (1+r_1)e^{2\gamma L}}{e^{2\gamma L} - r_1 r_2} \quad (4)$$

$$\begin{bmatrix} T_1 & -R_{l1} & & \cdots & 0 \\ -R_{l1} & T_2 & -R_{l2} & & \vdots \\ & \vdots & \vdots & \vdots & \\ \vdots & & -R_{lm-2} & T_{m-1} & -R_{lm-1} \\ 0 & \cdots & & -R_{lm} & T_m \end{bmatrix} \cdot \begin{bmatrix} I_{p1} \\ I_{p2} \\ \vdots \\ I_{pm-1} \\ I_{pm} \end{bmatrix} = \begin{bmatrix} E_{ind1} \\ E_{ind2} \\ \vdots \\ E_{indm-1} \\ E_{indm} \end{bmatrix} \quad (5)$$

$$V_k = \left(I_{k+1} - I_k\right) \cdot R_{li} \qquad k \in [0, m] \quad (6)$$

$$E_{\text{ind}} = I_A Z_{mA} + I_B Z_{mB} + I_C Z_{mC} \quad (7)$$

$$Z_{m.Carson} = \frac{\omega\mu}{8} + j\frac{\omega\mu}{2\pi}\ln\left(\frac{D_{eq}}{d_i}\right) \quad (8)$$

II. KEY FIGURES

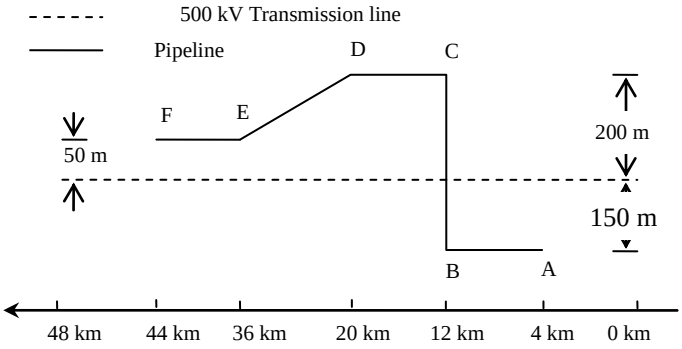

Figure 1. Layout of the power line – pipeline corridor

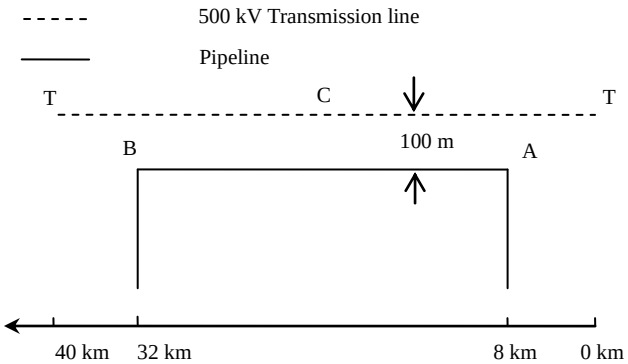

Figure 2. Layout of the power line – pipeline corridor

III. KEY RESULTS

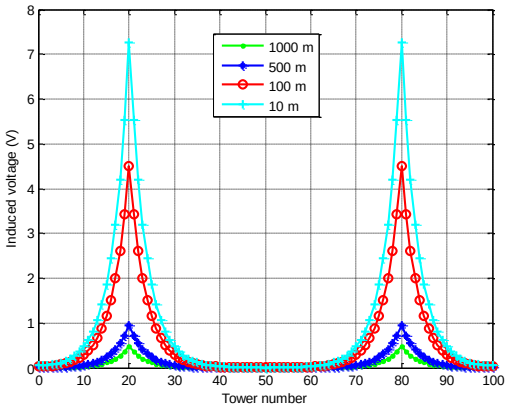

Figure 1. Effect of lateral distance on the induced voltage distribution

Modeling and Control of Discrete Event Systems Using Finite State Machines with Parameters and Their Applications in Power Grids

Junhui Zhao
Department of Electrical and Computer Engineering, Wayne State University, Detroit, MI 48201, USA,
Email: junhui.zhao@wayne.edu

***Abstract* — Control theories for discrete event systems modelled as finite state machines have been well developed over the years to address various fundamental control issues. However, finite state machine model has long suffered from the problem of state explosion that renders it unsuitable for some practical applications. To mitigate the problem of state explosion, we propose to employ both finite state machines and sets of parameters in modeling discrete event systems as Finite State Machines with Parameters (FSMwP). Our FSMwP can represent a broader class of discrete event systems with far smaller numbers of discrete states. Then we takes the advantage of both event disablement and enforcement in order to prevent the controlled system from venturing into the prohibited state space. We apply our theoretical results in optimal control of power distribution networks by modelling a distribution network by a FSMwP. We consider both conventional loads and PHEV loads. A supervisor is then designed to ensure the network is fully utilized and never overloaded.**

I. KEY EQUATIONS

The guiding equations of the safety controller are:

$$\begin{aligned}\mathrm{CFSMwP} &= \mathrm{FSMwP}_1 \| \ldots \| \mathrm{FSMwP}_n \\ &= (\Sigma_1, Q_1, \delta_1, P_1, G_1, (q_{o1}, p_{o1}), Q_{m1}) \| \ldots \| (\Sigma_n, Q_n, \delta_n, P_n, G_n, (q_{on}, p_{on}), Q_{mn}) \\ &= (\Sigma_1 \cup \ldots \cup \Sigma_n, Q_1 \times \ldots \times Q_n, \delta_1 \times \ldots \times \delta_n, P_1 \cup \ldots \cup P_n, G_1 \cup \ldots \cup G_n, \\ &\quad (q_{o1}, \ldots, q_{on}, p_{o1}, \ldots, p_{on}), Q_{m1} \times \ldots \times Q_{mn}) \\ &= (\Sigma, Q, \delta, P, G, (q_o, p_o), Q_m),\end{aligned}$$

$$I_q(k+1) = I_q(k) \wedge (\neg(\bigvee_{(q, g\wedge\sigma / p:=f(p), q')\in\delta\wedge\sigma\notin\Sigma_c} (g \wedge \neg I_{q'}(k)\big|_{p:=f(p)})) \vee (\bigvee_{(q, g\wedge\sigma / p:=f(p), q')\in\delta\wedge\sigma\in\Sigma_f} (g \wedge I_{q'}(k)\big|_{p:=f(p)}))).$$

$$\psi(r) = \begin{cases} \{\sigma \in \Sigma : (q, g\wedge\sigma / p := f(p), q') \in \delta \wedge \neg(g \wedge \neg I^*_{q'}\big|_{p:=f(p)})\} \cup (\Sigma - \Sigma_c) \\ \qquad \text{if } \neg(\bigvee_{(q, g\wedge\sigma / p:=f(p), q')\in\delta\wedge\sigma\in\Sigma_c} (g \wedge \neg I^*_{q'}\big|_{p:=f(p)})) \\ \{\sigma \in \Sigma_f : (q, g\wedge\sigma / p := f(p), q') \in \delta \wedge (g \wedge I^*_{q'}\big|_{p:=f(p)})\} \\ \qquad \text{otherwise.} \end{cases}$$

II. KEY FIGURES

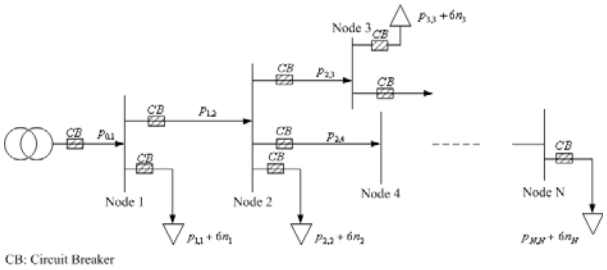

Figure 1. A Distribution Network with N Nodes.

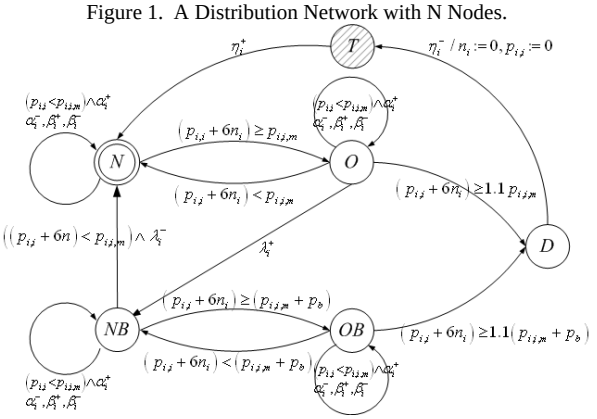

Figure 2. FSMwP Model for Local Load at Node *i*.

III. KEY RESULTS

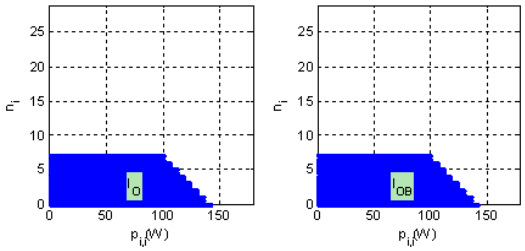

Figure 3. Safety area when β is uncontrollable event of State *O* and State *OB*.

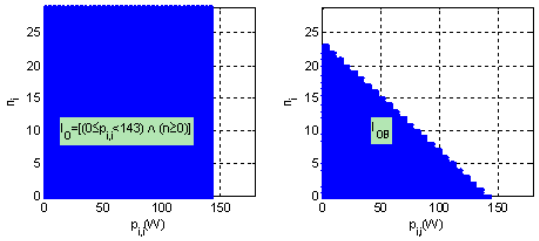

Figure 4. Safety area when β is enforceable event of State *O* and State *OB*.

A Third-Order Sliding-Mode Controller for DC/DC Converters with Constant Power Loads

Yue Zhao and Wei Qiao
Department of Electrical Engineering, University of Nebraska-Lincoln, Lincoln, NE 68503-0511, USA,
Email: yue.zhao@huskers.unl.edu and wqiao@engr.unl.edu

***Abstract*— Incorporating a medium voltage DC (MVDC) integrated power system is an important goal for future surface combatants and submarines. Several technical challenges still need to be solved and instability of constant power loads (CPLs) is one of key issues. The purpose of this paper is to present an assessment of the negative incremental impedance instability of constant power loads in MVDC shipboard power system, and focuses on design criteria of sliding mode controllers for DC/DC converters with constant power loads. The proportional-integral-derivative (PID) based third-order sliding mode controller is proposed, and tested under different operations and in presence of significant variation in load and input voltage with Matlab Simulink. Furthermore, the system level analysis and simulation results of controller tested in one generator DC system are also presented.**

I. KEY EQUATIONS

The guiding equations of the third-order sliding-mode controller for DC/DC converters with constant power loads are:

$$\begin{cases} \dfrac{di_L}{dt} = \dfrac{v_{in}}{L}d - \dfrac{v_o}{L} \\ \dfrac{dv_o}{dt} = \dfrac{1}{C}(i_L - \dfrac{P}{v_o}) \end{cases} \tag{1}$$

$$s = \left(\frac{d}{dt} + \lambda\right)^2 \left(\int_0^t \tilde{x}dt\right) = \dot{\tilde{x}} + 2\lambda\tilde{x} + \lambda^2 \int_0^t \tilde{x}dt \tag{2}$$

$$s = a_1\dot{e}_v + a_2 e_v + a_3 \int e_v dt \tag{3}$$

$$d^* = \frac{1}{v_{in}}[k_1 i_C + k_2(V_{ref} - v_o) + v_o] \tag{4}$$

II. KEY FIGURES

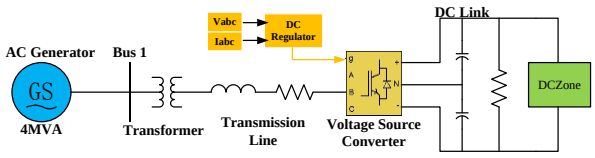

Figure 1. One-generator MVDC system with a constant power load.

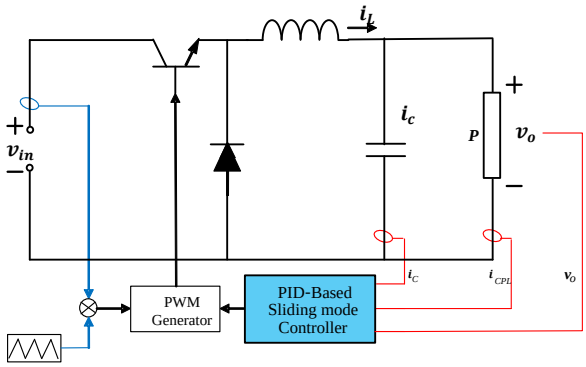

Figure 2. Schematic diagram of the buck converter with a constant power load controlled by the third-order SMC.

III. KEY RESULTS

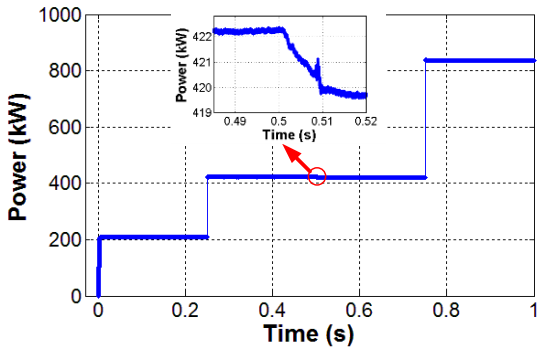

Figure 3. Load power waveform with its detail while load shedding and DC link voltage drop.

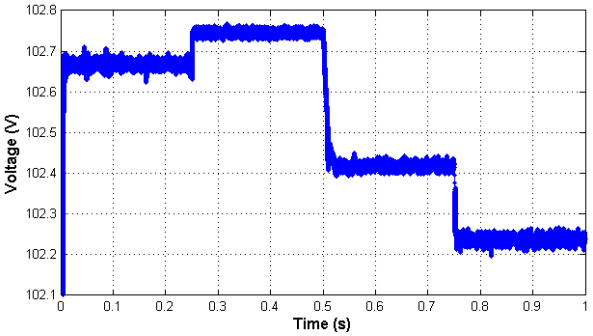

Figure 4. The load voltage response during step changes in load power and DC link voltage drop.

Understanding Power System Oscillations Using Time-Domain Simulations

Alicia Allen
Department of Electrical and Computer Engineering, University of Texas at Austin, Austin, TX 78756, USA,
Email: *aliciajallen@gmail.com*

***Abstract*— Synchronous generators within an interconnected, dynamic power system produce electromechanical oscillations which can be analyzed to reveal the state of the power system. The most recent analysis consists of real-time estimation of modal frequencies, damping, and the mode shape. However, because power systems in the real world are so large it is difficult to obtain data to study and understand how these electromechanical oscillations arise. It is simpler first to study a simulation of a small power system that can be manipulated to create conditions similar to events occurring on the grid. This poster presents such a power system simulation in order to better understand electromechanical oscillations and analyze the state of the system based on the measured oscillations. The two-area power system simulation is developed in PSCAD/EMTDC and is based on [Kundur]. The two areas comprise a weak system and are separated by a long transmission line, with two synchronous generators and a large load located in each area. Analysis of the simulation output is completed in MATLAB. One type of analysis is used to determine the state of the power system, or system stability. A ring down analysis (Prony Analysis) is used to estimate modal frequencies and damping for transient events such as a generating unit trip or step-increase in load. The accuracy of these methods is also examined.**

I. KEY EQUATIONS

For the ring down analysis, the k^{th} mode in the measured signal can be represented as the following equation:

$$y(k) = \sum_{i=1}^{L} A_i e^{\sigma_i k} \cos\left(2\pi f_i \cdot k + \theta_i\right) \qquad (1)$$

II. KEY FIGURES

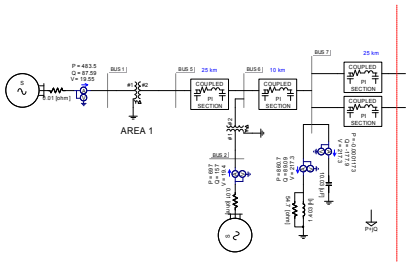

Figure 1. Area 1 of Two-Area Test System

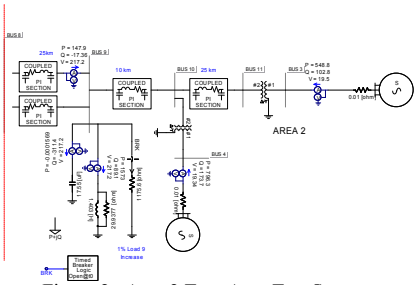

Figure 2. Area 2 Two-Area Test System

III. KEY RESULTS

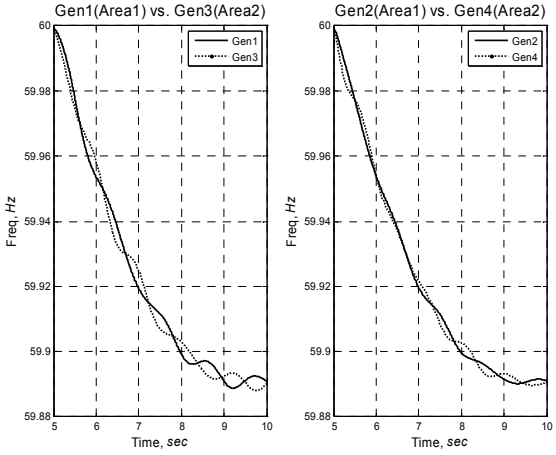

Figure 2. Frequency drop caused by 2.5% step increase in load

Table 1. Prony analysis results on Gen1 Frequency signal show modal frequency and damping (α)

Amplitude	θ	α	Modal Freq
0.0373	0.1028	-0.3011	0.1321

An Enhanced Hybrid State Estimator for Wide Area Monitoring of Power Systems

Markos Asprou and Elias Kyriakides
KIOS Research Center, Department of Electrical and Computer Engineering, University of Cyprus, Nicosia, Cyprus,
Email: asprou.markos@ucy.ac.cy *and* elias@ucy.ac.cy

***Abstract*— Synchronized measurement technology (SMT) is rapidly deployed in power systems, finding applications in many functions of the Supervisory Control and Data Acquisition System (SCADA). The incorporation of synchrophasors provided by the Phasor Measurement Units (PMUs), in the state estimation process has great impact on the state estimator accuracy improvement. In this paper, the incorporation of synchronized measurements in the state estimator (along with the existing conventional measurements) is examined. As a result, a hybrid state estimator that incorporates pseudo power flow measurements is presented. The performance of the estimator is assessed and compared to the conventional state estimator as well as to other hybrid state estimators proposed in the literature.**

I. KEY EQUATIONS

The guiding equations of the proposed state estimator are:

$$J(\mathbf{x}) = [\mathbf{z} - \mathbf{h}(\mathbf{x})]\mathbf{R}^{-1}[\mathbf{z} - \mathbf{h}(\mathbf{x})] \quad (1)$$

$$\mathbf{x}^{k+1} = \mathbf{x}^{k} + [\mathbf{G}(\mathbf{x}^{k})]^{-1}\mathbf{H}^{T}(\mathbf{x}^{k})\mathbf{R}^{-1}[\mathbf{z} - \mathbf{h}(\mathbf{x}^{k})] \quad (2)$$

$$P_{ij_{pseudo}} = V_i I_{ij} \cos(\theta_i - \theta_{ij}) \quad (3)$$

$$Q_{ij_{pseudo}} = V_i I_{ij} \sin(\theta_i - \theta_{ij}) \quad (4)$$

The equation used for the state estimator performance indicator is:

$$\sigma_s^{\,2} = \frac{1}{M}\sum_{i=1}^{M}\sum_{k=1}^{N}(\mathbf{x}(k) - \hat{\mathbf{x}}(k)_{(i)})^2 \quad (5)$$

II. KEY FIGURES

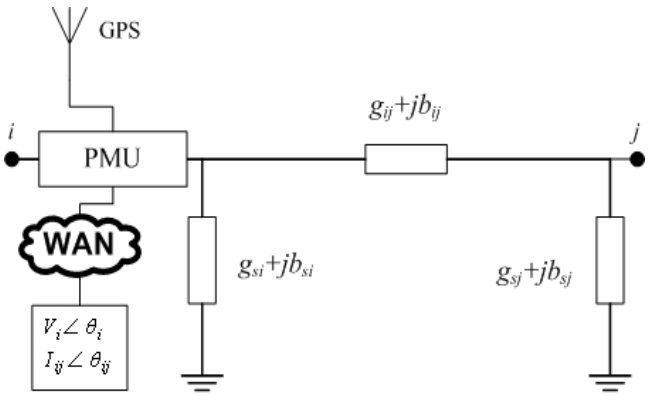

Figure 1. Transmission line representation in a pi model

III. KEY RESULTS

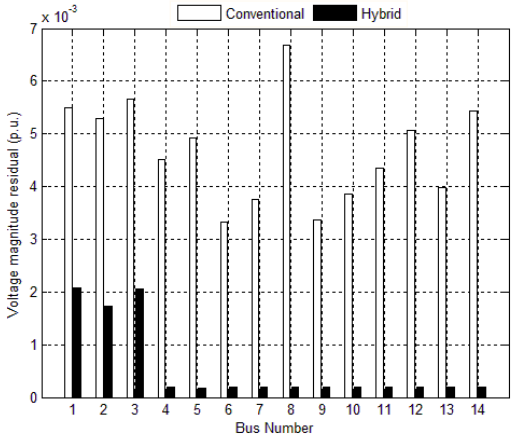

Figure 2. Voltage magnitude residuals for IEEE 14 bus system

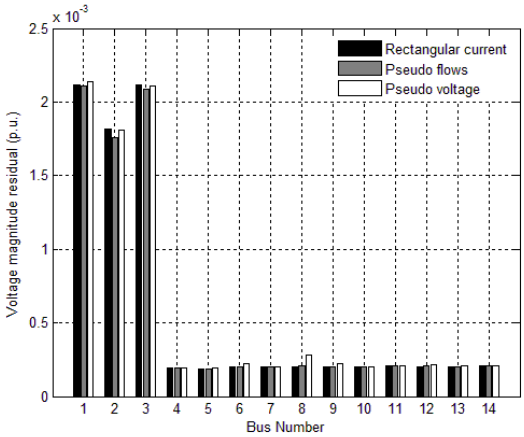

Figure 3. Voltage magnitude residuals for IEEE 14 bus system

TABLE I
PERFORMANCE OF HYBRID STATE ESTIMATORS USED IN THE IEEE 14, 30 AND 118 BUS TEST SYSTEMS

Type of estimator	IEEE 14 bus system	IEEE 30 bus system	IEEE 118 bus system
Hybrid using rectangular form of currents	$1.5929\text{x}10^{-5}$	$4.0782\text{x}10^{-5}$	$6.8610\text{x}10^{-4}$
Hybrid using pseudo flows	$1.5637\text{x}10^{-5}$	$4.1309\text{x}10^{-5}$	$6.8774\text{x}10^{-4}$
Hybrid using pseudo voltage	$1.5823\text{x}10^{-5}$	$4.8669\text{x}10^{-5}$	$7.092\text{x}10^{-4}$

Electromechanical Mode Estimation Validation using Recursive Residual Whiteness Testing

Zheng Cao, Luke Dosiek, and John W. Pierre

Department of Electrical and Computer Engineering, University of Wyoming, Laramie, WY 82071, USA
Email: zcao@uwyo.edu and pierre@uwyo.edu

Abstract: The electromechanical modes, which are described by their frequency, damping and shape of the oscillation, are important in the stability property of a power system. Therefore, it is always important to monitor the system in real time and obtain an estimate of the modes. One method for estimating the modes is to use an AR(Autoregressive) model to model the system and apply the RLS(Recursive Least-Squares) algorithm to update the estimates. Validating the mode estimation, or showing that the estimated modes are reasonable given the data, is an equally important problem.

One method of testing the validity of the estimated modes is to examine if the residual prediction errors resulting from the RLS are white. In this poster, a way of recursively updating an estimate of the whiteness of the residuals is presented. If the residuals are not white, then it is an indicator that the estimated electromechanical modes are not valid, or at least not accurate enough. The results in this poster are presented for a 17-machine model of the western North American power grid and for actual measurement data from WECC.

I. KEY EQUATIONS

The guiding equations for mode estimation validation are:

$$\hat{y}(k \mid \underline{\theta}) = -\sum_{i=1}^{n} a_i y(k-i) \quad (1)$$

$$E(k) = y(k) - \hat{y}(k \mid \underline{\theta}) \quad (2)$$

$$\hat{\theta}(t) = \arg\min_{\underline{\theta}} \sum_{k=n+1}^{t} \lambda^{t-k} \varepsilon^2(k \mid \underline{\theta}) \quad (3)$$

$$\hat{R}_{\varepsilon}(t,\tau) = \lambda \hat{R}_{\varepsilon}(t-1,\tau) + (1-\lambda)\varepsilon(t)\varepsilon(t-\tau) \quad (4)$$

II. KEY FIGURES

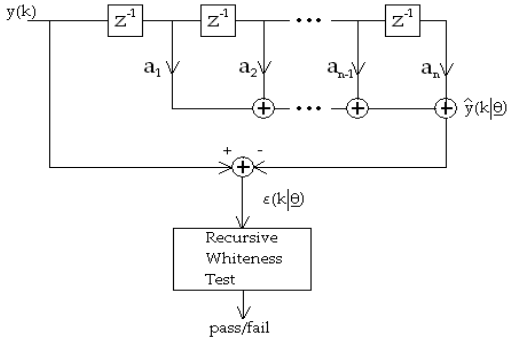

Figure 1. AR Model and Whiteness Testing

III. KEY RESULTS

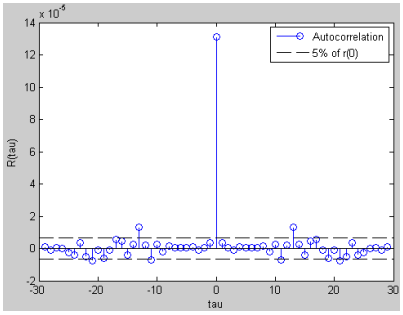

Figure 2. Too low of an order(n=10) and not white, demonstrated by some terms being above the threshold

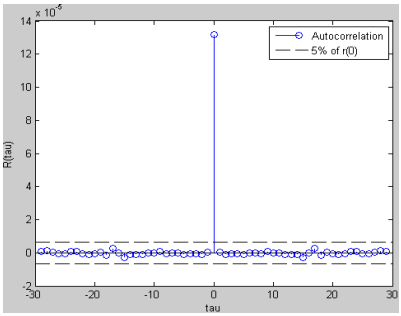

Figure 3. Appropriate order(n=30) and white

A Predictive Out of Step Protection Scheme based on PMU enabled Dynamic State Estimation

Evangelos Farantatos, *Student Member, IEEE*, Renke Huang, *Student Member, IEEE*, George J. Cokkinides, *Senior Member, IEEE*, and A. P. Meliopoulos, *Fellow, IEEE*

***Abstract*— In this paper, a dynamic state estimator (DSE) is initially presented that can capture with high fidelity the electromechanical dynamics of the system. The described DSE is performed in a decentralized way, on the substation level based on local measurements which are globally valid. The substation based DSE uses data from relays, PMUs, meters, FDRs etc in the substation only, thus avoiding all issues associated with transmission of data and associated time latencies. This approach enables very fast DSE update rate which can go up to more than 60 executions per second. The state is defined as the collection of the voltage phasors at each bus of the system and is extended to include internal states (algebraic or dynamic) of the devices, for example the torque angle and the rotor speed of a generator or the magnetic flux linkage of a transformer.**

In this paper we also propose a predictive out of step protection scheme which is based on an energy approach. Specifically, stability monitoring is performed on the basis of Lyapunov Energy functions and Lyapunov direct method. The total energy of a generator that experiences a fault is monitored continuously as the sum of its kinetic and potential energy based on the DSE results. For a clearing time t_c, if the total generator energy is less than the peak (barrier) value of its potential energy then the system is stable. If the total energy becomes higher than the barrier value then instability is detected. Thus monitoring of the trajectory of the total energy as the disturbance is evolving can lead to the calculation of the exact time that the system loses its synchronism and becomes unstable, and as a result provides us with the exact time that the out of step relay should trip the generator.

I. KEY EQUATIONS

DSE: min $J(x,y)=\eta^T W\eta$

where: $\eta = z - h(x,y)$, (1)

$$W = diag\left[\frac{1}{\sigma_v^2}\right].$$

The best estimate of the system state is obtained from the Gauss-Newton iterative algorithm:

$$\hat{x}^{j+1} = \hat{x}^j + (H^T W H)^{-1} H^T W (z_a - h(\hat{x}^j)), \quad (2)$$

Out of Step Relaying Application: The potential energy and the kinetic energy of the generator can be calculated as:

$$E_{potential} = \int_{\delta_s}^{\delta} \left(P_{e\_post}(\delta(t)) - P_m\right) d\delta \quad (3)$$

$$E_k = \frac{1}{2} M \omega^2(t)$$

II. TEST SYSTEM

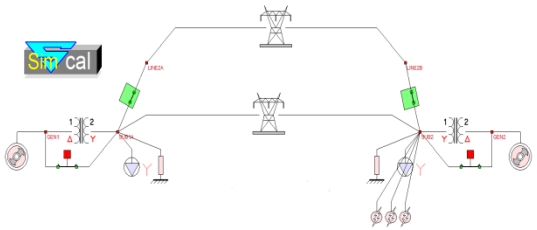

Fig. 1. One-line diagram of the two unit test system.

III. KEY RESULTS

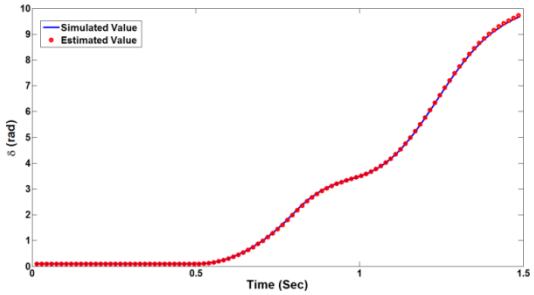

Fig. 2. Generator Estimated and Simulated Torque Angle

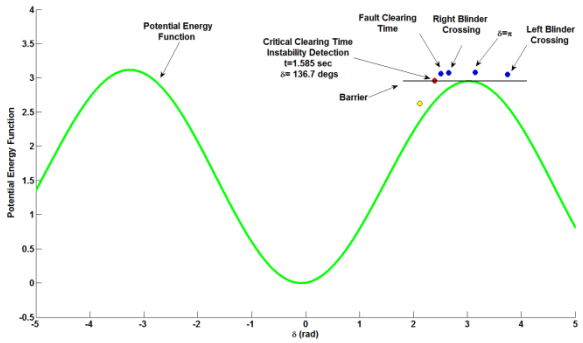

Fig 3: Proposed Out of Step Protection Scheme-Total and potential energy trajectory of the system.

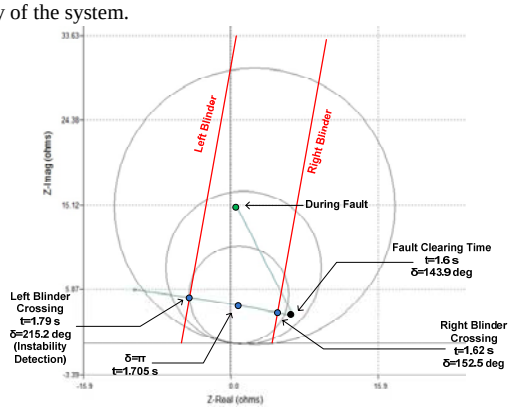

Fig 4: Comparison of proposed method with present protection schemes

A synchrophasor based distribution system state estimator for increased observability and control

Daniel A. Haughton Gerald T. Heydt
Arizona State University, Tempe, AZ 85280
Email: {dhaughto; Heydt} @asu.edu

Abstract— Present distribution systems often lack the level of observability and infrastructure needed to enable more sophisticated levels of visualization and control as envisioned in a Smart Grid. A synchrophasor based distribution state estimator (DSE) is proposed to enhance the level of visualization, automation and operational control at the distribution level. The DSE process is an analog to state estimators in transmission networks, but the mathematical formulation and measurement vectors have been modified to facilitate a more robust calculation procedure and include new measurement technologies into distribution systems. By taking synchronized phasor measurements across distribution systems, network visualization, power flow control, energy management and demand-side response functions, fault location and system reconfiguration are more easily facilitated. Enhancing the level of sensory data enables the development of applications that are consistent with the vision for a Smarter Grid. Technical details of the DSE and sample results are presented.

I. KEY EQUATIONS

$$hx = z + \eta \tag{1}$$

$$r = hx - (z + \eta) \tag{2}$$

$$\frac{\partial}{\partial x}(r^t r) = 0 \tag{3}$$

$$\hat{x} = h^+ z \tag{4}$$

When the state estimation formulation is developed using synchrophasors based complex quantities,

$$r^H r = (z_r - h_r x_r + h_i x_i + \eta_r)^2 + (z_i - h_i x_r - h_r x_i + \eta_i)^2. \tag{5}$$

$$\frac{\partial}{\partial x_r} r^H r = 0 \qquad \frac{\partial}{\partial x_i} r^H r = 0 \tag{6}$$

$$\begin{bmatrix} \hat{x}_r \\ \hat{x}_i \end{bmatrix} = \begin{bmatrix} h_r & -h_i \\ h_i & h_r \end{bmatrix}^+ \begin{bmatrix} z_r \\ z_i \end{bmatrix} + \begin{bmatrix} h_r & -h_i \\ h_i & h_r \end{bmatrix}^+ \begin{bmatrix} \eta_r \\ \eta_i \end{bmatrix} \tag{7}$$

$$h = \begin{bmatrix} [U] & -[Y_{bus}] \\ [0] & [U] \\ [U] & [0] \\ [h_{LM}] & [0] \end{bmatrix} \tag{8}$$

$$\hat{x} = \begin{bmatrix} \hat{I} \\ \hat{V} \end{bmatrix}, \qquad z = \begin{bmatrix} [0_{state}] \\ [V_{meas}] \\ [I_{meas}] \\ [I_{line}] \end{bmatrix}, \tag{9}$$

II. KEY FIGURES

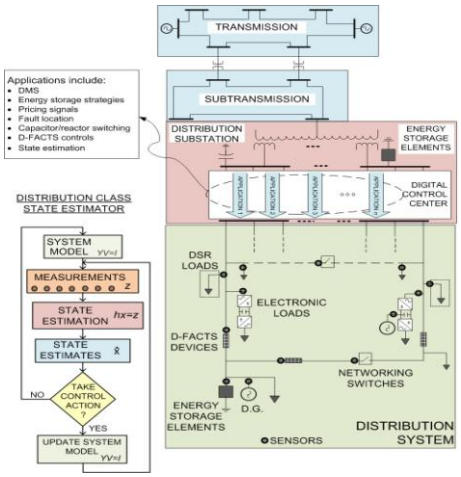

Figure 1. The distribution class state estimator in a Smart Grid

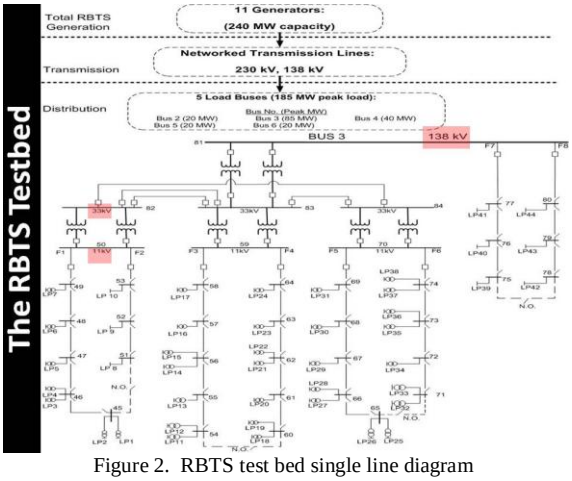

Figure 2. RBTS test bed single line diagram

III. KEY RESULTS

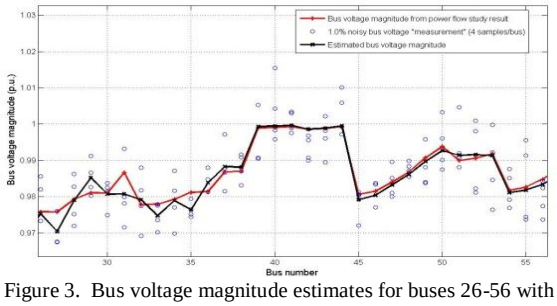

Figure 3. Bus voltage magnitude estimates for buses 26-56 with 1.0% pseudorandom noise in the measurement vector

A Flexible Integrated Phasor System Design for PMU Data Concentrating

Xinyu Tony Jiang, Jeff Hui, and Joe H. Chow
Department of Electrical, Computer, and Systems Engineering, Rensselaer Polytechnic Institute, Troy, NY 12180, USA,
Email: *jiangx4@rpi.edu*, *huij@rpi.edu* and *chowj@rpi.edu*

***Abstract*— Recently, many utility companies have been adding phasor measurement capabilities to their systems, and with this comes the need for phasor data concentrator (PDC) systems for collecting and processing phasor data. Some of the challenges that a PDC system has to address include support for different phasor streaming protocols, ease of configuration and data access, and efficient storage and retrieval of phasor data.**

In this poster, we present a PDC design, called the Flexible Integrated Phasor System (FIPS), to provide a flexible and open source solution for independent system operators and transmission owners to collect and access their phasor data (Fig. 1). FIPS is being developed for the Linux platform and supports common phasor streaming formats such as IEEE C37.118 and IEEE 1344. The system uses a XML format to define all its data sources, destinations, and how data is routed between the sources and destinations. Control of FIPS and access to the stored data are both provided through a web-based interface (Fig. 2).

Due to the high sampling rate and time series nature of phasor measurements, FIPS has an integrated database system that stores the phasor data as binary files. Data from each phasor channel is stored as a series of files, with each file containing a specified time span of data (Fig. 3). The data is stored in strictly sorted order according to timestamp and thus can be retrieved efficiently using a binary search algorithm. FIPS uses a MySQL database to store phasor channel metadata and to look up the location of phasor data binary files during data retrieval requests.

The first FIPS will be deployed on New York Power Authority (NYPA)'s phasor network. In this application, FIPS will store data from up to 25 PMUs and forward selected phasor data to PDCs outside of NYPA.

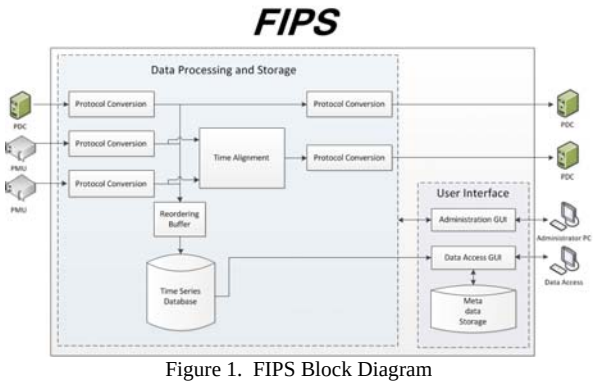

Figure 1. FIPS Block Diagram

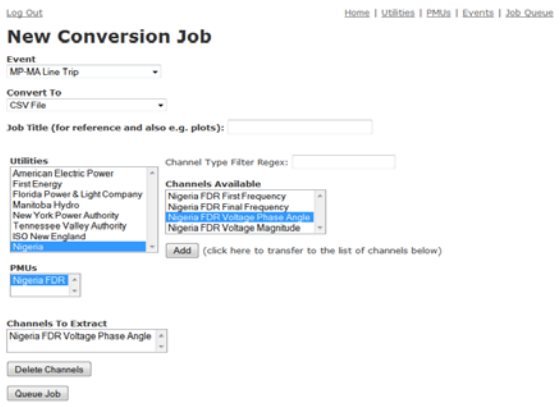

Figure 2. FIPS Web-based Data Access Interface

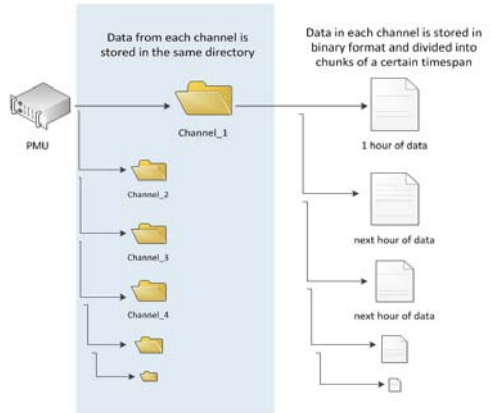

Figure 3. FIPS Data Storage Organization

Scalable Integrated Situational Awareness Systems for Smart Grids

Bipul Luitel and Ganesh K. Venayagamoorthy
Real-Time Power and Intelligent Systems Laboratory, Department of Electrical and Computer Engineering, Missouri University of Science and Technology, Rolla, MO 65409, USA,
Email: iambipul@ieee.org and gkumar@ieee.org

***Abstract*— It is important to monitor different components of a smart grid for situational awareness and predictive state estimation. As the size of the power system in smart grid increases, the number of components and variables to be monitored also increases, which makes the problem of predictive state estimation challenging. Neural networks have been successfully shown to be able to predict the speed deviations of generators and bus voltages in the power system. Different neural networks have been used to independently predict these signals for situational awareness. However, traditional approaches to neuro-identification of power system parameters are not scalable and start to show performance degradation as well as become computationally infeasible for practical implementation in a large system. Cellular neural networks (CNN) are more scalable forms of neural networks which utilize 'divide and conquer' strategy to solve a large problem. Each cell of the CNN consists of a simultaneous recurrent neural network connected to the neighboring cells in such a way that it accurately represents the connectivity of the actual components in a smart grid. In this work, an integrated approach to situational awareness is proposed where a single cellular neural network is used for both speed deviation as well as bus voltage identification. The CNN is implemented in a parallel hardware platform such as CPU/GPU cluster in order to benefit from its inherent concurrency and thus reducing computational complexity.**

I. EQUATIONS

Equations (1) and (2) show outputs of a typical cell in a CNN used for integrated situational awareness system. Consider *Area 1* in Fig. 1, the speed deviation is predicted using (1). As seen in (2), speed deviation and bus voltage are coupled through V_{ref1} which propagates across the network through other cells as shown by (3). *Wi* and *Wo* are the input and output weights of a speed network and *Vi* and *Vo* are that of the voltage network.

$$\hat{\omega}_1(t+1) = f\left(V_{ref1}, \omega_1(t), \hat{\omega}_2(t), \hat{\omega}_4(t), Wi_1(t), Wo_1(t)\right) \quad (1)$$

$$\hat{V}_1(t+1) = f\left(V_{ref1}, V_1(t), \hat{V}_5(t), Vi_1(t), Vi_1(t)\right) \quad (2)$$

$$\hat{V}_5(t+1) = f\left(V_5(t), \hat{V}_1(t), \hat{V}_6(t), Vi_5(t), Vo_5(t)\right) \quad (3)$$

II. FIGURES

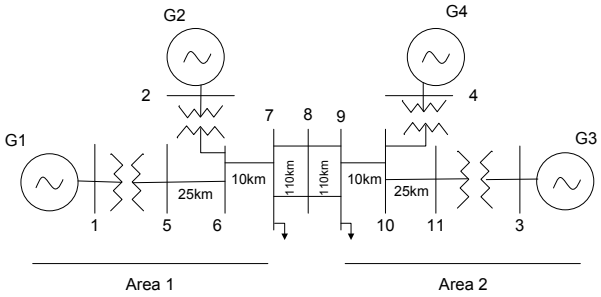

Fig 1. Two-area four-machine system

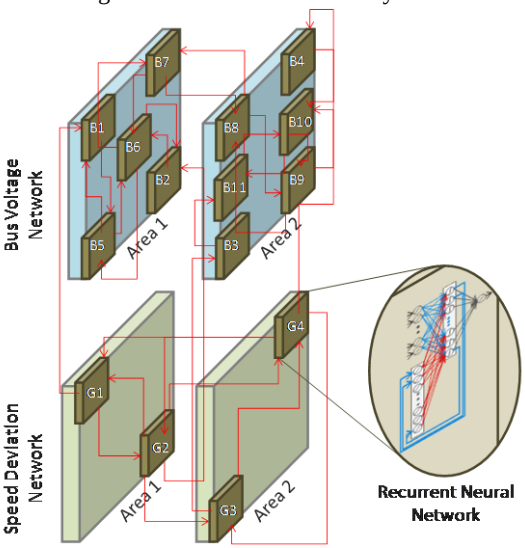

Fig 2. Cellular neural networks implementation of an integrated situational awareness system for a two-area four-machine system. Vertical cross-section separates different areas and horizontal cross section separates different networks (voltage, speed etc.).

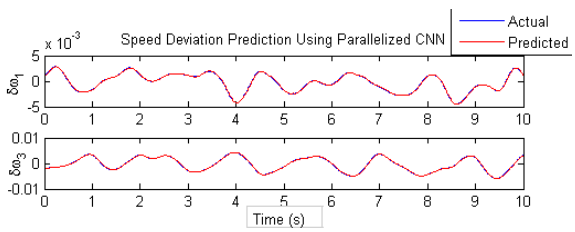

Fig 3. Preliminary results obtained for generator speed deviation predictions using cellular neural networks implemented on a CPU cluster.

Fast Out-Of-Step Detection in Large Power System Using State Plane Analysis

Binod Shrestha, Rama Gokaraju and Mohindar Sachdev
Department of Electrical and Computer Engineering, University of Saskatchewan, Saskatoon, SK. Canada
Email: *bis094@mail.usask.ca, rama.krishna@usask.ca and sachdev@sasktel.net*

***Abstract*— Disturbances in power system cause oscillation in machine rotor angles and result in stable or unstable power swing. Power swing can cause unwanted relay operation at different network location, which can aggravate further the power system disturbances and possibly leads to cascading outages and power blackouts. Such a loss will have a huge economic and social impact. Instability detection for operational reliability hence carries major importance especially when it is a large power system. This work proposes a new fast and accurate out-of-step detection technique for large power system based on state plane analysis (SPA). Using SPA, power system dynamics is represented by trajectories so that its mathematical model is replaced by a simple graphical plot, known as state plane trajectories. With the help of these trajectories during and after disturbance, stability limits is predicted with reduced computational effort resulting faster power swing detection. An algorithm is hence developed using SPA and is implemented to detect instability based on wide area measurement. The proposed approach performs online coherency analysis to group the generators into two critical clusters after the disturbance happens in the system. Two groups of generator are then reduced to OMIB equivalent system and the instability is determined using proposed algorithm. Whenever the two equivalent areas lose synchronism, out-of-step tripping is carried out on the critical lines at which the system is separating. An additional logic using state plane of the derivative of state variables is introduced to detect multi-swing instability in the system and tested with the multi-swing cases. The approach is tested in IEEE 39 bus test system using electromagnetic transient simulation tool (PSCAD™). Test results have shown that the proposed technique is robust, fast, accurate and computationally efficient so that it can easily be implemented in a numerical relay.**

I. Key Equations

The motion of partial centers of angles of group 'A' and group 'S' as shown in figure 2 is described by Eq. 1 and 2.

$$M_s\ddot{\delta}_s = \sum_{l\in s} P_{ml} - P_{el} \tag{1}$$

$$M_a\ddot{\delta}_a = \sum_{k\in a} P_{mk} - P_{ek} \tag{2}$$

One machine infinite bus (OMIB) equivalent of two-machine system is obtained using following relations.

$$\delta \triangleq \delta_s - \delta_a \tag{3}$$

$$M\ddot{\delta} = P_m - (P_c + P_{max}\sin(\delta - \gamma)) \tag{4}$$

where,

$$M = \frac{M_a M_s}{M_T},\quad M_T = \sum_{i=1}^{n} M_i \tag{5}$$

$$P_m = (M_a \sum_{l\in s} P_{ml} - M_s \sum_{k\in a} P_{mk}) M_T^{-1} \tag{6}$$

$$P_e = (M_a \sum_{l\in s} P_{el} - M_s \sum_{k\in a} P_{ek}) M_T^{-1} \tag{7}$$

State plane representation of OMIB equivalent system is given by Eq. 8.

$$\begin{bmatrix}\dot{\delta}\\ \dot{\omega}\end{bmatrix} = \begin{bmatrix}\omega\\ P'_m - P'_c - P'_{max}\sin(\delta - \gamma)\end{bmatrix} \tag{8}$$

II. Figures

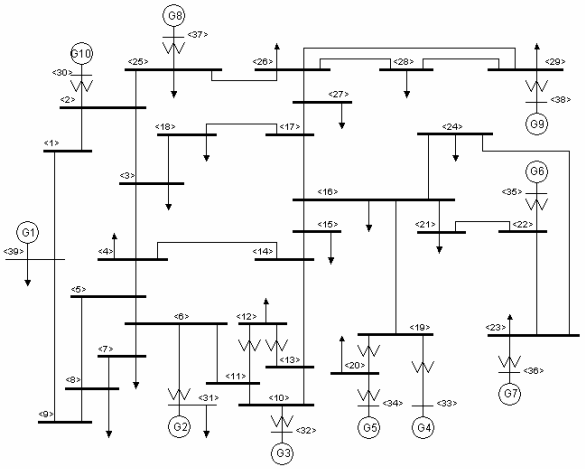

Figure 1. IEEE 10 machines 39 buses New England test system

Figure 2. Equivalent two-machine system

Multi-channel methodology for a system wide measure of complex dynamics in power systems

Ralph Wilson and Sanjeev Srivastava
The Center For Advanced Power Systems, Florida State University, Tallahassee, FL 32310, USA,
Email: rbw07@fsu.edu and sanjeev@caps.fsu.edu

***Abstract*— Power systems are dynamical systems whose structure consists of a network of interdependent components. Some of these components may exhibit nonlinear behavior. It has increasingly been seen that certain nonlinear behaviors are responsible for various faults and failures. More recently, researchers in the field of complex systems have begun to further understand the multiple interactions of dynamical systems on a network, as well as emergence of nonlinear dynamics on networks. In the past, measures of "statistical complexity" have been proposed as a tool for the investigation and characterization of dynamical components. Previous work has examined time series dynamics of single components, and characterized their complexity. We now look at extending the methodology to a system wide measure. The original methodology was based on using a single variable measurement and using it to reconstruct a state space for the component. The extension of this methodology will involve constructing a "global" state space from each components which will constitute the state space of the entire system. Similar methodologies have been used to study EEG dynamics in the brain. Power systems are particularly well suited for such analysis, as they do not suffer from the measurement difficulties that EEG data do. Global entropy and complexity will be examined. The work will be motivated by the development of complexity measures to quantify the impact of additional non-linear elements and behaviors on power systems.**

I. Key Ideas

The time-delay embedding methodology takes a time series $X=\{x_1, x_2, .. x_N\}$ consisting of N scalar measurements, and creates *m*-dimensional vectors as

$$X_n = \left\langle x_n, x_{n+\tau}, x_{n+2\tau} \ldots x_{n+(m-1)\tau} \right\rangle \qquad (1)$$

where τ is an integer called the "time lag". *m* is called the embedding dimension. In general, if the measurements taken from the system are not scalars, but vectors consisting of measurements from each component, we may create a "multi-embedding", where we construct vectors of these vectors, each with their own time lag, and embedding dimension. The vectors constructed as such lie in a reconstructed state space where geometric structure corresponds to the behavior of the various components in the system.

We will define the following as the basis of our calculations with reconstructed time series. Given a reconstructed vector X_i, define

$$C_i^m(r) = \{\text{number of } X_j \mid d(X_i, X_j) \le r\}$$

where $d(X_i, X_j)$ is the maximum of the component-wise differences between X_i and X_j.

From this, we can approximate the family of Renyi entropies. For instance, for a system with n distinct states that are a state space partition of into hypercubes of size ε, the i^{th} state having probability $p_i(\varepsilon)$, the Renyi entropy of order μ is given as

$$H_\mu(X,\varepsilon) = \frac{1}{1-\mu}\log\sum_{i=1}^{n} p_i(\varepsilon)^\mu \qquad (2)$$

with (μ>0). It can be shown that as $\mu \to 1$, $H_\mu(X) \to H(X)$, the Shannon entropy. $H_\mu(X)$ may be approximated by

$$H_\mu(X,\varepsilon) \approx \frac{1}{1-\mu}\log\left(\frac{1}{N_0}\sum_{i=1}^{N_0}\left(\frac{1}{N_0}\sum_{j\neq i}^{N_0}(C_j^m(r))\right)^{\mu-1}\right)$$

, where r= ε/2.

The ApEn statistic is a simplification of this, first proposed by Pincus,

$$ApEn(m,r) = \phi^{m+1}(r) - \phi^m(r) \qquad (3)$$

where

$$\phi^m(r) = \frac{1}{N_0}\sum_{i=1}^{N_0}\log C_i^m(r). \qquad (4)$$

Our past research has modified this so that it is a measure of complexity which is a nonlinear function of entropy. This measure will be extended to the multichannel methodology.

PMU-Based Monitoring of Rotor Angle Dynamics

Jie Yan, *Student Member, IEEE* Chen-Ching Liu, *Fellow, IEEE* Umesh Vaidya, *Member, IEEE*

***Abstract*— On-line monitoring of rotor angle stability in wide area power systems is an important task to avoid out-of-step instability conditions. In recent years, the installation of Phasor Measuremnt Units (PMUs) on the power grids has increased significantly and, therefore, a large amount of real-time data is available for on-line monitoring of system dynamics. This poster proposes a PMU-based application for on-line monitoring of rotor angle stability. A technique based on Lyapunov exponents is used to determine if a power swing leads to system instability. The relationship between rotor angle stability and Maximal Lyapunov Exponent (MLE) is established. A computational algorithm is developed for the calculation of MLE in an operational environment. The effectiveness of the monitoring scheme is illustrated with a 200-bus system model.**

I. KEY THEORY

MLE Stability Criterion: Consider a continuous-time dynamical system and assume that all Lyapunov exponents are nonzero. Then the steady state behavior of the system consists of a fixed point. Furthermore, if the MLE is negative, then the steady state behavior is an attracting fixed point.

II. KEY FIGURES

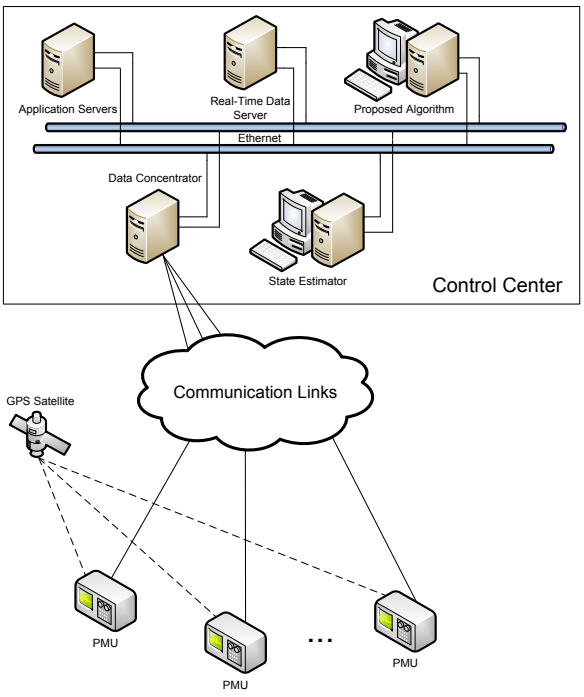

Fig. 1 Concept for monitoring of rotor angle stability

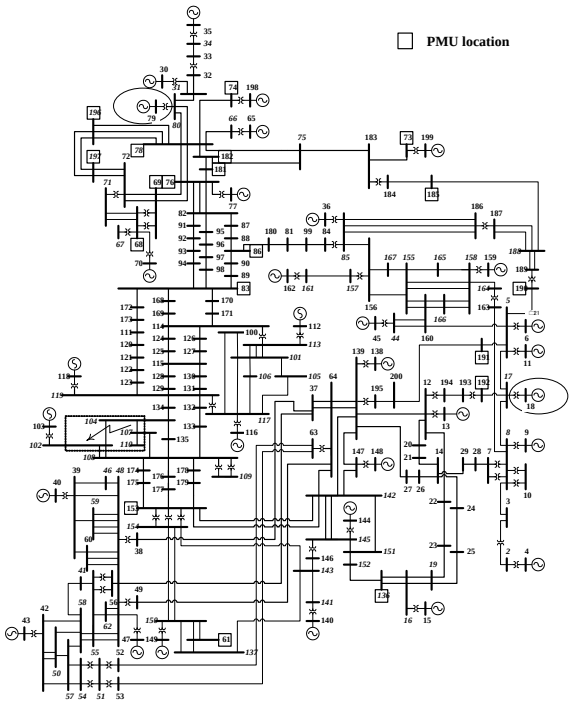

Fig. 2 A 200-bus system

III. KEY RESULTS

Table I
Simulation results of 200-bus system

3-phase fault	Clearing	Time-domain simulation result	$\lambda_{t=5}$
Bus 18	Generator 18	unstable	0.2958
Bus 30	Generator 30	unstable	0.1421
Bus 35	Generator 35	unstable	0.1559
Bus 36	Generator 36	unstable	0.4526
Bus 40	Generator 40	stable	-0.1588
Bus 43	Generator 43	stable	-0.0964
Bus 45	Generator 45	unstable	0.4102
Bus 47	Generator 47	stable	-0.0816
Bus 65	Generator 65	unstable	0.1164
Bus 70	Generator 70	unstable	0.1065
Bus 32	Line 32-31	unstable	0.2782
Bus 64	Line 64-142	stable	-0.1049
Bus 74	Line 74-78	unstable	0.4460
Bus 83	Line 83-168	stable	-0.0434
Bus 104	Line 104-102	stable	-0.3635
Bus 108	Line 108-174	stable	-0.3144
Bus 114	Line 114-171	stable	-0.1026
Bus 119	Line 119-131	stable	-0.1919
Bus 122	Line 122-123	stable	-0.2977
Bus 145	Line 145-151	stable	-0.3150

Quantification of Emission Reduction from Electricity Network with the Integration of Renewable Resources

M. A. Abdullah, A. P. Agalgaonkar, and K. M. Muttaqi
Integral Energy Power Quality and Reliability Centre, School of Electrical, Computer and Telecommunications Engineering, University of Wollongong, Wollongong, New South Wales, 2522, Australia,
Email: maa267@uowmail.edu.au

***Abstract*— Integration of renewable energy resources into the electricity network is one of the strategies for overall emission reduction in the network. The quantification of emission offset from renewable distributed generation (DG) needs to be incorporated in planning to assess the effectiveness of integrating these resources from emission reduction perspective. In this paper, a numerical method is proposed for quantifying the emission reduction from distribution network with the integration of renewable resources by examining the coincident hours between the time varying nature of load and generation. The factors influencing annual emission reduction are also identified along with the use of energy curtailment strategy for emission reduction. Embodied emissions for energy from grid and renewable DG systems are also used for quantification of overall emission reduction. The proposed methodology has been tested on a practical distribution network and results are presented.**

I. KEY EQUATIONS

The major equations for quantification of emission reduction from integration of renewable resources into the electricity network are:

$$E_{Total}(h) = E_{Grid}(h) + E_{DG}(h) \quad (1)$$

$$E_{Total}(h) = \alpha_{Grid} \times W_{Load}(h) - \left(\alpha_{Grid} - \alpha_{DG}\right) \times \varphi(h) \times {}^{DG}P_{cap} \quad (2)$$

$$E_{reduction}(h) = \left(\alpha_{\text{Grid}} - \alpha_{\text{DG}}\right) \times \varphi(\text{h}) \times {}^{\text{DG}}\text{P}_{\text{cap}} \quad (3)$$

$$\text{Re}duction = \left(\frac{\alpha_{\text{Grid}} - \alpha_{\text{DG}}}{\alpha_{\text{Grid}}}\right) \times \left(\frac{\sum_{\text{h}} \varphi(\text{h})}{\sum_{\text{h}} \text{W}_{\text{Load}}(\text{h})}\right) \times {}^{\text{DG}}\text{P}_{\text{cap}} \quad (4)$$

$$W_{Curt}(h) = \left(\varphi(h) \times {}^{DG}P_{cap} - \lambda_{curtl} \times W_{Load}(h)\right) \times H\left(h, {}^{DG}P_{cap}\right) \quad (5)$$

$$\text{Re}duction = \left(\frac{\alpha_{Grid} - \alpha_{DG}}{\alpha_{Grid}}\right) \times \frac{\sum_{h}\left\{\varphi(h) \times {}^{DG}P_{cap} - W_{Curt}(h)\right\}}{\sum_{h} W_{Load}(h)} \quad (6)$$

II. KEY FIGURES

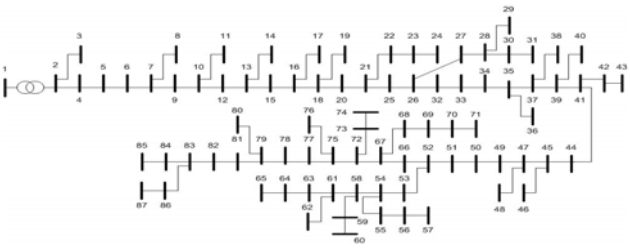

Figure 1. Test System

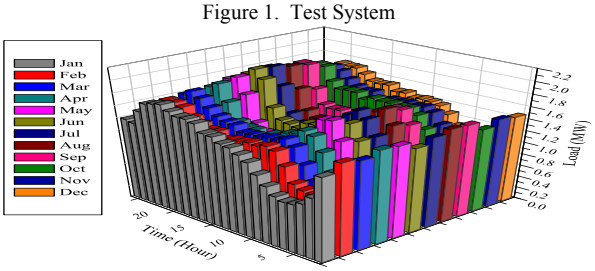

Figure 2. Average Daily Load Curve for a Year

III. KEY RESULTS

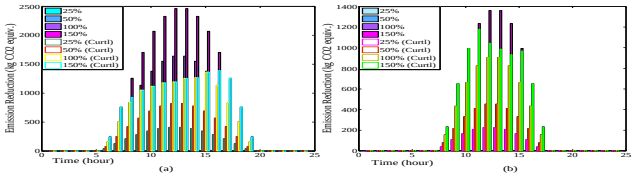

Figure 3. Average Hourly Emission Reduction from Solar PV Generation System with and without Energy Curtailment Strategy for: (a) January, and (b) July

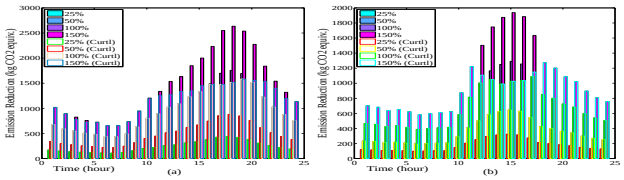

Figure 4. Average Hourly Emission Reduction from Wind Energy Conversion System with and without Energy Curtailment Strategy for: (a) January, and (b) July

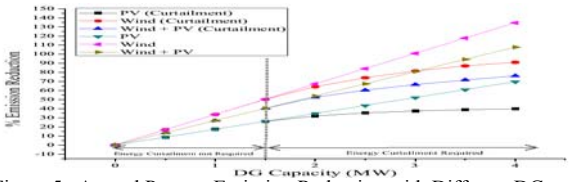

Figure 5. Annual Percent Emission Reduction with Different DGs

Railway power supply investment decisions considering the voltage drops – assuming the future traffic to be known – an MINLP formulation

Lars Abrahamsson and Lennart Söder
School of Electrical Engineering, Division of Electric Power Systems, Royal Institute of Technology (KTH), Teknikringen 33, SE 100 44 Stockholm, Sweden, Email: lars.abrahamsson@ee.kth.se and lennart.soder@ee.kth.se

***Abstract*— A fast approximator that uses aggregated railway power supply system information has been developed. The approximator studies the impacts of voltage drops on the traffic flow. The weaker the power system and the heavier the traffic, the greater the voltage drops. And the greater the voltage drops, the more limited the maximal attainable tractive force on the locomotives. That approximator is in this paper used as a constraint in a railway power supply system investment decision program, where investment decisions are assumed to be realized immediately, and there is no preexisting power supply system to consider. The traffic forecasts are in this first approach assumed to be perfect. Previously, a similar model has been presented as a DNLP program, a program class that does not allow binary variables. Therefore, a reformulation of the program to an MINLP program has been made. This stepwise creation of the planning program makes evaluating it easier.**

I. Key Equations

The space limits of this extended abstract would not allow printing the equations for calculating the number of trains in traffic for each power section using binary variables. Those equations constitute a great proportion of the contributions of this work. In Figure 1, it is however shown an example of what these equations do.

Other important equations are the two suggested alternative operating cost equations related to voltage-drop caused reduced tractive effort of electric trains:

$$OC = \sum_{a_d} (130 - v(a_d)) \tag{1}$$

$$OC = \sum_{a_d} t(a_d)\,(130 - v(a_d)) \tag{2}$$

where t denotes the number of trains in a power section, and v the average velocity of trains in that power section.

II. Key Figures

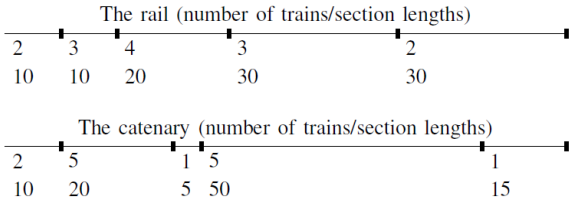

Figure 1. An illustration of how the numbers of trains in the rail sections are converted over to the number of trains in the power sections. First respective rows represent the number of trains, whereas the second rows represent the section lengths in km. Vertical lines represent train stops and electrical connections respectively.

III. Key Results

$c(a_v)$ [km]	$d(a_d)$ [km]	$v(a_d)$ [km/h]	$t(a_d)$ [train units]
104.4	104.4	123.4	10.8
283.7	179.3	123.4	4.9
388.6	105.0	123.4	10.7
466.0	77.4	123.4	12.9
576.6	110.6	123.4	10.3
725.1	148.5	123.4	7.3
N/A	174.9	123.4	5.2

Table I. Results using cost function (1)

$c(a_v)$ [km]	$d(a_d)$ [km]	$v(a_d)$ [km/h]	$t(a_d)$ [train units]
95.7250	95.7250	124.6138	10.0580
300.0000	204.2750	120.3964	5.9420
389.3315	89.3315	124.7296	10.4220
458.5422	69.2107	125.3178	11.2864
549.0499	90.5077	124.7266	10.3334
715.7898	166.7399	122.0082	7.3266
N/A	184.2102	121.3268	6.6315

Table II. Results using cost function (2)

Student Friendly Economic Dispatch Problem Analysis Toolbox in Power System

Most. Nahida Akter and A. B. M. Nasiruzzaman
Department of Electrical and Electronic Engineering, Rajshahi University of Engineering & Technology, Rajshahi, 6204, Bangladesh
Email: nahidalaboni@gmail.com and nasiruzzaman@ieee.org

Abstract— **Economic dispatch is one of the most challenging problems of power system. The Genetic Algorithm (GA) based solution techniques are more promising than other techniques due to its capability of global searching, robustness, and it does not require derivative information. Here we present a genetic – fuzzy based toolbox for solving economic dispatch problem based on MATLAB GUI. The toolbox is built with undergraduate students keeping in mind. Thermal power plants with second order cost function model can be simulated. Comprehensive help file is provided to help understand student's basic concepts of optimal dispatch, GA and fuzzy logic based optimization problem.**

I. KEY EQUATIONS

The guiding equations are very basic:

$$C_t = \sum_{i=1}^{n} \alpha_i + \beta_i P_i + \gamma_i P_i^2 \quad (1)$$

$$P_{i(\min)} \le P_i \le P_{i(\max)} \quad i = 1, 2, ..., n \quad (2)$$

$$P_i = \frac{P_i^{\max} - P_i^{\min}}{2^{bit} - 1} \quad (3)$$

$$f = \frac{1}{1 + \dfrac{P_D - P_L - \sum_{i=1}^{n} P_i}{P_D}} \quad (4)$$

II. KEY FIGURES

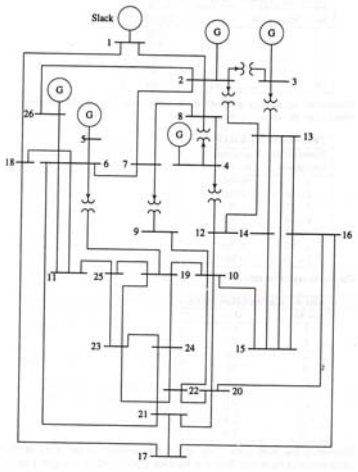

Figure 1. Test System-26 Bus Power System

III. KEY RESULTS

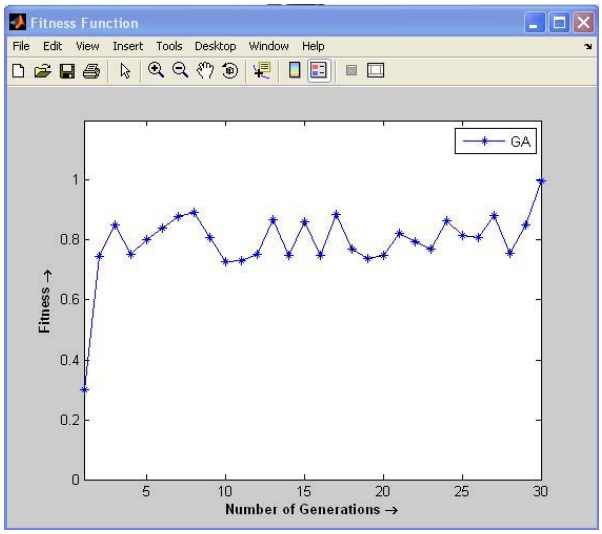

Figure 3. Fitness function vs. Generation

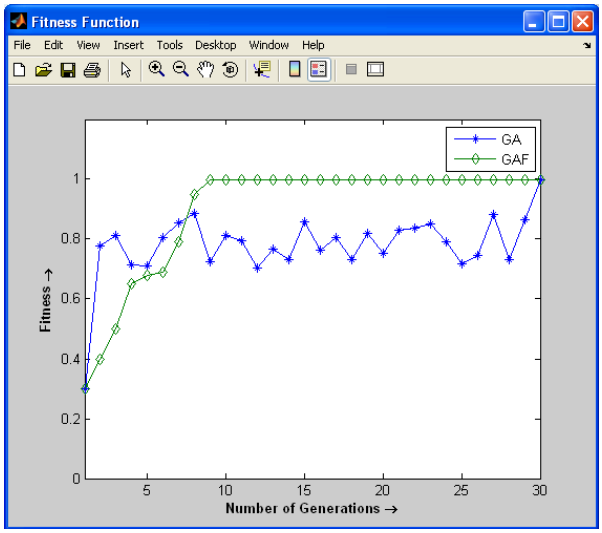

Figure 3. Comparison of Convergence in GA and GA-Fuzzy Algorithms

Techniques for Improving Precision and Construction Efficiency of a Pattern Classifier in Composite System Reliability Assessment

Bordin Bordeerath and Panida Jirutitijaroen
Department of Electrical and Computer Engineering, National University of Singapore, 119077, Singapore,
Email: *elebordi@nus.edu.sg* and *elejp@nus.edu.sg*

Abstract— **Pattern Classifiers have been widely utilized to improve computational efficiency in composite power system reliability assessment using Monte Carlo simulation. Construction of a classifier for reliability assessment demands sufficient amount of training vectors so that success and failure states can be effectively differentiated. The traditional way to obtaining such training vectors is to sample the states in accordance with their original distributions. This leads to the requirement of a large number of training vectors to construct an effective classifier; and, this number grows even larger for a highly reliable system. Additionally, a highly imbalanced set of training vectors, i.e. number of success states are much more than that of failure states, can lower efficiency of a classifier. On the other hand, an obtained classifier may not be able to classify the states with acceptable level of precision. This paper proposes the techniques to address the aforementioned issues. The first technique is based on worsening system reliability to obtain balanced amount of success and failure states for training patterns. This technique enhances construction efficiency of a classifier in general and also solves imbalance issue. The second is based on relaxed decision boundary which is used to improve precision of general classifiers. Various case studies are conducted on IEEE-RTS 79 in order to justify the proposed techniques. Results show that the proposed techniques outperform traditional methodologies in terms of both precision and construction efficiency of a classifier.**

I. KEY FIGURES

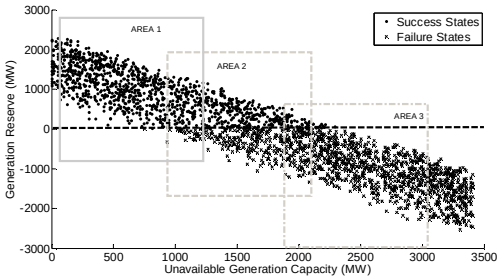

Figure 1. Sampled areas of different methodologies

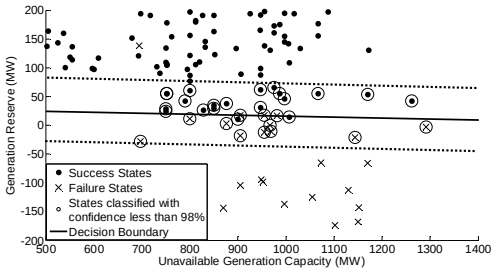

Figure 2. Relaxed decision boundary

II. KEY RESULTS

TABLE I
ACCURACY COMPARISON OF CASE 1: 2 DIMENSIONAL SPACE

Indices	Traditional Decision Boundary	Relaxed Decision Boundary
TP	99,870	99,880
TN	130	120
FP	7	0
FN	16	6
NMR	12.3077 %	5 %
OMR	0.023 %	0.006%

TABLE II
ACCURACY COMPARISON OF CASE 2: 4 DIMENSIONAL SPACE

Indices	Traditional Decision Boundary	Relaxed Decision Boundary
TP	99,868	99,862
TN	132	138
FP	59	0
FN	9	3
NMR	6.8182 %	2.1739 %
OMR	0.068 %	0.003 %

TABLE II
COMPARISON OF RELIABILITY INDICES

Indices	SQ-MC	NSQ-MC	Proposed NSQ-MC
LOLP	0.001251	0.001274	0.001250
EENS (MWh/yr)	1216.014	1263.12	1288.95
LOLF (occ./yr)	2.550725	2.608509	2.440011
LOLD (hr/occ.)	4.288428	4.374379	4.320063

Pollutant Emission Modeling for Sustainable Water Delivery

Timothy H Carter[1], Stephen S. Miller[2], Ian A. Hutt[2], Caisheng Wang[3], Shawn P. McElmurry[1], and Carol J. Miller[1]

[1]Department of Civil & Environmental Engineering, Wayne State University, Detroit, MI
[2]Commonwealth Associates Inc., Jackson, MI
[3]Department of Engineering Technology, Wayne State University, Detroit, MI

***Abstract*— This poster presents the development of a model that links electric power consumption to associated pollutant emissions as a function of time throughout the day. The model is applied to the task of sustainable water transmission and distribution for large urban areas. The price of electricity at a particular location (i.e. the Locational Marginal Price or LMP) is used to determine the type of electric generator that is "on the margin" at any given time. The marginal unit is the generator that will be affected by changes in electric power demand. Pollutant emission factors for each type of power generator are obtained using data available from the US Environmental Protection Agency (EPA). Thus, the model is used to predict changes in emissions based on an incremental change in electric power consumption. When input into control algorithms for water distribution networks, this model can be used to shift pumping loads to account for an optimal reduction in pollutant emissions. The pilot study has been conducted for the Detroit Water and Sewerage Department network where electric power dispatch is controlled by the Midwest Independent System Operator (MISO). Historical power generation data is used to validate the approach. While sustainable water delivery is the primary goal of this research, the model will have applications across all fields for anyone who wishes to reduce environmental impact associated with electric power consumption.**

I. Key Equations

The guiding equations of the pollutant model are:

$$LMP_i = \lambda_{REF} - \sum_{n=1}^{N} \mu_n \phi_{ni} + (\frac{1}{PF_i} - 1)\lambda_{REF} \quad (1)$$

$$HR = \frac{E_{input}}{E_{Output}} \quad (2)$$

$$C_{avg} = \sum_{i=1}^{n} C_i * \frac{Q_i}{Q_T} \quad (3)$$

$$MC_{avg} = HR_{avg} * C_{avg} \quad (4)$$

II. Key Figures

Figure 1. Map of U.S. Power Markets

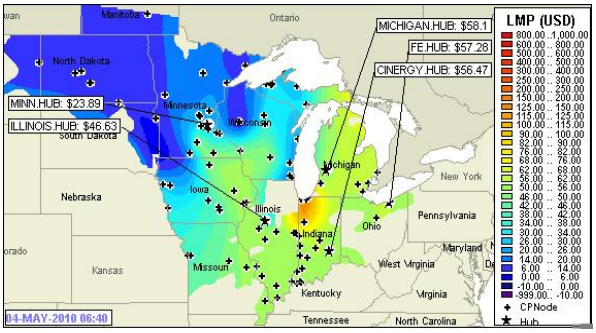

Figure 2. MISO Real-time LMP Map

III. Key Results

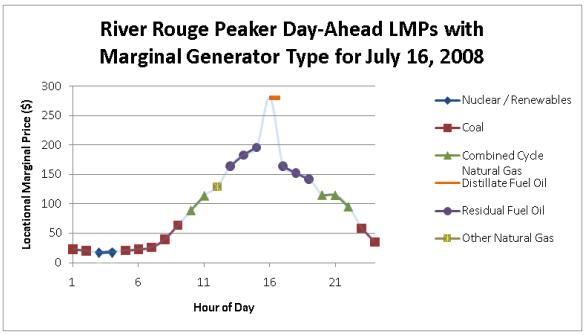

Figure 3. LMP curve for the River Rouge Peaker with marginal generator types for July 16, 2008.

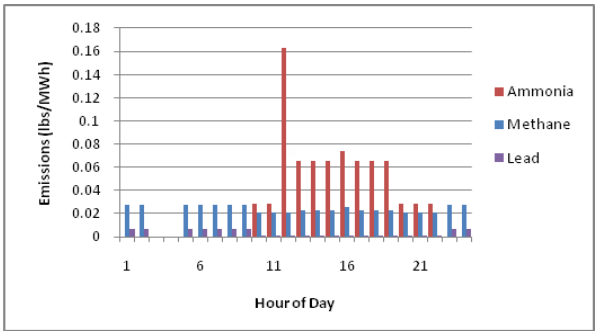

Figure 4. Estimated emissions of three toxic pollutants (NH_3, CH_4, and Pb) for the marginal generator unit type as a function of time based on hourly averaged historical day-ahead LMPs for the River Rouge Peaker on July 16, 2008.

Determination of Critical Sensitivity Indices for Large Scale Solar PV Investment Models

Indrajit Das, Wajid Muneer, Claudio Canizares and Kankar Bhattacharya
Department of Electrical and Computer Engineering, University of Waterloo, Waterloo, ON N2L 3G1, Canada,
Email: idas@uwaterloo.ca , wmuneer@uwaterloo.ca , ccanizares@uwaterloo.ca and kankar@uwaterloo.ca .

Abstract **– Large scale solar photovoltaic (PV) generation is now a viable, economically feasible and clean energy supply option. Lucrative incentive schemes, such as the Feed-in-Tariff (FIT) in Ontario, have in recent times, attracted large scale investments in solar PV generation. In a previous work [1], the authors have presented an investor-oriented planning model for optimum selection of PV investment decisions. In this research, a method for determining the critical Sensitivity Indices (SI) for the solar PV investment model is proposed. The proposed method is based on the application of Duality Theory on the Karush-Kuhn-Tucker (KKT) optimality conditions of the optimization model. The advantage of this model is that the indices are simultaneously determined for all the model parameters using a single step approach. A case study is carried out for the province of Ontario, based on a GAMS & MATLAB model, which maximizes the Net Present Value (NPV) of an investor's profit in solar PV generation and allows to determine the SIs of the model parameters with respect to the objective function.**

KEY EQUATIONS

Optimization Model:

Maximize: NPV of Solar PV Investments

Subject to the following constraints:

- Supply Demand Balance
- Energy Generation from Solar PV sources
- Line Flow Limits
- Power Angle Limits
- Dynamic Constraint on PV Capacity Addition
- Annual Budget Limit
- Total Budget Limit

Sensitivity Indices Model:

$$Max\ z = f(x,a)$$
$$\text{s.t.: } h(x,a) = b : \lambda$$
$$g(x,a) \le c : \mu$$

Assuming parameter $p = [a\ b\ c]^T$, the SI's can be computed using:

$$(\nabla_x f(x,p))^T dx + (\nabla_p f(x,p))^T dp - dz = 0$$

$$(\nabla_x h(x,p))^T dx + (\nabla_p h(x,p))^T dp = 0$$

$$(\nabla_x g_j(x,p))^T dx + (\nabla_p g_j(x,p))^T dp = 0; \forall\, j \in J; \mu_j \neq 0$$

$$\big(\nabla_{xx} f(x,p) + \textstyle\sum_k \lambda_k \nabla_{xx} h_k(x,p) + \sum_j \mu_j \nabla_{xx} g_j(x,p)\big)dx +$$
$$\big(\nabla_{xp} f(x,p) + \textstyle\sum_k \lambda_k \nabla_{xp} h_k(x,p) + \sum_j \mu_j \nabla_{xp} g_j(x,p)\big)dp +$$
$$\nabla_x h(x,p)d\lambda + \nabla_x g(x,p)d\mu = 0;\ \ \forall\, j \in J;\ \forall\, k \in l$$

KEY RESULTS

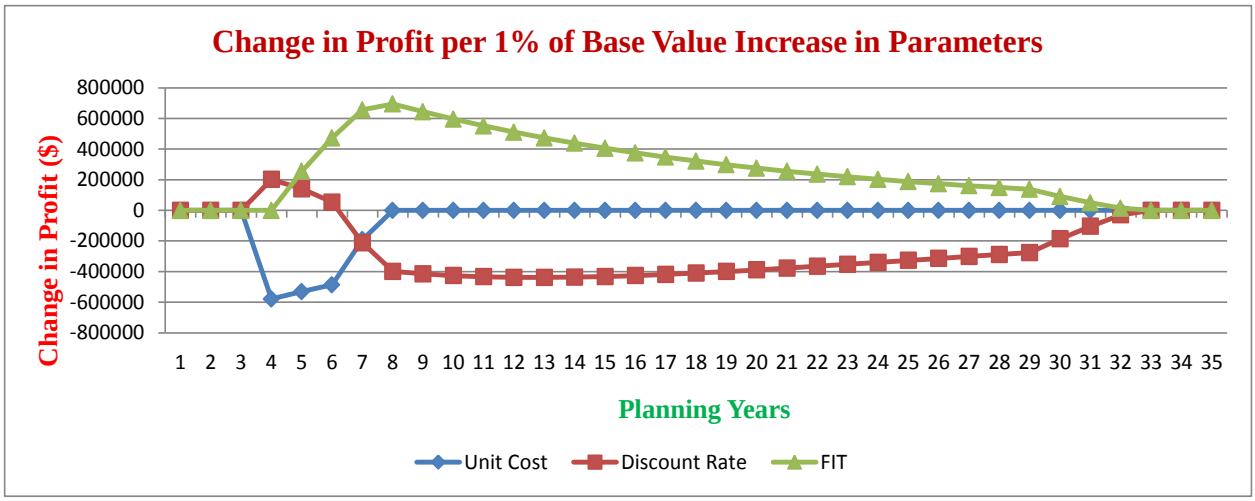

Figure 1: Comparison of Sensitivity Indices of various significant parameters

[1] W. Muneer, K. Bhattacharya, C. Canizares, 'Large-Scale Solar PV Investment Models, Tools and Analysis: The Ontario Case', IEEE Transactions on Power Systems, in print.

Campus-Wide Power Infrastructure: Preliminary Study into Smart Grid Application

Andrew Drees
Department of Electrical and Computer Engineering, Michigan Technological University, Houghton, MI 49931, USA,
Email: amdrees@mtu.edu

Abstract— **A sweeping system improvement known as the smart grid offers the campus the automated system that it needs. The smart grid vision proposes to install intelligent electronic devices (IEDs) into the campus electrical distribution system. The IEDs would then rely on the existing University communications backbone. Utilization of these IEDs is an important step to making the power system become transparent. Transparency allows system operators to quickly identify problems and get accurate meter readings at the accuracy and speeds only a computer can offer. However, if any upgrade is to succeed first a proper examination of current system must be performed. The examination can best be made through the use of a power flow analysis. The power flow analysis provides the foundations and planning insight required to update the existing campus electrical distribution system. Once system operators have a solid foundation from which to work and the communications system has been established the next step is to tie them together by developing a method to visualize all the new data streaming in as clearly, and as quickly as possible. The Michigan Technological University campus offers a unique opportunity for this research as the campus is primarily a micro-grid and would be relatively easy to scale the techniques and practices found here to the greater distribution system.**

I. KEY FIGURES

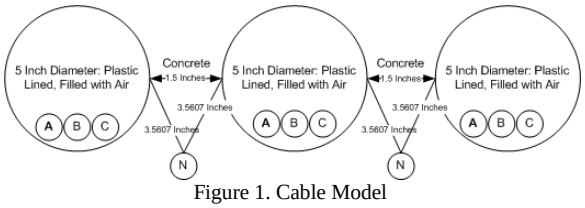

Figure 1. Cable Model

Figure 2.GIS Visualization Diagram

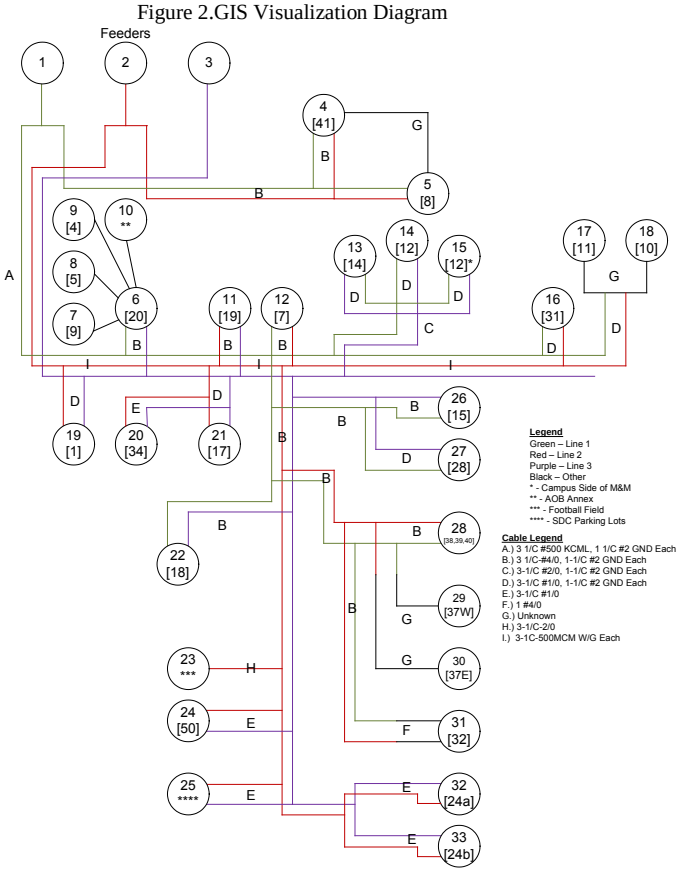

Figure 3.Campus One-Line Diagram

Reliability Assessment of Cyber-Physical Power Systems

Bamdad Falahati and Yong Fu
Department of Electrical and Computer Engineering, Mississippi State University, Mississippi State, 39762, USA
Email: *bf229@msstate.edu*, *fu@ece.msstate.edu*

Abstract—A cyber-power system, as a type of cyber-physical systems, contains two interconnected infrastructures: a power network and a cyber network. The cyber network has been employed for monitoring, protecting and controlling the power network. Without the cyber network, the efficient and reliable operation of the power network is actually unattainable. The interdependency generally means that the correct and appropriate operation of one element depends on existence and proper function of some elements. This paper studies the cyber-power interdependencies in smart grids and categorizes interdependencies between cyber and power networks.

In this paper two types of interdependencies are defined. One is the Element-Element interaction which is for the interaction between elements interconnected between cyber and power networks. The other is Network-Element interaction which evaluates the impact of the performance of one network on the element in other network. The proposed classification permits to assess adverse effects of failures in cyber network on the power network operation. The proposed reliability assessment method is applied for a micro grid in five different scenarios and results are compared.

I. Key Equations

Reliability Evaluation formulation:

$$Order(\Phi_i) = \sum_{j=1}^{n_E} \varphi_{i,j}$$

$$p_i = \prod_{j=1}^{n_E} A_j^{(1-\varphi_{i,j})} U_j^{\varphi_{i,j}}$$

$$U_j = 1 - A_j = \frac{E\lambda_j}{E\lambda_j + E\mu_j}$$

Optimization problem formulation for the cyber network:

$$Minimize \quad \sum_{k=1}^{n_R}\sum_{i=1}^{n_L} \zeta_{i,k}$$

Subject To:

$$\sum_{i=1}^{n_G} S_{i,k} = \sum_{i=1}^{n_L} D_{i,k} - \sum_{i=1}^{n_L} \zeta_{i,k}$$

$$\sum_{j=1}^{n_N} \beta_{ij} \times \delta_{j,k} = S_{i,k} - D_{i,k} + \zeta_{i,k} \qquad 0 \le \zeta_{i,k} \le 1$$

$$\zeta_i = \text{int}\left(\sum_{k=1}^{n_R} \zeta_{i,k} \Big/ n_R \right)$$

II. Key Flowchart

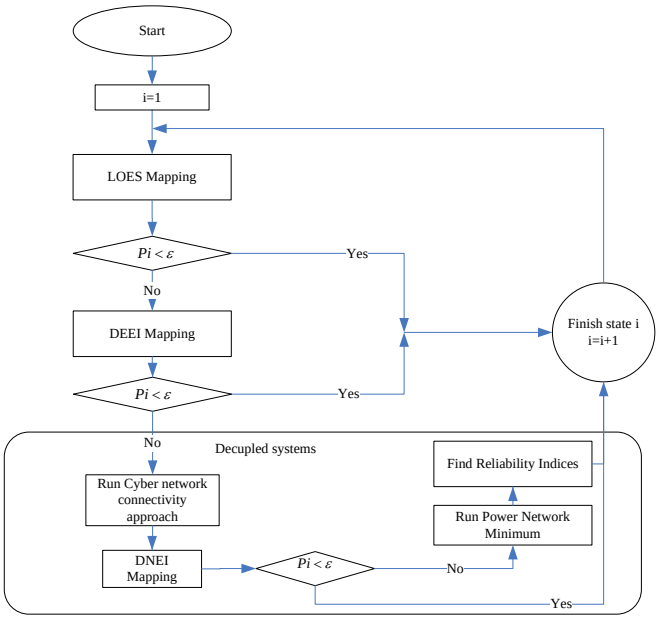

Fig. 1. Reliability assessment procedure

III. Key Results

TABLE I
RELIABILITY RESULTS OF A MICRO GRID

No	Scenario	LOLP	EENS(p.u)
1	Failure in the power system	0.0321	0.03252
2	Failure in controllers	0.07788	0.08
3	Failure in communication network	0.27663	0.3498
4	Failure in the controllers and power system	0.1075	0.1116
5	Failure in the communication network and power system	0.2988	0.3723

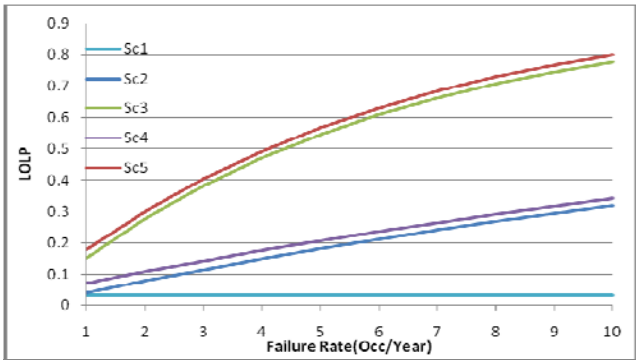

Fig. 2. LOLP of the cyber-power system vs failure rates

Dual-tree M-band Wavelet Transform and Composite Very Short-term Load Forecasting

Che Guan[1], *Student Member, IEEE,* Peter B. Luh[1], *Fellow, IEEE,* Wen Cao[2], Laurent D. Michel[1], Kwok Cheung[3], *Senior Member, IEEE*

1. Department of Electrical and Computer Engineering, University of Connecticut, Storrs, CT 06269-2157, USA,
2. Stern School of Business, New York University, NY 10012, USA,
3. Alstom Grid, Redmond, WA 9805, USA,

Email: che.guan@engr.uconn.edu

***Abstract*— Very short-term load forecasting predicts the load over one hour into the future in five-minute steps. Accurate load forecasting is critical for automatic generation control and resource dispatch. A method of multiple-level neural networks trained by hybrid Kalman filters has been presented to capture the complicated features of the load components. However, it is hard to decompose the load into appropriate frequencies. In this paper a method of dual-tree M-band wavelet neural networks trained by hybrid Kalman filters is further developed. It decomposes the load into several frequency components with uniform bandwidths. To reduce computation complexity, these components are grouped. Separate neural networks trained by hybrid Kalman filters are applied to capture different features of individual grouped components, and results are combined. To generate better forecasting results, multiple load forecasting methods needs the integration of their results. A composite forecast is developed to deliver a mixing prediction. For methods which are based on Kalman filters and have covariance matrices on the forecast load, these dynamic covariance matrices are used for the combination. Otherwise, static covariance matrices derived from historic forecasting accuracy are used for the combination. Individual variances are then estimated and approximated combined to construct the final confidence interval. Testing results demonstrate the effects of the dual-tree M-band wavelet decomposition and the accuracy of the composite forecasting based on ISO New England data.**

I. Key Equations

To generate better forecasting results, multiple load forecasting methods needs the integration of their results, a composite forecast is developed to mix multiple methods for VSTLF with CI estimation:

$$\Lambda_j(t) = N\{z(t); \hat{z}_j(t \mid t-1), S_j(t)\}, \quad (1)$$

$$\mu_j(t) = \Lambda_j(t) \cdot \bar{c}_j \Big/ \left(\sum_{j=1}^{3} \Lambda_j(t) \cdot \bar{c}_j\right),$$

$$where \ \ \bar{c}_j = \sum_{j=1}^{3} p_{ij}\mu_i(t-1),\ j = 1,2,3, \quad (2)$$

$$\hat{z}(t+1 \mid t) = \sum_{j=1}^{3} \mu_j(t) \cdot \hat{z}_j(t+1 \mid t), \quad (3)$$

$$S(t+1) = \sum_{i=1}^{3} \mu_i(t) S_i(t+1), \quad (4)$$

where $z_j(t)$ represents the load, $\mu_j(t)$ is the mixing weight, $\Lambda_j(t)$ is the likelihood functions, and $S_j(t)$ is the covariance matrices with superscript j=1, 2, 3 representing MWNNBP, DMWNNHKF and IMM.

II. Key Figures

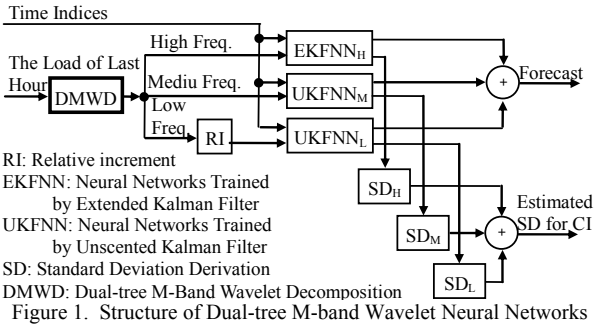

Figure 1. Structure of Dual-tree M-band Wavelet Neural Networks Trained by Hybrid Kalman Filters (DMWNNHKF)

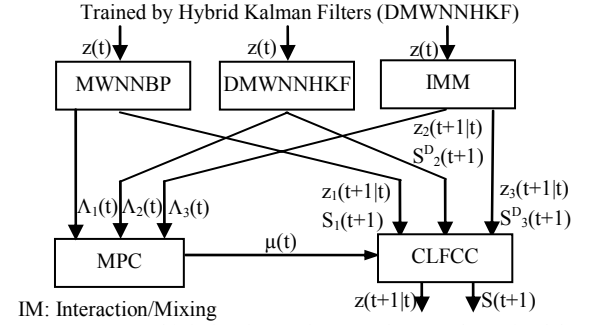

Figure 2. Structure of Composite Forecasting with Confidence interval Estimation (Integrating MWNNBP, DMWNNHKF & IMM)

III. Key Results

Composite Forecasting Effectively Integrating MWNNBP, DMWNNHKF and IMM

min.	MAE (MW)	MAPE (%)	His. SD (MW)	Est. SD (MW)	One-σ Coverage (%)
5	16.64	.1136	17.08	30.72	86.10
10	24.84	.1687	26.35	43.59	85.19
15	31.26	.2118	33.44	53.33	84.18
20	36.98	.2505	40.34	62.94	84.62
25	42.70	.2883	47.24	71.23	83.84
30	48.72	.3285	54.00	79.77	83.15
35	54.92	.3691	61.65	89.13	82.92
40	61.55	.4134	69.32	98.33	82.37
45	68.31	.4571	76.45	107.68	82.26
50	74.73	.4998	83.16	116.20	81.71
55	81.38	.5442	90.05	125.66	81.82
60	87.89	.5875	96.93	134.57	81.43

The Impact of Integrating Distributed Generation on the Losses in the Smart Grid

Yiyun Guo, Yufeng Lin and Mingjie Sun
University College London, London, WC1E 6BT, United Kingdom,
Xiamen Electric Power Industry Bureau, Xiamen, 361004, China,
Email: yiyun.guo.10@ucl.ac.uk , yflin@eee.hku.hk and smj821121@163.com

***Abstract*— The impact of distributed generation (DG) on losses is of great interest in the smart grid research area. This paper analyses how DG locations, automatic voltage controls, generator types, and the operating modes of DG devices impact on the losses of a distribution system. The topology of the grid is selected from the practical distribution network in Xiamen, which is one of the four pilot smart distribution grid cities in China. The Shapley Value method is used to identify each DG device's individual impact on these losses. Results show that the losses are reduced most significantly when the DG devices operate in the constant current and voltage control modes, followed by the power factor control mode. The induction machine bus could increase the losses. In addition, according to the Shapley Values of the DG devices, the individual impacts of DG devices on losses are location-dependent. The method proposed in this paper has been applied to the Xiamen smart grid.**

I. KEY EQUATIONS

The guiding equations of the immune based controller are:

$$X(i)=\sum_{s}\frac{(|s|-1)!(n-|s|)!}{n!}*[V(s)-V(s-i)] \quad (1)$$

II. KEY FIGURES

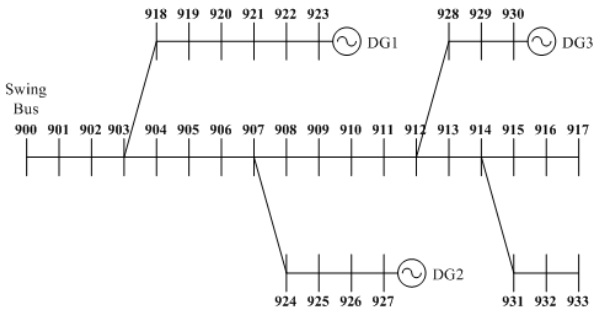

Figure 1. Diagram of the practical Xiamen distribution network.

- Case I: DG devices are connected at the end of the branches 923, 927, 930, respectively.
- Case II: DG devices are connected at the joint points 903, 907, 912 of the distribution grid.

III. KEY RESULTS

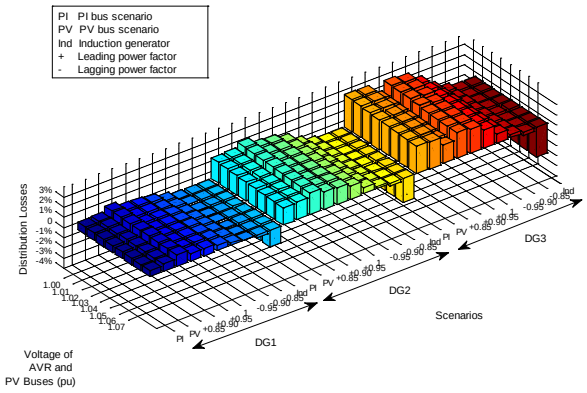

Figure 3. Shapley Values of DG devices in case I.

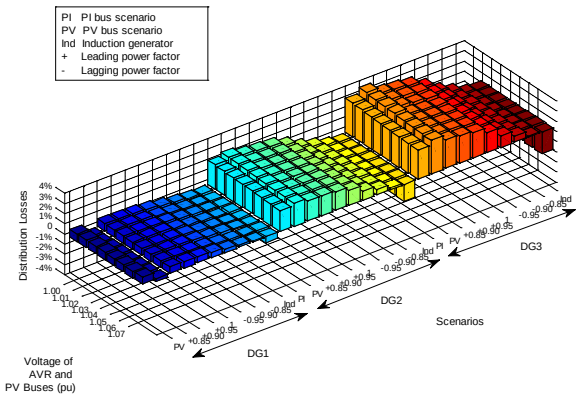

Figure 4. Shapley Values of DG devices in case II.

IV. CONCLUSION

Synchronous machine based DG can reduce losses. The induction machine would cause high losses to the grid.

The lower the AVR setting point, the greater the reduction in losses once DG devices are used.

The losses decrease if the DG devices operate with leading power factors

If the DG devices are installed at the end of the branches, more losses can be reduced.

System Constraints Effects on Optimal Dispatch Schedule for Battery Storage Systems

Jesse Hill, Chika Nwankpa
Department of Electrical and Computer Engineering
Drexel University
Philadelphia, PA 19104
jrh62@drexel.edu nwankpa@ece.drexel.edu

Abstract – As the demand to develop more green and cost efficient means of supplying power to customers grows, we need to look at the solution from another angle. From the customer viewpoint, this paper identifies an efficient manner in which to utilize available resources. These resources include traditional utility sources, renewable solar, and battery storage. This paper looks at how constraints set can affect the optimal solution.

In particular, a distributed generation set-up for a residential customer will have constraints placed on the utilization of the resources and the exact effects of these constraints will be examined for their results on the final solution.

I. KEY EQUATIONS

$$\min \sum_{i=1}^{7} \sum_{j=1}^{24} c_{ij} . * x_{ij} \quad (1)$$

$$s_{ij} + b_{ij} + x_{ij} = l_{ij} \; \forall \, i,j \in Z^{+} \quad (2)$$

$$B_o + \sum_{i=1}^{present} \sum_{j=1}^{present} b_{ij} \leq B_{min} \quad (3)$$

$$B_o + \sum_{i=1}^{present} \sum_{j=1}^{present} b_{ij} \geq B_{max} \quad (4)$$

$$B_o + \sum_{i=1}^{End} \sum_{j=1}^{24} b_{ij} \geq b_o \quad (5)$$

II. KEY RESULTS

Sample Dispatch Schedule			
Time (Hr)	Battery (kWh)	Time (Hr)	Battery (kWh)
1	2.0	13	0.0
2	0.4	14	1.0
3	-0.4	15	-1.0
4	-1.0	16	1.0
5	-1.0	17	-1.0
6	0.0	18	2.0
7	0.0	19	0.4
8	0.0	20	-1.0
9	0.0	21	-1.0
10	0.0	22	1.6
11	0.0	23	-1.0
12	0.0	24	-1.0

Table 1 – Sample Dispatch Schedule

Base Case Data			
Hour	Load (kWh)	Solar (kWh)	LMP ($/kWh)
1	0.565	0	0.0307
2	0.502	0	0.0289
3	0.477	0	0.0282
4	0.467	0	0.0279
5	0.464	0	0.0272
6	0.542	0	0.0288
7	0.761	0	0.0337
8	0.900	0.0293	0.0387
9	0.848	0.1744	0.0414
10	0.859	0.5739	0.0438
11	0.867	0.7543	0.0449
12	0.892	0.8924	0.0458
13	0.921	1.0089	0.0472
14	0.958	0.9726	0.0488
15	0.920	0.8838	0.0484
16	1.074	0.6483	0.0511
17	1.130	0.5275	0.051
18	1.433	0.3597	0.0528
19	1.446	0.0467	0.0514
20	1.294	0	0.0489
21	1.254	0	0.0488
22	1.340	0	0.0496
23	1.224	0	0.0448
24	0.853	0	0.0372

Table 2 – Load, Solar, and LMP Profiles for Base Case

Base Case Simulation Results		
Metric	Do-Nothing	Default Settings
Objective Function	0.9743	0.6138
Switching Operations	N/A	10
Cycles	N/A	5
Savings	N/A	36.96%
Cycles/Savings Ratio	N/A	0.135

Table 3 – Base Case Results

III. KEY FIGURES

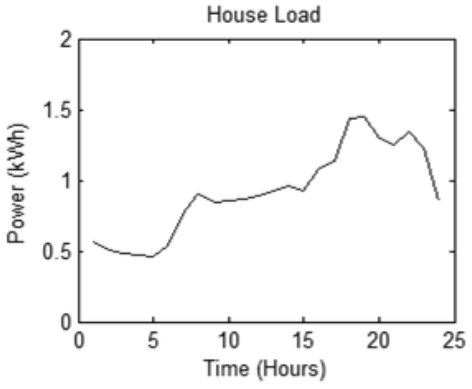

Figure 1 – Residential Customer Load

Heuristic Optimal Restoration Based on Constructive Algorithms for Smart Grids

Qinran Hu, Sarina Adhikari and Fangxing(Fran) Li
The Department of Electrical Engineering and Computer Science, the University of Tennessee (UT), Knoxville, TN 37996, USA,
Email: qhu2@utk.edu, sadhikar@utk.eduand fli6@utk.edu

***Abstract*— Among many challenges of Smart Grid, fast and efficient service restoration in distribution systems is clearly a vital factor for achieving better service reliability, especially considering that up to 90% of power system outage events originate in distribution systems. This paper proposes two heuristic optimization algorithms for fast online restoration for future smart grids. The algorithms are based on constructive approaches to restore the supply of loads after a fault in a very short time. These two algorithms are both fast but different in the objective of optimization. Specifically, the first algorithm minimizes the load imbalance among available substations in post-fault restoration strategy; meanwhile, the second minimizes the total number of switching operations. Essentially, these two algorithms start with all operable switches open, and at each step, close the switch that results in the least increase in the objective function. Besides, several sample systems are run to demonstrate the algorithms in detail. And the test results verify the effectiveness of the proposed algorithms though comparing with other methods.**

I. KEY EQUATIONS

Capacity Factor:

$$\mathrm{CF} = \frac{L_{sum}}{SS_{cap}} \tag{1}$$

Minimal Loading Imbalance:

$$Min\ F = [Max(CF_i) - Min(CF_i)] + Penalty \cdot UL, \quad i \in N_s \tag{2}$$

Minimal Switching Operation:

$$Min\ F = N_{SO} + Penalty \cdot UL \tag{3}$$

$$s.t. \quad S(i) \le S_{cap}(i); i \in N_{SS} \tag{4}$$

$$N_{SS} = \{S(i), \forall i \text{ such that } S(i) > 0\} \tag{5}$$

$$DG(i) \le \mu \cdot Min(DG_{cap}(t)); i \in N_{DG} \tag{6}$$

$$N_{DG} = \{DG(i), \forall i \text{ such that } DG(i) > 0\} \tag{7}$$

$$N_s = N_{ss} \bigcup N_{ss} \tag{8}$$

$$\sum_{j=1}^{sj} L(j) \le Line_{cap}(j);\ j = 1 \sim n_{Line} \tag{9}$$

$$S_{rc}(L_i) \le 1; i = 1 \sim n_L \tag{10}$$

II. KEY FIGURES

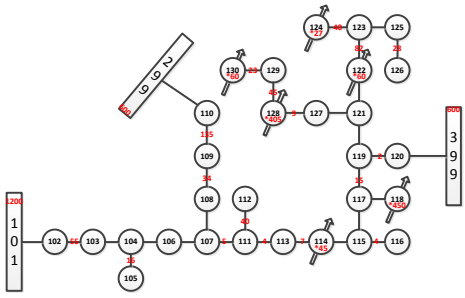

Figure 1. IEEE 34 bus test system

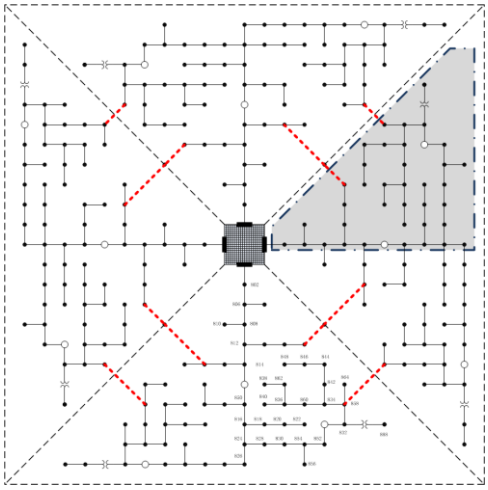

Figure 2. Complex system with interconnections and DGs

III. KEY RESULTS

TABLE I. Simple system case

Method	Time Used	# of comparisons
Exhaust Algorithm	0.0780 s	8192
Minimal Loading Imbalance	0.0156 s	208
Minimal Switch Operation	0.0156 s	153

TABLE II. Complex system case

Method	Time Used	# of comparisons
Exhaust Algorithm	>1hr	4.195×10^{29}
Minimal Loading Imbalance	< 1s	7056
Minimal Switch Operation	< 1s	5922

A Two-stage Stochastic Economic Dispatch Model with Minimum Frequency Constraints

Yen-Yu Lee and Ross Baldick
Department of Electrical and Computer Engineering, the University of Texas at Austin
Email:yenyu@mail.utexas.edu and ross.baldick@engr.utexas.edu

***Abstract*—In this paper, a new economic dispatch model is proposed as a two-stage stochastic linear program. This model optimizes the expected operation cost under various types of uncertainties, including forced generation outages, demand uncertainty, and variability of wind. The post-contingency transmission constraints are considered to guide the locational allocations for reserves. In addition, minimum frequency constraints are enforced to incorporate the effects of under-frequency load shedding. Small- and medium-scale system examples are provided to demonstrate the value of the model. That is, incorporating minimum frequency and post-contingency transmission constraints are significant in determining the optimal schedules of energy and reserves.**

I. Key Equation

The objective of the stochastic economic disaptch (SED) model is to minimize the expected operation costs, subject to pre- and post-contingency operation constraints:

$$\begin{aligned}
\min \quad & p_0 C_e(x) + C_r(r^{\mathrm{SP}}, r^{\mathrm{FS}}, r^{\mathrm{NS}}) \\
& + \sum_{\omega\in\Omega} p_\omega Q\left(x, r^{\mathrm{SP}}, r^{\mathrm{FS}}, r^{\mathrm{NS}}, a_\omega, \delta_\omega\right) && \text{(1a)} \\
\text{s.t.} \quad & \sum_{i\in\mathcal{N}} x_i = \sum_{i\in\mathcal{N}} d_i && \text{(1b)} \\
& \sum_{i\in\mathcal{N}} H_{\ell i}(x_i - d_i) \le b_\ell,\ \forall \ell \in \mathcal{L}' && \text{(1c)} \\
& x_i + r_i^{\mathrm{SP}} \le u_i \overline{g}_i,\ i \in \mathcal{N} && \text{(1d)} \\
& x_i \ge \underline{g}_i,\ i \in \mathcal{N} && \text{(1e)} \\
& r_i \le u_i \overline{g}_i^{\mathrm{SP}},\ i \in \mathcal{N} && \text{(1f)} \\
& r_i^{\mathrm{FS}} \le (1-u_i)(\alpha_i)\overline{g}_i,\ i \in \mathcal{N} && \text{(1g)} \\
& r_i^{\mathrm{FS}} + r_i^{\mathrm{NS}} \le (1-u_i)\overline{g}_i,\ \forall i \in \mathcal{N}, && \text{(1h)}
\end{aligned}$$

where the recourse problem Q is formulated as:

$$\begin{aligned}
& Q(x, r^{\mathrm{SP}}, r^{\mathrm{FS}}, r^{\mathrm{NS}}, a_\omega, \delta_\omega) \\
& = \min\ C_e^{\mathrm{S}}(x_\omega^{\mathrm{S}}) + C_e^{\mathrm{R}}\left(x_\omega^{\mathrm{R}}\right) + v^{\mathrm{LL}}\Big(\sum_{k\in\mathcal{K}} e_{k\omega}^{\mathrm{S}} + t_{\mathrm{R}} \sum_{i\in\mathcal{N}} \ell_{i\omega}^{\mathrm{R}}\Big) \\
& \quad \text{s.t. minimum frequency constraints,} \\
& \qquad \text{post-contingency power balance constraint,} \\
& \qquad \text{post-contingency transmission constraints,} \\
& \qquad \text{frequency restoring constraint,} \\
& \qquad \text{reserve restoring constraints,} \\
& \qquad \text{generation and load shedding limits.}
\end{aligned} \tag{2}$$

The shortfall in stored kinetic energy to meet the nominal frequency is expressed as follows:

$$\begin{aligned}
e_{k\omega} &= e_{k-1,\omega} - e_{k\omega}^{\mathrm{S}} + \text{energy consumed during } \Delta t_k \\
&\quad - \text{energy generated during } \Delta t_k \\
&= e_{k-1,\omega} - e_{k\omega}^{\mathrm{S}} + \left[\Delta t_k q_{k-1,\omega} + \frac{1}{2}\Delta t_k^2 \left(\sum_{i\in\mathcal{N}} m_{i\omega}\right)\right] \\
&\quad - \left[\Delta t_k y_{k-1,\omega} + \frac{1}{2}\Delta t_k (y_{k\omega} - y_{k-1,\omega})\right],\ k = 1, \ldots, K,
\end{aligned} \tag{3a}$$

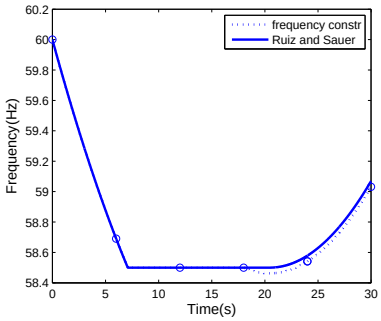

Fig. 1: Estimated frequency excursion.

TABLE I: Costs and unserved energy for the 118 bus system.

	SED	ED-S[a]
Expected cost	41419.40	74299.86
Unserved energy	0.0629	3.4274
Under-Freq. Load Shedding	0.0152	0.0304

[a]Economic dispatch with fixed system-wide reserve requirement.

II. Key Results

Figure 1 shows that the frequency constraints produce good approximation of frequency excursion, compared to the approach proposed by Ruiz and Sauer[1]. Table I shows the expected operation costs according to (1a) and the expected unserved energy in the 118 bus example. The SED model indeed generates an energy and reserves schedule that is much more resilient to system contingencies, compared to the models with deterministic reserve criteria. In addition, the estimated amount of under-frequency load shedding is not negligible and should be included into the model.

[1]P. Ruiz and P. Sauer, "Spinning contingency reserve: Economic value and demand functions, " *IEEE Transactions on Power Systems*, vol. 23, no. 3, pp. 1071-1078, Aug. 2008.

Quantifying Spinning Reserve in Systems with Significant Wind Power Penetration

Guodong Liu and Kevin Tomsovic
Power Engineering Laboratory, Department of Computer Science and Electrical Engineering, The University of Tennessee, Knoxville, TN 37916, USA, Email: *gliu5@utk.edu* and *tomsovic@utk.edu*

***Abstract*—With increasing wind power penetration in many power systems, the requirement of spinning reserve has become an important concern. Adequate reserves are directly related to the reliability and economy of the system. In this work, a new probabilistic method is proposed to maintain a uniform system reliability level in each dispatch interval by quantifying different levels of spinning reserve. The method considers the probability distribution of forecast errors of wind and load, as well as generator forced outage rate by using the Expectation of Demand Not Served (EDNS) as an evaluation index. The proposed method is solved by sequential quadratic programming. Simulation on the IEEE Reliability Test System shows the method by varying required reserves can maintain desired level of reliability. The relationships of uncertainties on required system reserve are verified.**

***Index Terms*—Spinning reserve, wind power forecast error, load forecast error, EDNS, reliability, probabilistic method.**

I. Key Equations

$$E_{DNS}^{t} = \sum_{k \in S} C_k^t P_k$$

$$\begin{aligned} C_k^t &= E\left(e_d - \sum_{i\in A} r_i^t + \sum_{m\in U} P_m^t \mid e_d > \sum_{i\in A} r_i^t - \sum_{m\in U} P_m^t\right) \\ &\quad \cdot P\left(e_d > \sum_{i\in A} r_i^t - \sum_{m\in U} P_m^t\right) \\ &= \frac{\sigma_d}{\sqrt{2\pi}} e^{-\frac{\left(\sum_{i\in A} r_i^t - \sum_{m\in U} P_m^t\right)^2}{2\sigma_d^2}} \\ &\quad - \left(\sum_{i\in A} r_i^t - \sum_{m\in U} P_m^t\right) \\ &\quad \cdot \left(1 - \Phi\left(\frac{\sum_{i\in A} r_i^t - \sum_{m\in U} P_m^t}{\sigma_d}\right)\right) \end{aligned}$$

II. Key Figures

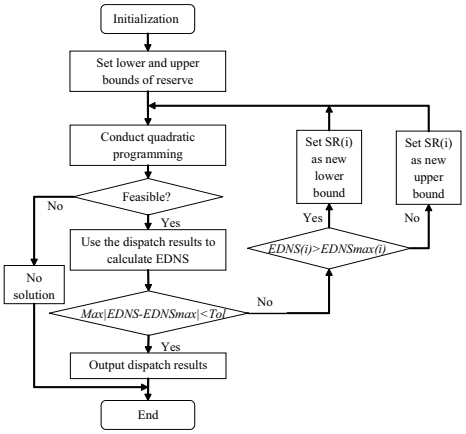

Figure 1. Iterated optimization scheme

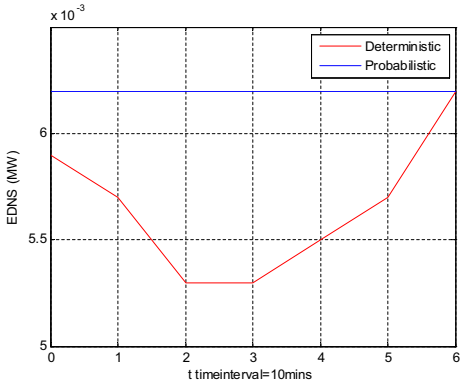

Figure 2. EDNS value of two methods

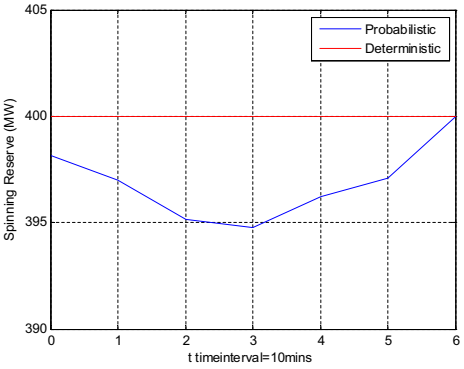

Figure 3. Spinning reserve of two methods

III. Key Results

Affine Decision Rules-Based Power Systems Planning under Multiple Uncertainties

Diego Mejia and James McCalley
Electric Power and Energy Systems, Department of Electrical and Computer Engineering, Iowa State University, Ames, IA 50010, USA,
Email: diegomej@iastate.edu and jdm@iastate.edu

***Abstract*— This work proposes, develops, and implements a methodology for making investment decisions regarding the power system capacity in an environment full of uncertainties. Investment decisions that are usually obtained in power capacity planning tools when uncertainties are not considered properly may yield to poor future performance of the system. An approach based on both the recourse philosophy of stochastic programming and the safe representation of uncertain linear constraints through robust optimization that avoids the use of scenario trees is implemented. The resulting investment decisions are arbitrarily set up as affine functions of revealed information in the past (realized uncertainties), which provides an effect of the relevant uncertainties on future investment decisions. The capacity expansion plan of a 14-technology, 5-region aggregated version of the US power system that considers multiple uncertainties (investment cost, fuel prices, power demand, carbon emissions policies, capacity credit of wind and solar power, capacity factors, among others) is implemented. Results show the flexibility of the planning solution since investment decisions are adjusted according the realization of uncertainties.**

I. KEY EQUATIONS

The investment decisions (wait-and-see variables) at any geographical location for any power production technology at time are arbitrarily set as affine functions of past information:

$$Investment_t = affine(1, U_t, U_{t-2}, \ldots, U_{t-k})$$

Where $U_t, U_{t-2}, \ldots, U_{t-k}$ are pieces of the information sets available at time t, and at $t=0$, investment decisions are the here-and-now variables (there is no any information available). This type of decision rule is basically the underlying philosophy of stochastic programming; however, in this work we do not sample data from any random population to generate scenario trees, which are computationally intractable when even a small number of uncertainties are considered. What we actually do is modeling the uncertainty as it is, i.e., as a continuous random or uncertain variable; and then, use the theory of the robust counterpart to obtain an equivalent optimization problem protected against uncertainty.

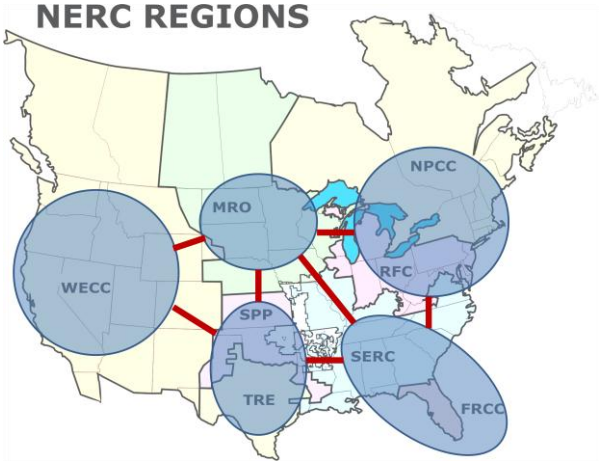

Figure 1. 5-Region US Power System Aggregation

II. KEY RESULTS

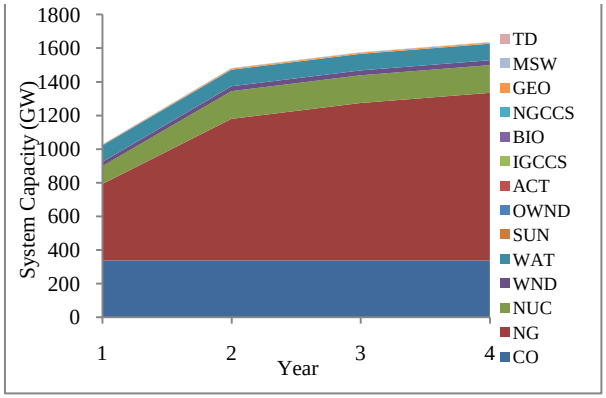

Figure 2. Expectation of the evolution of the total system capacity (year 1 represents 2008 US installed capacity)

III. KEY COMMENTS

- ✓ Optimization problem with 819,364 constraints and 59,827 decision variables.
- ✓ Natural Gas Combined Cycle (NGCC), nuclear, wind, solar, and geothermal are part of the here-and-now capacity additions.
- ✓ After year 2, NGCC power investments are highly affected by fluctuations in both coal and natural gas prices.
- ✓ Under expected situations, the power consistently would flow from west and mid-west to the east coast.

Generator-Transmission Maintenance Planning Prioritization Method with Pareto Optimal Set

Chihaya Murakami, Kiyotaka Matsushita and Sinichi Iwamoto

Power Systems Laboratory, Department of Electrical Engineering and Bioscience, Waseda University, Tokyo, 169-8555, Japan.
Email:murakami.chihaya.pwrs@gmail.com

***Abstract*--The electric power utilities have installed many electric power facilities in the high economic growth period. And these facilities have aged because they have been used for a long time. Therefore, they should be replaced anytime soon. But we have to make maintenance plans in advance to replace them. Although the power system maintenance takes place intensively in spring and autumn which have less power demand, the low demand period may decrease by the load leveling effects with electric vehicle charging and the advancing electrification rate. Therefore the updates of the electric power facilities have to be carried out in shorter terms, and the power system maintenance plans should be made more efficiently. For this reason, we propose a transmission planning prioritization method using Pareto Optimal Set considering generator maintenance. Here we evaluate the total heavy-loaded power flows, critical clearing times, maximum real power margins, CO_2 emissions, fuel costs, and transmission losses. Finally we carry out simulations with IEEJ EAST 30-machine 107 bus system to confirm the validity of the proposed method.**

I. KEY EQUATIONS

One of the objective functions used in this paper is shown below.

$$f_2 = \text{Fuel Cost} = a + b \cdot P + c \cdot P^2 \quad (1)$$

$$P_{\max -i} = K_{c-i} \cdot P_{Load-i} \quad (2)$$

$$f_3 = PM_{\max -i} = P_{\max -i} - P_{Load-i} \quad (3)$$

$$f_5 = \text{CO2 Emission} = A \cdot P \quad (4)$$

$$f'_m = \sum f_m \quad (5)$$

where f : objective function, a, b, c : Generator fuel cost constants, Kc : maximum load factor, $\square_i$: bus number, A : CO_2 emissions constant.

II. KEY FIGURES

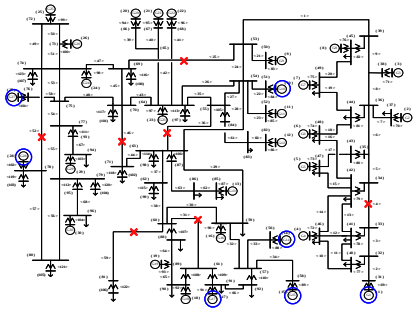

Figure 1. IEEJ EAST 30-machine system model

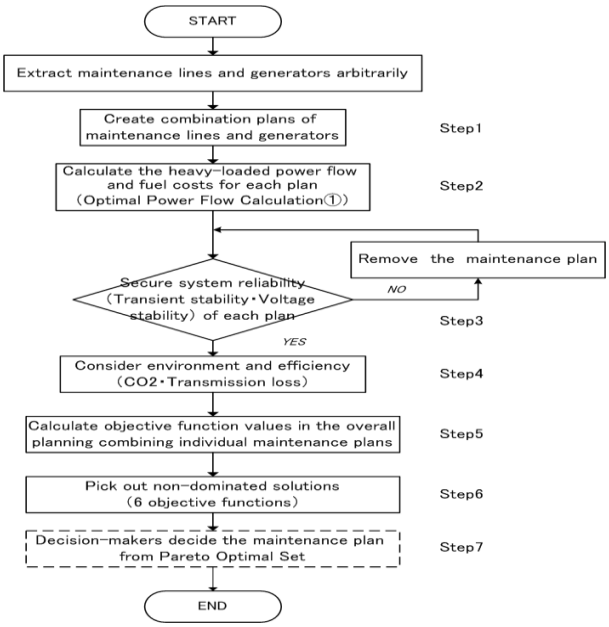

Figure 2. Flowchart of the proposed maintenance plan

III. KEY RESULTS

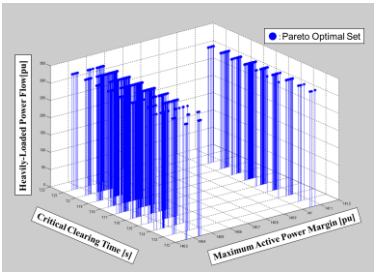

Figure 3. Non-dominated solutions for functions of system stability

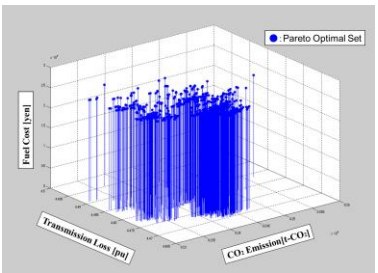

Figure 4. Non-dominated solutions for functions of additional value for power system

The validity of the proposed method has been confirmed from the simulation results and the proposed method would be useful for decision-makers..

Toward a More Flexible Generator Cost Function: A U-Shaped Supply Function

Ajinkya Paralikar[1], Kory W. Hedman[1], Richard P. O'Neill[2], and Eric A. Krall[2]
[1] School of Electrical, Computer, and Energy Engineering, Arizona State University, Tempe, AZ 85287, USA
[2] Federal Energy Regulatory Commission, 888 1st St NE, Washington, DC 20002, USA,
Email: aparalik@asu.edu, khedman@asu.edu, richard.oneill@ferc.gov, and eric.krall@ferc.gov

***Abstract*— In many ISOs, the cost function of a generator is assumed to be monotonically non-decreasing starting at a minimum operating level, which is generally greater than zero. Traditionally, this minimum operating level is treated as a hard constraint, a constraint that cannot be violated, i.e., it is assumed that generators cannot operate below this minimum operating level. Due to various approximations in the bid format, a generator may not be able to express its true cost structure. As a result, generators may submit a minimum operating level that is not based on a physical requirement of the generator. Instead, this minimum operating level is guided by the economic operation of the generator. This minimum operating level is often called the 'eco-min'. As a result, this minimum operating level should be ideally treated as a soft constraint as opposed to a hard constraint that should never be violated no matter the cost. Modeling this minimum operating level as a soft constraint would allow the generator to operate below its defined 'eco-min'.**

Such modeling approaches have been already adopted by the industry. The true cost function would allow operation below the 'eco min', but at higher costs. The cost to operate below the eco-min may be higher due to less efficient heat rates and/or greater pollution. With simple modifications, market models can be modified to accommodate these cost functions, which are more indicative of the generator's true supply function.

In this paper, we have developed a dispatch optimization formulation based on a soft constraint for the eco-min. This is mathematically modeled as a U-shaped supply function for generators. This function is monotonically non-decreasing from the eco-min to its maximum capacity limit and is monotonically non-increasing from the generator's actual minimum operating level, defined by the physical limitations of the plant, to its eco-min. By developing of a U-shaped supply function, we are able to more accurately model the cost structure of a generator. Furthermore, the modeling of the eco-min as a truly soft constraint adds flexibility to the dispatch optimization problem.

This research develops a multi-period unit commitment formulation with U-shaped supply functions and examines the implications of a soft constraint for the eco-min.

I. Key Equations

The guiding equations of this dispatch optimization formulation are:

$$\text{Minimize: } \sum_g \sum_s c_{gs} P_{gs} + \sum_g SU_g v_g + \sum_g \sum_s c^{-}_{gs} P^{-}_{gs} \quad (1)$$

$$\sum_g P_{g,s,t} - \sum_g P^{-}_{g,s,t} = d_t \quad \text{for all } t \quad (2)$$

$$P_{g,1,t} \geq P_{g,1}^{min} u_{g,t} - \Sigma_s P^{-}_{g,s,t} \quad \text{for all } g,t \quad (3)$$

$$P_{g,1,t} \leq P^{max}_{g,1} u_{gt} \quad \text{for all } g,\ t \quad (4)$$

$$0 \leq P_{g,s,t} \leq P_{g,s}^{max} u_{g,t} \quad \text{for all } g,t,s > 1 \quad (5)$$

$$0 \leq P^{-}_{g,s,t} \leq P^{-}_{g,s}{}^{max} u_{g,t} \quad \text{for all } g,\ s,t \quad (6)$$

$$v_{g,t} - w_{g,t} = u_{g,t} - u_{g,t-1} \quad \text{for all } g,\ t \quad (7)$$

$$\Sigma_s (P_{g,s,t} - P_{g,s,t-1}) \leq RU_g u_{g,t-1} + R^{SU}_g v_{g,t} \quad \text{for all } g,t \quad (8)$$

$$\Sigma_s (P_{g,s,t-1} - P_{g,s,t}) \leq RD_g u_{g,t} + R^{SD}_g w_{g,t} \quad \text{for all } g,\ t \quad (9)$$

$$\Sigma^{t}_{q=t-UTg+1} v_{g,q} \leq u_{g,t} \quad \text{for } g,t \in \{UT_g \ldots T\} \quad (10)$$

$$\Sigma^{t}_{q=t-DTg+1} w_{g,q} \leq 1 - u_{g,t} \quad \text{for } g,t \in \{DT_g \ldots T\} \quad (11)$$

$$u_{g,t} \in \{0,1\} \quad \text{for all } g,\ t \quad (12)$$

$$0 \leq v_{g,t} \leq 1 \quad \text{for all } g,\ t \quad (13)$$

$$0 \leq w_{g,t} \leq 1 \quad \text{for all } g,\ t \quad (14)$$

$$r_{g,t} \leq R^{SP}_g \quad \text{for all } g,t \quad (15)$$

$$r_{gt} \leq \sum_s P^{max}_{g,s} u_{g,t} - \sum_s P_{g,s,t} \quad \text{for all } g\ t \quad (16)$$

II. Key Figure

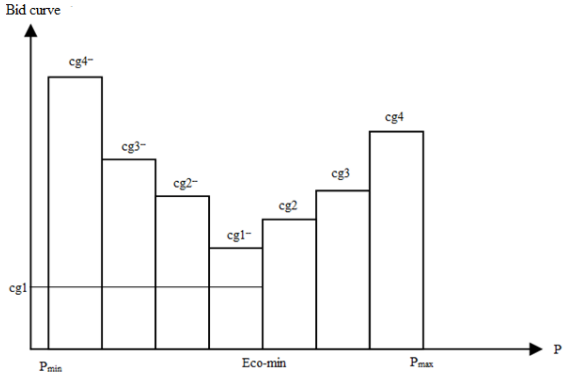

Figure 1. U-shaped supply function

Coordinated Operation of Energy Hubs in Smart Grids

Isha Sharma, Dr. Claudio A. Cañizares, and Dr. Kankar Bhattacharya
Department of Electrical and Computer Engineering
University of Waterloo, Waterloo, Ontario, N2L 3G1, CANADA,
Email: *{i4sharma, ccanizar, kankar}@uwaterloo.ca*

***Abstract*— In this work a bi-level optimization problem for an Energy Hub is presented that seeks to achieve an optimum solution where two different sets of entities seek to optimize their own (often conflicting) objectives independently. At the macro-hub level, which in this case is the distribution system operator, typical objectives may include load shape modification and peak reduction. At the micro-hub level, which is typically the customer level, cost minimization is envisaged as a likely objective. In this research, the micro-hub model comprises a residential load with the objective of minimizing the cost of energy consumption from the customer's point of view. At the macro-hub level, the optimization model is geared toward the distribution system operator that incorporates the changing load dynamics of customers, while minimizing the total energy drawn from substations. Energy price, system emission profiles, weather forecast information and customer load parameters are used as inputs to the bi-level optimization framework.**

I. KEY EQUATIONS

The macro-hub optimization model includes a detail three-phase model of distribution system components [1]. The distribution system operation objective is to minimize the energy drawn from the substation as follows, but other objectives such as minimizing the number of switching operations can be incorporated as well:

$$min\ J = \sum_{h} P_{sub_h} \tag{1}$$

$$\text{s.t.} \begin{bmatrix} \bar{V}_{l,s} \\ \bar{I}_{l,s} \end{bmatrix} = \begin{bmatrix} A & B \\ C & D \end{bmatrix} \begin{bmatrix} \bar{V}_{l,r} \\ \bar{I}_{l,r} \end{bmatrix} \tag{2}$$

The ABCD parameters in (2) are constants for series elements except for load tap changers (LTCs) which depend on the setting of tap positions during operation.

$$A_t = W \begin{bmatrix} 1+\Delta S_t Tap_{a,t} \\ 1+\Delta S_t Tap_{b,t} \\ 1+\Delta S_t Tap_{c,t} \end{bmatrix} \text{ and } D_t = A_t^{-1} \tag{3}$$

The wye-connected loads are represented on a per-phase basis, as follows:

- Constant power loads:

$$V_{p,L} I^*_{p,L} = P_{p,L} + Q_{p,L} \tag{4}$$

- Constant impedance loads:

$$V_{p,L} = Z_{p,L} I_{p,L} \tag{5}$$

- Constant current loads:

$$\left|I_{p,L}\right|(\angle V_{p,L} - \angle I_{p,L}) = \left|Io_{p,L}\right| \angle \theta_{p,L} \tag{6}$$

- Capacitor banks:

$$V_{p,C} = X_{p,C} I_{p,C} \tag{7}$$

For delta-connected loads and capacitors banks, (4)-(7) can be used by replacing the line variables with line-to-line variables.

The micro-hub operational model represents different components of a residential customer including detailed energy consumption, energy storage and energy production [2],[3]. The objective function considered, is minimization of customer's total cost of energy (8).

$$min\ J = \sum_{t\in T} \sum_{i\in A} C_i P_i S_i(t) \tag{8}$$

$$\text{s.t.} \sum_{i\in T} P_i S_i(t) \le P_t^{\max} \tag{9}$$

The operational constraints (9) include various energy consumption devices such as fridge, air conditioning/heating, water heater, dish washer, stove, washer, dryer, etc.

II. KEY FIGURE

Figure shows the overall bi-level optimization framework to determine the optimal operation of the macro-hub.

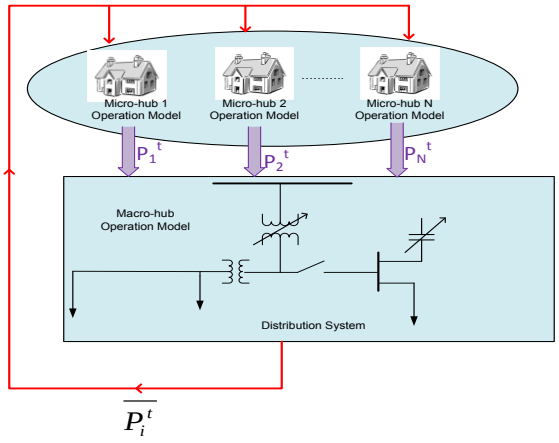

Figure 1: Bi-level optimization framework for Energy Hubs

References
[1] S. Paudyal, C. Cañizares, K. Bhattacharya, "Optimal Operation of Distribution Feeders in Smart Grids," *IEEE Trans. Industrial Electronics,* Early Access. Apr. 2011.
[2] M. Chehreghani Bozchalui, S. A. Hashmi, H. Hassen, K. Bhattacharya and C. A. Cañizares, "Optimal Operation of Residential Energy Hubs in Smart Grids - Part I: The Concept and Mathematical Modeling," *IEEE Trans.on Smart Grids*, April 2011.
[3] M. Chehreghani Bozchalui, S. A. Hashmi, H. Hassen, K. Bhattacharya and C. A. Cañizares, "Optimal Operation of Residential Energy Hubs in Smart Grids - Part II: Simulations and Implementation Aspects," submitted to *IEEE Trans. on Smart Grids*, April 2011.

Modeling the impact of wind ramping events on thermal power plant emissions

Karen Studarus and Richard D. Christie
Wind Integration Research Laboratory, Department of Electrical Engineering,
University of Washington, Seattle, WA 65409, USA,
Email: studarus@uw.edu and christie@ee.washington.edu

***Abstract*—The integration of wind energy into the electricity market promises to reduce harmful emissions by reducing the consumption of fossil fuels; however, naively assuming an even swap of clean MWh for dirty MWh oversimplifies and overstates the emissions reductions from renewable generation. Increases in stochastic wind generation have resulted in new operating regimes for other generators, including increased operation at partial load and more frequent startups and shutdowns. Emissions transients are sometimes observed several hours after a ramping event. This work examines whether those transients produce statistically significant deviations in total emissions from those predicted by the unit's input-output characteristic. Examination hourly emissions from 4148 thermal plants between 2007 and 2010 as reported to the Environmental Protection Agency (EPA) reveals that such transients in carbon dioxide (CO_2), nitrous oxide (NO_x), and sulfur dioxide (SO_2) do not produce statistically significant differences in total emissions from those predicted by a steady state model. Therefore, total CO_2, NO_x, and SO_2 emissions are not affected by wind-ramp caused transients, do not need to be incorporated into the dispatch algorithm and are not a barrier to wind energy utilization.**

***Index Terms*—Coal, energy resources, Event detection, natural gas, pollution measurement, power generation dispatch, power generation economics, power system modeling, wind energy.**

I. Key Equations

The statistic summarizing excess emissions during one ramping event is:

$$X_{event} = \frac{\sum_{n=1}^{N}(O_n - E_n)}{N \cdot E_{Pmax}} \quad (1)$$

Where O_n is the observed emissions at one sample during the ramping event, E_n expected emissions, E_{Pmax} the expected emissions at capacity and N the duration of the event.

II. Key Figures

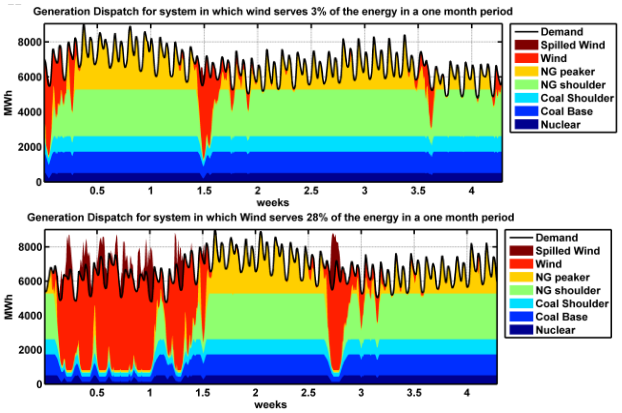

Figure 1. Increased utilization of wind energy results in higher variance operation of thermal generators.

III. Key Results

The analysis in this work examined more than a hundred thousand ramping events to conclude that CO_2, NO_x and SO_2 emissions totals are not affected by transients in generator output from ramping. Increased emission due to increases in wind penetration may be accurately computed using steady state emissions models for thermal power plants.

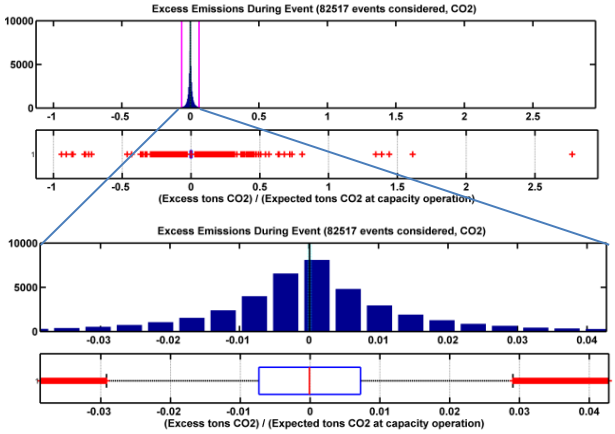

Figure 3. Carbon dioxide (CO2) excess emissions are zero mean. Both histogram and box plot portray the same events. Vertical pink bars on the histogram show a 95% confidence interval for excess emissions modeled as a zero mean gaussian. The box plot shows median (veritcal red bar), 25th-75th quartiles (blue box), 3 sigma (whiskers), and outlying points (red + symbols.). The bottom image is zoomed in on the 95% confidence interval of the first

Integrated Retail and Wholesale Power System Operation with Smart Grid Functionality

Auswin George Thomas[a], Pedram Jahangiri[b], Chengrui Cai[c], Huan Zhao[d], Dionysios Aliprantis[e] and Leigh Tesfatsion[f]

Department of Electrical and Computer Engineering [{a,b,c,e}] and Department of Economics[{d,f}]
Iowa State University, Ames, Iowa, USA
Email: *(agthomas, pedramj, ccai, hzhao, dali, tesfatsi)@iastate.edu*

***Abstract*—In this project we are developing the IRW Power System Test Bed, an agent-based test bed permitting the integrated study of retail and wholesale power systems operating over realistically rendered transmission and distribution grids. This test bed seams together AMES; an open source agent-based test bed developed at Iowa State University that incorporates the basic architecture of U.S. restructured wholesale power markets, and GridLAB-D, an open-source electric energy distribution platform developed by DOE researchers at Pacific Northwest National Laboratory that permits detailed empirically-based simulations of end-user loads. Research topics under study by means of the IRW test bed include: the reliability and efficiency implications of introducing price-sensitivity of demand for retail customers as realized through demand response, demand dispatch, and/or price-sensitive demand bidding; the dynamic effects of increased penetration of consumer-owned distributed energy resources, such as PV generation and plug-in electric vehicles; and the development of agent-based algorithms for smart device implementation.**

I. KEY FIGURES

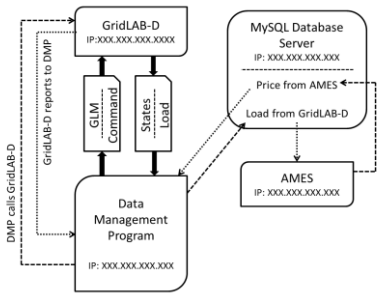

Figure 1. Structure of the Test Bed

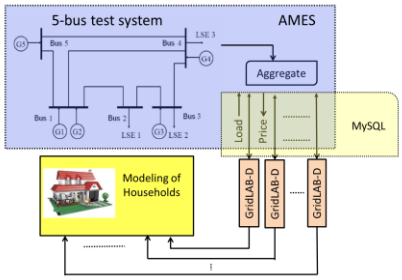

Figure 2. Initial Test Case

II. KEY RESULTS

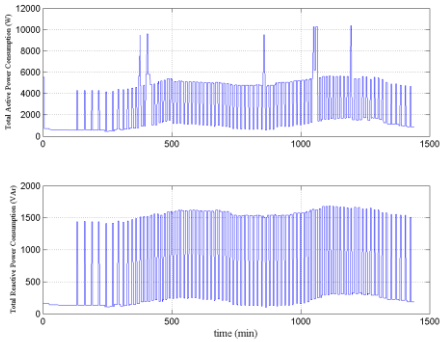

Figure 3. Active and Reactive power consumption of a household

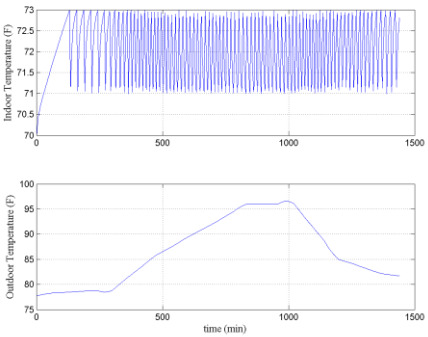

Figure 4. Variation of a household's indoor temperature to an HVAC cooling set-point of 72° F

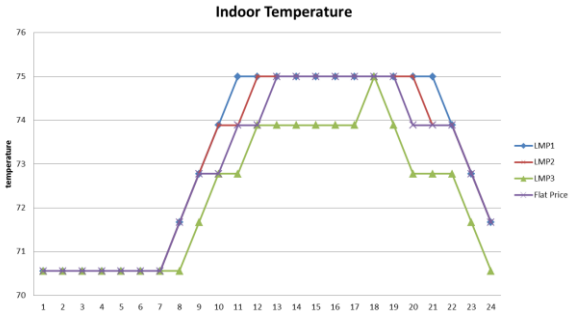

Figure 5. Variation of HVAC set-points for indoor temperature that achieves an optimal trade-off between comfort and energy costs for a home resident conditional on dynamic LMPs.

Hardware Prototype of a Multi-Agent Grid Management System

Jerry Thompson
Advanced Power and Electricity Research Center, Lane Department of Computer Science and Electrical Engineering,
West Virginia University, Morgantown, WV 26505, USA,
Email: jthomp12@mix.wvu.edu

***Abstract*— In an effort to improve the reliability of today's power systems, it is necessary to design a control structure capable of not only providing supervisory control and data acquisition, but also the ability to fully identify and resolve disturbances to the system. Due to the vast range of disturbance scenarios, the desired architecture must be able to operate effectively even when multiple communication ties are lost, as well as be able to convey critical information to the network operator. To meet these objectives, this paper explores the mechanics of a decentralized Multi-Agent Grid Management System (MGMS) and its ability to locate and isolate a fault prior to restoring service to applicable power zones. The scheme has a hierarchal structure which provides network operating information sampled through many points of interests within the network, while providing multiple paths for data transfer. Agents will interact directly with reconfiguration hardware allowing self healing potential. The inherent decentralization of the system will permit the performance of system subsets when communication failure occurs. The mechanics and operation of one system fulfilling these objectives will be explored.**

I. KEY FIGURES

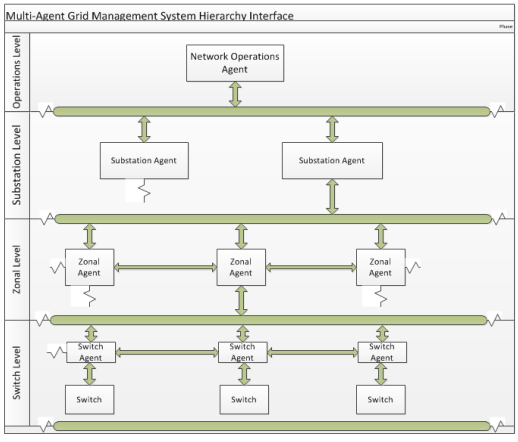

Figure 1. Decentralized System Structure

.

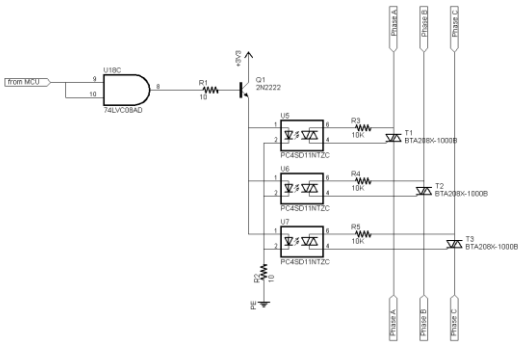

Figure 2. Electronic Switch Schematic

II. KEY RESULTS

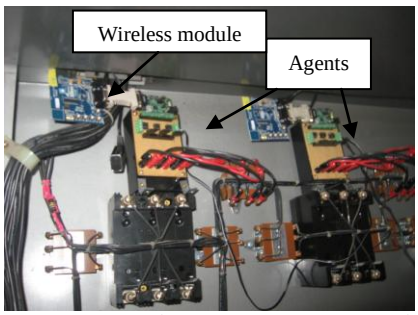

Figure 3: Deployment of agent control system using flexible communications

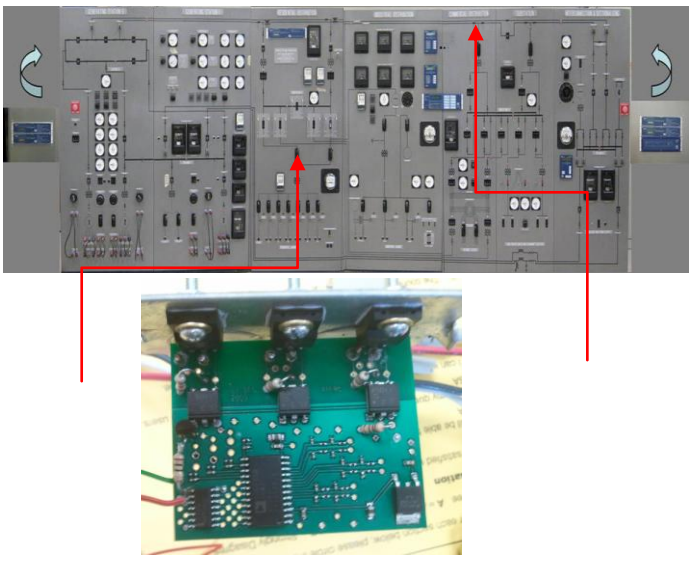

Figure 4. Implementation of Electronic Switches

New Security Tools for Real-Time Operation of Power System

Qin Wang and James D. McCalley
Department of Electrical and Computer Engineering, Iowa State University, Ames, IA 50010, USA,
Email: wangqin@iastate.edu and jdm@iastate.edu

***Abstract*— New security tools are developed for real-time operation of power system with the purpose of modernizing the electric grid while enhancing security and reliability of energy infrastructure. The tools include risk-based optimal power flow (RBOPF), which is further extended to Risk-based (RB) security-constrained optimal power flow (SCOPF), and high-speed extended-term time domain simulation (HSET-TDS). The benefit of RB-SCOPF model lies in its ability to improve the economic performance of power system while enhancing the system's overall security level, thus enabling the system operators to make a tradeoff between cost reduction and the level of the system's security during operation. A nested Benders decomposition with multi-layer linear programming method is proposed to solve the RB-SCOPF model, and has been tested on the ISO New England bulk system. For the HSET-TDS, a high-speed HH4 integrator is developed with VDHN nonlinear solver and SUPERLU linear solver. Test on the PJM bulk system indicates that the approach is feasible and efficient.**

I. KEY EQUATIONS

The compact form of Risk-based SCOPF model is shown in (1):

$$\begin{aligned} &\underset{x_0,\ldots,x_{NC},u_0}{\text{Min}} \quad f_0(\boldsymbol{x_0},\boldsymbol{u_0}) \\ &s.t. \quad \boldsymbol{g}_k(\boldsymbol{x}_k,\boldsymbol{u}_0)=0 \quad k=0,\ldots,NC \\ &\qquad \boldsymbol{h}_0(\boldsymbol{x}_0,\boldsymbol{u}_0)\le \boldsymbol{h}_0^{max} \\ &\qquad \boldsymbol{h}_k(\boldsymbol{x}_k,\boldsymbol{u}_0)\le K_C\times \boldsymbol{h}_k^{max} \quad k=1,\ldots,NC \\ &\qquad \sum_{k=0}^{NC} Risk_k(Pr_k,\boldsymbol{x}_k)\le K_R\times Risk_{max} \end{aligned} \tag{1}$$

II. KEY FIGURES

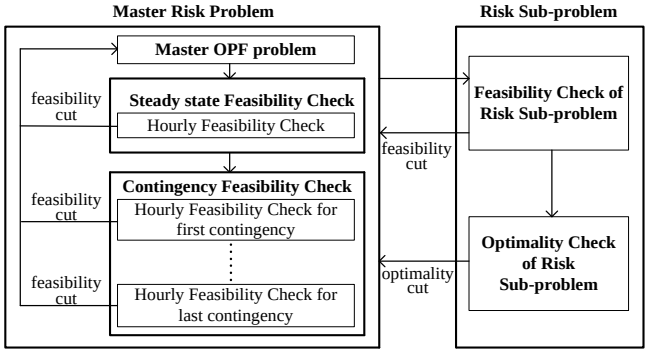

Figure 1. Multi-layer Benders decomposition to solve RBSCOPF

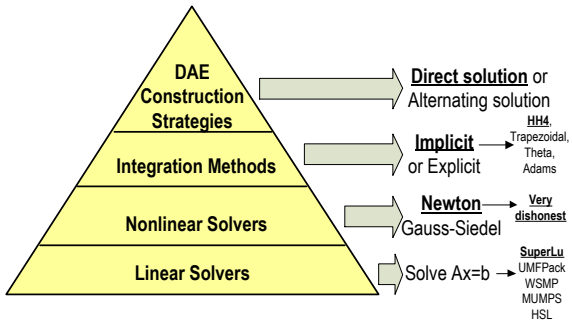

Figure 2. Sequential design to solve HSET-TDS

III. KEY RESULTS

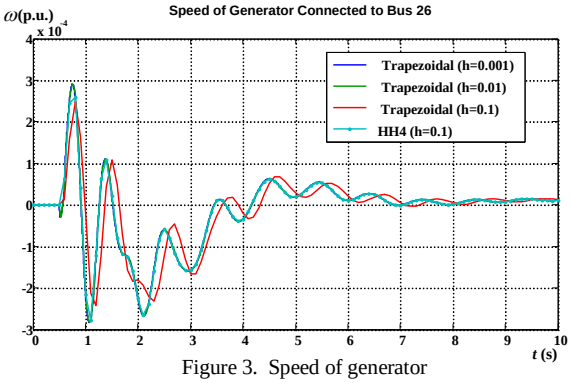

Figure 3. Speed of generator

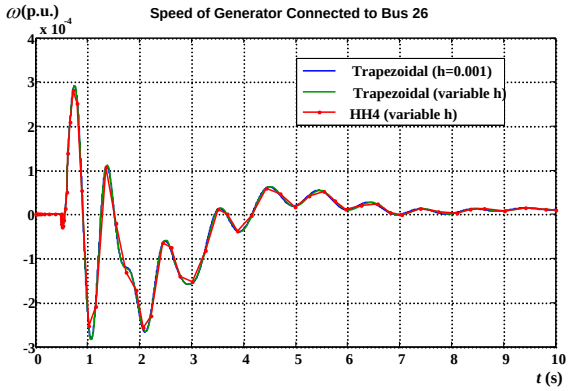

Figure 4. Speed of generator

Table 1. RB-SCOPF test result on ISO New England bulk system

Constraints	SCOPF	RBOPF	RB-SCOPF		
			HSM (K_C=1, K_R=0.5)	ESM ($\bar{K}_C$=1.05, K_R=0.5)	EESM ($\bar{K}_C$=1.20, K_R=0.5)
Risk	18.2690	9.1345	9.1345	9.1345	9.1345
Cost ($/hr)	684642.50	605407.32	728899.10	610611.54	605542.08
ASI	24.5466	24.0768	24.5458	24.0824	24.0848
CEI	850.02	80.14	254.83	197.42	219.65

The Stochastic Unit Commitment with Reliability Constraints

Peng Xiong and Panida Jirutitijaroen
Department of Electrical and Computer Engineering, National University of Singapore, 21 Lower Kent Ridge Road, 119077, Singapore
Email: g0800452@nus.edu.sg and elejp@nus.edu.sg

***Abstract*—This paper addresses unit commitment (UC) problem in a probabilistic manner. Two major sources of uncertainty in short-term generation scheduling, namely, the contingencies of generation failures and load uncertainty, are modeled separately. The first type is expressed by a number of selected outage scenarios, while the second is handled by the proposed reliability constraints, which barely increase the problem sizes, so little extra computational burden is caused. This UC formulation helps the operator to achieve desired reliability performance, in terms of the probability that electricity demand is met over the entire decision period. Implementation and assessment of this method, together with the resultant performance under various reliability requirements, are provided in this paper to demonstrate the effectiveness of the proposed approach. The influence of different types of uncertainty on the produced decisions is also examined in the case studies. Numerical tests show that the unit commitment decisions generated by the presented formulation are well adapted to system uncertainties.**

I. KEY EQUATIONS

The formulation of the stochastic unit commitment:

$$\min \ \mathrm{E}_{\omega}\left\{\begin{array}{l}\sum_{m\in\mathcal{M}}\mathcal{S}_m\left(\mathbf{u}_m(\omega)\right)\\ +\sum_{\substack{m\in\mathcal{M}\\ t\in\mathcal{T}}}\mathcal{G}_m\left(u_{mt}(\omega),g_{mt}(\omega)\right)+\sum_{t\in\mathcal{T}}CL\cdot l_t(\omega)\end{array}\right\} \tag{1}$$

$$\sum_{m\in\mathcal{M}} g_{mt}(\omega)+l_t(\omega)=D_t,\quad \forall t,\omega \tag{2}$$

$$g_{mt}(\omega)+r_{mt}(\omega)\le u_{mt}(\omega)\cdot\overline{G}_m,\ \forall m,t,\omega \tag{3}$$

$$-g_{mt}(\omega)+\le -u_{mt}(\omega)\cdot\underline{G}_m,\ \forall t,\omega \tag{4}$$

$$\left(\mathbf{u},\mathbf{g},\mathbf{r}\right)\in\mathcal{F}(\omega) \tag{5}$$

$$\sum_{m\in\mathcal{M}}\left[g_{mt}(\omega)+r_{mt}(\omega)\right]+M\left(1-\rho(\omega)\right)\ge sc_t(\omega),\quad \forall t,\omega \tag{6}$$

$$\eta_t(\omega)\ge\max_{k\in\mathcal{K}}\left\{A_t^k\cdot sc_t(\omega)+B_t^k\right\},\quad \forall t,\omega \tag{7}$$

$$q(\omega)\ge\sum_{m\in\mathcal{M}}\eta_t(\omega),\quad \forall\omega \tag{8}$$

$$\sum_{\omega\in\Omega}\pi_\omega\cdot q(\omega)\le\alpha^{\max} \tag{9}$$

II. KEY FIGURES

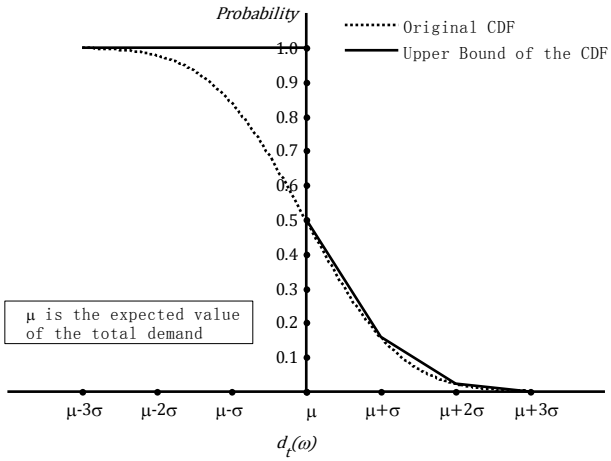

Figure 1. Approximated Cumulative Distribution Function

III. KEY RESULTS

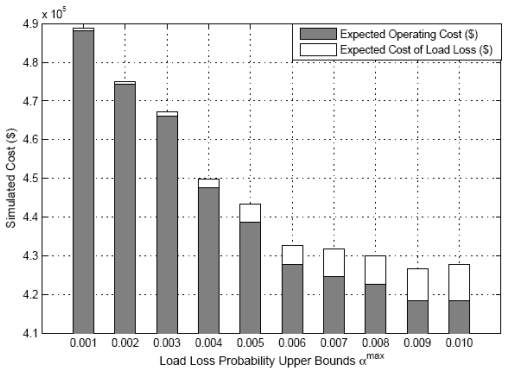

Figure 2. Simulated Cost under Different Reliability Requirements

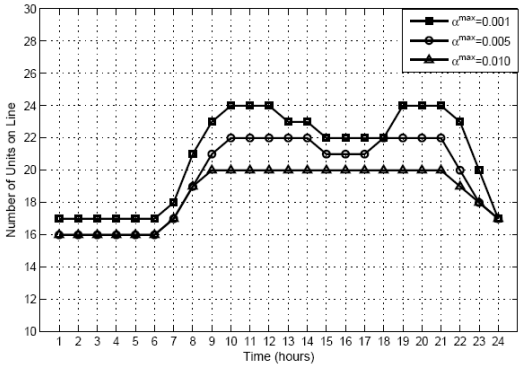

Figure 3. Decisions under Different Reliability Requirements Expressed by the Numbers of Online Units

Integrated Maintenance Scheduling of Generators and Transmission Lines Based on Fast Group Searching Optimizer

J. P. Zhan[1], Y. J. Yin[1], C. X. Guo[1] and Q. H. Wu[2]
1. Department of Electric Engineering, Zhejiang University, Hangzhou 310027, Zhejiang Province, China;
2. Department of Electrical Engineering & Electronics, the University of Liverpool, Liverpool L69 3GJ , UK,
Email: zhanjunpeng@zju.edu.cn, yinyujuan@zju.edu.cn, guochuangxin@zju.edu.cn and q.h.wu@liverpool.ac.uk

***Abstract*—This paper presents a new model for the integrated maintenance scheduling (IMS) of generators and transmission lines, which is formulated as a high dimensional, mix-integer and highly constrained optimization problem. The advantage of the new model is that the number of integer variables is greatly reduced in comparison with that in the traditional IMS model in a large scale power system. Besides, a fast group search optimizer (FGSO) algorithm is developed to solve the new IMS model, whose objective is to minimize the total costs of maintenance and power production. The effectiveness of the new model and the FGSO has been evaluated on the IEEE reliability test system. Simulation results show that the new model is successfully solved by FGSO and particle swarm optimizer (PSO). FGSO consumes much less time to find a near optimal solution and has better convergence performance in comparison with GSO and PSO.**

I. Key Equations

The objectives and constraints of the IMS model:

$$\sum_{t=1}^{T}\sum_{i=1}^{I} C_{it}\cdot(x_i == t)+\sum_{t=1}^{T}\sum_{k=1}^{K} C'_{kt}\cdot(x'_k == t) + \sum_{t=1}^{T}\sum_{i=1}^{I} c_{it}P_{it} \quad (1)$$

$$\sum_{m=0}^{d_{i_1}-1}\left((x_{i_1}+m)==t\right)+\sum_{m=0}^{d_{i_2}-1}\left((x_{i_2}+m)==t\right)\le 1,\forall t \quad (2)$$

$$\sum_{i=1}^{I}\sum_{m=0}^{d_{i_1}-1}\left((x_{i_1}+m)==t\right)\le n_{us},\forall t \quad (3)$$

The behaviors of producers, scroungers and rangers in FGSO:

$$\begin{cases} d_{i_j}^k = 0,\ j=1,2,...,n-t_d-1 \\ d_{i_j}^k = \sin(\varphi_{i_{(j-1)}}^k)\cdot\prod_{q=j}^{n-1}\cos(\varphi_{i_q}^k),\ j=n-t_d,...,n-1 \\ d_{i_n}^k = \sin(\varphi_{i_{(n-1)}}^k) \end{cases} \quad (4)$$

$$\begin{cases} X_z = X_p^k + \text{circshift}\left(r_1 l_{\max} D_p^k(\varphi^k),k\right) \\ X_r = X_p^k + \text{circshift}\left(r_1 l_{\max} D_p^k(\varphi^k + r_2\theta_{\max}/2),k\right) \\ X_l = X_p^k + \text{circshift}\left(r_1 l_{\max} D_p^k(\varphi^k - r_2\theta_{\max}/2),k\right) \end{cases} \quad (5)$$

$$X_i^{k+1} = X_i^k + r_3(X_p^k - X_i^k) \quad (6)$$

$$X_i^{k+1} = X_i^k + \text{circshift}\left(l_i D_i^k(\varphi^{k+1}),k\right) \quad (7)$$

II. Key Figures

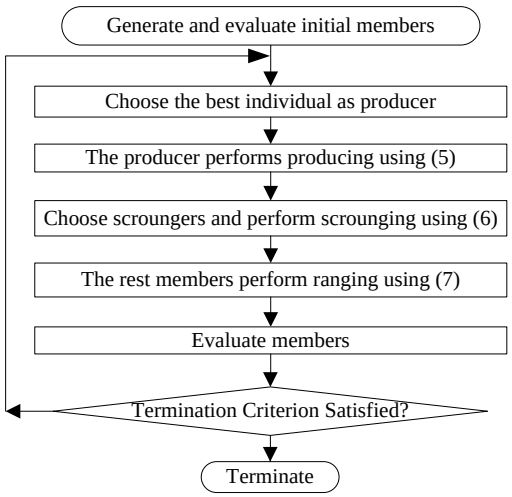

Figure 1. Flowchart of Fast Group Search Optimizer

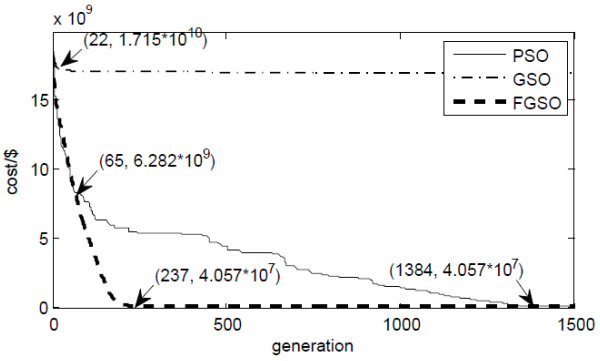

Figure 2. The Convergence Speed of PSO, GSO and FGSO in Case 1.

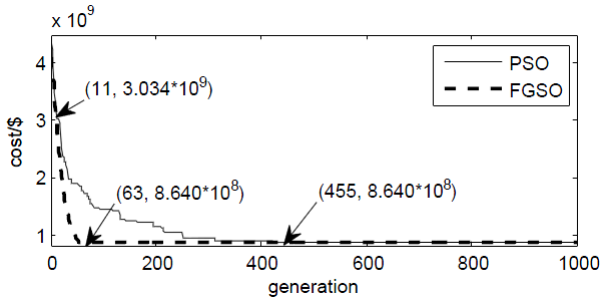

Figure 3. The Convergence Speed of PSO and FGSO in Case 2.

Wind Turbine Imbalance Fault Detection Using Current Signals

Xiang Gong and Wei Qiao
Department of Electrical Engineering, University of Nebraska - Lincoln, NE 68588, USA,
Email: xiang.gong@huskers.unl.edu and wqiao@engr.unl.edu

***Abstract* — The penetration of wind power has increased greatly over the last decade in the United States and across the world. Online condition monitoring and fault detection is an effective means of not only increasing the reliability but also reducing the costs associated with operation and maintenance of wind turbine generators (WTGs). This work investigates and proposes a 1P-invariant method for wind turbine imbalance fault detection by using the WTG stator current signals. Simulation and experimental results verify the availability of the proposed method. By using the proposed 1P-invariant power spectrum density (PSD) method, the imbalance faults of the wind turbine can not only be discovered but also be quantified and evaluated by the location and degree of the excitation in the stator current PSD of the wind generator.**

I. KEY EQUATIONS

The horizontal component of the force F_c caused by imbalance faults is:

$$F_c = F_{im} \cdot \sin(\omega t + \varphi) \qquad (1)$$

II. KEY FIGURES

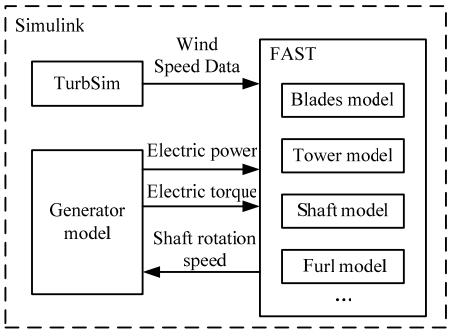

Figure 1. Simulation Model

Figure 2. The Wind Tunnel Used in the Experiments

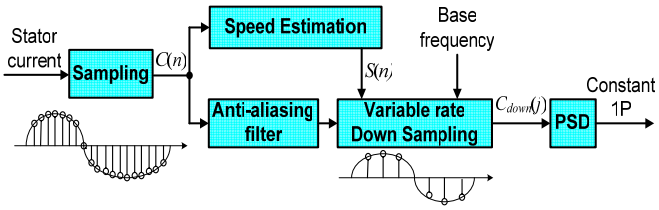

Figure 3. 1P-invariant PSD Method

III. KEY RESULTS

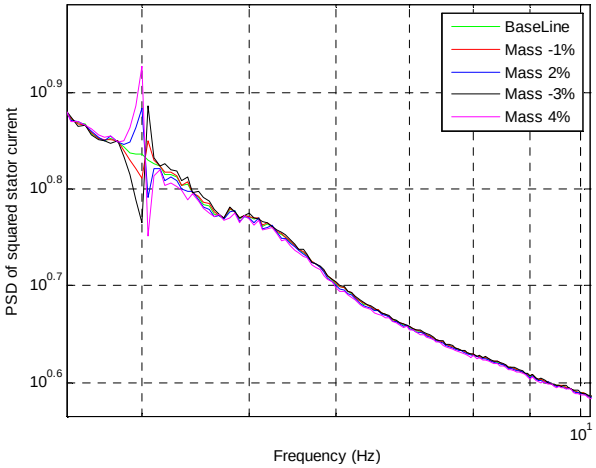

Figure 4. The Simulation Results

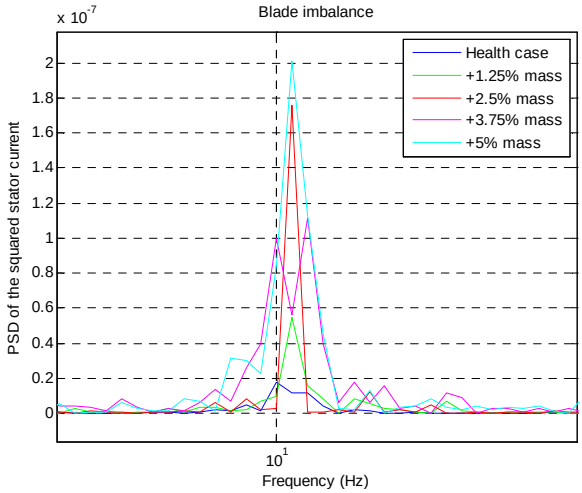

Figure 5. The Experimental Results

An Intrusion and Defense Testbed in a Cyber-Power system Environment

Junho Hong, *Student Member, IEEE,* Chen-Ching Liu, *Fellow, IEEE*

School of Electrical, Electronic and mechanical Engineering, University College Dublin, Ireland

Email: *junho.hong@ucdconnect.ie, liu@ucd.ie*

***Abstract*— The proposed testbed of the cyber-power system consists of power system simulation, substation automation, and the SCADA system. Scenarios for substation cyber security intrusions and anomaly detection concepts have been proposed. An attack tree method can be used to identify vulnerable substations and intrusions through remote access points. Specific substation vulnerability scenarios have been tested. Temporal anomaly is determined by data and information acquired at different time points. This is a metric to determine the anomaly between two snapshots. In a distributed intrusion detection algorithm, distributed agents are trained with a large number of scenarios and intended for real-time applications. In a distributed environment, if an anomaly is detected by one agent, it is able to distribute critical information to other agents in the network.**

I. KEY FRAMEWORK

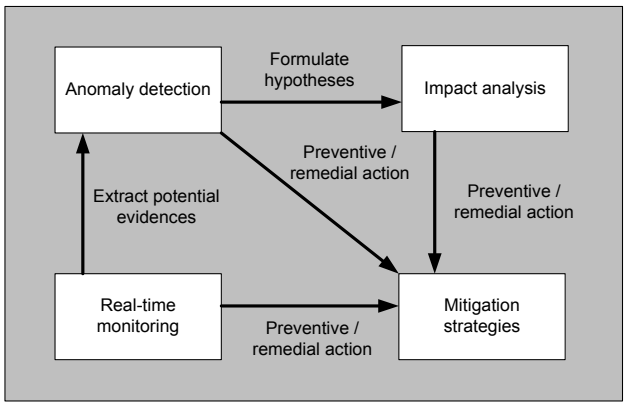

Fig. 1. RAIM Framework

II. CYBERSECURITY TESTBED

1) Control center: There are 2 communication protocols for control centers, e.g., ICCP and DNP 3.0 over TCP/IP.

2) Power system and substations: The testbed contains 3 parts - power system simulator, user interface and Intelligent Electronic Device (IED).

3) Attacker: : It is assumed that the substation has remote access points such as dial-up, and VPN for personnel or site engineers.

4) Cyber-physical system: Cyber security tasks can be divided into 2 parts, i.e., before intrusion and after intrusion.

III. KEY RESULTS

The results of the research program to date are:

- Testbed for cybersecurity has been established;
- Cyber security benchmarking scenarios are defined;
- Two computational algorithms for anomaly detecti-on have been developed;
- Plan of linkage between UCD and ISU through the ICCP has been developed.

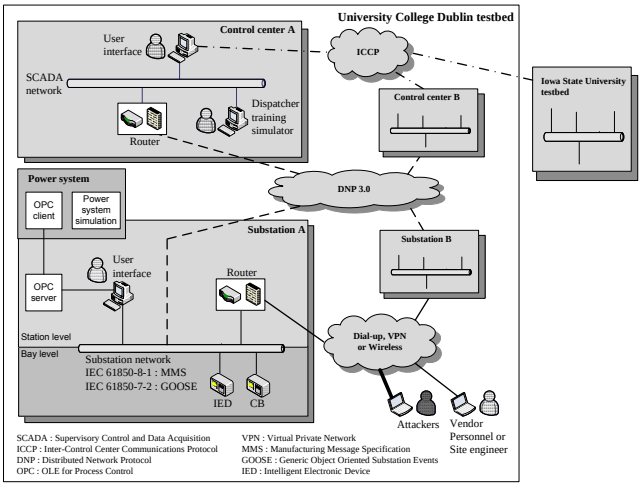

Fig. 2. Testbed for Cyber Security

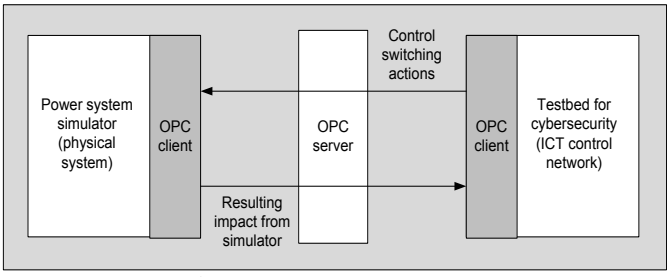

Fig. 3. Integration of Power System Simulator and Testbed ICT Network

Fault Current Contribution from Type I Wind Turbine-Generators

[1]Dustin F. Howard, [1]Jose Restrepo, [2]Travis Smith, [2]Michael Starke, [1]Jie Dang, and [1]Ronald G. Harley
[1]School of Electrical and Computer Engineering, Georgia Institute of Technology, Atlanta, GA, 30332, USA.
[2]Oak Ridge National Laboratory, Oak Ridge, TN, 37831, USA.
Email: dhoward@gatech.edu, restrepo@ieee.org, smithtm@ornl.gov, starkemr@ornl.gov, jdang3@gatech.edu, and rharley@ece.gatech.edu

***Abstract*— Increasing fault current contribution from wind farms into the utility network presents new engineering challenges for utility protection engineers. Traditionally, sequence component networks are used to calculate fault currents for relay settings, but there is at present uncertainty on the appropriate sequence component models of the various wind generator types for inclusion into protection calculation software. This work includes the development of a sequence component model for Type I wind turbine-generators. Time-domain transient simulations of wind turbine-generator fault currents are run using several popular power system simulation packages, including PSCAD/EMTDC, EMTP-RV, and SimPowerSystems; these results are compared with the calculations based on the sequence network circuits, and found to have good agreement.**

I. Key Equations

V' and X' for the induction machine are given by

$$X' = X_1 + \frac{X_m X_2}{X_m + X_2} \tag{1}$$

$$V' = nV_{IB}e^{j30^\circ} + jI_{gen}(X' + X_{line} + X_{trans}) \tag{2}$$

The fault currents for the three phase fault and single line to ground fault are calculated using:

$$I_{gen} = I_{SC} = \frac{V'}{jX'} \tag{3}$$

$$I_a = I_a^+ + I_a^- = \frac{V' - V_{a'g}^+}{jX'} - \frac{V_{a'g}^-}{jX'} = \frac{V' - V_{a'g}^+ - V_{a'g}^-}{jX'} \tag{4}$$

II. Key Figures

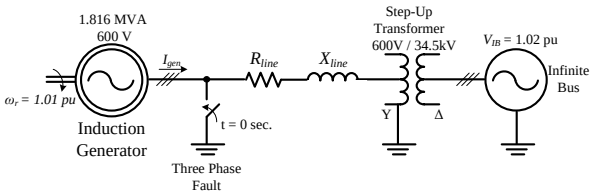

Fig. 1. PSCAD simulation setup for fault current analysis of wind turbine generator.

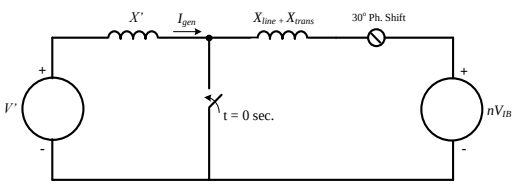

Fig. 2. Simplified positive sequence network using the V' and X' parameters.

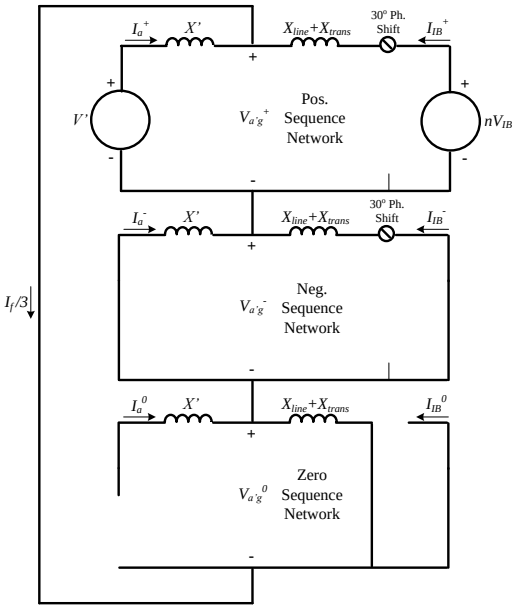

Fig. 3. Sequence network for single line to ground fault.

III. Key Results

RMS fault currents from time-domain simulations:

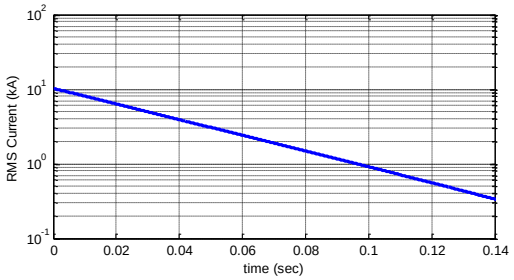

Fig. 4. RMS phase A current during a three phase fault.

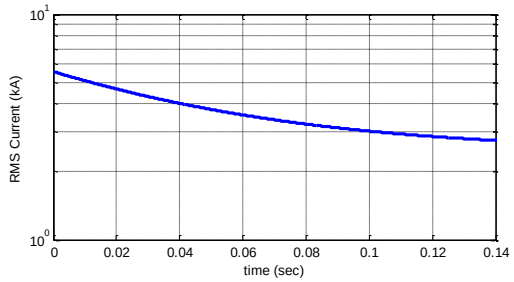

Fig. 5. RMS phase A fault current for single line-to-ground fault.

A User Interface technique for HMI of IED based on IEC 61850

Yonghwan Jo, Taewan Kim, MyeonSong Choi, Seungjae Lee, Byeongho Lee*, Hyunsung Kim*, Chulhee Cho*
Next-generation Power Technology Cent, Electrical engineering, Myongji University, South Korea
Hyundai Heavy Industries Co., ltd*, South Korea
Email: topboyman@nate.com, twkim@mju.ac.kr, mschoi@mju.ac.kr, sjlee@mju.ac.kr
byeongho@hhi.co.kr, hskim10@hhi.co.kr, choch_sp@hhi.co.kr

***Abstract*—IEC 61850 is an international standard for substation automation and recently a system based on IEC 61850 has become most-widely accepted practice due to its many advantages. The substation based on IEC 61850 has internal IED(Intelligent Electronic Device). They are required to process more functions and have to execute more UI(User Interface) data than the existing IED.**

Many companies are recently developing the IED-loaded TFT-LCD because of the market expansion and they are investing consistently on HMI(Human Machine Interface) technique. A technique needed to apply for the IED based on IEC 61850 which are able to realize the screen faster, to control variable functions more easily, and to handle larger data than before.

When applying existing UI technique, one screen is realized by making one UI screen and the data related to the one UI screen was coded directly on the screen. Therefore, the more functions increases, the increase of UI screen occurs, which results in larger size and slower speed of the program.

This paper proposes an advanced UI technique to improve the problems. [Figure 5]Similar static screens are realized by only one UI screen with the technique. [Figure 3]Configure files containing basic information (menu, data value, description, password, etc.) of IED and all information for static screens are necessary to apply proposed UI technique. The configure files are similar with SCD (Substation Configuration Description) which is utilized in substation based on IEC 61850.

The proposed technique results in faster booting speed and reduction of the program size as a number of X by realizing only one [Figure 4]UI screen due to reduction of UI screens from number of [Figure 1]N to number of [Figure 2]N-X. Also the proposed technique creates the screen by changing only the text inside the screen but leaving the configuration of screen alone. The technique leads to a significant procedure reduction (creation of new screen, labels, buttons, etc.) on UI screen realization which results faster processing speed.

I. KEY FIGURES

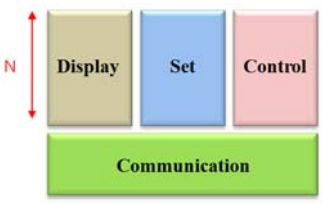

Figure 1. Existing UI structure

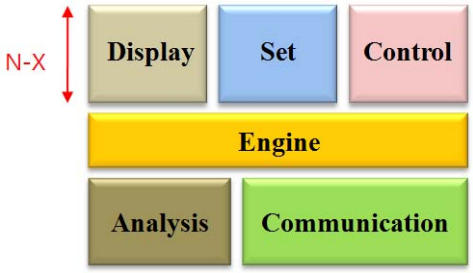

Figure 2. Proposed UI structure

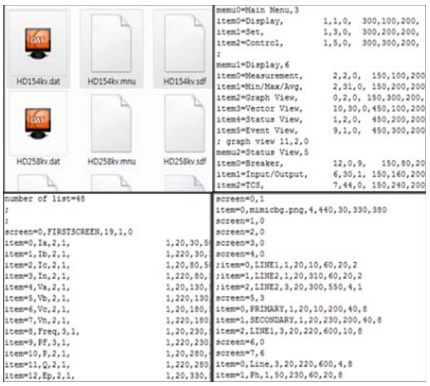

Figure 3. Configure files

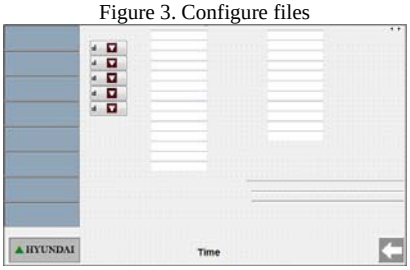

Figure 4. Default UI screen

II. REALIZATION RESULT

Figure 5. Realized screen

Special Protection Schemes (SPSs) with Smart Transmission Switching

Akshay Korad and Kory W. Hedman
School of Electrical, Computer, and Energy Engineering, Arizona State University, Tempe, AZ 85287, USA,
Email: akorad@asu.edu and Kory.Hedman@asu.edu

***Abstract*— Special protection Schemes (SPSs), also known as Remedial Action Schemes (RAS), are an essential part of grid operations as they can be used to improve the reliability of the grid and improve the operational efficiency. Today, SPSs are established based on the operators' past knowledge of the system as well as ad-hoc methods. It is extremely difficult to solve such a complex nonlinear, non-convex combinatorial network problem in real time. Hence, current SPSs are developed offline. The benefit of doing so is that they are developed in advance, the corrective action is predetermined, and SPSs are setup to automatically respond once the predefined contingency occurs; the drawback is that they may be less accurate since the status of the system must be predicted. A systematic tool for the identification of new and advanced SPSs involving transmission switching that can be used to improve system reliability as well as to increase operational flexibility to improve system efficiency is presented. The Direct Current Optimal Power Flow (DCOPF) formulation is used to model the network flow for the electric grid. The candidate switching actions is identified by the use of the smart transmission switching DCOPF formulation. The formulation will be modified to determine the operating states by which the corrective action will be effective. Furthermore, the corrective action would also need to be confirmed with an AC power flow model to ensure that the switching action is AC feasible. The proposed method is implemented on Reliability Test System (RTS) – 1996.**

I. KEY EQUATIONS

Minimize:

$$\sum_t \sum_g \left(c_g P_{gt} + c_g^{SU} v_{gt} + c_g^{SD} w_{gt} + c_g^{NL} u_{gt} \right) \quad (1)$$

s.t.

$$\sum_{\forall k(n,.)} B_k(\theta_{nt} - \theta_{mt}) - \sum_{\forall k(.,n)} B_k(\theta_{nt} - \theta_{mt}) + \sum_{\forall g(n)} P_{gt} = d_{nt}, \forall n,t \quad (2)$$

$$P_k^{\min} \le B_k(\theta_{nt} - \theta_{mt}) \le P_k^{\max}, \forall k,t \quad (3)$$

$$\sum_{\forall k(n,.)} B_k(\gamma_{kt}^c - \theta_{mt}^c) - \sum_{\forall k(.,n)} B_k(\gamma_{kt}^c - \theta_{mt}^c) + \sum_{\forall g(n)} P_{gt}^c = d_{nt}, \forall n,t \quad (4)$$

$$P_{kc}^{\min} z_{kt}^c \le B_k(\gamma_{kt}^c - \theta_{mt}^c) \le P_{kc}^{\max} z_{kt}^c, \forall k,t \quad (5)$$

$$\theta_{nt}^c - \gamma_{kt}^c + (1 - z_{kt}^c N1_k^c)\theta^{rec} \ge 0, \forall k,t \quad (6)$$

$$\theta_{nt}^c - \gamma_{kt}^c - (1 - z_{kt}^c N1_k^c)\theta^{rec} \le 0, \forall k,t \quad (7)$$

$$P_g^{\min} u_{gt} \le P_{gt} \le P_g^{\max} u_{gt}, \forall g,t \quad (8)$$

$$v_{g,t} - w_{g,t} = u_{g,t} - u_{g,t-1}, \forall g,t \quad (9)$$

$$\sum_{q=t-UT_g+1}^{t} v_{g,q} \le u_{g,t}, \forall g, t \in \{UT_g,..,T\} \quad (10)$$

$$\sum_{q=t-DT_g+1}^{t} w_{g,q} \le 1 - u_{g,t}, \forall g, t \in \{DT_g,..,T\} \quad (11)$$

$$P_{g,t} - P_{g,t-1} \le R_g^{+} u_{g,t-1} + R_g^{SU} v_{g,t}, \forall g,t \quad (12)$$

$$P_{g,t-1} - P_{g,t} \le R_g^{-} u_{g,t} + R_g^{SD} w_{g,t}, \forall g,t \quad (13)$$

$$P_{gt}^c - P_{gt} \le R_g^{+c}, \forall g,c,t \quad (14)$$

$$P_{gt} N1_g^c - P_{gt}^c \le R_g^{-c}, \forall g,t \quad (15)$$

$$0 \le v_{g,t} \le 1, \forall g,t \quad (16)$$

$$0 \le w_{g,t} \le 1, \forall g,t \quad (17)$$

$$u_{g,t} \in \{0,1\}, \forall g,t \quad (18)$$

$$z_{kt}^c \in \{0,1\}, \forall k,t \quad (19)$$

II. KEY FIGURES

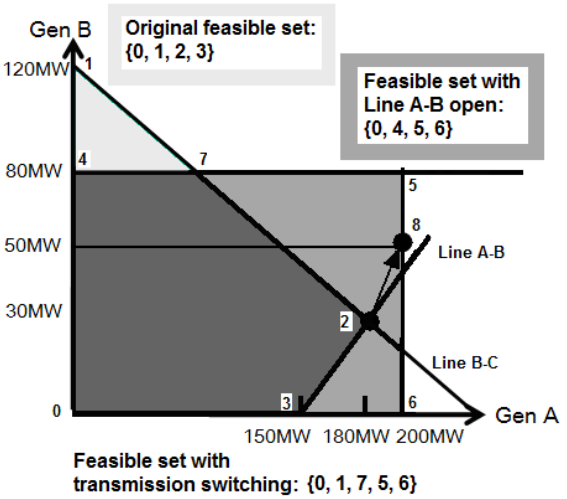

Figure 1. Optimal Transmission Switching's Influence on the Feasible Set

Wind Turbine Imbalance Fault Detection Using the Hilbert-Huang Transform

Clark Lacy, Xiang Gong, and Wei Qiao
Department of Electrical Engineering, University of Nebraska-Lincoln, Lincoln, Ne 68588, USA,
Email: clarklacy@gmail.com

***Abstract*— The Hilbert-Huang Transform (HHT) is a relatively new method of representing a signal in both the time and frequency domains. This method utilizes Empirical Mode Decomposition to separate a signal into a set of sinusoidal waveforms that satisfy the following requirements of an IMF, (1) in the dataset, the number of extrema and the number of zero-crossings must either be equal or differ at most by one; and (2) at any point the mean value of the envelope containing the dataset is zero. The frequency and amplitude of each IMF can then be calculated using the Hilbert Transform and its properties. This work studies the use of the HHT method for wind turbine imbalance fault detection using the wind generator's stator current measurements, which are nonlinear, non-stationary signals due to the variable-speed operation of the wind turbine.**

I. KEY EQUATIONS

The guiding equations of the immune based controller are:

$$H[x(t)] = \frac{1}{\pi} PV \int_{-\infty}^{\infty} \frac{x(\tau)}{t-\tau} d\tau = y(t) \quad (1)$$

$$z(t) = x(t) + jy(t) = a(t)e^{j\theta(t)} \quad (2)$$

$$a(t) = \sqrt{x^2(t) + y^2(t)} \quad (3)$$

$$\theta(t) = \tan^{-1}\left(\frac{y(t)}{x(t)}\right) \quad (4)$$

$$w(t) = \frac{d\theta(t)}{dt} \quad (5)$$

II. KEY FIGURES

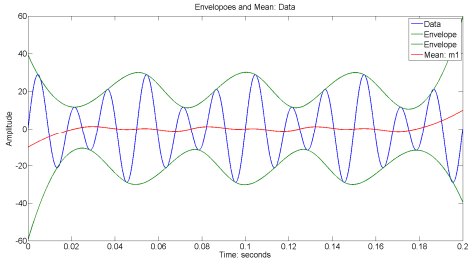

Figure 1. Original Data with Envelopes and the Corresponding Mean of the Two Envelopes.

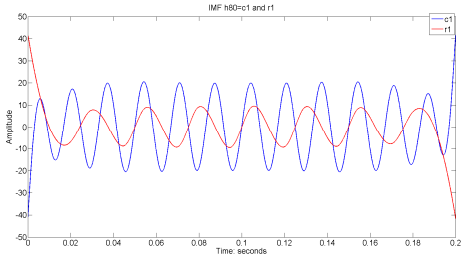

Figure 2. The Two Primary Components of the Original Data After Sifting

III. KEY RESULTS

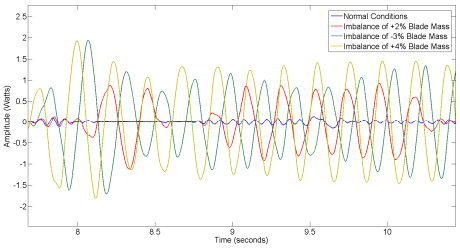

Figure 3. Third Extraction of Data for the Four Simulations of the Imbalance Faults

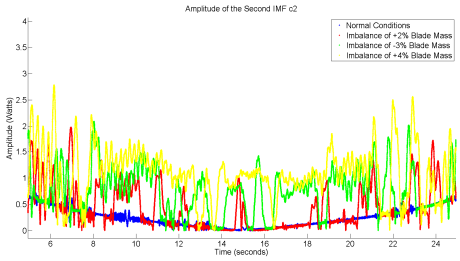

Figure 4. Amplitude of Third Extraction from Data for the Four Simulations of the Imbalance Faults

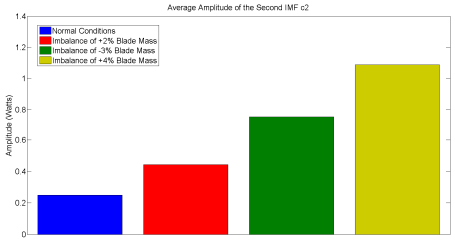

Figure 5. Average Amplitude of Third Extraction from Data for the Four Simulations of the Imbalance Faults

Selective Ground Fault Protection Algorithm For DC Traction Systems

Won-Seok Lee, Sang-Hee Kang
Department of Electrical Engineering, Myongji University
Email: iamaseouler@gmail.com and shkang@mju.ac.kr

***Abstract*— Most DC traction systems are ungrounded to minimize the stray current which can increase the potential of the rail. The ground faults in the DC railway systems are usually detected by a potential relay, 64P. Upon detecting a ground fault, the potential relay right away initiates the tripping of the corresponding breakers to ensure the safety of the electric facilities. However, a conventional 64P relay has some shortcomings. Even though it can detect a ground fault very well, it is unable to identify the faulted line and the faulted region as well. Thus, a ground fault occurs, in Figure 1, for example, all four breakers in substation B and all four breakers in substation C will be tripped out by each 64P. Moreover, there can be the worst case which all four breakers in substation A are also tripped by the operation of the 64P installed at substation A. It is obviously desirable that the feeder breaker at the right up-line (RU) in the substation B and the feeder breaker at the left up-line (LU) in the substation C should be tripped out selectively when a fault occurs as in Figure 1. A selective ground fault protection algorithm for a DC traction system is suggested in this paper. To apply the suggested algorithm, a high speed ground switch controlled by power electronic devices should be installed parallel to the 64P as in Figure 2. The high fault current after a ground fault can flow through the ground switch during very short time, 100 [ms], for example, in this paper. The proposed algorithm is able to identify the faulted feeder as well as the faulted region. The operating process of the proposed algorithm is as follows. A ground fault is detected by the 64P, which operates the ground switch on. A faulted feeder can be preselected after comparing the integrated currents calculated with four feeder currents in a substation. The highest integrated current is the one from the faulted feeder. The pick-up information of the preselected feeder is transferred to the remote substation to be compared with the pick-up information of the remote substation. The pick-up information of the remote substation also comes to the local substation. If the two pick-up results from each end are same, it is finally decided to ignite the breaker of the feeder. The DC traction system is modeled with PSCAD/EMTDC and a traction load consists of DC motors and a inverter based on PWM.**

I. KEY EQUATIONS

Figure 3 and eq. (1) explain how to integrate each feeder current.

$$\Delta I = \int_{t_F}^{t_W} (I_F - I_{pre})dt \ \ [A \cdot S] \qquad (1)$$

t_F : Time of fault detection
t_W: Time to end integration
I_F : Fault current
I_{pre}: Pre-fault current

II. KEY FIGURES

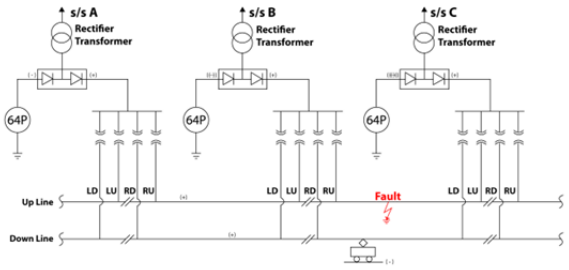

Figure 1. Conventional protective relaying scheme for ground faults in a DC traction system

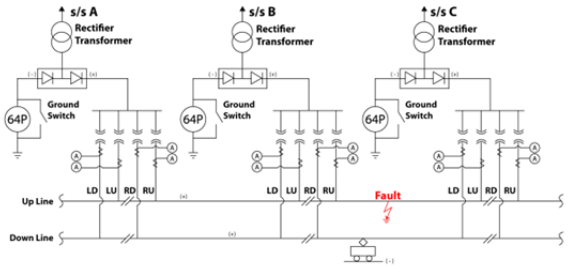

Figure 2. Proposed protective relaying scheme for ground faults in a DC traction power system

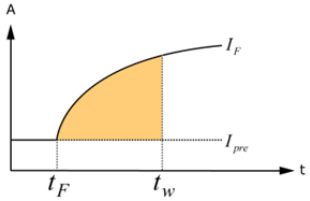

Figure 3. Typical fault current and current integration

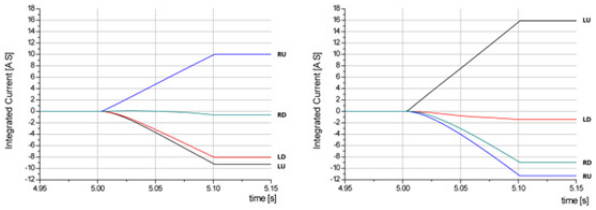

Figure 4. Integrated feeder currents at s/s B (left) and at s/s C (right)

III. KEY RESULTS

Figure. 4 shows the integrated feeder currents at substation B and C when a ground fault occurs at the up-line between substation B and C and a traction load is in the center of the down-line between substation B and C. Figure. 4 shows that the proposed algorithm successfully detects the faulted feeder.

Coordination of Protection and VSC-HVDC Systems for Mitigating Cascading Failures

Rujiroj Leelaruji and Luigi Vanfretti
School of Electrical Engineering, Department of Electric Power Systems
Royal Institute of Technology (KTH), Stockholm, Sweden
Email: rujiroj.leelaruji@ee.kth.se and luigi.vanfretti@ee.kth.se,

***Abstract*— This poster proposes a methodology to coordinate protection relays with a VSC-HVDC link for mitigating the occurrence of cascading failures in stressed power systems. The methodology uses a signal created from an evaluation of the relay's status and simplifications of certain system parameters. This signal is sent to a Central Control Unit (CCU) which determines corrective action in order to reduce the risk of cascading failures.**

We hypothesize that if the operation of protective devices is coupled to the potential relief capacity of VSC-HVDC, then cascading failures can be avoided. To this aim, we propose a control strategy coupling protection systems and VSC-HVDC that can mitigate tripping propagation of the transmission lines.

I. KEY EQUATIONS

The components involved in this study are modelled as following:

Overcurrent Relays (Inverse characteristic):

$$t(I) = \frac{A}{M^P - B} + C \tag{1}$$

Relay tripping variable:

$$x_r = \begin{cases} \int_0^{T_0} \frac{1}{t(I)}\, dt & |I| \geq 1.2 I_P \\ 0 & |I| < 1.2 I_P \end{cases} \tag{2}$$

Non-linear load with exponential recovery:

$$\frac{dx_p}{dt} = \frac{1}{T_{Lp}}(-x_p + P_s(V_L) - P_t(V_L)) \tag{3}$$

$$P_L = x_p + P_t(V_L)$$

VSC-HVDC (Injection model):

$$E_i = \frac{1}{U_i}\sqrt{(P_{si}^2 + Q_{si}^2)X_{eq_i}^2 - U_i^4 + 2X_{eq_i}U_i^2(Q_{si} + \frac{U_i^2}{X_{eq_i}})}$$

$$\delta_i = \begin{cases} \theta_i - \arcsin(-\frac{P_{si}X_{eq_i}}{U_i E_i}) & \cos(\theta_i - \delta_i) > 0 \\ \theta_i - \left[\pi - \arcsin(-\frac{P_{si}X_{eq_i}}{U_i E_i})\right] & \cos(\theta_i - \delta_i) < 0 \end{cases} \tag{4}$$

II. KEY FIGURES

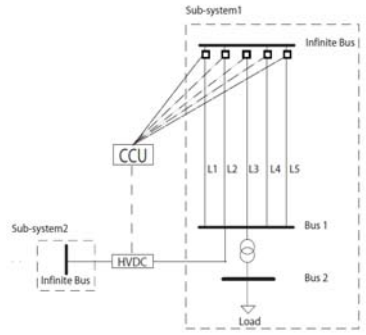

Figure 1. Single-Load-Infinite-Bus (SLIB) system

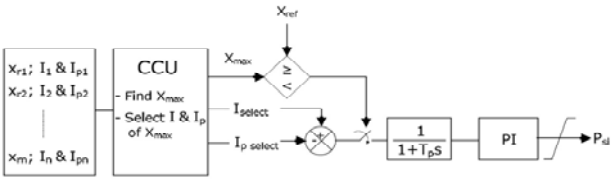

Figure 2. Coordination of the protection relays and the VSC-HVDC injection model

III. KEY RESULTS

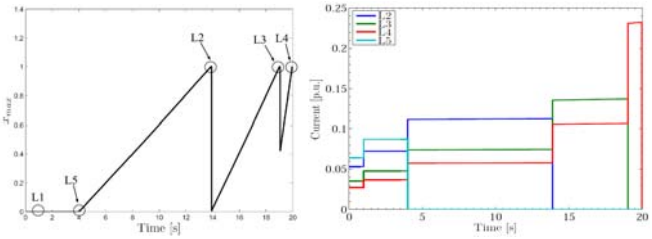

Figure 3. Tripping indicator and Line current profile without coordination between protection and VSC-HVDC systems

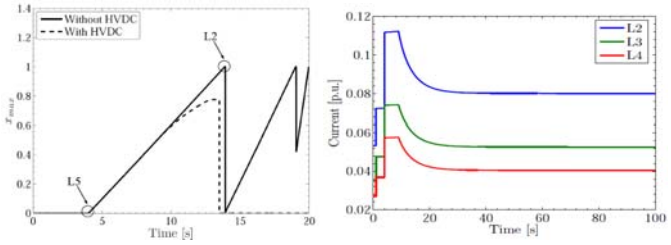

Figure 4. Tripping indicator and Line current profile with coordination between protection and VSC-HVDC systems

A New Technique of Faults Detection in De-Energized Distribution Feeders

Xun Long, Wilsun Xu and Yun Wei Li
Power Disturbance & Signaling Research Laboratory, Department of Electrical and Computer Engineering,
University of Alberta, Edmonton, AB, Canada, T6G 2V4
Email: xlong@ualberta.ca, wxu@ualberta.ca and yunwei.li@ece.ualberta.ca

***Abstract*— Re-energizing an overhead distribution feeder safely is a major consideration for utility's safe work practice. One way to improve the safety is to determine if the feeder still experiences short circuits before it is energized. In this paper, a novel fault detection technique is proposed to detect if a de-energized distribution system still experiences short-circuit faults. The proposed method involves injecting a thyristor-generated controllable signal into the de-energized feeder. The feeder voltage and current responses are analyzed to determine if a fault still exists. A thyristor gating control strategy and fault detection algorithm is also developed in this work to detect all possible types of faults that can happen in a system. Furthermore, a stalled motor or a shunt connected capacitor bank in the downstream may also behaves like a short-circuit. Therefore, a fault detection algorithm based on the analysis of the harmonic impedance of the de-energized system is developed as well. The effectiveness of the proposed method has been verified through theoretical analysis, computer simulations and lab tests.**

I. KEY EQUATIONS

The guiding equations of the thyristor-based scheme for detecting faults in a de-energized system are:

$$v_{signal}(t) = \frac{Z_{load} + Z_{line}}{Z_{load} + Z_{line} + Z_{sys} + 2Z_{xform}} \sqrt{2}E \sin(\omega t + \delta) \quad (1)$$

$$L_{eq} \frac{di_{signal}(t)}{dt} + R_{eq} i_{signal}(t) = V_{signal}(t) \quad (2)$$

$$\left| I_{signal}(t) \right| = \frac{\sqrt{2}E}{\left| Z_{eq} \right|} [\sin(\omega t + \delta_1) - e^{-R_{eq} t / L_{eq}} \sin \delta_1] \quad (3)$$

$$dV(j\omega) = Z(j\omega) * dI(j\omega) \quad (4)$$

$$Z(f) = R(f) + jX(f) = R_{load} + j2\pi f (L_{load} + L_{line}) \quad (5)$$

II. KEY FIGURES

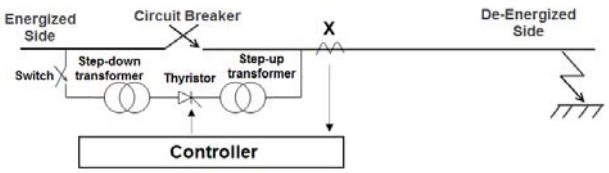

Figure 1. Single-line representation of the proposed fault detection method

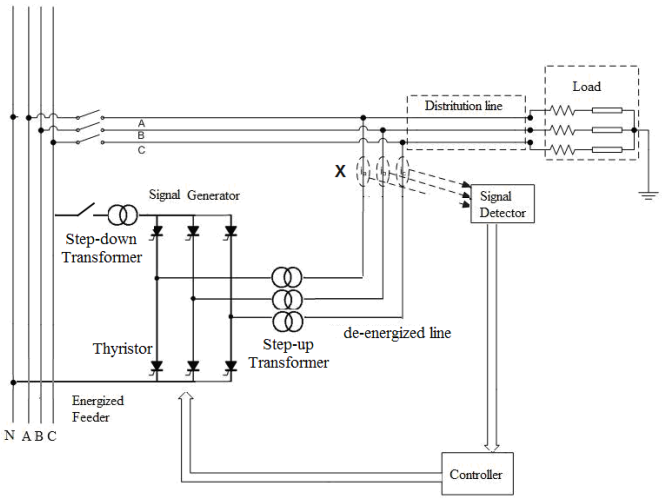

Figure 2. Three-phase thyristor bridge based fault detection scheme.

III. KEY RESULTS

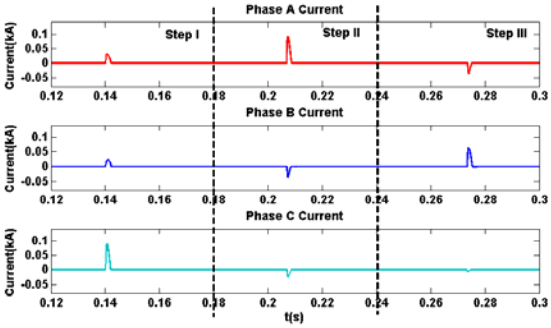

Figure 3. Three-phase detection signals under multiple faults.

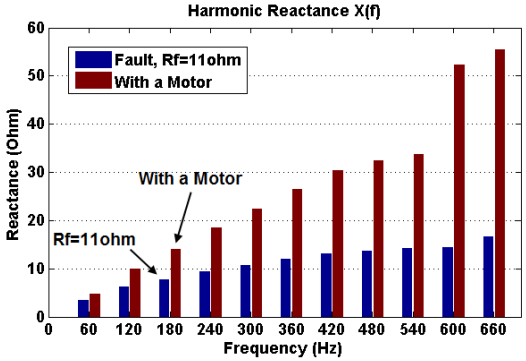

Figure 4. Lab test result. (Distinguish a fault from a stalled motor by utilizing harmonic reactance)

Stator Current-Based Fault Diagnosis of Wind Turbines using ALE & Wiener Filter

Dingguo Lu and Wei Qiao
Power and Energy Systems Laboratory, Department of Electrical Engineering, University of Nebraska-Lincoln, Lincoln, NE 68588-0511, USA,
Email: stan1860@huskers.unl.edu and wqiao3@unl.edu

***Abstract*—Fault diagnosis is a preliminary process for condition monitoring on wind turbines. This research presents the application of an optimal Adaptive Line Enhancer (ALE) and Wiener Filter on fault diagnosis using the stator current measured from the wind turbine generator terminals. In this research, signal refers to the components in measurements that are induced by faults, while noise refers to the dominant components in measurements that are not related to faults. Under this definition, the signals measured from the faulted components will have a low signal-to-noise ratio (SNR), which makes fault detection difficult. The optimal ALE is proposed using an adaptive Wiener Filter as a fault diagnostic tool. Original data is filtered by a Lowpass Filter first and the output is used as the input of the ALE. Since the system is a time-varying system, the tap-weight vector of the Wiener filter is updated based on the Fast Block Least-Mean-Squares (FBLMS) algorithm. The output of ALE is then analyzed in both time domain and frequency domain. The pattern changes of the output can indicate whether there exists any fault within a wind turbine. The simulation results have shown that the proposed method is effective for the fault diagnosis on wind turbines operating at variable loads.**

I. KEY EQUATIONS

The guiding equations of the optimal ALE based Wiener Filter and FBLMS are:

1). Filtering

$$\mathbf{x}_F(k) = FFT(\tilde{\mathbf{x}}(k)) \quad (1)$$

$$\mathbf{y}(k) = \text{last L elements of } IFFT(\mathbf{x}_F(k) \otimes \mathbf{w}_F(k)) \quad (2)$$

2). Error estimation

$$\mathbf{e}(k) = \mathbf{d}(k) - \mathbf{y}(k) \quad (3)$$

3). Tap-weight adaption:

$$\mathbf{e}_F(k) = FFT\left(\begin{bmatrix} \mathbf{0} \\ \mathbf{e}(k) \end{bmatrix}\right) \quad (4)$$

$$\mathbf{w}_F(k+1) = \mathbf{w}_F(k) + 2\mu(\mathbf{x}_F^*(k) \otimes \mathbf{e}_F(k)) \quad (5)$$

4). Tap-weight constraint

$$\mathbf{w}_F(k+1) = FFT\left(\begin{bmatrix} \text{first N elements of } IFFT(\mathbf{w}_F(k+1)) \\ \mathbf{0} \end{bmatrix}\right) \quad (6)$$

II. KEY FIGURE

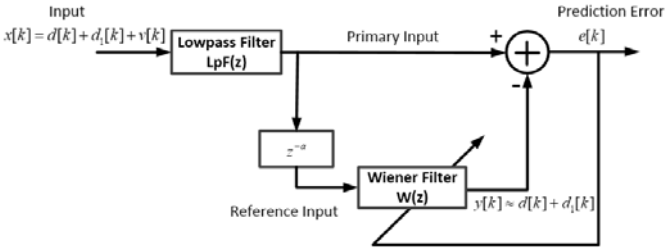

Figure 1. Optimal ALE as fault diagnostic tool

III. KEY RESULTS

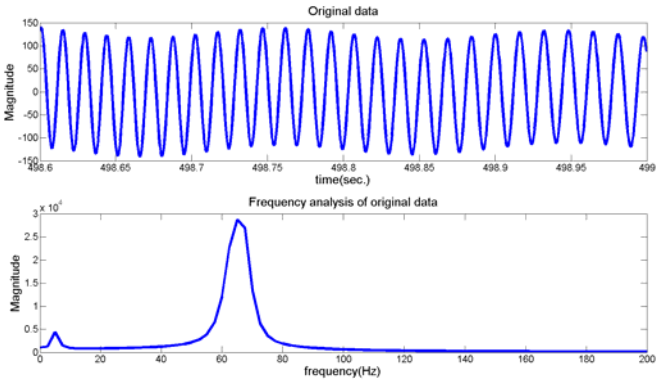

Figure 2. Original data used to train the optimal ALE, where large energy is found around both5Hz and 65Hz

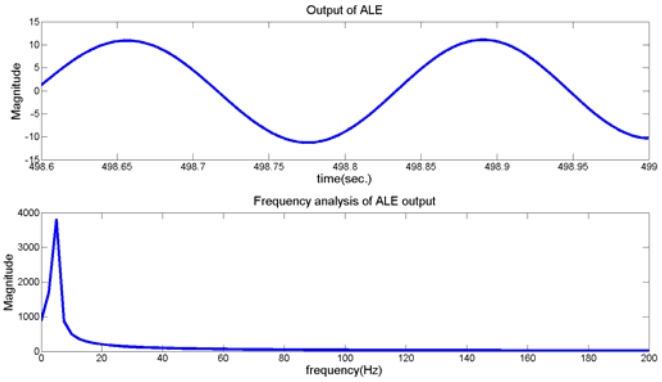

Figure 3. Performance of the optimal ALE, where large energy is found around only 5Hz

Detection of Forced-Response Disturbances in Power Systems

Russell C. Martin, Luke A. Dosiek, and John W. Pierre
Department of Electrical and Computer Engineering, University of Wyoming, Laramie, WY 82071, USA
Email: rcmartin@uwyo.edu pierre@uwyo.edu ldosiek@uwyo.edu

***Abstract*— In power systems, unwanted forced responses within the system can occur. This happens for various reasons, such as a rogue controller on a generator. These forced responses show up in synchrophasor measurements. It is desirable to be able to accurately detect these oscillations in order to better understand what causes them. Such oscillations have been linked to power system instability, even though they can often vary across a wide range of measurable magnitude. The frequencies of these disturbances can be very close to system electromechanical modes. Also, these oscillations are not to be confused with transients caused by line-switching and load shedding within the power system. If the forced oscillations present are of low magnitude, to distinguish them it may be necessary to eliminate the presence of the power system electromechanical modes as well as observe a long record length of collected data. A detection method for such oscillations can be implemented with the availability of system-wide data collected from Phasor Measurement Units (PMUs). This detection method utilizes multiple signal processing techniques in order to estimate presence and characteristics. A whitening filter can be constructed from a recent parametric estimate of power system modes, and statistical analysis applied in order to pick out present sinusoids. The proposed detection scheme has been numerically implemented on simulated power system data as well as real-world PMU data, and results are presented in this poster.**

I. Key Equations

$$H(z) = \frac{1}{A(z)}\text{; AR Transfer Function of estimated order} \quad (1)$$

$$W(z) = \frac{1}{H(z)}\text{; Filter to whiten electromechanical modes} \quad (2)$$

II. Key Figures

Note: Location of individual PMUs, exact time of measurement, and raw data is confidential. Both PMUs shown in these figures have the same filtering applied to either set of data.

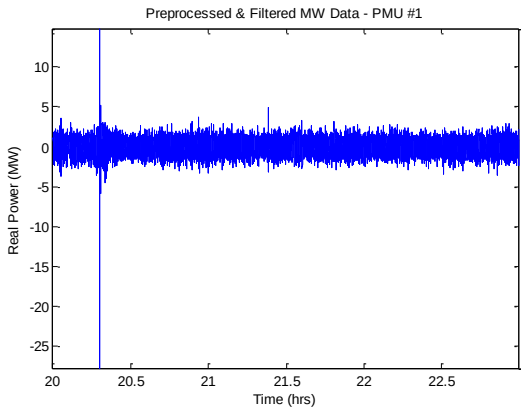

Figure 1: Three hours of power data from PMU #1. After processing the data, a clear "event" is present just after the 20th hour.

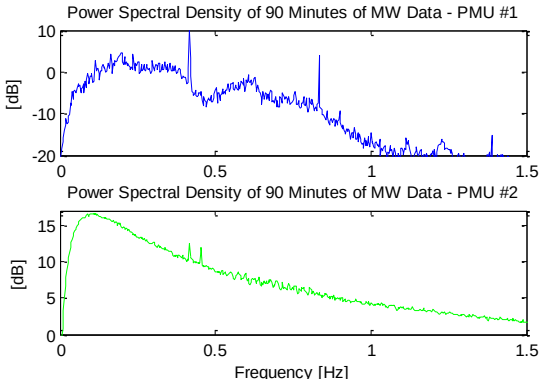

Figure 2: PSDs of two geographically separated PMUs over a 90-minute time-synchronized period. This shows the same forced oscillation at 0.42Hz occurring at both PMUs, over an hour after the "event" shown in Figure 1.

III. Key Results

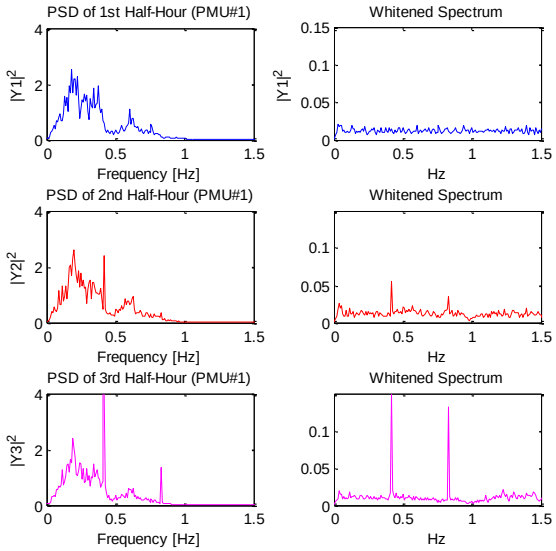

Figure 3: The same 90-minute period broken into 30-minute segments. The whitening filter allows early detection of the forced oscillation and associated harmonic.

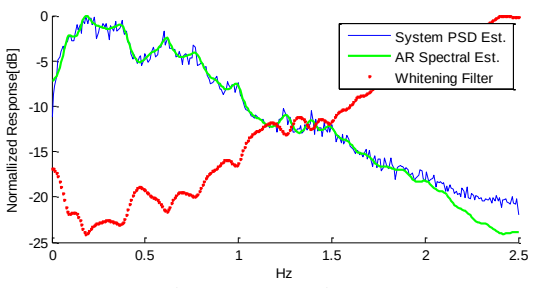

Figure 4: From the first 30 minutes of data seen in Figure 3 (no oscillation present), use Recursive-Least Squares to construct an AR spectral estimate of the system and construct the whitening filter.

Testing POTT Scheme Based on International Electrotechnical Commission (IEC) 61850

José Ruiz and Kirpal Doad
Power System Laboratory, Department of Electrical Engineering, University of Tennessee at Chattanooga, Chattanooga, TN 37403, USA
Email: *Jose-Ruiz@mocs.utc.edu and sgw333@mocs.utc.edu*

***Abstract*—IEC 61850 describes rules for integration of protection, control, measurement, and monitoring functions within a power system network at the process and station control levels. Earlier envisioned for substation automation, IEC 61850 has shown potential in eliminating substation wiring and enhancing interoperability between vendors and systems. Thus efforts are now being made to expand it to cover substation-to-control center and substation-to-substation-automation. This study implemented the International Electrotechnical Commission (IEC) 61850 standard in a Permissive Overreach Transfer Trip (POTT) scheme to protect a 34.76 mile, 161 kV transmission line using Generic Object Oriented Substation Events (GOOSE) messaging in the laboratory. Two digital line protection relays were placed at each end of the line to protect the transmission line via the POTT communication scheme. Faults were simulated at different points on the line using two modern relay test sets. It is observed that the average maximum and minimum time delay between fault occurrence and the POTT operation is around 24.6 ms and 8.18 ms respectively under laboratory conditions for source impedance ratios (SIR) of 1.0 and 0.58.**

I. KEY FIGURES

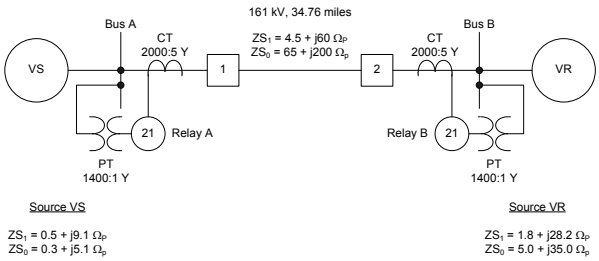

Figure 1. Test System

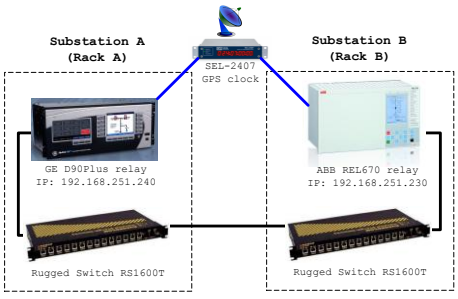

Figure 2. Communication Scheme

II. KEY RESULTS

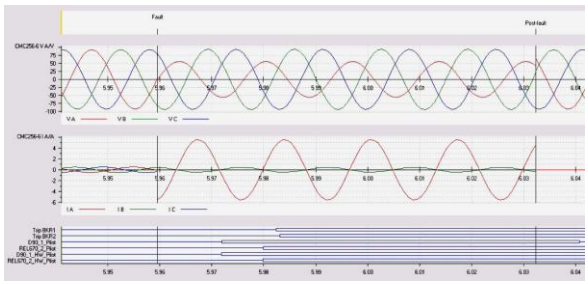

Figure 3. Breakers and Permissive trip signals on GOOSE messages and hard-wired Comparison for an A-G fault at 90% of the transmission line applied to relay A

Fault Type and Location	Relay A			Relay B		
	Average Time (cycles)	Max Time (cycles)	Minimum Time (cycles)	Average Time (cycles)	Max Time (cycles)	Minimum Time (cycles)
3-phase 10%	0.49	0.52	0.47	1.41	1.50	1.35
A-G 10%	0.52	0.54	0.49	1.41	1.46	1.39
B-C-G 10%	0.61	0.64	0.59	1.44	1.54	1.37
B-C 10%	0.62	0.64	0.60	1.42	1.48	1.35
3-phase 90%	1.35	1.49	1.22	1.41	1.47	1.35
A-G 90%	1.38	1.49	1.23	1.45	1.52	1.40
B-C-G 90%	1.32	1.37	1.25	1.41	1.49	1.37
B-C 90%	1.38	1.44	1.33	1.48	1.55	1.41

Table 1. Performance Comparison for POTT with IEC 61850

Fault Type and Location	Relay A			Relay B		
	Average Time (cycles	Max Time (cycles	Minimum Time (cycles	Average Time (cycles	Max Time (cycles	Minimum Time (cycles
3-phase 10%	0.50	0.53	0.47	1.45	1.54	1.40
A-G 10%	0.51	0.54	0.49	1.44	1.52	1.39
B-C-G 10%	0.61	0.62	0.59	1.45	1.53	1.30
B-C 10%	0.62	0.64	0.61	1.49	1.53	1.42
3-phase 90%	1.48	1.55	1.43	1.48	1.54	1.39
A-G 90%	1.47	1.56	1.42	1.49	1.56	1.43
B-C-G 90%	1.49	1.57	1.37	1.47	1.57	1.38
B-C 90%	1.50	1.55	1.44	1.46	1.48	1.43

Table 2. Performance Comparison for POTT with Hard-wired

Trending and Condition Monitoring of Wind Turbine SCADA data

Author: Shane Ryan, *Student Member, IEEE*; Advisor: Prof. Chen Ching Liu, *Fellow, IEEE.*
Department of Electrical, Electronic and Mechanical Engineering, University College Dublin, Belfield, Dublin, Ireland
Email: *shane.ryan.4@ucdconnect.ie*; *liu@ucd.ie*

***Abstract*- Wind turbines are going to take up a sizeable fraction of the green energy put forward in reducing greenhouse gases globally within the next century. With this surge in their production and usage, optimal operation and maintenance procedures are essential to their technical and economic development. Wind turbines produce vast amounts of supervisory control and data acquisition (SCADA) data on their various components to monitor their condition whilst the turbine is running. There is a need to develop data analysis methods to utilise this information in the most efficient way possible. It is required to simplify and produce the data in a manner where particular trends towards component failure can be deduced. Data analysis centres on the power curve of the wind turbines and a method to reduce data point quantity of yearly scatter plots of power curves containing up to 50000 data points. These plots are compared against the official vendor power curve taken from the turbine manual and the theoretical wind power curve. The results for the 70 wind turbines show that in general, the turbines perform well with only two turbines exhibiting noticeable underperformance. These turbines are examined in detail and the first turbine is found to have an erratic pitching issue which is familiar to the DSO and is an open issue with the turbine vendor and the DSO. The second turbine is underperforming for an unknown reason and hypotheses are put forward with the support of graphs of various SCADA outputs. Ideas for implementation of this mean power curve into a potential alarm system with upper and lower alarm limits applied to the power curve are also put forward. The DSO is looking further into this problem, by analyzing the profile of the surrounding land causing aerodynamic issues.**

I. KEY EQUATIONS

$$\bar{P}_{a,b,c..} = \frac{X_1 + X_2 + .. X_n}{X_n}$$

$$\bar{V} = 0.5,1.0,1.5 \ldots; \begin{cases} 2.5 \leq V \geq 4 \\ 10 \leq V \geq 20 \end{cases}$$

$$\bar{V} = 4.0,4.25,4.5,4.75,5.0 \ldots; \quad \{4 \leq V \geq 10$$

$$D = \frac{P_x}{P_{nom}}$$

II. RESULTS

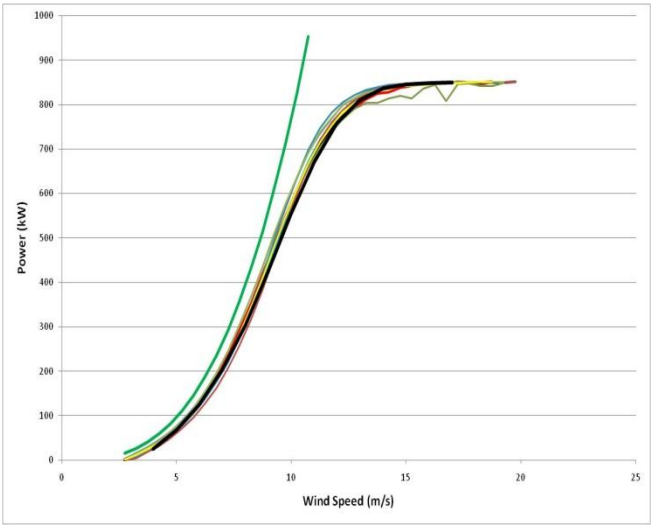

Figure 1. Power Curve comparison

Field:	[UnitID]	[AvgWindSpeed]	[AvgPower]	[AvgPitchAng]
Table:	WTShortHist	WTShortHist	WTShortHist	WTShortHist
Sort:				
Show:	☑	☑	☑	☑
Criteria:		>=12	<840	<20

Figure 2. Data Filtering after curve analysis to centralize on period of underperformance.

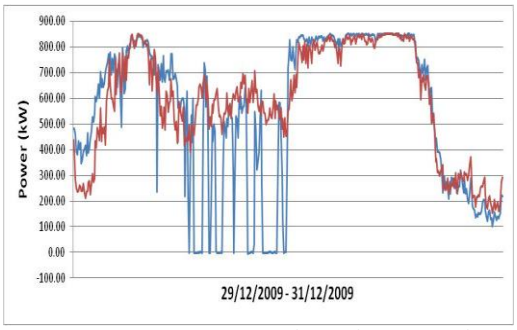

Figure 3. 3-day Power plot of identified period of underperformance, optimally performing turbine plotted against underperforming turbine.

Trouble Call Analysis Using Artificial Immune System Techniques

Laxman Subedi, Anil Pahwa and Sanjoy Das
Electrical and Computer Engineering, Kansas State University, Manhattan, KS 66502, USA,
Email: laxman@ksu.edu, pahwa@ksu.edu and sdas@ksu.edu

***Abstract*—Loss of power means loss of revenue to industry and businesses, and overall inconvenience to customers. The first step of outage management is to know where the problem is. This part of outage management is usually called Trouble Call Analysis in the utility jargon. The utilities typically depend on customers to call and inform them of the problem by entering their addresses. After sufficient calls are received, the utility is able to pinpoint the location of the outage. The biggest challenge is to determine the sufficient level of calls before declaring the location of outage. Incorrect location would lead to wasted crew time and delay in service restoration. On the other hand waiting too long to make the diagnosis will also delay restoration of power to the customers. This research focuses on using artificial immune system techniques to analyze the trouble calls and determine the location of the outage. The idiotypic network model was used modeling protective devices as antibodies and customer trouble calls as antigens. Different call scenarios were created using the test circuit system. The differential equation was solved in MATLAB using the call scenarios. The output of the simulation identifies the probable faulty device based for that particular call scenario. Based on the given calls, the algorithm predicted the likely fault location in the initial cases. The algorithm is to be tested on a real circuit with known customer calls.**

I. KEY EQUATIONS

The dynamics of the system based on the idiotypic network model can be described using a set of differential equations in the form as below:

$$\frac{dx_i}{dt} = c\left[\sum_{j=1}^{N} m_{ji}x_i x_j - k_1\sum_{j=1}^{N} m_{ij}x_i x_j + \sum_{j=1}^{n} n_{ji}x_i y_j\right] - k_2 x_i \quad (1)$$

The modified algorithm for the system is given as:

$$\frac{dx_i}{dt} = c\left[-k_1\sum_{j=1}^{N} m_{ij}x_i x_j + \sum_{j=1}^{n} n_{ji}x_i y_j\right] - k_2 x_i \quad (2)$$

$$\frac{dx_i}{dt} = c\left[-(Suppression) + (Stimulation)\right] - (Death\ rate) \quad (3)$$

II. KEY FIGURES

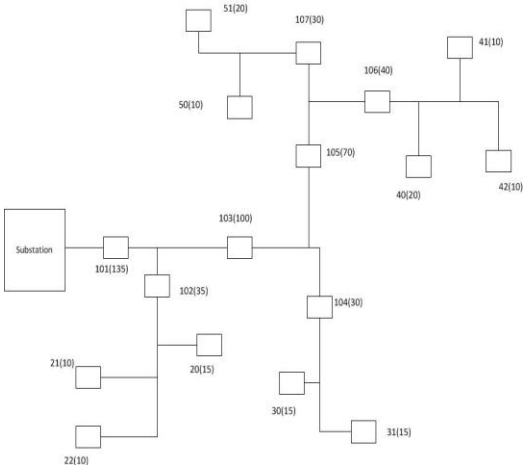

Figure 1: Test circuit system

The squares represent the protective devices each with its own unique number and number of customers is given in brackets.

III. KEY RESULTS

Calls Scenario: 1 call from 40, 1 call from 41, 1 call from 42

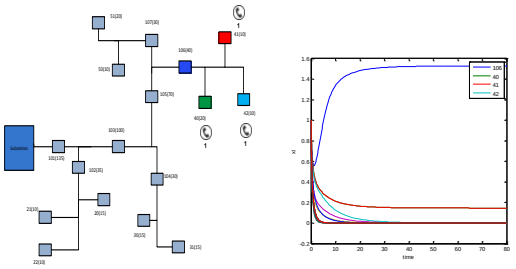

Figure 2: Results for call scenario 1

Calls Scenario2: 1 call from 40, 1 call from 41, 1 call from 42, 1 call from 50, 1 call from 51

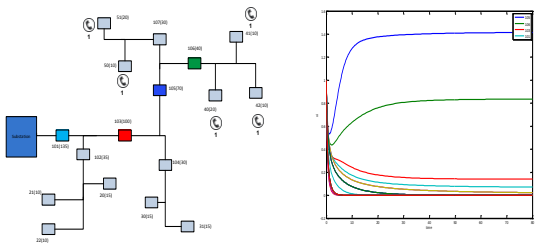

Figure 3: Results for call scenario 2

Multi-Kernel Support Vector Classifier for Fault Diagnosis of Transformers

Yujuan Yin, Junpeng Zhan and Chuangxin Guo
College of Electrical Engineering, Zhejiang University, Hangzhou, Zhejiang, China
Email: yinyujuan@zju,.edu.cn, zhanjunpeng@zju.edu.cn and guochuangxin@zju.edu.cn

***Abstract*—Dissolved gas analysis (DGA) has proved to be one of the most useful techniques to detect the incipient faults of power transformers. This paper presents a novel method named multi-kernel support vector classifier (MKSVC), to analyze the DGA for fault diagnosis of transformers. Different from the conventional support vector machine (SVM), MKSVC uses a combined kernel formed through a linear combination of several basis kernels. In MKSVC, each basis kernel extracts a specific type of information from the training data, providing a partial description of the data. Given many partial descriptions of the data, a convex optimization is obtained by a linear combination. Thus, the learning problem can be solved by iteratively computing this optimization problem. The MKSVC method is evaluated using 318 fault data in comparison with several commonly used methods. The diagnostic results show that the diagnostic accuracy of MKSVC prevail those of the commonly used methods.**

I. KEY EQUATIONS

The guiding equations of multi-kernel support vector classifiers are:

$$\begin{cases} \min_{ff_l,b,\xi,d_l} \quad \frac{1}{2}\sum_{l=1}^{M}\frac{1}{d_l}\| ff_l \|^2 + C\sum_{i=1}^{N}\xi_i \\ subject\ to: \\ y_i\sum_{l=1}^{M} ff_l(x_i) + y_i b \geq 1-\xi_i \\ \sum_{l=1}^{M} d_l = 1 \\ \xi_i \geq 0,\ d_l \geq 0 \end{cases} \tag{1}$$

$$\begin{cases} \max_{\alpha} \quad -\frac{1}{2}\sum_{i,j}\alpha_i\alpha_j\sum_l d_l K_l(x_i,x_j) + \sum_i \alpha_i \\ with \\ \quad \sum_i \alpha_i y_i = 0 \\ \quad C \geq \alpha_i \geq 0 \end{cases} \tag{3}$$

$$f(x) = \sum_{i=1}^{N}\sum_{l=1}^{M}\alpha_i y_i d_l K_l(x_i,x) + b \tag{4}$$

II. KEY FIGURES

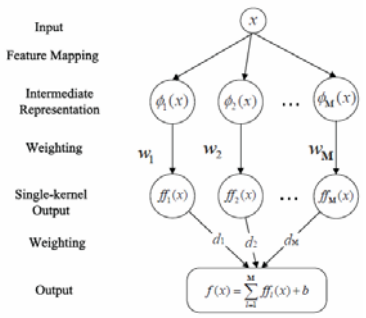

Figure 1. Support vector machine with multi-kernel learning

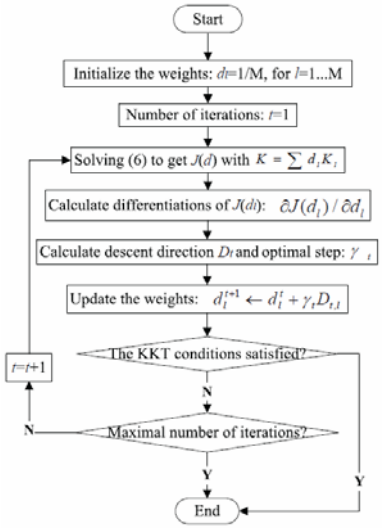

Figure 2. The flow chart of the SimpleMKL algorithm

III. KEY RESULTS

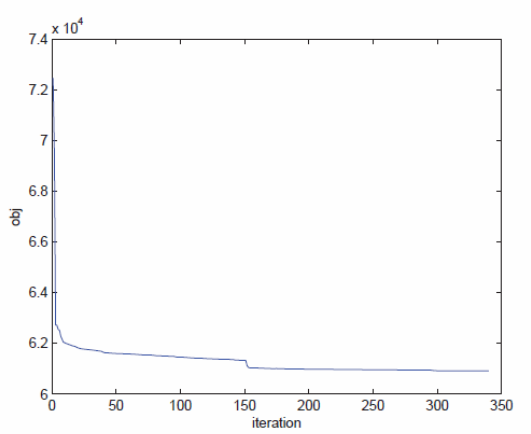

Figure 3. The variation tendency of the value of the objective function

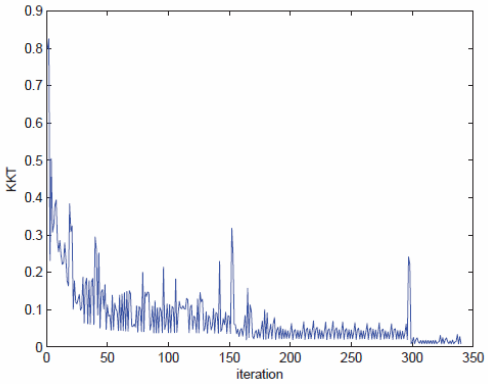

Figure 4. The variation tendency of the KKT constraints

Linear Analysis of the KTH-NORDIC32 System

Yuwa Chompoobutrgool and Luigi Vanfretti
Electric Power Systems, KTH Royal Institute of Technology, Stockholm, SWEDEN
Email: *yuwa@ee.kth.se* *and* *luigiv@kth.se*

***Abstract*— A set of important dynamic properties of power systems are those related with small-signal (or linear) stability. Understanding dynamic responses of a power system is a vital key in assessing the system's characteristics. Once these characteristics of the system have been well-understood, the response of the system to some disturbances may be anticipated. In this study, the linear analysis of the KTH-NORDIC32 system, a conceptualization of the Swedish power system and its neighbors, is presented using the eigenanalysis method. Time-domain simulations are used to verify and to assess the behavior of the linearized system. Two studies are conducted for the model validation; (1) a small perturbation induced by a 3φ fault and (2) a step change at an AVR's voltage reference. The objectives of this poster are to present the linear analysis results of the study system and to assess the small-signal dynamic characteristics of the network.**

I. KEY EQUATIONS

The equations used in eigenanalysis to determine the eigenvalues λ_i, damping ratio ξ_i, and eigenvectors v_i are

$$\det(\lambda I - A) = 0; \text{ (1) where } \quad \lambda_i = \sigma_i \pm j\omega_i$$

$$\xi_i = \frac{-\sigma_i}{\sqrt{\sigma_i^2+\omega_i^2}} \qquad (2)$$

$$Av_i = \lambda_i v_i \qquad (3)$$

II. KEY RESULTS

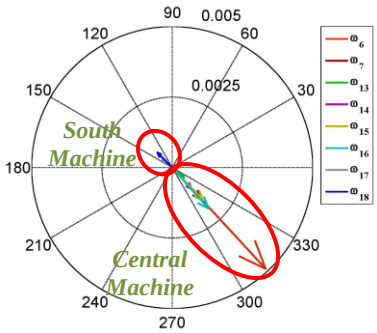

Figure 1. Mode shapes of the generator speed, 0.73-Hz inter-area mode

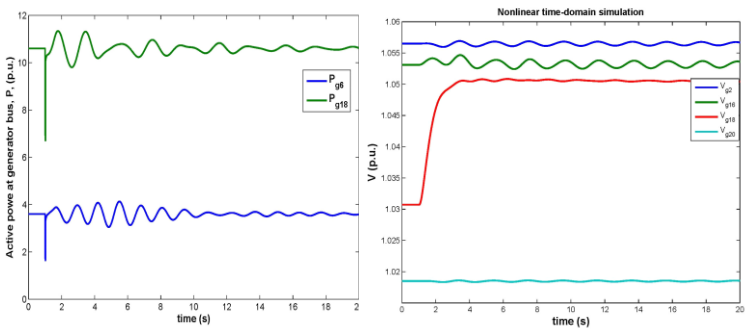

(a) (b)

Figure 2. (a) Active power responses after applying a 3-φ fault at Bus4044. (b) Voltage responses after applying a 2% step change at V_{ref} of the AVR at G_{18}

III. KEY FIGURES

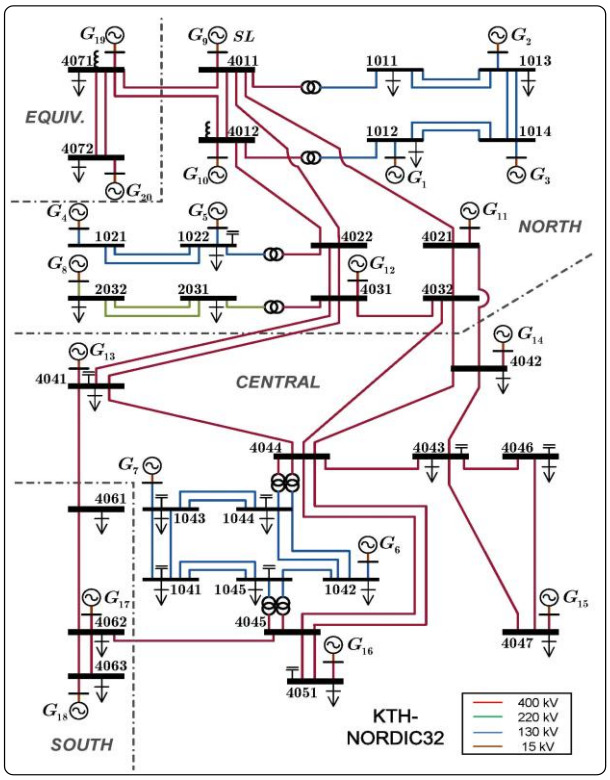

Figure 3. KTH-NORDIC32 System

An Approach to Control Photovoltaic Generator to Damp Low Frequency Oscillations in Emerging Distribution Systems

Sudarshan Dahal, Mithulananthan Nadarajah and Tapan Saha
School of Information Technology and Electrical Engineering, The University of Queensland, Australia
Email: *sdahal@itee.uq.edu.au*, *mithulan@itee.uq.edu.au*, and *saha@itee.uq.edu.au*

***Abstract*— Factors like diminishing fossil fuels and environmental concerns are driving the integration of locally available energy resources at a distribution level. As a result, a number of stability issues have become a concern for utilities at distribution systems. One of the important stability concerns is the small signal stability caused by electromechanical or other low frequency oscillations. The oscillations with lower values of frequency and damping may cause instabilities. In such cases, a suitable control methodology must be applied to ensure the stability of an emerging distribution system. In this paper, a methodology to control the power factor of photovoltaic generator (PV) is proposed for enhancement of system stability. The impact of PV power factor control on a low damped mode is assessed by using both eigenvalue sensitivity and time domain analysis. An appropriate signal for the proposed controller is identified by residue technique. The effectiveness of the controller is tested in IEEE 43 bus test distribution system with distributed generators. Results show that reactive power support from PV is better for damping of critical mode.**

I. KEY EQUATIONS

The guiding equations of the PV generator and controller are:

$$\frac{C}{2}\frac{dv_{dc}^2}{dt} = P_{PV} - P_{DC} \tag{1}$$

$$\begin{cases} P = \frac{3}{2}\left(v_{SD}i_D + v_{SQ}i_Q\right) \\ Q = \frac{3}{2}\left(v_{SQ}i_D - v_{SD}i_Q\right) \end{cases} \tag{2}$$

$$\frac{\partial \lambda_i}{\partial S_{PV}} = \frac{\psi_i^T\left(\frac{\partial A}{\partial S_{PV}}\right)\phi_i}{\psi_i^T.\phi_i} \tag{3}$$

II. KEY FIGURES

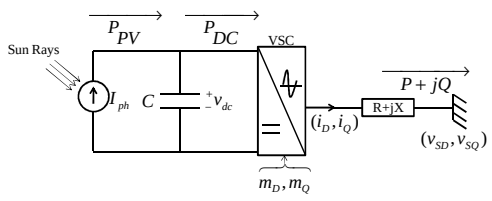

Figure 1. Schematic diagram of a grid connected PV system.

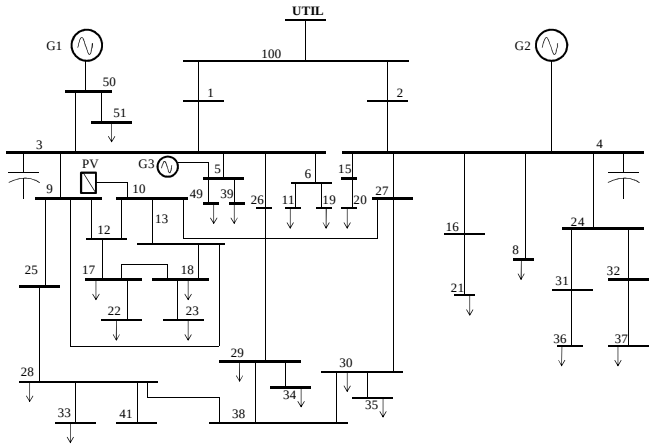

Figure 2. Test Distribution Network

III. KEY RESULTS

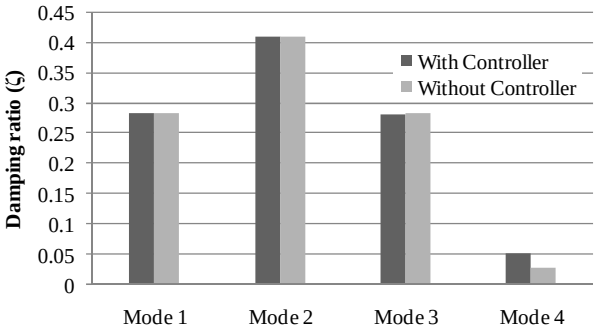

Figure 3. Comparison of damping ratios with and without controller.

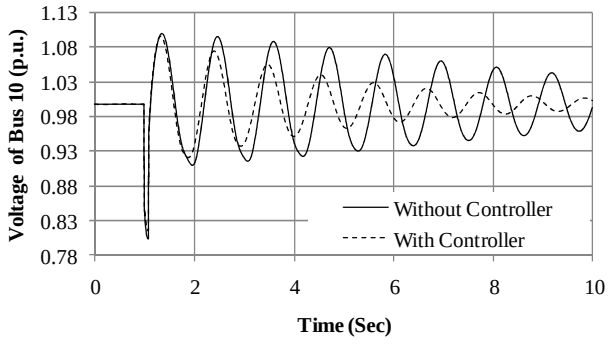

Figure 4. Comparison of time domain responses of voltage at Bus 10 with and without controller

Relating Residuals to Mode Estimate Accuracy for Stability Analysis

Jim Follum and John Pierre
Department of Electrical and Computer Engineering,
University of Wyoming, Laramie, WY
Email: {jfollum, pierre}@uwyo.edu

Ning Zhou
Advanced Power and Energy Systems Group, Pacific Northwest National Laboratory, Richland, WA
Email: ning.zhou@pnl.gov

***Abstract*—This paper proposes a method for determining electromechanical mode estimate accuracy by relating mode estimate error to residual values. Using a 17-machine model with varying levels of load noise, mode frequency and damping ratio (DR) were estimated using Prony analysis and residuals were calculated. Residuals were found to increase proportionally to the root mean squared error (RMSE) of mode estimates as noise levels increased, revealing a distinctly linear relationship. Knowledge of this relationship could help inform system operators of the level of confidence they can place in mode estimates. With the relationship established, a method of predicting mode estimate error based on residuals was developed. After obtaining initial mode estimates, various levels of white Gaussian measurement noise were added to the initial ringdown. Prony analysis was applied for each noise level to obtain new mode estimates. The residual values for each noise level were linearly related to deviations of mode estimates from initial estimates. The slope of the applied linear regression was used to estimate the initial mode error based on the initial residuals. The potential of this method to evaluate the confidence level of mode estimates is examined.**

I. KEY EQUATIONS

The equations to relate residual values from Prony analysis to mode estimate error through a slope are:

$$\hat{y}(k) = \sum_{i=1}^{P} \hat{B}_i * \hat{z}_i^{\,k} \tag{1}$$

$$\varepsilon[k] = y[k] - \hat{y}[k] \tag{2}$$

$$S_{MAX} = \max|\varepsilon[k]| \tag{3}$$

$$S_{RMS} = \sqrt{\frac{1}{K}\sum_{k=1}^{K} \varepsilon[k]^2} \tag{4}$$

$$\epsilon_\lambda = \mathrm{m} * \mathrm{S}_* \tag{5}$$

II. KEY FIGURES

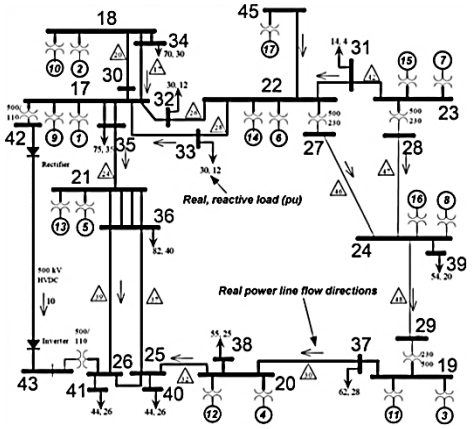

Figure 1. One-line diagram of the 17-machine model

III. KEY RESULTS

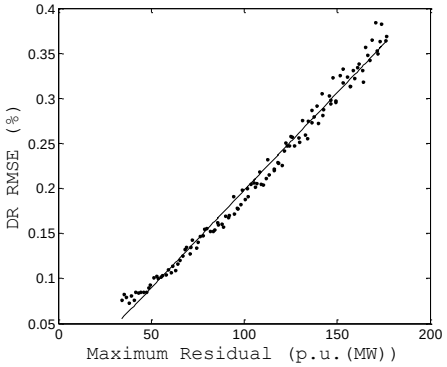

Figure 2. Trend line relating DR estimate error to residual values.

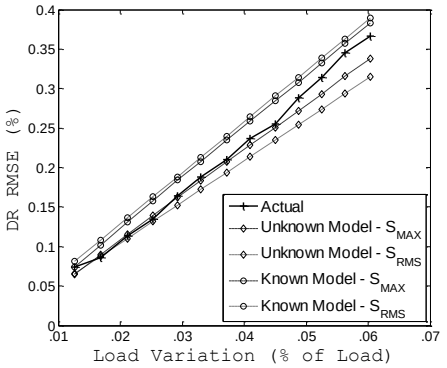

Figure 4. Mode DR RMSE prediction using derived slopes and residual values in real-world conditions (unknown model) and simulation conditions (known model).

A Real-Time Wide-Area Excitation Control to Enhance Transient and Oscillatory Stabilities

Ramtin Hadidi and Benjamin Jeyasurya
Faculty of Engineering & Applied Science, Memorial University of Newfoundland, St. John's, NL, Canada, A1B 3X5,
Email: r.hadidi@mun.ca and jeyas@mun.ca

***Abstract*— A real-time control scheme based on wide-area measurements and excitation control of generators is introduced in this paper. The wide-area measurements are preprocessed in a central unit. The processed data are then used by stability agents which are decentralized and autonomous. The goals of these controllers are to stabilize the system after severe disturbances and mitigate the oscillations afterward. A reinforcement learning algorithm is used to design the controllers. The proposed method extends the stability boundary of the system and achieves the above goals without losing any generator or load area and without any knowledge of the disturbances causing the response. The effectiveness of the proposed control scheme is illustrated through case studies on IEEE 39-bus power system.**

I. KEY EQUATIONS

The key equations for reinforcement learning algorithms are:

$$R_t = r_{t+1} + \gamma r_{t+2} + \gamma^2 r_{t+3} + \ldots = \sum_{k=0}^{\infty} \gamma^k r_{t+k+1} \quad (1)$$

$$Q^*(s,a) = E\left\{ r_{t+1} + \gamma \max_{a'} Q^*(s_{t+1}, a') \middle| s_t = s, a_t = a \right\} \quad (2)$$

The equations for data preprocessing are:

$$\delta_{COA} = \frac{\sum_{i=1}^{N} \delta_i H_i}{\sum_{i=1}^{N} H_i} \quad (3)$$

$$\omega_{COSP} = \frac{\sum_{i=1}^{N} \omega_i H_i}{\sum_{i=1}^{N} H_i} \quad (4)$$

$$\Delta\delta_i = \delta_i - \delta_{COA} \quad (5)$$

$$\Delta\omega_i = \omega_i - \omega_{COSP} \quad (6)$$

II. KEY FIGURES

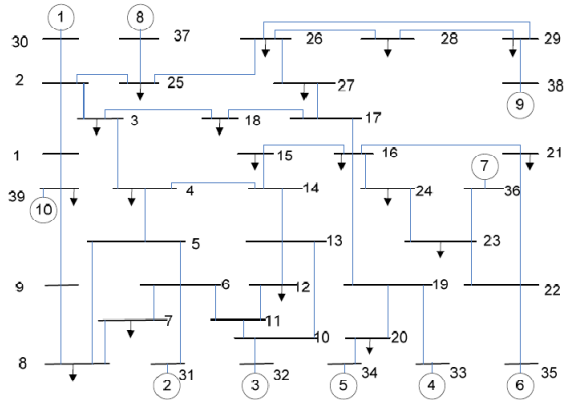

Figure 1. Test System

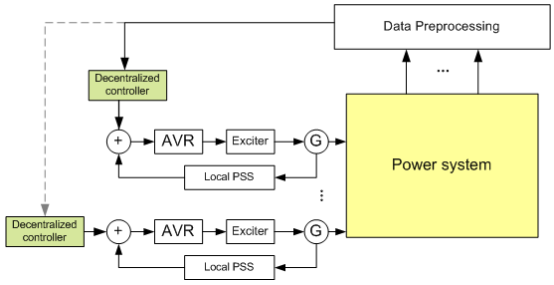

Figure 2. The proposed control structure

III. KEY RESULTS

Table 1 Sample list of the improvement on the system stability

Fault Bus	Line removed	Generator selected	Critical clearing time improvement
16	16-21	6,7	20 ms
4	4-6	10	30 ms
26	26-27	9	13ms
4	4-14	10	25ms
4	4-5	10	28ms

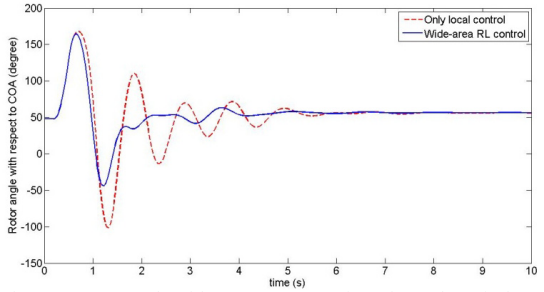

Figure 3. Rotor angle with respect to COA for a three-phase fault at bus 26 cleared after 320 ms by tripping line 25-26

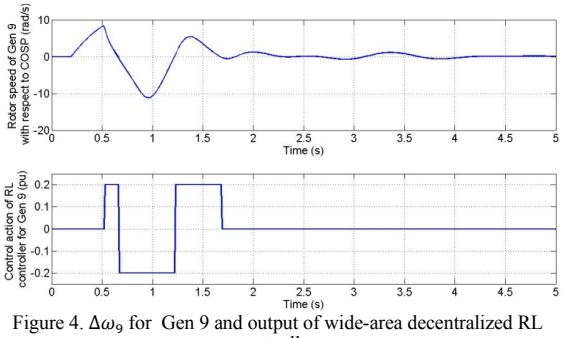

Figure 4. $\Delta\omega_9$ for Gen 9 and output of wide-area decentralized RL controller

Flatness-Based Automatic Generation Control with High Penetration of Wind Energy

Maryam H Variani and Kevin Tomsovic
Dept. of Electrical Engineering and Computer Science
University of Tennessee, Knoxville, TN 37996, USA,
Email: mhassani@utk.edu and tomsovic@utk.edu

***Abstract*— Existing energy systems are characterized by multiple, largely hierarchical systems for transient stability control, load frequency control, voltage control, power quality control, or distribution protection. To allow for distributed generation and alternative energy units, we propose these controls should be replaced by a two-tier approach of local control operating within a global context of situational awareness. In local control, individual components and individual loads operate in a manner to follow some desired trajectory based on local observations. The desired trajectory is determined by the context of the overall system needs for reliability, speed, and robustness. Flatness as an extension of controllability is a key to enabling planning and optimization at various levels of the grid in this structure. In this study, implementation of flat control on automatic generation control (AGC) of a multi-area system with high penetration of wind energy is investigated. The local control tracks the desired frequency and relative angle at the generator bus under normal operations. Simulation results demonstrate the promising performance of the proposed control strategy in comparison with conventional controllers.**

I. KEY EQUATIONS

The guiding equations of the flatness based controller are:

$$\dot{\delta}_{(i)} = \omega_{(i)} - \omega_0$$

$$\ddot{\delta}_{(i)} = \frac{1}{2H}\left(P_{m(i)} - \sum_{\substack{j=1 \\ i\neq j}}^{n} \frac{\delta_{(i)} - \delta_{(j)}}{X_{ij}} - P_L - D\left(\omega_{(i)} - \omega_0\right) \right)$$

$$\delta_{(i)}^{(3)} = \frac{1}{2H}\left(\frac{1}{\tau_T} P_{gv(i)} - \frac{1}{\tau_T} P_{m(i)} - \sum_{\substack{j=1 \\ i\neq j}}^{n} \frac{\dot{\delta}_{(i)} - \dot{\delta}_{(j)}}{X_{ij}} - D\ddot{\delta}_{(i)} \right)$$

$$\delta_{(i)}^{(4)} = \frac{1}{2H}\left(\begin{array}{l} \frac{1}{\tau_T \tau_g} u - \frac{1}{\tau_T \tau_g} \frac{\omega_{(i)} - \omega_0}{R} - \left(\frac{1}{\tau_T \tau_g} + \frac{1}{{\tau_T}^2} \right) P_{gv} \\ + \frac{1}{{\tau_T}^2} P_m - \sum_{\substack{j=1 \\ i\neq j}}^{n} \frac{\ddot{\delta}_{(i)} - \ddot{\delta}_{(j)}}{X_{ij}} - D\dddot{\delta}_{(i)} \end{array} \right)$$

II. KEY FIGURES

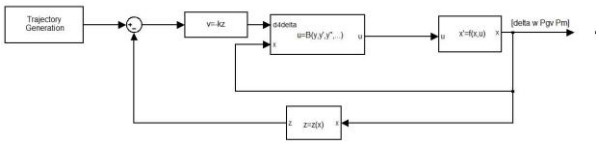

Figure 1. Flatness-Based control block diagram.

III. KEY RESULTS

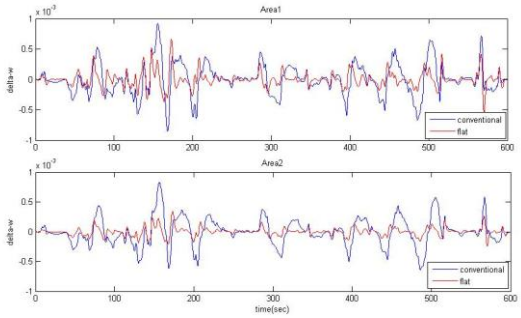

Figure 2. frequency deviations (pu).

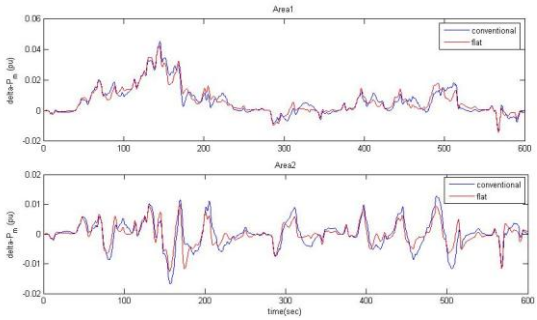

Figure 3. mechanical power deviations (pu).

Optimal Transient Stability Control Based on OMIB Equivalents and Trajectory Sensitivities

Yulong Huang[1,2], Claudio A. Cañizares[2], and Mingbo Liu[1]

1. School of Electric Power Engineering, South China University of Technology, Guangzhou, China, 510641;
2. Department of Electrical and Computer Engineering, University of Waterloo, Ontario, Canada, N2L 3G1

Email: yulong.h@mail.scut.edu.cn, ccanizar@uwaterloo.ca, and epmbliu@scut.edu.cn

***Abstract*— An optimal transient stability control (OTSC) quadratic model based on a one-machine-infinite-bus (OMIB) equivalent and a trajectory sensitivity method is proposed in this paper to maintain power system stability. The proposed OTSC is used to determine the generator voltage regulator reference set points. An OMIB equivalent is used to introduce a strict transient stability criterion into the OTSC model, and a trajectory sensitivity method and a stability index margin are proposed here to enhance computational efficiency by avoiding the need for searching critical stable trajectories for unstable faults. The effectiveness of the proposed method is demonstrated and verified on the 10-machine, 39-bus New England benchmark system, as well as on a real 692-Bus, 138-Machine system.**

I. KEY EQUATIONS

The equations or constraints representing the transient stability margins are:

$$A_U = -\frac{1}{2} M \hat{\omega}_u^2 \tag{1}$$

$$A_S \approx \frac{1}{2} P_a(t_r)(\delta_r - \delta_{cct}(t_r)) \tag{2}$$

$$\rho_U = \frac{A_U}{W_C} = -\left(\frac{\hat{\omega}_u}{\hat{\omega}_c}\right)^2 \tag{3}$$

$$\rho_S \approx \frac{P_a(t_r)(\delta_r - \delta_{cct}(t_r))}{M \hat{\omega}_c^2} \tag{4}$$

$$\phi(t'_u, \lambda_{t_e}) = \rho_{\min} - \rho_U \le 0 \tag{5}$$

The optimal transient stability control model is proposed as follows:

$$\begin{aligned} \min \quad & F = (V^k_{ref_{t_e}} + \Delta V^{k+1}_{ref_{t_e}} - V^0_{ref_{t_e}})^T \Gamma (V^k_{ref_{t_e}} \\ & \qquad + \Delta V^{k+1}_{ref_{t_e}} - V^0_{ref_{t_e}}) \\ \text{s.t.} \quad & 0.5 V^k_{ref_{t_e}} \le V^k_{ref_{t_e}} + \Delta V^{k+1}_{ref_{t_e}} \le 1.5 V^k_{ref_{t_e}} \\ & V_{R_{\min}} \le V_R\left(t, V^k_{ref_{t_e}}\right) + V_{R_{V_{ref\,t_e}}}\left(t, V^k_{ref_{t_e}}\right) \Delta V^{k+1}_{ref_{t_e}} \le V_{R_{\max}} \\ & \qquad \forall t \in [\tilde{t}_e, \tilde{t}'_e] \\ & V_{\min} \le V\left(t, V^k_{ref_{t_e}}\right) + V_{V_{ref\,t_e}}\left(t, V^k_{ref_{t_e}}\right) \Delta V^{k+1}_{ref_{t_e}} \le V_{\max} \\ & \qquad \forall t \in [\tilde{t}_e, \tilde{t}'_e] \\ & \phi(t'_u, V^k_{ref_{t_e}}) + \phi_{V_{ref\,t_e}}(t'_u, V^k_{ref_{t_e}}) \Delta V^{k+1}_{ref_{t_e}} \le 0 \end{aligned} \tag{6}$$

II. KEY FIGURES

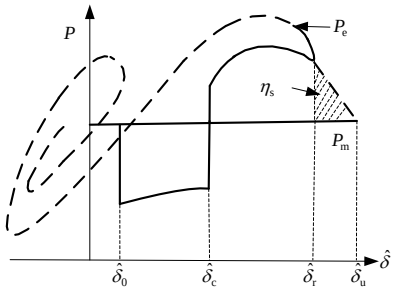

Fig. 1. Power-angle characteristics of OMIB equivalent system under stable conditions

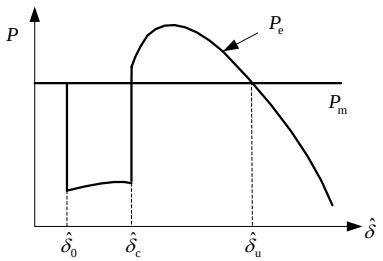

Figure 2. Power-angle characteristics of OMIB equivalent system under "generally" unstable conditions

III. KEY RESULTS

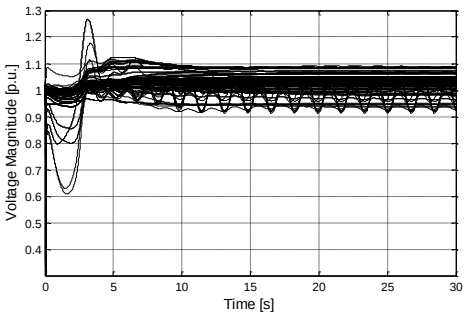

Figure 3. Generator terminal voltages of a real 692-Bus, 138-Machine system after OTSC.

Toward Modeling and Control of Synchrophasor-enabled Frequency Regulation in the Electric Energy Systems

Qixing Liu and Marija Ilić
Department of Electrical and Computer Engineering, Carnegie Mellon University, Pittsburgh, PA 15213, USA,
Email: lqx@cmu.edu and milic@ece.cmu.edu

***Abstract*— This poster concerns the problem of regulating stable frequency within the standards defined by the industry. At present frequency regulation is implemented using automatic generation control (AGC) and it is not designed to guarantee a desired performance for the rage of disturbances of interest. Instead, it is based on several assumptions that are not likely to hold as the system dynamics becomes harder to predict than in the past. Fortunately, recent progress with the sensor technologies, synchro-phasors in particular, can be used to enhance today's AGC and relax the inherent assumptions. In this poster we briefly summarize assumptions underlying today's AGC and the models being used. We next present our work in progress that considers availability of fast, spatially dispersed, synchro-phasors for sensing frequency dynamics. A new modeling approach is introduced first. Next, this model is used to illustrate systematic control design for stabilizing and regulating frequency over the ranges of operating conditions. Performance improvement based on this new model is illustrated on a small system in which disturbances are created by the hard-to-predict wind power variations.**

In short, the conventional AGC uses a single Area Control Error (ACE) to drive a PI controller to regulate frequency of each control area. A control area is a subsystem of the electric power grid that is responsible to balance supply and demand. If each control area regulates its own supply-demand imbalance, namely its own ACE, the imbalance of the entire interconnection comprising several control areas will be regulated. This approach assumes strong electrical connection inside of each control area and it is based on a model which represents each area as an equivalenced single generator. However, in the environment of newly evolving smart power grids participants such as renewable power plants and price-responsive loads introduce considerable random disturbances at a much faster time scale than a regular step change disturbance. In this environment a steady state is never reached. Swings among internal generators need to be considered since the strong assumption about the control area behaving as a single generator no longer holds. As a result, the PI control using a scalar ACE signal becomes incapable of balancing the imbalances and frequency deviations may become unacceptably high. The need for a model which is dynamic and more systematic control design becomes inevitable. For the first time more detailed synchro-phasor spatial measurements are available and this makes it possible to design AGC using more detailed spatial measurements and more accurate temporal measurements. In this poster we present an enhanced AGC model by taking the internal electrical distance of a control area into consideration. Each generator within a control area is modeled using its reduced-order model based on singular perturbation technique. It is explained how this carefully designed model captures the dynamics of interest. The problem of the minimal frequency regulation is then posed as an optimal feedback control design problem based on the proposed reduced-order model. The feedback information about the key output variables is available through the implementation of sychro-phasor-enabled technologies. A proof-of-concept model and simulation are presented and the results are compared with those obtained using the ACE-based AGC system.

I. KEY FIGURES

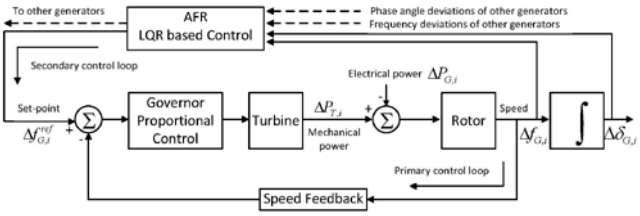

Figure 1. Block diagram of the proposed Advanced Frequency Regulator (AFR) approach

II. KEY RESULTS

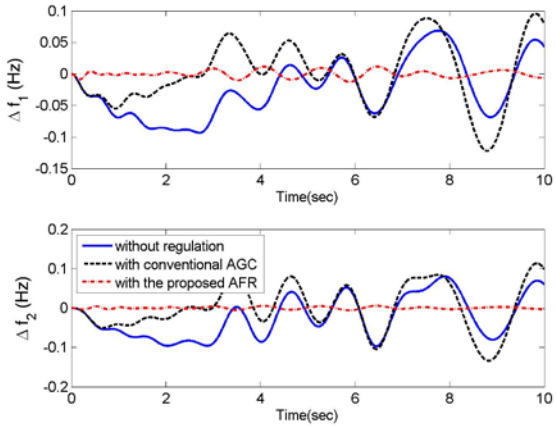

Figure 2. Performance Comparison for the proposed AFR approach and the conventional AGC approach in a 3-bus test power system with 2 synchronous generators; and 1 wind power plant as the disturbance

Observer-based Nonlinear Excitation Control of Power Systems

M. A. Mahmud[1], H. R. Pota[1], and M. J. Hossain[2]
[1]School of Engineering & Information Technology, The University of New South Wales at Australian Defence Force Academy (UNSW@ADFA), Canberra, ACT 2600, Australia
[2]School of Information Technology & Electrical Engineering, University of Queensland, St. Lucia, Brisbane, QLD 4072, Australia
Email: Md.Mahmud@student.adfa.edu.au, H.Pota@adfa.edu.au, *and* *m.hossain9@uq.edu.au*

***Abstract*— The stable operation of power systems can be ensured by using high-performance controllers which regulate the system under diversity of operating conditions. The design of nonlinear controller under wide variation of operating region is still now a challenging task. Feedback linearization technique can provide stability of power systems over a large range of operation. But the problem associated with this technique is that it is essential to measure all the state variables of power systems which are very difficult in practice. These difficulties can be resolved by implementing observer. Here, a nonlinear observer is designed based on the zero dynamic design principle of feedback linearization. Then using the observed states of power systems, a nonlinear excitation controller is designed. Finally, the performance of this controller is tested on a single machine infinite bus (SMIB) system.**

I. KEY EQUATIONS

The guiding equations of the immune based controller are:

$$\dot{\delta} = \omega \tag{1}$$

$$\dot{\omega} = -\frac{D}{2H}\omega + \frac{1}{2H}\left(P_m - \frac{V_s E'_q}{x'_{d\Sigma}}\sin\delta\right) \tag{2}$$

$$\dot{E}'_q = -\frac{1}{T'_d}E'_q + \frac{1}{T_{do}}\frac{x_d - x'_d}{x'_{d\Sigma}}V_s\cos\delta + \frac{1}{T_{do}}E_f \tag{3}$$

II. KEY FIGURES

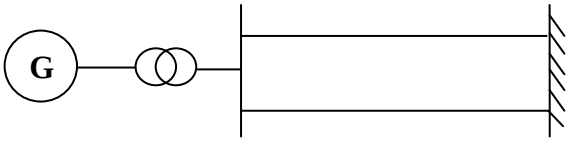

Figure 1. Test System

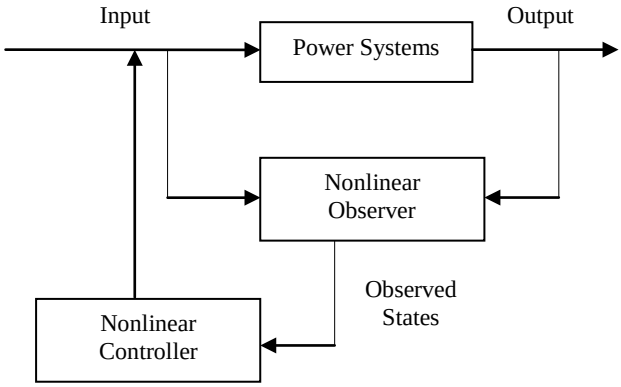

Figure 2. Observer-based Nonlinear Controller

III. KEY RESULTS

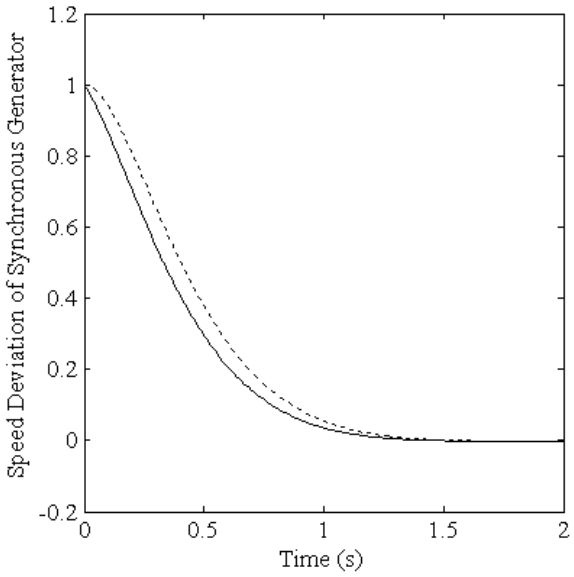

Figure 3. Speed deviation of synchronous generator (The solid line represent the speed deviation for exact linearizing excitation controller, whereas the dashed line represents the same for observer-based excitation controller)

Adaptive Dynamic Programming for SVC Secondary Voltage Control in a Smart Grid

Joseph Makasa and Ganesh K. Venayagamoorthy
Real-Time Power and Intelligent Systems Laboratory, Department of Electrical and Computer Engineering, Missouri University of Science and Technology, Rolla, MO 65409, USA,
Email: jkm6g7@mst.edu and gkumar@ieee.org

***Abstract*— Plug-in Electric Vehicles (PEVs) and Wind farms are both of intermittent nature and pose new stability control challenges that cannot be adequately implemented using traditional control methods. The use of Adaptive Dynamic Programming (ADP) based on neural networks for enhancement of reactive power support and optimal voltage control is explored. An Echo State Network (ESN) is used to estimate Voltage Stability Load Index (VSLI) of local and remote buses. The proposed ADP method is investigated on a modified IEEE 68 bus system implemented on a Real-time Digital Simulator (RTDS) and DSP platform.**

I. KEY FIGURES

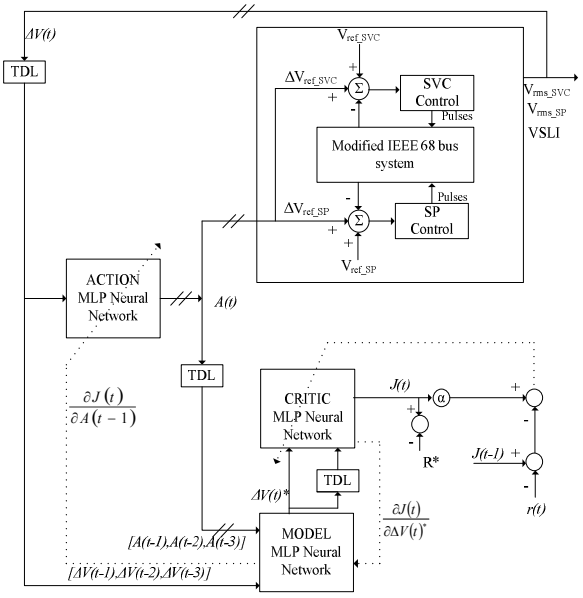

Figure 1. Proposed ADP Controller for Voltage Control

Adaptive Dynamic Programming based on Heuristic Dynamic Programming (HDP) has the following equations:

$$A(t) = [\Delta V_{ref\_SP}, \Delta V_{ref\_SVC}] \quad (1)$$

$$J(t) = (V_{rms}, \Delta V_{ref\_SP}, \Delta V_{ref\_SVC}, VSLI) \quad (2)$$

$$U(t) = A_1(VSLI_{39SS} - VSLI_{39}(t))^2 + A_2(VSLI_{44SS} - VSLI_{44}(t))^2 + A_3(VSLI_{49SS} - VSLI_{49}(t))^2 \quad (3)$$

The actor network minimizes the cost-to-go function *J(t)* by providing inputs *A(t)* to the plant and the critic network. The utility function (3) is based on VSLI obtained using the neural identifier based on echo state neural network structure below (figure 2)

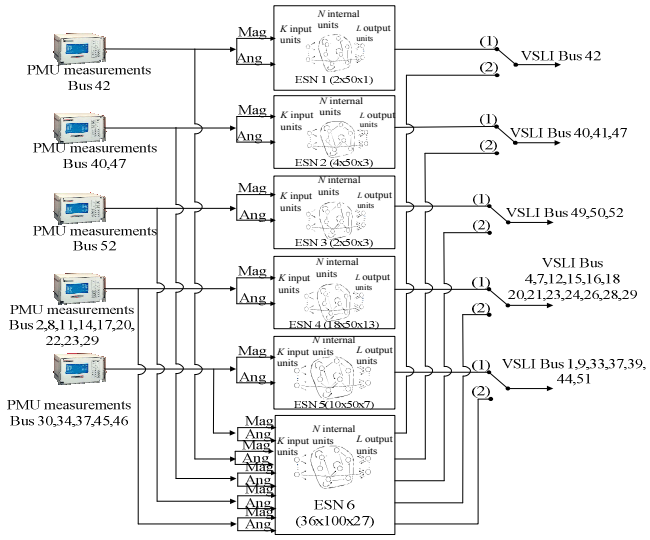

Figure 2. Estimation of VSLI

II. SVC VOLTAGE CONTROL

The utility along with measurements of bus voltage at buses 39, 44, and 49 are used for ADP control of SVC. The results will be compared with that of traditional controller shown below.

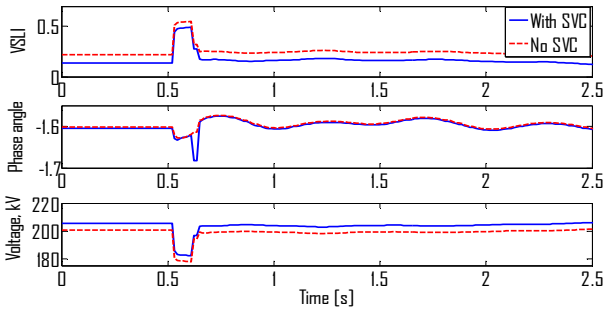

Figure 3. SVCcontrol with a traditional PI controller at bus 39

The SVC improves the voltage profile of bus 39 and the VSLI is lower. During the fault, VSLI is lower with SVC compared with the case with no SVC. In this project performance of the ADP controller is compared with that of the traditional controller.

Performance of Power Oscillation Damping Controllers with Different Static Load Characteristics

Nilesh Modi, Tapan Kumar Saha, N. Mithulananthan
School of Information Technology & Electrical Engineering,
The University of Queensland, Brisbane 4072, Australia
Email: nilesh@itee.uq.edu.au, saha@itee.uq.edu.au and mithulan@itee.uq.edu.au

***Abstract*— Low-frequency inter-area oscillations are threat to secure operation of power systems. Power system stabilizer and Power oscillation damping controllers are used to provide damping to oscillatory modes. Such oscillatory modes, inter-area modes in particular, are significantly affected by change in operating conditions and load characteristics. In this paper, influence of load characteristics on performance of two distinct power oscillation damping controllers is being examined. The interaction between load characteristic and performance of power oscillation damping controller is explored in terms of damping contribution by individual controller on inter-area mode. Eigenvalue analysis approach is used to evaluate the performance of power oscillation controllers, which are designed based on residue compensation technique and H∞ loop-shaping technique respectively. This paper also addresses the dynamic behaviour of the two controllers under different operating conditions and load characteristics.**

I. KEY EQUATIONS

The key equations for static load model representation are:

$$P = P_o\left(a_1\left(\frac{V}{V_o}\right)^{mp1} + a_2\left(\frac{V}{V_o}\right)^{mp2} + a_3\left(\frac{V}{V_o}\right)^{mp3}\right)k_p \quad (1)$$

$$Q = Q_o\left(b_1\left(\frac{V}{V_o}\right)^{mq1} + b_2\left(\frac{V}{V_o}\right)^{mq2} + b_3\left(\frac{V}{V_o}\right)^{mq3}\right)k_p \quad (2)$$

The key equations for controller design based on residue compensation are:

$$\phi = 180° - \arg(R_i) \quad (3)$$

$$\alpha = \frac{T_{lead}}{T_{lag}} = \frac{1-\sin\left(\phi/m\right)}{1+\sin\left(\phi/m\right)} \quad (4)$$

$$T_{lag} = \frac{1}{\omega_i\sqrt{\alpha}};\ T_{lead} = \alpha T_{lag} \quad (5)$$

The key equations for controller design based on H_∞ loop-shaping techniques are:

$$G_S = W_2 G W_1 \quad (6)$$

$$G_P = (M + \Delta_M)^{-1}(N + \Delta_N)^{-1} \quad (7)$$

$$Gp = \{M + \Delta_M\}^{-1}\{N + \Delta_N\}^{-1} : \left\|\Delta_M \quad \Delta_N\right\| < \varepsilon \quad (8)$$

$$\left\| \begin{bmatrix} K \\ I \end{bmatrix} (I - GK)^{-1} M^{-1} \right\|_\infty \le \gamma \quad (9)$$

II. KEY RESULTS

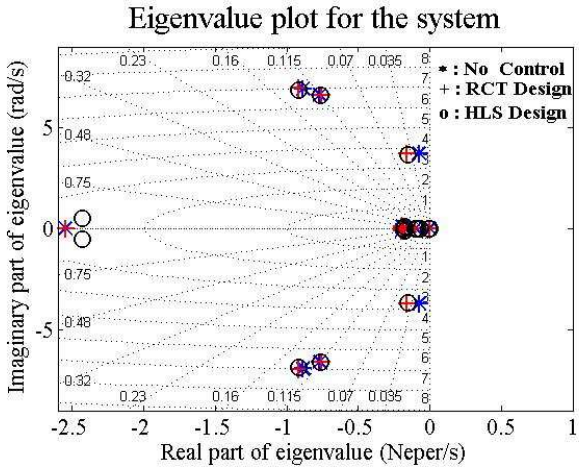

Figure 1. Eigenvalue Plot with and without POD. '*' No Control, '+' RCT Design and 'o' HLS Design

TABLE I: PERFORMANCE OF PODS UNDER CONTINGENCY

Type of Load	RCT		HLS	
	DR (%)	Freq. (Hz)	DR (%)	Freq. (Hz)
Const P	6.8	0.488	8.5	0.496
Const I	6.8	0.487	8.5	0.492
Const Z	7.4	0.488	8.8	0.493
Exp 1	6.9	0.488	8.5	0.493
Exp 2	6.7	0.488	8.4	0.492
Exp 3	6.7	0.487	8.4	0.492
PIQZ	6.8	0.488	8.5	0.492
PZQP	7.4	0.488	8.8	0.493
PPQI	6.5	0.482	8.5	0.489

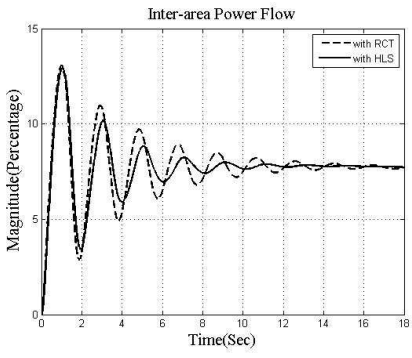

Figure 2: Power flow in line between bus 9 and 10 – $P_{9\text{-}10}$.

Modeling and Stability Analysis of a Microturbine as a Distributed Energy Resource

Ehsan Nasr Azadani, *Student Member, IEEE*, Claudio Cañizares, *Fellow, IEEE*, and Kankar Bhattacharya, *Senior Member, IEEE*
Power and Energy System Group, Department of Electrical and Computer Engineering,
University of Waterloo, CANADA,
Email: *ehsan.nasr33@gmail.com*

Abstract— **One of the Distributed Energy Resources (DER) for supplying electric and thermal energy to residential and commercial loads is micro-turbines (MTs). MTs are useful for efficient peak shaving because of easy controllability and quick start capability. This paper discusses the dynamic behaviour of a split shaft MT as a DER. The MT-Generator (MTG) is represented using an appropriate stability model of an MT coupled with a synchronous generator. This model also incorporates a speed controller to maintain constant speed at different loads. In this MTG model, both transient and slow dynamics are taken into account. Based on this model, voltage, angle, and transient stability studies are carried out. Voltage stability studies are performed based on PV curves; small perturbation stability studies are carried out based on eigenvalue analyses of the linearized system models; and transient stability studies are performed by time domain simulations to study contingencies. The MTG model is developed in PSAT, which is a MATLAB-based toolbox for power system studies, and tested using a simple grid, feeder, and load test system.**

I. KEY EQUATIONS

The basic equations of the MT model are:

$$\dot{Mt_1} = \frac{(K_a \times temp) - Mt_1}{\tau_s} \quad (1)$$

$$temp = (VCE \times \omega_{mt}) \times (1 - \omega_{min}) + \omega_{min} - (k_f \times\times Mt_2) \quad (2)$$

$$\dot{Mt_2} = (Mt_1 - Mt_2)/\tau_f \quad (3)$$

$$\dot{Mt_3} = (Mt_2 - Mt_3)/\tau_{ecr} \quad (4)$$

$$\dot{Mt_4} = (Mt_3 - Mt_4)/\tau_{cd} \quad (5)$$

$$P = \omega_{mt} \times [1.3 \times (Mt_4 - 0.23) + 0.5 \times (1 - \omega_{mt})] \quad (6)$$

II. KEY FIGURES

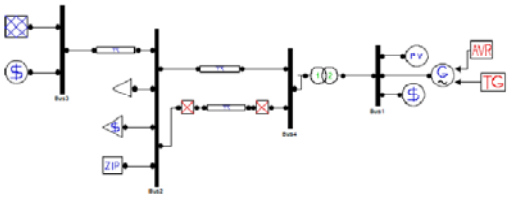

Figure 1. Test System

III. KEY RESULTS

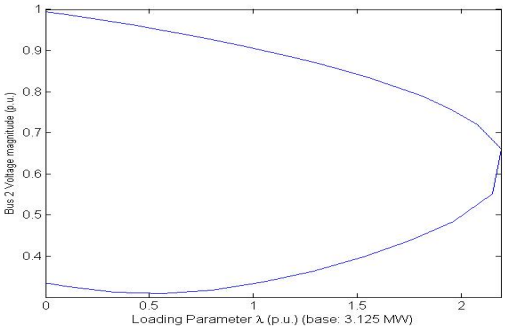

Figure 2. PV curve (Bus 2)

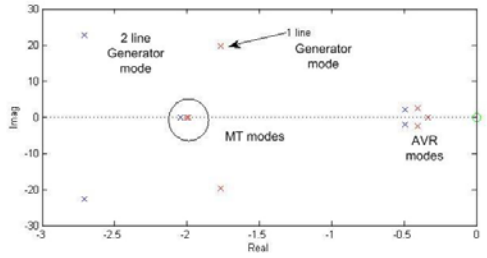

Figure 3. Eigenvalues of the MTG model

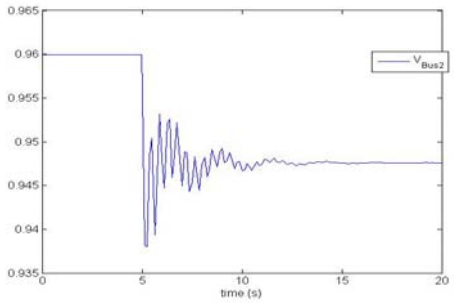

Figure 4. Time domain simulation for a Line trip (Bus 2 voltage magnitude)

Time Evaluation of Voltage Stability for System Planning Study

Ryuichi Ogahara, Yuya Suzuki, and Shinichi Iwamoto

Power Systems Laboratory, Department of Electrical Engineering and Bioscience, Waseda University, Tokyo, 169-8555, JAPAN
Email: ogahara.ryuichi.pwrs@gmail.com

***Abstract*— This paper proposes a new systematic scheme for voltage stability control in power systems. Recently, renewable energy and distributed generations have been introduced in power systems because of the worldwide social interests concerning environmental problems. However, renewable energies such as photovoltaic and wind power generations have unstable characteristics dependant on natural power. Therefore, power systems have steadily grown more complicated, and sill lead to a voltage instability phenomenon problem. This may cause large power outages. However, the voltage stability in power systems has been handled as a static condition problem in many cases, and considered peak load situation where the load is expected to increase in the future. However, when a large amount of renewable energy penetration is advanced, it is thought that it is necessary to treat a time evaluation of voltage stability. In this paper, we propose a voltage stability control scheme. Finally we carry out simulations for one machine with a one load model system to confirm the validity of the proposed method.**

I. KEY EQUATIONS

The dynamic load models shown below are applied to simulations.

$$\begin{cases} P_L = P_{LO} \cdot (tV)^{\alpha} \\ Q_L = Q_{LO} \cdot (tV)^{\beta} \end{cases} \quad \cdots\cdots (1)$$

[Objective Function]

Minimize

$$g = w_1 x_{SVC}^{\ 2} + w_2 x_{Series}^{\ 2} + w_3 x_{NAS}^{\ 2} \quad \cdots\cdots (2)$$

[Equality Constraint]

$$\begin{bmatrix} a & b & c \end{bmatrix} \begin{bmatrix} x_{SVC} \\ x_{Series} \\ x_{NAS} \end{bmatrix} = t_{cl} \quad \cdots\cdots (3)$$

Where

wi: weight, a,b,c: sensitivities for controllers

II. KEY FIGURES

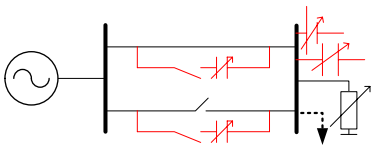

Figure 1. Test System

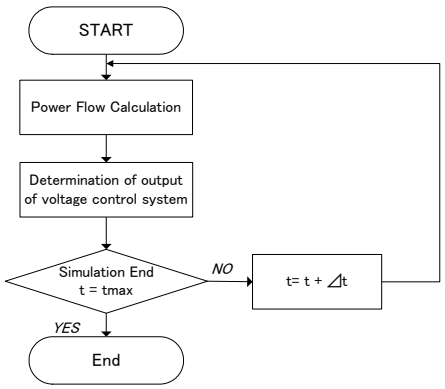

Figure 2. The flowchart of the voltage calculation

III. KEY RESULTS

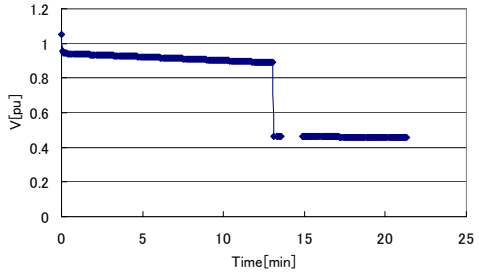

Figure 3. The load voltage(before)

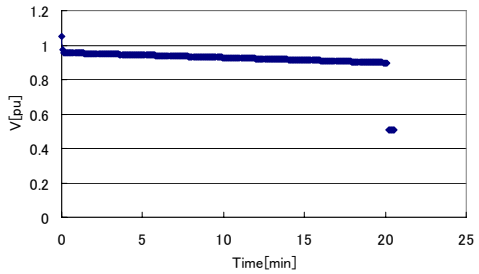

Figure 4. The load voltage(proposed method)

In the result, the voltage collapse time has been extended to 19.7[min] from 13.13[min]. The result is close to the targeted time of 20[min]. Delaying the voltage collapse time enables an operator to take measures to prevent voltage collapse. Moreover, if it is not possible to deal with this problem by setting up voltage control facilities, we can consider another system planning method, which is to add a transmission line to another substation.

Transient Stability Prediction Using Recurrent Neural Network

P.K Olulope[1], Ganesh K. Venayagamoorthy[1], K.A Folly[2] , S.Chowdhury[2], SP. Chowdhury[2]
[1]Real-Time Power and Intelligent Systems Laboratory, University of Science and Technology, Rolla, MO 65409, USA,
[2]Department of Electrical Engineering, University of Cape Town, South Africa
Email:ollpau002@uct.ac.za

***Abstract*— August 2003 blackout in USA, Canada, Sweden, and Denmark shows that the security margin of the grids is compromised. As the present day's grid continues to increase in complexities due to vast integration of renewable energy and other power electronics devices, the need arises to provide fast and versatile simulation techniques. Simulation techniques that will possess capability to deliver results of the status of the interconnected power system in real time and under large disturbances in order to avert occurrences of catastrophic event before its happen. This study focuses on application of recurrent neural network in transient stability prediction of power system. To evaluate the performance of RNN, a modified IEEE 14 Bus system containing integrated hybrid Wind/Solar PV distributed generations developed in DIgSILENT is used. Time domain simulation was first conducted over wide range of operating conditions. The data collected was trained using a conjugate gradient back propagation with one step secant Quasi- Newton algorithm. Among other training algorithm that was investigated, it was discovered that one secant is most applicable to use because it is faster with reduce memory capacity and lower mean square error. The input vector is presented sequentially with time delay and the training is done in batches. The data from DIgSILENT is later reduced using principal component analysis (PCA). To validate the result, a comparison of the result was made with DIgSILENT and Multi-layer neural network (MLP). The results show effectiveness of RNN in predicting transient stability status of power system.**

I. KEY EQUATIONS

The guiding equations of the recurrent neural network are:

$$a^1(t) = tansig\{w^1 \times \mathrm{P}^1(t) + w^1 \times a^1(t-1) + bias\} \quad (1)$$

$$\delta_{max}(t) = purelin\{w^2 \times a^1(t) + bias\} \quad (2)$$

$$\mathrm{Y{=}SI{=}MAX}\ \{\max(\delta_i - \delta_i^0)\}\ i = 1,2,3 \ldots . N_G \quad (3)$$

II. KEY FIGURE

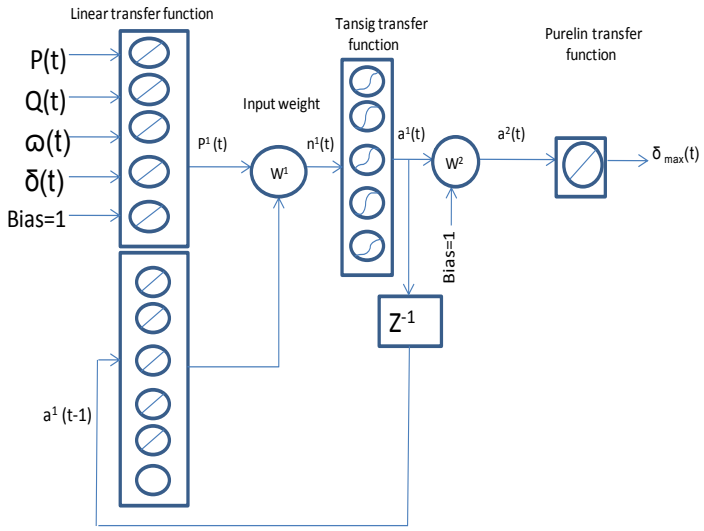

Figure1. RNN architecture

III. KEY RESULTS

Table I: Comparison between MLP and RNN.

ANN Types	Time (s)	msereg(mse with regularization)	%Predicted correctly	% Not correctly predicted	Regression Analysis
MLP	0.17	0.1243	97.1	2.9	0.88553
RNN	0.08	0.02822	98.6	1.4	0.95433

Table II: Comparing Prediction time of DIgSILENTand RNN

Fault clearing time (s)	Time of loss of synchronism with (DIgSILENT) (s)	Time used to predict instability with (RNN) (s)
0.02	35.9	0.08
0.03	36.2	0.09
0.04	36.5	0.10

Coordination of Underexcitation Limiter, Loss of Excitation Protection and Generator Control

Eli Pajuelo, Dr. Ramakrishna Gokaraju, Dr. Mohindar S. Sachdev
Power Systems Research Group, Department of Electrical and Computer Engineering, University of Saskatchewan, Saskatoon, SK S7L 6J3, Canada,
Email: elp168@mail.usask.ca , rama.krishna@usask.ca

***Abstract*— This poster provides a review of considerations for coordination between underexcitation limiter (UEL), loss of excitation protection (LOE) and automatic voltage regulator (AVR). The objective is always to allow a control action to bring any temporary abnormal condition back to normal. At the same time, the range of control should take advantage of the full capability of the generator, in particular during severe system disturbances. In this context, a protective operation is made to prevent damage to the machine, only after control efforts were unsuccessful to correct the problem. An example system to illustrate modeling, response, control and protection settings, in a practical scenario is included.**

I. Key Figures

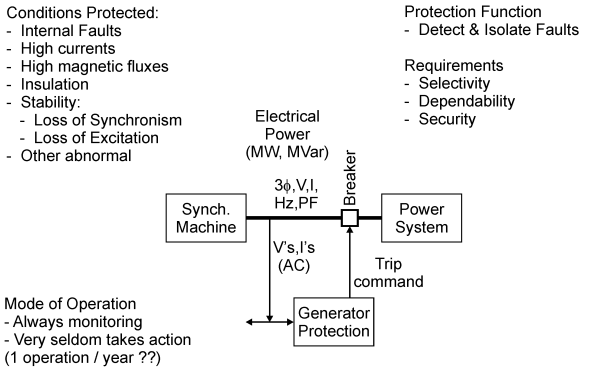

Figure 1. Synchronous Generator Protection Considerations

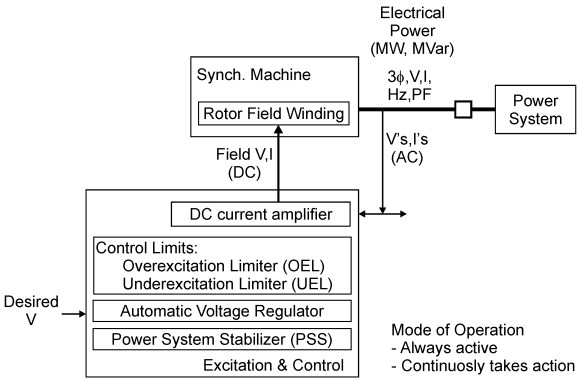

Figure 2. Synchronous Generator Excitation Control Considerations

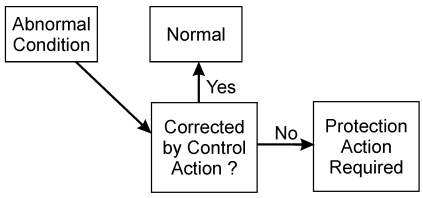

Example:
- Excitation suddenly dropped
- Underexcitation Limiter (UEL) control action
  - Tries to return it to normal levels
- Excitation does not recover
- Loss of Excitation (LOE) protection action
  - Confirms the loss of field and trips de unit out of service

Coordination is not always in place !!

Figure 3. Protection and Control Coordination

II. Key Results

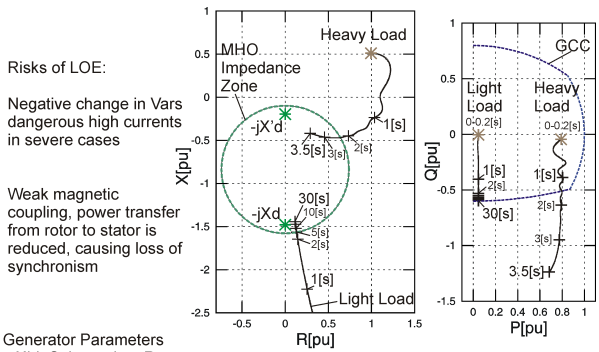

Figure 4. Loss of excitation condition, protection should operate

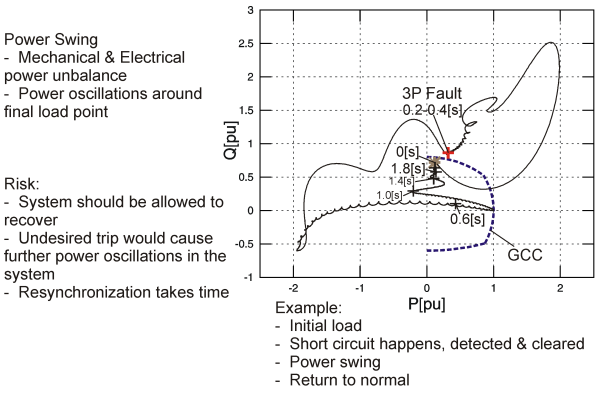

Example:
- Initial load
- Short circuit happens, detected & cleared
- Power swing
- Return to normal

Figure 5. Power swing condition, only control should operate

Large Area Small Signal Stability Enhancement of AC Networks Based on Multi-Infeed HVDC Configuration

Sahar Pirooz Azad, Reza Iravani, and Josephe Euzebe Tate
Department of Electrical and Computer Engineering, University of Toronto, Toronto, ON M5S 3G4, Canada
Email: Sahar.piroozazad@utoronto.ca, iravani@ecf.utoronto.ca, and zeb.tate@utoronto.ca

***Abstract*— The small signal stability of power systems has remained a concern for power engineers for the past several decades. Large power transfers over long distances in response to growing loads are major contributing factors for instability phenomena in power systems including small signal instability. Although HVDC transmission is usually installed for reasons aside from stability, reported studies have shown that the stability of the power system can be improved by judicious control of the HVDC system. The main focus of this study is to damp the inter-area low frequency oscillations of the systems by rerouting the flow of power in the power system. In order to reroute the power, we should be able to control the flow of power in the entire network. For this purpose, a multi-infeed DC (MIDC) configuration in multi-areas is proposed. In this configuration an MIDC system overlaid on an AC transmission network which is already in place to allow for increased transfer capability between geographically diverse generators and loads, is utilized to adjust the power flow in the entire network. Small signal instability due to interactions among the constituents HVDC links is a potential problem for MIDC systems. One way to determine the interaction level between the HVDC links is to use the short circuit ratio (SCR) definition for MIDC systems, known as multi-infeed SCR (MSCR). In this study, this criterion has been used to evaluate the impact of the location of HVDC links on the oscillation damping capability of the MIDC system. Simulation results show that a MIDC configuration in multi-areas with HVDC links installed on bus-bars with high MSCR leads to damped low frequency oscillations under small disturbances and a fast recovery after a fault in the system.**

I. Key Equations

The single-infeed SCR and multi-infeed SCR (MSCR) are defined as (1) and (2).

$$SCR_i = \frac{1}{Z_{Li}} \quad (1)$$

$$MSCR_i = \frac{1}{\sum_{m=1}^{K} Pdc_i Z_{i,m}} \quad (2)$$

II. Key Tables

Table 1. MSCR and SCR for WSCC system with two HVDC links

HVDC #	MSCR (case 1)	MSCR (case 2)	SCR
HVDC1	2.5	3.9	4.7
HVDC2	2.5	4.1	5.1

III. Key Figures

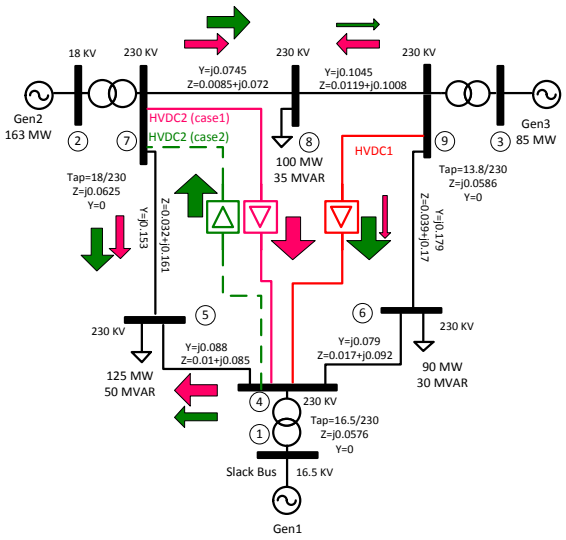

Figure 1. WSCC Network with a Multi-Infeed HVDC Configuration

IV. Key Results

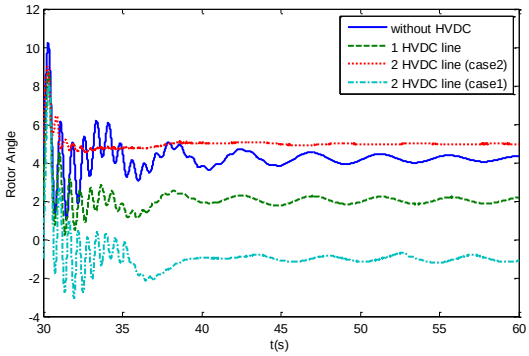

Figure 1. Generator 2 rotor angle trajectory with a 3-phase fault

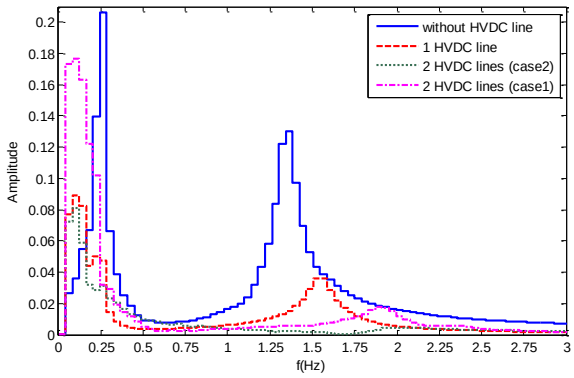

Figure 3. The single-sided amplitude spectrum of bus 7 phase angle

Simulation Platform to Study the Effect of Large Scale Integration of Wind Power in Small Signal Stability

Linash P Kunjumuhammed and Stefanie Kuenzel
Control and Power Research Group, Department of Electrical and Electronic Engineering,
Imperial College London, UK
Email: linash.p.k@imperial.ac.uk, stefanie.kuenzel06@imperial.ac.uk

***Abstract*— With large scale integration of wind power into electrical networks, the small signal stability of the power system becomes an important concern. The stochastic nature of wind power output will create unpredictable operating scenarios in power systems which will have a huge impact on damping of small signal stability modes. If right measures are not being taken, it could affect the power transfer capacity of the entire system, which in turn will negate the advantage obtained by using renewable generation. In this study, a MATLAB/SIMULINK based simulation platform is developed to study a power system with both synchronous generators and wind farms. The output of synchronous generators, wind farms, and loads are represented using a probabilistic model. The NETS-NYPS test system with 16-machines and 68-buses is used to validate the model. Different feasible operating scenarios of the power system are generated to study the variation in the inter-area oscillation mode damping.**

I. KEY EQUATIONS

Following set of equations summarize the dynamics of an electrical power system.

$$\begin{bmatrix} \dot{x}_{dfig} \\ \dot{x}_{synch} \\ \dot{x}_{facts} \end{bmatrix} = A \begin{bmatrix} x_{dfig} \\ x_{synch} \\ x_{facts} \end{bmatrix} + Bu \quad (1)$$

$$y = C \begin{bmatrix} x_{dfig} \\ x_{synch} \end{bmatrix} + Du \quad (2)$$

Where $x_{dfig} = [i_{qs}, i_{qr}, e'_{qs}, e'_{ds}]$, $x_{synch} = [\delta, \omega, E'_q, E'_d, E_{fd}, x_{exc}, x_{pss}]$ and x_{facts} are the state variables of DFIGs, synchronous generator, and the FACTS devices, respectively. The x_{synch} includes state variables related to the excitation system (x_{exc}) and PSS (x_{pss}) of synchronous generators.

II. KEY RESULTS

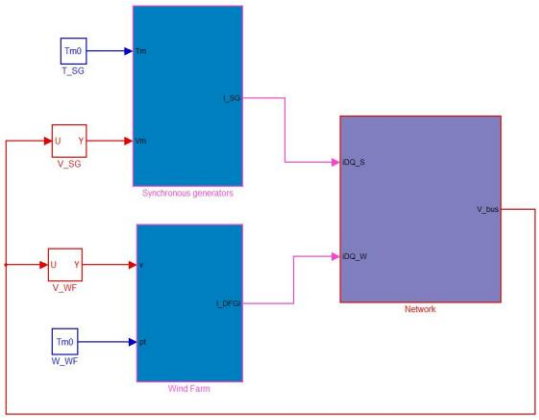

Figure 1. Schematic diagram of simulation platform

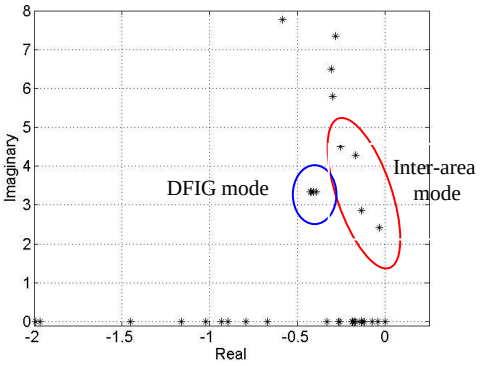

Fig. 3 Open loop eigenvalues of the system with five wind generators under nominal operating condition

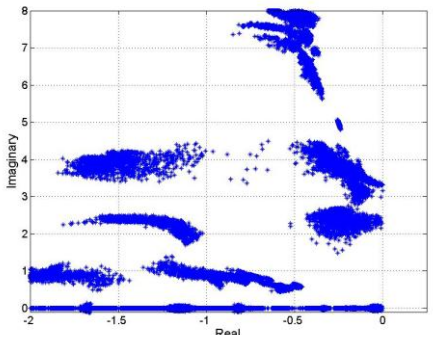

Fig. 4 Variation in inter-area modes of the system with all synchronous generators for several operating conditions

Fault-Tolerant Wide-Area Control of Power Systems

Felix Rafael Segundo Sevilla[1], Imad Jaimoukha[1], Balarko Chaudhuri[1] and Petr Korba[2]
[1]Control and Power Research Group, Department of Electrical and Electronic Engineering, Imperial College London, London, SW7 2AZ, UK and [2]ABB Corporate Research, Baden, Switzerland
Email: f.segundo-sevilla09@imperial.ac.uk i.jaimoukha@imperial.ac.uk b.chaudhuri@imperial.ac.uk and petr.korba@ch.abb.com

Abstract— **Despite effectiveness of wide-area control for power oscillation damping (POD), most utilities are still reluctant to deploy it for improving their system dynamic performance. One of their major concerns is the consequences of problems in communication channels leading to loss of signals in the worst case. In this poster, a fault-tolerant (FT) control scheme is proposed to guard against potential loss of one or more, but not all, remote signals. The controller is designed to ensure stringent specifications for the fault free nominal plant and minimal specifications for asset on off-nominal plants mimicking potential loss of signals. The control design problem is solved in a linear matrix inequality (LMI) framework. Effectiveness of such a fault-tolerant controller in the face of loss of feedback signals is demonstrated through a case study on the reduced equivalent of the Nordic system. Also the conservativeness of the controller is compared against a conventional one (ORD).**

I. Key Equations

The guiding equations of the fault tolerant controller are:

$$G(s) = \left[\begin{array}{c|c} A & B \\ \hline C & 0 \end{array}\right] \quad C = \begin{bmatrix} c_1^T & c_2^T & \cdots & c_{ny}^T \end{bmatrix}^T \tag{1}$$

$$G_i(s) = \left[\begin{array}{c|c} A & B \\ \hline C_i & 0 \end{array}\right] C_i = \begin{bmatrix} {c_1^i}^T & {c_2^i}^T & \cdots & {c_{ny}^i}^T \end{bmatrix}^T \tag{2}$$

$$c_j^i = \begin{cases} 0, & i = j \\ c_j, & i \neq j \end{cases} \quad \begin{matrix} i = 1, \cdots, ny \\ j = 0, \cdots, ny \end{matrix} \tag{3}$$

$$K(s) = \left[\begin{array}{c|c} A_k & B_k \\ \hline C_k & 0 \end{array}\right] \tag{4}$$

$$\lambda_c \left(\begin{bmatrix} A & BC_k \\ B_k C_i & A_k \end{bmatrix} \right) \in \lambda_d(\theta_i) \tag{5}$$

II. Key Figures

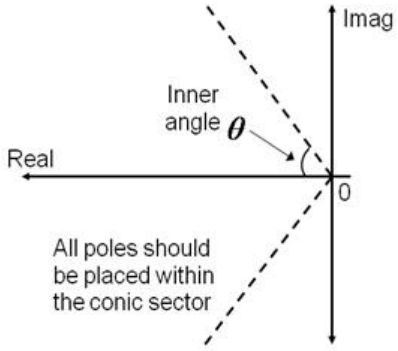

Figure 1. Pole placement criteria.

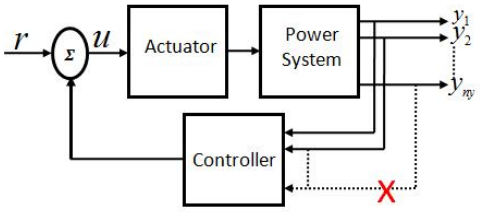

Figure 2. Block diagram of the closed loop system.

III. Key Results

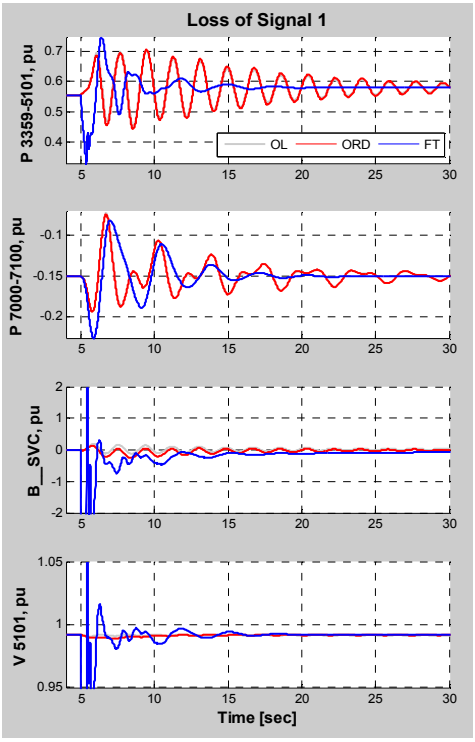

Figure 3. Dynamic response of the FT and ORD controllers following the loss of signal 1 in the closed loop system.

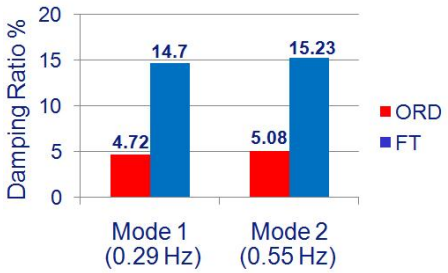

Figure 4. Damping ratio comparison of the oscillatory modes following the loss of signal 1.

Wind Turbines with Energy Storage for Power Smoothing and FRT Enhancement

Guoyi Xu, Lie Xu and D. J. Morrow
School of Electronics, Electrical Engineering and Computer Science, Queen's University of Belfast, Stranmillis Road, Belfast, BT9 5AH, UK.
Email: *gxu03@qub.ac.uk; l.xu@ee.qub.ac.uk; dj.morrow@ee.qub.ac.uk*

***Abstract*— The continued development of high power wind turbines raises the standards of operation requirement. This paper evaluates the ability of an energy storage device with a bidirectional dc-dc converter connected to the dc link of a direct driven wind turbine for output power smoothing and fault ride through enhancement. Method based on simple dc voltage measurement and coordinated dc voltage loops of the grid side dc-ac and the energy storage dc-dc converters are proposed to provide a versatile power smoothing control. Further studies on wind turbine fault ride through (FRT) capability in the presence of energy storage and dc damping resistor are outlined. Simulation results with Matlab/Simulink based on a 3 MW wind turbine are presented to validate the effectiveness of the proposed power smoothing strategy. It also shows that with energy storage, the size of the dc damping resistor can be reduced.**

I. KEY EQUATIONS

The equations of the grid side converter and ESS controller are:

$$P_{Grid}=C\cdot V_{dc}[k_{p\_dc}\Delta V_{dc}+k_{i\_dc}\int\Delta V_{dc}dt] \quad (1)$$

$$P_{ESS}=C\cdot V_{dc}\cdot k_d\cdot\Delta V_{dc} \quad (2)$$

II. KEY FIGURES

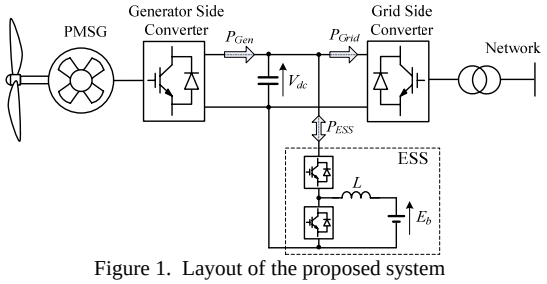

Figure 1. Layout of the proposed system

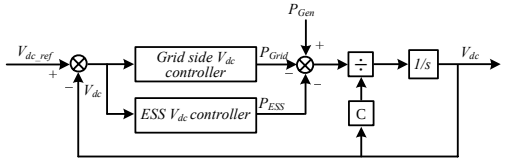

Figure 2. Diagram of the dc control system

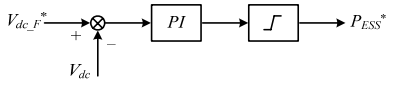

Figure 3. FRT control block of ESS

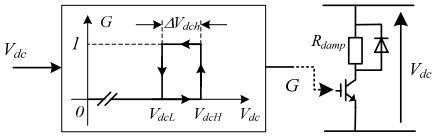

Figure 4. Control of damping resistor

III. KEY RESULTS

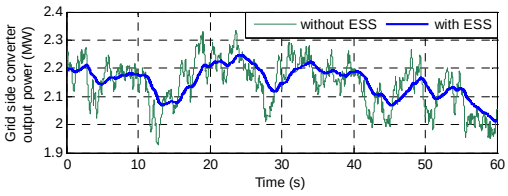

(a) 10 Hz bandwidth for grid side converter

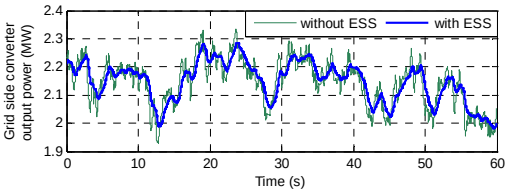

(b) 20 Hz bandwidth for grid side converter

Figure 5. Grid side converter output power

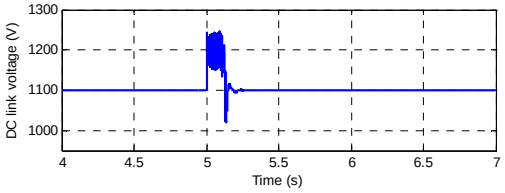

(a) DC link voltage

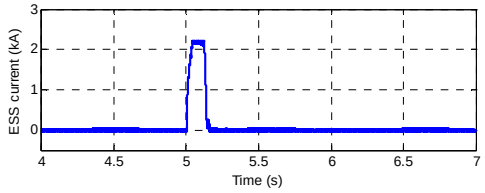

(b) ESS absorbed current

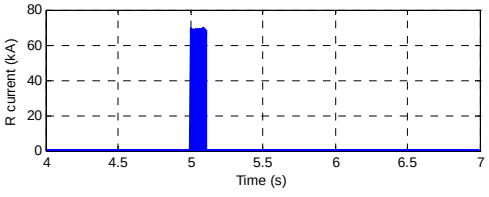

(c) Damping resistor current

Figure 6. Simulation result of fault ride through

A Novel Energy-Based Dissipative Excitation Control for Synchronous Generators

Zhe Zhang and Wei Qiao
Department of Electrical Engineering, University of Nebraska-Lincoln, Lincoln, NE 68588-0511, USA
Email: zhezhangx@gmail.com and wqiao@engr.unl.edu

***Abstract*— The highly complex, dynamic behavior and nonlinearity of power systems, together with their almost continuously time varying nature, have posed a great challenge to power system control engineers for decades. The traditional AVR and PSS, which are designed based on linear control theory, have shown their limitations in handling serious malfunctions. This paper presents a novel approach for designing generator excitation controllers by describing the power system as a port-controlled Hamiltonian system (PCHS). The proposed energy-based dissipative controller, which is also of the port-controlled Hamiltonian form, can be viewed as a feedback control technique that exploits the coupling between a physical power system and an energy-based controller to efficiently remove energy from the power system. A single machine infinite bus (SMIB) power system is developed in the MATLAB/SIMULINK environment to evaluate the performance of the energy-based dissipative controller. Simulations are carried out to compare the proposed controller with the traditional AVR and AVR+PSS in damping the transient power oscillations of the power system.**

I. KEY EQUATIONS

The three-dimensional flux decay model is of the form:

$$\dot{\delta} = \omega_0 \Delta\omega_m \tag{1}$$

$$2H\Delta\dot{\omega} = P_m - D_m\Delta\omega_m - E_q{}'U_t \sin\delta / x_d{}' \tag{2}$$

$$T_{do}\dot{E}_q{}' = -x_d E_q{}' / x_d{}' + (x_d - x_d{}')U_t \cos\delta / x_d{}' + E_{fd} + u_f \tag{3}$$

The output of the port-controlled Hamiltonian system is of the form:

$$y = \frac{x_d E_q{}'}{2Hx_d{}'(x_d - x_d{}')} - \frac{U_t \cos\delta}{2Hx_d{}'} - \frac{E_{fd}}{2H(x_d - x_d{}')} \tag{4}$$

The fixed-order, energy-based hybrid dynamic controller is of the form:

$$\dot{x}_c(t) = J_c(x_c(t))\frac{\partial H_c^T(x_c(t))}{\partial x_c} + G_c(x_c(t))u_c(t) \tag{5}$$

$$y_c(t) = G_c^T(x_c(t))\frac{\partial H_c^T(x_c(t))}{\partial x_c} \tag{6}$$

The controller is designed of the form:

$$u_f = K(y_c - y) \tag{7}$$

$$u_c = K(y - y_c) \tag{8}$$

The resetting set $Z \subset D_P \times D_C$ is given by:

$$Z = \left\{(x_p, x_c) \in D_P \times D_C : \frac{d}{dt}H_c(x_c) = 0 \text{ and } H_c(x_c) > 0\right\} \tag{9}$$

II. KEY FIGURES

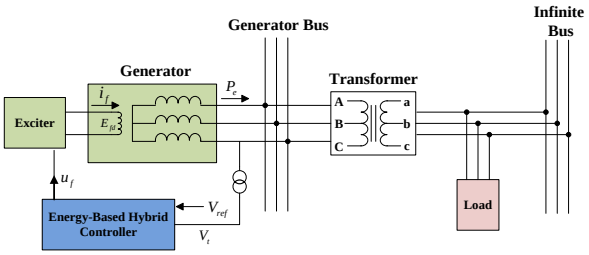

Fig. 1. The single machine infinite bus system

III. KEY RESULTS

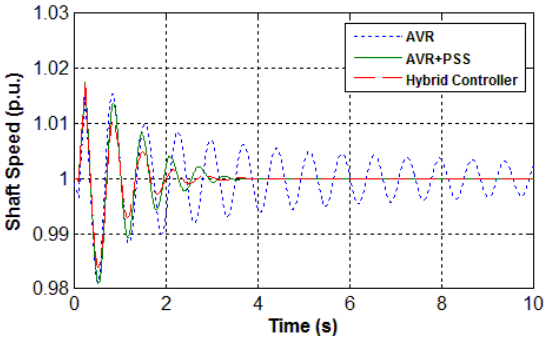

Fig. 2. Comparison of the generator shaft speed for AVR, AVR+PSS and energy-based dissipative controller for a 150-ms three-phase short-circuit.

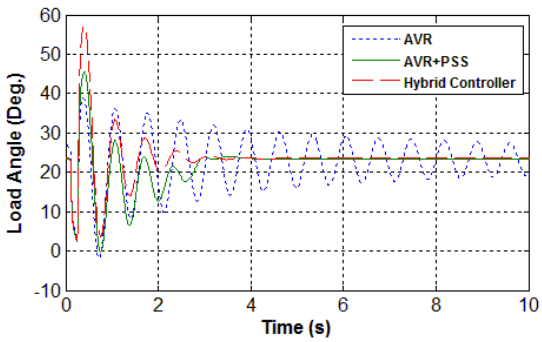

Fig. 3. Comparison of the load angle for AVR, AVR+PSS and energy based dissipative controller for a 150-ms three-phase short-circuit.

A Grid Compatible Methodology for Reactive Power Compensation in Renewable Based Distribution System

T. Aziz, U. P. Mhaskar, T. K. Saha and N. Mithulananthan
School of ITEE, The University of Queensland, Australia.
Email: taziz@itee.uq.edu.au

***Abstract*— The penetration level of renewable based distributed generation (DG) has increased rapidly in recent years. Grid standards demand small DG units to operate with constant power factor control mode and large DG units with voltage control mode. As a result, small DG units are exposed to the problem of slow voltage recovery due to contingencies like fault. This paper proposes a new sensitivity index based methodology for placement of shunt reactive power compensators to support voltage at load bus and generator bus under steady state and transient conditions. Two different test systems with diverse network and load configurations have been used to test and verify the proposed methodology.**

I. KEY FIGURES

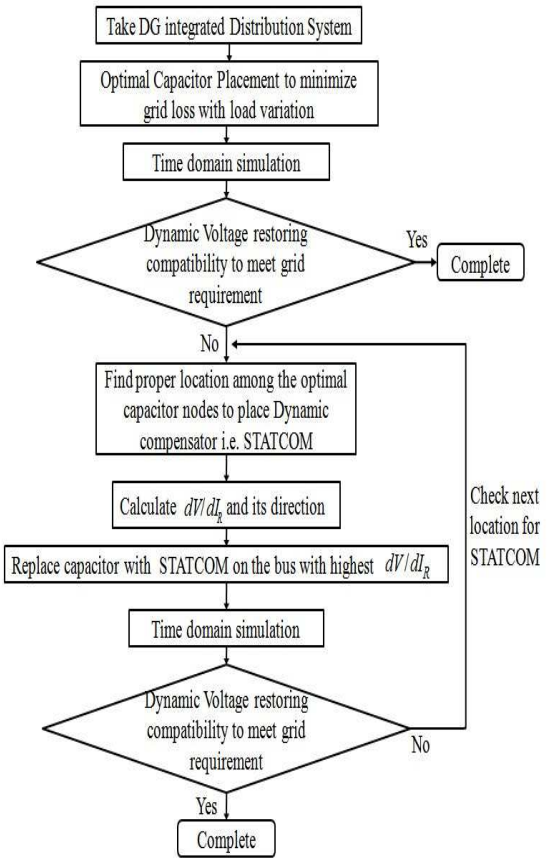

Figure 1. Flow-chart for the solution algorithm

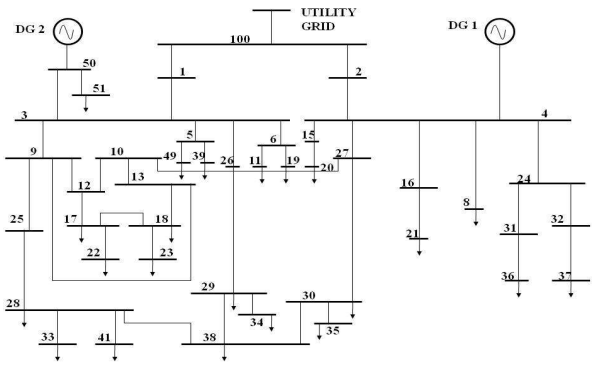

Figure 2. 43 Bus Test System

II. KEY RESULTS

TABLE I
OPTIMAL CAPACITOR SOLUTION FOR 43 BUS SYSTEM

Optimal Node	Capacitor Size (MVAr)	Sensitivity index	
		dV/dQ (Vpu/MVAr)	dV/dI_R (Vp.u/Ip.u.)
49	0.6	0.044	0.20 (Capacitive)
29	0.6	0.046	0.25 (Capacitive)
21	0.6	0.088	0.33 (Capacitive)
51	0.6	0.046	0.2 (Capacitive)
41	0.6	0.048	0.2 (Capacitive)
25	0.6	0.006	0.03 (Capacitive)
30	0.6	0.047	0.25 (Capacitive)
39	**1.1**	**0.044**	**-0.25 (Inductive)**
17	1.1	0.055	0.25 (Capacitive)
35	1.2	0.049	0.2 (Capacitive)
18	1.2	0.048	0.2 (Capacitive)
37	1.2	0.068	0.33 (Capacitive)
33	1.2	0.049	0.25 (Capacitive)

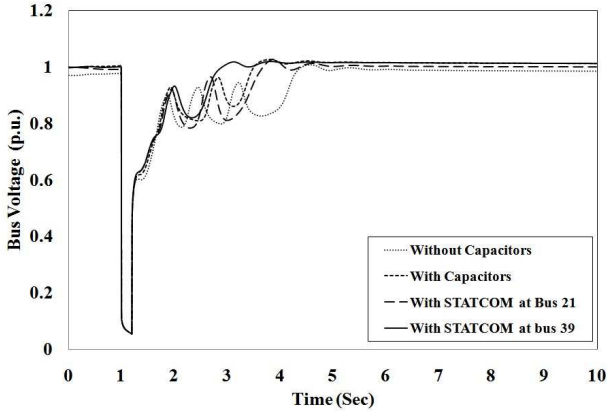

Figure 3. Performance Comparison for voltage restoration at bus 4 (base load)

Reactive Power Compensation in Low-Power Mode: Implementing Controlled Shunt Reactors

Yury Dvorkin
Sensors, Energy, and Automation Laboratory, Department of Electrical Engineering, University of Washington, Seattle, WA 98105, USA,
Email: dvorkin@u.washington.edu

Dmitry Rimorov
Moscow Power Engineering Institute, Moscow 141090, Russia

***Abstract*—Reactive power compensation in electrical grids uses well-known components called thyristor controlled shunt reactors (CSR). CSRs are commonly used to maintain dynamic stability of the power system in hard transient processes caused by faults or emergent switching. This paper presents a study for the application of CSRs for secure, reliable, and efficient power delivery through a high-voltage (over 500 kV) transmission line, in a static, low-power mode. The low-power mode is peculiar because it consists of excessive amounts of reactive power generated to the grid by the transmission line, which is due to high capacitance of line conductors. Therefore, even a relatively short high-voltage transmission line is exposed to a serious risk of overvoltage that can exceed nominal voltage of the transmission line by up to 60%. The authors consider the performance of a CSR, when installed in the middle of a 1200 km transmission line, and then investigate its influence on voltage control across the transmission line. Next, the authors introduce a control strategy for real-time regulation of the CSR admittance to compensate for redundant reactive power. Finally, the authors evaluate implementation costs of the CSR and conclude about the efficiency of the proposed technology, when compared to other FACTS devices.**

I. Key Equations

The guiding equations of the proposed paper are:

$$V(x) = V_i \cdot \left| ch\left(\gamma_0 \cdot l_x\right) + \frac{S_i^*}{V_i^2} \cdot Z_0 \cdot sh\left(\gamma_0 \cdot l_x\right) \right| \quad (1)$$

$$Q_{CSR} = Q_1 - \left(\frac{V_2^2}{Z_{12}} \cos(\alpha_{12}) - \frac{V_2 \cdot V_3}{Z_{12}} \cos(\delta_{12} - \alpha_{12}) \right) \quad (2)$$

$$Y_{CSR} = \frac{Q_{SCR}}{V_2^2} \quad (3)$$

II. Key Figures

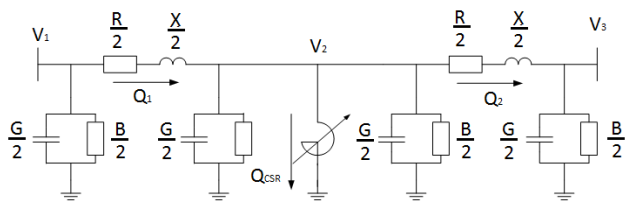

Figure 1. Schematic representation of the considered power line.

III. Key Results

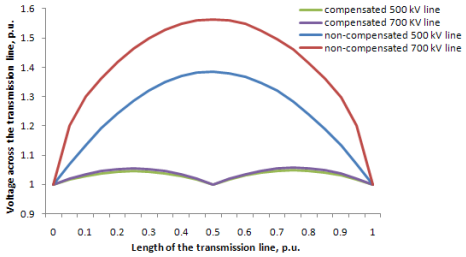

Figure 2. Illustration of the voltage regulation effect for 500 kV and 500 kV transmission lines with the CSR.

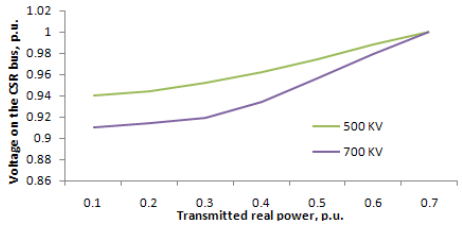

Figure 3. Voltage characteristics on the CSR bus for both 500 kV and 700 kV transmission lines.

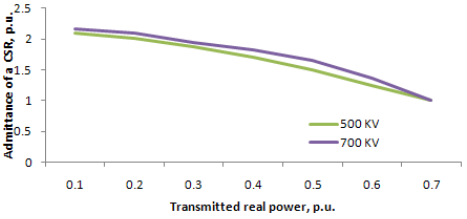

Figure 4. Proposed controlled strategy for the CSR's admittance in low-power modes.

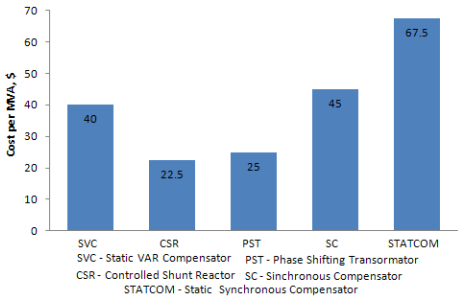

Figure 5. Comparison between cost per MVA for the CSR and other FACTS devices.

Thermal Impact on IGBTs of the Grid-Connected STATCOM

Lakshmi GopiReddy[1], Leon Tolbert[1, 2], Burak Ozpineci[1, 2], Yan Xu [2], Tom Ritzy[2]

[1]*University of Tennessee, 414 Ferris Hall, Knoxville, TN 3799-2100*
[2]*Oak Ridge National Laboratory, P.O. Box 2008 MS-6070, Oak Ridge, TN 3783-6070*
Email: lgopired@utk.edu, Tolbert@utk.edu, ozpinecib@ornl.gov, xuy3@ornl.gov, ritzydt@ornl.gov

***Abstract*— Most of the failures in IGBTs are caused by thermal fatigue. Hence, the thermal analysis of IGBTs for each particular application is an important step in determining their lifetime. In this paper, the thermal analysis of the STATCOM is presented for two different applications, power factor correction and harmonic elimination. The STATCOM model is developed in EMTP for the above mentioned functions. The analytical equations for average conduction losses in IGBT and diode are derived. The electro thermal model is used to estimate the temperature of the IGBT. A comparative analysis of the thermal stresses on the IGBT with various parameters such as power factor, harmonic frequency and harmonic amplitude is presented as a basis for future reliability testing of IGBTs in FACTS applications.**

As the power factor of the load decreases, the inverter losses increase and the temperature increase is inverted parabolic in shape with a maximum of temperature rise at Φ= 90°. The losses in the inverter are proportional to the load current and the power factor angle. The losses due to harmonic compensation of purely harmonic load are independent of the frequency of the harmonics and dependent on the amplitude of the harmonic. The temperature rise of IGBT for a purely harmonic inverter load of 50A of 5th harmonics and that for a 50A of 7th harmonics is similar as demonstrated by simulation. Simulation results would be validated by experimental work. The case of STATCOM operation for simultaneous power factor correction and harmonic load on the junction temperature of IGBT and diode, and in effect on the reliability of the IGBT and STATCOM would be presented.

Key Equations-

Conduction losses in IGBT and diode for power factor correction-

$$P_{cond\_i} = (I_l \times \sin\Phi) \times \left(\frac{V_{on\_i}}{2\pi} + \frac{I_l \times \sin(\Phi) \times R_{oni}}{8} \right) \quad (1)$$

$$P_{cond\_d} = (I_l \times \sin\Phi) \times \left(\frac{V_{on\_d}}{2\pi} + \frac{I_l \times \sin(\Phi) \times R_{fd}}{8} \right) \quad (2)$$

Conduction losses in IGBT and diode for single harmonic load compensation-

$$(P_{cond\_i})_h = I_h \times \left(\frac{V_{on\_i}}{2\pi} + \frac{I_h \times R_{oni}}{8} \right) \quad (3)$$

$$(P_{cond\_d})_h = I_h \times \left(\frac{V_{on\_d}}{2\pi} + \frac{I_h \times R_{fd}}{8} \right) \quad (4)$$

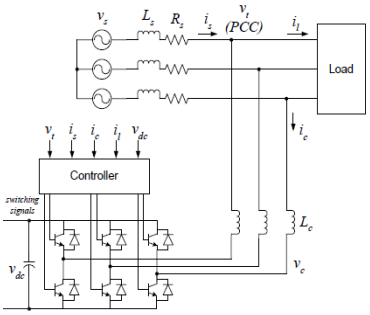

Figure 1. Model of the STATCOM connected to Power System

I. KEY RESULTS

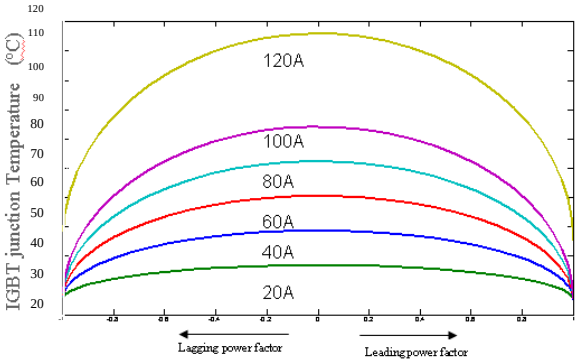

Figure 2. The variation of junction temperature of IGBT with power factor obtained from EMTP simulation

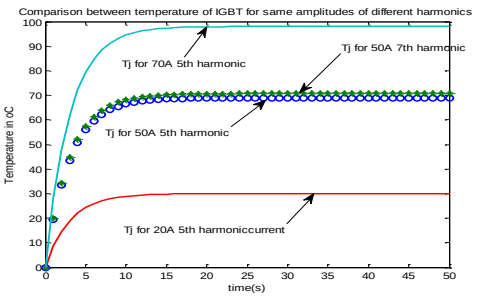

Figure 3. The junction temperature of IGBT varying with time for different two load harmonics, 5th and 7th, at same amplitudes, 50A, and also different amplitudes (20A, 50A and 70A) of 5th harmonic.

Conduction Losses for harmonic load compensation

$$P_{cond\_i} = (I_1 \times \sin\Phi)\left\{ \frac{V_{on\_i}}{2\pi} + I_1 \times \sin(\Phi) \times R_{oni} \times \left\{ \frac{1}{8} + \frac{1}{\pi} \sum_h \frac{M_{2h}}{(h-2) \times h \times (h+2)} \right\} \right\} + \sum_{\substack{h=2n+1 \\ h \neq 3^*y}}^{N} I_h \times \left(\frac{V_{on\_i}}{2\pi} + \frac{I_h \times R_{oni}}{8} \right) \quad (5)$$

$$P_{cond\_d} = (I_1 \times \sin\Phi) \times \left\{ \frac{V_{on\_d}}{2\pi} + I_1 \times \sin(\Phi) \times R_{fd} \times \left\{ \frac{1}{8} + \frac{1}{\pi} \sum_h \frac{M_{2h}}{(h-2) \times h \times (h+2)} \right\} \right\} + \sum_{h=2n+1}^{N} I_h \times \left(\frac{V_{on\_d}}{2\pi} + \frac{I_h \times R_{fd}}{8} \right) \quad (6)$$

Low Voltage Profile – a Big Problem for Dispersed Generation

N. K. Roy, M. A. Mahmud, and H. R. Pota
School of Engineering and Information Technology
The University of New South Wales at Australian Defence Force Academy (UNSW@ADFA)
Canberra ACT 2600, Australia
Email: N.Roy@student.adfa.edu.au, Md.Mahmud@student.adfa.edu.au, H.Pota@adfa.edu.au

***Abstract*—This paper presents the simulation results showing the effect of lower and higher penetration of distributed wind generation on the voltage profile in distribution systems. The analysis is carried out over a test distribution system representative of the Kumamoto area in Japan. A squirrel cage induction type wind generator is connected at bus 10 for this analysis. The analyses show that high wind penetration exhibits low voltage profile in the distribution system. This under voltage problem can trip low voltage main circuit breaker resulting in an entire plant shutdown. To work electrical equipments properly, it is essential to keep the system voltage within permissible limit (0.95 pu). A dispersion level phenomenon is proposed in this paper to solve this problem. Dispersion level is the ratio of the number of buses that have wind generator to the number of load bus in the system. If wind generators are distributed in different buses of the entire distribution network keeping the penetration level same then the voltage profile of the system is significantly improved.**

I. KEY EQUATIONS

The dynamics of the shaft of wind generator (WG) can be represented as follows [1]:

$$\dot{\omega}_m = \frac{1}{2H_m}\left[T_{ae} - K_s\lambda - D_m\omega_m\right] \quad (1)$$

$$\dot{\omega}_g = \frac{1}{2H_g}\left[K_s\lambda - T_{ae} - D_g\omega_g\right] \quad (2)$$

$$\dot{\lambda} = 2\pi f\left(\omega_m - \frac{1}{N_g}\omega_g\right) \quad (3)$$

A simplified transient model of a squirrel cage induction generator (SCIG) can be described by the following algebraic-differential equations [2]:

$$\dot{E}'_{qr} = -\frac{1}{T'_o}\left[E'_{qr} - (X - X')I_{dg} + s\omega_s T'_o E'_{dr}\right] \quad (4)$$

$$\dot{E}'_{dr} = -\frac{1}{T'_o}\left[E'_{dr} + (X - X')I_{qg} - s\omega_s T'_o E'_{qr}\right] \quad (5)$$

$$\dot{s} = \frac{1}{2H_g}\left(T_m - T_e\right) \quad (6)$$

A synchronous generator (SG) with third order model is also connected at bus 15.

II. KEY FIGURES

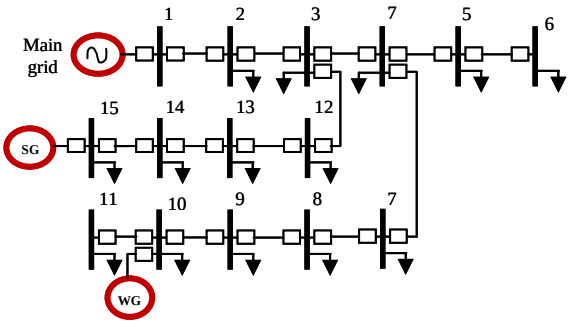

Figure 1. Single line diagram of Kumamoto 15-bus distribution test system

III. KEY RESULTS

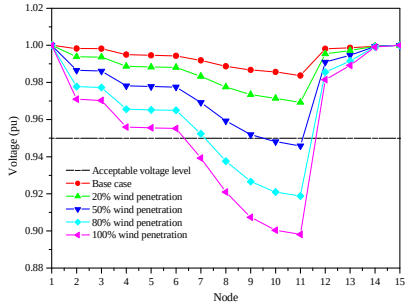

Figure 2. Nodal voltages of the distribution system with distributed wind generation for different penetration level (0.8 pf lagging)

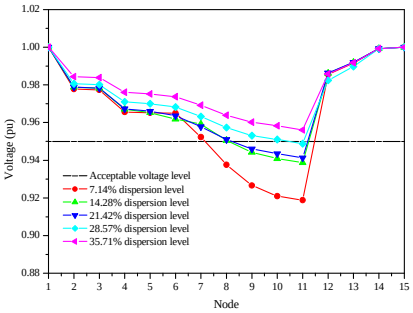

Figure 3. Nodal voltages of the distribution system for different dispersion level (80% wind penetration level)

Reference

[1] M. J. Hossain, H. R. Pota, V. Ugrinovskii, and R. A. Ramos, "Simultaneous STATCOM and Pitch Angle Control for Improved LVRT Capability of Fixed-Speed Wind Turbines," IEEE *Transactions on Sustainable Energy*, vol. 1, no. 3, October 2010.
[2] C. W. Taylor, *Power System Voltage Stability*, New York: McGraw-Hill, 1994.

Ultra-capacitor Integration to Improve Dynamic Real and Reactive Power Conditioning

Deepak Somayajula and Mariesa L. Crow
Department of Electrical and Computer Engineering, Missouri University of Science and Technology,
Rolla, MO 65409, USA,
Email: dbsv2b@mail.mst.edu and crow@mst.edu

***Abstract*—Power system grid has many power quality and reliability problems like voltage sags, swells, real and reactive power imbalances which can be detrimental to the grid. Such real and reactive imbalances can be compensated with the help of shunt and series filters which will act as power conditioners. In this paper the integration of an ultra-capacitor through a dc-dc bidirectional boost converter is proposed for improving the dynamic performance real and reactive power conditioners. The series and shunt filters are back to back inverters which will filter out voltage and current harmonics in the grid. However, both the filters need real and reactive power support from an additional source apart from the dc-link capacitor. The dc-dc converter and control design are very important in this regard. It is observed that the ultra-capacitor integration is ideally suited for providing good real power support for the series filter which compensates for voltage sags and swells. And it is also observed that the dc-dc converter helps in maintaining a stiff dc-link voltage which helps in the operation of the shunt filter. The simulation model of the overall system is developed in PSCAD and the simulation results agree well with the observations.**

I. Main Figures

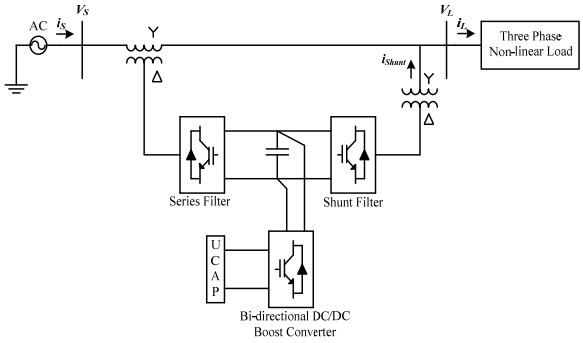

Figure 1. Block diagram of the System

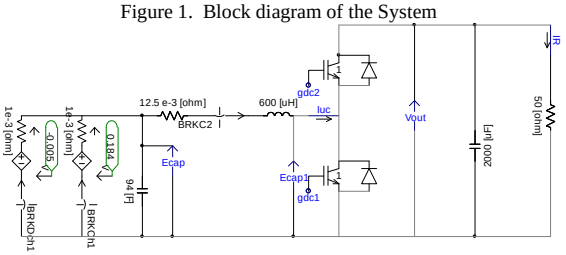

Figure 2. Ultra-capapacitor and Dc-dc converter model in PSCAD

II. Simulation Results

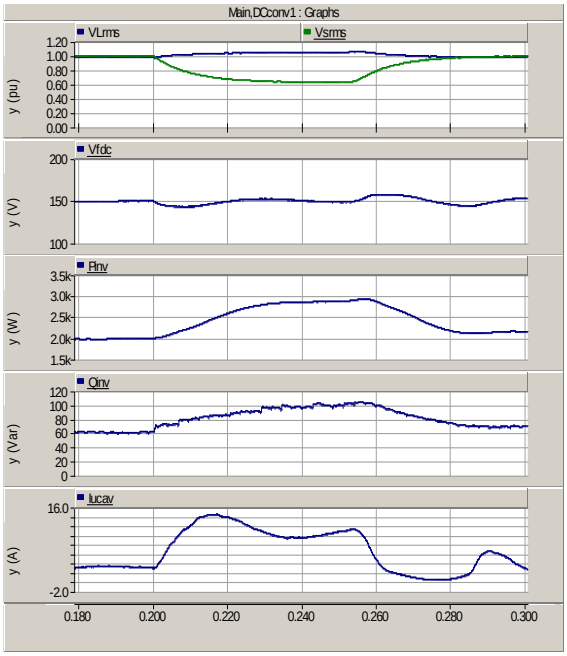

Figure 3. Dc-dc converter providing real and reactive power support to the Series filter during voltage sag

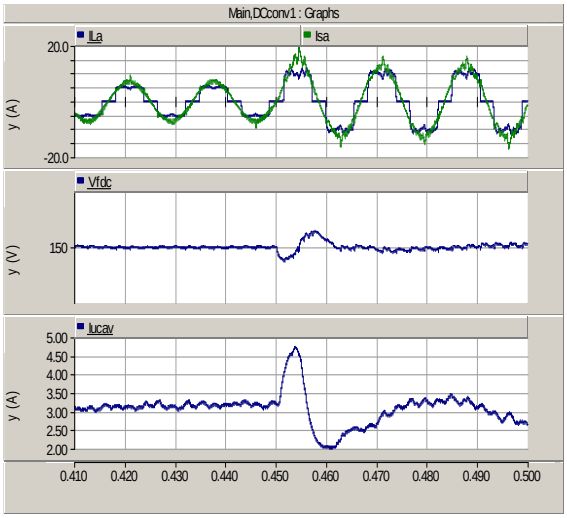

Figure 4. Dc-dc converter providing stiff link voltage support to the Shunt filter during dynamic load changes

Shunt Capacitor Renewal Planning with a Cost Leveling Strategy using the Condition Age Model

Ken Suzuki, Yuta Tanaka, and Shinich Iwamoto
Power Systems Laboratory, Department of Electrical Engineering and Bioscience, Waseda University, Tokyo 169-8555, Japan
Email: suzuki.ken.pwrs@gmail.com

***Abstract*— With the past high economic growth period in Japan, the demand for power has been increasing sharply year by year. Therefore, Shunt Capacitors (SCs), as a new Japanese utility, have been installed along with the predicted demand in order to maintain the voltage profile and stability. Meanwhile, some SCs have aged because they have been used for a long time, and thus, have to be replaced sometime soon. Recently, economic evaluation techniques have caught the interest of asset management for power systems. Therefore we propose a renewal planning method using an aged SC model and SC life cycle costs, considering failure rates. Also, from the point stability, this paper deals with the voltage stability L-index which is appropriate to control SC. In addition, it is used the SC grouping method that is possible to confirm which SCs are important in the power system. Finally, we run simulations for the IEEJ 30 machine 115 bus system to confirm the validity of the proposed method.**

I. KEY EQUATIONS

Equations (1), (2) are used for the failure rate model.

$$FR = A \quad ;(COA \le B) \qquad (1)$$

$$FR = A + C\left(e^{D(COA-B)} - 1\right) \quad ;(COA > B) \qquad (2)$$

where, A～D: Constant values, COA: Condition age

Equation (3) shows the life cycle cost model of SC.

$$SCLCC(i) = \sum IC + \sum MC + \sum REMC + \sum REPC \qquad (3)$$

where, IC: Installation cost, MC: Maintenance cost, REMC: Removal cost, REPC: Repair cost

Equations (4), (5) are related to voltage stability.

$$L_j = \left| 1 - \sum_{i=1}^{N} F_{ji} \frac{V_i}{V_j} \angle\left(\theta_{ji} + \delta_i - \delta_j\right) \right| \qquad 0 \le L_j \le 1 \qquad (4)$$

$$L_{group\ i} = L_{change\ i} - L_{first\ i} \qquad (5)$$

where, L: Voltage stability index-L.

II. KEY FIGURES

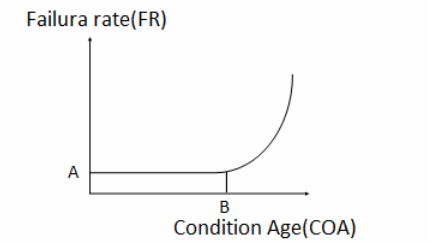

Figure 1. The conditon age modl (Failure rate model)

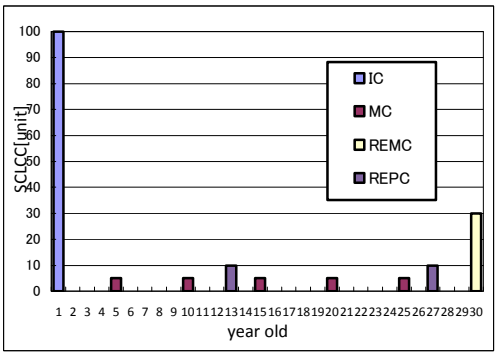

Figure 2. The life cycle cost model of SC

III. KEY RESULTS

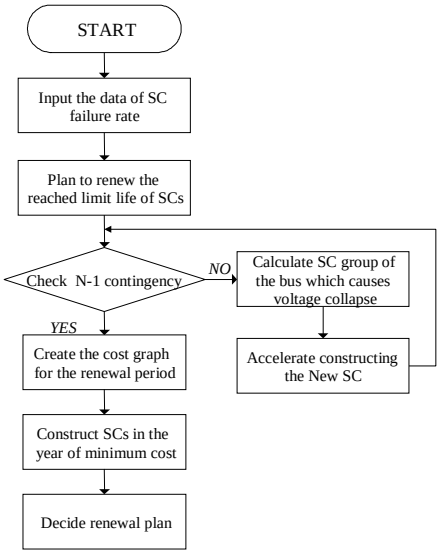

Figure 3. The flowchart of the proposed method

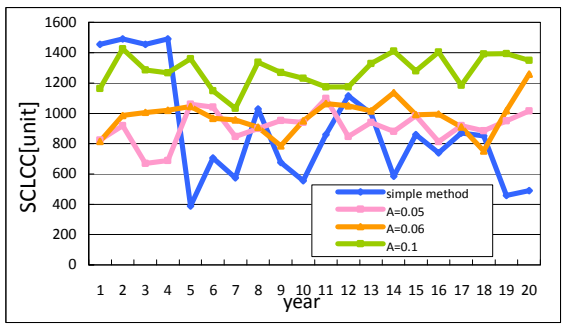

Figure 4. SCLCC during renewal period

It is confirmed that the proposed method which employs the condition age model is very effective for cost leveling strategy.

Reactive Power Planning using Different VAr Devices

Yurong Wang[1], Qiulan Wan[1], and Fangxing Li[2]
1. School of Electrical Engineering, Southeast University, Nanjing, China 210096; 2. Department of Electrical Engineering and Computer Science, The University of Tennessee, Knoxville, TN37996, USA,
Email: yurongwang@seu.edu.cn, qlwan@seu.edu.cn and fli6@utk.edu

***Abstract*— Abstract: Besides the classical shunt capacity banks (SCB), FACTS devices, such as SVC and STATCOM, are widely implanted in practice since the FACTS type devices can provide fast dynamic response characteristics. In this work, based on the different dynamic or static operation performance, mixed allocation of SCB and SVC are investigated, the corresponding compensation capacities are optimized. The reactive power planning model is built considering both short term and long term system stability constraints with cost-based objective function. Case study based on the IEEE 39-bus system clearly indicates that, short term stability constrained reactive power planning can effectively make the most advantages of SVC, the optimal allocation of different types of VAr devices can satisfy different levels of stability constraints.**

I. KEY EQUATIONS

The guiding equations of short term stability indices are:

$$V_{dip} = \frac{V_0 - V_s}{V_0} = \frac{\Delta V}{V_0} \times 100\% \quad (1)$$

Indices for Site Selection of SVC

$$VDI = \begin{cases} |V_{dip}| & if\ |V_{dip}| \geq 0.25 \\ 0 & else \end{cases} \quad (2)$$

$$LVDI = \left\{ \sum_{t \ni (t_{cl}, t_f)} t/T \,|V(t) < 0.8V_0, \forall t \right\} \quad (3)$$

$$R_i = \omega_1 VDI_i + \omega_2 LVDI_i \quad (4)$$

Objective function and parts of constraints of the optimization model for reactive power planning:

for Shunt Capacitor:

$$\min \alpha \sum_{k=1,\cdots,N_L} T^{(k)} P_{loss}^{(k)} + \beta \sum_{i=1,\cdots,Nc} Q_{ci} y_i \quad (5)$$

For SVC:

$$\min \sum (C_{fix\_i} + C_{vi} Q_{Ci}) \quad (6)$$

Constraints:

$$H(x,u,p) = 0 \quad (7)$$

$$g_{\min} \leq g(x,u,p) \leq g_{\max} \quad (8)$$

$$\sum_{i=1}^{n} y_i = N_c \quad (9)$$

$$\delta_{\min} \leq \delta_i(t) - \delta_{COI}(t) \leq \delta_{\max} \quad \forall i \in N_g \quad (10)$$

$$V_{dip}(t) = \frac{V_s(t) - V_0}{V_0} = \frac{\Delta V(t)}{V_0} \times 100\% \leq 25\% \quad (11)$$

$$\delta_i^t - \delta_i^{t-1} - \frac{\Delta t}{2}(\omega_i^t - \omega_i^{t-1} - 2)\omega_N = 0 \quad (12)$$

$$\omega_i^t - \omega_i^{t-1} - \frac{\Delta t}{2M_i}(2P_{mi} - P_{ei}^t - P_{ei}^{t-1}) = 0 \quad (13)$$

II. KEY FIGURES

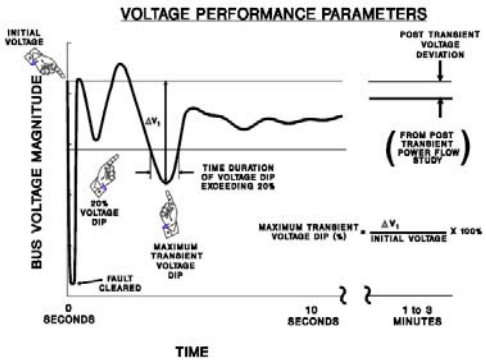

Figure 1. WECC Standard for Short Term Voltage Performance Criteria

III. KEY RESULTS

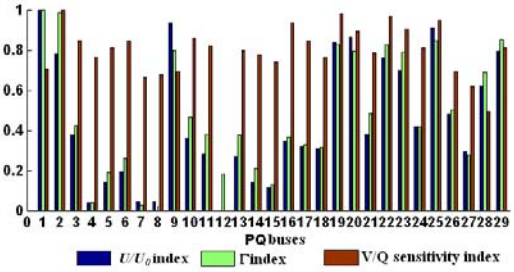

Figure 2. The standardized Values of Three Voltage Related Indices at stable base case at load buses

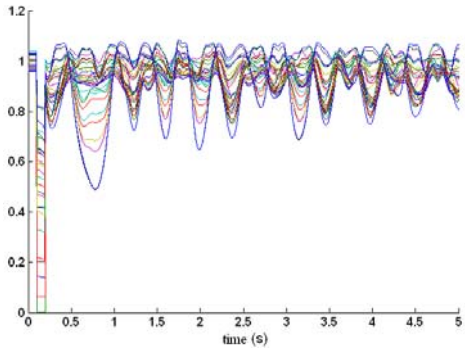

Fig. 3. The load bus voltages with three-phase fault during transient process

Voltage and PQ Control with Inverter-based Photovoltaic Systems

Sarina Adhikari*, Yan Xu, Fangxing Li*,**, Huijuan Li*, John D. Kueck**, Isabelle B. Snyder****

**The University of Tennessee, Knoxville, TN 37996, USA*
(e-mail: sadhikar@utk.edu; fli6@ut.edu; hli26@utk.edu)
***Oak Ridge National Laboratory, Oak Ridge, TN 37831, USA*
(e-mail: xuy3@ornl.gov; lif1@ornl.gov; kueckjd@ornl.gov; snyderib@ornl.gov)

***Abstract*— Distributed energy resources (DER) are relatively small-scale generators or energy storage units that are located in close proximity to load centers. The DERs that are integrated to the grid with the power electronic converter interfaces are capable of providing nonactive power in addition to active power. Hence, they are capable of regulating the voltages of weak electrical buses in distribution systems. This paper discusses voltage control capability of photovoltaic (PV) systems as compared to the traditional capacitor banks. The simulation results prove the effectiveness of dynamic voltage control capability of inverter-based PVs. With proper control algorithms, active and nonactive power supplied from DERs (e.g., solar PVs) can be controlled independently. This paper also presents the scenario of controlling active and nonactive power supplied from a PV array to track and supply the local load. The simulation is carried out in EMTP-RV environment.**

Key Equations

The underlying equations for voltage control, PQ control and modeling of Solar PV are as follows:

$$v_c^*(t) = v_t(t)\left[1 + K_P\left(V_t^*(t) - V_t(t)\right) + K_I\int_0^t\left(\left(V_t^*(t) - V_t(t)\right)dt\right)\right] \quad (1)$$

$$v_{c1}^* = \left[1 + K_{P1}(I_{cn}{}^* - I_{cn}) + K_{I1}\int_0^t (I_{cn}{}^* - I_{cn})dt\right]v_t(t) \quad (2)$$

$$\alpha^* = K_{P2}(I_{ca}{}^* - I_{ca}) + K_{I2}\int_0^t (I_{ca}{}^* - I_{ca})dt \quad (3)$$

$$I = I_{PV} - I_o\left[\exp\left(\frac{V+R_sI}{V_{therm}a}\right) - 1\right] - \frac{V+R_sI}{R_{sh}} \quad (4)$$

I. KEY FIGURES

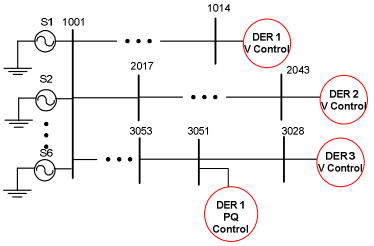

Figure 1. The test system.

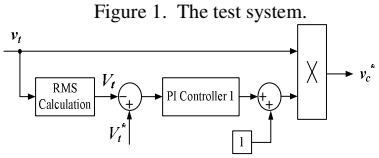

Figure 2. Control diagram for voltage regulation

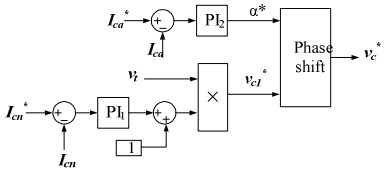

Figure 3. Active and Nonactive power Control diagram

II. KEY RESULTS

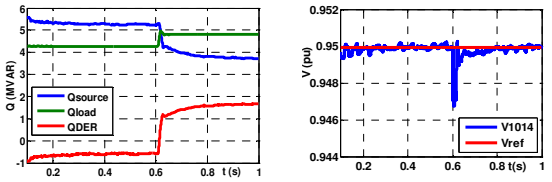

Figure 4. Nonactive power of the system and voltage profile of bus 1014.

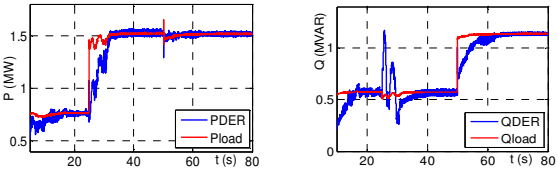

Figure 5. Active and Non-active power from the PV.

A Novel High Frequency Multi-Port Power Converter for Hybrid Sustainable Energy Conversion Systems

Mahmoud M. Amin and Osama A. Mohammed
Energy Systems Research Laboratory, Department of Electrical and Computer Engineering, Florida International University, Miami, FL 33174, USA,
Email: mneam001@fiu.edu and mohammed@fiu.edu

***Abstract*— This poster presents a new high frequency multiport power converter (HFMPC) feasible for hybrid sustainable energy conversion systems. This HFMPC is a highly integrated, ultra fast power converter module solution for low and medium power applications. It is designed to be the interface part between hybrid sustainable energy sources and dc-bus system. Also, it has ability for parallel integrated renewable sources connection representing dc-microgrid and sharing same dc-bus voltage level. The main advantages of this invented module, when compared to conventional converters, are higher efficiency, power density, reliability and durability of all power converter components, as well as less overall operational costs. The bulk dc-output power can either supply dc-loads or be injected into local ac-grid through a power inverter module system. The developed HFMPC is designed to provide superior power management for rapid control prototyping and is also highly suitable for various applications such as: DC-distribution infrastructure systems, Grid connected systems, Plug-in hybrid Electric Vehicles (PHEVs), and Adjustable Speed Drives (ASDs). A 72 kW prototype was tested in order to investigate the overall performance and to verify the effectiveness of the invented HFMPC.**

I. KEY EQUATIONS

The guiding equations of the proposed system control strategies are:

$$P_{wt} = 0.5\,\pi\,\rho\,v^3\,R^2\,C_P(\lambda,\beta) \quad (1)$$

$$i_o = (zFk\,(P_{H2} + P_{O2})/Rh)\,.\,exp\,(-\Delta G/RT) \quad (2)$$

If $V_{dc} > V_{dc\_up}$, then charging: $V^r_{dc} = V_{dc\_up}$

If $V_{dc} < V_{dc\_low}$, then discharging: $V^r_{dc} = V_{dc\_low}$ (3)

If $V_{dc\_low} \le V_{dc} \le V_{dc\_up}$, then no control (rest).

II. KEY FIGURES

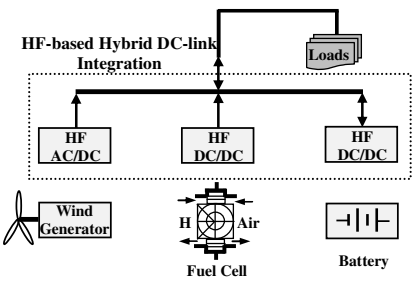

Figure 1. Test System

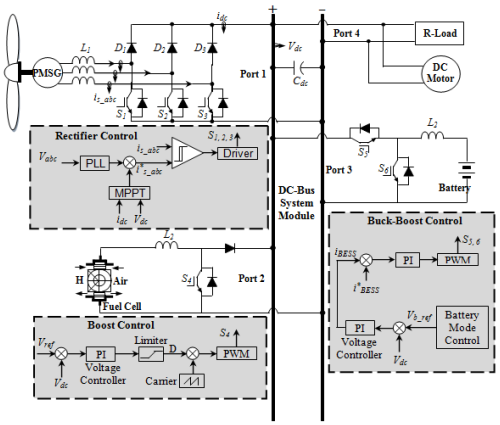

Figure 2. Proposed Controller for the HFMPC

III. KEY RESULTS

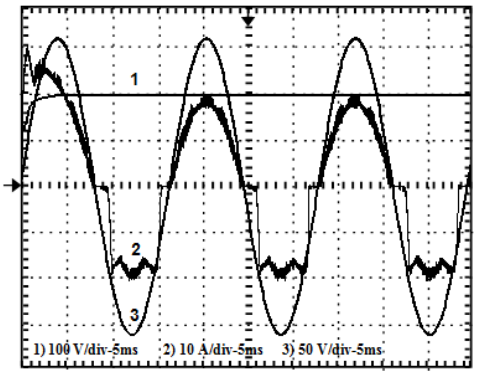

Figure 3. DC-bus output voltage (1-200 V/div, 5ms), rectifier current (2-5 A/div, 5ms), and generator voltage (3-50 V/div, 5ms).

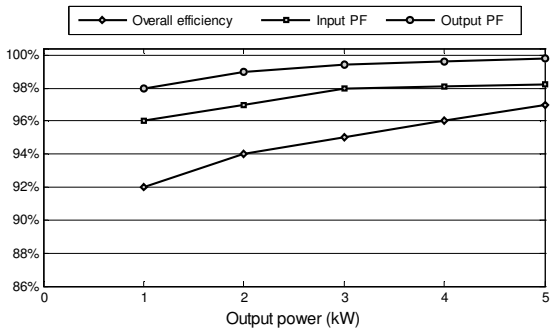

Figure 4. Efficiency, input, and output PF versus output power.

LCC Based MTDC for Grid Integration of Large Onshore Wind Farms in Northwest China

Xia Chen, Weixing Lin, Haishun Sun, Jinyu Wen, *Member, IEEE*,
Naihu Li, *Member, IEEE*, and Liangzhong Yao
College of Electrical & Electronic Engineering, Huazhong University of Science and Technology, Wuhan, China.
Email: cxhust@foxmail.com

***Abstract*—In recent years, many large onshore wind farms are constructed or under construction all over the world. In northwest region of China, the planned capacity of onshore wind farms has reached over 20GW in total. However, the locations of those wind farms are very remote and far away from load centers, and their distance to load centers are beyond 1000km. Therefore, it's of primary importance to address the issues concerned with bulk wind power transmission over long distance. This paper is aimed at development and application of using the line-commutated converter based multi-terminal HVDC (LCC-MTDC) technology for grid integration of large remote onshore wind farms located at Northwest China region. The studies have firstly focused on the design of LCC-MTDC system configuration and its parameters, taking into consideration the practical operation requirements for wind farm grid integration. The control strategy for the LCC-MTDC operation is then proposed, and the comparison in control strategy with and without coordinated operation is also carried out and verified by PSCAD/EMTDC simulation. Various operation scenarios such as ac fault on rectifier and inverter sides are simulated to investigate the system performance during disturbances. Results show that the proposed LCC-MTDC configuration and its control strategy are effective and the LCC-MTDC system is well controlled over the whole operating range.**

I. KEY EQUATIONS

The equations of the converter 1 could be obtained:

$$V_1 = V_{d0I1} + (R_{I1} + sL_{I1} + R_1)I_{I1} \quad (1)$$

$$V_{d0R1} = V_1 + (sC_1V_1 + I_{I1})R_1 + (R_{R1} + sL_{R1})I_{R1} \quad (2)$$

$$I_{R1} = \frac{1}{R_3}\left[V_1 + (sC_1V_1 + I_{I1})R_1 - V_3\right] + (sC_1V_1 + I_{I1}) \quad (3)$$

The relation between output current I_d and the measured current I_m could be expressed below:

$$I_m = \frac{1}{1+sT_m} I_d \quad (4)$$

Therefore, the state equation of MTDC can be written as follows:

$$\begin{aligned} \dot{\mathbf{x}} &= A\mathbf{x} + Bu \\ y &= C\mathbf{x} \end{aligned} \quad (5)$$

In which, $u = [v_1, v_2, v_3, v_4]^T$, $y = [I_{R1}, I_{R2}, I_{I1}, I_{I2}]^T$.

II. KEY FIGURES

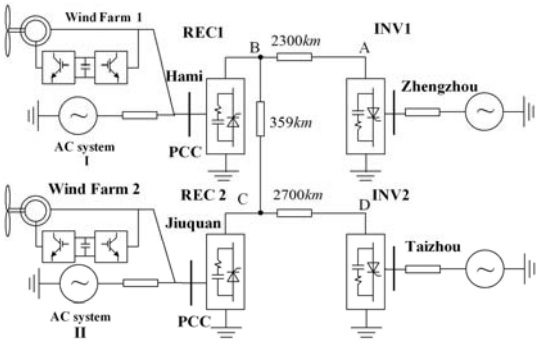

Figure 1. Four-terminal HVDC configuration

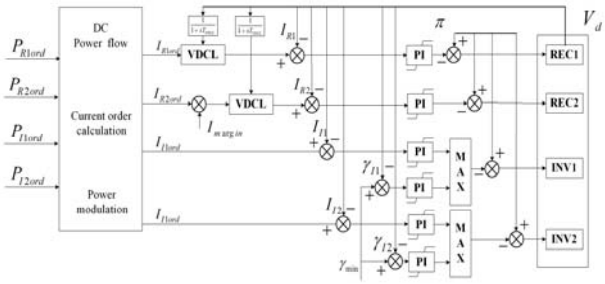

Figure 2. Comprehensive control strategy for MTDC

III. KEY RESULTS

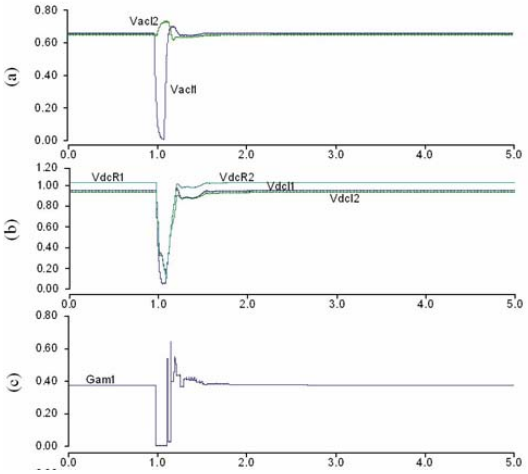

Figure3. Simulation results with the ac fault on INV1 side

Impact of Large Scale Penetration of Photovoltaic Systems on Power System Performance

Sara Eftekharnejad Advisors: Gerald T. Heydt, Vijay Vittal
Power Systems Engineering Research Center, School of Electrical, Computer and Energy Engineering, Arizona State University, Tempe, AZ 85287, USA,
Email: seftekha@asu.edu

***Abstract*— With the rapid and unprecedented structural and market based changes in power systems, new concerns have arisen regarding the reliable and secure operation of the system. Replacing conventional fossil fuel based generation with renewable energy resources such as photovoltaic (PV) systems is one of the structural changes that might impact the steady state as well as dynamic behavior of power systems. The electric power output from a PV system is variable and is highly dependent on weather conditions. As the penetration levels of PV systems increase, the variability in the power output from such sources could result in more significant impacts on system performance. This work first investigates the steady state voltage behavior of the system with various PV penetration levels. Next, the dynamic behavior of the system in terms of system frequency, bus voltages and phase angles, under various levels of disturbances based on variability is investigated. A portion of the WECC system is selected for this study with a relatively large amount of energy exchange to the neighboring areas. Light load conditions are selected for study purposes, since the system is more likely to be affected under these operating conditions. While these results are analytically justified, different methods are suggested to mitigate the increased voltages, caused by increased PV generation, in the system.**

I. KEY FIGURES

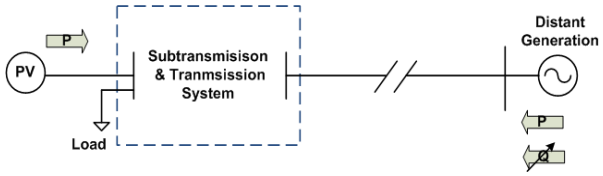

Figure 1. Simple Representation of the System Topology.

II. KEY RESULTS

Both static and dynamic analyses are performed to examine the impact of large scale penetration of the photovoltaic resources on system behavior.

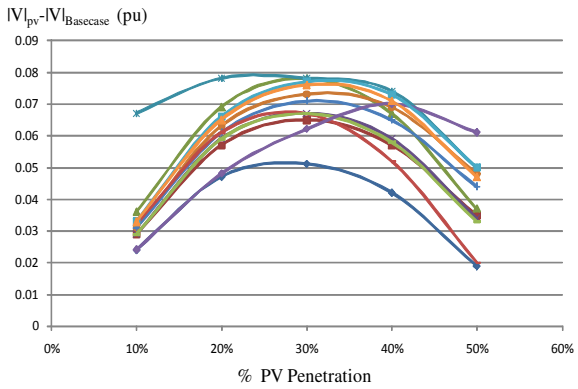

Figure 2. Steady State Voltages of the System under Study with Different Generation Levels of the PV Systems.

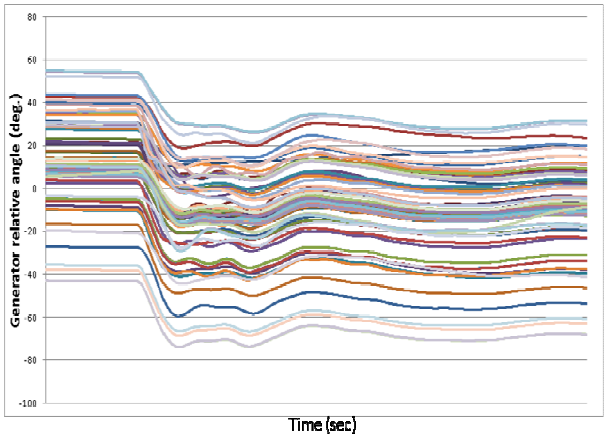

Figure 3. Generator Relative Angles while the Output of the Residential PVs are Dropped. .

Analysis of Wind Generation Impacts on Ontario System Operation

Amr El-Mazariky[1] Kankar Bhattacharya[1] Jatin Nathwani[2]
[1]Department of Electrical and Computer Engineering
[2]Department of Management Sciences
University of Waterloo, Waterloo, ON N2l 3G1, Canada,
Email: aelmazar@uwaterloo.ca , kankar@uwaterloo.ca and nathwani@uwaterloo.ca

***Abstract*— In recent years, energy policies in Ontario have been driven towards a clean and green economy and to this effect, the Government of Ontario has set a goal to eliminate all coal-fired generation by the end of 2014. Wind energy is one of the most mature amongst the renewable energy technologies. It is clean and abundant, and given Canada's wind profile and wind energy potential, Ontario has focused on increasing the installed wind generation capacities to compensate for the phasing-out of coal-fired generation. According to the Canadian Wind Energy Association, 20% of Canada's electricity demand could be supplied by wind energy by 2025. An expansion of installed wind generation requires a closer examination of the location and quality of wind resources and a detailed understanding of its operational impacts on the Ontario transmission grid. In this work, comprehensive analysis is carried out using Ontario's market demand for on- and off-peak periods, to examine the contribution of wind generation during these periods. The on- and off- peak market demands are defined as the maximum and minimum hourly market demand for a certain day respectively. The statistical method used for correlation analysis, is the Pearson Product-Moment Correlation Coefficient.**

I. KEY EQUATIONS

The guiding equations of the Pearson Product-Moment Correlation Coefficient are:

$$\rho_{X,Y} = \frac{\mathrm{cov}(X,Y)}{\sigma_X \sigma_Y} \quad (1)$$

$$\mathrm{cov}(X,Y) = E[(X - \mu_X)(Y - \mu_Y)] \quad (2)$$

$$\sigma_X = \sqrt{E[(X - E(X)^2)]}, \ \sigma_Y = \sqrt{E[(Y - E(Y)^2)]} \quad (3)$$

$$\mu_X = E(X), \ \mu_Y = E(Y) \quad (4)$$

II. KEY FIGURES

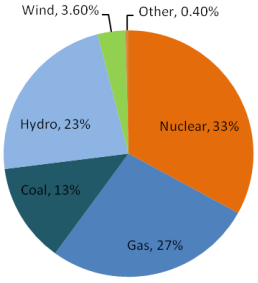

Figure 1. Ontario's Current Electricity Supply Mix (Feb 20, 2011)

III. KEY RESULTS

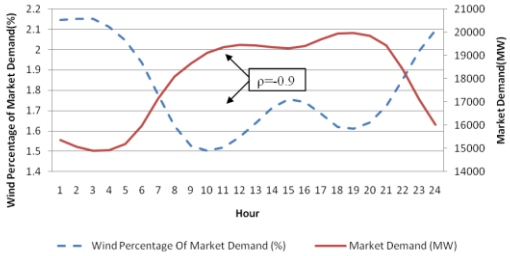

Figure 2. Yearly Average - Wind Generation Percentage of Market Demand Vs Market Demand (2010)

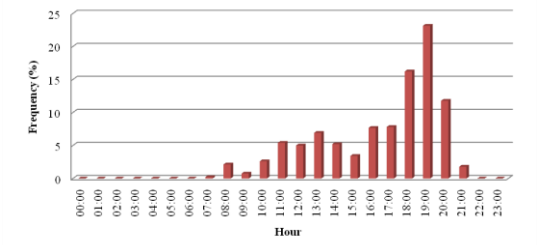

Figure 3. Occurrence of Daily Market Peak Demand (2007-2010)

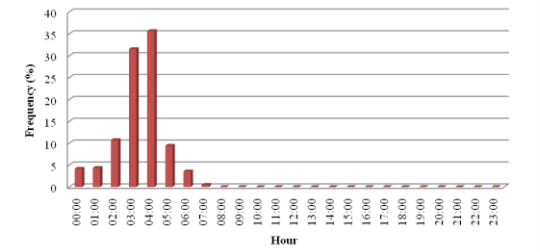

Figure 4. Occurrence of Daily Market Off-Peak Demand (2007-2010)

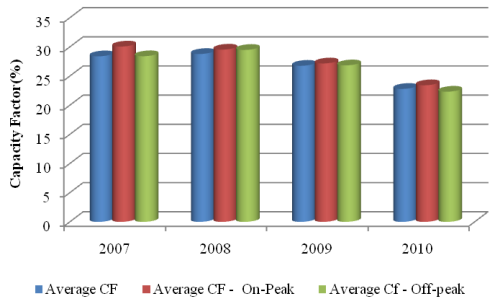

Figure 5. Annual-Average Wind Generation Capacity Factor in Ontario

Probabilistic Power Flow in Transmission System with Photovoltaic Generation

Miao Fan, *Student Member, IEEE*, Vijay Vittal, *Fellow, IEEE*, Gerald T. Heydt, *Fellow, IEEE* and Raja Ayyanar, *Senior Member, IEEE*

School of Electrical, Computer, and Energy Engineering, Arizona State University, Tempe, AZ 85287, USA, Email: miao.fan@asu.edu, vijay.vittal@asu.edu, heydt@asu.edu and rayyanar@asu.edu

***Abstract*— Photovoltaic (PV) power generation is becoming an increasingly important renewable energy resource due to its ability to produce emission-free electric power including both distributed generation and dedicated commercial sized plants. PV generation is a variable resource because its production is influenced by ever-changing weather conditions. PV generation has the potential to cause a significant impact on power system reliability since its total installed capacity is projected to increase at a significant rate. This study focuses on the influence of PV generation on transmission system reliability. To evaluate the influence of PV generation uncertainty, this research applies the probabilistic power flow (PPF) algorithm. In this algorithm, a novel probabilistic model of PV generation is developed to obtain the probability density function (PDF) of the PV generation production based on the environmental conditions which determine PV generation behavior. The correlation between individual loads is considered in the algorithm, since loads are highly correlated to the time of day. The proposed approach is tested on the IEEE 39-bus (New England) system. The proposed algorithm is strongly relevant to the operating and planning studies of the transmission systems with PV generation installed.**

I. KEY EQUATIONS

The guiding equations of the PPF algorithm are:

$$\begin{cases} y = g(x) \\ z = h(x) \end{cases} \tag{1}$$

$$\begin{cases} \Delta x = J^{-1}\Delta y = S\Delta y \\ \Delta z = G\Delta x = GS\Delta y = L\Delta y \end{cases} \tag{2}$$

$$\begin{cases} \Delta x_i = \sum_{k=1}^{n} a_{ik}\Delta y_k \\ \Delta z_j = \sum_{k=1}^{n} b_{jk}\Delta y_k \end{cases} \tag{3}$$

$$f_{\Delta x_i}(\Delta x_i) = \frac{1}{|a_{i1}|} f_{\Delta y_1}(\frac{\Delta y_1}{a_{i1}}) * \frac{1}{|a_{i2}|} f_{\Delta y_2}(\frac{\Delta y_2}{a_{i2}}) * \cdots * \frac{1}{|a_{in}|} f_{\Delta y_n}(\frac{\Delta y_n}{a_{in}})$$

$$f_{\Delta z_j}(\Delta z_j) = \frac{1}{|b_{j1}|} f_{\Delta y_1}(\frac{\Delta y_1}{b_{j1}}) * \frac{1}{|b_{j2}|} f_{\Delta y_2}(\frac{\Delta y_2}{b_{j2}}) * \cdots * \frac{1}{|b_{jn}|} f_{\Delta y_n}(\frac{\Delta y_n}{a_{jn}}) \tag{4}$$

$$P = rA\eta(1 - k\Delta T) \tag{5}$$

$$f_P(P) = \int_{-\infty}^{\infty} \frac{\Gamma(\alpha+\beta)}{\Gamma(\alpha)\Gamma(\beta)} \left(\frac{P_M}{R_M}\right)^{\alpha-1} \left(1 - \frac{P_M}{R_M}\right)^{\beta-1} \frac{k}{\sqrt{2\pi}\sigma} e^{-\frac{k^2}{2\sigma^2}\left(\frac{P}{P_M}-1\right)^2} |P_M|^{-1} dP_M \tag{6}$$

II. KEY FIGURES

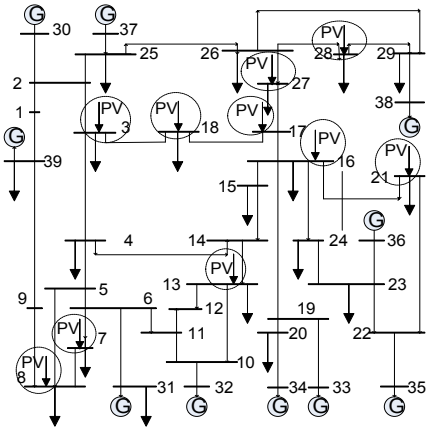

Figure 1. Test System

III. KEY RESULTS

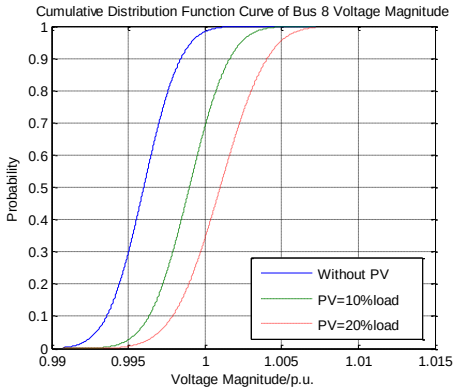

Figure 2. CDF curve of bus 8 voltage magnitude in different PV generation penetrations

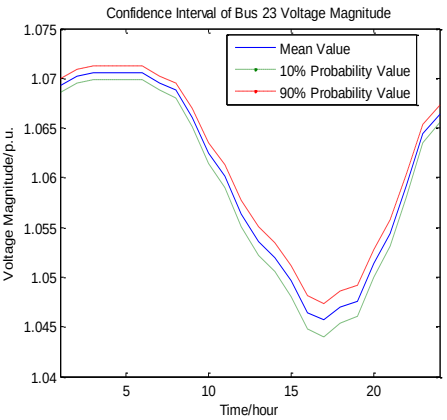

Figure 3. Confidence interval of bus 23 voltage

Renewable and Modular Micro-Source for Smart Grid Applications

Undergraduate Design Team:

Preston Finnie, Matthew Bixler, Justin Shipley, Sebastian Hoyos, Ryan Ricono

Faculty Mentors:

Drs. Sukumar Kamalasadan and Valentina Cecchi

Power, Energy and Intelligent Systems Laboratory (PEISL), Department of Electrical and Computer Engineering, University of North Carolina at Charlotte, Charlotte, NC, USA,
Email: *pfinnie@uncc.edu* and *vcecchi@uncc.edu* and *skamalas@uncc.edu*

Abstract— **The scope of the project is to design, test, and construct a modular, transportable, renewable micro-source that retains plug-and-play capabilities. The power source should possess hybrid production capabilities via the implementation of photovoltaic array and PEM-hydrogen fuel cell. In addition, the source should be capable of generating and conditioning power suitable for use in stand-alone as well as grid-tie applications. Complimentary to these design requirements, the system should have a fully integrated protection scheme and control algorithm to ensure optimized safety and efficiency during operation. A Simulink model will be constructed to replicate the physical system, it will include all major sub-systems including power generation, condition, storage, as well as an integrated control-structure algorithm. Test results acquired from the physical system will be used to validate the model.**

I. Design Requirements

1. *Fuel Cell* and *Photovoltaic Cells* serve as primary *renewable* sources.
2. *Modular*, *transportable*, and possess *plug-and-play* capabilities.
3. *Condition*, *store*, and *deliver* generated power.
4. Function in *grid-tie* and *stand-alone* applications.
5. Sustain *500-Watt* load.

II. System Design

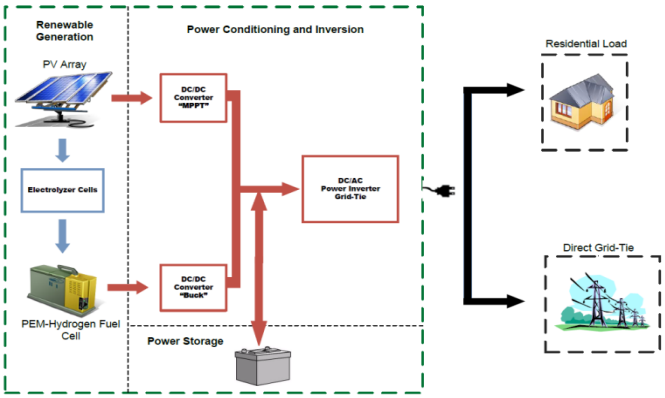

Figure 1. System Topography

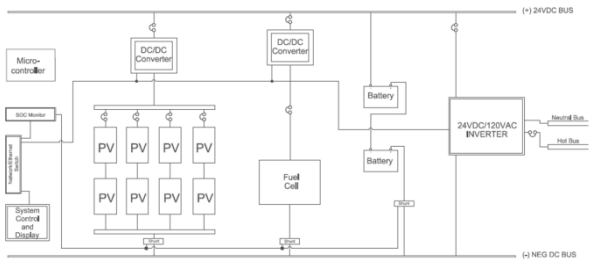

Figure 3. One-Line Schematic

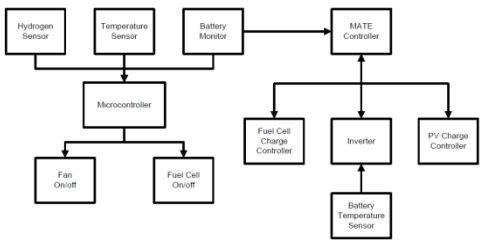

Figure 4. Control Architecture

Assessment of Wind Generation Curtailment

Yingzhong Gu, Omar Urquidez, Peter Thevanh, Jacob Jacobson,

James Carroll, Alan Hise, and Chung Wang

Department of Electrical and Computer Engineering, Texas A&M University, College Station, TX 77840, USA,
Email: *gyzdmgqy@tamu.edu*

***Abstract*— The development of wind energy has increased substantially in the past decade all over the globe. However, due to power system operating reliability and security requirements as well as other practical limitations, not all of the wind production potential can be utilized. The amount of renewable resource production potential that is wasted and thus under consideration is significant.**

Our research focuses on wind generation curtailment and subsequent under-utilization of wind resource potential. Several related factors have been modeled and analyzed such as transmission lines congestion, units' ramping constraints, wind forecast errors.

A simulation platform has been developed for wind curtailment modeling ERCOT in capacity, location, system constraints and pricing. IEEE RTS-24 buses system is used to analyze and verify those wind curtailment situations.

I. KEY EQUATIONS

The mathematic formulation of the proposed model is presented as follows:

$$\max: \sum_{k=k_0}^{T}\sum_{i\in D} B_i\left(P_{Di}^k\right)+\sum_{i\in S} E_i^T \hat{\lambda}_i^T-\sum_{k=k_0}^{T}\sum_{i\in G}\left[C_i^G\left(P_{Gi}^k\right)+C_i^{RG}\left(P_{RGUi}^k,P_{RGDi}^k\right)+C_i^{RS}\left(P_{RSUi}^k,P_{RSDi}^k\right)\right] \quad (1)$$

Subject to

$$\sum_{i\in G} P_{Gi}^k=\sum_{i\in D} P_{D_i}^k \quad k=k_0,\cdots,T \quad (2)$$

$$E_i^{k-1}-E_i^k=\Delta t\cdot P_{Gi}^k \quad i\in S, k=k_0,\cdots,T \quad (3)$$

$$\sum_{i\in G} P_{RSUi}^k=D_{RSU}^k \quad k=k_0,\cdots,T \quad (4)$$

$$\sum_{i\in G} P_{RSDi}^k=D_{RSD}^k \quad k=k_0,\cdots,T \quad (5)$$

$$\sum_{i\in G} P_{RGUi}^k=D_{RGU}^k \quad k=k_0,\cdots,T \quad (6)$$

$$\sum_{i\in G} P_{RGDi}^k=D_{RGD}^k \quad k=k_0,\cdots,T \quad (7)$$

$$\left|\boldsymbol{F}^k\right|\le \boldsymbol{F}^{\max} \quad k=k_0,\cdots,T \quad (8)$$

$$\Delta t\left(P_{Gi}^k-P_{Gi}^{k-1}\right)\le P_i^{RMP} \quad i\in G,\ k=k_0,\cdots,T \quad (9)$$

$$P_{Gi}^k+P_{RSi}^k+P_{RGi}^k\le P_{Gi}^{\max},\ k=k_0,\cdots,T \quad (10)$$

$$P_{RGi}^k+P_{RSi}^k-P_{Gi}^k\le -P_{Gi}^{\min},\ k=k_0,\cdots,T \quad (11)$$

$$E_i^{\min}\le E_i^k\le E_i^{\max},\ i\in S,\ k=k_0,\cdots,T \quad (12)$$

$$P_{Gi}^{\min}\le P_{Gi}^k\le P_{Gi}^{\max},\ k=k_0,\cdots,T \quad (13)$$

$$P_{RSUi}^{\min}\le P_{RSUi}^k\le P_{RSUi}^{\max},\ k=k_0,\cdots,T \quad (14)$$

$$P_{RSDi}^{\min}\le P_{RSDi}^k\le P_{RSDi}^{\max},\ k=k_0,\cdots,T \quad (15)$$

$$P_{RGUi}^{\min}\le P_{RGUi}^k\le P_{RGUi}^{\max},\ k=k_0,\cdots,T \quad (16)$$

$$P_{RGDi}^{\min}\le P_{RGDi}^k\le P_{RGDi}^{\max},\ k=k_0,\cdots,T \quad (17)$$

$$P_{Di}^{\min}\le P_{Di}^k\le P_{Di}^{\max},\ k=k_0,\cdots,T \quad (18)$$

II. KEY FIGURES

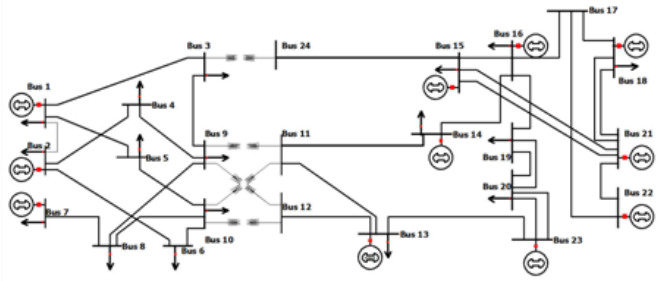

Fig. 1. IEEE RTS-24 System (Modified)

III. KEY RESULTS

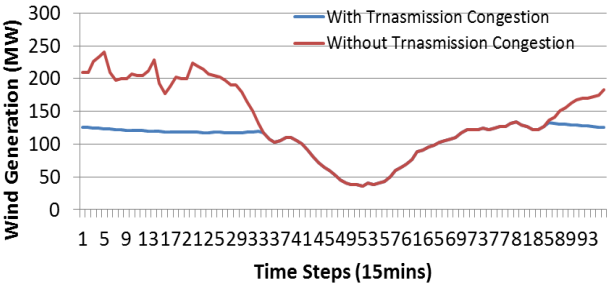

Fig. 2. Local Congestion Caused Wind Curtailment

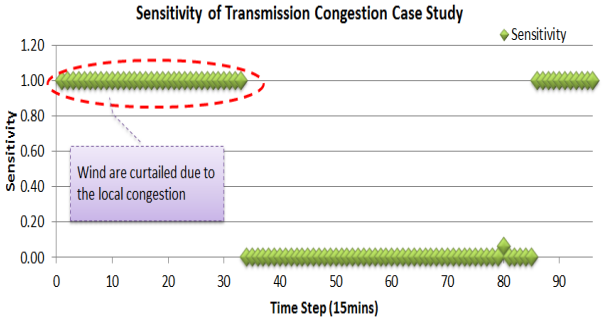

Fig. 3. Sensitivity Analysis of Wind Curtailment

A Selection Method of Output Control Generators Considering Voltage Stability for Large Penetration of PVs

Aye Mya Mya Hlaing, Keita Tokumitsu, Shinichi Iwamoto
Power Systems Laboratory, Department of Electrical Engineering and Bioscience, Waseda University, 169-8555, Tokyo Japan
Hirokazu Achiwa, Kosei Sato, Hisanori Ito, Chubu Electric Power Company, Nagoya, 461-8640, Aichi, Japan
Email: *aye.hlaing.pwrs@gmail.com*

***Abstract*—In Japan, the Japanese government has the target for the penetration of Photovoltaic (PV) power to reach 53GW by 2030. However, large penetration of PV power will cause several problems in power systems. If a large amounts of PV power comes in, thermal power generators have to reduce their outputs in order to take the balance. With this concerns, arise about the reactive output decrease and voltage drops. To solve that problem, in this paper, we propose a selection method for output control (reduce) generators considering the voltage stability. In this method, we use the voltage stability index VMPI (Voltage Margin Proximity Index) and VMPI-i. Simulations are run using the IEEJ WEST 10 machine O/V system model to verify the effectiveness of the proposed method.**

I. KEY EQUATIONS

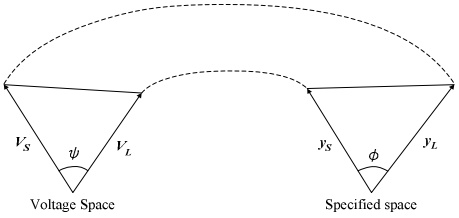

$$\mathrm{VMPI} = \Phi = \begin{cases} \cos^{-1}\dfrac{y_s^{t}\cdot y_L}{\|y_s\|\cdot\|y_L\|} & \left(\|y_L\| > \|y_s\|\right) \\ -\cos^{-1}\dfrac{y_s^{t}\cdot y_L}{\|y_s\|\cdot\|y_L\|} & \left(\|y_L\| < \|y_s\|\right) \end{cases}$$

II. KEY FIGURES

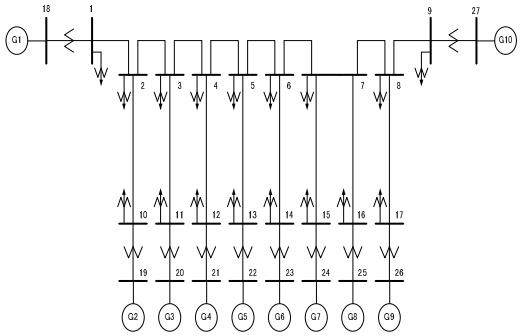

Figure 1. IEEJ West 10 Machine O/V system model

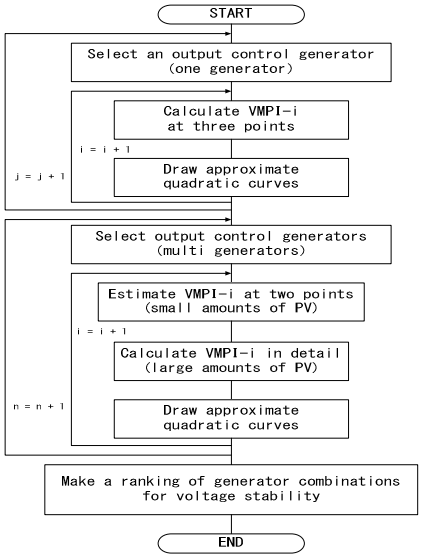

Figure 2. Flowchart of the proposed method

III. KEY RESULTS

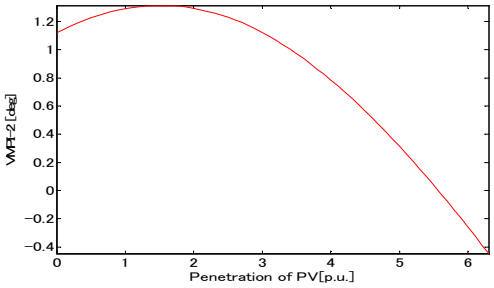

Figure 3. Variation of VMPI-2 for penetration of PV

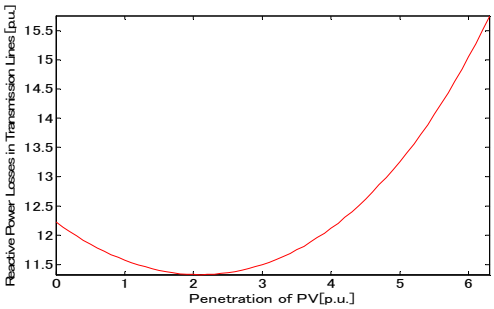

Figure 4. Variation of reactive power losses in transmission lines for penetration of PV

According to the proposed method, we can take good care to the variation of reactive power losses and it is really effective to calculate combinations of output control generators for multiple cases of PV outputs, accurately.

A Framework for the Investigation of Impacts of Wind Energy Penetration on Unscheduled Flows in Bulk Interconnections

Manish Mohanpurkar, *Student Member IEEE*,
Advanced Power Engineering Laboratory, Department of Electrical and Computer Engineering,
Colorado State University, Fort Collins, CO 80523, USA,
Email: manishm@rams.colostate.edu

***Abstract*— Deregulated power systems are characterized by numerous interconnections between areas and zones. Advantages are increased security and reliability of supply, lower operating costs, and increased Available Transfer Capacity (ATC). However, interconnections also introduce challenges such as propagation of system events over wider areas and unscheduled flow of electricity.**

Unscheduled flows (USFs) are a result of electricity trades in a competitive market not based on the electrical nature of interconnected system. USFs are undesirable power flows in the interconnected power systems with reference to the desired or contract paths. The power flow between any two buses will occur through all the possible parallel paths determined by the impedances, rather than the contract paths. Deviation of power flow leads to forced participation of utilities and other assets that may not directly be involved in particular trades. USFs are known to reduce the ATC, increase transmission losses with operation at or near stability limits, and complicate cleared transmission pricing. Within a given network USFs are attributed to fictitious minor loop flows. Hence, to determine or accommodate the effects of USFs, several techniques are available in literature. A linear model to estimate minor loop flows using the topology of the system, and the difference of the actual branch flows and the expected load flows as a measurement is an established method. These estimates are then used in designing a 'contribution factor' (CF) for the various GENCOs participating in that market period. USFs can be effectively accommodated by associating a cost and also in overcoming the non-applicability of superposition theorem. The basis of above approach was conventional power flow algorithms. Coordinating councils identify transmission paths which are prone to USFs from the historical load flow data and are termed as qualified paths. A straightforward technique of identifying a qualified path is transmission line operation at 97% or more of its rated value for more than 100 hours during the past 36 months.

Wind energy promises to be a front runner amongst renewable energy resources. Wind farms involve transmission infrastructure expansion, thus further increasing parallel paths. Wind being inherently variable imparts a stochastic nature to the power injected into the grid. Impacts of wind energy penetration on the load flow and especially the nature of USFs on the qualified paths need to be investigated. The methodology is based on probabilistic load flows followed by appropriate estimation techniques. Probability density functions (pdf) for minor loop flows are an expected outcome of the approach. Confidence intervals will be obtained from the pdfs of the line flows such that an equivalent metric is developed in order to identify a qualified path. Probabilistic load flow (Monte Carlo or convolution method) is the backbone of this approach with stochastic wind generation added to the system. MC simulations though computationally tedious will be performed and used as reference with the assistance of advanced computational facilities. The poster will provide a pictorial representation of the estimation and accommodation of USFs with conventional generation (present state) and with conventional and wind generation mix (future state) in a bulk interconnection.

In the transmission system, the nature of the pdf of USFs, impact on ATC, and transmission expansion, and accommodation of USFs on a market and/or technical level are the technical fronts of investigation. Suggesting cost effective solutions over the existing cost prohibitive is also an objective. Hence, a suitable proposal of estimating and accommodating USFs under stochastic conditions has been presented via this extended abstract and the intended poster.

I. KEY EQUATIONS

The linear system of equations used to model minor loop flows in interconnected systems is:

$$H*x = z \quad (1)$$

where: H = Incidence matrix
z = Difference branch flows
x = Minor loop flow values

Pseudoinverse is one of the most commonly used techniques to estimate minor loop flows (x) in such cases. Pseudoinverse of H matrix is:

$$H^{+} = (H^{T}H) * H^{T} \quad (2)$$

II. KEY FIGURE

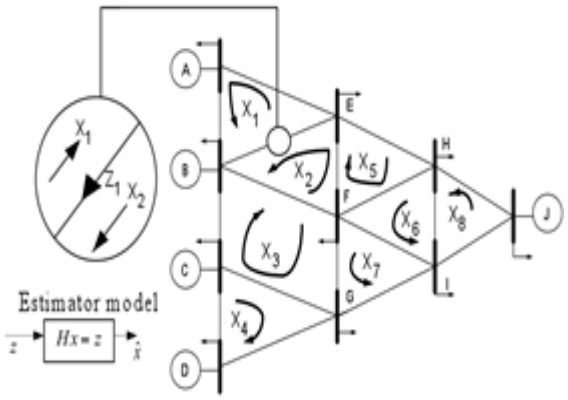

Figure 1: Interconnected Network Displaying Minor Loop Flows

Image Processing Tools for Predicting the Time of Cloud Shadow Arrivals to Photovoltaic Systems

Yazmin Najera and W. Mack Grady
Department of Electrical and Computer Engineering.
The University of Texas at Austin, Austin, Texas, USA
Email: yazminnajera@gmail.com and grady@mail.utexas.edu

***Abstract*— This document presents two solutions for detecting clouds from sky images and for predicting the arrival time of cloud shadows to an area of interest, in this case an area of solar panels. Solar panels are used to produce energy from the sun in areas without access to electricity from central power plants and are increasingly being used by people who want to have the flexibility of being disconnected from the main power grid. Unfortunately, the volatility of cloud motion makes photovoltaic (PV) power unreliable for those who want a steady production of electricity. Knowledge about expected drops in power generation due to cloud shadows in PV systems can improve the performance of microgids by granting users the flexibility to turn on alternative forms of power generation, such as fuel cells, or power storage devices such as batteries, to keep the same loads working uninterruptedly. The solutions provided in this document combine different image processing tools such as SIFT, Libnetpbm and GIMP to find clouds and their velocities from sky images taken at about 5 seconds apart.**

I. Key Equations

The average velocity estimation equations are:

$$Average\ distance\ traveled = \frac{1}{k}\sum_{i=1}^{k}\sqrt{(x_i - x'_i)^2 + (y_i - y'_i)^2} \quad (1)$$

$$Average\ angle = \frac{1}{k}\sum_{i=1}^{k}\tan^{-1}\left(\frac{y'_i - y_i}{x'_i - x_i}\right) \quad (2)$$

The estimated time of arrival estimation equation is:

$$t = \frac{d_{to-sun}}{Avg_{cloud-speed}} \quad (3)$$

II. Key Figures

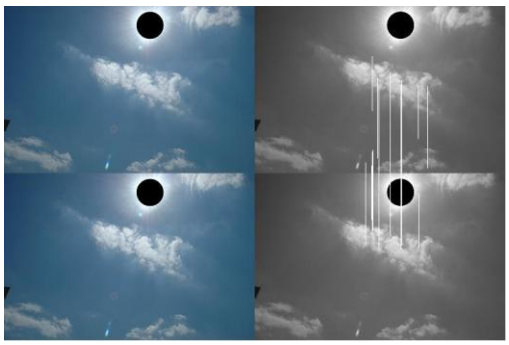

Figure 1. Images taken 5 minutes apart matched by SIFT. The matched points can be used to get an average distance of cloud travel. *Left column: original images. Right column: images analyzed and matched by SIFT*

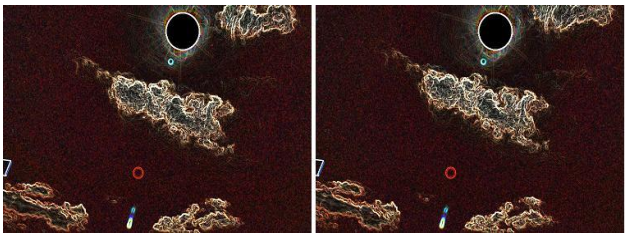

Figure 2. Images Analyzed by GIMP to find Edges (in white).

III. Key Results

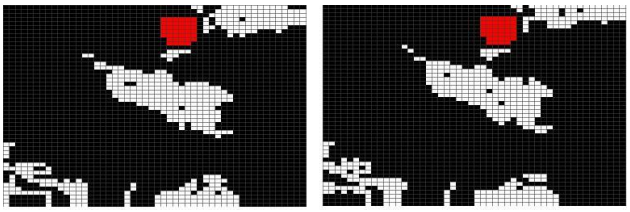

Figure 3. Images Analyzed by Program Using Libnetpbm. The Majority of the Clouds were Recognized Correctly. The Images can be used to Predict the Arrival Times of Clouds to the Sun.

Renewable Energy-Based Power Electronics Teaching Lab

David S. Ochs and Ruth Douglas Miller
Department of Electrical and Computer Engineering, Kansas State University, Manhattan, KS 66506, USA
Email: daveochs@ksu.edu and rdmiller@ksu.edu

***Abstract*— The field of power electronics is experiencing rapid growth, due in large part to greater use of renewable energy sources in power systems. This paper describes a project to provide a way to better prepare students to work with power electronics, specifically as applied to renewable energy. An outline of an undergraduate or graduate lab course in power electronics is presented, with every lab and project having direct applications to renewable energy systems. The labs will make use of power electronics equipment specifically made for classroom settings. The equipment will be well protected and will allow students to focus on the overall design and performance of power electronics circuits, without having to spend a great amount of time on minute details. As part of the lab course, students will build and test such circuits such as choppers, single-phase and three-phase inverters, rectifiers, and filters. They will also design PID controllers and sinusoidal pulse-width modulation (PWM) as part of two major projects: designing and implementing a maximum power point tracker (MPPT) for a solar array, and a three-phase grid tie inverter for a permanent magnet wind turbine. The labs will be integrated into an existing course on wind and solar engineering at Kansas State University, with the goal that they will eventually be the basis for a standalone undergraduate or graduate lab course on power electronics.**

I. Key Equations

The guiding equations for some of the circuits students will be working with are:

Boost MPPT:

$$V_{pv} = V_{dc\ link}(1-k) \quad (1)$$

Single-phase full bridge inverter:

$$v_o = \sum_{n=1,3,5\ldots}^{\infty} \frac{4V_s}{n\pi} \sin(nwt) \quad (2)$$

Sinusoidal PWM inverter:

$$V_o = V_s \left(\sum_{m=1}^{p} \frac{\partial_m}{\pi} \right)^{1/2} \quad (3)$$

II. Key Figures

A. *Solar Labs*

1) Classifying solar panels
2) Choppers/intro to MPPTs
3) MPPT control & chopper w/ PV panel
4) Single-phase inverters
5) Final solar project: boost MPPT with inverter

B. *Wind Labs*

1) Permanent magnet synchronous generators & induction generators
2) Rectifiers
3) 3 phase inverters
4) Final wind project: 3 phase grid tie inverter with sinusoidal PWM

C. *Other Labs*

1) Snubber circuits
2) Overcurrent and overvoltage protection
3) Heatsinksing

Table 1. Class Outline

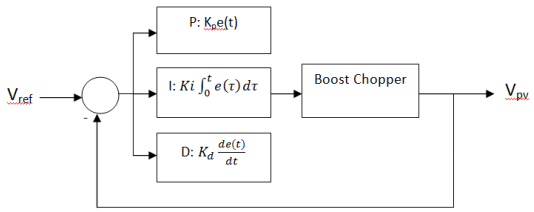

Figure 1. Boost MPPT Control System

III. Key Results

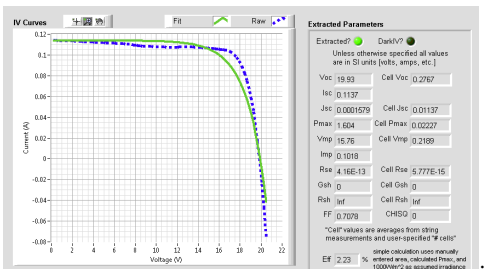

Figure 2. IV Curve taken with Keithley 2400 Sourcemeter and IVStat 3.1 software for 10W Photovoltaic Panel

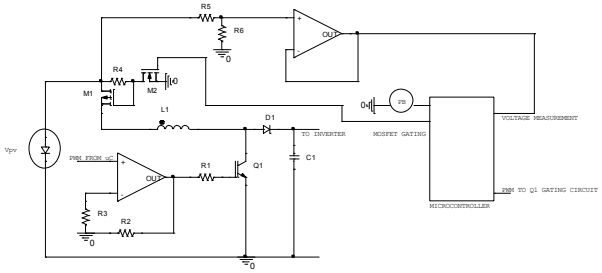

Figure 3. Boost MPPT circuit

Novel Configurations for Photovoltaic Farms to Reduce Partial Shading Losses

M. Z. Shams El-Dein, *Student Member, IEEE*, M. Kazerani, *Senior Member, IEEE*, and M. M. A. Salama, *Fellow, IEEE*
Power and energy Group, Electrical and Computer Engineering Department, University of Waterloo, Waterloo, ON N2L 3G1, Canada,
Email: *mshamsel@uwaterloo.ca*

***Abstract*— Partial shading is the condition of having different insolation levels at different parts of a photovoltaic structure. This structure can be a module, array or farm. The difference in insolation levels causes mismatch in the elements of the photovoltaic structure. This mismatch has undesirable effects such as reduction in generated power from the elements of the structure and hot spots inside the structure. The severity of these effects can be considerably reduced by reconnecting the structure in such a way that mismatch is reduced. This paper proposes novel configurations for modules inside farms, that result in considerable reduction in partial shading losses. Also this paper introduces a novel mathematical formulation for insolation level mismatch. This formula can be used for comparative evaluation of different photovoltaic configurations. The improvement over the existing photovoltaic configurations has been demonstrated by simulation results.**

I. KEY EQUATIONS

The guiding equations for insolation level mismatch are :

$$\hat{I}_c = \frac{\sum_{j=1}^{n} I_j}{n} \quad (1)$$

$$\Delta I_j = \frac{I_j - I_c}{I_c} \quad (2)$$

$$\Delta I_c = \sqrt{\sum_{j=1}^{n} (\Delta I_j)^2} \quad (3)$$

$$\Delta \hat{I}_c = \frac{\sum_{i=1}^{m} \Delta I_{ci}}{m} \quad (4)$$

II. KEY FIGURES

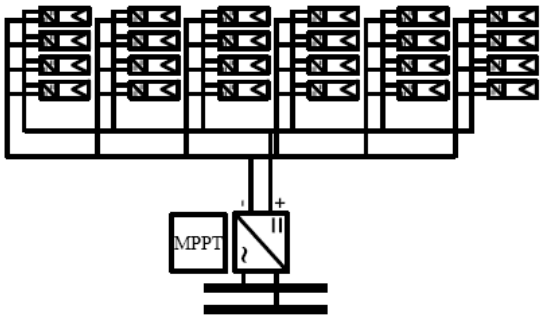

Figure 1. Modified Central Inverter Configuration

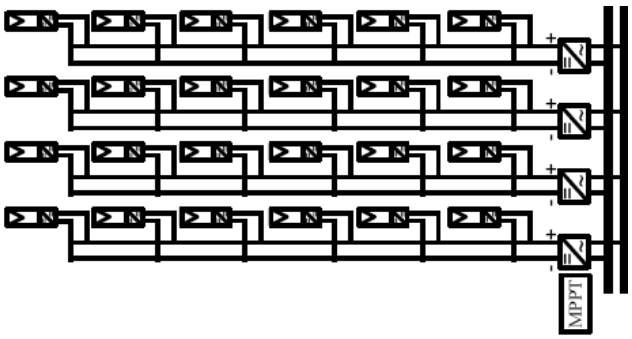

Figure 2. Modified String inverter configuration

III. KEY RESULTS

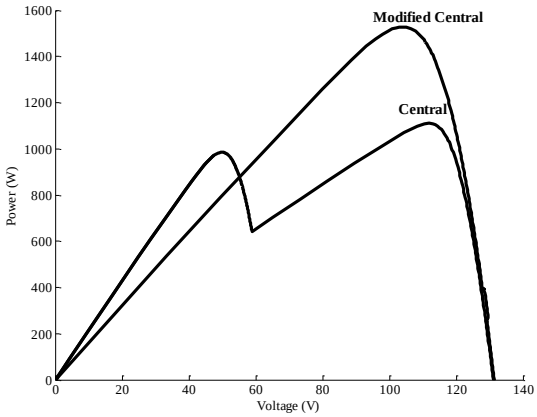

Figure 3. Farm *P-V* characteristics for case study 1.

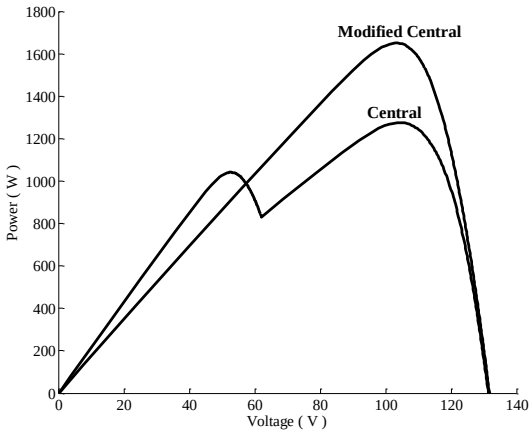

Figure 4. Farm *P-V* characteristics for case study 2.

Latin Hypercube Sampling Techniques for Power Systems Reliability Analysis with Renewable Energy Sources

Zhen Shu and Panida Jirutitijaroen
Department of Electrical and Computer Engineering, National University of Singapore 119077, Singapore
Email: a0017032@nus.edu.sg and elejp@nus.edu.sg

***Abstract*— This paper proposes Latin Hypercube Sampling (LHS) methods for reliability analysis of power systems including renewable energy sources, with an emphasis on the fluctuation of bus loads and intermittent behavior of renewable generations such as wind and solar power. The LHS methods that are applicable for systems with correlated random variables – system load and renewable generation are proposed. Reliability indices such as loss of load expectation and loss of load probability are estimated. Results from Monte Carlo (MC) sequential sampling, MC non-sequential sampling, and that from the proposed LHS methods are compared. It is shown that the proposed methods are as accurate as the other sampling methods while requiring much less CPU time. Two case studies modified from the Electric Reliability Council of Texas (ERCOT) and IEEE Reliability Test System (IEEE RTS) are presented to demonstrate the performances of the proposed sampling methods.**

I. Key Problem and Equations

Power system reliability analysis using LHS considering correlation between time dependent sources:

$$COV = \frac{\sqrt{Var(\hat{E}[f])}}{\hat{E}[f]} = \frac{1}{\hat{E}[F]}\sqrt{\frac{\mathrm{Var(f)}}{\mathrm{N_S}}} \quad (1)$$

$$P(G_r = G_{ri} \cap L = L_j) = \frac{Length\ of\ Time\ (When\ G_r = G_{ri}, L = L_j)}{Total\ length\ of\ Observed\ Time} \quad (2)$$

$$s_{jk} = F_j^{-1}\left(\frac{\tau_{jk} - rand_{jk}}{n}\right) \quad (3)$$

$$Error_{Index} = \frac{\overline{Index} - \overline{Index_{SS}}}{\overline{Index_{SS}}} \times 100\% \quad (4)$$

II. Key Figures

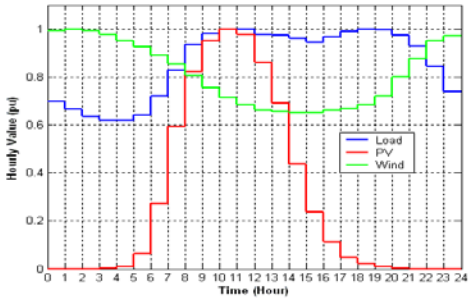

Figure 1. Hourly Values of Load, PV, and Wind

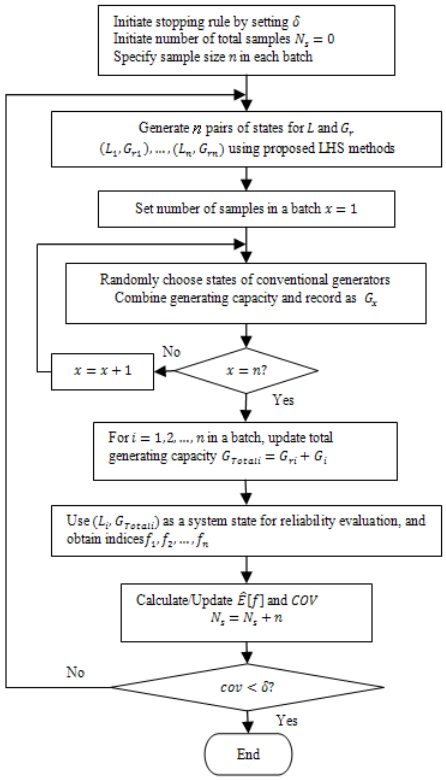

Figure 2. Flow Chart of Implementation of Proposed LHS Approach

III. Key Results

Table I ERCOT System with Wind

Methods	Indices				Error	
	LOLP (%)	EUE (MW)	No. States	CPU Time(s)	LOLP (%)	EUE (%)
SS without wind	0.6914	15.735	11890	2916		
SS	0.4913	10.815	13670	3314	0	0
RS	0.3786	8.077	3297	255	-22.94	-25.32
LD	0.4926	10.892	2662	148	0.26	0.71
LHS_LD	0.4902	10.812	1539	58	-0.22	-0.03
SLR	0.4844	10.522	2893	106	-1.41	-2.71
LHS_SLR	0.4906	10.648	1189	45	-0.14	-1.54
MLR	0.4883	10.660	2349	103	-0.61	-1.43
LHS_MLR	0.4930	10.689	1184	43	0.36	-1.17
JP	0.4950	10.794	2559	120	0.76	-0.20
LHS_JP	0.4872	10.776	1091	26	-0.83	-0.36
LHS_RC	0.4586	9.882	1459	119	-6.65	-8.63

Table II IEEE RTS with PV

Methods	Indices				Error	
	LOLP (%)	EUE (MW)	No. States	CPU Time(s)	LOLP (%)	EUE (%)
SS without PV	1.5478	5.034	11092	2508		
SS	0.9021	3.089	12584	2769	0	0
RS	1.1505	3.779	826	79	27.53	22.33
LD	0.8971	3.091	1759	87	-0.56	0.07
LHS_LD	0.9031	3.112	786	33	0.11	0.74
SLR	0.9113	3.190	2315	92	1.02	3.26
LHS_SLR	0.9109	3.157	742	31	0.97	2.20
MLR	0.9110	3.173	2280	90	0.98	2.72
LHS_MLR	0.9080	3.135	605	25	0.65	1.48
JP	0.8941	3.079	2490	91	-0.89	-0.34
LHS_JP	0.9060	3.086	557	15	0.43	-0.11
LHS_RC	0.9524	3.228	761	58	5.58	4.50

Multi-State Representation of Variable Wind Generation Profiles for Power System Reliability Studies

Anubhav Sinha, Student Member, IEEE Advisors: R. Ayyanar, Senior Member IEEE, V. Vittal, Fellow IEEE and G. T. Heydt Life Fellow IEEE
Department of Electrical, Computer and Energy Engineering, Arizona State University, Tempe, AZ 85287, USA
Email: anubhav.sinha@asu.edu, rayyanar@asu.edu, Vijay.Vittal@asu.edu and gheydt@asu.edu

***Abstract*— While evaluating the reliability of a power system, conventional generating units are represented to be operating in either a fully available or a forced out state. Defining the service availability of a wind generator in a similar manner would result in erroneous values of forced outage rate (FOR) and loss-of-load probability (LOLP) calculations since the output of wind generators is variable and highly dependent on the wind velocity throughout the day. This paper proposes calculation of an equivalent-FOR (EFOR) for a system that includes wind generation by approximating a range of reduced power outputs as a separate operational state. The EFOR is henceforth calculated as a weighted mean of the FOR of each state. This approach leads to a more accurate reliability calculation for a power system. The effectiveness of using multiple power output states is demonstrated by conducting FOR and LOLP calculation on MATLAB for different states and analyzing its benefits on calculation precision. A graphic user interface (GUI) based tool is developed to calculate the capacity outage table (COT) and LOLP for an inputted set of generation and load demand data.**

I. KEY EQUATIONS

For conventional generators the FOR is defined as:

$$FOR = \frac{FOH}{FOH + SH} \tag{1}$$

where,
FOH: Forced outage hours
SH: Service hours

The power output of a wind generator varies drastically depending upon the time of the day (Figure 2). Even if a wind generator operates continuously throughout the day, the immensely reduced output during daytime must be viewed as a significant partial outage. To account for the output variability, an equivalent-FOR is defined, over a period of time (state), as follows:

$$EFOR = \frac{\sum_{i}^{n}\left(\frac{SH_i}{AH} \times \frac{G_i}{R}\right)}{AH} \tag{2}$$

where,
SH_i: Service hours in i^{th} state
AH: Total available hours
G_i:Generation during i^{th} state (MW)
R: Rating of the generation unit (MW)

Based on the EFOR values of each state, a COT is constructed which contains all the capacity states with each outage multiplied by its probability. Thereafter, using the load duration curve, system reliability is assessed by calculating the LOLP as follows:

$$LOLP = \sum_{j} P_j T_j \tag{3}$$

where,
P_j= Capacity state probability
T_j= Duration for which a given magnitude of outage occurs

II. KEY FIGURES

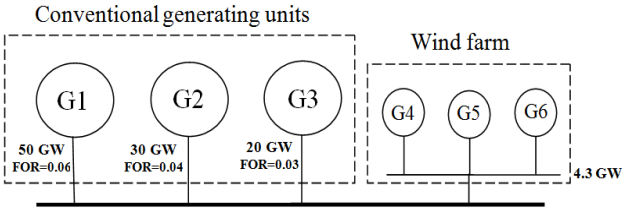

Figure 1. Test system

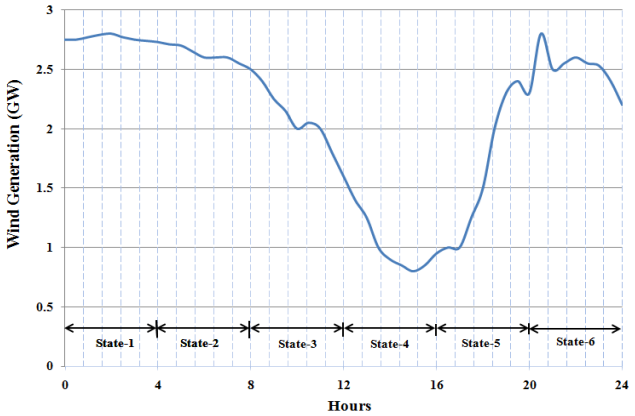

Figure 2. Wind generation profile discretised into six states

III. KEY RESULTS

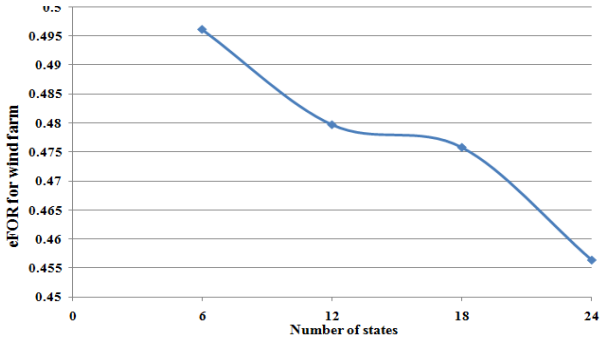

Figure 3. Result demonstrating an increased accuracy in EFOR calculation with increasing number of states

Steady-State Analysis of a Renewable Energy Inverter

Perlekar Tamtam and Dr. Ward Jewell
Wichita State University, Electrical Engineering and Computer Science Deportment,
Wichita, KS 67260, USA
Email: pxtamtam@wichita.edu and wardj@ieee.org

***Abstract*— As the penetration of small solar photovoltaic (PV) generators increases on a power system, it is important for electric power system operators and planners to fully understand the operating characteristics of PV inverters and battery systems. This paper presents detailed results of steady-state testing on one commercial inverter system with lead acid battery storage. The project will continue with transient testing of the same inverter system and development of models for the inverter and batteries.**

A. Connection of steady-state tests

Eight six-volt batteries are connected in series to obtain 48 V of output voltage. These batteries are connected to the DC terminals of two parallel inverter/chargers through over current circuit breakers. Six terminals are on the AC side of the inverter/charger—two terminals for AC input, two terminals for AC output, and two terminals for ground. AC input terminals are connected to the power supply via AC breakers, and AC output terminals are connected to the load via other breakers. The input and output terminals of the inverter are connected to a surge protector to protect the inverter from excessive high voltage [1]. There are two communication ports—RJ45 and RJ11. The MATE is connected to the inverter/charger by an RJ45 cable, and to the computer by an RS-232 cable to communicate with computer software (watt plot software). Figure 1 shows a test equipment connection diagram for the steady-state analysis.

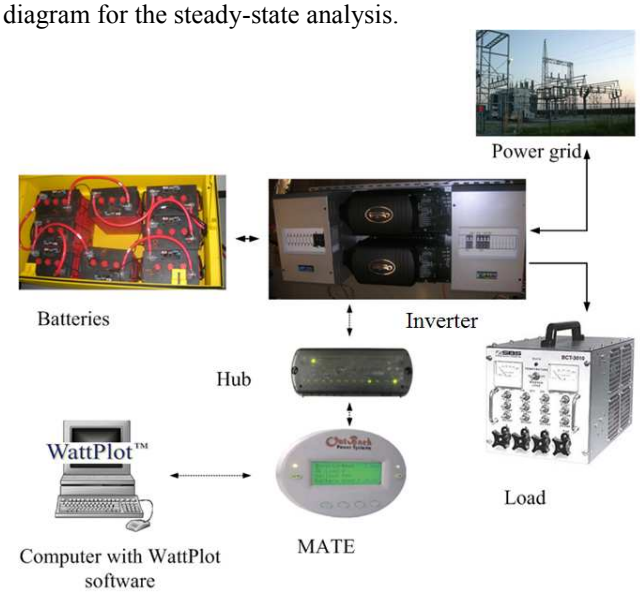

Figure 1 Test equipment connections

B. Inverter test results

V_{DC}	P_{DC}	V_{AC}	P_{AC}	Power Loss	Efficiency
48.8	761.28	122	629	132.28	82.05
48.00	1444.8	122.2	1262.66	182.14	87.39
47.6	2137.24	122.3	1882.67	254.57	88.81
46	2787.6	121.9	2493.34	294.26	89.44
45.2	3457.8	121.3	3087.66	370.14	89.29
44.4	4146.96	120.9	3648.67	498.29	87.98

Table **1** Performance table of inverter/charger while discharging through resistive load

V_{DC}	P_{DC}	V_{AC}	P.F	P_{AC}	Power Loss	Efficiency
51.6	864.3	121.5	0.93	976	111.7	88.55
52.4	1226.16	121.0	0.95	1416	189.84	86.59
53.2	1840.72	120.5	0.96	2098.3	257.6	87.72
54.4	2552	119.1	0.98	2892.3	340.3	88.23
55.2	3085.36	118.3	0.99	3465.3	380	89.03
56	3637.2	117.6	0.99	4046.2	409	89.89

Table 2 Performance table of inverter/charger while charging batteries

C. Transient analysisb (Future Work)

By using Lab View software we plan to generate distorted AC waveforms, which will simulate disturbances that the inverter will encounter on the AC power system. We will also use Lab View with historical solar data to generate the output voltage and power profile of a DC power supply that is simulating PV modules. An analog to digital converter will transfer this waveform to the AC load testing system and programmable DC power supply. These systems will then take the data from Lab View and generate the AC waveform that is supplied to the inverter. Data will be collected from the inverter by a digital storage oscilloscope. At this time, we have all the equipment and are looking for real-time data of distorted waveforms from any solar panels.

References

[1] Manual on " Outback Power Systems FLEXware Surge Protector FW-SP-ACA, FW-SP-250, FW-SP-R User's Guide," available at http://www.outbackpower.com/pdfs_spec/OutBackCatalog.pdf.

Impact to the Volatility of Electricity Price under High-Penetration Wind Power

Yanli Wei and Fangxing (Fran) Li
Department of Electrical Engineering and Computer Science, The University of Tennessee, Knoxville TN 37996, USA,
Email: ywei9@utk.edu and fli6@utk.edu

***Abstract*— There is an increasing need to understand the impact from high-penetration wind power on various aspects in power system operation. This paper presents a methodology to evaluate impacts on the market price volatility from the intermittent wind power. The proposed methodology first considers the uncertainty of wind power using a probabilistic distribution of wind speed in combination with the rated speed-MW curve. The correlation among different wind power plants is also modeled. With these statistical models, a Monte Carlo simulation can be used to assess the probabilistic distribution of the price signals, i.e., the probabilistic LMP distribution. Since the computational effort of Monte Carlo simulation (MCS) is intensive, a lookup table is proposed as a preprocessing to greatly simplify the Monte Carlo simulation. The proposed approach is tested with the PJM 5-bus system and the IEEE 118-bus system. Rules of thumb are drawn regarding the probabilistically calculated LMP and the correlation coefficients.**

I. KEY EQUATIONS

The correlation model among the wind farms are:

$$W_s \sim N(\mu, \sigma) \tag{1}$$

$$\phi(w_{s1}, w_{s2}) = \frac{1}{2\pi\sigma_{ws1}\sigma_{ws2}\sqrt{1-\rho_{ws}^2}} \exp[-\frac{z_{ws}}{2(1-\rho_{ws}^2)}] \tag{2}$$

$$z_{ws} = \frac{(Ws_1 - \mu_{ws1})^2}{\sigma_{ws1}^2} - \frac{2\rho_{ws}(Ws_1 - \mu_{ws1})(Ws_2 - \mu_{ws2})}{\sigma_{ws1}\sigma_{ws2}} + \frac{(Ws_2 - \mu_{ws2})^2}{\sigma_{ws2}^2} \tag{3}$$

$$\mu = (\mu_{ws1}, \mu_{ws2}) \tag{4}$$

$$\Sigma = \begin{bmatrix} \sigma_{ws1}^2 & \rho_{ws}\sigma_{ws1}\sigma_{ws2} \\ \rho_{ws}\sigma_{ws1}\sigma_{ws2} & \sigma_{ws2}^2 \end{bmatrix} \tag{5}$$

$$\rho_{ws} = \frac{\mathrm{cov}(W_{s1}, W_{s2})}{\sigma_{ws1}\sigma_{ws2}} = \frac{E[(W_{s1} - \mu_{ws1})(W_{s2} - \mu_{ws2})]}{\sigma_{ws1}\sigma_{ws2}} \tag{6}$$

The economic dispatch model is:

$$\text{Min} \sum_{i=1}^{N} C_{c,i} \times G_{c,i} + \sum_{i=1}^{N} C_{w,i} \times G_{c,i} \tag{7}$$

$$\text{s.t.} \sum_{i=1}^{N} G_{c,i} + \sum_{i=1}^{N} G_{w,i} - \sum_{i=1}^{N} D_i = 0 \tag{8}$$

$$\sum_{i=1}^{N} GSF_{k-i} \times (G_{t,i} + G_{w,i} - D_i) \le F_k^{\max}, \text{ for } k \in \{\text{all lines considering both directions}\} \tag{9}$$

$$G_{c,i}^{\min} \le G_{c,i} \le G_{c,i}^{\max} \text{ for } i \in \{\text{all conventional generators}\} \tag{10}$$

$$G_{w,i}^{\min} \le G_{w,i} \le G_{w,i}^{\max} \text{ for } i \in \{\text{all wind generators}\} \tag{11}$$

II. KEY FIGURES

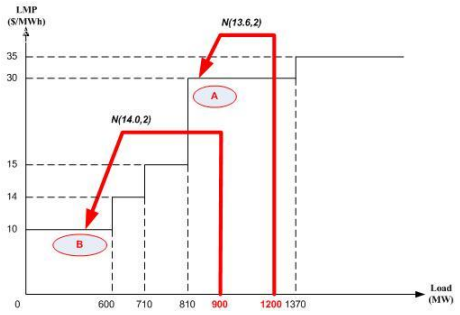

Fig. 1. Two cases showing the impact on actual operating point for the PJM 5-bus system.

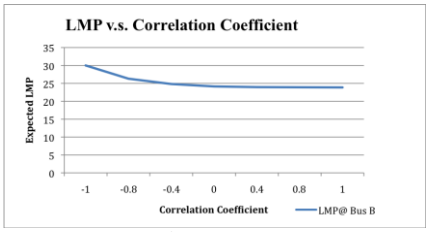

Fig. 2. Increasing pattern of the expected LMP versus correlation coefficient.

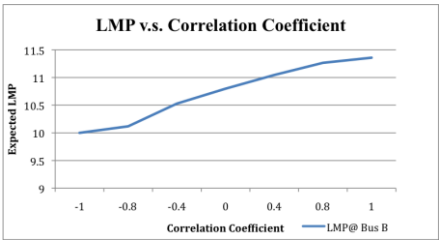

Fig. 3. Decreasing pattern of the expected LMP versus correlation coefficient.

Payment Cost Minimization Considering Wind Energy Effects and Transmission Constrains

Yao Xu, Qinran Hu and Fangxing Li
The Department of Electrical Engineering and Computer Science, the University of Tennessee (UT), Knoxville, TN 37996, USA,
Email: yxu25@utk.edu, qhu2@utk.edu and *fli6@utk.edu*

Abstract— **The penetration of wind sources to the power system network has been increasing in the recent years. The wind energy tends to be unsteady because of the effects of the natural and meteorological conditions. With the unstable wind energy, the payment cost and the location marginal price (LMP) will vary in different cases. In this paper, the payment cost minimization (PCM) problem with the effects of the wind energy and transmission constrains are presented. The wind generation is modeled as the normal distribution. Considering the variable wind generation and the line capacity, the changeable LMP at each bus can be obtained. Then, with the probabilistic wind generation and LMP, the expected value of the minimum payment cost can be calculated. To avoid the local minima and get global optimal PCM, the genetic algorithm is applied to solve PCM in this paper. The presented model and solution methodology are tested and the numerical results of the examples show that the proposed formulation and the solution can greatly reduce the consumer payments.**

I. KEY EQUATIONS

Wind generation distribution:

$$G_t = N(\mu_t, \delta_t^2) \tag{1}$$

$$P_i = \int_{G_{i-1}}^{G_i} \varphi(u)du = \phi(G_i) - \phi(G_{i-1}) \tag{2}$$

$$\varphi(x) = \frac{1}{\delta_t \sqrt{2\pi}} e^{-\frac{(x-\mu_t)^2}{2\delta_t^2}} \tag{3}$$

LMP Model Based on DCOPF:

$$\min \sum_{i=1}^{N} c_i \times G_i \tag{4}$$

$$s.t. \quad \sum_{i=1}^{N} G_i = \sum_{i=1}^{N} D_i \tag{5}$$

$$\sum_{i=1}^{N} GSF_{k-i} \times (G_i - D_i) \le Limit_k \tag{6}$$

$$G_i^{\min} \le G_i \le G_i^{\max} \tag{7}$$

$$LMP_i = \frac{\partial \psi}{\partial D_i} = \lambda + (\sum_{k=1}^{M} \mu_k \times GSF_{k-i}) \tag{8}$$

Payment Cost Minimization Problem

$$\min \sum_{t=1}^{T} ((\sum_{i=1}^{N_d} LMP_i(t) \times d_i(t)) + \sum_{i=1}^{N_g} (x_i(t) \times S_i(t))) \tag{9}$$

The expected value of the PCM

$$E(PCM) = \sum_{i=1}^{n} (PCM_i \times P_i) = \sum_{i=1}^{n} (PCM_i \times (\int_{G_{i-1}}^{G_i} \varphi(u)du)) \tag{10}$$

II. KEY FIGURES

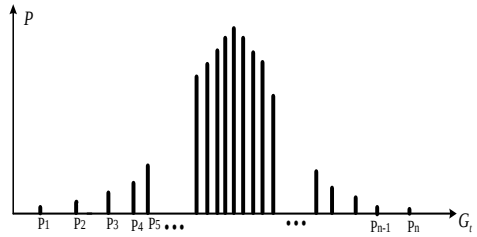

Figure 1. Probability mass function of wind generation

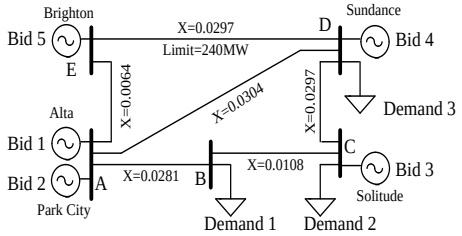

Figure 2. The PJM 5-bus system

III. KEY RESULTS

TABLE I PJM 5 BUS SYSTEM DEMAND

Hour	Demand	Hour	Demand	Hour	Demand
1	856.186	9	996.48888	17	1002.1281
2	822.24711	10	1002.9253	18	1018.7815
3	814.33671	11	1014.2224	19	988.53664
4	832.015	12	1007.7137	20	986.29921
5	847.51063	13	1007.9577	21	974.21134
6	870.35328	14	1007.0279	22	968.86929
7	954.66749	15	1010.5921	23	964.39934
8	960.32833	16	1018.5397	24	959.15532

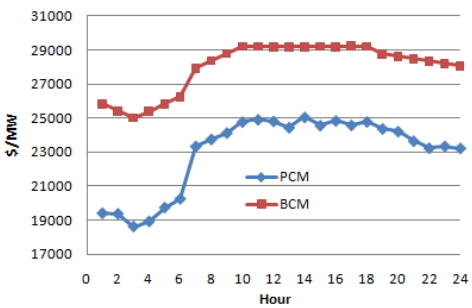

Figure 3. Hourly Expected Value of PCM and BCM

Short-Term Solar Power Prediction Using an RBF Neural Network

Jianwu Zeng and Wei Qiao
Department of Electrical Engineering, University of Nebraska-Lincoln, Lincoln, NE 68588, USA,
Email: *jzeng@huskers.unl.edu* and *wqiao@engr.unl.edu*

***Abstract*—This paper proposes a radial basis function (RBF) neural network-based model for short-term solar power prediction (SPP). Instead of predicting solar power directly, the model predicts transmissivity, which is then used to obtain solar power according to the extraterrestrial radiation. The proposed model uses a novel two-dimensional (2D) representation for hourly solar radiation and uses historical transmissivity, sky cover, relative humidity and wind speed as the input. Simulation studies are carried out to validate the proposed model for short-term SPP by using the data obtained from the National Solar Radiation Database (NSRDB). The performance of the RBF neural network is compared with that of two linear regression models, i.e., an autoregressive (AR) model and a local linear regression (LLR) model. Results show that the RBF neural network significantly outperforms the AR model and is better than the LLR model. Furthermore, the use of transmissivity and other meteorological variables, especially the sky cover, can significantly improve the SPP performance.**

I. Key Equations

The three prediction models, autoregressive (AR) model and RBF neural network model are expressed as:

$$\hat{y} = a_1 x_{t-1} + a_2 x_{t-2} + \cdots + a_p x_{t-p} + e_t \quad (1)$$

$$\hat{y} = \sum_{i=1}^{n} w_i \phi(x, c_i, \sigma_i) + w_0 \quad (2)$$

II. Key Figures

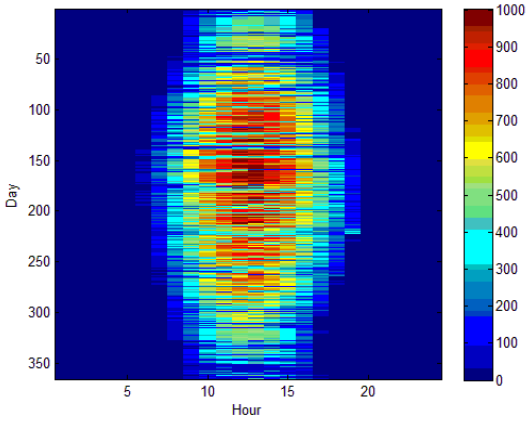

Figure 1. A 2D image view of the solar radiation data.

III. Key Results

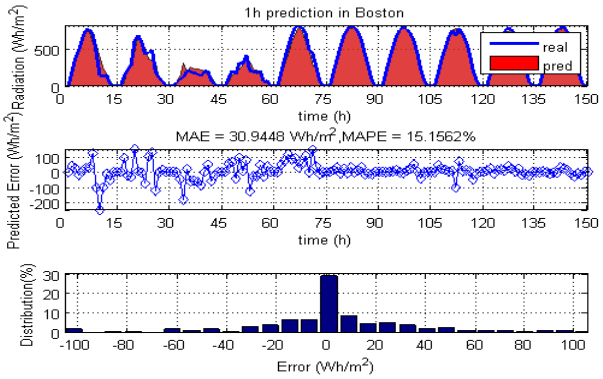

Figure 2. One-hour-ahead prediction in Boston using the RBF neural network.

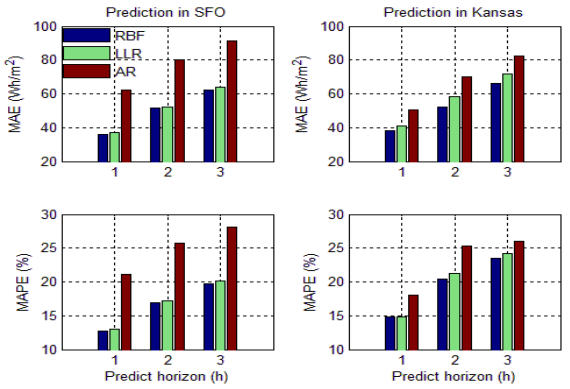

Figure 3. Comparison of the MAEs and MAPEs of the AR, LLR, and RBF neural network-based prediction models.

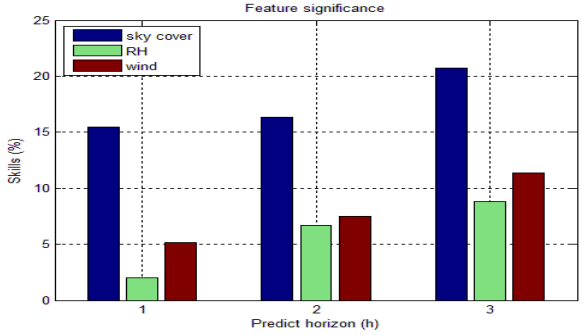

Figure 4. Comparison of feature significance in Boston

Transmission Switching Forensics

Clayton Barrows and Seth Blumsack
Department of Energy and Mineral Engineering, Penn State University, University Park, PA 16802,
Email: cpb155@psu.edu and sethb@psu.edu

***Abstract*— Removal of specific transmission lines from operation ("transmission switching") can reduce the costs associated with power system operation. This phenomenon, known as Braess' Paradox, could be avoided in electric transmission networks through the use of high-quality "smart grid" data and emerging technologies that would make the topology of the power grid adaptable to real-time system conditions. The "optimal transmission topology" problem has been posed in previous research, but is infeasible to solve globally due to the size of real power systems. We analyze the optimal transmission switching results of previous research on the RTS-96 network to determine network properties that identify the optimal number and location of transmission switches. Additionally, we decompose the results of Optimal Transmission Switching to determine the marginal contribution of each switched line to cost savings. As expected, none of the examined network properties successfully identify optimally switched lines. However, our analysis of marginal switching contribution draws conclusions that will enable solution heuristics for the optimal transmission switching problem on larger systems.**

I. Key Figures

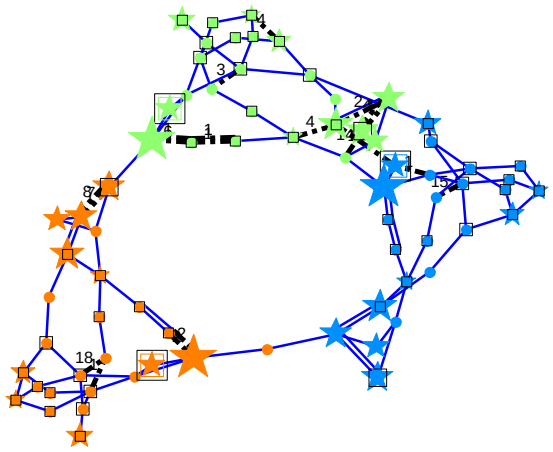

Figure 1. RTS-96 Network. The dashed lines represent the # of hours that each branch is removed from service. The relative size of stars and squares represent the respective amount of peak, un-switched generation and load at each bus.

II. Key Results

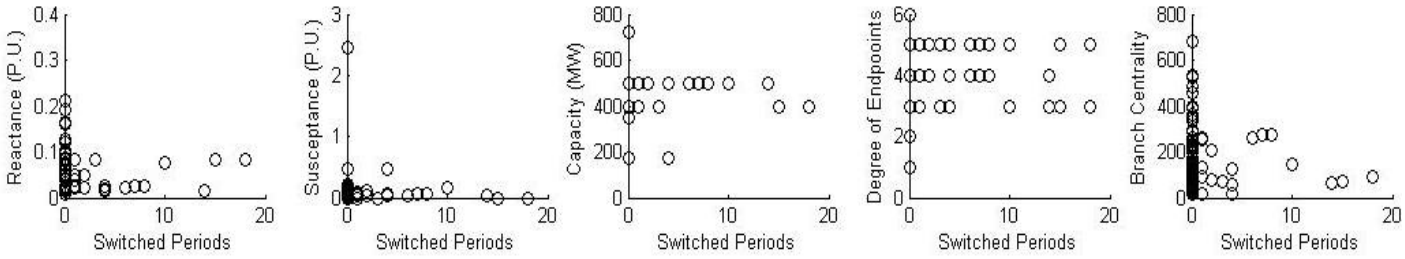

Fig. 2. Various transmission line parameters are plotted as functions of the number of periods each transmission line is removed from service.

TABLE I - Marginal Savings as % of Un-switched System Cost

	Periods (Hours)																							
Lines	**1**	**2**	**3**	**4**	**5**	**6**	**7**	**8**	**9**	**10**	**11**	**12**	**13**	**14**	**15**	**16**	**17**	**18**	**19**	**20**	**21**	**22**	**23**	**24**
109-111	-0.01	---	---	---	---	---	-0.01	---	1.93	4.20	4.63	4.70	4.63	4.70	4.70	4.45	4.36	4.36	3.87	3.72	3.72	---	---	---
112-113	---	---	---	---	---	---	---	---	---	---	---	---	---	---	---	---	---	---	---	---	---	---	---	0.11
113-215	-0.27	0.00	0.00	0.00	0.00	0.00	-0.27	---	---	---	-2.51	---	---	---	-2.52	---	---	---	---	---	---	---	-3.35	---
201-202	0.00	---	---	---	---	---	0.00	---	---	---	---	---	---	---	-0.02	---	---	---	---	---	---	---	---	-0.06
209-211	---	---	---	---	---	---	0.35	---	---	---	3.74	---	---	---	---	---	---	---	---	---	---	---	1.99	---
215-216	---	---	---	---	---	---	---	---	---	---	---	0.15	0.10	---	0.15	-0.02	---	---	---	---	---	---	---	---
215-221	---	---	---	---	---	---	---	---	---	---	---	-0.24	-0.24	---	---	---	---	---	---	---	---	---	---	---
217-218	---	0.00	0.00	0.00	0.00	0.00	---	0.17	0.24	0.33	0.32	---	---	0.32	---	---	---	---	---	0.35	0.35	0.34	---	0.16
218-221	---	---	---	---	---	---	---	---	---	---	---	---	---	---	---	0.03	---	---	---	---	---	---	---	---
218-221	---	---	---	---	---	---	0.00	---	---	---	---	---	---	---	0.03	---	0.03	---	0.03	---	---	---	---	---
219-220	---	---	---	---	---	---	---	---	0.25	---	---	---	---	---	---	---	---	---	---	---	---	---	---	---
219-220	---	---	---	---	---	---	---	---	---	---	---	---	---	---	---	---	---	---	---	0.50	---	---	---	---
220-223	---	---	---	---	---	---	---	---	0.18	---	---	0.27	0.28	0.27	---	0.29	0.30	---	---	---	---	---	---	---
220-223	---	---	---	---	---	---	---	---	---	---	---	---	---	---	---	---	---	---	---	0.34	---	---	---	---
309-311	0.20	---	0.00	---	---	---	0.20	1.75	3.42	4.29	4.50	4.44	4.50	4.44	4.44	4.47	4.39	4.39	4.12	4.02	4.02	---	---	1.06
310-311	---	0.00	---	---	---	---	---	---	---	---	---	---	---	---	---	---	---	---	---	---	---	---	---	---
318-321	0.00	---	---	---	---	---	---	---	-0.01	---	---	-0.03	-0.03	-0.03	-0.03	-0.03	---	---	---	---	---	---	---	---
318-321	---	---	---	---	---	---	0.00	-0.01	---	---	---	-0.03	-0.03	-0.03	---	-0.03	---	---	-0.03	-0.03	---	---	---	---
320-323	-0.01	---	---	---	---	---	---	---	---	---	---	---	---	---	---	---	---	---	---	---	---	---	---	0.02
320-323	---	---	---	---	---	---	---	---	---	---	---	---	---	---	---	---	---	0.17	0.18	---	---	---	---	---
# Sw'd[1]	6	3	3	2	2	2	7	3	6	3	5	7	7	6	7	7	4	3	5	6	3	1	2	5
Cost $k[2]	7.27	7.26	7.25	7.25	7.25	7.25	7.27	7.34	7.44	7.54	7.59	7.60	7.59	7.60	7.60	7.56	7.55	7.55	7.51	7.50	7.50	7.51	7.44	7.31
Σ[3]	-0.01	0.00	0.00	0.00	0.00	0.00	0.03	0.19	0.60	0.88	1.07	0.93	0.92	0.97	0.68	0.92	0.91	0.89	0.82	0.89	0.81	0.03	-0.14	0.13
Savings[4]	0.00	0.00	0.00	0.00	0.00	0.00	0.05	0.19	0.55	0.82	1.03	0.76	0.76	0.93	0.72	0.86	0.89	0.84	0.74	0.83	0.72	0.03	0.00	0.10

[1]#switched lines produced by Optimal Transmission Switching. [2] Total system cost of the un-switched system in thousands of dollars.
[3] Σ represents the sum of the marginal % savings of all of the switched lines for each hour. [4]Optimal Transmission Switching % savings.

Low-Frequency AC Transmission for Offshore Wind Power

Hao Chen*, Dionysios C. Aliprantis* and A. P. Sakis Meliopoulos†
*Department of Electrical and Computer Engineering, Iowa State University, Ames, IA 50011 USA
Email: {chenh, dali}@iastate.edu
†School of Electrical and Computer Engineering, Georgia Institute of Technology, Atlanta, GA 30332 USA
Email: a.meliopoulos@ece.gatech.edu

***Abstract*—Offshore wind power plants are expected to represent a very significant component of the future electric generation portfolio due to space availability and better wind energy potential in offshore locations. The integration of offshore wind power plants with the onshore main power grid is still subject of active research. Within the power plant, a DC collection grid has become a feasible alternative. For the transmission system, besides high-voltage AC (HVAC) and high-voltage DC (HVDC) technology, a low-frequency AC (LFAC) transmission system has also been recently proposed, but has not yet been fully analyzed. In this paper, a novel LFAC transmission system using thyristor-based converters is proposed to connect offshore wind power plants with the main power grid. An analytical methodology to obtain the steady-state operating point of the LFAC system, taking into account the operational constraints of the thyristor-based converters at the sending and receiving ends is developed. Two optimization problems for minimizing the transmission loss, by controlling the receiving end voltage magnitude and the transmission frequency as a function of transmitted wind power are formulated. A numerical case study for a hypothetical 50 mile-long offshore transmission line is used to demonstrate the operation characteristics of the LFAC system. In general, the LFAC system has higher reliability and lower cost compared to voltage source converter-based HVDC, and can transmit power over longer distances compared to a 60-Hz line. The LFAC transmission could be optimal for medium distance transmission (somewhere in between HVAC and HVDC).**

I. Key Equations

Based on the operational constraints of the thyristor-based converters, given the transmission line length and transmitted wind power, Two optimization problems (named 'OPT-1' and 'OPT-2') can be formulated to minimize the transmission loss. For OPT-1, V_R is varied and ω_e is set to $2\pi 20$ rad/s. For OPT-2, both V_R and ω_e are varied. OPT-1 and OPT-2 can be formulated as:

$$\min g\left(V_S, \omega_e\right) \tag{1}$$

subject to

$$h\left(V_S, V_R, \omega_e\right) = 0\,, \tag{2}$$

$$0.6V_R^{\max} \le V_R \le V_R^{\max}\,, \tag{3}$$

$$V_R \ge \sqrt{\frac{B}{9M^2} - A}\,, \tag{4}$$

$$V_S \ge \frac{1}{3M}\,, \tag{5}$$

$$\frac{V_S}{\omega_e} \le \frac{V_S^{\max}}{\omega_e^{\max}}\,, \tag{6}$$

$$0 < \omega_e \le \omega_e^{\max}\,, \tag{7}$$

II. Key Figures and Results

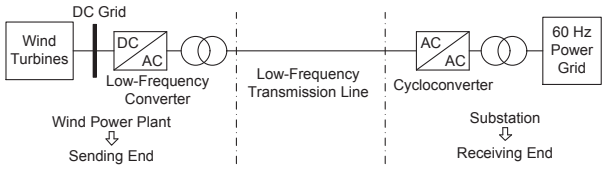

Fig. 1. LFAC transmission system.

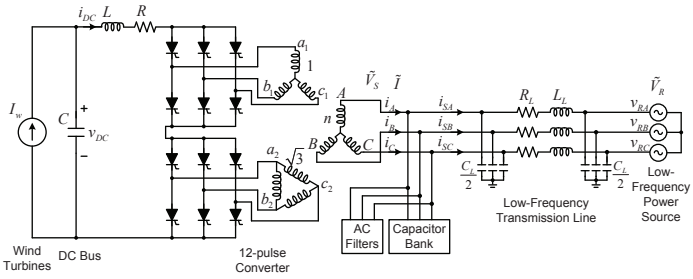

Fig. 2. Simplified model of LFAC transmission system.

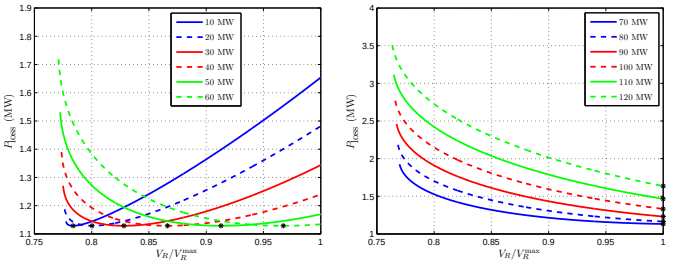

(a) $P_w = 10 \sim 60$ MW (b) $P_w = 70 \sim 120$ MW

Fig. 3. Transmission power loss corresponding to OPT-1.

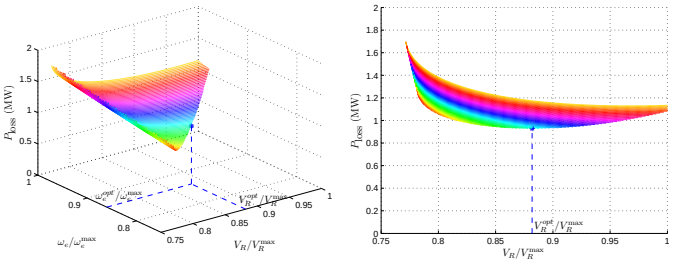

(a) 3-D plot (b) Projection onto V_R–P_{loss} plane

Fig. 4. Transmission power loss corresponding to OPT-2 ($P_w = 60$ MW).

Operation of Doubly Fed Induction Generators with VSC-HVDC Transmission

Katherine Elkington, Hector Latorre and Mehrdad Ghandhari
Electric Power Systems Laboratory, School of Electrical Engineering, Royal Institute of Technology, Sweden
Email: *katherine.elkington@ee.kth.se* and *hector.latorre@ee.kth.se*

***Abstract*— In this article we investigate the interaction of a wind park and a VSC-HVDC link in a power system. The wind park is comprised of doubly fed induction generators, which are induction generators whose rotors are connected to the grid through converters, which can be utilised for control in the power system. We examine the effect of using a power oscillation damping (POD) scheme in wind turbines and VSC-HVDC links based on the idea of a Single Machine Equivalent equivalent, which is often used in controllable components, and show how this damping method can be coordinated with wind power production. This is done by gain scheduling, where the optimal gains of the feedback signals are a function of wind power production. We present the combined impact of the components on power oscillation damping and voltage support.**

I Key Equations

$$u_1 = k_1(\omega_C - \omega_{NC})\sin(\delta_C - \delta_{NC})$$
$$u_2 = -k_2(\omega_C - \omega_{NC})\cos(\delta_C - \delta_{NC}) \quad (1)$$

$$\omega_C = M_C^{-1}\sum_{i\in C} M_i\omega_i \qquad \omega_{NC} = M_{NC}^{-1}\sum_{j\in NC} M_j\omega_j \quad (2)$$

$$\delta_C = M_C^{-1}\sum_{i\in C} M_i\delta_i \qquad \delta_{NC} = M_{NC}^{-1}\sum_{j\in NC} M_j\delta_j \quad (3)$$

$$\max_{k_1} \zeta_{\text{mode}} \ : \ \zeta_{\text{mode}} \le \zeta_i \ \forall i \quad (4)$$

II Key Figures

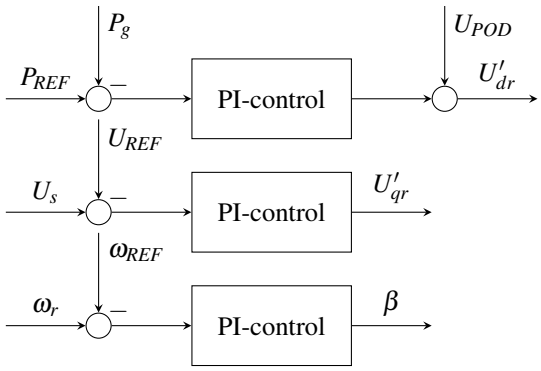

Figure 1: Basic Control Scheme

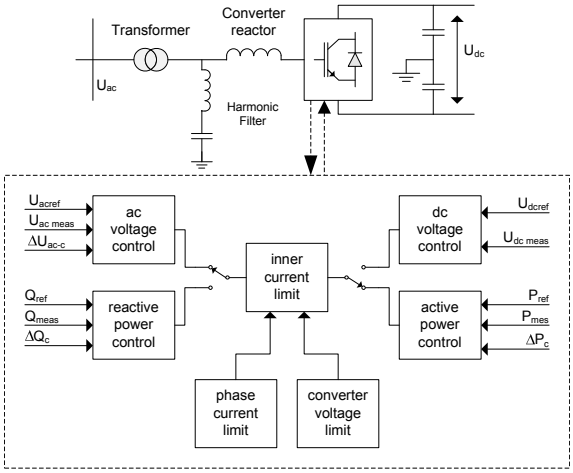

Figure 2: Control VSC-HVDC

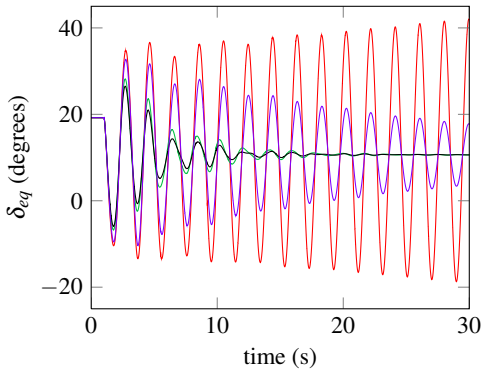

Figure 3: No POD [red], POD only in wind park [blue], POD only in VSC-HVDC [green] and POD in wind park and VSC-HVDC [black]

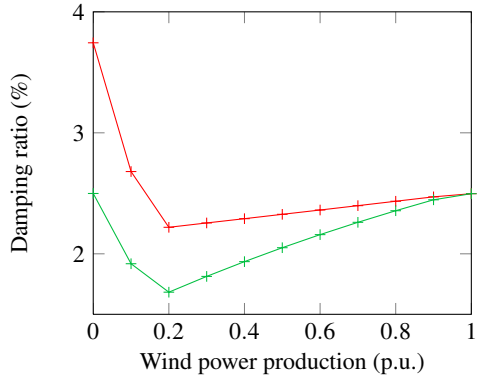

Figure 4: Damping ratio with coordination [red] and without coordination [green]

Impact of AC Grid Faults on VSC-HVDC Off-Shore Wind Network

Lina He (Advisor: Prof. Chen-Ching Liu)
School of Electrical, Electronic and Mechanical engineering,
University College Dublin, Belfield, Dublin 4, Ireland,
Email: Lina.He@ucdconnect.ie

***Abstract*— An off-shore wind farm based on permanent magnet synchronous generators (PMSG) is connected to the ac grid through a VSC-HVDC link. Due to the use of pulse width modulation (PWM) control, the active and reactive power can be independently adjusted. The wind farm side VSC (WFVSC) uses a constant active power, which allows the collection of power from the wind farm to be transferred to the dc side. To balance the input and output of HVDC, the grid side VSC (GSVSC) is assigned to control the dc voltage at a constant. Also, the GSVSC can supply reactive power for the ac grid. When the ac grid encounters an ac fault near the point of common coupling (PCC), the PCC voltage rapidly declines. This in turn reduces the power transmission capability of GSVSC. As the WFVSC injected power cannot be reduced instantaneously, the unbalanced power in HVDC will lead to charging of dc capacitors. This can result in a severe dc overvoltage, which reduces the reliability of costly HVDC devices. In addition, the dc overvoltage can increase the wind farm terminal voltage. Excessive voltage at the wind farm terminal might cause wind turbines to be tripped by its overvoltage protection. This in turn leads to a deficit in generation, causing voltage and frequency problems in the ac system. A HVDC off-shore wind network is developed for computer simulations. To identify the impact of ac faults on the HVDC grid, ac faults close to PCC are studied, and the simulation results of the test system are presented.**

I. KEY EQUATIONS

The decoupling controller equations are:

$$v_d = -(K_{ip} + \frac{K_{iI}}{s})(i_q^* - i_q) + \omega L i_q + v_{sd} \quad (1)$$

$$v_q = -(K_{ip} + \frac{K_{iI}}{s})(i_d^* - i_d) - \omega L i_d + v_{sq} \quad (2)$$

II. KEY FIGURES

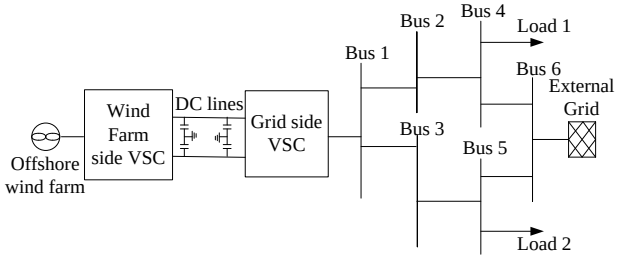

Figure 1. Test System

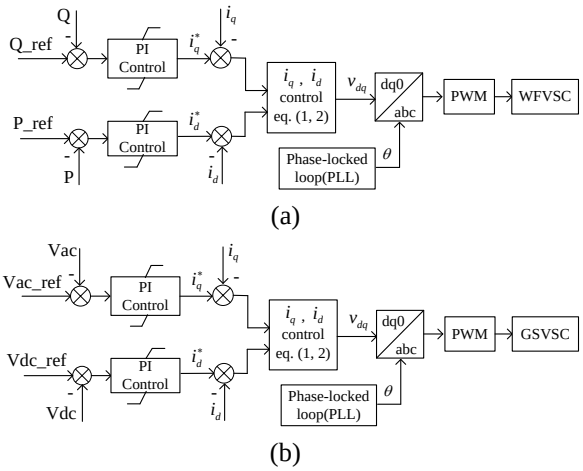

Figure 2. Controller Configurations: (a) WFVSC , (b) GSVSC

III. KEY RESULTS

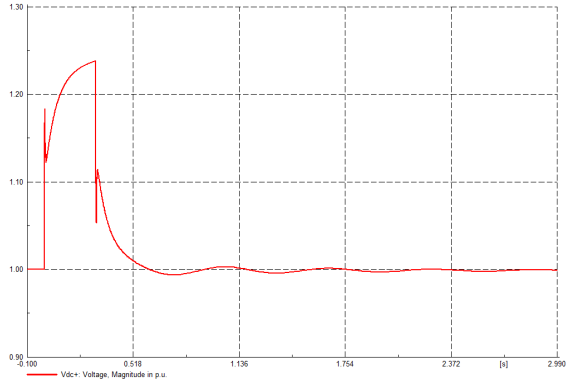

Figure 3. Positive Pole DC Voltage of HVDC Off-shore Wind Network Under Three-Phase Short-Circuit Fault at Line 1-3

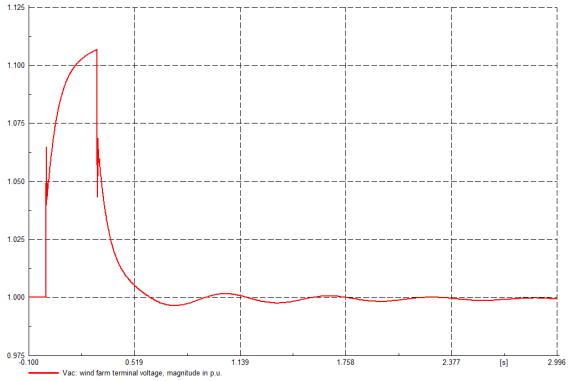

Figure 4. Wind Farm Terminal Voltage of HVDC Off-Shore Wind Farm Network Under Three-Phase Short Circuit Fault at Line 1-3

Analyses of the modifications in the π circuits for inclusion of frequency influence in transmission line representation

Leonardo S. Lessa, Afonso J. Prado, Sérgio Kurokawa, José Pissolato Filho and Luiz F. Bovolato
Transient Electromagnetic Studies Laboratory, Department of Electrical Engineering, UNESP - University of São Paulo State, Ilha Solteira, Brazil,
Email: nardolessa@yahoo.com.br, afonsojp@uol.com.br, kurokawa@dee.feis.unesp.br, pisso@dsce.fee.unicamp.br and bovolato@dee.feis.unesp.br

***Abstract*— In this article, a transmission line is represented by state equations through mono-phase π circuits. The line parameters are considered for both conditions: frequency independent, using the classical structure of π circuits and frequency dependent, using modified π circuits. It is determined the reasonable number of π circuits and the number of blocks composed by parallel resistor and inductor (modified π circuits) for reduction of numerical oscillations. It is simulated the numerical routine with and without the effect of frequency in the longitudinal parameters. State equations and π circuits are used, representing the transmission line composing a linear system which is solved by numerical routines based on the trapezoidal rule. The effect of frequency on the longitudinal line parameters is synthesized by resistors and inductors in parallel and this representation is analyzed in details.**

I. MATHEMATICAL MODEL

Using the trapezoidal rule, the linear system is:

$$\left[I-\frac{T}{2}A\right]x[k+1]=\left[I+\frac{T}{2}A\right]x[k]+\frac{T}{2}B[u[k]+u[k+1]] \quad (1)$$

I matrix is the identity one. The other elements are:

$$x^T=\begin{bmatrix}x_1 & \cdots & x_n\end{bmatrix} \quad (2)$$

$$x_k^T=\begin{bmatrix}i_{k0} & i_{k1} & i_{k2} & \cdots & i_{km} & v_k(t)\end{bmatrix} \quad (3)$$

$$B^T=\begin{bmatrix}\frac{1}{L_0} & 0 & 0 & \ldots & 0 & 0\end{bmatrix} \quad (4)$$

$$A=\begin{bmatrix}D & A_H & 0 & \cdots & 0\\ A_L & D & A_H & \ddots & \vdots\\ 0 & A_L & \ddots & \ddots & 0\\ \vdots & \ddots & \ddots & D & A_H\\ 0 & \cdots & 0 & A_L & D\end{bmatrix} \quad (5)$$

For frequency influence, each π circuit presents:

$$A_H=\begin{bmatrix}0 & 0 & \cdots & 0\\ \vdots & \ddots & \cdots & \vdots\\ 0 & \cdots & \ddots & \vdots\\ -1/C & 0 & \cdots & 0\end{bmatrix} \quad (6)$$

$$A_L=\begin{bmatrix}0 & \cdots & 0 & 1/L_0\\ \vdots & \ddots & \cdots & 0\\ \vdots & \cdots & \ddots & \vdots\\ 0 & 0 & \cdots & 0\end{bmatrix} \quad (7)$$

$$D=\begin{bmatrix}-\frac{\sum R}{L_0} & \frac{R_1}{L_0} & \cdots & \frac{R_m}{L_0} & -\frac{1}{L_0}\\ \frac{R_1}{L_1} & -\frac{R_1}{L_1} & 0 & \cdots & 0\\ \vdots & 0 & \ddots & 0 & \vdots\\ \frac{R_m}{L_m} & \vdots & 0 & -\frac{R_m}{L_m} & 0\\ \frac{2}{C} & 0 & \cdots & 0 & -\frac{G}{C}\end{bmatrix} \quad (8)$$

II. TESTING MODEL

The transmission line represented by a π circuit cascade with frequency independent parameters is:

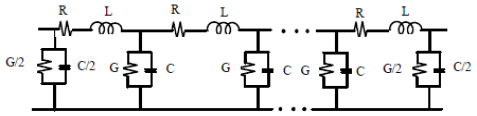

Figure 1: A cascade of π circuits without frequency influence.

The effect of frequency on the longitudinal line parameters is introduced by RL parallel associations. It is represented by:

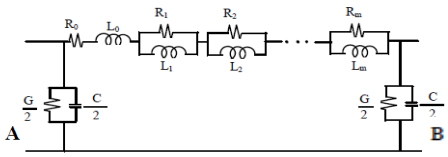

Figure 2: Inserting the effect of frequency in a π circuit unity.

III. OBTAINED RESULTS

It is shown the output voltages at the receiving line end for a step voltage source at the sending line end.

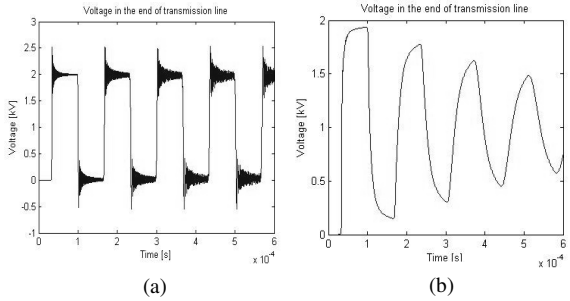

(a) (b)

Figure 4: transmission line (a) without the effect of frequency, (b) with the effect of frequency.

Dynamic simulation of HVDC interconnection in large power system

Minh X. Bui, Mai H. Nguyen, and Tapan K. Saha
Queensland Geothermal Energy Centre of Excellence and School of Information Technology & Electrical Engineering
The University of Queensland, Brisbane, QLD-4072, Australia
Email: buixuanmin82@yahoo.com, huongmai@itee.uq.edu.au and saha@itee.uq.edu.au

***Abstract*— This paper develops a controller for a line commutated converter HVDC in order to improve the transient stability of the power system. This controller is based on the integration of a frequency modulation to the HVDC control scheme. The HVDC model based on CIGRE benchmark model is used for dynamic simulation to investigate the system's operation when subjected by faults and large disturbances. The results of time domain simulations prove that the proposed HVDC controller provide a significant improvement in transient stability and voltage stability of the system. The VDCOL is also proved to be a critical part of the HVDC control scheme for stabilizing the AC systems connected by a HVDC link. HVDC can help to improve the transient stability of the network although more reactive power compensation is required. Simulations are implemented on the simplified Southern Eastern (SE) Australian power system using the Power Factory software package.**

I. KEY FIGURES

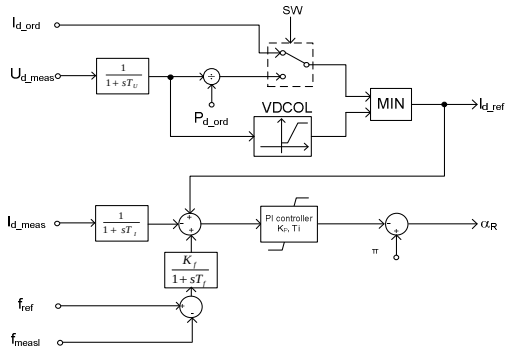

Figure 1. Proposed rectifier controller model

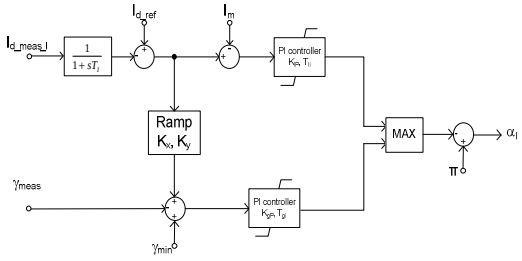

Figure 2. Inverter controller model

II. KEY RESULTS

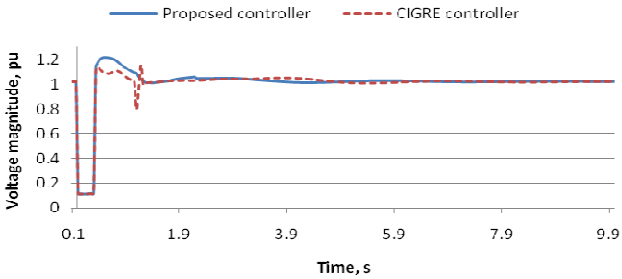

Figure 3. Voltage magnitude of bus 217 with fault at rectifier terminal

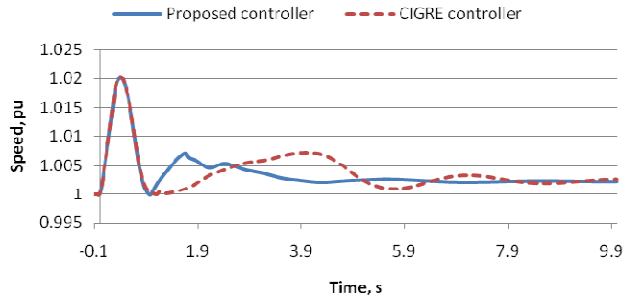

Figure 4. Speed of BPS2 with fault at rectifier terminal

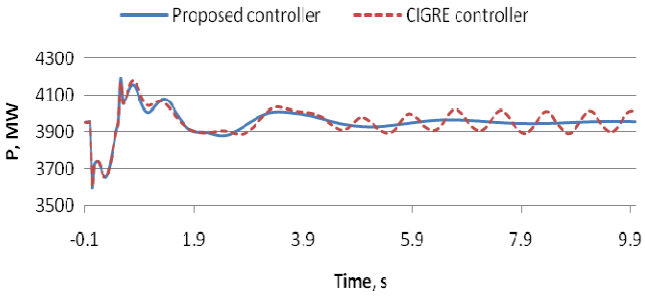

Figure 5. Active power generation of BPS2 with fault at inverter terminal

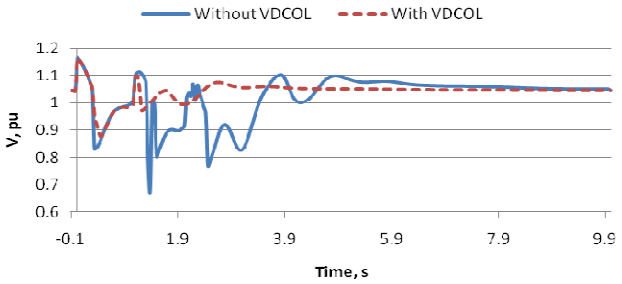

Figure 6. Voltage magnitude of bus 102 with fault at inverter terminal

Preliminary Analysis of MV Cable Lines Models for High Frequency Harmonic Penetration Studies

R. Langella, *Senior Member, IEEE*, **L. Nugnes**, **F. Pilo**, *Member, IEEE*, **G. Pisano**, *Member, IEEE*, **G. Petretto**, **S. Scalari**, **A. Testa**, *Fellow, IEEE*

***Abstract*— The large penetration of distributed generation requires accurate line and cable models in a frequency range much wider than the classical interval, 0-2.5 kHz, used for traditional harmonic and interharmonic penetration studies. In the paper, the behavior of MV cable lines is considered in the frequency range from 0 to 100 kHz, with reference to a case-study. Models based on the classical Π and Γ line equivalent circuits are considered. Reference is made to open and short circuited line input terminals conditions. A comparison of the performances of different complexity models, in terms of output terminal impedance magnitude accuracy, is developed**

I. KEY EQUATIONS

The guiding equations are:

$$\overline{Z}_{1,2} = \overline{B} = \overline{Z}_0 \sinh \overline{K}x = \sqrt{\overline{Z}/\overline{Y}} \sinh \sqrt{\overline{Z}\overline{Y}},$$
$$\overline{Y}_{1,0} = \overline{Y}_{2,0} = \frac{\overline{A}-1}{\overline{B}} = \frac{\overline{Y}}{2} \frac{tgh\sqrt{\overline{Z}\overline{Y}}/2}{\sqrt{\overline{Z}\overline{Y}}/2}, \quad (1)$$

$$\overline{Z} = r_s + j\omega l_s \quad (2)$$

$$\overline{Y} = g_s + j\omega c_s \quad (3)$$

II. KEY FIGURES

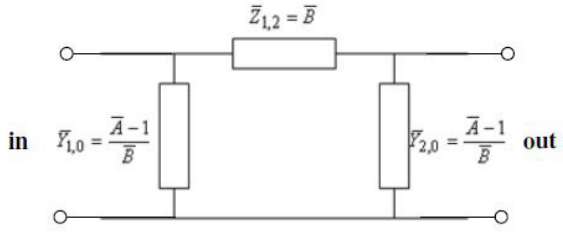

Figure 1. Distributed Parameters Model of a finite length line as two-port.

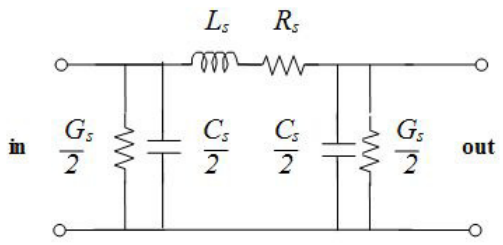

Figure 2. Model of a line based on a single Π equivalent.

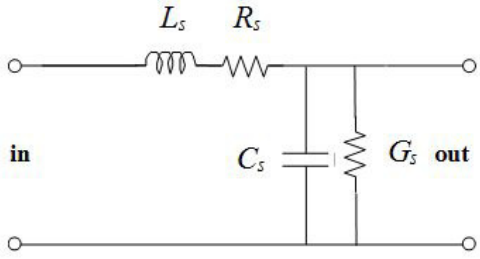

Figure 3. Model of a line based on a single Γ equivalent.

III. KEY RESULTS

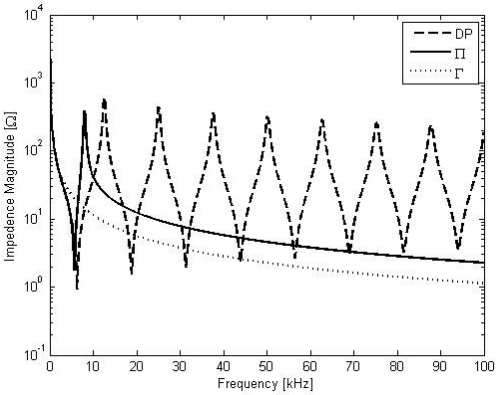

Figure 4. Output Impedance Magnitude versus frequency (0-100 kHz) for a 3 km length cable for open circuited input; models: Distributed Parameters (DP, dashed lines), Π equivalent (solid lines) and Γ equivalent (dotted lines).

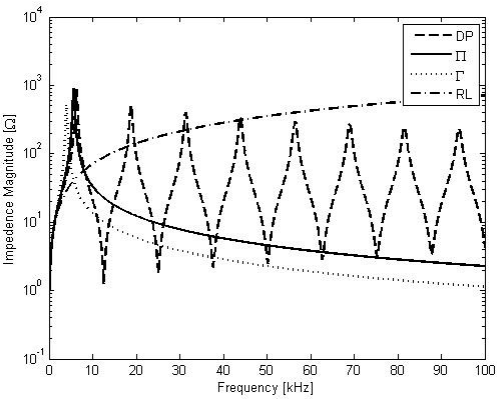

Figure 5. Output Impedance Magnitude versus frequency (0-100 kHz) for a 3 km length cable for short circuited input; models: Distributed Parameters (DP, dashed lines), Π equivalent (solid lines) and Γ equivalent (dotted lines) and RL equivalent (dash-dotted line).

A New Protection Principle for HVDC Transmission Lines Based on Fault component of Voltage and Current

Luhua Xing, Qing Chen, Zhanjun Gao, Zhaoyuan Fu
School of Electrical Engineering Shandong University, Shandong Jinan 250061, China,
Email: xingluhua@mail.sdu.edu.cn and qchen@sdu.edu.cn

***Abstract*—The paper presents a new main protection for double circuit transmission lines of bipolar HVDC transmission system，which is based on the variation characteristics of fault component of voltage and current. By a set threshold for the ratio of amplitudes of the fault components of voltage on bipolar lines, faults outside HVDC lines can be excluded, and the fault line can be distinguished. The polarities of the fault component of currents at the ends of the fault line are different for internal faults, while are the same for external faults. Accordingly, internal faults and external faults can be distinguished. The principle can be applied for bipolar neutral grounding at both ends and monopolar metallic return mode operation. Simulation results based on PSCAD/EMTDC for a practical HVDC transmission system demonstrate that the fault line can be rapidly selected and internal faults and external faults can be distinguished by the protection. Lightning disturbances can be excluded by the proposed criterion. The protection criterion can move accurately for internal faults with high transition resistance and lightning induced faults. The calculation requirement of the protection criterion can be satisfied with sampling frequency in the range of 10 kHz~100 kHz.**

I. KEY EQUATIONS

The fault detection criterion is:

$$\begin{cases} |\Delta u_{Ri}| > k_R \\ |\Delta u_{Ii}| > k_I \end{cases} \quad (1)$$

Where i=1, 2.

Protection criterions for double circuit dc lines can be described as:

For internal faults on line 1:

$$\begin{cases} |\Delta u_{R1}| / |\Delta u_{R2}| > k_{R2} \\ |\Delta u_{I1}| / |\Delta u_{I2}| > k_{I2} \\ p = sign(M\Delta i_{R1}) \times sign(M\Delta i_{I1}) = -1 \end{cases} \quad (2)$$

For internal faults on line 2:

$$\begin{cases} |\Delta u_{R2}| / |\Delta u_{R1}| > k_{R3} \\ |\Delta u_{I2}| / |\Delta u_{I1}| > k_{I3} \\ p = sign(M\Delta i_{R2}) \times sign(M\Delta i_{I2}) = -1 \end{cases} \quad (3)$$

II. KEY FIGURES

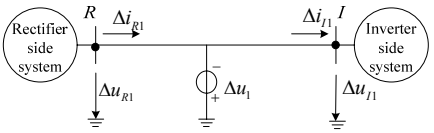

Figure1. Fault superimposed circuit of internal faults on line 1

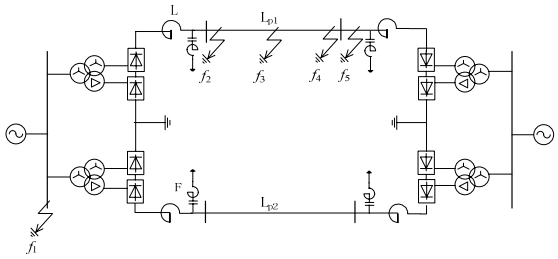

Figure2. A ±660kV HVDC Transmission System

III. KEY RESULTS

Table 1.Magnitudes and Ratios of Fault Component of Voltages under Conditions with Different Fault Positions and Transition Resistances

Fault positions	Value of TR(Ω)	$\|\Delta u_{R1}\|$ (p.u)	$\|\Delta u_{I1}\|$ (p.u)	$\|\Delta u_{R1}\|/\|\Delta u_{R2}\|$	$\|\Delta u_{I1}\|/\|\Delta u_{I2}\|$
f_1	0	0.409	0.396	1.002	1.001
	200	0.115	0.136	1.001	0.998
f_2	0	1.167	0.891	**7.481**	**1.757**
	200	0.595	0.427	**8.488**	**1.564**
	600	0.298	0.222	**10.64**	**1.523**
f_3	0	0.999	0.913	**10.46**	**5.265**
	200	0.466	0.531	**10.81**	**4.307**
	600	0.210	0.293	**11.46**	**2.93**
f_4	0	0.887	0.841	**1.958**	**8.271**
	200	0.407	0.618	**1.612**	**35.90**
	600	0.209	0.334	**1.518**	**14.01**
f_5	0	0.881	1.002	**1.939**	**9.843**
	200	0.406	0.616	**1.586**	**33.46**
	600	0.209	0.335	**1.513**	**14.23**
CF		0.525	0.573	1.001	1.000

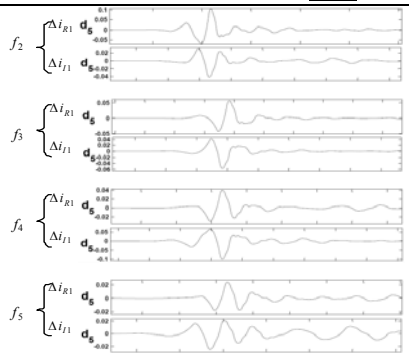

Figure 3. Wavelet transform five level coefficients of Δi_{R1} and Δi_{I1} for line to ground faults at f_2, f_3, f_4 and f_5 (sampling frequency of 100 kHz)

Coordination between DFIG-based Wind Farm and LCC-HVDC Transmission Considering Limiting Factors

Haiping Yin, Lingling Fan and Zhixin Miao
Department of Electrical Engineering, University of South Florida, Tampa, FL 33620, USA,
Email: fll@ieee.org

Abstract— **For wind farms with thyristor-based line current commuting (LCC)-HVDC delivery systems, reactive power must be provided for the HVDC converters to ensure normal operation. When the wind speed increases, the capability to provide reactive power by a doubly-fed induction generator (DFIG) wind farm decreases. Meanwhile, there is increase in reactive power loss in the transformer and ac lines. As a consequence, the reactive power transmitted to the LCC-HVDC could be reduced. Coordination of the DFIG wind farm terminal voltage and HVDC rectifier voltage is necessary to make sure the required reactive power is supplied to the HVDC converters. The goal of this paper is to investigate the upper and lower limits for the rectifier ac bus voltage. An integrated DFIG-based 200 MW wind farm with a simplified HVDC-link connection is studied in Matlab/Simulink. Time-domain simulation results are given to confirm the analysis.**

I. KEY EQUATIONS

For a monopole, 12-pulse inverter of HVDC-link, the relationship of AC/DC voltage and current of rectifier are shown as below:

$$V_{dr} = \frac{3}{\pi}\sqrt{6}V_{ac}\cos\alpha \quad (1)$$

$$V_{dr} = I_{dc}R + V_{di} \quad (2)$$

$$P_{dc} = V_{dr}I_{dc} \quad (3)$$

$$Q_{ac} = P_{dc}\tan\varphi \quad (4)$$

II. KEY FIGURES

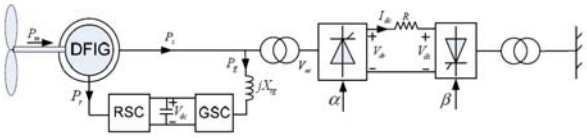

Figure 1. Study System

Figure 1. P/Q Limit and Operating Points of DFIG under Different Wind Speeds.

III. KEY RESULTS

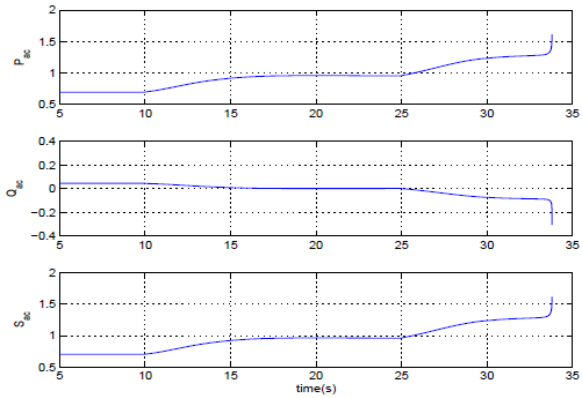

Figure 2. Dynamic Responses of Active Power, Reactive Power, Apparent Power at the ac Bus under Wind Speed Changes, Wind Speed Increases from 9m/s to 10m/s at 10s, and Increase from 10m/s to 11m/s at 25s. V_{ac} = 0. 993.

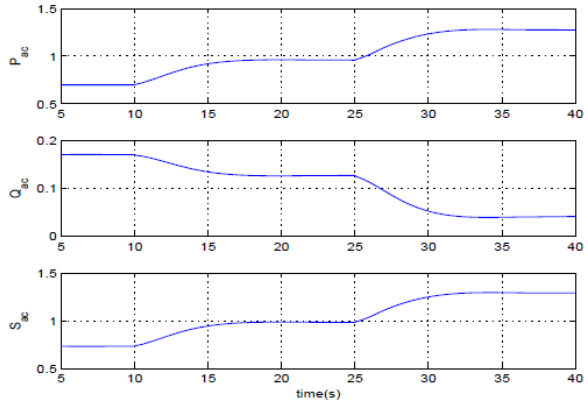

Figure 3. Dynamic Responses of Active Power, Reactive Power, Apparent Power at the ac Bus under Wind Speed Changes, Wind Speed Increases from 9m/s to 10m/s at 10s, and Increase from 10m/s to 11m/s at 25s. V_{ac} = 0. 98.